(2)

Marine Physical Laboratory

AD-A239 961

Freely Drifting Swallow Float Array: August 1990 NATIVE 1 Experiment (First Deployment)

G. L. D'Spain, W. S. Hodgkiss, G. L. Edmonds, and M. Darling

MPL Technical Memorandum 426
February 1991

Approved for public release; distribution unlimited.

91 8 29 030

University of California, San Diego
Scripps Institution of Oceanography

91-09294

UNCLASSIFIED

SECURITY CLASSIFICATION OF THIS PAGE

REPORT DOCUMENTATION PAGE

Form Approved OMB No. 0704-0188

1a. REPORT SECURITY CLASSIFICATION
UNCLASSIFIED

1b. RESTRICTIVE MARKINGS

2a. SECURITY CLASSIFICATION AUTHORITY

2b. DECLASSIFICATION / DOWNGRADING SCHEDULE

3. DISTRIBUTION / AVAILABILITY OF REPORT
Approved for public release; distribution unlimited.

4. PERFORMING ORGANIZATION REPORT NUMBER(S)
MPL-U-4/91 [MPL Technical Memorandum 426]

5. MONITORING ORGANIZATION REPORT NUMBER(S)

6a. NAME OF PERFORMING ORGANIZATION
University of California, San Diego

6b. OFFICE SYMBOL *(If applicable)*
MPL

7a. NAME OF MONITORING ORGANIZATION
Office of Naval Research
Department of the Navy

6c. ADDRESS *(City, State, and ZIP Code)*
Marine Physical Laboratory
Scripps Institution of Oceanography
San Diego, California 92152

7b. ADDRESS *(City, State, and ZIP Code)*
800 North Quincy Street
Arlington, VA 22217-5000

8a. NAME OF FUNDING / SPONSORING ORGANIZATION
Office of Naval Research

8b. OFFICE SYMBOL *(If applicable)*
ONR

9. PROCUREMENT INSTRUMENT IDENTIFICATION NUMBER
N00014-89-D-0142

8c. ADDRESS *(City, State, and ZIP Code)*
800 North Quincy Street
Arlington, VA 22217-5000

10. SOURCE OF FUNDING NUMBERS

PROGRAM ELEMENT NO.	PROJECT NO.	TASK NO	WORK UNIT ACCESSION NO.

11. TITLE *(Include Security Classification)*
FREELY DRIFTING SWALLOW FLOAT ARRAY: AUGUST 1990 NATIVE 1 EXPERIMENT (FIRST DEPLOYMENT)

12. PERSONAL AUTHOR(S)
G. L. D'Spain, W. S. Hodgkiss, G. L. Edmonds, and M. Darling

13a. TYPE OF REPORT	13b. TIME COVERED	14. DATE OF REPORT *(Year, Month, Day)*	15. PAGE COUNT
tech memo	FROM _____ TO _____	February 1991	

16. SUPPLEMENTARY NOTATION

17. COSATI CODES			18. SUBJECT TERMS *(Continue on reverse if necessary and identify by block number)*
FIELD	GROUP	SUB-GROUP	Swallow floats, geophone and hydrophone time series, particle velocity and pressure spectra

19. ABSTRACT *(Continue on reverse if necessary and identify by block number)*

Representative data collected by the Marine Physical Laboratory's (MPL) set of Swallow floats during event 1 of the NATIVE 1 experiment are presented in this report. The deployment location was in the northwest Atlantic Ocean around 31° 15.6′ N, 74° 53.2′ W, almost 600 km east of Savannah, Georgia. Nine midwater Swallow floats were deployed; two equilibrated at a depth of about 400 meters and the remaining seven were staggered about every 100 meters starting at 1100 meters down to 1700 meters. They were put into the water at about the geometric center of a triangle, whose sides were approximately 6.5 km in length, formed by the three remaining floats which were tethered to the 3180-meter-deep ocean bottom by 3.05-meter lines.

20. DISTRIBUTION / AVAILABILITY OF ABSTRACT
☐ UNCLASSIFIED/UNLIMITED ☒ SAME AS RPT ☐ OTIC USERS

21. ABSTRACT SECURITY CLASSIFICATION
UNCLASSIFIED

22a. NAME OF RESPONSIBLE INDIVIDUAL	22b. TELEPHONE *(Include Area Code)*	22c. OFFICE SYMBOL
W. S. Hodgkiss	(619) 534-1798	MPL

DD Form 1473, JUN 86 *Previous editions are obsolete*

SECURITY CLASSIFICATION OF THIS PAGE
UNCLASSIFIED

DTIC
COPY
INSPECTED
6

Accession For
NTIS GRA&I
DTIC TAB
Unannounced
Justification
By
Distribution/
Availability Codes
Dist | Avail and/or Special
A-1

Freely Drifting Swallow Float Array: August 1990 NATIVE 1 Experiment (First Deployment)

G. L. D'Spain, W. S. Hodgkiss, G. L. Edmonds, and M. Darling

Marine Physical Laboratory
Scripps Institution of Oceanography
San Diego, CA 92152

ABSTRACT

Representative data collected by the Marine Physical Laboratory's (MPL) set of Swallow floats during event 1 of the NATIVE 1 experiment are presented in this report. The deployment location was in the northwest Atlantic Ocean around 31° 15.6′ N, 74° 53.2′ W, almost 600 km east of Savannah, Georgia. Nine midwater Swallow floats were deployed; two equilibrated at a depth of about 400 meters and the remaining seven were staggered about every 100 meters starting at 1100 meters down to 1700 meters. They were put into the water at about the geometric center of a triangle, whose sides were approximately 6.5 km in length, formed by the three remaining floats which were tethered to the 3180-meter-deep ocean bottom by 3.05-meter lines.

This report presents the Swallow float deployment positions both in plan view and in depth, the other acoustic sensors in the experiment (the TSVLA, the VEDABS vertical line array, and a set of sonobuoys of various designs), the known signal sources during the experiment (the research vessels NADC 38 and Gyre, the ELF towed source, and the SUS charges), a summary of the Swallow float log, and representative Swallow float data. The Swallow float data are composed of a) general indications of data quality, b) battery voltage, compass heading, and automatic gain control (AGC) measurements, c) the 8 kHz acoustic localization ping arrivals, and d) the infrasonic acoustic data. The infrasonic data include the RMS levels of the pressure and the three components of particle velocity for all floats over the whole duration of the experiment, selected pressure and particle velocity time series, and selected pressure spectra and horizontal active intensity spectra. A description of the Swallow float infrasonic data acquisition system, along with calibration curves, is given in Appendix 1.

The Swallow float data set is of extremely high quality: 99.9 percent of the recorded data passed data quality screening tests. However, a few problems, which had only minimal impact on the quality of the data set, occurred. First, bottom-tethered float 11, which appeared to operate flawlessly throughout the experiment, failed to ascend upon recall and was lost. Second, float 4's infrasonic hydrophone somehow became disconnected from its electronic circuitry before deployment and recorded no usable data. Finally, the sensitivity of float 2's hydrophone at the lowest infrasonic frequencies apparently increased suddenly by 6 dB midway through the experiment.

A number of interesting features can be seen in a preliminary look at the data. First, the Swallow floats were clearly able to hear the 7, 10, and 16 Hz tones generated by the towed ELF source; signal-to-noise ratios of 15 dB or greater are common. The directionality of the sound field at these three frequencies, as measured by the active acoustic intensity spectrum, shows the expected behavior; i.e., net energy flow away from the source. Second, the two SUS charge events involved the detonation of 22 and 18 charges, respectively, with a few detonations being recorded prior to the events. Third, the T phase generated by an earthquake in the Leeward Islands of the Caribbean was

recorded by all the floats. Fourth, the geophones in seven of the nine midwater Swallow floats recorded disturbances of a non-acoustic nature; the two shallowest floats at 400 meters were especially affected. These non-acoustic disturbances may have been caused by nekton near the floats. Fifth, a broad spectral peak at 0.47 Hz appears to be due to a water-column resonance, i.e., the fundamental "organ pipe" mode. Finally, six acoustic arrivals of unknown origin, each with about a 1 minute duration, were recorded by the floats. They occurred at 16:49 Z, 20:20 Z, and 21:24 Z on 4 August, and 7:20 Z, 8:57 Z, and 9:50 Z on 5 August. Their sources may be identifiable once further analysis of the data is done.

Table of Contents

Introduction

I. Swallow Float Deployment Geometry
   a) Plan View of the Deployment/Retrieval Positions
   b) Deployment Depths

II. Other Receivers, Known Sound Sources, and Environmental Data
   a) Other Receiving Systems in the Experiment
   b) The ELF Towed Source and the Gyre, the NADC 38, and the SUS Charges
   c) Environmental Data

III. Summary of NATIVE 1 Swallow Float Log

IV. Swallow Float Data - General Indication of Data Integrity
   a) Data Quality Screening Results
   b) Unique Aspects of Certain Floats in this Deployment

V. Battery Voltage, Float Heading, AGC Level, and Percentage of Clipped Points
   a) Battery Voltage
   b) Float Heading
   c) AGC Level
   d) Percentage of Clipped Points

VI. The 8 kHz Surface and Bottom Bounce Data

VII. The 8 kHz Interelement Range Data

VIII. RMS Pressure and Particle Velocity
   a) Midwater Swallow Floats
   b) Non-Acoustic Disturbances in the Midwater Swallow Float Geophone Data
   c) Bottom-Tethered Swallow Floats

IX. Geophone and Hydrophone Time Series
   a) SUS Charge Arrivals
   b) T Phase Arrival from the Leeward Islands' Earthquake
   c) Non-Acoustic Disturbances in the Midwater Swallow Float Geophone Data
   d) Unknown Acoustic Arrivals

X. Particle Velocity and Pressure Spectra
   a) LOFAR Grams of Float 2's Auto Spectra
   b) Hydrophone Pressure Spectrum vs Geophone-Data-Derived Pressure Spectrum
   c) The Rise Towards the Microseismic Peak
   d) Comparison of Spectral Levels on the Three Geophone Components
   e) Spectra of the T Phase Arrival from the Leeward Islands' Earthquake
   f) Time Series of ELF Signal Spectra

Acknowledgements

References

Appendix 1 - Swallow Float Infrasonic Data Acquisition System

Appendix 2 - Caribbean Area Map and Preliminary Determination of Epicenters

Figures

Introduction

The Marine Physical Laboratory's (MPL) Swallow floats are independent, neutrally buoyant, and freely drifting sensor systems. They are capable of measuring simultaneously the acoustic pressure and the three orthogonal components of the acoustic particle velocity in the infrasonic frequency band from 0.2 to 25 Hz [1]. Figure 1 is a schematic drawing of a typical midwater Swallow float. Contained within a 0.432-meter-diameter glass sphere are the three orthogonally-oriented geophones for measuring infrasonic particle velocity, a magnetic compass, and the necessary hardware and electrical power to record up to 20 hours of digitized data. Mounted outside of the float's glass sphere are the omni-directional ceramic hydrophone for measuring infrasonic pressure and the International Transducer Corporation (ITC) hydrophone which is part of the 8 kHz localization system.

The Swallow floats were deployed twice during the August, 1990 NATIVE 1 (Noise And Transmission loss In VLF Environments) experiment [2]. This experiment marked only the second time in which all the floats were equipped with both infrasonic hydrophones and geophones. The following table summarizes the time periods over which the Swallow floats recorded data.

Deployment	Event Number	Data Recording		No. of Floats Deployed (No. with Full Data Tapes)
		Start Time	Approx End Time	
1	1	16:30 Z, 4 Aug	11:30 Z, 5 Aug	12 (11)
2a	3	10:00 Z, 10 Aug	05:00 Z, 11 Aug	2 (2)
2b	4	04:00 Z, 12 Aug	23:00 Z, 12 Aug	9 (9)

Note that in the first deployment, 12 floats were deployed but only 11 were recovered; a bottom-tethered float, for some unexplained reason, could not ascend from the ocean bottom.

The purpose of this report is to present a preliminary analysis of the Swallow float data collected during the first deployment, located around 31.3° N, 74.9° W. These data include the results of a general screening for Swallow float data quality (Section IV), the battery voltage, compass heading, and automatic gain control (AGC) measurements (Section V), the 8 kHz acoustic localization ping arrivals (Sections VI and VII), and the infrasonic pressure and particle velocity data (Sections VIII, IX, and X). Before the discussion of the Swallow float data, the float deployment and retrieval locations (Section I), and a brief summary of the other components of the NATIVE 1 experiment (Section II), are given. Also, Section III gives a summary o the Swallow float log during the entire NATIVE 1 experiment.

Note that all times given in this report are in Greenwich Mean Time (GMT), indicated by "Z". Local Eastern Daylight Time can be obtained by subtracting four hours from GMT time.

I. Swallow Float Deployment Geometry

a) Plan View of the Deployment/Retrieval Positions

Figure I.1 shows a plan view of the deployment and retrieval positions of the Swallow floats with respect to point "D" (31° 15.6′ N, 74° 53.2′ W) in the first deployment (event 1). The scale of the axes used in the plot is the same as that in the deployment geometry plots for previous Swallow float experiments. Floats 9, 10, and 11 (indicated in the figure by "9", "A", and "B", respectively) were tethered to the ocean bottom by 3.05-meter-long lines in a triangular pattern 6.5 km (3.5 nm) on a side. Float 11, the southernmost bottom float, could not ascend to the surface and was lost. The nine freely drifting midwater floats were deployed in a tight cluster near point D. The two shallowest floats, floats 0 and 1 (at about 400 meters depth) were recovered to the north of point D, whereas the deeper floats (between the depths of 1100 and 1700 meters) drifted to the southwest during the experiment.

For comparison, the plan view of the Swallow float deployment and retrieval positions with respect to point "D2" (31° 13.3′ N, 74° 38.8′ W) in the two parts of the second deployment (events 3 and 4) is shown in Figure I.2. The deployment positions are connected by solid lines. Floats 9 and 10, bottom tethered by 6.3-meter-long lines, were deployed for event 3; their deployment positions are at the ends of the northernmost line in the figure. The remaining floats, eight midwater floats and bottom-tethered float 8, were deployed for event 4. All floats drifted to the south and southwest during the deployment. Note that the scale of this figure is larger than in Figure I.1; to show this, a triangle the size of the bottom float triangle in Figure I.1 is plotted in Figure I.2. In fact, the surface area encompassing the float deployment and retrieval positions in this deployment is more than 6 times larger than the surface area encompassing any previous experiment.

b) Deployment Depths

The true deployment depths of the Swallow floats as a function of time in the first deployment of the NATIVE 1 experiment are shown in Figure I.3. The set of horizontal dotted lines, starting at about 400 meters depth, are measurements of the float depths, obtained by converting the travel times of the surface bounce arrivals to depth using the harmonic mean of the sound speed. (A discussion of this 8 kHz localization data is given in Section VI). The following table provides a comparison between the planned deployment depth and the average depth actually achieved for each of the floats.

Float ID Number	Planned Deployment Depth (m)	Actual Deployment Depth (m)
0	300	415
1	300	393
2	1100	1121
3	1200	1213
4	1300	1330
5	1400	1481
6	1500	1580
7	1600	1531
8	1700	1671
9	bottom	3174
10	bottom	3186

The actual deployment depths of all floats except float 0 are within 100 meters of the planned depth; the average difference is 59 meters. The shallowest seven floats equilibrated at depths deeper than planned, whereas floats 7 and 8 equilibrated at shallower depths. These results are excellent, especially since this was the first deployment of the Swallow floats in the Atlantic Ocean.

The lower horizontal axis of Figure I.3 gives the record number in which the surface bounce detection was made. This axis is actually a measure of time elapsed since the synchronization of the floats at 08:30 Z, 4 August. Since each record is 45 seconds long, the conversion from record number to minutes is made by multiplying the record number by 0.75. Each float was programmed to ping every 12 records; this is the horizontal spacing between each of the dots in a given line. The waviness of the midwater floats' dotted lines, due to their depths changing as a function of time, is probably indicative of the presence of internal waves. Note that previous float deployments in the northeast Pacific Ocean have shown a larger amplitude of float oscillation in depth (e.g., [3] and [4]).

Also included in Figure I.3 is a sound speed profile calculated using Generalized Digital Environmental Model data [5] for 31.0° N, 75.0° W provided by Janice Boyd at the Naval Oceanographic and Atmospheric Research Laboratory (NOARL) and an equation relating salinity, temperature, and depth to sound velocity [6]. The upper horizontal axis of the plot gives the sound velocity in meters/sec.

The planned float depths in the second float deployment are plotted in Figure I.4. The two bottom floats 9 and 10 in the first part of the second deployment are marked by "X"s in the plot. The remaining nine floats for event 4 are floats 0, 1, and 2 at 300 meters, floats 3, 4, 5, 6, and 7 at 3100 meters, and bottom-tethered float 8. The true deployment depths will be determined during a future analysis of these data.

The midwater floats in the deployments are equipped with 3 orthogonally-oriented infrasonic geophones as well as infrasonic hydrophones. The simultaneous measurement of the three components of acoustic particle velocity and acoustic pressure permits a complete characterization of the sound field at a given point in the ocean [7]. The bottom-tethered floats contain only a vertical component geophone and a hydrophone since the horizontal geophone components are typically heavily contaminated by tether effects.

II. Other Receivers, Known Sound Sources, and Environmental Data

a) Other Receiving Systems in the Experiment

Three other receiving systems were deployed near the Swallow float array during event 1 of NATIVE 1. These were 1) the test, steerable, vertical line array (TSVLA) operated by the Naval Air Development Center (NADC) in Warminster, Pa., 2) a versatile, experimental, data acquisition buoy system (VEDABS) vertical line array deployed by personnel from the Naval Oceanographic and Atmospheric Research Laboratory (NOARL), and 3) a set of air-launched sonobuoys of various designs deployed and monitored by NADC. The TSVLA is a large aperture, vertical array of 21 hydrophones. It drifts freely in the water column in order to reduce ocean-current-induced self noise. Analog data are sent up an electrical cable to a surface float which then transmits it to a receiving ship. The array motion is decoupled from that of the surface float by sea anchors located on the array. Due to a weak surface float transmitter, the NADC 38 remained within a few kilometers of the array during event 1.

The VEDABS number 1 was deployed near site D just before event 1 and was equipped with a very slow (≈ 0.2 inches per sec), 28-track, analog tape recorder capable of continuously recording up to 156 hours of data. The vertical line array connected to the VEDABS was also large in aperture and it also contained 21 hydrophones. (The additional 7 tracks available on the tape recorder were used for time code recording, synchronization, etc). Two other VEDABS/vertical line arrays were deployed in NATIVE 1. Number 2 also contained an analog tape recorder and was put near site D2. Number 3, actually an ADABS (AEAS data acquisition buoy system), contained an experimental digital data acquisition system and was not deployed until the 6th of August, after event 1 was completed. The following table lists the deployment times and locations of the three VEDABS arrays.

Deployment Times and Locations of the VEDABS Arrays in NATIVE 1

VEDABS Number	Deployment Time (Anchor Reached Bottom)	Deployment Location (Determined by Ship Survey)
1	14:13 Z, 3 August	31° 16.07′ N, 74° 52.43′ W
2	22:43 Z, 3 August	31° 13.35′ N, 74° 38.79′ W
3	18:23 Z, 6 August	31° 16.99′ N, 74° 53.57′ W

As part of all five Swallow float experiments between 1987 and 1989, personnel from NADC have co-deployed sonobuoys of various designs with the floats. Comparisons between the sonobuoy and Swallow float data have been made (e.g., [8]). Also, the table on p. 2 of [4] presents a sample listing of the types of sonobuoy designs which have been used. The NATIVE 1 experiment was no exception; a number of sonobuoys were air-deployed by NADC during the Swallow float recording period in events 1, 3, and 4. In addition, sonobuoys were used to make acoustic signature measurements of the two research vessels in the experiment, the Gyre and the NADC 38. The results of these acoustic signature tests, as well as the deployment times and locations of the sonobuoys in the experiment, will hopefully be obtained from NADC in the future.

b) The ELF Towed Source and the Gyre, the NADC 38, and the SUS Charges

As part of event 1 of NATIVE 1, a low frequency source belonging to NADC was towed at a 400 ft (121.9 meter) depth on a predominantly north-south course by the research vessel Gyre. Figure II.1 shows a plan view of the track of the Gyre during the Swallow float data recording period in event 1 (i.e., the 20-hour period from 16:30 Z, 4 Aug to 12:30 Z, 5 Aug). The ship positions were obtained from the handwritten log kept by Paul Bucca aboard the Gyre. They are either GPS fixes when available or Loran-C fixes otherwise; the large jumps in longitude in the ship track are due to a change in navigation method. The locations in minutes are with reference to 31° N and 74° W. Both axes of the plot have a range of 45 minutes, with the length of the x axis decreased by a factor of 0.857 in order to account for the latitude of the site. The triangle in the figure is formed by the bottom-tethered Swallow floats and the stars indicate

the locations of 14 expendable bathythermographs (XBT) deployed from the Gyre. The ship was located to the north-northeast of the Swallow floats at the beginning of their recording period, it steamed across the array to the south-southwest over a distance of almost 80 km, and then it reversed direction and returned along approximately the same course. The large "*" in the figure marks the position of the ship at 8:20 Z, 5 August; it is referred to in Section Xe.

The towed source, called ELF (for Extremely Low Frequency), simultaneously transmitted a pair of tones, either 7 Hz and 10 Hz or 10 Hz and 16 Hz, during three separate time periods in event 1. The track of the Gyre during these three periods are plotted with solid curves in Figure II.1; the dotted curves indicate the ship track during the two periods when the source was silent. The schedule of the ELF tone transmissions, obtained from the LOFAR grams presented in Section X, is given in the following table.

Transmission Schedule of the ELF Source

Frequency Pair	Swallow Float Record Interval	Time Interval	Ship Position at Start and End of Interval
7 and 10 Hz	640 to 1121	16:30 Z to 22:31 Z, 4 Aug	31° 27.46′ N, 74° 49.20′ W to 31° 05.25′ N, 74° 55.47′ W
7 and 10 Hz	1280 to 1560	00:30 Z to 04:00 Z, 5 Aug	30° 57.74′ N, 74° 57.49′ W to 30° 45.52′ N, 75° 00.35′ W
10 and 16 Hz	1880 to end	08:00 Z to 12:30 Z, 5 Aug	31° 00.21′ N, 74° 55.75′ W to 31° 18.32′ N, 74° 51.31′ W

Note that the LOFAR grams indicate that for a short time at the end of the 10-16 Hz broadcast period, the 7 Hz tone was also being transmitted.

This data-derived schedule agrees well with the actual ELF deployment log given in reference [16]. The table below summarizes the information in [16] on the ELF transmission schedule and source level during the Swallow float recording period in event 1.

Source Level for the ELF (dB re 1 μ Pa @ 1 m)

GMT Time (Date)	Frequency 7 Hz	10 Hz	16 Hz
16:30-22:30 (4 Aug)	164.1	166.1	off
00:30-02:42 (5 Aug)	164.2	166.2	off
02:42-04:00 (5 Aug)	164.2 --> 163.2	165.2	off
08:00-08:08 (5 Aug)	off	162.2	off
08:08-08:15 (5 Aug)	off	162.2	162.8
08:15-08:26 (5 Aug)	off	161.1	161.8
08:26-12:30 (5 Aug)	off	160.1	160.8

Because of the depth of the source (122 meters ± 7 meters [16]) with respect to the sound velocity profile (re Figure I.3), much of the source-generated energy arriving at the floats has interacted with the bottom. This feature of the ELF-generated sound field is shown qualitatively by the ray tracing picture in Figure II.2. Only the rays leaving the source in a ± 20 degree interval about the horizontal are plotted. Therefore, knowledge of the geoacoustic properties of the bottom is extremely important in modeling the ELF acoustic field. The transmission loss of the ELF tones as a function of range to the Swallow floats will be calculated once the locations of the floats as a function of time have been determined.

The personnel on board the NADC 38 were responsible for deploying the VEDABS array, the TSVLA, and the Swallow floats. Because of a weak surface transmitter on the TSVLA array, the ship remained near the float array during event 1. In order to remain as quiet as possible, either one of both of the ship's engines were stopped at intermittent times during the experiment [NADC 38 engineering log]. However, ship maneuvering was necessary during certain periods (e.g., to remain close to the TSVLA and to retrieve an air-dropped package) so that NADC 38-generated signals are present in the data. Therefore, navigation information for this ship will be important in the interpretation of the Swallow float data. In addition, acoustic signature tests using sonobuoys were conducted for both the Gyre and the NADC 38. The results of these tests, as well as the navigation information, will hopefully be provided by NADC in the

future.

A number of SUS charges were air-dropped from P-3 aircraft during event 1. Swallow float time series of the arrivals from these charge detonations are discussed in part a of Section IX. A total of 22 detonations were recorded in the first SUS event (from 22:50 Z to 23:15 Z, 4 Aug) and 18 were recorded in the second SUS event (from 23:49 Z, 4 Aug to 00:09 Z, 5 Aug). A few other SUS charge arrivals also appear in the data. A SUS charge deployment log, including deployment times and locations, charge size, and detonation depth, will hopefully be obtained from NADC.

c) Environmental Data

As shown by the stars in Figure II.1, a total of 14 expendable bathythermographs (XBT) were deployed from the Gyre during the Swallow float recording period in event 1. All were Sippican model T-5 XBTs, which have a maximum depth of 1830 meters. The following table lists the time and location of these XBT deployments, as recorded in Paul Bucca's log.

The Gyre XBT Deployment Times and Locations in Event 1

XBT Number	Deployment Time	Deployment Location
1	16:50 Z, 4 Aug	31° 26.50′ N, 74° 49.34′ W
2	17:20 Z, 4 Aug	31° 24.71′ N, 74° 49.86′ W
3	17:40 Z, 4 Aug	31° 23.47′ N, 74° 51.26′ W
4	17:47 Z, 4 Aug	31° 23.04′ N, 74° 51.34′ W
5	20:05 Z, 4 Aug	31° 14.51′ N, 74° 53.17′ W
6	22:15 Z, 4 Aug	31° 06.32′ N, 74° 55.12′ W
7	22:25 Z, 4 Aug	31° 05.67′ N, 74° 55.34′ W
8	00:05 Z, 5 Aug	30° 59.29′ N, 74° 57.20′ W
9	02:38 Z, 5 Aug	30° 50.18′ N, 74° 59.47′ W
10	04:20 Z, 5 Aug	30° 45.75′ N, 75° 00.46′ W
11	06:36 Z, 5 Aug	30° 54.45′ N, 74° 57.39′ W
12	08:40 Z, 5 Aug	31° 02.91′ N, 74° 55.37′ W
13	10:25 Z, 5 Aug	31° 09.96′ N, 74° 54.29′ W
14	12:30 Z, 5 Aug	31° 18:32′ N, 74° 51.31′ W

A wealth of other environmental information were also collected. The sensors used for this purpose include expendable current profilers (XCP), a conductivity, temperature, depth (CTD) instrument, air-launched XBTs (AXBT), a 3.5-kHz ocean bottom profiler, a National Data Buoy Center (NDBC) weather buoy, a tropical oceanic global atmospheric (TOGA) meteorological buoy, and ship-mounted anemometers. In addition, basic weather observations were recorded on both the Gyre and the NADC 38. Bruce Gomes at NOARL is responsible for writing a report on these environmental measurements. It will be available in early 1991 [2].

Finally, radar surveys of surface shipping near the deployment site were conducted by S-3 aircraft during the experiment. This information will hopefully be obtained from NADC.

III. Summary of NATIVE 1 Swallow Float Log

Note: All times are in standard Greenwich Mean Time. To obtain local eastern daylight time, subtract 4 hours. Also, all position fixes in which the minutes are given to three decimal places are Global Positioning System (GPS) fixes; those to two decimal places are Long Range Navigation (Loran-C) fixes.

25 July 1990

Swallow float scientific party from the Marine Physical Laboratory in San Diego arrives in Key West, Fla. for NATIVE 1 experiment. Personnel are Greg Edmonds, head electronics engineer, Marvin Darling, head electronics technician, and Gerald D'Spain, postdoctoral researcher.

28 July 1990

13:30 Finish checkout of Swallow float 1) acoustic release circuit, 2) acoustic transpond circuit, 3) synchronization and writing of two records, and 4) localization pings by floats 0 and 1. All floats are operating perfectly.

31 July 1990

20:00 The NADC 38 departs the NADC pier, Key West detachment, for the test site.

3 August 1990

00:00 Arrive at station "D", 31° 15.6′ N, 74° 53.2′ W. NADC personnel begin deployment of six SSQ 57D sonobuoys in order to measure the acoustic signals of The NADC 38 and The Gyre.

4 August 1990

07:24 Begin checkout of floats for the 0830 synchronization time for event 1.

07:45 All float transponder circuits, acoustic release circuits, timed release settings, and OAR flashers are operating properly.

08:30:00 Synchronously start all 12 Swallow floats for event 1. All floats' programs are running properly.

08:48 The floats are disconnected from the synchronization cable. Two complete localization ping cycles are finished and all floats are pinging at the correct time. Float 7's localization ping sounds different from the other floats' pings. A check of the Swallow Float Sea Assembly Log shows that float 7's localization circuit has a 4400 p-p voltage, a level which may be too high. The voltage level will be checked and possibly changed during float refurbishing between events 1 and 3. Each float's radio beacon will be activated and checked at time of float deployment.

09:29 Midwater float 8 deployed at 31° 15.737′ N, 74° 52.715′ W.

09:32 Midwater float 7 deployed at 31° 15.724′ N, 74° 52.735′ W.

09:34 Midwater float 6 deployed at 31° 15.715′ N, 74° 52.772′ W.

09:37 Midwater float 5 deployed at 31° 15.700′ N, 74° 52.820′ W.

09:39 Midwater float 4 deployed at 31° 15.636′ N, 74° 52.852′ W.

09:42 Midwater float 3 deployed at 31° 15.616′ N, 74° 52.867′ W.

09:44 Midwater float 2 deployed at 31° 15.619′ N, 74° 52.889′ W.

09:51 Midwater float 1 deployed at 31° 15.591′ N, 74° 52.975′ W.

09:55 Midwater float 0 deployed at 31° 15.570′ N, 74° 53.003′ W.

10:02 Begin VHF ADF radio check of midwater floats to determine if any floats have failed to descend from the surface. No floats appear to be on the surface.

10:10 Depart for bottom float 9's deployment site.

10:29 Bottom float 9 deployed at 31° 16.381′ N, 74° 55.153′ W.

10:45 The OAR flasher on float 11 is not flashing; replace flasher.

10:59 Bottom float 10 deployed at 31° 16.586′ N, 74° 51.047′ W.

11:29 Bottom float 11 deployed at 31° 13.399′ N, 74° 53.131′ W.

12:30 The ship is now back near point D. Lower hydrophone into the water off the starboard side in order to listen for the float localization pings and perform an acoustic survey of the float positions.

12:45 All floats' localization pings are audible.

13:49 Begin an acoustic survey of the float positions at 31° 15.048′ N, 74° 54.044′ W.

14:00 Finish acoustic survey at this ship position.

14:46 Have received a report that radio contact with the Test Steerable Vertical Line Array (TSVLA) has been lost. Ship is returning to the TSVLA deployment site.

14:55 Closest point of approach to the TSVLA. NADC personnel begin to deploy kytoon.

15:15 Begin float acoustic survey at survey point 1, 31° 16.77′ N, 74° 53.05′ W Loran-C. Bruce Gomes estimates that the Loran-C longitude fixes are offset from the GPS position fixes by 0.6′ to the west.

15:58 Begin float acoustic survey at survey point 2, 31° 15.07′ N, 74° 52.77′ W Loran-C.

16:30 Problems continue with a weak radio signal from the TSVLA. Therefore, instead of leaving the area, the NADC 38 will drift near the TSVLA, i.e., near site D, during event 1.

20:25 Begin to listen for float localization pings at 31° 14.928′ N, 74° 56.107′ W. All float pings are audible.

23:25 Begin to listen for float localization pings at 31° 16.291′ N, 74° 52.090′ W. All float pings are audible.

5 August 1990

10:05 Begin to listen for float localization pings at 31° 15.922′ N, 74° 54.676′ W. The pings for all floats, except float 1, are audible.

11:33 Begin to listen for float localization pings at 31° 15.674′ N, 74° 55.511′ W. All float pings are audible. Float 1 appears to be the greatest distance from the ship.

11:46 Slant range to float 1 is 8673 meters. Ship position is 31° 15.729′ N, 74° 55.602′ W.

15:25 Recover surface float on the TSVLA. Start to retrieve the TSVLA.

16:26 Acoustically survey the float positions.

16:45 Finish recovery of TSVLA and prepare to pass supplies to The Gyre.

17:28 Begin the process of recovering the Swallow floats. Acoustically survey the float positions.

17:38 Acoustically release float 0.

18:14 Float 0 is on the surface since its radio beacon signal is detected

18:44 Recover float 0 at 31° 17.870′ N, 74° 52.313′ W. Its program is still running.

18:54 Acoustically release float 1.

19:45 Float 1 is on the surface.

20:13 Recover float 1 at 31° 19.407′ N, 74° 52.076′ W. Its program is still running.

20:56 Acoustically release float 2.

20:59 Acoustically release float 3.

21:00 Acoustically release float 4.

22:25 Float 2 is on the surface.

22:27 Float 4 is on the surface.

22:56 Recover float 2 at 31° 14.204′ N, 74° 54.226′ W. Its program is still running.

23:00 Float 3 is on the surface.

23:12 Recover float 4 at 31° 13.770′ N, 74° 54.218′ W. Its program is still running.

23:30 Recover float 3 at 31° 13.364′ N, 74° 54.409′ W. Its program is still running.

23:47 Acoustically release float 5.

23:48 Acoustically release float 6.

23:51 Acoustically release float 7. Note that float 7 does not appear to be issuing the long-duration ping which floats generate after release. However, the change with time in the slant range to float 7 is consistent with it ascending to the surface.

6 August 1990

01:40 Float 5 is on the surface.

01:45 Float 6 is on the surface.

02:15 Recover float 6 at 31° 13.204′ N, 74° 54.967′ W. Its program is still running.

02:26 Recover float 5 at 31° 13.112′ N, 74° 54.824′ W. Its program is still running.

02:42 Float 7 is on the surface.

02:50 Acoustically release float 8.

02:51 Acoustically release float 11.

03:10 Recover float 7 at 31° 12.968′ N, 74° 55.021′ W. Its program is still running.

04:43 Float 8 is on the surface.

05:20 Recover float 8 at 31° 13.006′ N, 74° 54.641′ W. Its program is still running.

05:30 The slant range to float 11 is 3838 meters. The float does not appear to be ascending to the surface, even though it is issuing a long-duration ping.

05:41 Acoustically release float 9.

06:20 The slant range to float 11 is 3207 meters.

06:29 The ship position is 31° 13.227′ N, 74° 53.376′ W.

07:00 Float 11 appears to still be on the bottom. This float's galvanic time release (GTR) will corrode around 20:30, 6 August (plus or minus 3 hours) and its timed release is set for 7 August, 07:00.

07:34 Acoustically release float 10.

08:58 Recover float 9 at 31° 16.040′ N, 74° 54.794′ W. Its program is still running.

10:40 Float 10 is on the surface.

11:19 Recover float 10 at 31° 16.479′ N, 74° 51.147′ W. Its program is still running.

21:31 Slant range to float 11 is 3198 meters and the ship position is 31° 13.401′ N, 74° 53.279′ W.

22:31 Begin to refurbish float 10 for the second deployment.

23:30 Check slant range to float 11; it still is not ascending.

7 August 1990

02:50 Check slant range to float 11; it still is not ascending.

03:00 Quit refurbishing float 10 for the evening.

04:15 Check slant range to float 11; it still is not ascending.

10:40 Check slant range to float 11; it still is on the bottom.

10:45 Resume refurbishing of float 10.

12:17 For the second and third deployments, the tether lines for the bottom floats will be increased from 10 ft (3.05 m) to 20.7 ft (6.3 m) and a second GTR, in addition to the GTR connecting the float base plate to the tether, will be placed 8 in. (0.20 m) from the anchor. The longer tether line will hopefully prevent the 8 kHz transducer from becoming entangled in debris on the ocean bottom and the second GTR will prevent the entanglement of a bottom float in its tether line from allowing the float to ascend to the surface.

12:28 Finish refurbishing float 10.

12:45 Begin refurbishing float 9 for the second deployment.

16:12 Finish refurbishing float 9.

16:25 Begin refurbishing float 0 for the third deployment.

19:40 Finish refurbishing float 0.

19:45 Begin refurbishing float 1.

21:23 Check range to float 11. It is still on the bottom.

22:45 Finish refurbishing float 1.

8 August 1990

10:00 Observe the day counter decrement by one for the floats which have already been refurbished.

10:20 Check range to float 11. It is still on the bottom.

10:34 Begin refurbishing float 2.

12:45 Finish refurbishing float 2.

13:10 Begin refurbishing the deep (3100 meter) midwater floats for the third deployment. These five floats, floats 3, 4, 5, 6, and 7, will be equipped with extra 2-lb ballast weights connected by 6-hour GTRs in order to speed their descent to equilibrium depth. Begin refurbishing float 4 first; floats 3 and 5 will be refurbished last since their infrasonic hydrophone data acquisition systems recorded unusually low pressure autospectral levels in the July, 1989 Downslope Conversion experiment.

15:20 Finish refurbishing float 4.

16:08 Begin refurbishing float 6.

18:48 Finish refurbishing float 6.

18:50 Begin refurbishing float 7. Because of an odd-sounding localization ping, the transformer setting is changed so that a lower voltage is applied to the localization hydrophone for pinging. In the battery check, the transponder voltage is anomalously low.

20:35 A quick battery recharge is begun for the four batteries in the transponder circuit.

21:23 Stop the quick battery recharge for the four batteries in float 7's transponder circuit. Circuit voltage has increased.

21:30 Begin long-term battery recharge for float 7's transponder circuit batteries.

22:19 The voltage from float 7's transponder circuit batteries is not increasing. A faulty battery cell is suspected. Since the three remaining battery cells appear to be good, the float will be deployed anyway.

22:20 Stop the battery recharge for float 7's transponder circuit batteries.

23:18 Finish refurbishing float 7.

9 August 1990

11:10 Check the day counter setting for the floats which have already been refurbished. All settings are correct except for float 6; its day counter is not decrementing since its clock alarm was not set during refurbishing.

11:52 Begin refurbishing float 8. It will be reconfigured as a bottom float, i.e., its horizontal geophone components will be shorted out and 18 dB of gain will be removed from the vertical geophone component data acquisition system.

12:15 Check range to float 11. It is still on the bottom and so appears to be lost forever.

13:10 Finish refurbishing bottom float 8.

13:16 Begin refurbishing float 3.

15:25 Finish refurbishing float 3.

16:25 Begin refurbishing float 5. Replace OAR flasher holder on float 5. If the flasher holder was already broken prior to the first deployment, then this new holder will result in the float equilibrating at a depth greater than the desired 3100 meters.

17:50 Finish refurbishing float 5. All eleven Swallow floats are now ready to be redeployed.

17:55 Check whether all floats are powered down and whether their day counters are properly set. Everything is okay except for the day counter on float 6.

10 August 1990

01:00 Prepare to synchronously start all three bottom floats, floats 8, 9, and 10, for the second deployment. If float 9 and 10 operate properly, then float 8 will be powered down and used for the third deployment.

02:00:00 Synchronously start floats 8, 9, and 10 for the second deployment. All three floats are operating properly.

03:23 Deploy float 9 at 31° 13.495′ N, 74° 40.138′ W.

03:52 Deploy float 10 at 31° 13.072′ N, 74° 37.478′ W.

03:57 Power down float 8.

04:15 Check localization pings from floats 9 and 10.

11:30 Check localization pings from floats 9 and 10.

11 August 1990

11:41 Check whether the remaining nine floats are powered down and whether their day counters are correctly set. All is normal except for the day counter for float 6.

19:00 Begin preparation of nine remaining floats for the third deployment. They will be synchronously started at 20:00 Z, one hour earlier than in the test plan. The difference of 42 hours between this new synchronization time and the synchronization time for the second deployment is an integral multiple of 9 minutes. Therefore, the localization pinging of floats 9 and 10

in the second deployment will be synchronized with the pinging of floats 0 through 8 in the third deployment.

20:00:00 Synchronously start the nine remaining floats for the third deployment.

20:06 All floats are operating properly and are ready for deployment.

20:30 Deploy float 7 at 31° 08.957′ N, 74° 39.985′ W.

20:40 Deploy float 8 at 31° 09.494′ N, 74° 39.803′ W.

20:50 The ship hit float 6 during the attempt to deploy the float at 20:41, causing the external ballast to break off. Recover the float at 20:48 and begin to refit the float with a new ballast. Float 6's new ballast is a modified version of the original ballast for float 8 for the third deployment, before float 8 was reconfigured as a bottom float in order to replace float 11.

21:05 Finish attaching the new ballast to float 6. The float is now ready to be redeployed.

21:17 Deploy float 2 at 31° 12.355′ N, 74° 39.021′ W.

21:26 Deploy float 1 at 31° 12.260′ N, 74° 38.470′ W.

21:50 Redeploy float 6 at 31° 09.390′ N, 74° 39.862′ W.

22:36 Deploy float 5 at 31° 12.65′ N, 74° 41.47′ W (Loran-C fix).

22:50 Float 2 does not appear to be sinking since the VHF ADF detects its radio beacon signal. After attempts to locate the float, it was decided to wait until after sundown, when the float's OAR flasher will be visible. The other floats will be deployed during the remaining daylight time.

23:31 Float 2 is no longer on the surface since its radio beacon signal is not present.

23:59 Deploy float 0 at 31° 13.681′ N, 74° 39.951′ W.

12 August 1990

00:27 Deploy float 3 at 31° 13.136′ N, 74° 38.168′ W.

00:40 Deploy float 4 at 31° 13.073′ N, 74° 37.628′ W.

01:04 Begin to listen for the floats' localization pings. The pings for floats 0 and 7 cannot be detected.

01:13 Begin an acoustic survey of the floats' positions. The acoustic responses of all eleven floats are detectable.

02:21 Begin to listen again for the floats' localization pings. Only the ping for float 7 cannot be detected; it must be too weak due to the low transponder circuit voltage.

10:51 Begin to listen again for the floats' localization pings; only float 7's ping cannot be detected.

15:56 Begin a survey of the floats' positions; transpond off each float immediately after hearing its localization ping so that survey will not contaminate the localization data. All except float 7's response is detectable.

13 August 1990

00:13 Begin a survey of the floats' positions; the response of floats 1, 4, and 7 cannot be detected.

01:30 Begin another survey of the floats' positions; the response of floats 4 and 7 cannot be detected.

02:03 Acoustically release float 0.

02:18 Release float 1.

02:33 Release float 2.

02:43 Float 0 is on the surface.

03:16 Recover float 0 at 31° 05.605′ N, 74° 48.555′ W. Its program is still running.

03:17 Float 1 is on the surface.

03:56 Recover float 1 at 31° 03.272′ N, 74° 48.745′ W. Its program is still running.

04:21 Recover float 2 at 31° 02.624′ N, 74° 48.002′ W. Its program is still running.

06:27 Conduct another float survey. The response of float 4 is finally detected at a slant range of 16431 meters.

07:53 Recover float 9 at 31° 12.038′ N, 74° 41.125′ W. Its program is still running. This float's GTR must have corroded prematurely.

09:02 Release float 3.

09:03 Release float 5.

09:14 Release float 4. Its slant range is 13586 meters.

12:37 Float 4 is on the surface.

13:04 Recover float 4 at 30° 57.726′ N, 74° 34.500′ W. Its LED display shows "00", possibly indicating that the program was stopped by the acoustic release command.

13:07 Float 5 is on the surface.

14:24 Recover float 5 at 31° 01.874′ N, 74° 42.403′ W. Its program is still running.

16:24 Recover float 3 at 31° 03.475′ N, 74° 36.651′ W. Its program is still running.

17:27 Recover float 10 at 31° 09.247′ N, 74° 37.871′ W. Its program is still running. This float probably released on its timed release command, although it's possible that its GTR also corroded earlier.

17:59 Release float 8. Float 6 will be used as a tracer for float 7 since the latter float's acoustic localization circuit does not appear to be operating.

18:40 After monitoring the slant range to float 8, it does not appear to be ascending. It may be trapped on the ocean bottom, similar to float 11 in the first deployment. Hopefully, the corrosion of either (or both) of the two GTRs along float 8's tether line will allow the float to ascend.

18:46 Attempt to release float 7.

18:48 Release float 6.

19:15 In transit to the estimate of float 6's recovery position, float 7's radio beacon signal is detected. This float will be recovered first.

20:00 Recover float 7 at 31° 02.506′ N, 74° 47.588′ W. Its program is still running.

22:43 Recover float 6 at 31° 02.803′ N, 74° 45.429′ W. Its program is still running.

23:00 Begin transit back to bottom float 8's deployment position in order to wait for its GTRs to corrode.

14 August 1990

00:09 Recover float 8 at 31° 08.115′ N, 74° 40.226′ W. Its program is still running.

14:38 Slant range to float 11 is 7616 meters and the ship's position is 31° 16.353′ N, 74° 51.431′ W. The float is still functioning properly, but it is still on the ocean bottom.

14:45 Begin to remove the Swallow float data tapes from the second and third deployments.

20:50 Finish removing the data tapes from the 11 floats. All floats appear to have written full data tapes in all three deployments.

IV. Swallow Float Data - General Indication of Data Integrity

After being synchronously started and spending about a half second in performing an initialization, each float begins to accumulate data into a temporary buffer. Once 44 seconds of data have been accumulated, they are written to cassette tape during a one-second period in which no data are gathered by the float. This 45-second cycle, called a record, is repeated until the cassette tape is filled. In experiments conducted since 1989, the floats have been programmed to skip the writing of the first 640 records (8 hours) of data to tape in order to provide time for them to equilibrate at depth. Each record is composed of 9766 bytes. Appendix 1 of reference [3] contains a description of the format of the record, along with a comparison with the old record format used with geophone-only-equipped floats. The cassette tape can store up to 1600 records.

a) Data Quality Screening Results

The first step in the analysis of the Swallow float data is to scan all the floats' data files with a general screening program. This program checks each record for the proper location of resynchronization characters and the proper sum of byte values in a group prior to a checksum. The output from the screening program is given in Figure IV.1. Note that the cassette-tape-reading program attaches a zero-byte record with the same internal record number as the last record on the cassette tape onto the end of each float's data file; this allows the number of internal records to be determined. For example, float 0's last-written record was internal record number 2238. (The record number listed in the left-most column is assigned by the screening program itself). Since the internal record number begins with record 640, due to an 8-hour delay in data recording after float synchronization, float 0 wrote 1599 records onto tape.

An unusual situation occurred in float 10's data. Two records with zero bytes were written, the first with internal record number 2188 and the second with internal record number 2198. This may have been caused by a gap in float 10's cassette tape. That is, the transcribing program may have written the first zero-byte record upon encountering the gap, and then the second one was written upon reaching the end of tape. However, an examination of the data suggests that those records after record 2188 may have been written in a previous experiment.

The number of errors detected by the screening program is typical of that in other Swallow float deployments. For the data recorded by the 11 floats, only 0.1 percent of the records did not pass the data quality screening tests. Some of these errors may be correctable by making adjustments to the Swallow-float-cassette-tape-to-magnetic-tape transcribing hardware.

b) Unique Aspects of Certain Floats in this Deployment

As in all experiments, unexpected events occur which may affect a float's data. The following table is a listing of some of the unique aspects of given floats in this deployment. The data demonstrating these unique aspects are discussed in later sections.

Unique Aspects of Given Floats

FLOAT	COMMENTS
1	Its geophone data are extensively affected by non-acoustic disturbances.
1 and 7	Small leaks of the oil encasing the electrostrictive material in the infrasonic ceramic hydrophones on these two floats were discovered after the NATIVE 1 experiment.
2	The tape-recorder-generated contamination at the beginning of each record is significantly greater than in previous deployments. Also, the spectral levels around 5 Hz and below in the hydrophone channel increase rather suddenly around record 1520 and continue to slowly increase for the duration of the experiment. No corresponding increase is seen in any other channel's data.

3 and 5	These floats' infrasonic hydrophones still suffer from an as-yet unexplained decrease in sensitivity with decreasing frequency.
4	The infrasonic hydrophone on this float did not function.
7	The localization ping issued by this float sounded unusual.
10	The last 10 records appear to be data recorded in a previous experiment.
11	The float appeared to operate perfectly during event 1, but for some unknown reason, it could not ascend to the surface upon recall and was not recovered. It continued to issue localization pings for the full duration of NATIVE 1.

V. Battery Voltage, Float Heading, AGC Level, and Percentage of Clipped Points

The battery voltage, the compass reading, and the automatic gain control (AGC) level, measured once during each 45-second record, are plotted in Figures V.1 through V.11 for all Swallow floats.

a) Battery Voltage

The battery level for all floats remained constant at slightly more than 6 volts. In fact, the power supply is probably sufficient for four or five deployments without a battery recharge. The duration of the floats' deployment is instead determined by their tape recording capacity.

b) Float Heading

Installed on the inside of each of the Swallow float glass spheres, at the sphere's south pole, is a compass for determining the orientation of the sphere, and, thus, the orientation of the float's horizontal geophone components with respect to magnetic north. The compass heading during each 45-second record is shown in the middle plot of Figures V.1 through V.11. The floats typically twist back and forth at a characteristic period of between 25 minutes to an hour once they stabilize at depth. The amplitude of the twisting is on the order of ± 50°. However, a low frequency component of float 3's twisting had an unusually large amplitude of ± 270°. The twisting is believed to be caused by current shear and/or rotation due to the vertical motion caused by internal waves. Occasionally, a midwater float undergoes a complete rotation after stabilization. For example, float 7 underwent two complete rotations between records 1600 and 2000. In addition, float 1 performed a rapid rotation around record 1400; this rotation coincided with a decrease in the float's AGC level, as discussed in Part c of this section. As observed in previous deployments, the midwater floats' headings appeared to stabilize at about 300° to 360° near the end of the experiment (float 3 may be an exception). The force responsible for this stabilization is believed to be due to the interaction of a small, intrinsic magnetic field of the float, possibly due to the permanent magnets inside the geophone's components, with the earth's magnetic field.

The compass heading information is used to rotate the horizontal geophone components so that the + y axis points to true north and the + x axis points to true east. To do this, the variation of true north from magnetic north, about + 9° in this experiment, is obtained from a navigation chart of the deployment area. A float heading time series which is sampled at the same frequency as the infrasonic data is calculated by linearly interpolating between the headings recorded at the beginning and end of each Swallow float data record.

The compass headings for the two bottom-tethered floats, floats 9 and 10, usually remained approximately constant or varied slowly due to the constraining effects of the tether and the prevailing ocean current. However, around record 1900, float 10 performed two complete rotations. This period of large change in the bottom float's heading was probably caused by changes in the ocean current direction. Note that near the end of float 10's recording period, the heading jumped more than 200° to 340° and remained fixed for the remainder of the deployment. This may indicate that the compass became stuck; the Swallow float compasses can only withstand a tilt of 3° from vertical before sticking. However, as mentioned in the previous section, these data also may have been written in a previous experiment.

c) AGC Level

The AGC is a variable gain amplifier, with a range of 0 to 36 dB gain, which allows the full dynamic range of the eight-bit A/D converter to be used. The AGC gain always changes by approximately 0.5 dB steps between records. After a five-second delay in the record, if more than 0.5 percent of the points sampled on all components are clipped, then the AGC decreases by 0.5 dB. Otherwise, it increases. Because of the slow adjustment time of the AGC gain, amplitude information for large impulsive arrivals cannot be

obtained.

The bottom plot in each figure shows the automatic gain control (AGC) level during every 45-second record. For floats 0 and 2 - 8, these plots are quite similar in appearance. Therefore, the AGC plot for float 2 will be used as reference in the following discussion.

The large dips in gain centered near records 900 and 2175 are due to the passage of the Gyre over the top of the array; the first one occurred as the ship steamed towards the south and the second one resulted from its return (re Figure II.1). Just prior to, and shortly after, record 1200, the two SUS charge events caused decreases in the gain. Another decrease occurred at the end of the Gyre's leg 1, around record 1570. Between records 1580 and 1780, the AGC gain is stable and at its highest level in the deployment. During this time, the Gyre was at its greatest distance from the array, the ELF source was not broadcasting, and the NADC 38 was drifting quietly so that ambient sound field measurements could be made. Finally, just before record 1900, the ELF began broadcasting 10 Hz and 16 Hz tones simultaneously (re the table in Section IIb), resulting in a net decrease in gain of a few dB.

The appearance of float 1's AGC gain plot between records 1200 and 1800 is quite different from that of the other midwater floats' plots. Large dips in gain occur due to signals recorded by this float's geophones. Since no corresponding signals appeared in either float 1's hydrophone data or in the other floats' data, then the signals must be non-acoustic in nature. These signals are discussed in Section IX, where it is suggested that they result from biological activity near the float.

The differences in bottom floats' 9 and 10 AGC plots from the other floats' plots are due to another cause; contamination by tether effects. Even though 18 dB of gain was removed from the bottom floats' vertical geophone channel prior to the experiment, tether contamination can still be sufficiently large to dictate the AGC level. If the horizontal geophone components on the bottom floats had not been disconnected, the effect of tether contamination would have been even greater, causing a loss of resolution in the hydrophone data. Note, however, that float 10's AGC level appears to be free of tether contamination between records 1450 and 2000.

d) Percentage of Clipped Points

For the four data acquisition channels, the percentage of points which are clipped in each record are plotted in Figures V.12 through V.22. The horizontal axis scale used in these plots matches the scale used in the previous plots of this section. The data plotted here are actually the controlling factor in determining the AGC gain discussed previously; the sum of the percentage of clipped points over all four channels dictates whether the AGC level increases or decreases by 0.5 dB.

Except for a few periods of short duration, the number of clippped points is less than two percent. The hydrophone channel usually suffers from a greater degree of clipping than the geophone channels since the sensitivity of the hydrophone plus the fixed gain in the hydrophone channel is about 4 dB greater than that in the geophone channels (-182 dB re 1 V/μPa + 80 dB for the hydrophone versus about -201 dB re 1 V/μPa + 95 dB above 8 Hz for the geophones; re Appendix 1). The usefulness of these figures is in determining times when the spectral estimates cannot be trusted due to contamination by clipping. For example, float 1's geophone data are severely contaminated between records 1200 and 1800, whereas the other midwater floats' data are relatively free of contamination. Similarly, spectra involving the z axis geophone data from float 9 between records 1250 and 2000 and those from float 10 between records 1050 and 1400 are probably not usable.

VI. The 8 kHz Surface and Bottom Bounce Data

Each Swallow float possesses an 8 kHz hydrophone suspended 1.83 meters below its glass sphere (see Figure 1). The source strength of the hydrophone is 192 dB re 1 μPa at 1 meter. The floats periodically transmit and receive 10 msec acoustic pulses with a carrier frequency of 8 kHz in order to measure interfloat and float-to-surface acoustic travel times. The floats take turns pinging, with a given float transmitting 10 seconds into each 45 second period. For 12 floats, the period of cycling through all floats once is therefore 9 minutes.

Figures VI.1 through VI.11 are plots of each float's record of issuing its own pulses and receiving the subsequent returns from them. These plots show the raw data used to create Figure I.3. The vertical axes in the figures have been scaled from travel time to distance using 1500 m/s for the speed of sound in water. (Note that the float depths in Figure I.3 were calculated using the actual harmonic sound speed, and therefore are more accurate estimates of the true float depth). The horizontal axes are in units of Swallow float record number, but may be converted to elapsed experiment time using the conversion factor of 80 records per hour.

For the midwater floats, reflections are received primarily from the ocean surface, indicating the float depth. Variations in the arrival time of these reflections after the float has equilibrated in depth are indicative of the presence of higher-frequency internal waves. The higher-frequency internal wave activity in this experiment appears to be weaker than in previous northeast Pacific Ocean deployments, as mentioned in Section I. The equilibrium depths of the floats are controlled by the weight of the float release ballast, which must be carefully determined for each float prior to deployment. Equilibrium depth is an extremely sensitive function of ballast weight, i.e., a 1 gram change in ballast corresponds to approximately a 10 meter change in equilibrium depth. The compressibility of the float components as a function of depth must also be taken into account. Finally, an accurate density-versus-depth profile for the experiment location must be available. For these reasons and considering the fact that this experiment was the first Swallow float deployment in the Atlantic Ocean, the agreement between the planned and achieved float depths is excellent.

A surprising result from these data is that the two shallowest floats, floats 0 and 1, appear to get shallower in depth over the duration of the experiment. This has not been observed before. In previous deployments, the floats have tended to become deeper over time since their average density increases as they equilibrate in temperature with the surrounding, colder ocean. One possible explanation for the results in this experiment is that the floats moved into an area with a greater water density at 400 meters, making them more buoyant. The resulting horizontal density gradient must have been dynamically supported somehow, e.g., by current flow. The fact that these two floats moved to the north by more than two nautical miles during the experiment, whereas the deeper floats moved to the southwest, may indicate the presence of such a current flow. Alternatively, the floats may have remained at a constant depth, but only appeared to move upward because of a change in the shallow water temperature structure. That is, they may have moved into an area with a warm water lid, resulting in a higher sound speed and therefore an apparent decrease in depth.

Intermittent reflections from the ocean bottom are also recorded; for example, the two sets of returns between records 1600 and 2200 and between 3000 meters and 3600 meters in float 0's data (Figure VI.1), and the weak arrivals in float 8's data (Figure VI.9) which occur just prior to the surface reflection. In previous experiments, reflections from another float's glass sphere occassionally have been received. Reverberations after the initial pulse issuance are due to temperature-dependent resonance of the floats' glass shell [1] (the glass shell appears to be resonant at 8 kHz, the carrier frequency of the acoustic pulses) and/or depth-dependent volume scattering. Reverberations after the surface reflection arrival are also caused by scattering from the sea surface. The amount of reverberation is also dependent upon the ambient ocean noise level (the range pulse detector circuit compares the level in a 200-Hz band centered at 8 kHz to that in a broader band, 2 kHz, centered at 10.5 kHz) and upon the sensitivity of each float's range pulse detection circuit (e.g., float 0's detection circuit appears to be more sensitive than float 1's circuit and float 10's circuit is more sensitive than float 9's circuit).

Figures VI.10 and VI.11 pertain to floats 9 and 10, which were deployed to the ocean bottom using a large weight and 3.05-meter tether in order to provide a fixed coordinate system for the experiment. The

outgoing pulse return at 0 depth for these two floats is relatively longer because of backscattering from the ocean bottom.

VII. The 8 kHz Interelement Range Data

Figures VII.1 through VII.11 contain the record of pulses transmitted by one float and received by another. As in Figure VI.1 through VI.11, the vertical axes have been scaled from travel time to range using 1500 m/s for the speed of sound, and the horizontal axes are in units of record number.

In the figures showing the travel times between one midwater float and another, a short-duration direct path pulse arrival is shown followed by a longer-duration surface bounce pulse arrival. The duration of the direct path arrivals correspond approximately to the duration of the localization pulse (10 msec). The surface bounce arrivals are much longer in duration due to scattering by the ocean surface. Only the direct path information is used in the algorithm for locating the floats as a function of time. In these data, only five erroneous data points or dropouts exist, i.e.,

float 2 listening to float 8 near record 2100 (Figure VII.3h),

float 3 listening to float 8 around record 1800 (Figure VII.4h),

float 6 listening to float 1 around record 2150 (Figure VII.7b),

float 8 listening to float 6 just before record 1000 (Figure VII.9g), and

float 10 listening to float 0 around record 1800 (Figure VII.11a).

Therefore, almost all midwater float localization pings appear to be audible to all other floats, even in the case of a nearly 10 km separation (i.e., between floats 1 and 7 around record 1600; Figures VII.2g and VII.8b). Note that because of relative float clock drift, the reciprocal travel times between two floats must be averaged in order to obtain an accurate estimate of the true interfloat travel time.

Figures VII.10j,k and VII.11j,k contain the travel times between bottom tethered floats. Only the surface bounce arrival is audible between bottom floats; the direct path is not present. This is due to the upward-refracting sound velocity profile near the ocean bottom. The arrival time of surface bounces generated by float 11 and recorded by the other bottom floats is a linear function of time. Since the floats are tethered to the bottom, the true surface bounce travel time is constant and this linear dependence is a direct measure of float 11's clock drift with respect to the clocks in floats 9 and 10. Therefore, float 11's clock drift can be corrected using these data and the arrival times of float 11's localization pings recorded by the other floats can then be used in locating the floats.

VIII. RMS Pressure and Velocity

In order to quickly scan the infrasonic data from all channels of all floats, the root mean squared (RMS) pressure for the hydrophone and root mean squared velocity for the geophones were calculated. The results are plotted in Figures VIII.1 through VIII.11. These RMS time series have been corrected for the AGC gain, but are otherwise uncalibrated; the vertical axis is in units of volts at the A/D converter (re Appendix 1 for a block diagram of the infrasonic data recording system). Each RMS level value results from taking the square root of the average of the squared amplitude levels over a period of five seconds (or 250 points since the data sampling rate is 50 Hz). Since each record is 2250 points (45 seconds) long, then nine RMS power values are calculated for each record. The RMS value for the last five-second period of each record includes one second of zeros. The one second of zeros represents the time during which no data is sampled while data in a temporary buffer is being written to cassette tape.

a) Midwater Swallow Floats

The following discussion will again focus on the plots pertaining to float 2's data; Figures VIII.3a through VIII.3i. An obvious feature of float 2's plots are the spikes which occur once every record on the geophone components, particularly the x axis. These spikes are the result of the transient at the start of each record due to the power-up and power-down of the tape recorder between records. In order to prevent contamination by these transients, the first three seconds of each record are skipped in the calculation of the spectral estimates in Section X. The character of the transients changes somewhat, especially on the y axis, at each of the three times when the direction of the tape recorder reverses, around records 1035, 1435, and 1835.

The other major features of the RMS plots are the increase in levels due to the passage of the Gyre near records 900 and 2175 (19:45 Z, 4 Aug and 11:41 Z, 5 Aug) and the two sets of large spikes due to the SUS charge events beginning around record 1150 and 1225 (22:53 Z, 4 Aug and 23:49 Z, 4 Aug). Additional spikes occur simultaneously in the hydrophone and geophone data, e.g., near records 667, 734, 743, 946, 1024, 1032, 1047, 1550-1558, 1827, 1906, 1955, and 2026, suggesting that these are acoustic in nature. In particular, evidence is presented in the next two sections that strongly indicates that the spike at record 1906 is the result of the T phase arrival from an earthquake in the Leeward Islands in the Caribbean. Also, a few of the other spikes, e.g., at records 734, 743, 1024, and 1047, are caused by additional SUS charge detonations. The source(s) of the remaining spikes are as yet undetermined; their origin may be identifiable once SUS charge logs and navigation information for the NADC 38 are obtained.

The background RMS levels between records 1575 (04:11 Z, 5 Aug) and 1825 (07:19 Z, 5 Aug) are higher on the hydrophone channel than on the geophone channels. This is due to the difference of about 4 dB in channel sensitivity, i.e., -182 dB re 1 V/μPa + 80 dB for the hydrophone versus about -201 dB re 1 V/μPa + 95 dB above 8 Hz for the geophones (re Appendix 1).

b) Non-Acoustic Disturbances in the Midwater Swallow Float Geophone Data

Between records 720 and 740 in float 2's data (Figure VIII.3a), a prominent disturbance is recorded on the horizontal geophone components. However, no corresponding disturbance is present in the hydrophone data, indicating that the source is non-acoustic in nature. Such non-acoustic signals have appeared in previous Swallow float deployments (for example, see p. 28, end of second paragraph of reference [9]), but never to the extent seen here. The geophone data from all midwater floats except floats 3 and 5 show some evidence of such disturbances, with the data collected by float 1 being particularly affected. These non-acoustic signals are discussed further in the next section.

c) Bottom-Tethered Swallow Floats

Figures VIII.10a - 10h and VIII.11a - 11h show the RMS pressure and velocity plots for the bottom-mounted floats 9 and 10. The 18 dB of gain removed from the vertical geophone component system has not been taken into account in these plots. Recall that the horizontal geophones have been shorted out so that non-zero RMS levels are due to electronic self noise. For extended periods of time, the vertical component geophone data are contaminated by tether effects; re records 1110 to 2080 for float 9 and records 980 to 1430 for float 10. However, during several periods, notably after record 1670 in float 10's data, uncontaminated vertical geophone information can be obtained. Those periods in which tether contamination on the z axis geophone is predominant may indicate periods when ocean bottom current flow is significant, so that non-acoustic pressure fluctuations may also be contaminating the hydrophone data.

IX. Geophone and Hydrophone Time Series

Selected time series recorded by the geophones and the hydrophones, corrected for the AGC level but otherwise uncalibrated, are presented in this section. Each figure shows the time series recorded by a given float's component over a 12-record (9 minute) period. The record numbers are given on the left hand side of the figures. The data are sampled at 50 Hz (re Appendix 1), so that 2200 points from each channel are collected in the 44 seconds of each record; the 45th second of the record is composed of 50 zeros. Only every other sampled point is plotted. The scale of the plots' vertical axis is given at the top of each figure.

The time periods selected for plotting are;

Swallow Float Infrasonic Time Series

Record Sequence	GMT Time (Date)	Float Channels	Comments	Figure Numbers
1164 - 1175	23:03 - 23:12 (4 Aug)	6x,y,z,p	A sequence of nine SUS charges.	IX.1
1140 - 1187	22:45 - 23:21 (4 Aug)	6z	The first set of 22 SUS charges.	IX.2
1220 - 1255	23:45 - 00:12 (4-5 Aug)	6z	The second set of 18 SUS charges.	IX.3
1900 - 1911	8:15 - 8:24 (5 Aug)	all operating float channels	Arrival of T Phase from Leeward Islands' earthquake.	IX.4-14
1280 - 1291	00:30 - 00:39 (5 Aug)	1x,y,z,p	Non-acoustic disturbance occurs extensively.	IX.15
2020 - 2031	9:45 - 9:54 (5 Aug)	6x,y,z,p	Acoustic arrival of unknown source.	IX.16

a) SUS Charge Arrivals

The time series from records 1164 to 1175 (23:03 Z to 23:12 Z, 4 Aug) for all four infrasonic channels on float 6 are plotted in Figures IX.1a through IX.1d. This period of time occurred during the first set of SUS charge detonations. Arrivals from 9 detonations are recorded, generally with a separation of 50 to 55 seconds. However, the time delay between the detonations in records 1165 and 1167 is about 70 seconds, and, apparently, a charge which would have generated arrivals in record 1172 did not detonate. The individual phases in each of the detonation arrivals will be identified once the locations of the SUS charge drops are obtained. Note that the arrival appearing 10 seconds after the beginning of record 1170 is due to the float's localization ping. It is best recorded on the vertical axis geophone whereas it saturates the hydrophone channel front-end, resulting in a temporary loss in sensitivity.

A comparison of the SUS charge signal-to-noise ratio (SNR) for each of the channels cannot be made since the arrivals result in clipping. For example, it appears from the plots that the SNR was highest on the z axis geophone and lowest on the hydrophone. However, the arrivals recorded by the hydrophone probably suffered from a greater degree of clipping, especially since the background sound recorded by the hydrophone usually dictates the AGC gain (re Section Vd).

In order to determine the number of SUS charge detonations during the two SUS charge events, the z axis geophone data recorded by float 6 were plotted over two time periods. The first time period is composed of four figures, Figures IX.2a through IX.2d, covering records 1140 to 1151, 1152 to 1163, 1164 to 1175, and 1176 to 1187 (22:45 Z to 23:21 Z, 4 Aug), and the second time period, in Figures IX.3a through IX.3c, covers records 1220 to 1231, 1232 to 1243, and 1244 to 1255 (23:45 Z, 4 Aug to 00:12 Z, 5 Aug). A total of 22 detonations were recorded during the first time period and 18 were recorded during the

second period. Note that for each of the time periods, the duration of the arrivals from a given detonation increases.

The float localization pings occur 10 seconds into records 1146, 1158, 1170, and 1182, and records 1230, 1242, and 1254. Also, an 8-second sequence of zeros occurs at the end of record 1162 because of a missing resynchronization character; re the Data Screening Results table discussed in Section IVa.

b) T Phase Arrival from the Leeward Islands' Earthquake

The next set of figures, Figures IX.4 through IX.14 show a 12-record (9-minute) sequence of uncalibrated time series recorded by all properly operating components of all floats. (The vertical geophone component data collected by bottom float 9 was not plotted since it was heavily contaminated by tether effects during this time). The sequence covers records 1900 to 1911 (8:15 Z to 8:24 Z, 5 Aug). A large arrival occurs in record 1906 which causes clipping on the horizontal geophone components and the hydrophone. The predominance of the arrival on the horizontal geophone components suggests that the source was at long range.

In Appendix 2 are copies of the "Preliminary Determination of Epicenters" from the National Earthquake Information Center. Indicated by an arrow and an asterisk is the listing of the magnitude 3.3 earthquake which occurred in the Leeward Islands of the Caribbean during event 1. It was a distance of 1950 km ($\Delta = 17.5°$) from the deployment site. Assuming a 1.5 km/sec average propagation speed, the T phase should arrive on 5 August at about 08:20:13 Z (= 07:58:33 Z + $\frac{1951 \text{ km}}{1.5 \text{ km/sec}}$). This calculated arrival time corresponds exactly to the time when Swallow float records 1906 and 1907 were recorded. Further evidence that the arrival in record 1906 is the T phase from the Leeward Islands' earthquake will be presented in the next section.

The initial T phase energy begins to arrive near the end of record 1905. It remains at a relatively low level until 15 to 20 seconds into record 1906, when significant clipping occurs on the horizontal geophone components and on the hydrophone, and an arrival is discernible on the vertical geophone component. This arrival structure is determined to a large extent by the dispersive properties of the oceanic waveguide. Both the shallowest floats and the bottom floats easily detected the T phase arrival, suggesting that its energy nearly fills the water column. Note a second arrival appears to occur in the second half of record 1907.

Two other features are notable in these time series. First, the degree of contamination at the beginning of each record from the power-up and power-down of the cassette tape recorder a) varies markedly from one float to the next for a given component, b) is greatest on the horizontal geophone components and is not present in the hydrophone data, and c) is fairly repeatable from one record to the next for a given float component. This last aspect of the contamination permits its removal by coherently averaging the time series over a set of records and subtracting the result from the original time series. The averaging must be done over records written on the same track of cassette tape since the tape recorder contamination can be dependent upon the direction of tape motion. Also, the effects of the contamination are reduced by skipping the first three seconds of each record in the calculation of the spectral estimates presented in the next section. Note that in some cases, the tape recorder transient produces a significant amount of long period (approximately 3 seconds) float rocking; re the x geophone components of floats 3, 7, and 8; Figures IX.7a, IX.11a, and IX.12a.

The second notable feature is that the geophone time series of both floats 0 and 1, Figures IX.4 and IX 5, show large signals arriving after the T phase arrival. Neither the hydrophone data recorded by these floats nor the data recorded by any of the other floats show such arrivals. These signals will now be discussed.

c) Non-Acoustic Disturbances in the Midwater Swallow Float Geophone Data

As mentioned previously, the geophone data collected during this experiment were affected by disturbances of an unknown cause. An extreme example is shown in Figures IX.15a through IX.15d, where the time series from record 1280 to 1291 (00:30 Z to 00:39 Z, 5 Aug) for all channels recorded by float 1 are plotted. Impulsive-like arrivals are often followed by long period float rocking on the horizontal geophone components. Only the higher-frequency part of the disturbances is recorded on the vertical geophone component. No associated signals appear in the hydrophone data. This fact, and the fact that no such signals appear in the other floats' data at this time, indicates these disturbances are non-acoustic in nature.

The following table lists the occurrences of these signals in each of the midwater floats' data.

Non-Acoustic Disturbances in Swallow Float Geophone Data

Float	Avg Depth (m)	Records with Disturbances
0	415	Intermittent, esp. between 1420-1560 and 1805-2100
1	393	Intermittent throughout and extensive, esp. between 1315-1470
2	1121	676, 698, 699, 700, 705, 733-734, 736-737, 1830
3	1213	None
4	1330	2018-2019
5	1481	None
6	1580	667-668, 693-694, 794-795, 882, 1799
7	1531	2089-2090
8	1671	795, 810

Because the disturbances occur in several floats' data, they are almost certainly real. That is, they were caused by something in, or a property of, the water column during the experiment rather than some system contamination. The frequency of occurrence of the disturbances is correlated with the depth of the float, with the two shallowest floats' data being most strongly affected. One possible explanation is that currents created by nekton near the floats may have caused the disturbances. The nekton may have been attracted by the 8 kHz float localization pings. For the shallowest floats, the float color may have also been attractive.

In one other experiment, the September, 1987 Swallow float experiment in the northeast Pacific Ocean, a single non-acoustic disturbance with a similar appearance occurred (re the end of the second paragraph on p. 28 of [9]). The float which recorded the disturbance was at about 2150 meters depth.

d) Unknown Acoustic Arrivals

Other large, unidentified arrivals occur in the data which generate spikes in both the RMS pressure and the RMS particle velocity plots for several floats. These arrivals are therefore acoustic in nature. The following table lists the records in which these arrivals occur.

Unknown Acoustic Arrivals in Swallow Float Data

Record	GMT Time (date)	Floats which Record Arrival
665-667	16:49 (4 Aug)	2 - 8, barely in 1, 9, 10
946	20:20 (4 Aug)	2 - 8, barely in 0, 9, 10
1032-1033	21:24 (4 Aug)	2 - 8
1827-1828	7:20 (5 Aug)	2 - 8, barely in 9, 10
1956-1957	8:57 (5 Aug)	0 - 10
2026-2027	9:50 (5 Aug)	0 - 10

The final set of plots in this section, Figures IX.16a through IX.16d, show the 4-component time series recorded by float 6 which encompass the last arrival listed in the table. Its character is very similar to that of the T phase arrival in records 1905 to 1906 discussed earlier. Evidence will be presented at a later date which indicates that the source direction is to the northeast, approximately perpendicular to the direction to the Leeward Islands' earthquake epicenter.

X. Particle Velocity and Pressure Spectra

Estimates of the calibrated autospectra for the geophone velocity components and for the hydrophone pressure component are presented in this section. Spectral estimates with two different frequency resolutions are calculated. Those with a 98 mHz resolution are made by dividing 40.96 seconds in a data record (obtained after skipping the first 3 seconds of data) into seven 10.24-second-long segments, with a 50 percent overlap between segments. The segments are fast Fourier transformed after using a Kaiser-Bessel window of $\alpha = 2.5$ to window the data. The resulting seven spectra within a record are incoherently averaged together. The averaged spectra for four consecutive records (equal to three minutes of data) are then incoherently averaged in order to further reduce the variance of the spectral estimates. For spectral estimates with a 24 mHz resolution, the segment length which is transformed is quadrupled to 40.96 seconds and the spectra for twenty consecutive records are incoherently averaged. For some of the plots in this section, additional averaging across records was done.

The autospectra are properly calibrated to units of dB re 1 $(\mu m/sec)^2/Hz$ for the geophone components and dB re 1 $(\mu Pa)^2/Hz$ for the hydrophone component. The pressure-particle velocity cross spectra are calibrated to units of dB re 1 $\mu Watts/m^2/Hz$. Refer to Appendix 1 for a description of the geophone and hydrophone data acquisition systems.

A guide to the plots in this section is given in the following table:

Swallow Float Spectral Estimates

Figure Numbers	Type of Plot	Record Interval	GMT Time Interval	Floats
X.1a-1b	LOFAR grams	640-2228	16:30, 4 Aug - 12:21, 5 Aug	2
X.2	Time series of pressure spectra at 5 Hz	640-2160	16:30, 4 Aug - 11:30, 5 Aug	2,6,7,8
X.3-11	Pressure spectra and spectral ratio	1580-1780	4:15-6:45, 5 Aug	0-8
X.12-20	Pressure spectra and spectral ratio	1200-1400	9:28-11:58, 9 July	0-8
X.21-24	2048-pt spectra on log freq scale	1580-1780 1200-1400	4:15-6:45, 5 Aug 9:28 - 11:58, 9 July	2-8 0-8
X.25-29	Comparison of geophone component spectra	1580-1780	4:15-6:45, 5 Aug	0-8
X.30-33	Pressure spectra just before and during T phase arrival	1900-1903 1904-1907	8:15-8:18, 5 Aug 8:18-8:21, 5 Aug	0-3, 5-8
X.34-37	Horizontal intensity just before and during T phase arrival	1900-1903 1904-1907	8:15-8:18, 5 Aug 8:18-8:21, 5 Aug	0-3, 5-8
X.38-39	Time series of pressure spectra and horizontal intensity at 7, 10 Hz	640-1120	16:30-22:30, 4 Aug	2,6
X.40-41	Time series of pressure spectra and horizontal intensity at 7, 10 Hz	1280-1560	00:30-4:00, 5 Aug	2,6
X.42-43	Time series of pressure spectra and horizontal intensity at 10, 16 Hz	1880-2160	8:00-11:30, 5 Aug	2,6

The measurements of the three orthogonal components of acoustic particle velocity can be used to calculate an equivalent pressure spectrum, $S_p^G(f)$, i.e.:

$$S_p^G(f) = (\rho_o c)^2 \sum_{j=1}^{3} S_{v_j}(f)$$

where $\rho_o \approx 10^3$ kg/m^3 is the fluid density, $c \approx 1500$ m/sec is the sound speed, and $S_{v_j}(f)$ is the jth geophone component autospectrum. The derivation of this geophone-data-derived pressure spectrum assumes that the sound field's kinetic energy density spectrum is equal to its potential energy density spectrum [7]. This assumption is not valid for many types of sound fields, but it is certainly true of those which are spatially homogeneous [7]. This point will be further discussed in the report on the energetics of the NATIVE 1 acoustic field.

a) LOFAR Grams of Float 2's Auto Spectra

The first two figures show gray level plots of float 2's geophone-data-derived pressure spectrum, Figure X.1a, and hydrophone pressure spectrum, Figure X.1b, as a function of time over the whole duration of float recording in event 1. Each spectrum in the plot was calculated by incoherently averaging 28 spectra, each estimated from 512 samples of data, over 4 consecutive records (3 minutes).

A number of the features of these plots have been discussed in previous sections. For example, the two SUS charge events appear as broad horizontal bands around records 1170 and 1240. The T phase arrival from the earthquake in the Caribbean results in the narrow horizontal line at record 1906. The six acoustic arrivals of unknown origin listed in the table in Section IX.d also appear as narrow horizontal lines, at records 666, 946, 1032, 1828, 1956, and 2027. Also, the non-acoustic disturbances in float 2's geophone data are particularly evident when comparing the appearance of the lower left corner of Figure X.1a with that of Figure X.1b.

These plots are also helpful in identifying narrow band signals in the experiment, indicated by the vertical dark bands in the two figures. For example, the operating schedule of the ELF source towed by the Gyre can be easily determined. From the start of the data recording (16:30 Z, 4 Aug) until record 1121 (22:31 Z, 4 Aug), the source was transmitting 7 Hz and 10 Hz simultaneously. It was turned off between records 1121 and 1280 in order to conduct the two SUS charge events. After record 1280 (00:30 Z, 5 Aug), it again transmitted 7 Hz and 10 Hz, until record 1560 (4:00 Z, 5 Aug). The source was turned off a second time between records 1560 and 1880 in order to permit measurements of the background sound field. After that, starting at record 1880 (8:00 Z, 5 Aug), the source then broadcast 10 Hz and 16 Hz for the remainder of the recording period. For a short period at the end of the experiment, i.e., after record 2140 (11:15 Z, 5 Aug), the 7 Hz tone appears to have been transmitted along with the 10-16 Hz tone pair.

Other narrow band features are prominent in the data; for example, at 8.2 Hz, 8.7 Hz, 9.2 Hz, 10.4 Hz, 14.4 Hz, 14.7 Hz, and 17.0 Hz. Some of these are most likely due to the Gyre; spectral lines at 10.4 Hz and 14.5 - 15 Hz appear to be loudest during the times of closest approach of this ship around records 900 and 2175. Intermittent lines appearing at 17 Hz and 20 Hz may also be Gyre-generated, although contributions from the NADC 38 cannot yet be ruled out. The NADC 38 remained near the float array during event 1 because of a weak surface transmitter on the TSVLA array. According to the ship's log, the NADC 38 began to move towards the TSVLA around 21:16 Z, 4 Aug, which corresponds to float record 1021. At this time, the sound levels between 12.5 Hz and 13 Hz increased to their highest levels in Figures X.1a and X.1b. The true source of the ship-generated spectral lines in these two figures will be more easily determined once the results of the acoustic signature tests are available. In addition, the directionality of the spectral lines (to be calculated and presented in a later report) along with the ships' navigation information can be used to help identify the correct source.

Noise "troughs" are centered on 5 Hz and around 10.25 Hz throughout the experiment. However, note that the low frequency levels recorded by float 2's hydrophone appear to suddenly increase by 5 dB around record 1520 and then slowly increase for the remainder of the experiment. Neither the geophone data from this float nor any of the data from the other floats show a corresponding increase. This point is illustrated in the plots in Figure X.2, where the spectral level in the 5.0 Hz bin is plotted as a function of

time over most of the experiment (from record 640 to 2160; i.e., 16:30 Z, 4 Aug to 11:30 Z, 5 Aug) for floats 2, 6, 7, and 8. The solid curve in each plot is for the geophone-data-derived pressure spectrum and the dotted curve is for the hydrophone pressure spectrum. The data from float 2 is plotted in the upper left plot, and the lower left, upper right, and lower right plots are for float 6, float 7, and float 8, respectively. The cause of this apparent problem with float 2's hydrophone is unknown at present. Note that the RMS pressure plots for float 2, discussed in Section VIII, do not show a noticeable jump around record 1520, indicating that the apparent increase in float 2's hydrophone sensitivity occurred only at the lower infrasonic frequencies.

b) Hydrophone Pressure Spectrum vs Geophone-Data-Derived Pressure Spectrum

A comparison of the geophone-data-derived pressure spectrum and the hydrophone pressure spectrum is shown in Figures X.3 through X.11. In the upper plots of the figures, the geophone-data-derived pressure spectrum is plotted with a solid curve and the hydrophone pressure spectrum is plotted with a dotted curve. The vertical axis of these plots is in units of dB re 1 $\mu Pa^2/Hz$, units familiar to underwater acousticians. The corresponding ratio of the two spectra appears in the lower plot in each figure. Spectral ratios greater than zero dB indicate that the geophone-derived spectral levels are greater than the hydrophone levels; negative spectral ratios indicate that the hydrophone levels are greater. The spectra are derived by averaging together the four-record-averaged spectral estimates over a 2.5-hour period between records 1580 and 1780 (4:15 Z to 6:45 Z, 5 Aug). This period of time was chosen since the Gyre was at its farthest distance from the deployment site after finishing leg 1 of the source tow and the ELF source was not broadcasting. The spectra estimated from data collected by all midwater floats are presented. However, note that the geophone data from float 0 are slightly contaminated and those from float 1 are heavily contaminated by the non-acoustic signals during this time. Also, float 4's hydrophone system recorded only electronic self noise during the experiment due to a faulty hydrophone-to-circuitry connection.

For comparison with Figures X.3 through X.11, the two pressure spectra and their spectral ratios estimated from data collected by all midwater floats during the July, 1989 experiment are presented in Figures X.12 through X.20. These data were obtained in 4100-meter-deep water about 150 km west of Pt. Arguello on the California coast [4]. These spectral estimates are also based on data collected over a 2.5-hour period; from 9:28 Z to 11:58 Z, 9 July, 1989 (records 1200 to 1400).

The background spectral levels above 5 Hz in the NATIVE 1 experiment are at about 75 dB re 1 $\mu Pa^2/Hz$ and are about 5 dB lower than those in the July, 1989 experiment. The lower background levels allow many more spectral peaks to be evident, causing the NATIVE 1 spectra above 5 Hz to appear "jagged" in nature. A peak at 3.7 Hz also appears in the NATIVE 1 spectra. A ship-generated peak of this amplitude at so low a frequency is unusual in the Swallow float data; it may have been generated by the NADC 38 which remained close to the deployment site in order to record the TSVLA data. Note that the lump of energy around 18-19 Hz in the July, 1989 data is absent in the NATIVE 1 data. Although the peak of this lump is harmonically related to the 9.3 Hz peak, part of this energy may also be biologically related. Signals with infrasonic energy content around 18 Hz are a common feature in Swallow float data collected between mid-summer and early fall in the northeast Pacific Ocean and have been associated with whales. Other features of the July, 1989 spectra are described in [7].

The spectral ratio plots show that the hydrophone pressure spectrum and the geophone-data-derived pressure spectrum generally agree to within a few decibels across most of the infrasonic frequency band in both experiments. The large peak at 0.3 Hz is the result of both float rocking and oscillation of the ITC localization transducer; in fact, ratios of spectra with finer frequency resolution show two peaks around 0.3 Hz. Both float rocking and transducer oscillation are efficiently coupled into the horizontal geophone components. The peak around 1.5 Hz in many of the plots is probably associated with float ballast rocking. The roll-off above 20 Hz is due to a difference in the corner frequency of the anti-aliasing filters in the geophone and the hydrophone channels.

The spectral ratios in August, 1990 and in July, 1989 for a given float typically show nearly identical features, unless something unusual occurred in either of the experiments. This suggests that pressure spectral ratios which differ from unity are due to errors in calibration and system contamination rather than

being due to the actual properties of the sound field. The following list gives comments on the comparison of the two experiments' spectral ratios for each of the midwater floats.

Spectral Ratios in August, 1990 (8-90) versus July, 1989 (7-89)

FLOAT	COMMENTS
0	Agreement is good, although values are slightly more positive in 8-90 because of non-acoustic contamination.
1	Can't make comparison because of extensive non-acoustic contamination in geophone data in 8-90.
2	Ratio is a dB or two more negative between a few Hz and 12-13 Hz in 8-90 than in 7-89, apparently because of a sudden increase in hydrophone sensitivity around record 1520. Below a few Hz, the ratio is much more positive in 8-90 because of increase in tape recorder contamination in the geophone data.
3	Agreement between 8-90 and 7-89 spectral ratio is good; both show a decreasing sensitivity with decreasing frequency in the hydrophone circuit.
4	Can't make comparison because of faulty hydrophone-to-circuitry connection in 8-90.
5	Agreement between 8-90 and 7-89 spectral ratio is good; both show a decreasing sensitivity with decreasing frequency in the hydrophone circuit below 4 Hz; although the peak around 1.5 Hz due to ballast rocking is much lower in 8-90. The troughs in the spectral ratio curves at 4, 6, and 8 Hz are due to self noise in the hydrophone circuitry which can be eliminated by further processing.
6	Agreement is good between both the 8-90 and 7-89 spectral ratio and between the hydrophone and geophone pressure spectra.
7	Agreement between 8-90 and 7-89 spectral ratio is good; both show a -2 dB value above 1-2 Hz.
8	Agreement is good, although greater float rocking at 0.3 Hz occurred in 8-90. The cause of the spectral ratio peak at 6.3 Hz in 8-90 is unknown.

The two infrasonic pressure spectra in these figures are estimated from data collected in completely different ways. That is, the two types of sensors measure different properties of the ocean's sound field and the electronics in the data acquisition channels are unique. The good agreement between the two spectra is confirmation of the high quality of the Swallow float infrasonic measurement system.

c) The Rise Towards the Microseismic Peak

The spectra presented previously in this section were plotted in linear frequency units. In order to examine the spectral levels at the lowest infrasonic frequencies, the Fourier transform length was quadrupled and the resulting spectral estimates were plotted on a log frequency scale. These spectra are shown in Figures X.21 through X.24. The plots for the data collected during event 1 of the NATIVE 1 experiment are shown in the left-hand plots (except for the lower left plot in Figure X.24) and those for the July, 1989 experiment are shown in the right-hand plots for comparison. The time periods over which the spectral estimates were made are the same 2.5-hour periods as in Figures X.3 through X.20, i.e., from 4:15 Z to 6:45 Z, 5 August, 1990 and from 9:28 Z to 11:58 Z, 9 July, 1989. The spectra in each row of each figure pertain to the data collected by a given float in the two experiments. Only the spectra for midwater floats 2 through 8 in the NATIVE 1 experiment were calculated since floats 0 and 1 were contaminated by non-acoustic signals during the time chosen for the analysis. However, these two floats' spectra from the July, 1989 experiment are presented in the bottom two plots of Figure X.24. Again, the solid curve in each plot is the geophone-data-derived pressure spectrum and the dotted curve is the hydrophone pressure spectrum.

The first point of note is the single or double peak structure of the geophone-data-derived pressure spectrum between 0.2 Hz and 0.5 Hz. These peaks are the result of float rocking and oscillation of the ITC localization transducer, as mentioned previously. They are smaller in amplitude in the NATIVE 1 spectra

since additional processing was done to reduce all forms of tape-recorder-generated contamination.

The second point of note is that the NATIVE 1 hydrophone spectra show a peak at about 0.47 Hz. Below this peak, the spectra are contaminated by electronic self noise. In contrast, the July, 1989 spectra show peaks around 0.17 Hz, the microseismic peak frequency, and 0.75 Hz. Both the 0.47 Hz peak and the 0.75 Hz peak may be due to the excitation of "organ pipe" modes, i.e., non-propagating, resonant, standing wave patterns in the vertical direction. The average water depth in event 1 of NATIVE 1 was about 3180 meters and the harmonic sound speed over the whole water column was 1506 m/sec. Therefore, the first organ pipe mode has a predicted frequency of 0.47 Hz (= 1506/3180), corresponding exactly to the frequency of the spectral peak. For July, 1989, the water depth was about 4060 meters, the harmonic sound speed was 1496 m/sec, and the predicted frequency of the first organ pipe mode is 0.37 Hz (= 1496/4060). The suggestion of a peak does occur at this frequency in some of the floats' spectra, especially that of float 4, but it certainly is not predominant. However, the predicted frequency of the second mode is 0.74 Hz, which matches the observed spectral peak frequency. The presence of these peaks makes it difficult to fit a simple power law relationship to these spectra, as is done, for example, by Kibblewhite and Ewans [10].

The absence of the microseismic peak in the NATIVE 1 data may be due to the relatively calms seas during the experiment. That is, the nonlinear wave-wave interaction source levels may have been so weak that the microseismic peak is buried in electronic self noise. The microseismic peak is present in the July, 1989 spectra since the seas were rough (the wind speed was 25-30 knots, gusting to 35-40 knots) and the swell was 11-13 feet [4].

d) Comparison of Spectral Levels on the Three Geophone Components

A comparison of the individual spectral levels on each of the three geophone components of all midwater Swallow floats in event 1 of NATIVE 1 is presented in Figures X.25 through X.29. The east-west axis (x) is plotted with a dashed curve, the north-south axis (y) is plotted with a dotted curve, and the up-down axis (z) is plotted with a solid curve. The ordinate of these plots is in units of dB re 1 $(\mu m/sec)^2/Hz$. By adding 123.5 dB (equal to 20 times the log of the characteristic impedance, $\rho_o c$) to the ordinate, standard pressure spectral units of dB re 1 $\mu Pa^2/Hz$ can be obtained. These spectra are estimated using the same data and the same procedure as the spectra in the upper plots of Figures X.3 through X.11.

The background levels on the two horizontal components are approximately equal and are about 6 dB greater than the background levels on the vertical geophone above 4 Hz. Therefore, in this frequency range, the properties of the horizontal component spectra dictate those of the geophone-data-derived pressure spectrum. Below 4 Hz, all three components have nearly identical spectral levels, except where float rocking, ballast motion, and localization hydrophone oscillation contaminate the horizontal component data. The north-south component spectrum contains more prominent peaks than the east-west component, probably because of the headings of the research vessels from the float array during this time.

The contaminating effect of the non-acoustic signals on the geophone spectral levels can be clearly seen in float 1's spectra; re the lower plot in Figure X.25. The offset of float 0's horizontal component spectra from its vertical component spectrum below 4 Hz, in the upper plot in Figure X.25, is also partially caused by the non-acoustic signals.

e) Spectra of the T Phase Arrival from the Leeward Islands' Earthquake

As discussed in Section IXb, the arrival in record 1906 of the Swallow float data occurred at exactly the expected arrival time of the T phase from the earthquake in the Leeward Islands of the Caribbean. Appendix 2 contains a map of the Caribbean area, showing the locations of the Leeward Islands' earthquake epicenter, indicated by a "*", and the deployment site at 31° 15.6′ N, 74° 53.2′ W, indicated by a "D". The epicenter has a range of 1950 km (Δ = 17.5°) and a heading of 135.6° from point D.

Figures X.30 through X.33 show a comparison of the pressure spectra recorded by midwater floats 0 - 3 and 5 - 8 just before (left-hand plots) and during (right-hand plots) the arrival of the T phase. Data from

float 4 are not presented because of its non-functioning infrasonic hydrophone. Both sets of spectra are based on 3 minutes (4 records) of data. The T phase arrival clearly increases the spectral levels between 1 and 15-20 Hz. However, its spectral shape is misleading since the arrival resulted in significant clipping. In fact, the increase in spectral levels above 20 Hz is probably due to contamination from clipping.

Note that, at the arrival time of the T phase from the Leeward Islands' earthquake, the Gyre was returning to the site from the south-southwest. Its position at this time is marked by a large "*" in Figure II.1. The ELF source, which the ship was towing, was simultaneously broadcasting 10 Hz and 16 Hz tones. The spectral peaks due to the ELF source are prominent features of the plots in Figures X.30 through X.33, especially the 16 Hz line.

The active acoustic intensity is a physically meaningful measure of the directionality of a sound field, i.e., it measures the magnitude and direction of net acoustic energy flux density [7]. Figures X.34 through X.37 show plots of the horizontal projection of the active acoustic intensity spectrum estimated from data collected by floats 0 - 3 and 5 - 8. These spectra were estimated over the same two periods of time as in Figures X.30 through X.33; the left-hand plots pertain to the 3-minute period just before the T phase arrival and the right-hand plots are for the period encompassing the arrival. The horizontal axes in the plots are in linear frequency units, from 0 to 25 Hz. The horizontal intensity magnitude per frequency is given by the lengths of each of the vectors in a given spectrum. To determine the magnitude in units of dB re 1 $\mu Watt/m^2/Hz$, the length of a vector is measured along the y axis, starting at the bottom of the plot at -80 dB re 1 $\mu Watts/m^2/Hz$. The direction of net energy flow is with respect to the compass given in the upper right corner of each spectrum.

For the data recorded prior to the arrival, three features are notable. First, the direction of acoustic energy flux is quite variable across the frequency band. Second, the direction of energy flux for the 10 Hz and 16 Hz tones generated by the ELF source is in the expected direction, i.e., to the north-northeast away from the source to the south-southwest. Variations from the expected direction are caused mostly by small errors in system calibration. Finally, a harmonically-related line pair occurs at 8.5 Hz and 17 Hz which shows energy flow mainly to the south. This line pair may have been generated by the NADC 38; this conjecture can be tested once the navigation information for this ship are obtained. Note that the directionality indicated by the data below 0.5 Hz is erroneous.

The horizontal active intensity spectra estimated from data collected during the time of the T phase arrival in record 1906 are shown in the right-hand plots. As mentioned previously, a significant degree of clipping occurred in the time series so that absolute spectral levels cannot be determined. However, from a few hertz up to 15-20 Hz, the spectra show an overwhelming flow of acoustic energy to the northwest. This direction of broadband energy flow is 180° from the heading of 136° of the Leewards Islands' earthquake epicenter, re the map in Appendix 2.

In summary, both the time of arrival and direction of broadband energy flux of the signal in record 1906 strongly suggest that it is the T phase arrival from the Leeward Islands' earthquake. The earthquake in Trinidad following the Leeward Islands' earthquake (re the "Preliminary Determination of Epicenters" in Appendix 2) does not appear to have been detected by the floats.

f) Time Series of ELF Signal Spectra

The final set of plots in this section, Figures X.38 through X.43, show time series of various spectra in the frequency bins corresponding to the tones broadcast by the towed ELF source. The upper two plots in each figure show the geophone-data-derived pressure spectral bin levels, plotted with solid lines, and the hydrophone pressure spectral bin levels, plotted with dotted lines, as a function of time. The ordinate of these plots range from 80 dB to 110 dB re 1 $\mu Pa^2/Hz$. The lower two plots in each figure show the horizontal projections of the active intensity spectral bin vectors versus time. The length of each vector determines the active intensity magnitude, in units of dB re 1 $\mu Watt/m^2/Hz$, and the direction of each vector is the direction of net energy flux, as in the intensity plots in part e of this section. The abscissa are in units of Swallow float record number (a measure of time) and are identical for all four plots in each figure. Only the data collected by floats 2, at 1120 meters depth, and float 6, at 1580 meters, are presented. The data over three different periods of time are plotted: Figure X.38, for float 2, and Figure X.39, for float 6, cover

the 6-hour period from 16:30 Z to 22:30 Z, 4 August (records 640 to 1120) when the source first began to broadcast 7 Hz (left-hand plots) and 10 Hz (right-hand plots); Figure X.40 (float 2) and Figure X.41 (float 6) cover the 3.5-hour period from 00:30 Z to 4:00 Z, 5 August (records 1280 to 1560) when the source restarted its broadcast of 7 Hz (left-hand plots) and 10 Hz (right-hand plots) after the SUS charge events; and Figure X.42 (float 2) and Figure X.43 (float 6) cover the 3.5-hour period from 8:00 Z to 11:30 Z, 5 August (records 1880 to 2160) when the source was broadcasting 10 Hz (left-hand plots) and 16 Hz (right-hand plots). Each spectral bin value was estimated by averaging over 4 records (3 minutes) of data and each frequency bin is 98 mHz wide.

The plots in Figures X.38 and X.39 clearly show the passage of the Gyre near the float array, around record 900, as it headed south (re Figure II.1). The pressure spectral levels reach their highest values around this time and the intensity vectors show large changes in direction over a short period of time; from energy flux to the south to energy flux to the north. The ship passed to the east of the array at its point of closest approach since energy flow occurs to the west during this time, and it passed closer to float 6 than to float 2 since the direction of energy flow changed more slowly in float 2's data. Interestingly, the return of the Gyre near the end of event 1 (re Figures X.42 and X.43) resulted in energy flow to the east in float 2's data and to the west in float 6's data, suggesting that the ship passed between these two floats. This occurrence was possible given that float 6 was recovered to the west of float 2's retrieval position; re Figure I.1.

One aspect of the pressure spectrum plots in these figures is that the troughs in the hydrophone pressure spectrum curves are typically deeper than those in the geophone-data-derived spectrum curves. This feature can be explained by considering the properties of a single normal mode. A normal mode is a standing wave pattern in the vertical direction which propagates in the horizontal direction. Because of this, the nodes/anti-nodes in the mode's pressure eigenfunction correspond to the nodes/anti-nodes of its horizontal particle velocity eigenfunction, whereas they correspond to the anti-nodes/nodes in the vertical particle velocity eigenfunction. For example, the pressure is zero at a pressure-release surface, whereas the vertical particle motion is maximum (the surface "gives way"). Likewise, the pressure is a maximum at a rigid boundary, whereas the vertical particle velocity is zero. Therefore, when nulls occur in the hydrophone pressure spectrum in the upper plots of Figures X.38 through X.43, the vertical particle velocity is maximum (or nearly so), causing the geophone-data-derived pressure nulls to be filled in. In general, the geophone-data-derived pressure spectrum is not necessarily equivalent to the hydrophone pressure spectrum. The two spectra are likely to differ when the spatial structure of the sound field is significant, i.e., when the field is spatially inhomogeneous [7], as is the case for the fields generated by the ELF source.

Once the float positions as a function of time have been determined, the transmission loss of the ELF tones as a function of range can be calculated. These calculations will be performed and presented at a later date.

Acknowledgements

We would like to thank the people from the Naval Air Development Center for their hospitality during the NATIVE 1 experiment. In particular, Bruce Steinberg was especially helpful and generous with his time. Also, the crew of the R/V NADC 38 was very responsive and patient. Special thanks are due to Bruce Gomes, the test director, whose diligent supervision of this experiment was a major contributor to its success.

This work was supported by the Naval Air Development Center in Warminster, PA, through Office of Naval Research contract # N00014-89-D-0142.

Appendix 1 - Swallow Float Infrasonic Data Acquisition System

A block diagram of the Swallow float infrasonic system appears in Figure A1.1. All midwater floats were equipped with three orthogonally-oriented Geo Space geophones and with a Ocean and Atmospheric Science (OAS) model E-4SD hydrophone. The bottom-tethered floats contained only a vertical component geophone and an infrasonic hydrophone; their horizontal geophone components were shorted out in order to prevent tether contamination from dictating the AGC gain level. The geophone channels will be described first, followed by a description of the hydrophone channel.

The water motion is first coupled into motion at the floats' geophones. The three orthogonal components of particle velocity at the geophone are then converted into voltages. The geophones are electromagnetic transducers in which a voltage is produced across a moving, conducting coil by its motion through the magnetic field lines produced by a permanent magnet [11]. The resulting voltage is proportional to the velocity of the coil with respect to the magnet. Constraining the coil to move in only one direction are elastic springs connecting the coil to the instrument casing. Laboratory tests have determined that the geophones can withstand a maximum tilt from vertical of about 15°. The geophone package for each midwater Swallow float is composed of three such transducers oriented to measure in three orthogonal directions.

The geophone amplitude and phase response was calculated using the theoretical equation of motion for this system [11]. (The amplitude response curve is nearly identical to the manufacturer's calibration curve provided with the geophones). Near-critical damping of the coil is achieved using a 60 kΩ shunt resistor. Note that the f^2 roll-off of the geophone amplitude response below the natural frequency of 8 Hz effectively pre-whitens the ocean ambient noise so that no additional pre-whitening needs to be implemented.

The three signals next undergo a fixed gain of 95 dB before being input to the automatic gain control (AGC). For the vertical geophone components on the bottom tethered floats, this fixed gain was reduced by 18 dB to 77 dB. Included in the geophone channel circuitry are nine RC circuits. Five of these RC circuits act as high pass filters, with poles located at 0.000034, 0.034, 0.07, 0.26, and 0.47 Hz, in order to eliminate DC bias and decrease ultra-low frequency self noise. The other four RC circuits act as low pass filters, with poles at 34, 34, 72, and 337 Hz, in order to eliminate AC coupling noise (i.e. "cross-talk"). These RC circuits are lumped together with the geophone channel "fixed gain" in Figure A1.1.

The water-borne pressure fluctuations (acoustic and non-acoustic) are converted into voltage fluctuations by the sensing material in the infrasonic hydrophone. The sensing material is electrostrictive; that is, it develops a voltage in response to an implied stress [12]. From laboratory tests, it has been determined that the sensing material is also pyroelectric, i.e. it generates a voltage in response to a change in temperature. The electrostrictive material in the OAS hydrophones is pre-polarized lead zirconate-titanate, a polycrystalline ceramic. The hydrophone has a sensitivity of -182 dB re 1 V/μPa and a frequency response which is flat (within ±1 dB) from 0 to 5 kHz. Because the ocean ambient noise spectrum increases as f^{-4} to f^{-6} below about 5 Hz [7], the voltage output by the hydrophone is then passed through a pre-whitening filter. This high-pass filter is comprised of two RC circuits in cascade. Both RC circuits have corner frequencies of about 8 Hz, the same as the natural frequency of the geophone components.

The "fixed gain" triangle for the infrasonic hydrophone channel in Figure A1.1 represents somewhat different circuitry than in the geophone channels. The fixed gain is set to 80 dB (rather than 95 dB), since the hydrophone is more sensitive than the geophones; -182 dB re 1 V/μPa for the hydrophone versus about -201 dB re 1 V/μPa above 8 Hz for the geophones. Also, since the hydrophone pre-whitening filter already includes two high pass RC circuits, only two additional high-pass circuits, with poles located at 0.034 and 0.47 Hz, were added. An additional equivalent high-pass RC circuit with resonant pole at 0.2 Hz is formed by the capacitance of the hydrophone itself (0.004 μf) and the resistance (200 MΩ) of a temperature-stable, metal film resistor. These three high-pass RC circuits are included in the "fixed gain" triangle along with four low-pass circuits, with poles at 34, 34, 72, and 339 Hz.

The hydrophone component voltage and all three geophone component voltages are then sent to a automatic gain control (AGC) amplifier. The AGC is a variable gain amplifier with a range of 0 to 36 dB gain which allows the full dynamic range of the eight-bit A/D converter to be used. The AGC gain always

changes between records by approximately 0.5 dB steps; if more than 0.5 percent of all data samples from the last 40 seconds of each record are clipped, then the AGC decreases by 0.5 dB. Otherwise, it increases. Plots of the AGC level for each float during every record are given in Section Vc.

Before being digitized, the signals are passed through a five-pole, four-zero, elliptic, anti-aliasing filter. Elliptic filters theoretically have the sharpest transition region for a given number of poles and circuit complexity. The filter frequency response and the pole-zero locations in the *s* plane are shown in Figure A1.2 [13,14]. Incoming signals are amplified by a maximum of 4.6 dB in the passband, which has a 0.28 dB equal ripple. The cut-off frequency (the highest frequency at which the amplitude gain is equal to the minimum passband gain) is 20 Hz, and the attenuation is 19.5 dB at the Nyquist frequency of 25 Hz. The maximum equal ripple level in the stop band is 50.1 dB below the level in the pass band and is first reached at 31 Hz. Before installation in the floats, all filters were adjusted so that broadband noise input to the filters yielded the same amplitude response and same null location at the filters' output.

The geophone channel response, including all components in the system except the AGC gain which varies over the time of the experiment (and excluding the 18 dB decrease in the fixed gain for the vertical geophone components on the bottom-tethered floats), is plotted in Figure A1.3. The hydrophone channel response, including all components in the channel except the AGC gain, is plotted in Figure A1.4. In deriving the phase response in Figure A1.4, it was assumed that no phase shift was introduced by the hydrophone's electrostrictive material in the conversion of pressure to voltage.

The channel voltage signals are then digitized at a 50 Hz sampling rate and put into a temporary buffer. After 44 seconds of data (equal to one data record) have accumulated in the buffer, a one second period of writing the data to cassette tape takes place. During this time, no data is sampled. The 45 second cycle then repeats until the cassette tape is full. The cassette tape can store up to 17 Mbytes of unformatted data, which is sufficient space for up to 1600 four-component data records.

Both the RMS plots discussed in Section VIII and the time series plots of Section IX have been corrected for the variable AGC level. No other adjustments have been made in these plots. The spectral plots of Section X, however, have been corrected for all electronic system gains including the geophone/hydrophone sensitivities and therefore report estimates calibrated to the input at the sensors.

Excellent agreement between the laboratory-measured and theoretically-predicted amplitude and phase responses of both the geophone and hydrophone channel circuitry, and the sensors themselves, has been obtained [1].

Appendix 2 - Caribbean Area Map and Preliminary Determination of Epicenters

On the following page is a map of the Caribbean area showing the location of the Leeward Islands' earthquake epicenter (the asterisk) and the deployment site of event 1 in the NATIVE 1 experiment (the "D"). Following the map are copies of four pages from the "Preliminary Determination of Epicenters" from the National Earthquake Information Center. On the copies are indicated the time periods in which the Swallow floats recorded data during events 1, 3, and 4 of NATIVE 1. Within these time periods, those earthquakes which are most likely to have generated detectable T phase arrivals have been marked by arrows. The T phase is that portion of the radiated seismic energy which somehow (probably through a downslope conversion mechanism [15]) gets coupled into the deep ocean sound channel. It has been the most commonly observed phase from earthquakes in the Swallow float data. The T phase generated by the Leeward Islands' earthquake during event 1, marked with an arrow and an asterisk, was probably detected by the floats, as discussed in the body of this report.

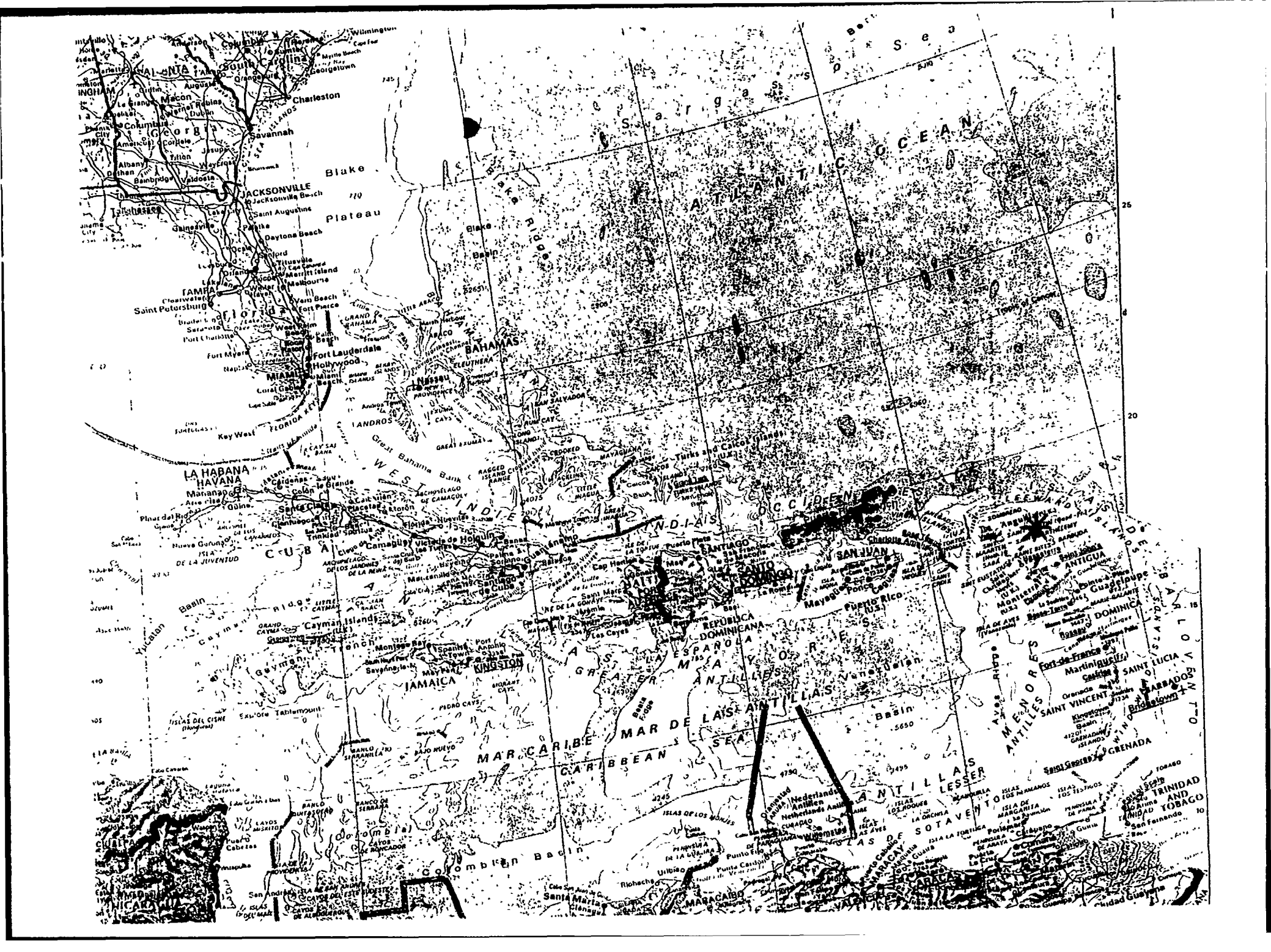
ATLANTIC OCEAN
Sargasso Sea
Blake Plateau
Blake Basin
Florida
Georgia
South Carolina
Charleston
Savannah
JACKSONVILLE
Tallahassee
Gainesville
Daytona Beach
Orlando
Melbourne
Titusville
Cocoa
Merritt Island
Vero Beach
Fort Pierce
TAMPA
Clearwater
Saint Petersburg
Sarasota
Fort Myers
Naples
West Palm Beach
Palm Beach
Fort Lauderdale
Hollywood
MIAMI
Miami Beach
Coral Gables
Key West
FLORIDA KEYS
BAHAMAS
Nassau
NEW PROVIDENCE
GRAND BAHAMA
ABACO
ELEUTHERA
SAN SALVADOR
RUM CAY
LONG ISLAND
CROOKED ISLAND
ACKLINS
MAYAGUANA
Turks and Caicos Islands (U.K.)
GREAT INAGUA
LITTLE INAGUA
ANDROS
Great Bahama Bank
Straits of Florida
CAY SAL BANK
GREAT EXUMA
RAGGED ISLAND CHAIN
ARCHIPIELAGO DE CAMAGUEY
LA HABANA
HAVANA
Mariano
Arroyo Arenas
Guira
Cárdenas
Colón
Jagüey Grande
Santa Clara
Placetas
Morón
Nuevitas
Florida
Trinidad
Sancti Spíritus
Ciego de Avila
Camagüey
Victoria de Holguín
Las Tunas
Bayamo
Guantánamo
Baracoa
CUBA
ISLA DE LA JUVENTUD
Nueva Gerona
Batabanó
Gulf of Batabanó
Cayman Ridge
Cayman Basin
Cayman Islands (U.K.)
Grand Cayman
Cayman Trench
Yucatan Basin
Yucatan
Gulf of Honduras
Belize
Guatemala
Honduras
Nicaragua
Costa Rica
Panama
Colombia
Colombian Basin
Monkey Rock
Serranilla Bank
Pedro Bank
Pedro Cays
Jamaica
Morant Cays
Port Antonio
Port Maria
Ocho Rios
Spanish Town
KINGSTON
Savanna-la-Mar
Negril Point
Negril
Montego Bay
Black River
Alligator Pond
Portland Bight
Portland Ridge
Jamaica Basin
Isla de Providencia
Isla de San Andrés
Cayos del Este Sudeste
Cayos de Albuquerque
Cayos de Roncador
Serrana Bank
Quitasueño Bank
Serranilla Bank
Banco Nuevo
Banco Serranilla
Banco Quitasueño
Isla del Cisne (Swan Is.)
Islas del Maíz (Corn Is.)
Cayos Miskitos
Puerto Cabezas
Laguna de Caratasca
Trujillo
Puerto Castilla
Roatán
Utila
Guanaja
Bay Islands
Belize City
Stann Creek
Punta Gorda
Livingston
Puerto Barrios
Izabal
Lake Izabal
Río Dulce
Gulf of Amatique
Chetumal
Bacalar
Chinchorro Bank
Cozumel
Isla Mujeres
Cancún
Isla Contoy
Arrecife Alacranes
Progreso
Campeche
Ciudad del Carmen
Laguna de Términos
Isla del Carmen
Frontera
Villahermosa
Tabasco
Veracruz
Alvarado
Tuxpan
Tampico
Ciudad Madero
Gulf of Mexico
Mississippi Delta
Mississippi
Louisiana
New Orleans
Lake Pontchartrain
Lake Maurepas
Mobile
Alabama
Mobile Bay
Pensacola
Florida Panhandle
Apalachicola
Cape San Blas
Port St. Joe
Panama City
Destin
Fort Walton Beach
Eglin Air Force Base
Choctawhatchee Bay
Santa Rosa Island
Gulf Breeze
Navarre
Perdido Key
Perdido Bay
Pascagoula
Gulfport
Biloxi
Bay St. Louis
Waveland
Pass Christian
Ocean Springs
Dauphin Island
Mobile Point
Fort Morgan
Gulf Shores
Orange Beach
Alabama Point
Grand Lagoon
Bayou La Batre
Theodore
Saraland
Satsuma
Citronelle
Chickasaw
Prichard
Creola
Axis
Semmes
Irvington
Wilmer
Grand Bay
Bayou Casotte
Escatawpa
Moss Point
Gautier
Ocean Springs
Biloxi
Gulfport
Long Beach
Pass Christian
Bay St. Louis
Waveland
Diamondhead
Kiln
Lakeshore
Slidell
Mandeville
Covington
Madisonville
Abita Springs
Hammond
Ponchatoula
Independence
Amite
Tangipahoa
Kentwood
Franklinton
Bogalusa
Columbia
Jackson
Clinton
Port Gibson
Vicksburg
Natchez
Woodville
Centreville
Brookhaven
McComb
Magnolia
Summit
Liberty
Fayette
Meadville
Lorman
Alcorn State University
Lorman
Hazlehurst
Crystal Springs
Wesson
Hazlehurst
Baxterville
Lumberton
Purvis
Columbia
Hattiesburg
Petal
Oak Grove
Gulfport
Biloxi
Ocean Springs
Pascagoula
Moss Point
Escatawpa
Gautier
Vancleave
Lucedale
George County
Agricultural High School
Leakesville
Wiggins
Stone County
Perkinston

CURRENT SHELVES
University of California, San Diego - Libraries
Received on: 09-04-90

U.S. DEPARTMENT OF THE INTERIOR
GEOLOGICAL SURVEY

NO. 31-90
AUG 23, 1990

PRELIMINARY DETERMINATION OF EPICENTERS

DAY	ORIGIN TIME UTC HR	MN	SEC	GEOGRAPHIC COORDINATES LAT		LONG		DEPTH	MAGNITUDES GS MB	Msz	SD	NO. STA USED	REGION, CONTRIBUTED MAGNITUDES AND COMMENTS
JUL 1990													
30	00	56	01.07	16.29	N	120.34	E	33 N			0.5	4	LUZON, PHILIPPINE ISLANDS
30	01	13	17.3	29.933	N	130.364	E	69	5.0		1.0	82	RYUKYU ISLANDS. Felt (III JMA) on Yaku-shima.
30	10	04	53.0•	4.330	S	10.638	W	10 G	4.8		1.0	35	NORTH OF ASCENSION ISLAND
30	10	11	55.2•	42.486	N	22.934	E	10 G			0.6	5	BULGARIA
30	12	32	22.6	45.666	N	26.429	E	12			1.1	15	ROMANIA
30	13	08	10.9%	45.949	N	0.009	W	21			0.9	13	FRANCE. ML 3.1 (LDG).
30	16	24	54.0•	41.288	S	88.337	W	10 G	4.9	5.1	1.0	19	WEST CHILE RISE
30	17	52	38.8	34.603	N	25.754	E	63 •	4.2		1.0	68	CRETE. MD 4.3 (HLW).
30	21	50	13.7•	54.301	N	164.737	W	33 N	4.6		1.1	17	UNIMAK ISLAND REGION
31	01	43	49.1•	42.371	N	126.743	W	10 G	4.0		0.9	12	OFF COAST OF OREGON
31	02	15	44.6	24.193	N	126.648	E	18 D	5.0		0.8	24	RYUKYU ISLANDS
31	02	52	14.9?	36.83	N	76.73	E	33 N	4.9		1.3	10	KASHMIR-XINJIANG BORDER REGION
31	03	17	29.4	42.404	N	126.633	W	10 G	4.8		1.0	42	OFF COAST OF OREGON
31	03	19	46.5	42.354	N	126.716	W	10 G	5.7	5.4	1.2	166	OFF COAST OF OREGON
31	04	28	47.1•	10.785	S	162.674	E	82 ?	5.0		1.2	18	SOLOMON ISLANDS
31	05	29	41.0•	16.374	N	120.889	E	23 •	4.6		1.3	9	LUZON, PHILIPPINE ISLANDS
31	06	49	31.8	37.253	N	21.495	E	58	4.7		1.1	139	SOUTHERN GREECE. MD 4.7 (ATH). Felt in Peloponnisos.
31	07	30	09.9?	18.45	N	94.53	W	33 N	4.4		1.0	9	GULF OF CAMPECHE
31	07	32	40.1&	34.456	N	106.862	W	8				14	NEW MEXICO. <SNM>. MD 3.3 (SNM). Felt in the Bernardo area.
31	09	15	17.6•	17.706	N	61.326	W	56 •	4.6		1.3	23	LEEWARD ISLANDS
31	09	55	15.3	14.199	N	91.172	W	75	4.4		1.3	57	GUATEMALA. Felt (II) at San Salvador, El Salvador. Also felt in southern Guatemala.
31	13	28	22.9	44.985	N	147.950	E	33 N	4.7		0.8	21	KURIL ISLANDS
31	13	37	28.7%	46.051	N	2.755	E	10 G			0.6	10	FRANCE. ML 2.3 (LDG).
31	13	49	21.2•	4.685	N	127.862	E	156 ?	4.9		1.2	14	TALAUD ISLANDS
31	15	58	54.8	43.011	N	17.798	E	27	4.7		1.2	135	YUGOSLAVIA. MD 4.7 (TTG), 4.8 (TRI). ML 4.8 (KBA). Felt (IV) in western Montenegro and at Titograd.
31	16	35	02.7	44.535	N	7.275	E	10 G			0.9	27	NORTHERN ITALY. ML 3.2 (LDG).
31	18	25	49.7	3.739	N	95.335	E	23 D	5.3	4.4	0.7	94	OFF W COAST OF NORTHERN SUMATERA
31	19	35	19.9?	18.89	N	67.07	W	10 G			0.2	4	MONA PASSAGE
31	19	51	02.47	36.67	N	8.88	W	10 G			0.6	9	WEST OF GIBRALTAR. mbLg 3.2 (MDD).
31	19	55	19.9?	23.68	N	123.23	E	10 G			1.2	6	SOUTHWESTERN RYUKYU ISLANDS
31	22	27	48.6•	15.382	N	146.842	E	46 •	4.6	4.2	1.3	37	MARIANA ISLANDS
31	23	15	18.4	43.813	N	17.822	E	40 •	4.7		1.3	115	YUGOSLAVIA. MD 4.6 (TRI), 4.4 (TTG). ML 4.6 (KBA). Felt (III) at Titograd.
31	23	49	45.5&	48.853	N	122.288	W	0	3.6			55	WASHINGTON. <SEA-P>. ML 3.5 (SEA). Felt (IV) at Deming.
AUG 1990													
01	02	04	27.9•	31.759	S	71.782	W	55 •	4.5		1.1	14	NEAR COAST OF CENTRAL CHILE
01	02	45	00.1	11.549	S	166.074	E	32 D	5.4	5.1	1.5	64	SANTA CRUZ ISLANDS. Ms 5.5 (BRK).
01	04	25	48 1•	16.415	N	120.785	E	20	4.4	4.0	1.4	13	LUZON, PHILIPPINE ISLANDS
01	09	04	40.5?	51.10	N	178.58	E	33 N	4.3		1.5	13	RAT ISLANDS, ALEUTIAN ISLANDS. ML 4.2 (PMR).
01	11	04	58.0?	7.91	S	123.04	E	203 ?	4.7		0.8	7	BANDA SEA
01	11	53	25.0•	14.439	S	73.692	W	33 N			0.4	8	PERU
01	12	19	54 0	41.621	N	22.326	E	10 G			0 7	7	YUGOSLAVIA. ML 2.1 (SKO).
01	14	54	04.7•	28.594	N	53.255	E	33 N	4.5	3.6	1.5	9	SOUTHERN IRAN
01	23	47	25.0%	36.210	N	27.193	E	33 N			1.4	6	DODECANESE ISLANDS. MD 3.8 (ATH).
02	00	09	47.3	31.721	S	71.653	W	54 •	4.9		1.1	30	NEAR COAST OF CENTRAL CHILE
02	00	53	30.3	38.465	N	23.686	E	10 G			1.3	9	GREECE. ML 2.8 (ATH).
02	02	41	35.7	17.100	N	121.034	E	10 G	4.8	4.3	1 5	37	LUZON, PHILIPPINE ISLANDS
02	04	51	04.1%	18.546	N	66.962	W	33 N			0.3	6	PUERTO RICO REGION
02	05	24	08.9	31 613	S	71.579	W	41	5.6	5.8	1.0	96	NEAR COAST OF CENTRAL CHILE. Ms 5.8 (BRK). Mo=2.0•10••18 Nm (PPT). Felt (V) at Illapel and (IV) Los Vilos and Santiago.
02	05	37	22.6&	19.846	N	155.618	W	22	4.8			48	HAWAII <HVO-P>. CL 4.9 (HVO). Felt (V) at Hilo, Honomu, Kamuela, Kurtistown, Oakala and Paauhau: (IV) at Hakalau, Hawi, Holualoa, Honokaa, Laupahoehoe, Papaaloa, Papaikou and Volcano. Also felt on Maui.
02	05	41	51.8?	33.20	S	69.17	W	33 N	4.6		0.8	15	CHILE-ARGENTINA BORDER REGION
02	05	58	14.0	10.881	S	166.270	E	33 N	5.2		0.9	42	SANTA CRUZ ISLANDS
02	08	46	39.5•	31.626	S	71.969	W	46 ?	4.3		1.2	15	NEAR COAST OF CENTRAL CHILE
02	11	01	01.4•	46.729	N	10.251	E	10 G			0 8	6	NORTHERN ITALY. ML 2.4 (VIE).
02	13	02	57.3&	36.625	N	121.272	W	6				14	CENTRAL CALIFORNIA. <BRK>. ML 2.5 (BRK).
02	15	03	25 8	6.549	S	105.320	E	33 N	5.3	5.4	1.2	77	SUNDA STRAIT
02	17	57	35.17	14.46	S	166.84	E	33 N	4.8		1 4	6	VANUATU ISLANDS
02	19	08	59 8?	22.64	N	94.59	E	153 •	4 8		1 3	22	BURMA
02	28	08	57 4&	36.967	N	121.275	W	7				7	CENTRAL CALIFORNIA. <BRK>. ML 2.4 (BRK).
02	22	05	22 9?	14.40	N	119.64	E	33 N	4.5		1 4	5	LUZON, PHILIPPINE ISLANDS
03	00	54	11 27	38.61	N	22.10	E	33 N			0 8	13	GREECE
03	04	52	19.7?	59 99	N	152.02	W	33 N			0 5	6	SOUTHERN ALASKA ML 3.7 (PMR).
03	07	50	57.8	31.707	S	71.842	W	31 D	4.5		1 0	28	NEAR COAST OF CENTRAL CHILE
03	08	17	16.5•	17.302	N	121.089	E	10 G	4 6		1 0	13	LUZON, PHILIPPINE ISLANDS
03	08	36	28 8•	15 232	S	173.141	W	37 D	5 1		1 1	36	TONGA ISLANDS
03	09	15	04.1	47.949	N	84.958	E	19	6.1	6 1	1 0	282	KAZAKH-XINJIANG BORDER REGION. Ms 5 8 (BRK). Mo=2 0•10••18 Nm (PPT) Eight people injured and about 500 buildings destroyed (VII) in the Akkol area, USSR. Felt (IV) at Ust-Kamenogorsk and Semipalatinsk; (III) at Pavlodar and Taldy-Kurgan. Also felt at Alma-Ata and Borovoy, USSR.
03	10	02	49 0	36 390	N	118.097	W	5 G			1 0	19	CENTRAL CALIFORNIA. ML 3 7 (BRK)
03	10	28	45 3?	15 70	S	173.92	W	33 N	5 2		0 7	12	TONGA ISLANDS
03	11	57	12 2	32 803	N	48 237	E	33 N	5 1	4 5	1 0	81	WESTERN IRAN Felt in the Andimeshk area

03	11	59	05.8•	7.282	S	129.265	E	125 ?	4.6		1.5	16	BANDA SEA
03	13	42	03.3	16.278	N	120.883	E	10 G	4.6		0.5	7	LUZON, PHILIPPINE ISLANDS
03	14	50	04.3	40.582	N	71.089	E	33 N	4.9		0.4	14	TAJIK SSR
03	15	07	17.1	32.988	N	48.364	E	33 N	5.0	4.1	0.9	38	WESTERN IRAN
03	15	43	31.9	29.210	N	142.288	E	33 N	4.8	4.7	1.0	33	SOUTH OF HONSHU, JAPAN
	16	55	09.2•	46.363	N	142.918	E	269 ?	4.6		0.5	22	SAKHALIN ISLAND
	20	55	54.2•	31.645	S	71.753	W	44 •	4.5		1.3	22	NEAR COAST OF CENTRAL CHILE
04	02	48	01.1?	43.68	N	146.91	E	33 N	4.9	3.7	1.0	10	KURIL ISLANDS
04	02	56	11.4?	6.08	S	147.78	E	33 N			0.4	6	EAST PAPUA NEW GUINEA REGION
04	03	56	53.3	45.589	N	26.370	E	160 •.	3.7		1.0	19	ROMANIA
04	05	05	37.2	0.062	S	99.598	E	75 D	5.4		1.0	26	SOUTHERN SUMATERA
04	05	28	28.0•	15.984	N	120.457	E	78 ?	4.8		1.2	22	LUZON, PHILIPPINE ISLANDS
04	07	29	29.0	39.551	N	20.367	E	44	5.0		1.2	86	GREECE-ALBANIA BORDER REGION
04	08	31	51.5	26.934	N	125.356	E	225 D	5.1		0.9	79	NORTHEAST OF TAIWAN
04	08	33	25.4•	39.575	N	20.640	E	10 G			1.3	10	GREECE-ALBANIA BORDER REGION
04	09	19	28.9	1.269	N	123.116	E	33 N	5.2	4.5	1.1	37	MINAHASSA PENINSULA
04	11	06	00.2	25.133	N	141.169	E	171 D	5.1		1.0	84	VOLCANO ISLANDS REGION
04	12	52	30.3•	29.514	N	103.357	E	33 N	4.9		1.4	19	SICHUAN PROVINCE, CHINA
04	17	20	15.5	59.049	N	151.686	W	83 ?			0.4	10	KENAI PENINSULA, ALASKA
04	20	38	19.4?	23.18	S	68.48	W	256 ?	3.8		0.9	7	NORTHERN CHILE
05	00	45	37.7?	38.51	N	20.80	E	33 N	4.1		1.3	20	GREECE
05	01	34	57.5	29.513	N	137.596	E	516 D	5.9		0.9	170	SOUTH OF HONSHU, JAPAN. mb 6 5 (BRK). Felt (II JMA) in parts of Kanto and Tohoku.
05	03	16	10.2	27.583	N	141.593	E	48 D	5.4		0.7	92	BONIN ISLANDS REGION. Felt (II JMA) on Chichi-shima.
05	03	36	24.3	36.388	N	141.883	E	42 D	5.7	6.0	0.8	178	NEAR EAST COAST OF HONSHU, JAPAN. Felt (IV JMA) at Mito and Choshi; (III JMA) at Fukushima, Onahama and Utsunomiya; (II JMA) at Sendai, Tokyo, Chiba and Yokohama.
05	06	52	13.6&	36.855	N	121.638	W	7	3.6			38	CENTRAL CALIFORNIA. <BRK>. ML 4.0 (BRK). Felt (IV) at Aromas, Castroville, Chualar, Monterey, San Juan Bautista, Tres Pinos and Watsonville.
05	07	13	01.8	35.088	N	139.042	E	37	5.4	4.5	0.6	98	NEAR S. COAST OF HONSHU, JAPAN. Felt (V) at Yokosuka.
05	07	24	36.6•	5.258	S	129.596	E	200 ?	4.8		1.2	15	BANDA SEA
05	07	58	32.6•	18.095	N	62.870	W	33 N			0.7	10	LEEWARD ISLANDS. MD 3.3 (TRN).
05	11	03	58.0%	10.448	N	61.495	W	10 G			1.3	6	TRINIDAD. MD 2.9 (TRN).
05	12	19	47.1•	14.857	N	91.589	W	67 D	4.4		1.1	38	GUATEMALA
05	13	10	11.8•	1.076	S	13.022	W	10 G	4.9		1.2	17	NORTH OF ASCENSION ISLAND
05	14	47	51.0	51.670	N	175.259	W	33 N	5.2	4.6	1.2	88	ANDREANOF ISLANDS, ALEUTIAN IS. Felt (IV) on Adak.
05	15	26	00.4?	15.21	N	121.25	E	10 G	4.9		1.6	18	LUZON, PHILIPPINE ISLANDS
05	17	42	32.2	1.013	S	13.962	W	10 G	5.6	6.2	1.1	125	NORTH OF ASCENSION ISLAND. Mo=5.0•10••18 Nm (PPT).
05	18	31	48 2	40.252	N	33.927	E	10 G	4.9		1.0	65	TURKEY. Felt in the Ankara area.
05	18	48	21.6	6.886	N	126.750	E	130 •	5.2		1 0	30	MINDANAO, PHILIPPINE ISLANDS
05	20	03	22.3?	18.64	N	65.79	W	27 •			0.6	7	PUERTO RICO REGION
05	21	18	45.3?	43.21	N	146.65	E	33 N	4.9		1.1	8	KURIL ISLANDS
	21	27	01.7	33.360	N	116.325	W	5 G			0.8	16	SOUTHERN CALIFORNIA ML 3.9 (NEIS). Felt (IV) at Borrego Springs and Warner Springs.
05	21	32	25.0•	42.406	N	1 036	E	10 G			0 9	9	PYRENEES. mbLg 3.3 (MDD). Felt (II) at Pobla de Segur, Spain.
05	23	11	14 4	35.861	N	137.606	E	10 G	4.1		0.9	7	HONSHU, JAPAN

First Deployment

Preliminary Map of Epicenters Listed in this PDE

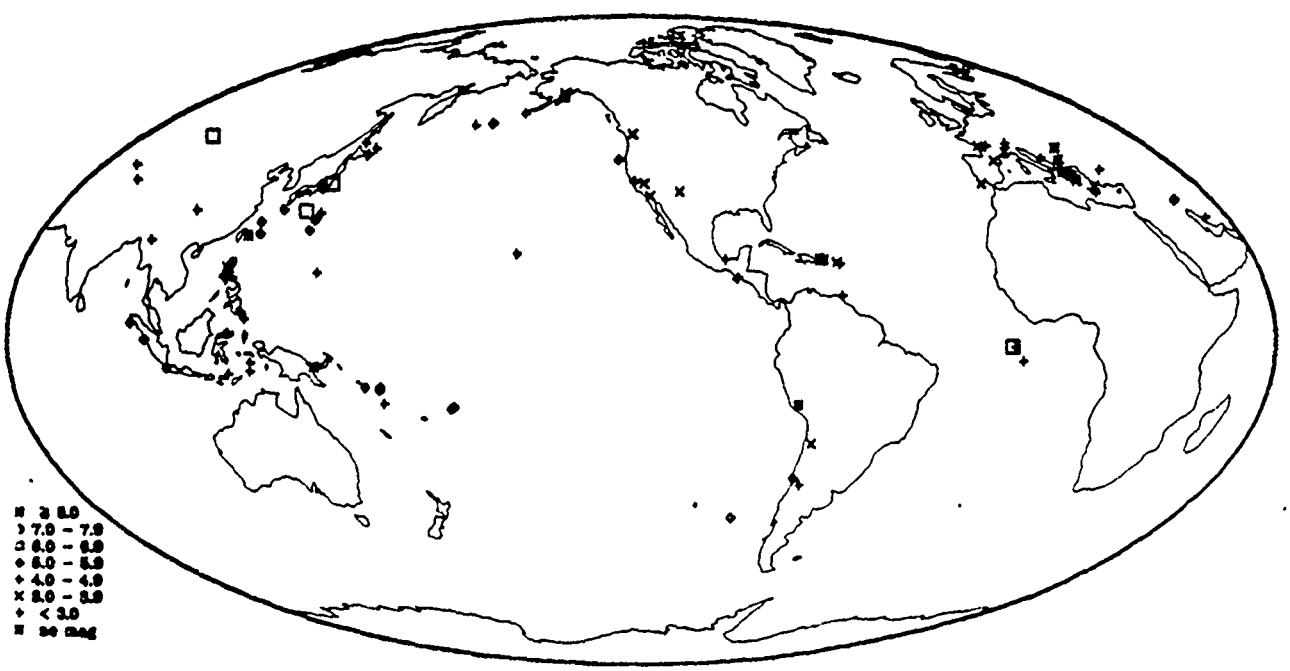

University of California, San Diego - Libraries
Received on: 09-10-90
CURRENT SHELVES

U.S. DEPARTMENT OF THE INTERIOR
GEOLOGICAL SURVEY

NO. 32-90
AUG 30, 1990

PRELIMINARY DETERMINATION OF EPICENTERS

DAY	ORIGIN TIME UTC HR MN SEC	GEOGRAPHIC COORDINATES LAT	LONG	DEPTH	MAGNITUDES GS MB	Msz	SD	NO. STA USED	REGION, CONTRIBUTED MAGNITUDES AND COMMENTS
AUG 1990									
06	02 38 41.1	16.284 N	120.589 E	39 D	5.3	4.4	0.9	78	LUZON, PHILIPPINE ISLANDS
06	03 26 16.1?	39.55 N	20.64 E	10 G			1.3	9	GREECE-ALBANIA BORDER REGION
06	03 29 02.0?	17.33 N	120.89 E	10 G	4.6	3.9	1.6	11	LUZON, PHILIPPINE ISLANDS
06	03 29 46.5?	43.09 N	10.21 E	10 G			0.8	10	CENTRAL ITALY
06	03 48 11.5?	7.95 S	129.99 E	149 ?	4.2		0.8	9	BANDA SEA
06	05 59 25.5&	43.994 N	7.542 E	10 G			0.4	5	NEAR SOUTH COAST OF FRANCE. ML 1.7 (GEN).
06	07 15 05.8?	43.84 N	21.06 E	10 G			1.5	6	YUGOSLAVIA
06	07 42 16.7&	44.235 N	7.419 E	10 G			0.3	8	NORTHERN ITALY. ML 1.9 (GEN).
06	08 40 01.9	24.100 S	66.853 W	182	4.6		1.2	53	SALTA PROVINCE, ARGENTINA
06	11 28 48.3•	10.365 S	75.149 W	33 N	5.0		1.3	11	PERU
06	13 59 10.9•	59.143 S	159.277 E	10 G	4.9	4.6	1.0	8	MACQUARIE ISLANDS REGION
06	16 23 17.3	16.153 S	173.447 W	83 D	5.2		0.9	72	TONGA ISLANDS
06	20 30 44.9	56.079 S	27.654 W	111 D	5.6		1.0	38	SOUTH SANDWICH ISLANDS REGION
07	00 02 07.3?	35.72 S	70.89 W	10 G			1.5	7	CHILE-ARGENTINA BORDER REGION
07	03 55 21.7	11.389 S	118.877 E	33 N	4.9		1.4	25	SOUTH OF SUMBAWA ISLAND
07	04 23 55.9?	16.04 N	121.37 E	33 N	4.4		0.4	7	LUZON, PHILIPPINE ISLANDS
07	05 05 56.4&	36.850 N	89.248 W	7				26	NEW MADRID, MISSOURI REGION. <SLM>. mbLg 3.0 (SLM). Felt (IV) at Wyatt, Missouri and (III) at Wolf Island, Missouri.
07	07 14 01.2?	19.01 S	65.67 E	10 G	5.1	4.8	0.1	7	MASCARENE ISLANDS REGION
07	08 26 20.7•	64.379 N	148.442 W	33 N			1.0	5	CENTRAL ALASKA. ML 2.9 (PMR).
07	10 35 04.6&	36.863 N	121.637 W	3				15	CENTRAL CALIFORNIA. <BRK>. ML 2.5 (BRK).
07	11 14 31.7	42.083 N	20.173 E	10 G			0.8	18	YUGOSLAVIA. ML 3.5 (TTG). Felt at Kukes, Albania.
07	13 49 43.6?	60.48 N	152.33 W	33 N			1.0	5	SOUTHERN ALASKA. ML 3.2 (PMR).
07	14 54 43.0•	42.083 N	144.894 E	37 •	4.9	4.0	1.1	24	HOKKAIDO, JAPAN REGION
07	18 39 47.8&	36.867 N	121.317 W	3				21	CENTRAL CALIFORNIA. <BRK>. ML 3.6 (BRK). Mo=7.6•10••14 Nm (BRK). Felt (III) at Aromas. Also felt at Moss Landing.
07	18 57 25.9?	61.32 N	147.75 W	33 N			1.5	6	SOUTHERN ALASKA. ML 2.7 (PMR).
07	19 22 07.6•	19.264 S	64.743 E	10 G	5.1	4.5	1.1	18	MASCARENE ISLANDS REGION
07	19 58 07.3•	8.667 N	126.339 E	88 •	4.4		1.1	13	MINDANAO, PHILIPPINE ISLANDS
07	20 43 23.4•	22.285 N	120.714 E	65 ?	4.3		1.1	11	TAIWAN
07	20 49 22.1	19.079 S	175.939 W	283	5.0		0.8	49	TONGA ISLANDS
07	21 35 00.7•	33.820 N	140.533 E	33 N	4.9		0.7	10	SOUTH OF HONSHU, JAPAN
07	21 44 07.1•	13.192 N	143.318 E	138	4.7		1.0	25	SOUTH OF MARIANA ISLANDS
07	22 34 22.6?	11.88 S	119.21 E	33 N	4.0		1.5	7	SOUTH OF SUMBA ISLAND
07	23 04 38.4•	40.073 N	19.697 E	10 G			1.4	6	ALBANIA. MG 3.1 (TIR). Felt at Vlora.
08	00 21 06.1	61.625 N	150.260 W	33 N			0.5	7	SOUTHERN ALASKA. ML 3.7 (PMR). Felt (III) at Palmer.
08	00 35 12.4	37.457 N	21 661 E	33 N	4.8	3.9	1.2	62	SOUTHERN GREECE
08	00 53 53.3•	61.523 N	151.121 W	33 N			0.5	6	SOUTHERN ALASKA. ML 2.9 (PMR).
08	06 17 03.4?	10.922 N	61.157 W	10 G			0.7	6	TRINIDAD. MD 3.2 (TRN).
08	08 21 59.3?	46.21 N	27 45 E	33 N			1.0	5	ROMANIA
08	10 10 57.6&	44.278 N	6.706 E	10 G			0.5	7	FRANCE. ML 2.0 (GEN).
08	11 10 53.5?	35.87 N	139.45 E	156 ?	5.0		1.5	11	NEAR S. COAST OF HONSHU, JAPAN
08	12 18 25.1	6.426 S	129.966 E	151 ?	4.7		1.3	22	BANDA SEA
08	14 19 50.0	44.463 N	7.272 E	10 G			0.3	12	NORTHERN ITALY. ML 2.2 (LDG).
08	14 42 38.7•	8.471 N	103.259 W	10 G	5.2	5.0	1.4	39	OFF COAST OF MEXICO
08	14 43 32.9•	42.818 N	19.455 E	10 G			1.2	5	YUGOSLAVIA
08	15 54 16.9	62.694 N	149.804 W	33 N			0.3	6	CENTRAL ALASKA. ML 3.3 (PMR).
08	19 27 08.1?	6.30 S	148 94 E	67 ?	4.8	3.5	0.9	12	NEW BRITAIN REGION
08	19 38 21.1?	15.17 N	120.58 E	10 G	4.3		1.3	7	LUZON, PHILIPPINE ISLANDS
08	19 54 41.3•	14.017 S	166.298 E	33 N	5.0	4.3	1.0	28	VANUATU ISLANDS
08	22 01 03.5?	9.92 N	103.32 W	10 G	4.4		1.2	16	OFF COAST OF MEXICO
09	23 27 46.4	16.261 N	120.631 E	20	4.9	4.4	1 1	44	LUZON, PHILIPPINE ISLANDS
09	02 06 36.8&	19.340 N	155 110 W	8	4.8			41	HAWAII <HVO-P>. MD 4 9 (HVO). Felt (V) at Hilo, Honomu and Pepeekeo; (IV) at Volcano; (III) at Honokaa, Mountain View, Paauilo, Pahala and Papaaloa.
09	02 36 33.9&	47.585 N	5 449 E	10 G			0 6	5	FRANCE. ML 2.4 (LDG).
09	02 42 07.8?	15.61 S	172.90 W	33 N	4.7		0 6	28	SAMOA ISLANDS REGION
09	05 32 03.7•	60 838 N	151.805 W	33 N			1 4	5	KENAI PENINSULA, ALASKA
09	06 28 24.9&	40.467 N	125 702 W	5	4.8			23	OFF COAST OF NORTHERN CALIFORNIA. <BRK>. ML 3.7 (BRK).
09	06 56 51.5•	13.155 S	112 048 W	10 G	5.1	4.6	0 9	38	NORTHERN EASTER I. CORDILLERA
09	07 33 54.4	7.270 S	129.167 E	131 •	5.0		1 1	28	BANDA SEA
09	09 38 45.0•	7.798 N	126.516 E	85 •	4.7		0.4	8	MINDANAO, PHILIPPINE ISLANDS
09	09 52 32.2?	15.02 S	72.25 W	33 N			0.6	6	SOUTHERN PERU
09	11 01 58.0&	45.597 N	1.898 E	10 G			0 6	6	FRANCE. ML 2.2 (LDG).
09	13 08 50.3•	6.543 S	127 505 E	416 ?	4 6		0.8	9	BANDA SEA
09	13 15 51 9	34.327 N	119.651 W	5 G			0.7	15	SOUTHERN CALIFORNIA ML 3.0 (NEIS) Felt (III) at Santa Barbara
09	14 58 26.4?	12 44 S	76 97 W	10 G			0 8	6	NEAR COAST OF PERU. Felt (IV) at Lima
09	17 53 44.0?	14 85 S	178 99 W	432 ?	4.3		0 2	7	FIJI ISLANDS REGION
09	18 12 47.1&	31.689 S	117 047 E	10 G			0.3	6	WESTERN AUSTRALIA
09	18 23 20.3?	19.45 N	109.15 W	10 G	4 0		1.0	20	REVILLA GIGEDO ISLANDS REGION
09	18 26 44.1	36.679 N	2.455 E	10 G			0.8	31	ALGERIA mbLg 3.7 (MDD)
09	19 16 57 0	43.985 N	7.416 E	10			0 9	37	NEAR SOUTH COAST OF FRANCE ML 3 4 (GEN), 3 2 (LDG).
09	19 45 59.7•	37.104 N	33 021 W	10 G	4 4		1 2	20	AZORES ISLANDS REGION
09	23 05 06 1%	43.976 N	8 448 E	10 G			0 3	5	CORSICA ML 1 7 (GEN)
10	00 16 17 3	4e.506 N	70 946 E	33 N	4.6		0 7	32	TAJIK SSR
10	01 51 19 5	0 064 S	122 924 E	177 D	5 3		1 1	66	MINAHASSA PENINSULA
10	02 50 09.8•	9.218 S	67 082 E	10 G	4 6		1 0	11	MID-INDIAN RISE
10	05 37 52.0	20.166 S	168 277 E	47 D	5 9	5 6	0 8	126	LOYALTY ISLANDS Ms 5 9 (BRK)
10	06 15 07 6•	15 748 S	176 722 W	37 ?	4 8		0 8	29	FIJI ISLANDS REGION

10	07	09	29.4?	63.55	N	144.79	W	33	N			0.3	5	CENTRAL ALASKA. ML 2.8 (PMR).
10	09	43	14.8%	44.963	N	7.265	E	10	G			0.3	9	NORTHERN ITALY. ML 2.8 (GEN).
10	11	07	46.8•	57.237	N	143.110	W	10	G			0.9	8	GULF OF ALASKA. ML 4.1 (PMR).
10	11	23	32.7	15.943	N	93.969	W	80		5.1		0.8	100	NEAR COAST OF CHIAPAS, MEXICO
10	11	41	30.8•	18.186	S	178.813	W	477		4.9		1.0	39	FIJI ISLANDS REGION
10	14	32	22.3	16.533	N	120.967	E	10	G	4.7		1.1	9	LUZON, PHILIPPINE ISLANDS
10	14	34	56.8	43.903	N	8.445	E	10	G			0.9	17	CORSICA. ML 2.8 (GEN). 2.7 (LDG).
10	15	00	00.7	57.390	N	33.036	W	10	G	4.8		1.1	57	NORTH ATLANTIC OCEAN
10	15	10	59.2?	58.21	N	30.71	W	10	G	4.3		0.5	19	NORTH ATLANTIC OCEAN
10	15	44	29.3	0.315	N	126.163	E	30	•	5.9	5.9	1.1	120	MOLUCCA PASSAGE
10	16	33	25.5	17.576	N	121.369	E	31		4.7		1.2	23	LUZON, PHILIPPINE ISLANDS. Felt (II) at Santa.
10	16	49	07.5•	0.319	N	126.163	E	93	?	4.9		1.5	16	MOLUCCA PASSAGE
10	17	47	39.3	19.677	S	177.520	W	392		5.8		0.9	138	FIJI ISLANDS REGION. mb 6.1 (BRK).
10	19	02	17.7	57.554	N	32.916	W	10	G	4.8	4.8	1.0	85	NORTH ATLANTIC OCEAN
10	21	11	48.7	6.535	N	60.243	E	10	G	5.4	5.2	1.1	96	CARLSBERG RIDGE
11	00	15	31.2?	18.28	S	178.73	E	33	N	4.9		0.8	12	FIJI ISLANDS
11	00	28	53.9	44.000	N	8.387	E	10	G			0.4	11	CORSICA. ML 2.3 (GEN). 2.1 (LDG).
11	02	15	57.8•	34.399	N	24.959	E	33	N	4.1		1.5	35	CRETE
11	02	45	18.9	6.869	S	130.389	E	127	?	5.1		1.1	39	BANDA SEA
11	02	59	54.9	0.871	S	78.528	W	5	G	5.0		1.2	99	ECUADOR. At least four people killed, 10 injured, considerable damage and landslides in the Pomasqui area. Felt strongly at Quito.
11	03	34	05.6•	0.291	S	78.710	W	5	G	3.9		1.2	8	ECUADOR
11	04	07	47.4%	43.984	N	8.395	E	10	G			0.3	7	CORSICA. ML 2.0 (GEN).
11	04	55	38.2•	28.416	N	127.985	E	21	D	4.5		1.3	14	EAST CHINA SEA
11	05	15	38.6?	36.06	N	24.47	E	72	?	3.5		0.8	5	SOUTHERN GREECE
11	05	31	47.1•	47.368	N	7.918	E	10	G			1.5	9	SWITZERLAND ML 3.3 (VIE), 3.1 (LDG).
11	06	09	38.6•	18.984	N	103.271	W	58	D	4.5		1.3	38	NEAR COAST OF MICHOACAN, MEXICO. Felt at Colima and Ciudad Guzman.
11	06	43	10.1•	40.932	N	22.644	E	10	G	3.6		1.3	19	GREECE. ML 3.8 (SKO).
11	06	45	48.8•	41.048	N	22.736	E	10	G			0.7	9	YUGOSLAVIA. ML 3.6 (SKO).
11	07	20	54.9?	32.75	S	179.98	W	419	?	4.7		1.0	8	SOUTH OF KERMADEC ISLANDS
11	07	49	16.4?	5.16	S	149.74	E	318	?	4.6		1.1	10	NEW BRITAIN REGION
11	08	00	15.2	22.104	S	171.079	E	133	D	5.1		1.1	45	LOYALTY ISLANDS REGION
11	09	22	56.5%	43.968	N	8.418	E	10	G			0.2	7	CORSICA. ML 2.3 (GEN).
11	10	25	46.0%	31.937	S	117.234	E	5	G			1.6	5	WESTERN AUSTRALIA
11	17	54	57.0	23.102	S	130.251	E	10	G			1.4	11	NORTHERN TERRITORY, AUSTRALIA
11	18	16	41.0?	16.33	S	71.77	W	132	•	3.9		1.0	10	SOUTHERN PERU. Felt (II) at Arequipa.
11	21	09	40.6	16.466	N	120.364	E	33	N	5.2	4.3	0.8	91	LUZON, PHILIPPINE ISLANDS
11	21	53	02.3&	36.803	N	121.557	W	2					19	CENTRAL CALIFORNIA. <BRK>. ML 2.6 (BRK)
11	22	04	32.4•	61.751	N	151.002	W	33	N	3.7		0.6	6	SOUTHERN ALASKA. ML 3.6 (PMR).
11	22	32	23.1•	17.600	S	73.899	W	33	N			1.2	9	OFF COAST OF PERU
11	23	17	30.9?	7.21	N	34.26	W	10	G	4.5	4.7	1.1	11	CENTRAL MID-ATLANTIC RIDGE
12	00	09	38.1	6.844	S	130.449	E	129	D	5.3		0.9	34	BANDA SEA
12	00	35	03.3	1.014	N	28.852	W	10	G	5.2	5.1	0.9	99	CENTRAL MID-ATLANTIC RIDGE
12	01	43	05.8•	14.978	N	146.820	E	33	N	4.3		1.4	10	MARIANA ISLANDS
12	02	54	49.8	51.188	N	5.440	E	10	G			0.9	19	NETHERLANDS. ML 3.1 (LDG) MD 2.7 (UCC)
12	03	04	15.2?	59.15	S	159.68	E	10	G	4.8	4.6	1.5	7	MACQUARIE ISLANDS REGION
12	05	35	19.2?	0.45	S	80.45	W	33	N			1.1	9	NEAR COAST OF ECUADOR
12	07	25	51.4•	5.819	S	151.594	E	47	•	4.7		0.9	12	NEW BRITAIN REGION
12	07	51	55.2	13.281	N	143.946	E	146		5.5		1.0	116	SOUTH OF MARIANA ISLANDS
12	08	30	18.0&	36.932	N	121.670	W	5					15	CENTRAL CALIFORNIA <BRK> ML 2.7 (BRK)
12	08	37	56.5&	36.927	N	121.683	W	11					17	CENTRAL CALIFORNIA. <BRK>. ML 3.3 (BRK) Mo=2.2e+10**14 Nm (BRK).
12	11	41	50.3%	43.146	N	3.819	E	10	G			0.8	8	NEAR SOUTH COAST OF FRANCE ML 2.8 (LDG)
12	11	55	54.6•	44.436	N	148.778	E	33	N	4.6		0.7	15	KURIL ISLANDS
12	13	53	25.4?	80.42	N	6.86	W	10	G	4.7		0.5	6	NORTH OF SVALBARD
12	15	19	53.8%	44.822	N	6.887	E	5	G			0.6	6	FRANCE ML 1.9 (GEN).
12	18	22	32.8•	43.845	N	16.781	E	10	G			1.2	7	YUGOSLAVIA
12	21	25	22.7	19.421	S	169.050	E	144	D	6.4		1.2	137	VANUATU ISLANDS
12	21	38	55.6	49.830	N	7.221	E	10	G			0.7	11	GERMANY ML 3.1 (LDG) MD 2.7 (UCC)
12	22	54	16.5	43.012	N	17.793	E	10	G			0.8	9	YUGOSLAVIA
12	23	00	17.0	43.024	N	17.762	E	10	G	4.3		1.6	77	YUGOSLAVIA MD 4.1 (TTG) Felt (V) in the Cetinje area
13	00	05	57.9?	20.71	S	168.36	E	34	D	4.9		1.1	17	LOYALTY ISLANDS

2nd Deployment Part a

2nd Deployment Part b

Preliminary Map of Epicenters Listed in this PDE

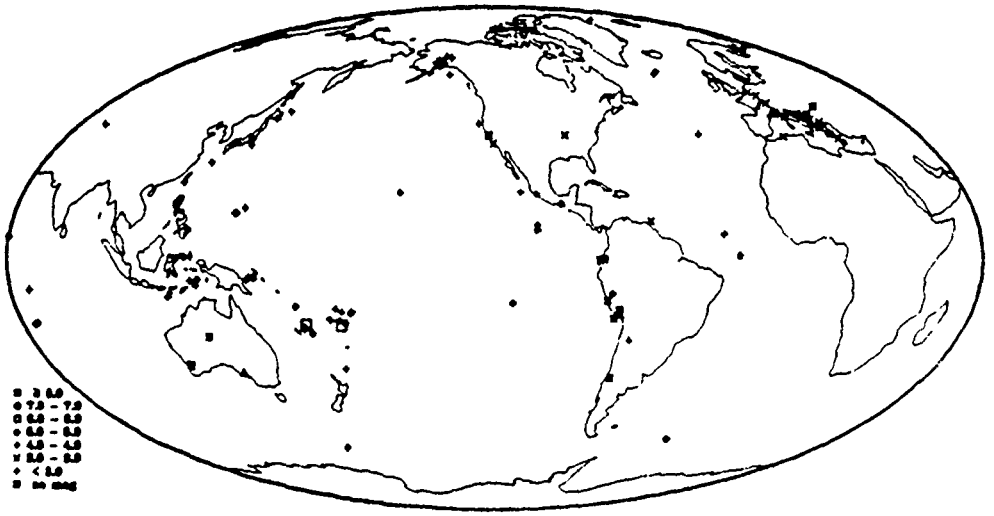

References

[1] G. L. D'Spain, W. S. Hodgkiss, and G. L. Edmonds, "The simultaneous measurement of infrasonic acoustic particle velocity and acoustic pressure in the ocean by freely drifting Swallow floats," accepted for publication in J. Oceanic Engin. (in press).

[2] "Data processing and analysis plan - noise and transmission loss in VLF environments - NATIVE 1" Naval Oceanographic and Atmospheric Research Laboratory, Stennis Space Center, MS (1990).

[3] G. L. D'Spain, R. L. Culver, W. S. Hodgkiss, and G. L. Edmonds, "Freely drifting Swallow float array: August 1988 trip report" MPL Tech. Mem. 407, Marine Physical Laboratory, Scripps Institution of Oceanography, San Diego, CA (1989).

[4] G. C. Chen, G. L. D'Spain, W. S. Hodgkiss, and G. L. Edmonds, "Freely drifting Swallow float array: July 1989 trip report" MPL Tech. Mem. 420, Marine Physical Laboratory, Scripps Institution of Oceanography, San Diego, CA (1990).

[5] W. J. Teague, M. J. Carron, and P. J. Hogan, "A comparison between the generalized digital environmental model and Levitus climatologies" J. Geophys. Res. 95 (C5), pp. 7167-7183 (1990).

[6] K. V. MacKenzie, "Nine-term equation for sound speed in the oceans" J. Acoust. Soc. Am., 70 (3), (1981).

[7] G. L. D'Spain, W. S. Hodgkiss, and G. L. Edmonds, "The energetics of the deep ocean's infrasonic sound field" accepted for publication in the March, 1991 issue of J. Acoust. Soc. Am., (in press).

[8] G. L. D'Spain and W. S. Hodgkiss, "Comparison of Swallow float, ocean bottom seismometer, and sonobuoy data in the VLF band" Marine Physical Laboratory, Scripps Institution of Oceanography, San Diego, CA (1988).

[9] G. L. D'Spain, W. S. Hodgkiss, and G. L. Edmonds, "Freely drifting Swallow float array: September, 1987 trip report" MPL Tech. Mem. 413, Marine Physical Laboratory, Scripps Institution of Oceanography, San Diego, CA (1989).

[10] A. C. Kibblewhite and K. C. Ewans, "Wave-wave interactions, microseisms, and infrasonic ambient noise in the ocean," J. Acoust. Soc. Am. 78 (3), pp. 981-994 (1985).

[11] M. Pieuchot, Seismic Instrumentation, vol. 2, from Handbook of Geophysical Exploration, Section I - Seismic Exploration, ed. K. Helbig and S. Treitel, Geophysical Press (1982).

[12] R. Urick, Principles of Underwater Sound, 3rd ed., McGraw-Hill, (1983).

[13] A. B. Williams, Electronic Filter Design Handbook, McGraw-Hill (1981).

[14] A. Antoniou, Digital Filters: Analysis and Design, McGraw-Hill (1979).

[15] R. H. Johnson, J. Northrop, and R. Eppley, "Sources of Pacific T phases" J. Acoust. Soc. Am., 68 (14), pp. 4251-4260 (1963).

[16] A. Brescia and J. McCandless, "The Extremely Low Frequency (ELF) projector source level reconstruction for the NATIVE 1 sea test, August 1990" NADC Tech. Mem. 5044-101290, Naval Air Development Center, Warminster, PA (1990).

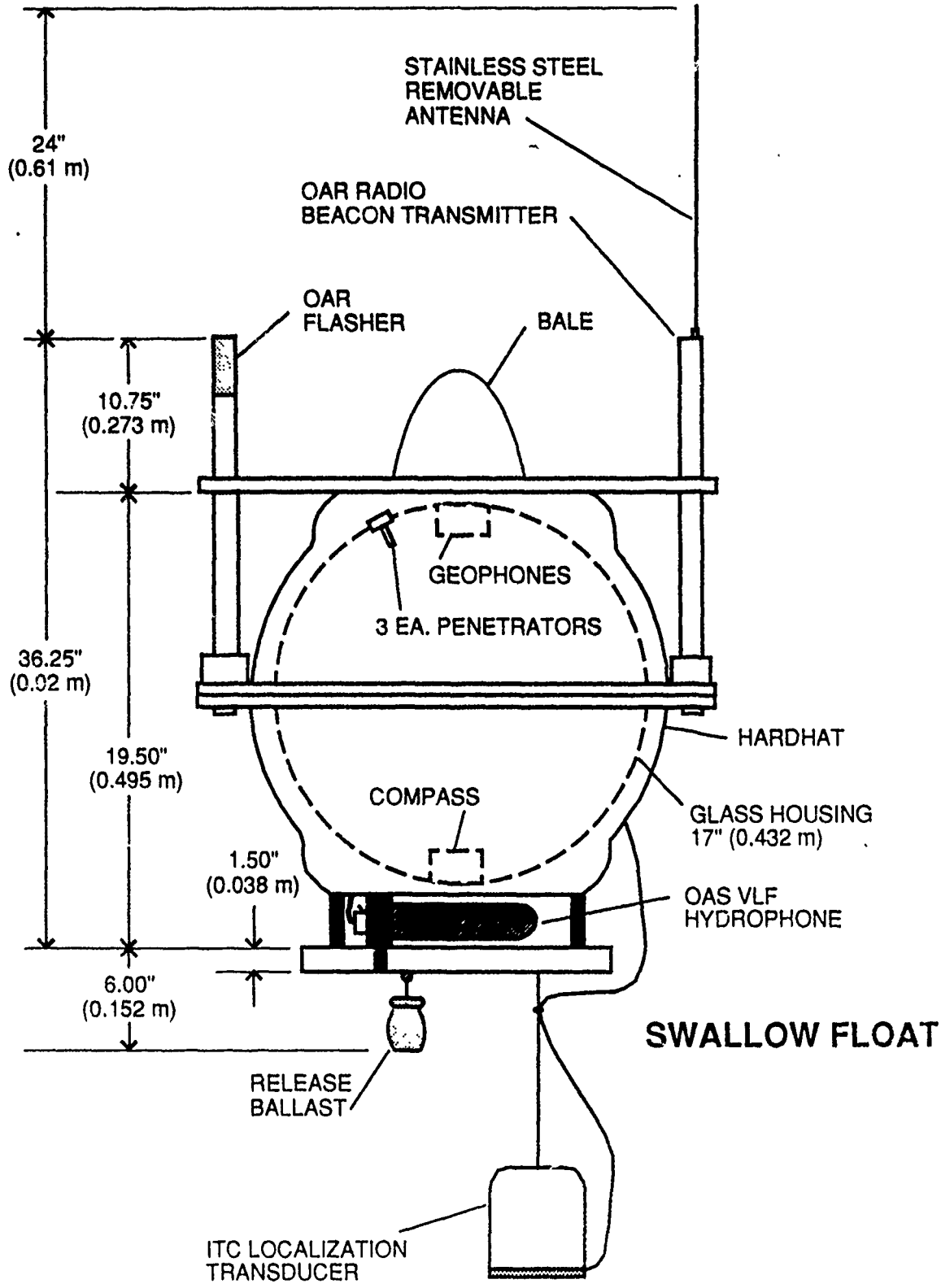
STAINLESS STEEL
REMOVABLE
ANTENNA
24"
(0.61 m)
OAR RADIO
BEACON TRANSMITTER
OAR
FLASHER
BALE
10.75"
(0.273 m)
GEOPHONES
3 EA. PENETRATORS
36.25"
(0.92 m)
HARDHAT
19.50"
(0.495 m)
COMPASS
GLASS HOUSING
17" (0.432 m)
1.50"
(0.038 m)
OAS VLF
HYDROPHONE
6.00"
(0.152 m)
SWALLOW FLOAT
RELEASE
BALLAST
ITC LOCALIZATION
TRANSDUCER

Figure 1

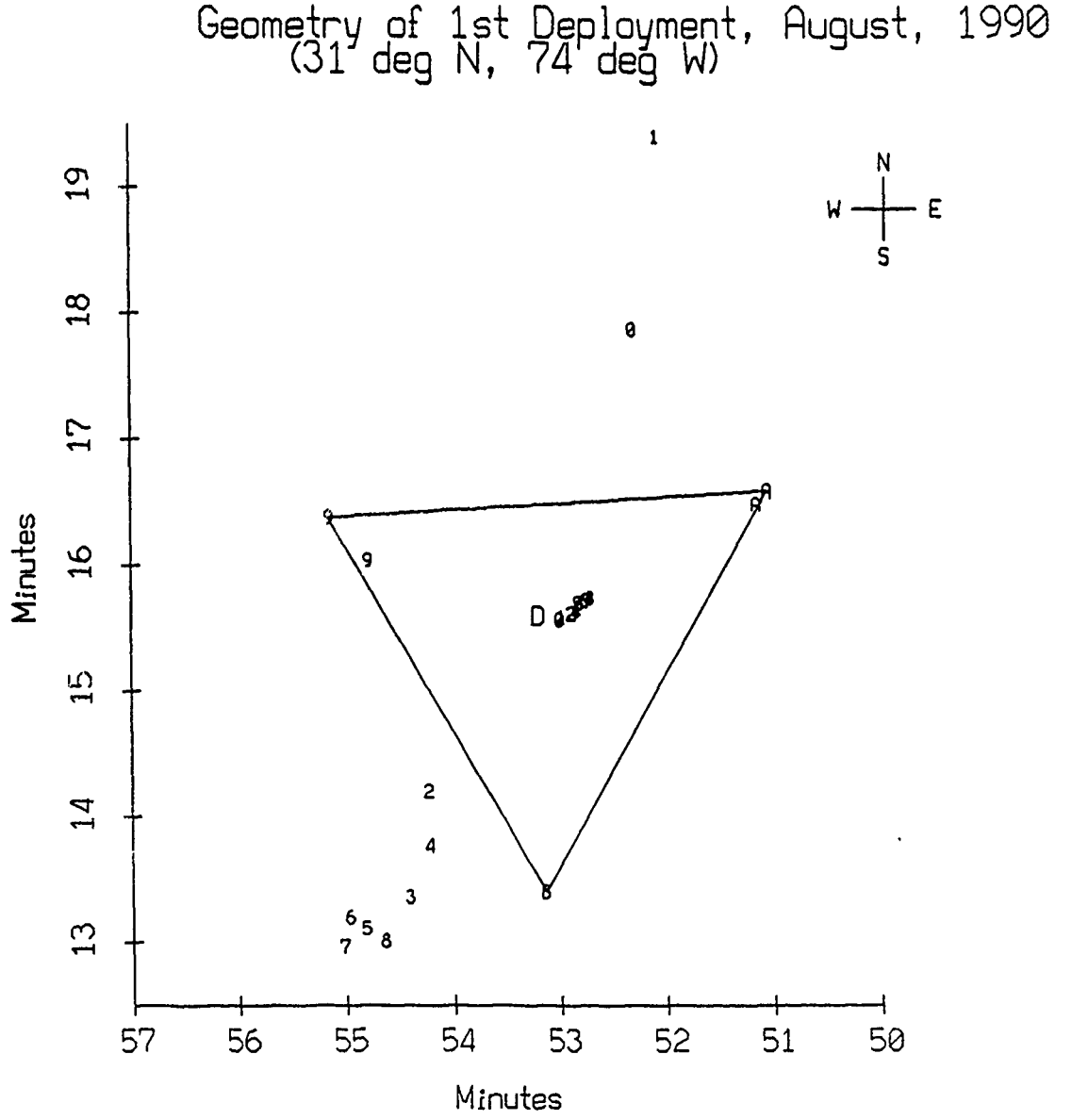
Geometry of 1st Deployment, August, 1990
(31 deg N, 74 deg W)
N
W
E
S
1
0
9
D
2
4
3
6
5
7
8
Minutes
19
18
17
16
15
14
13
57
56
55
54
53
52
51
50
Minutes

Figure I.1

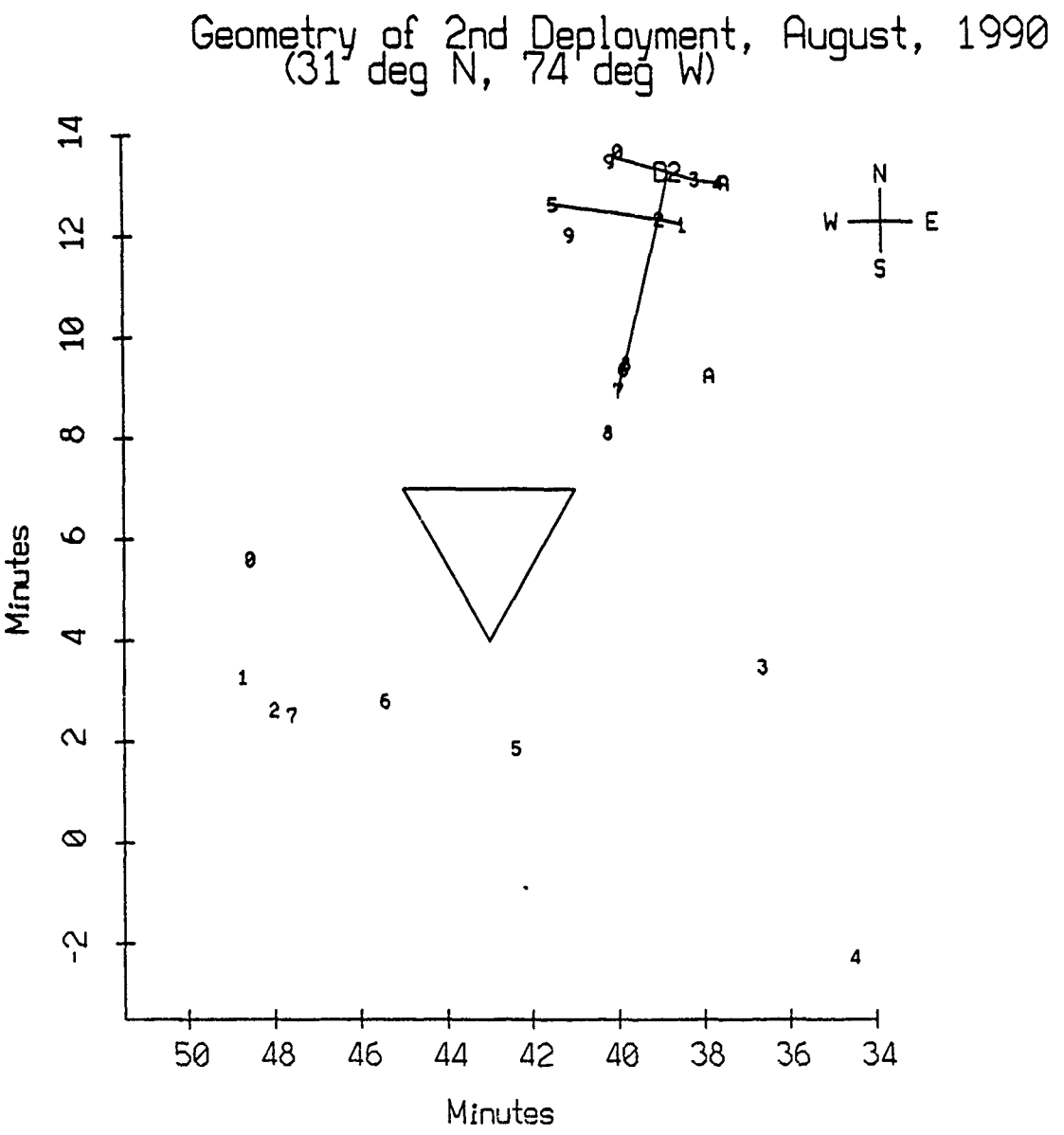
Geometry of 2nd Deployment, August, 1990
(31 deg N, 74 deg W)
N
W
E
S
Minutes
14
12
10
8
6
4
2
0
-2
50
48
46
44
42
40
38
36
34
Minutes

Figure I.2

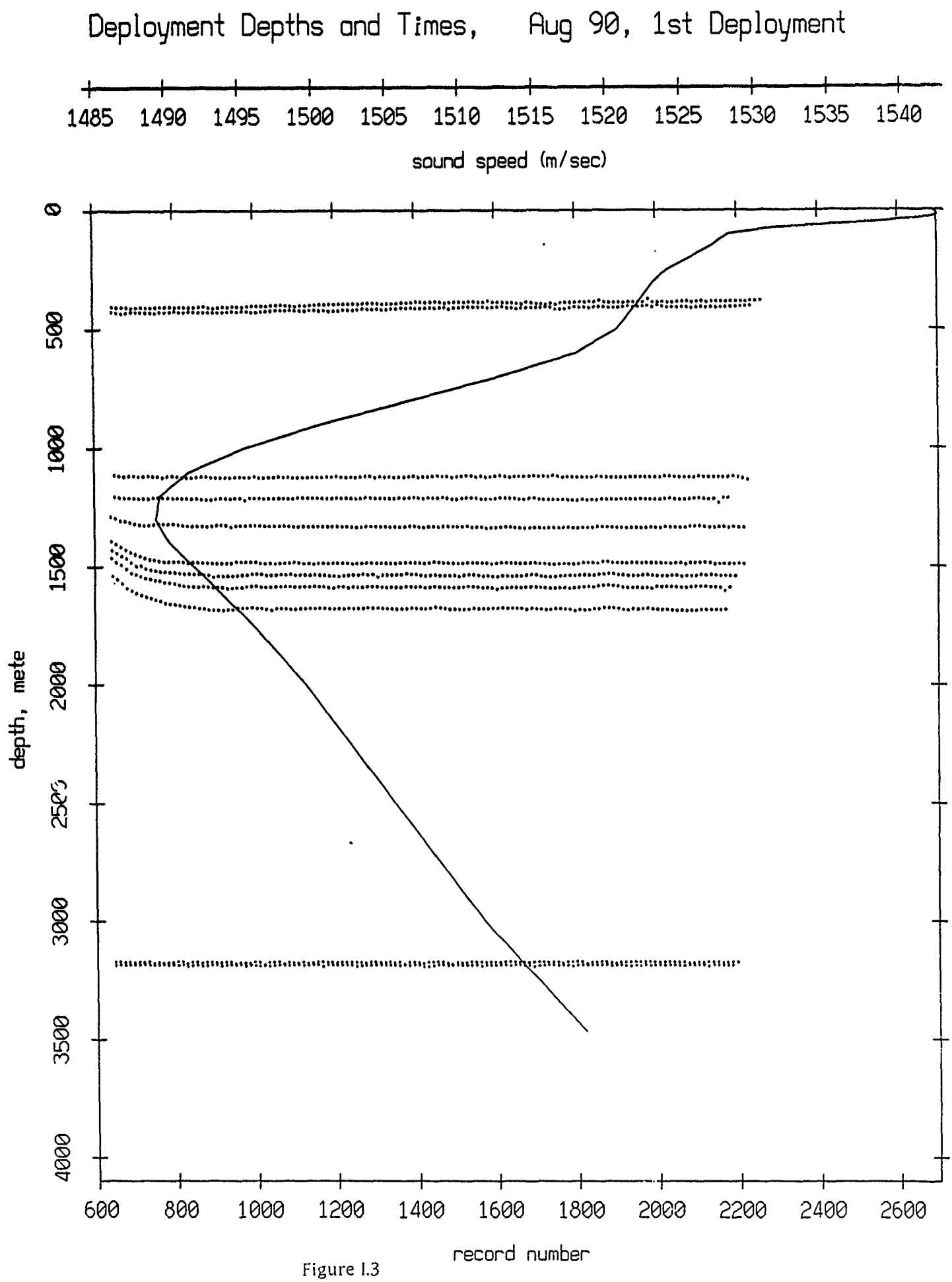
Deployment Depths and Times, Aug 90, 1st Deployment
1485 1490 1495 1500 1505 1510 1515 1520 1525 1530 1535 1540
sound speed (m/sec)
0 500 1000 1500 2000 2500 3000 3500 4000
depth, mete
600 800 1000 1200 1400 1600 1800 2000 2200 2400 2600
record number

Figure I.3

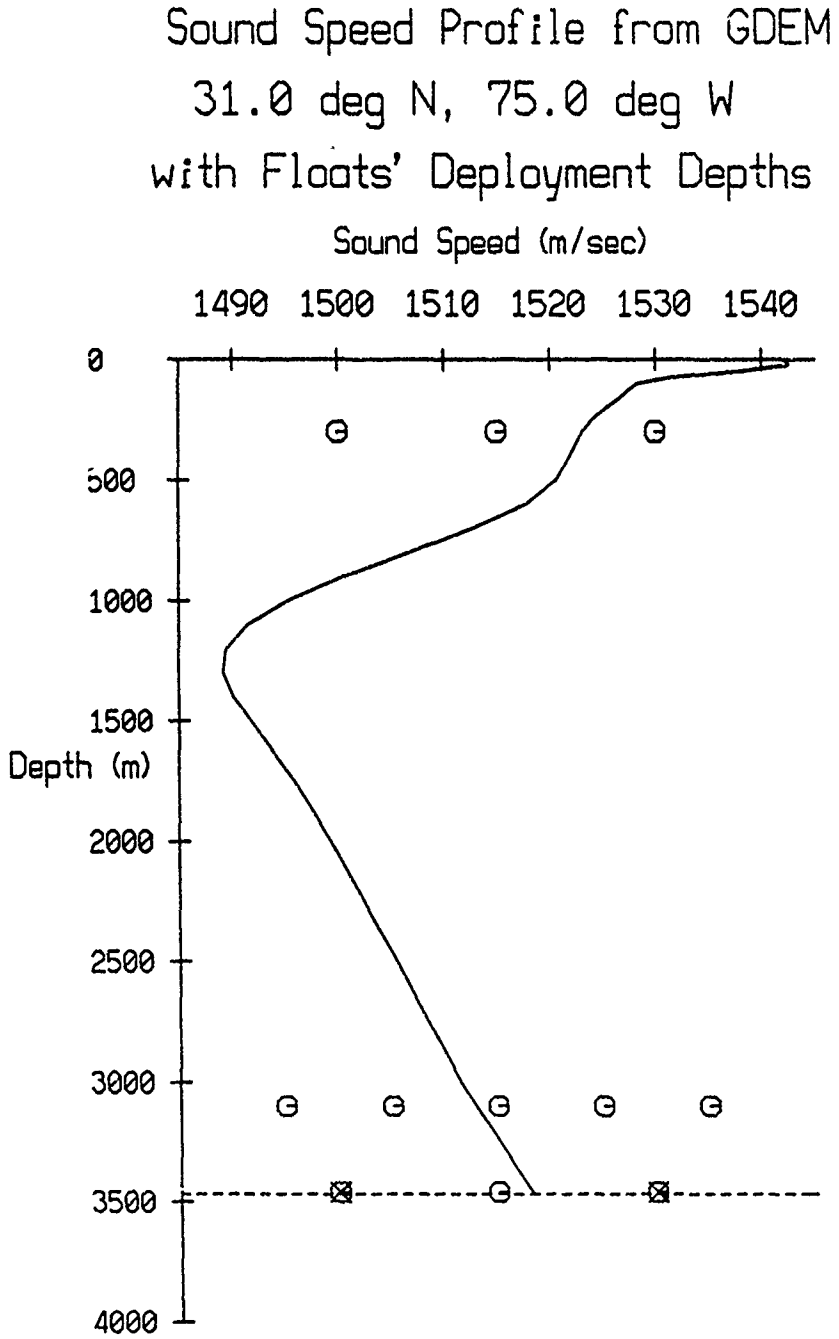
Sound Speed Profile from GDEM
31.0 deg N, 75.0 deg W
with Floats' Deployment Depths
Sound Speed (m/sec)
1490 1500 1510 1520 1530 1540
0
500
1000
1500
Depth (m)
2000
2500
3000
3500
4000

Figure I.4

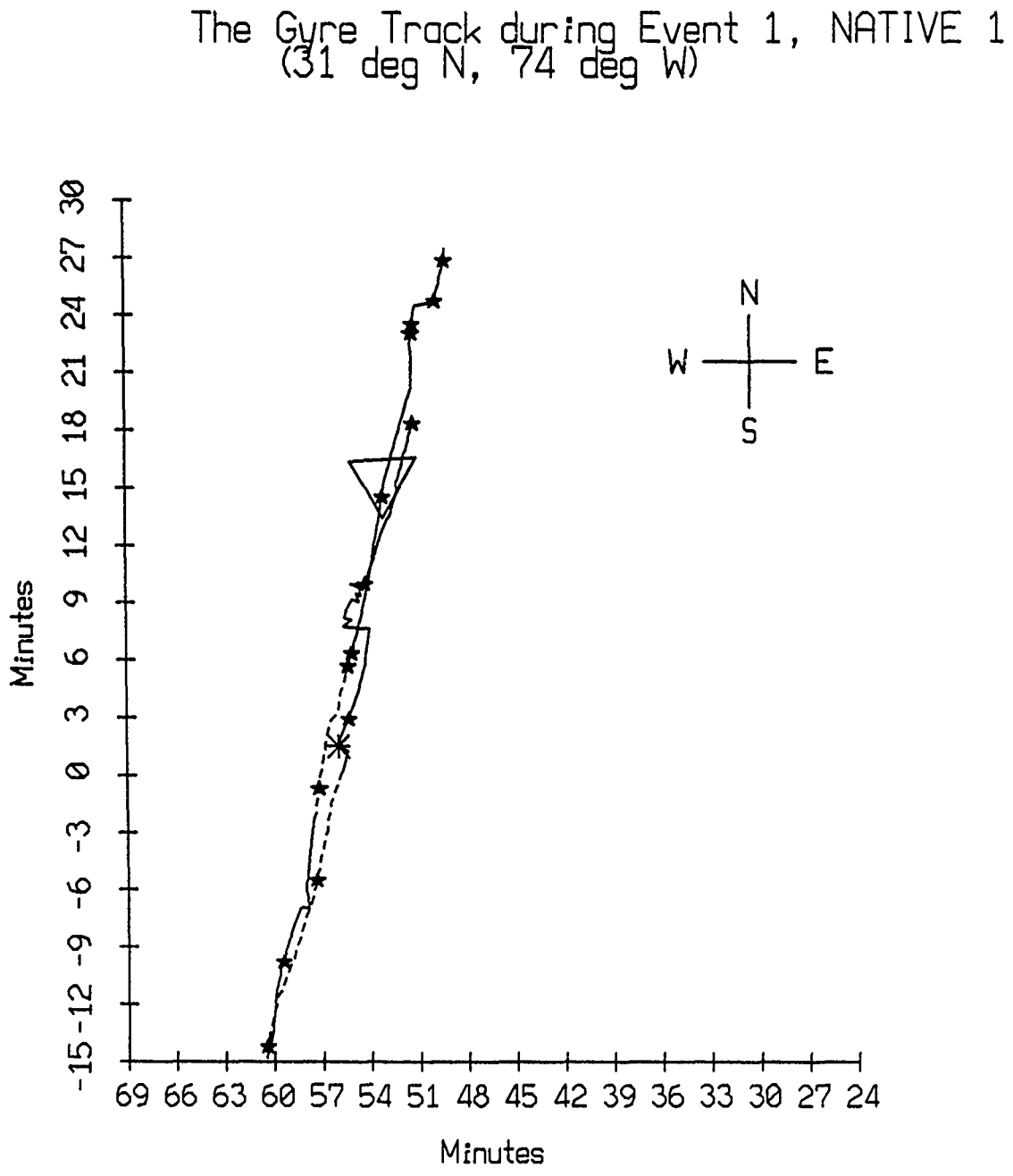
The Gyre Track during Event 1, NATIVE 1
(31 deg N, 74 deg W)
N
W
E
S
Minutes
30 27 24 21 18 15 12 9 6 3 0 -3 -6 -9 -12 -15
69 66 63 60 57 54 51 48 45 42 39 36 33 30 27 24
Minutes

Figure II.1

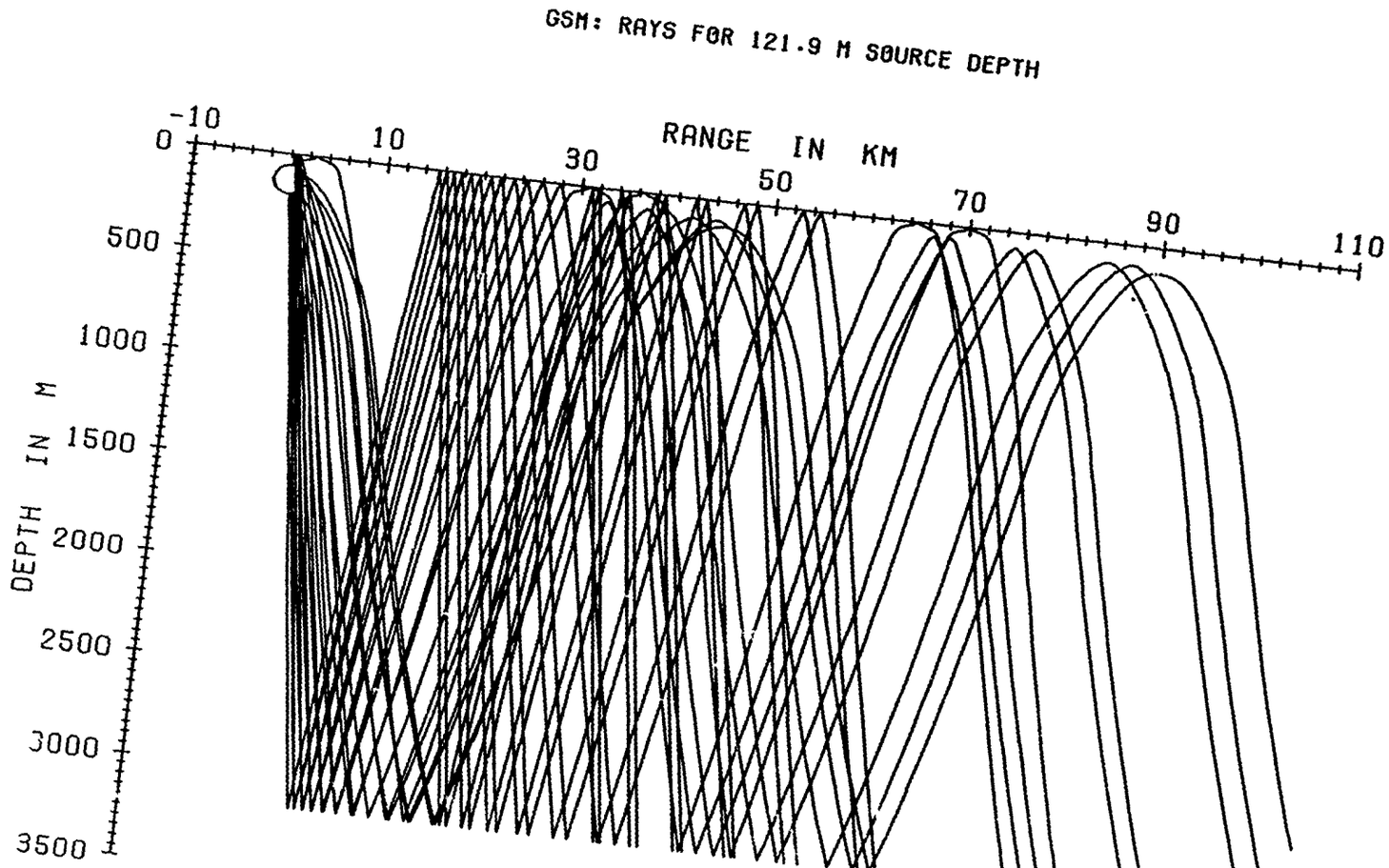
GSM: RAYS FOR 121.9 M SOURCE DEPTH
RANGE IN KM
-10
0
10
30
50
70
90
110
DEPTH IN M
500
1000
1500
2000
2500
3000
3500

Figure II.2

Aug 1990, 1st Deployment Data Screening Results

record number	internal record number	# of bytes written	first missing resync	pass header checksum?	pass range checksum?	# of failed acoustic checksums?
			Float 0			
797	1436	7018	0	yes	yes	1
798	****	2060	1	no	no	16
800	1438	7818	0	yes	yes	1
801	****	1250	1	no	no	8
1602	2238	0	0	yes	yes	0
			Float 1			
408	1047	9766	34	yes	yes	57
810	1449	4072	0	yes	yes	1
811	****	4952	1	no	no	43
1627	2265	8896	0	yes	yes	1
1628	****	198	1	no	no	1
1630	2266	0	0	yes	yes	0
			Float 2			
125	764	9766	59	yes	yes	32
1592	2230	0	0	yes	yes	0
			Float 3			
1157	****	9768	1	no	no	88
1544	2182	0	0	yes	yes	0
			Float 4			
788	1427	3718	0	yes	yes	1
789	3674	5348	1	no	no	46
1586	2223	0	0	yes	yes	0
			Float 5			
84	723	5196	0	yes	yes	1
85	****	5640	1	no	no	49
688	1326	7138	0	yes	yes	1

Figure IV.1a

Aug 1990, 1st Deployment Data Screening Results

record number	internal record number	# of bytes written	first missing resync	pass header checksum?	pass range checksum?	# of failed acoustic checksums?
689	****	1938	1	no	no	15
1580	2216	0	0	yes	yes	0
			Float 6			
523	1162	9764	76	yes	yes	15
1548	2186	0	0	yes	yes	0
			Float 7			
1056	1695	6716	0	yes	yes	1
1057	****	3426	1	no	no	29
1555	2192	0	0	yes	yes	0
			Float 8			
234	873	9766	0	yes	no	0
315	0	2	0	no	yes	0
316	-577	288	1	no	no	0
317	****	468	1	no	no	0
318	****	6442	1	no	no	57
1535	2170	0	0	yes	yes	0
			Float 9			
362	1001	9766	5	yes	yes	86
365	1004	9768	0	yes	yes	1
366	1005	9766	13	yes	yes	55
374	1013	9796	2	yes	no	88
1167	1806	9766	25	yes	yes	66
1557	2195	0	0	yes	yes	0
			Float 10			
379	1018	9766	4	yes	yes	87
1161	1	9768	1	no	no	88
1550	2188	0	0	yes	yes	0

Figure IV.1b

Aug 1990, 1st Deployment Data Screening Results						
record number	internal record number	# of bytes written	first missing resync	pass header checksum?	pass range checksum?	# of failed acoustic checksums?
1559	2198	0	0	yes	yes	0

Figure IV.1c

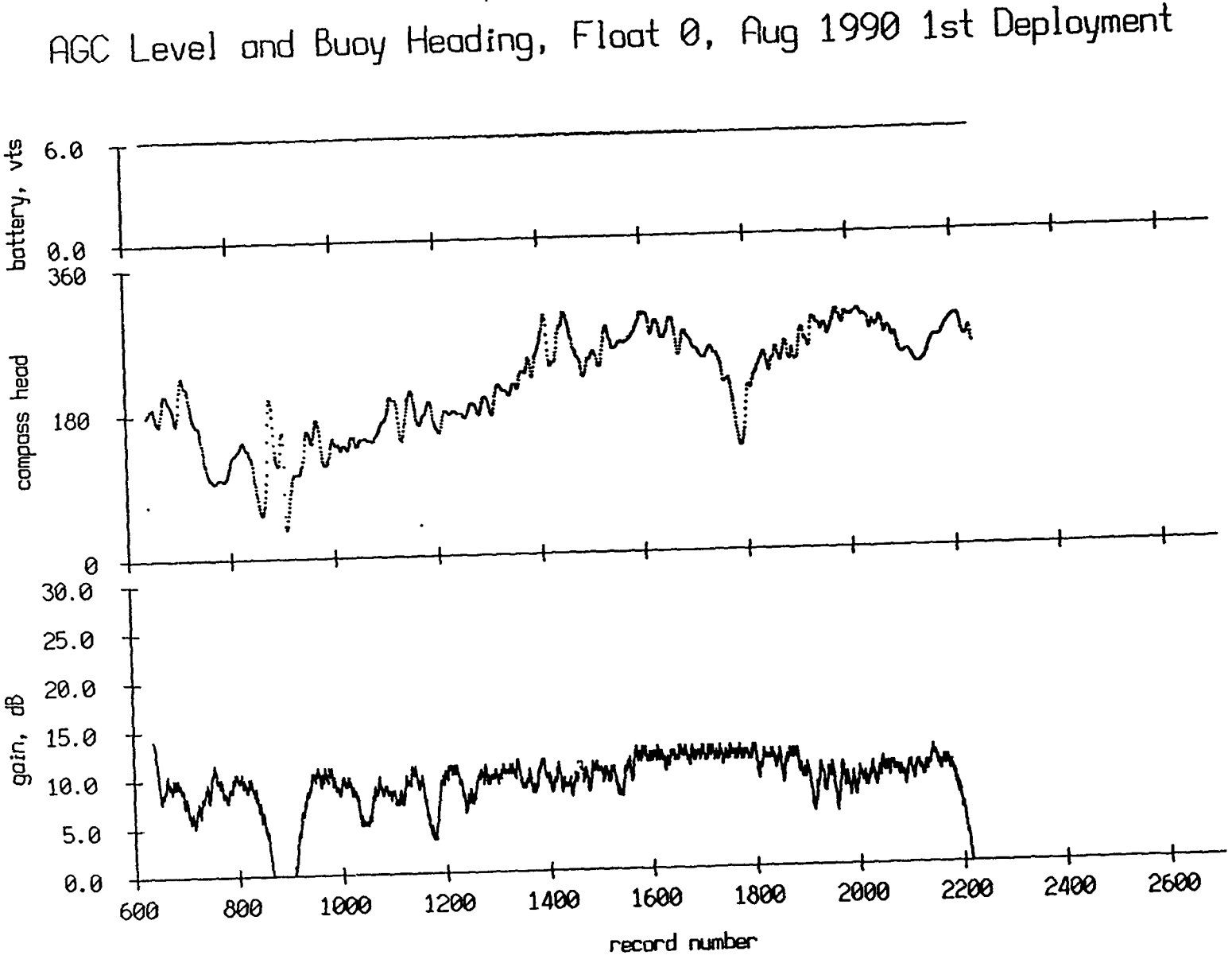
AGC Level and Buoy Heading, Float 0, Aug 1990 1st Deployment
battery, vts
6.0
0.0
compass head
360
180
0
gain, dB
30.0
25.0
20.0
15.0
10.0
5.0
0.0
600
800
1000
1200
1400
1600
1800
2000
2200
2400
2600
record number

Figure V.1

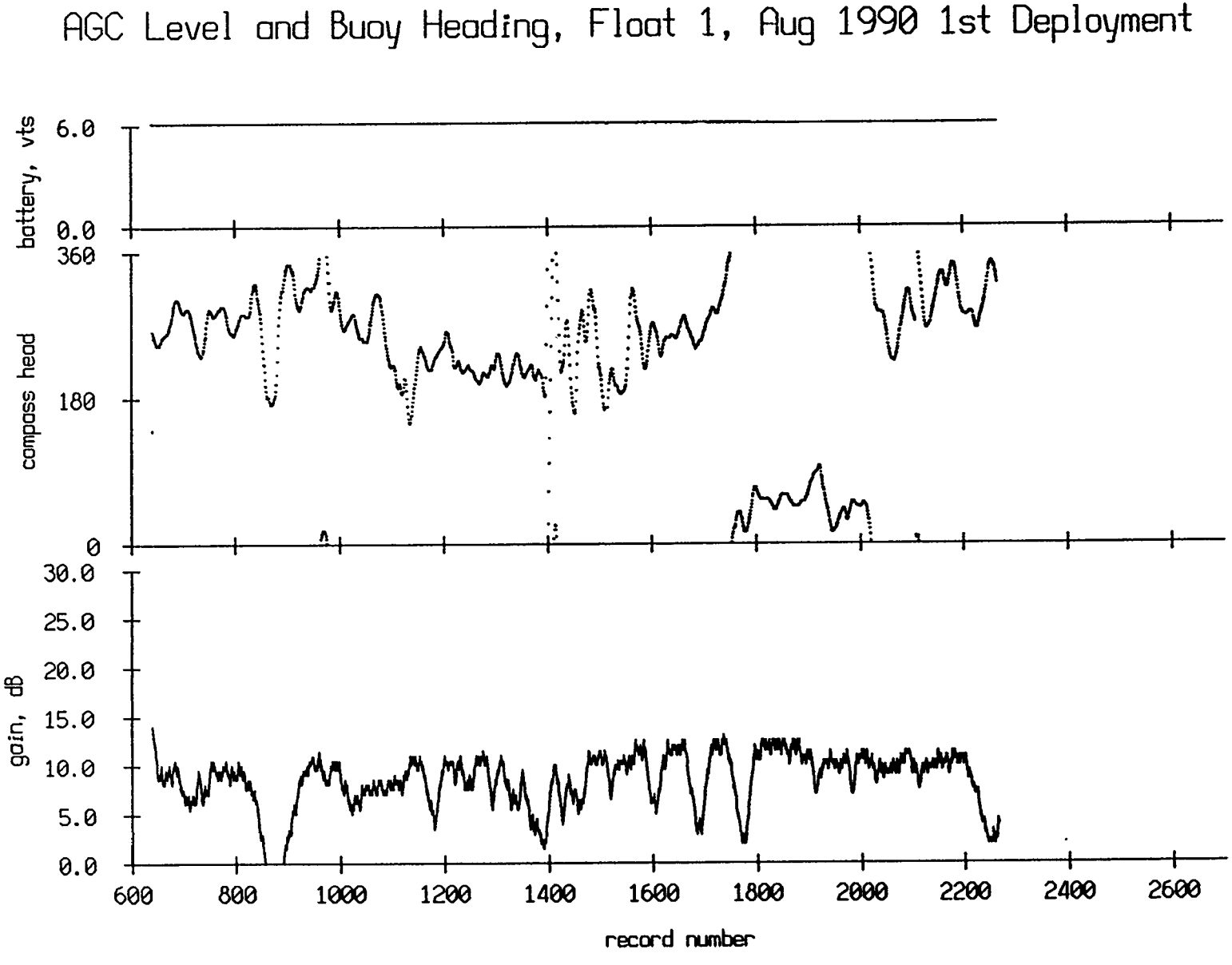
AGC Level and Buoy Heading, Float 1, Aug 1990 1st Deployment
battery, vts
6.0
0.0
compass head
360
180
0
gain, dB
30.0
25.0
20.0
15.0
10.0
5.0
0.0
600
800
1000
1200
1400
1600
1800
2000
2200
2400
2600
record number

Figure V.2

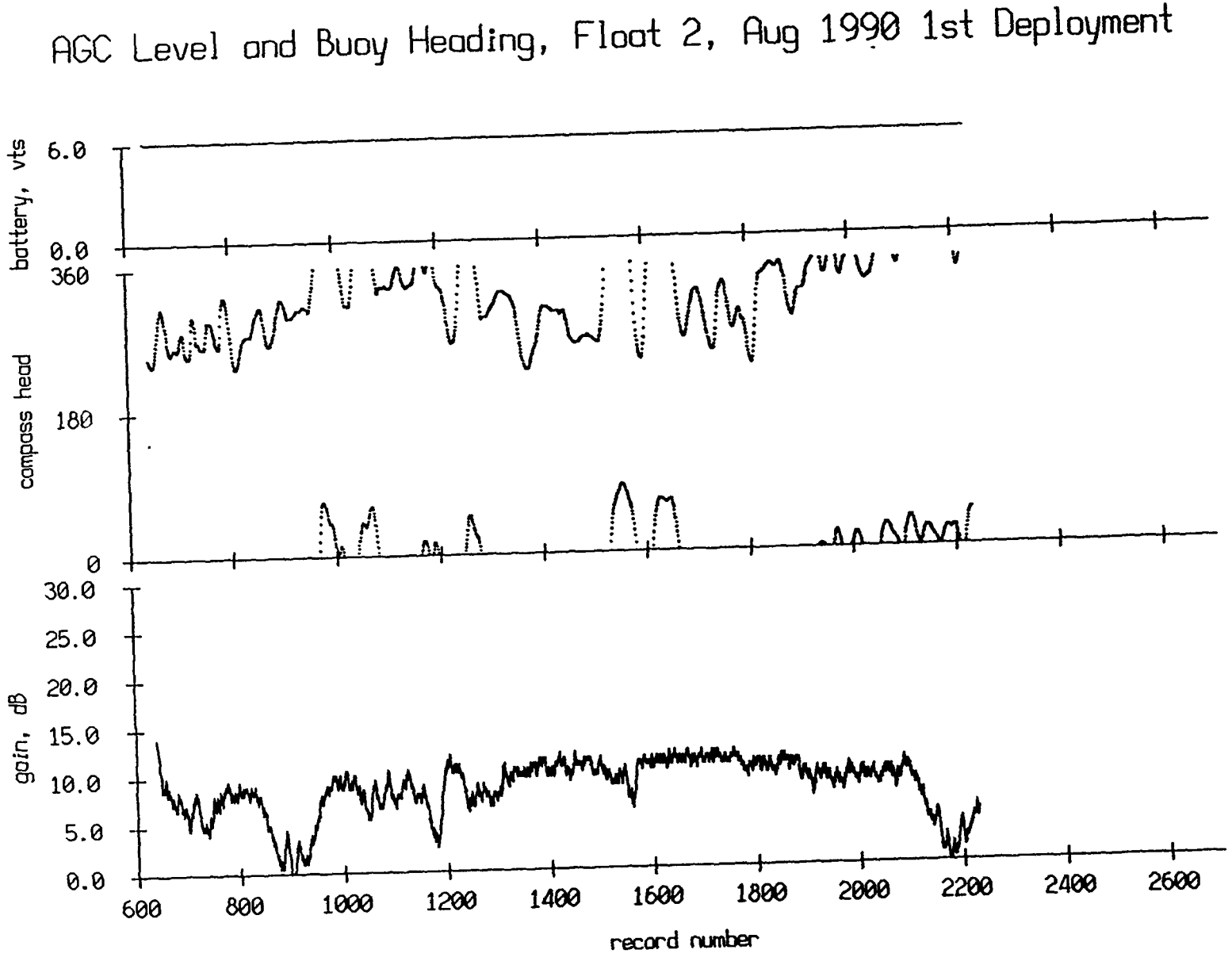
AGC Level and Buoy Heading, Float 2, Aug 1990 1st Deployment
battery, vts
6.0
0.0
compass head
360
180
0
gain, dB
30.0
25.0
20.0
15.0
10.0
5.0
0.0
600
800
1000
1200
1400
1600
1800
2000
2200
2400
2600
record number

Figure V.3

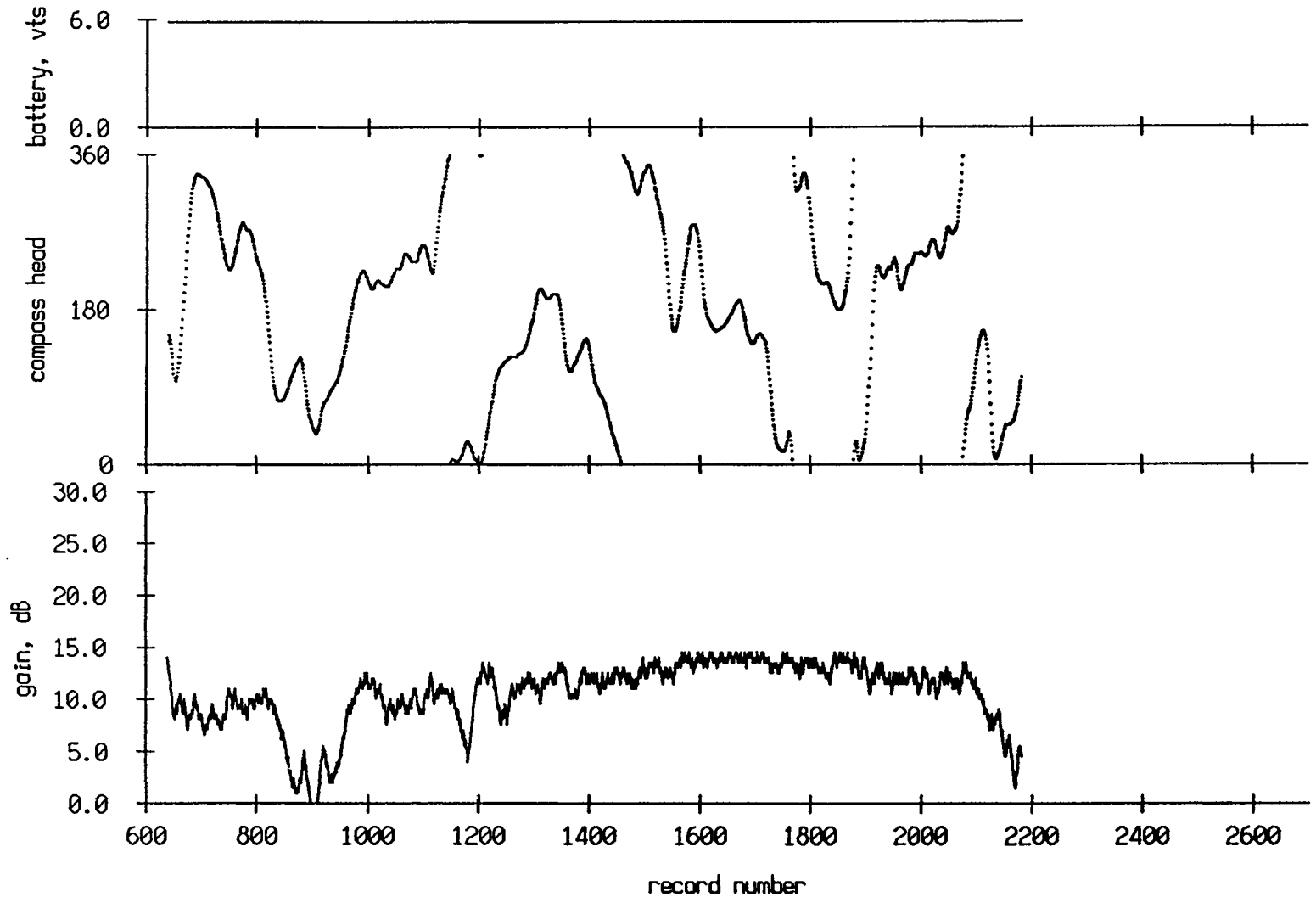
AGC Level and Buoy Heading, Float 3, Aug 1990 1st Deployment
battery, vts
6.0
0.0
compass head
360
180
0
gain, dB
30.0
25.0
20.0
15.0
10.0
5.0
0.0
600
800
1000
1200
1400
1600
1800
2000
2200
2400
2600
record number

Figure V.4

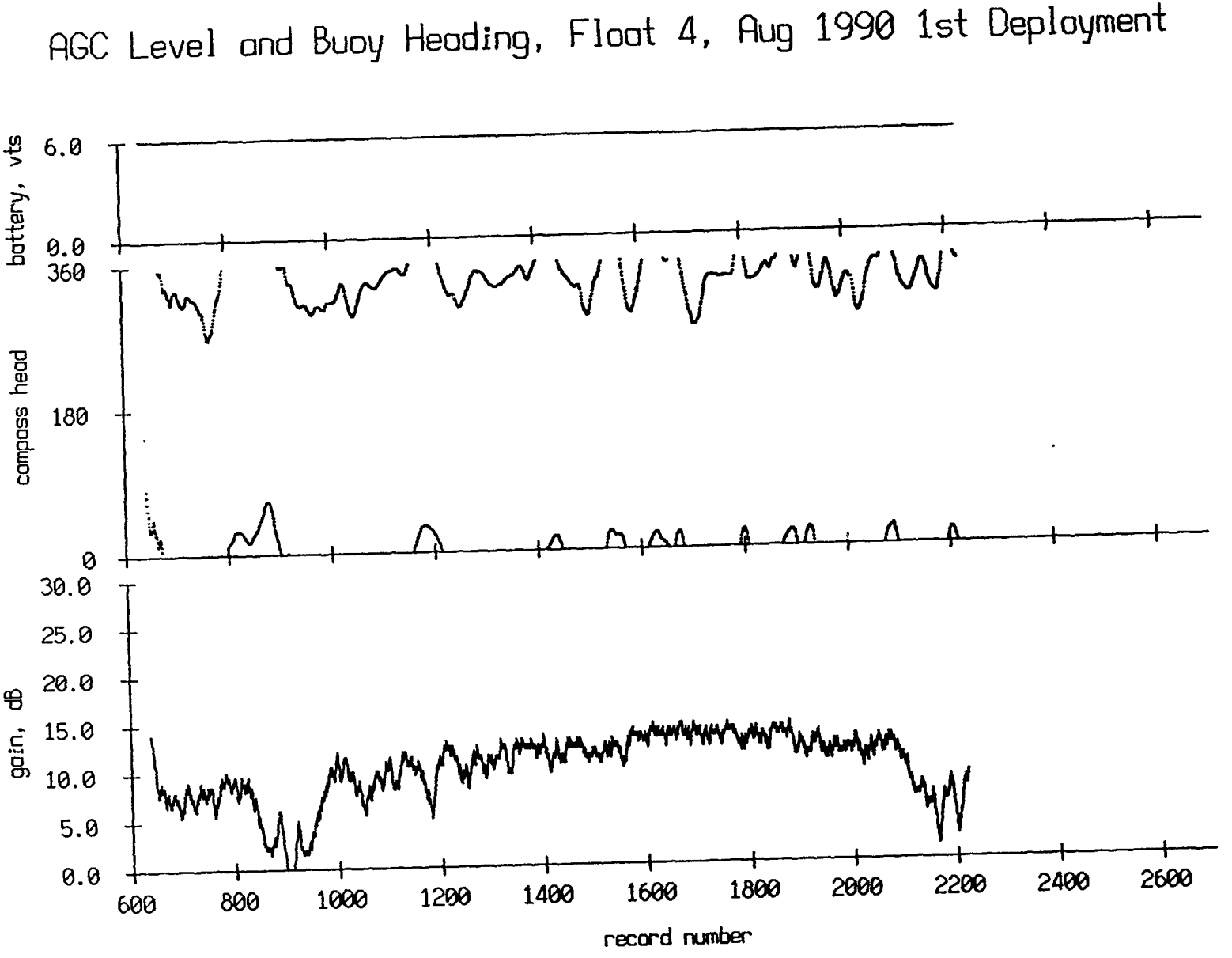
AGC Level and Buoy Heading, Float 4, Aug 1990 1st Deployment
battery, vts
6.0
0.0
compass head
360
180
0
gain, dB
30.0
25.0
20.0
15.0
10.0
5.0
0.0
600
800
1000
1200
1400
1600
1800
2000
2200
2400
2600
record number

Figure V.5

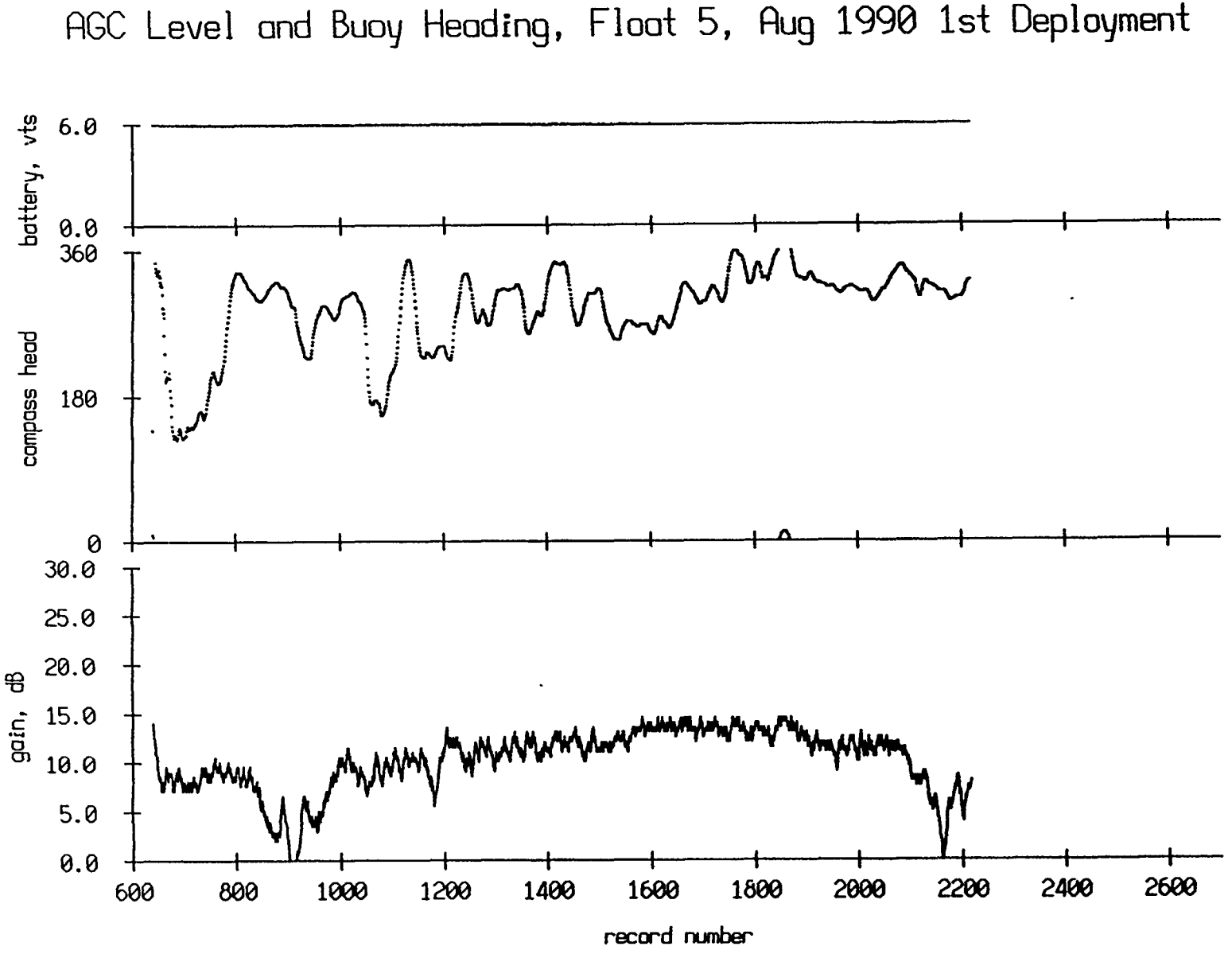
AGC Level and Buoy Heading, Float 5, Aug 1990 1st Deployment
battery, vts
6.0
0.0
compass head
360
180
0
gain, dB
30.0
25.0
20.0
15.0
10.0
5.0
0.0
600
800
1000
1200
1400
1600
1800
2000
2200
2400
2600
record number

Figure V.6

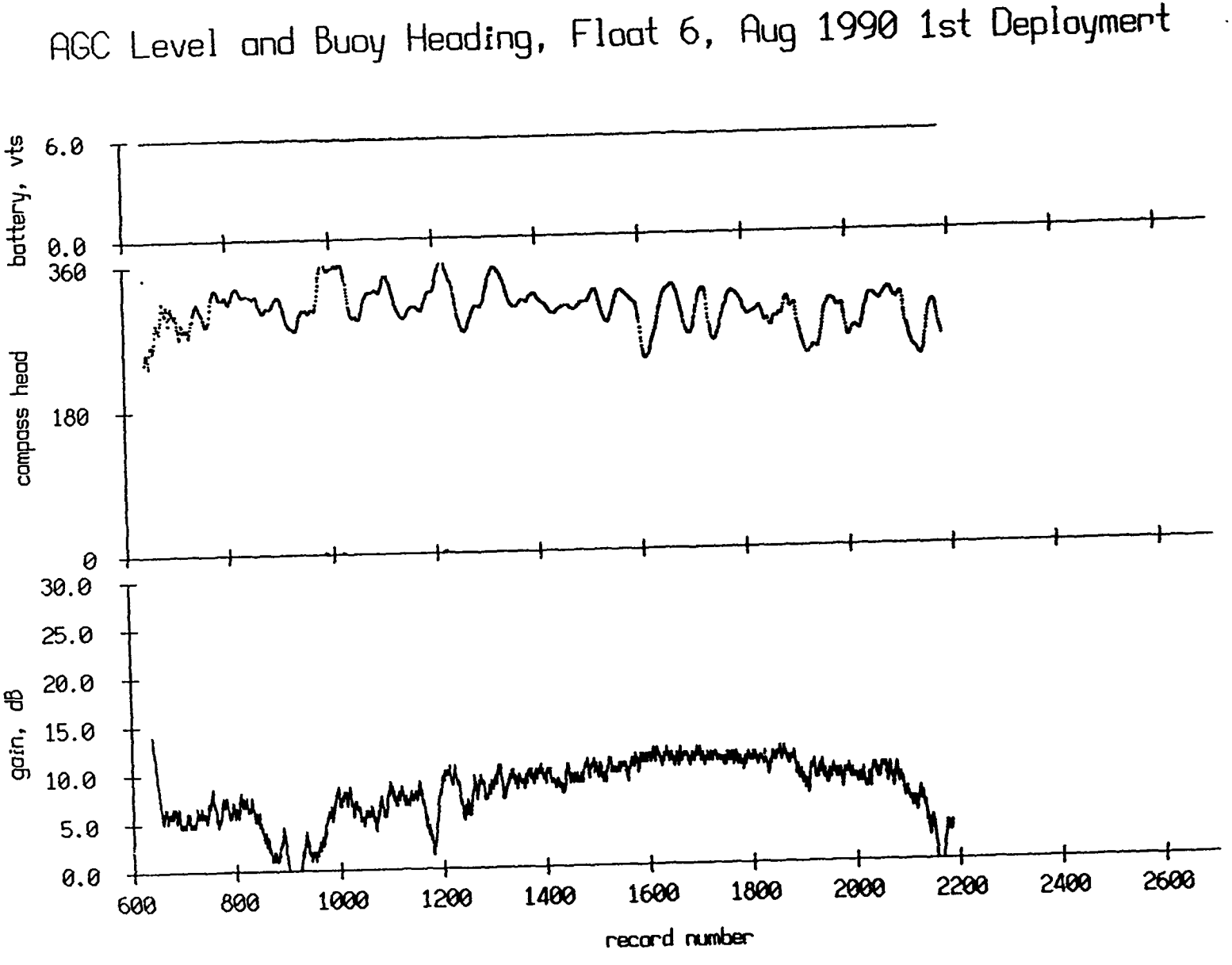
AGC Level and Buoy Heading, Float 6, Aug 1990 1st Deployment
battery, vts
6.0
0.0
compass head
360
180
0
gain, dB
30.0
25.0
20.0
15.0
10.0
5.0
0.0
600
800
1000
1200
1400
1600
1800
2000
2200
2400
2600
record number

Figure V.7

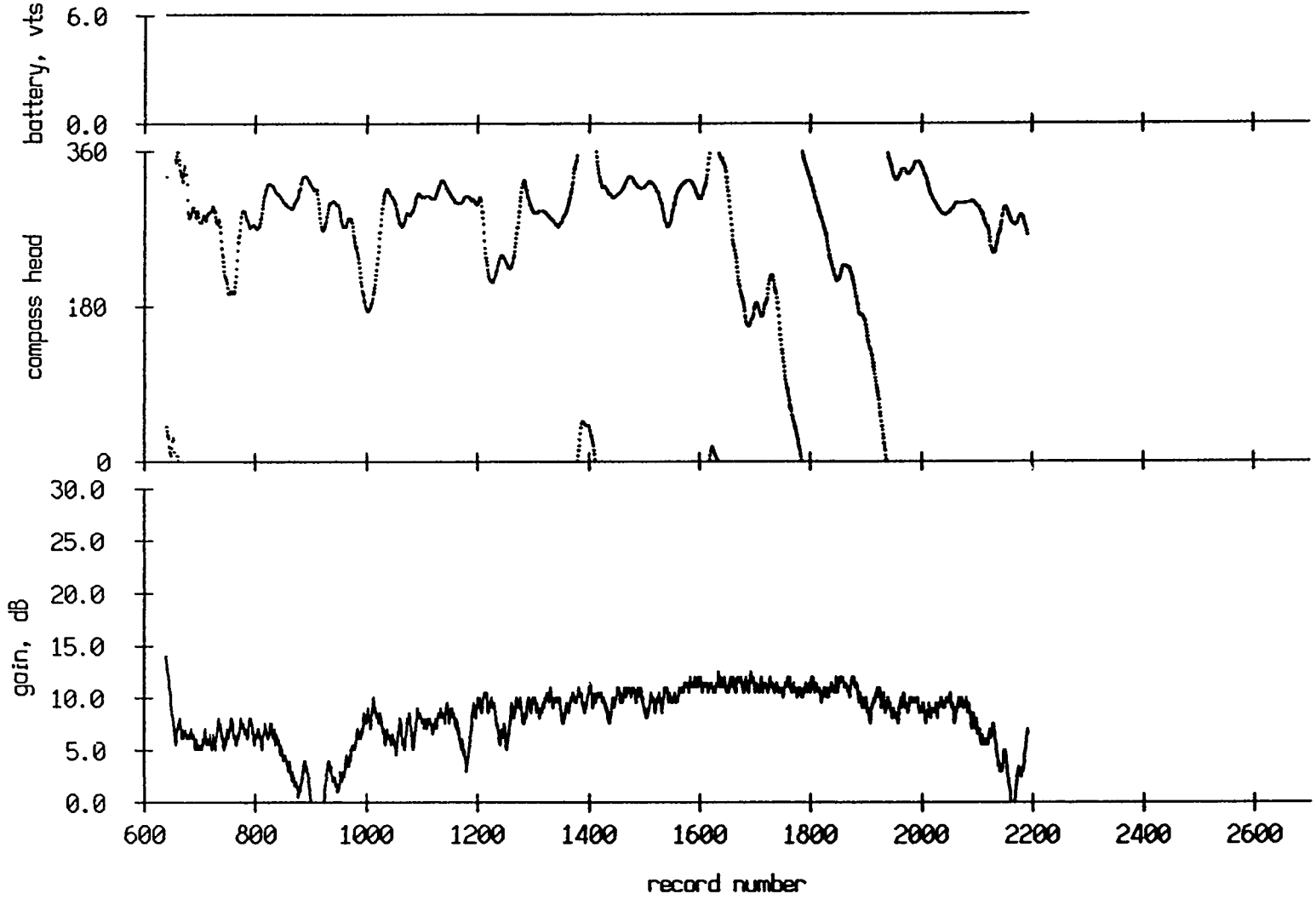
AGC Level and Buoy Heading, Float 7, Aug 1990 1st Deployment
battery, vts
6.0
0.0
compass head
360
180
0
gain, dB
30.0
25.0
20.0
15.0
10.0
5.0
0.0
600
800
1000
1200
1400
1600
1800
2000
2200
2400
2600
record number

Figure V.8

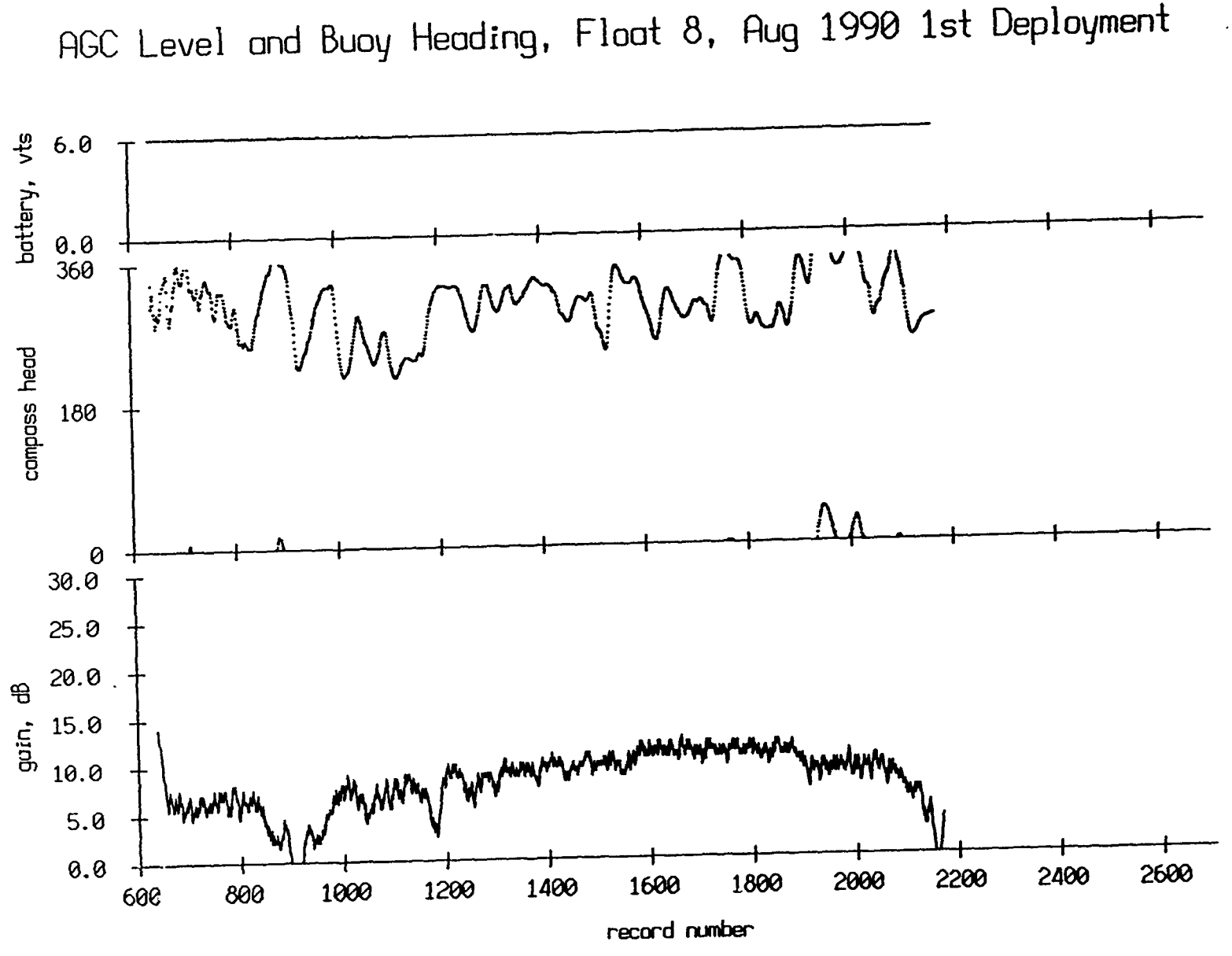
AGC Level and Buoy Heading, Float 8, Aug 1990 1st Deployment
battery, vts
6.0
0.0
compass head
360
180
0
gain, dB
30.0
25.0
20.0
15.0
10.0
5.0
0.0
600
800
1000
1200
1400
1600
1800
2000
2200
2400
2600
record number

Figure V.9

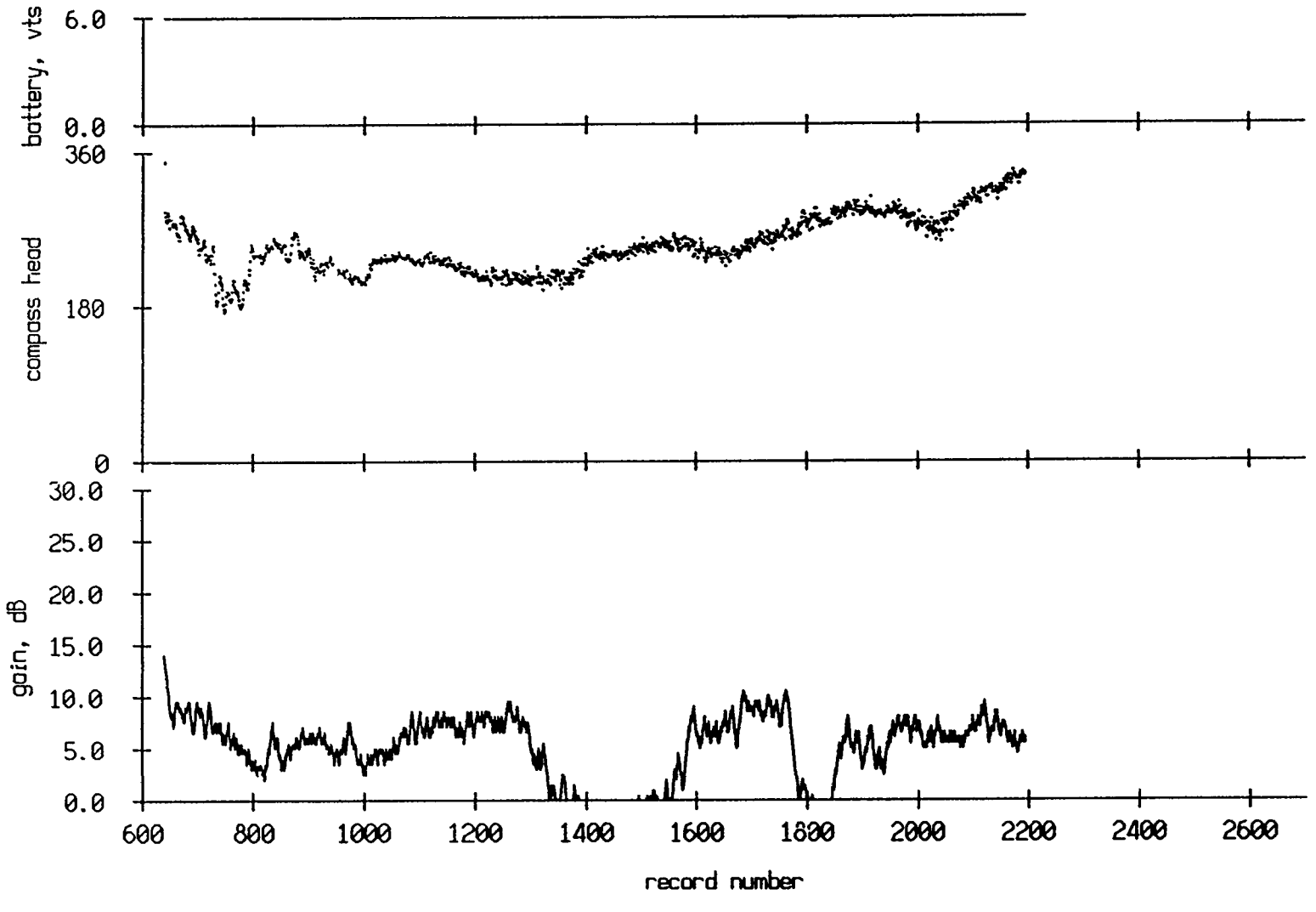
AGC Level and Buoy Heading, Float 9, Aug 1990 1st Deployment
battery, vts
6.0
0.0
compass head
360
180
0
gain, dB
30.0
25.0
20.0
15.0
10.0
5.0
0.0
600
800
1000
1200
1400
1600
1800
2000
2200
2400
2600
record number

Figure V.10

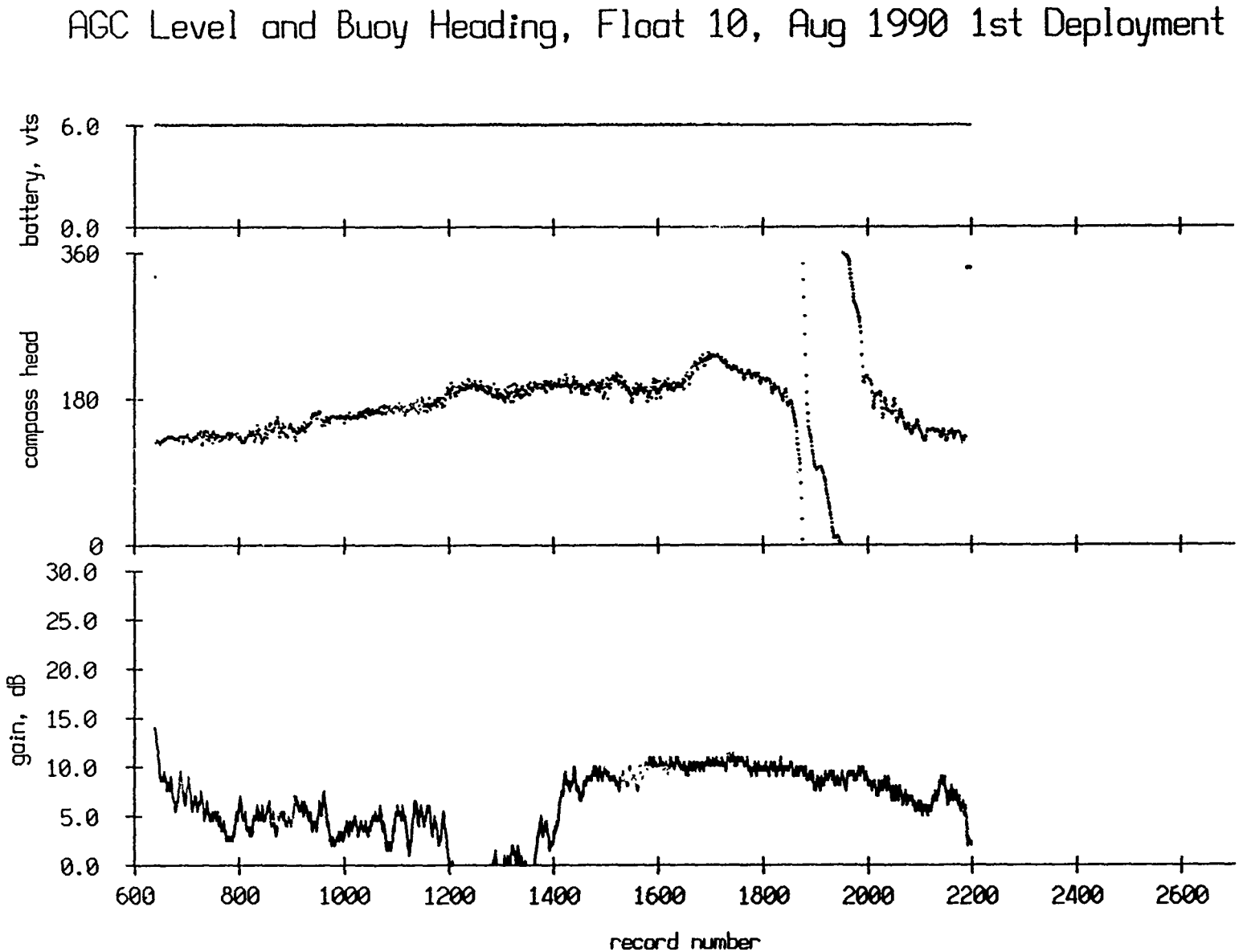
AGC Level and Buoy Heading, Float 10, Aug 1990 1st Deployment
battery, vts
6.0
0.0
compass head
360
180
0
gain, dB
30.0
25.0
20.0
15.0
10.0
5.0
0.0
600
800
1000
1200
1400
1600
1800
2000
2200
2400
2600
record number

Figure V.11

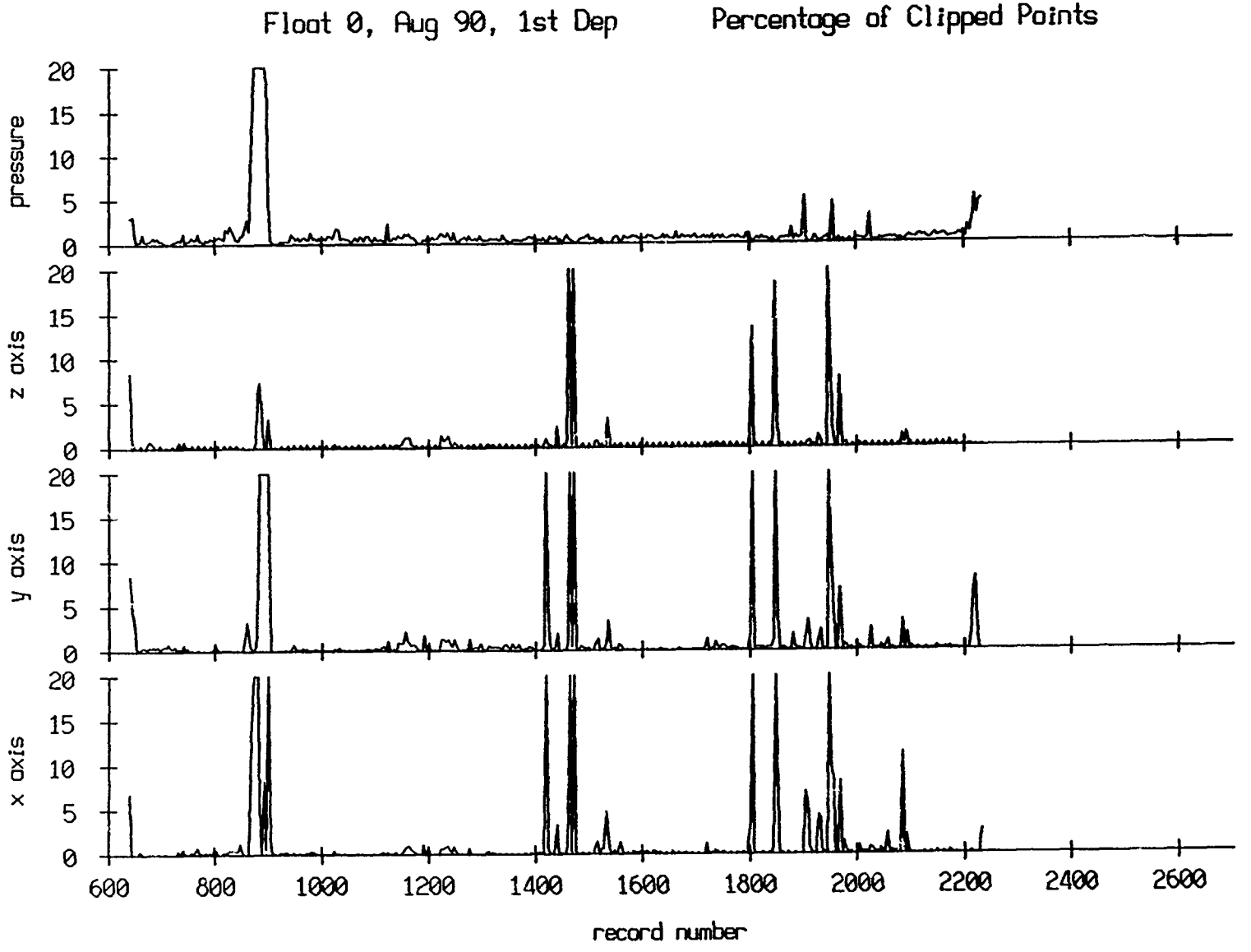
Float 0, Aug 90, 1st Dep
Percentage of Clipped Points
pressure
z axis
y axis
x axis
0
5
10
15
20
600
800
1000
1200
1400
1600
1800
2000
2200
2400
2600
record number

Figure V.12

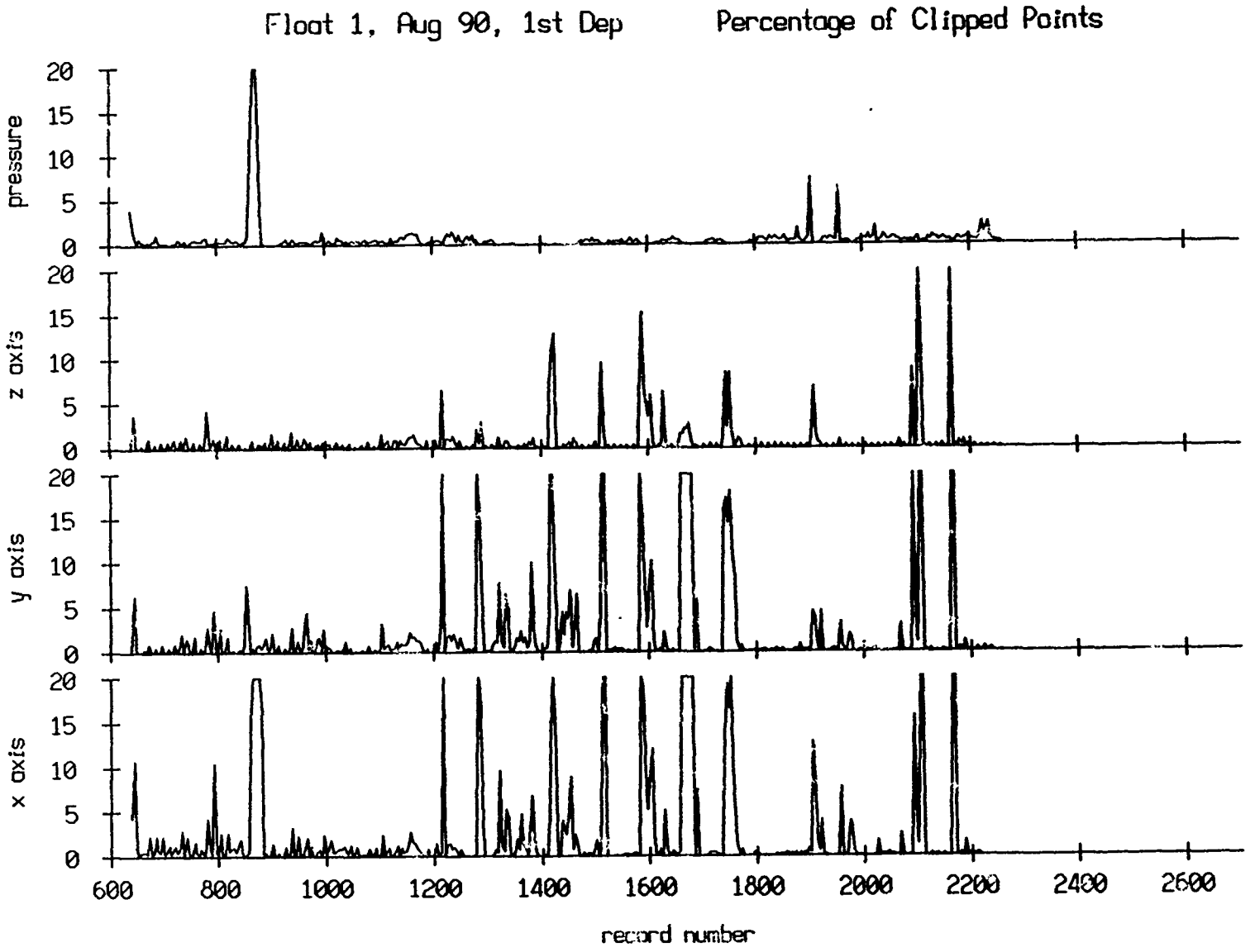
Float 1, Aug 90, 1st Dep
Percentage of Clipped Points
pressure
z axis
y axis
x axis
0
5
10
15
20
600
800
1000
1200
1400
1600
1800
2000
2200
2400
2600
record number

Figure V.13

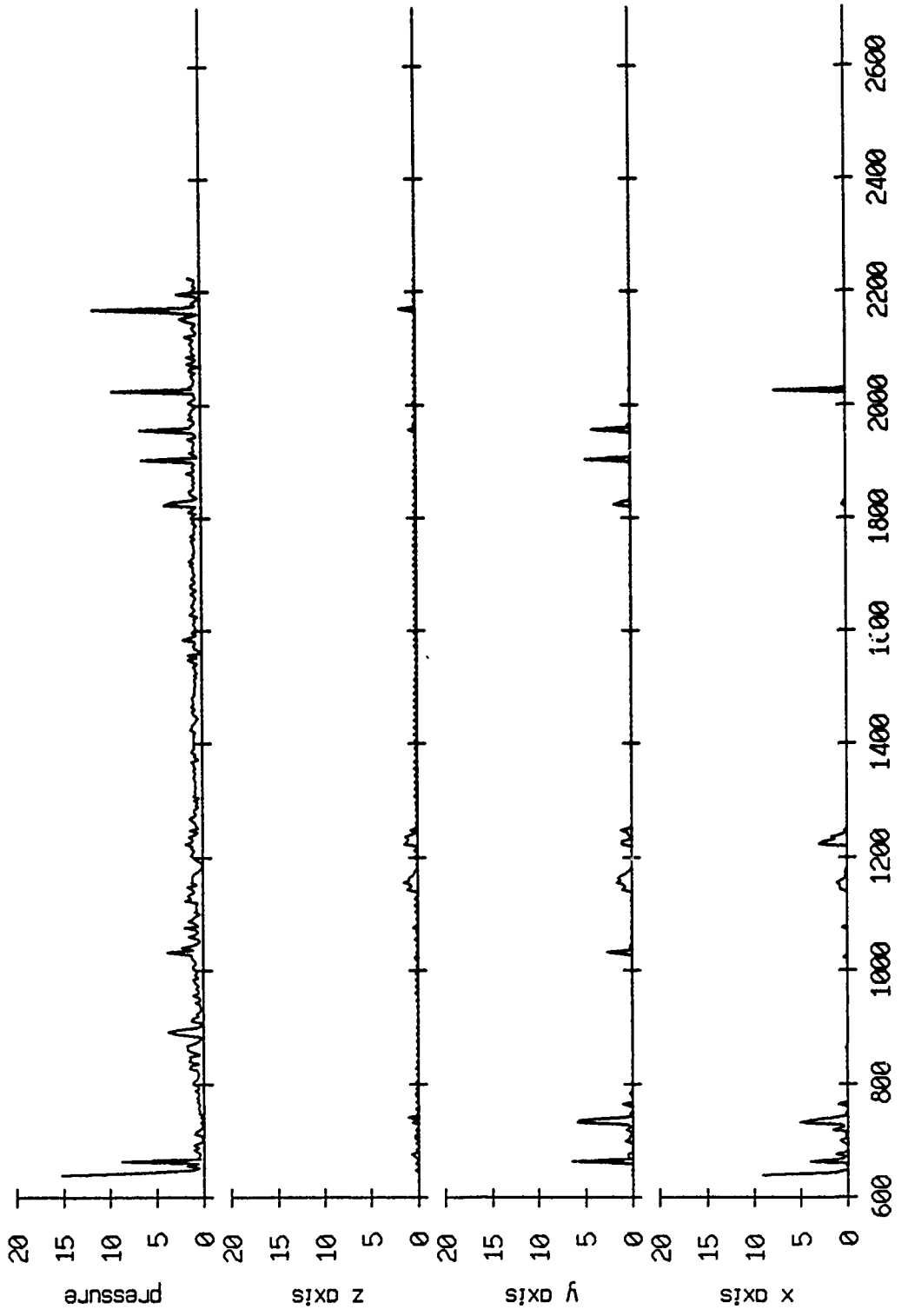
Float 2, Aug 90, 1st Dep
Percentage of Clipped Points
pressure
z axis
y axis
x axis
0
5
10
15
20
600
800
1000
1200
1400
1600
1800
2000
2200
2400
2600
record number

Figure V.14

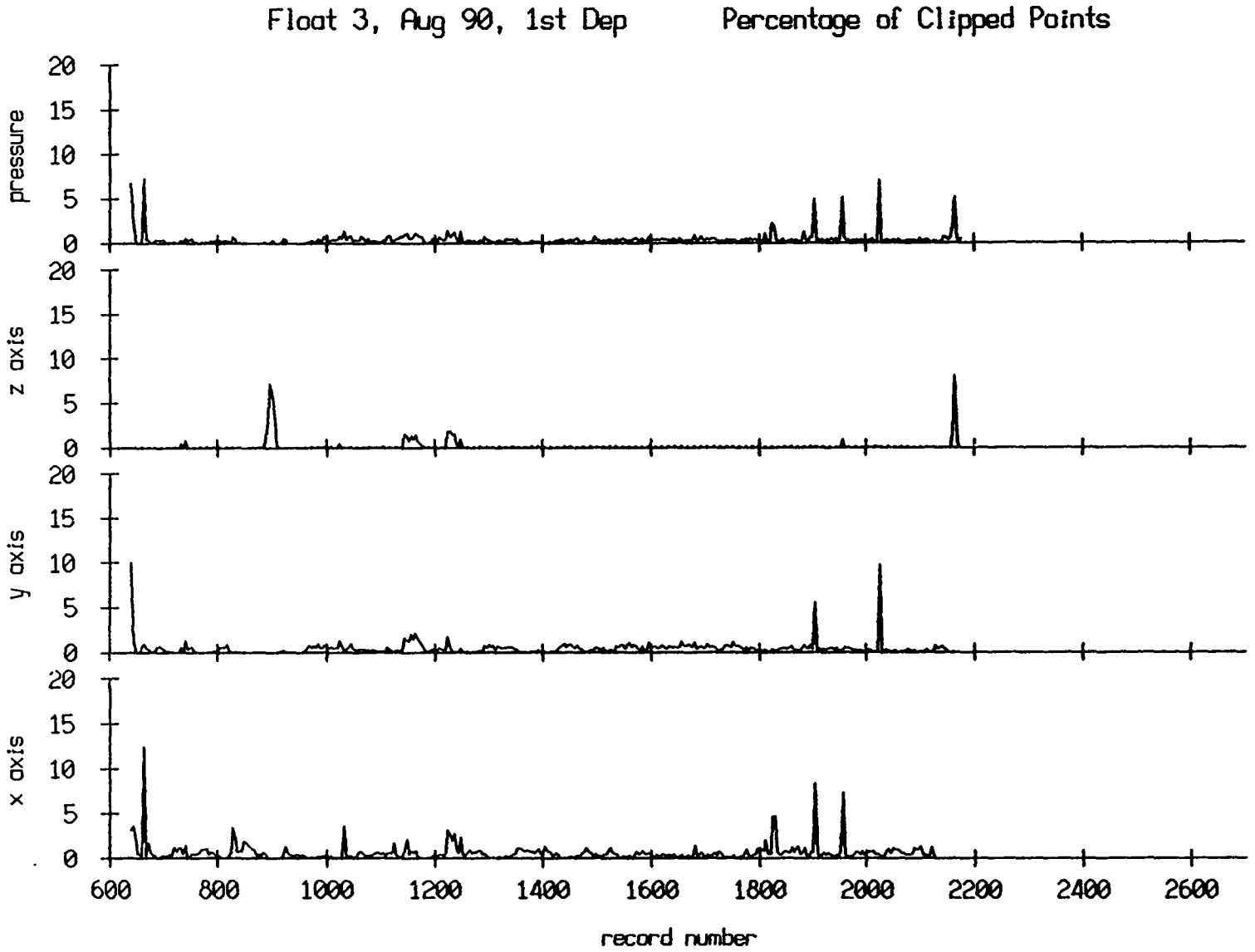
Float 3, Aug 90, 1st Dep
Percentage of Clipped Points
pressure
z axis
y axis
x axis
20
15
10
5
0
600
800
1000
1200
1400
1600
1800
2000
2200
2400
2600
record number

Figure V.15

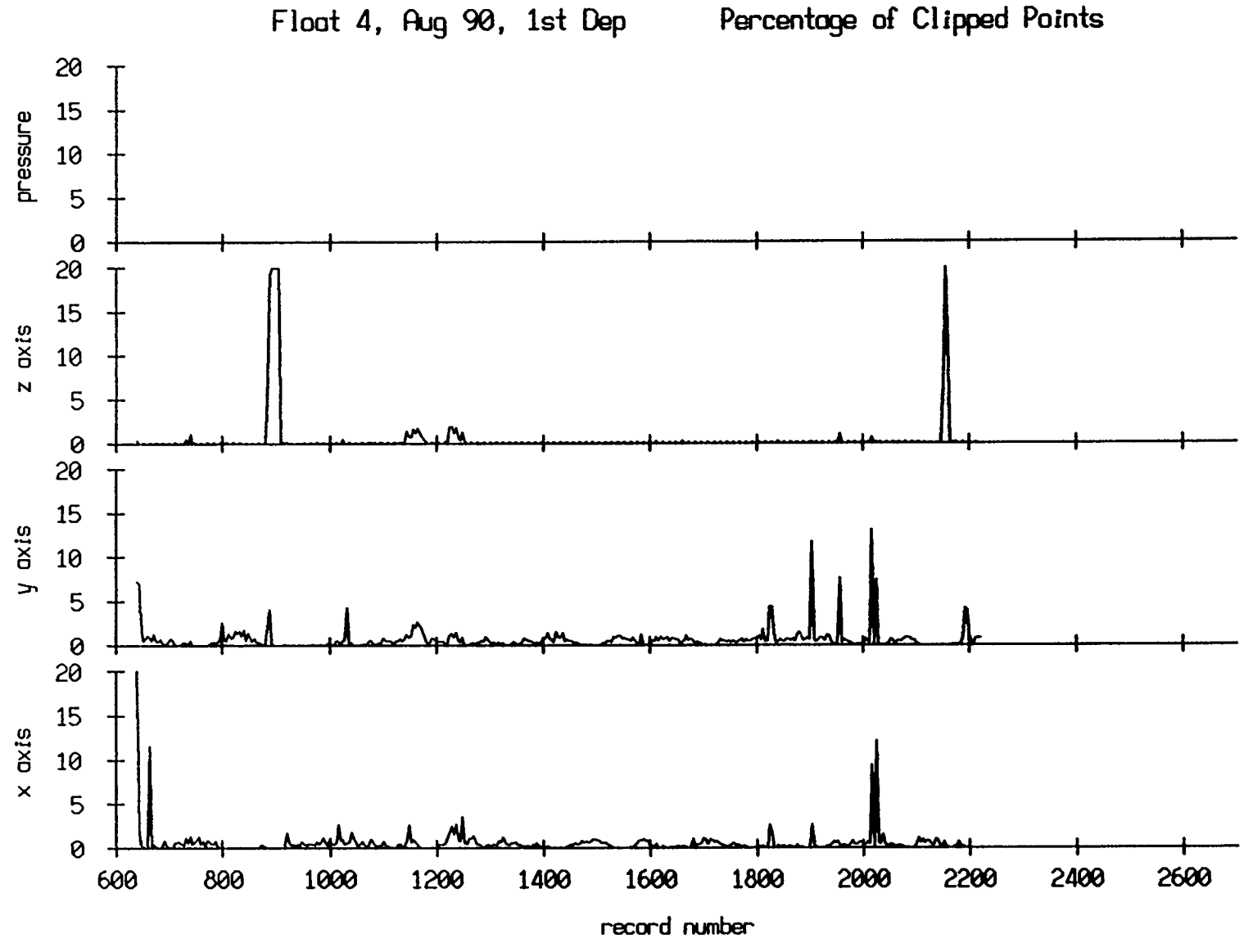
Float 4, Aug 90, 1st Dep
Percentage of Clipped Points
pressure
z axis
y axis
x axis
0
5
10
15
20
600
800
1000
1200
1400
1600
1800
2000
2200
2400
2600
record number

Figure V.16

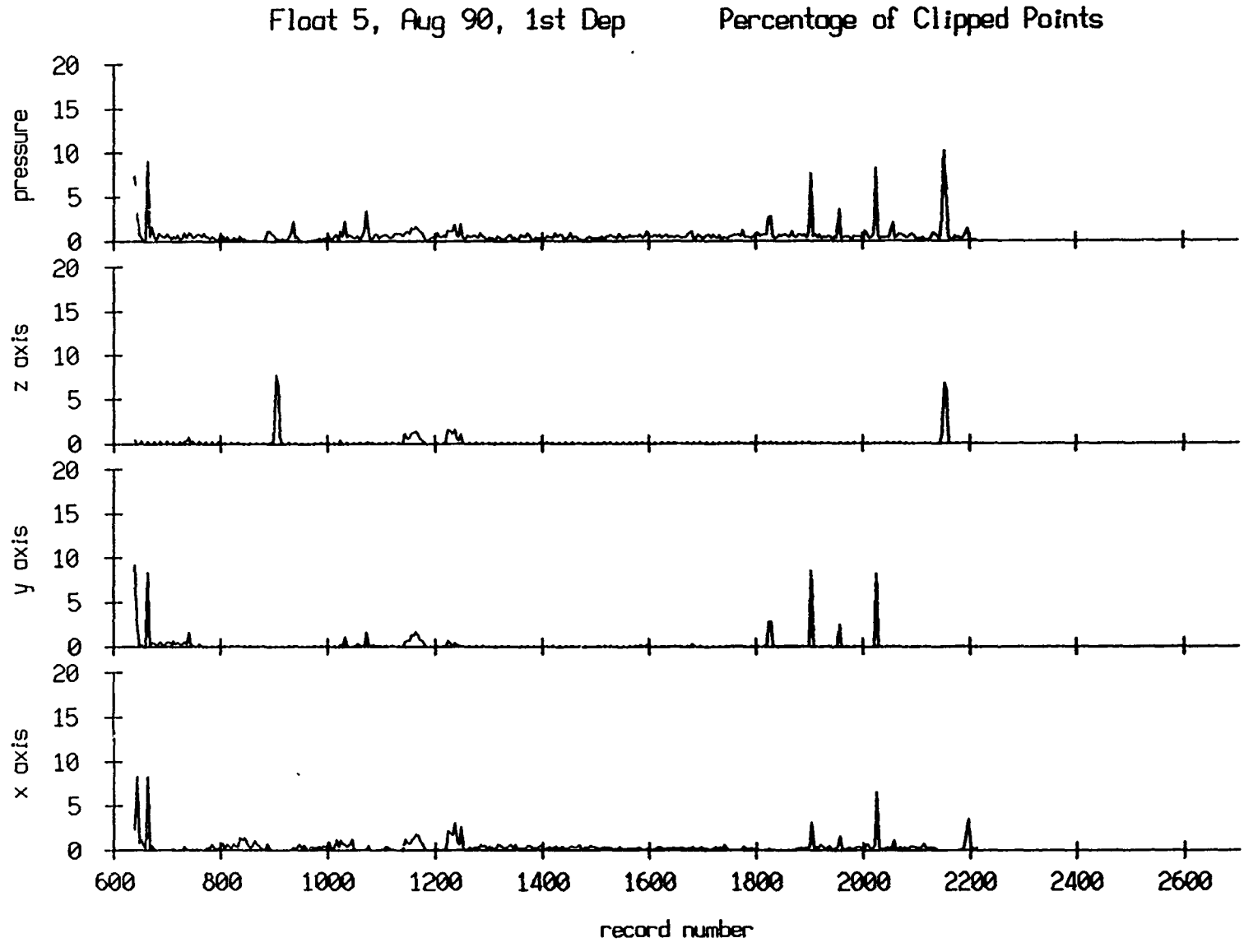
Float 5, Aug 90, 1st Dep
Percentage of Clipped Points
pressure
z axis
y axis
x axis
20
15
10
5
0
600
800
1000
1200
1400
1600
1800
2000
2200
2400
2600
record number

Figure V.17

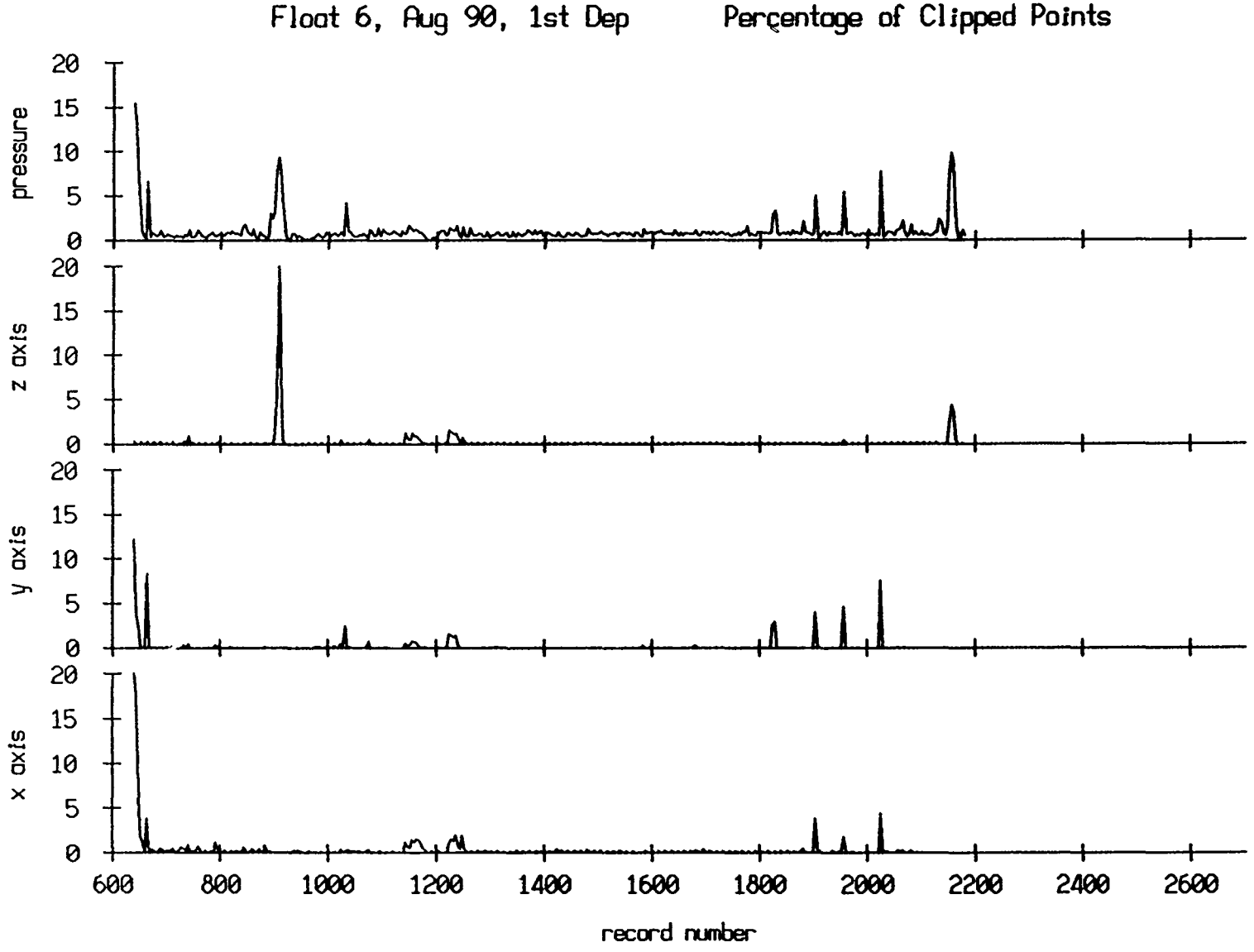
Float 6, Aug 90, 1st Dep
Percentage of Clipped Points
pressure
z axis
y axis
x axis
20
15
10
5
0
600
800
1000
1200
1400
1600
1800
2000
2200
2400
2600
record number

Figure V.18

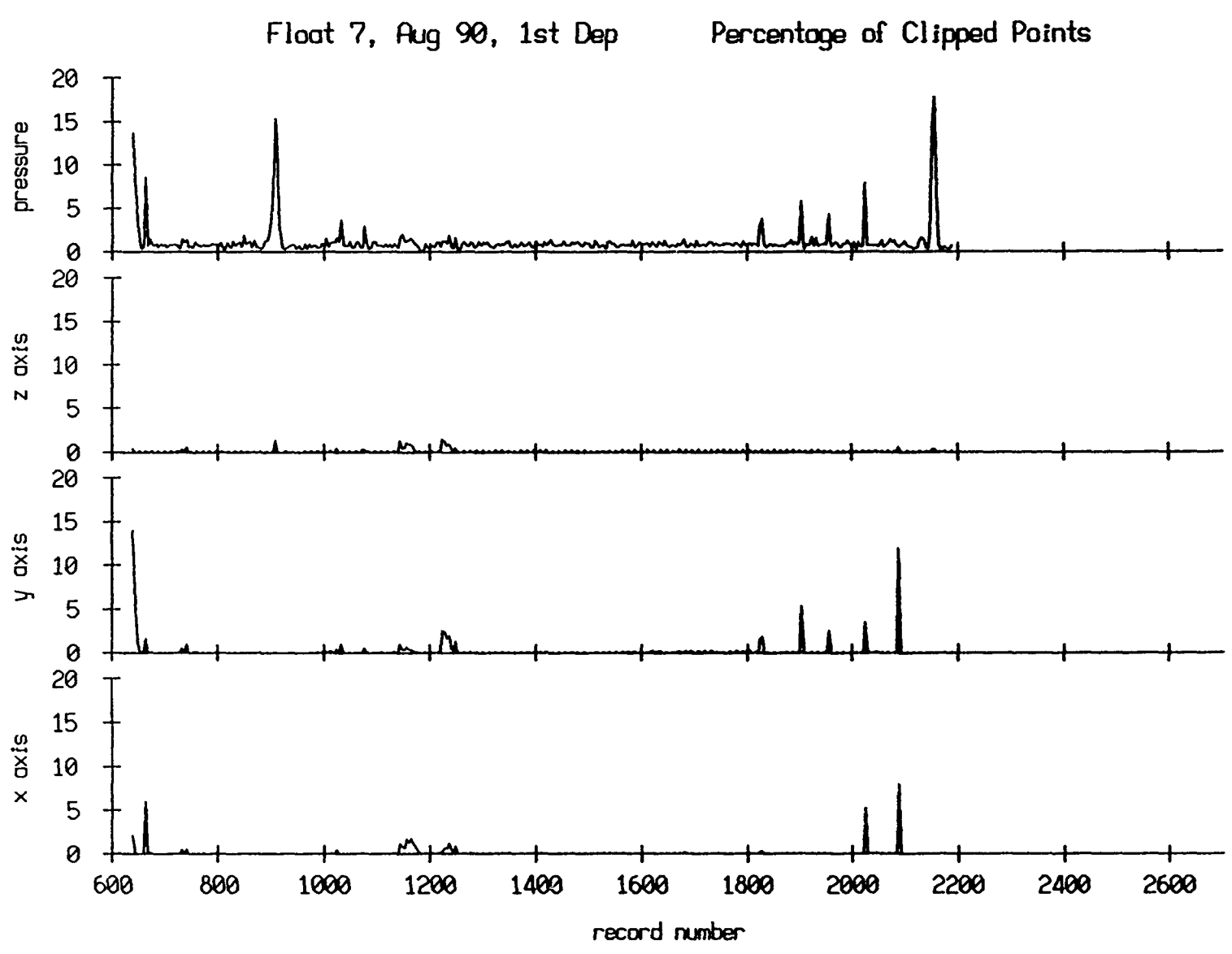
Float 7, Aug 90, 1st Dep
Percentage of Clipped Points
pressure
z axis
y axis
x axis
20
15
10
5
0
600
800
1000
1200
1400
1600
1800
2000
2200
2400
2600
record number

Figure V.19

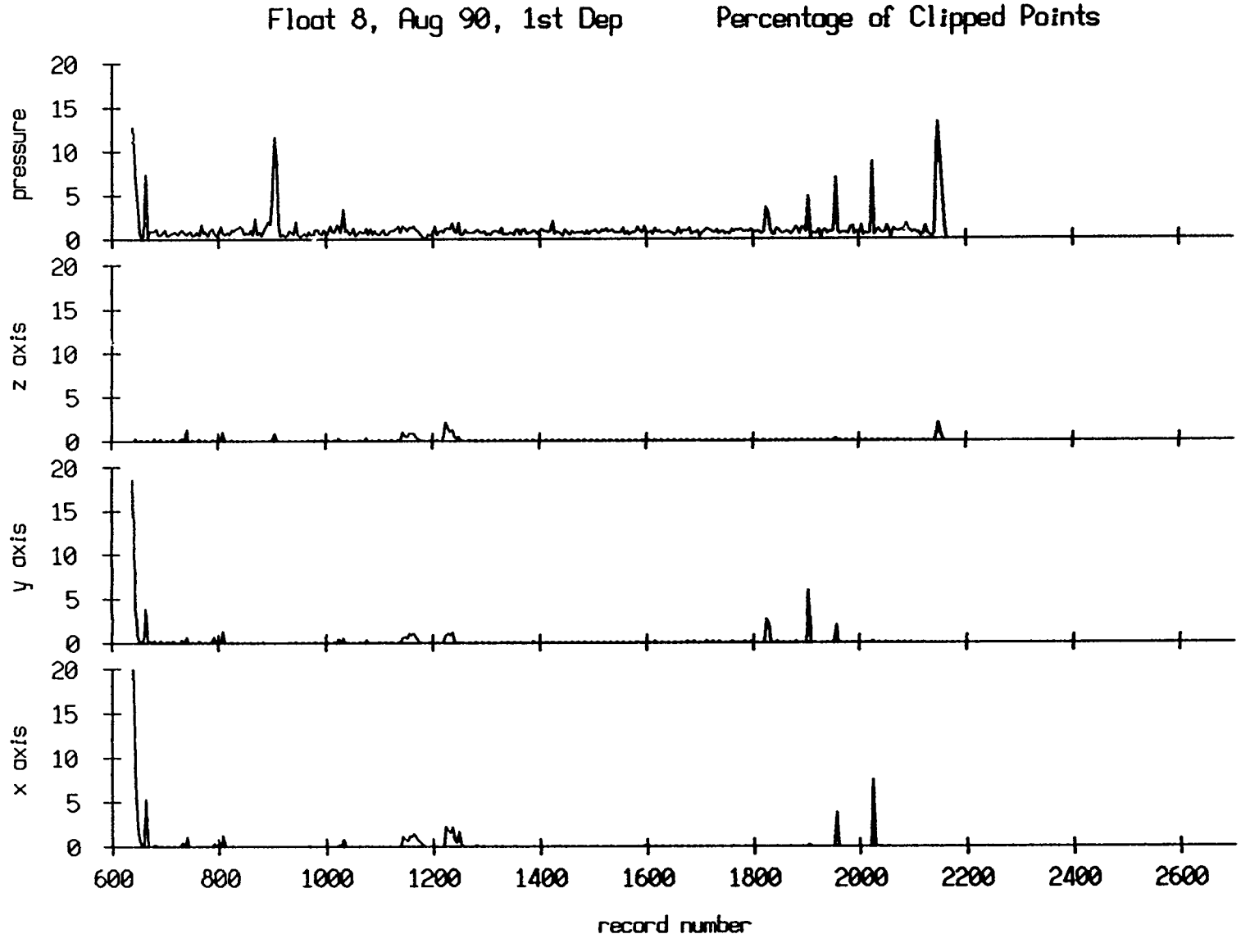
Float 8, Aug 90, 1st Dep
Percentage of Clipped Points
pressure
z axis
y axis
x axis
20
15
10
5
0
600
800
1000
1200
1400
1600
1800
2000
2200
2400
2600
record number

Figure V.20

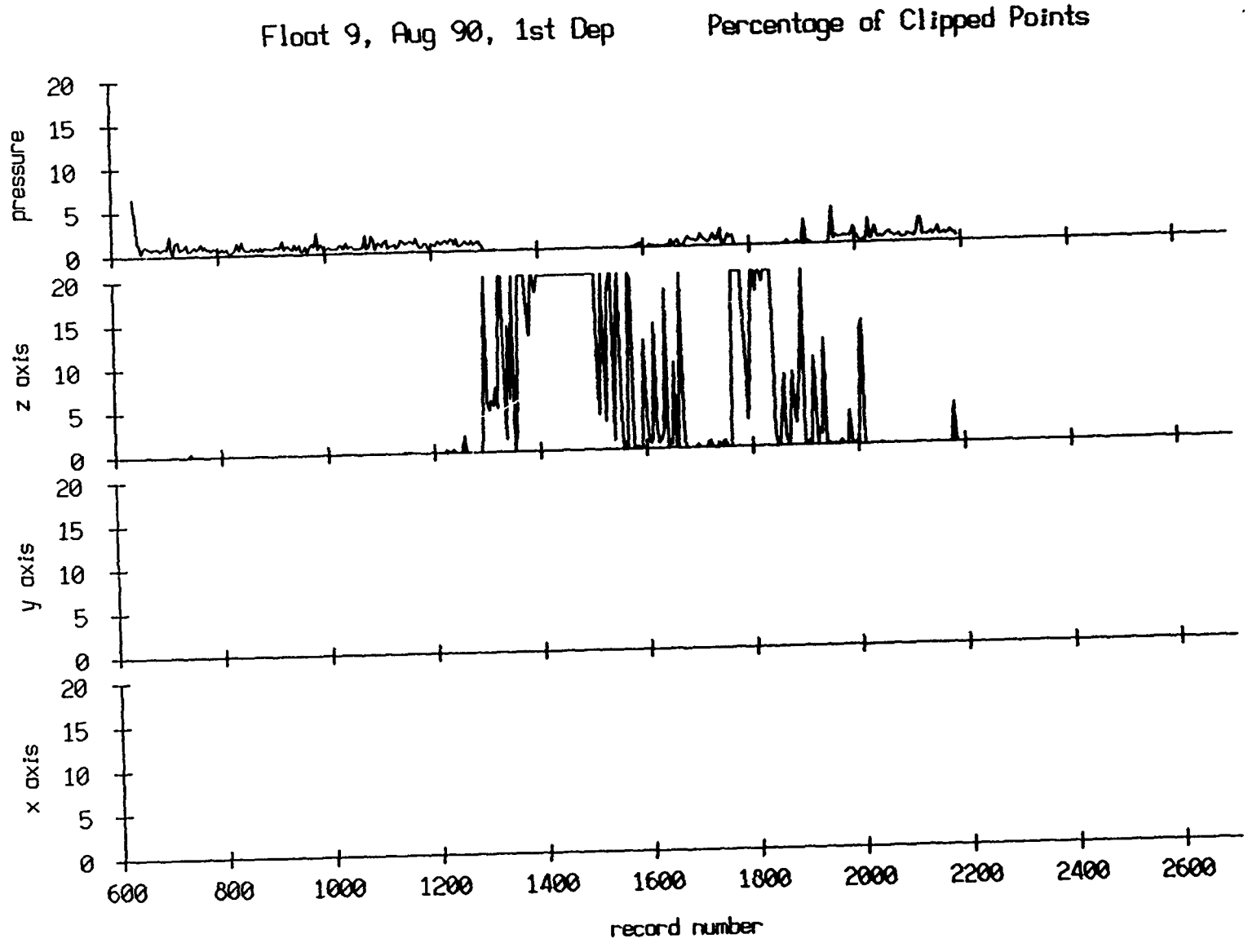
Float 9, Aug 90, 1st Dep
Percentage of Clipped Points
pressure
z axis
y axis
x axis
20
15
10
5
0
600
800
1000
1200
1400
1600
1800
2000
2200
2400
2600
record number

Figure V.21

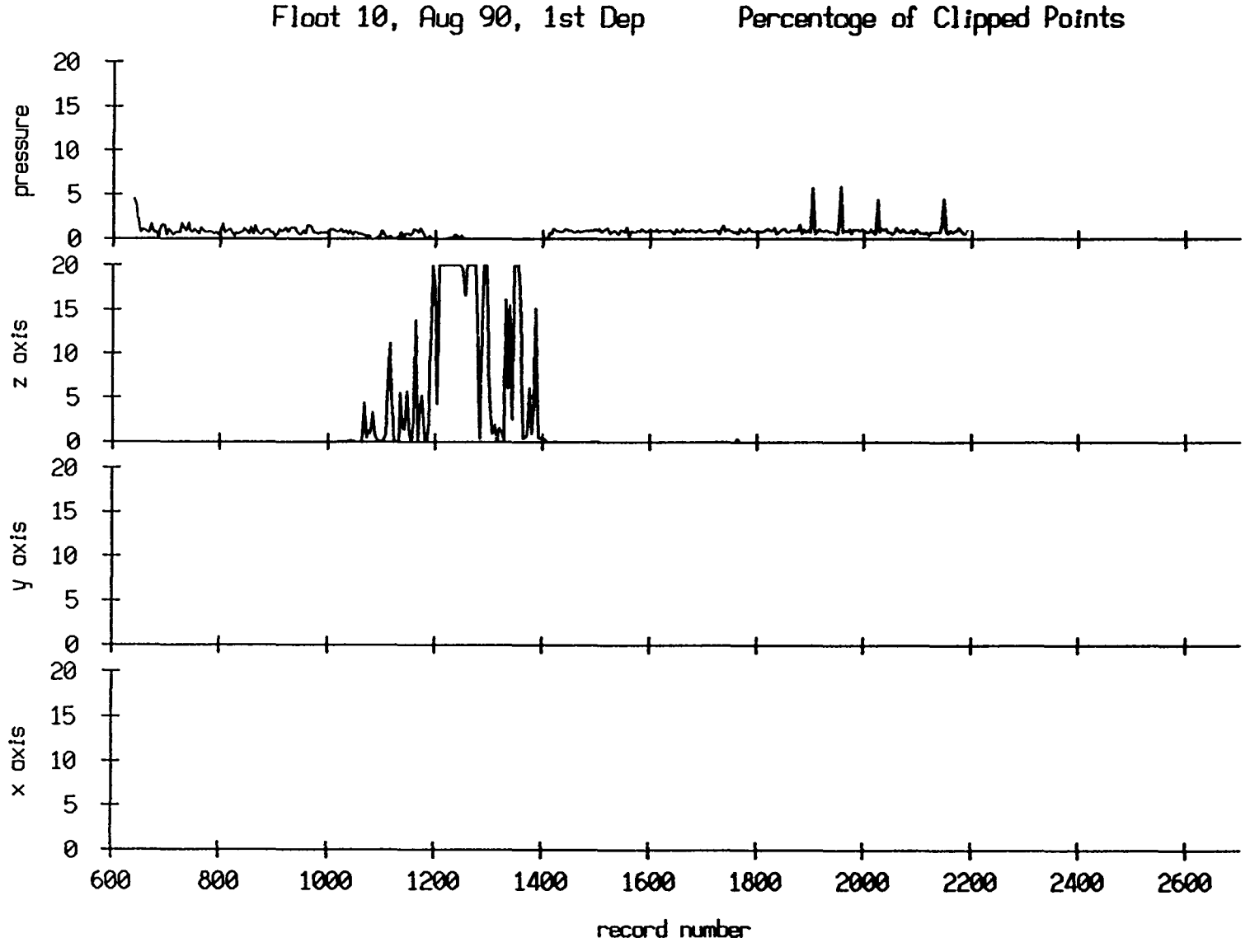
Float 10, Aug 90, 1st Dep
Percentage of Clipped Points
pressure
z axis
y axis
x axis
20
15
10
5
0
600
800
1000
1200
1400
1600
1800
2000
2200
2400
2600
record number

Figure V.22

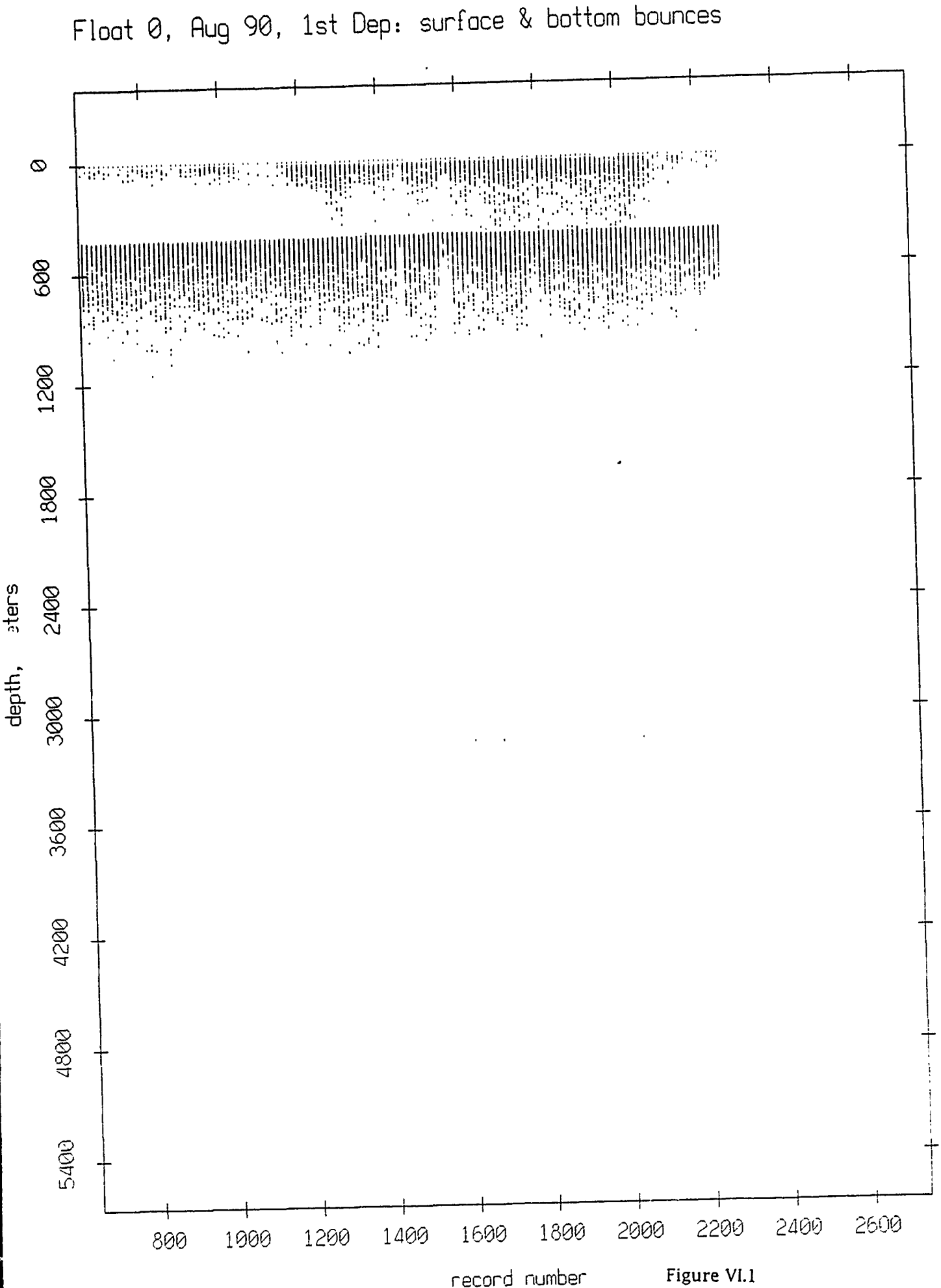
Float 0, Aug 90, 1st Dep: surface & bottom bounces
0
600
1200
1800
2400
3000
3600
4200
4800
5400
depth, eters
800
1000
1200
1400
1600
1800
2000
2200
2400
2600
record number

Figure VI.1

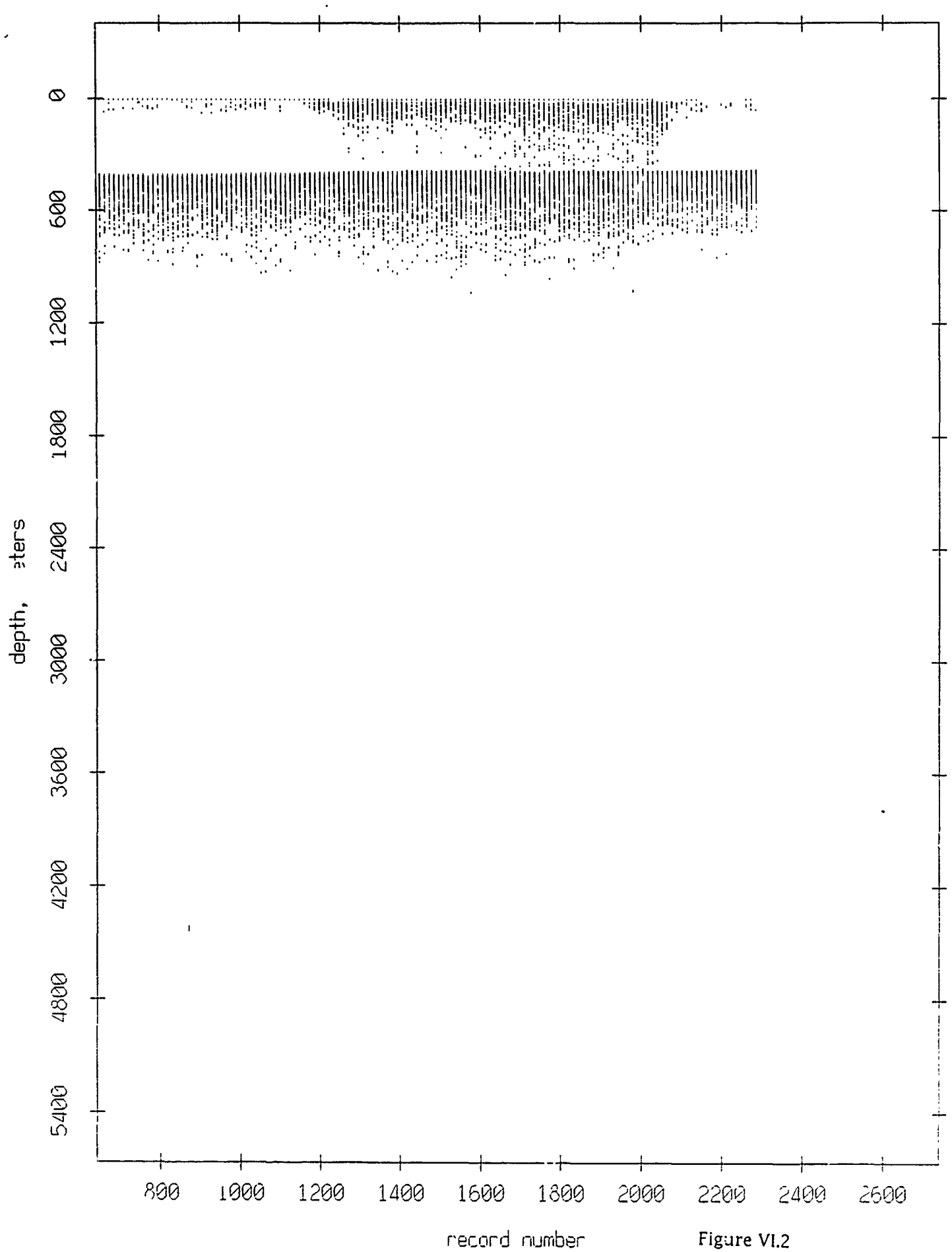
Floot 1, Aug 90, 1st Dep: surface & bottom bounces
depth, meters
0
600
1200
1800
2400
3000
3600
4200
4800
5400
800
1000
1200
1400
1600
1800
2000
2200
2400
2600
record number

Figure VI.2

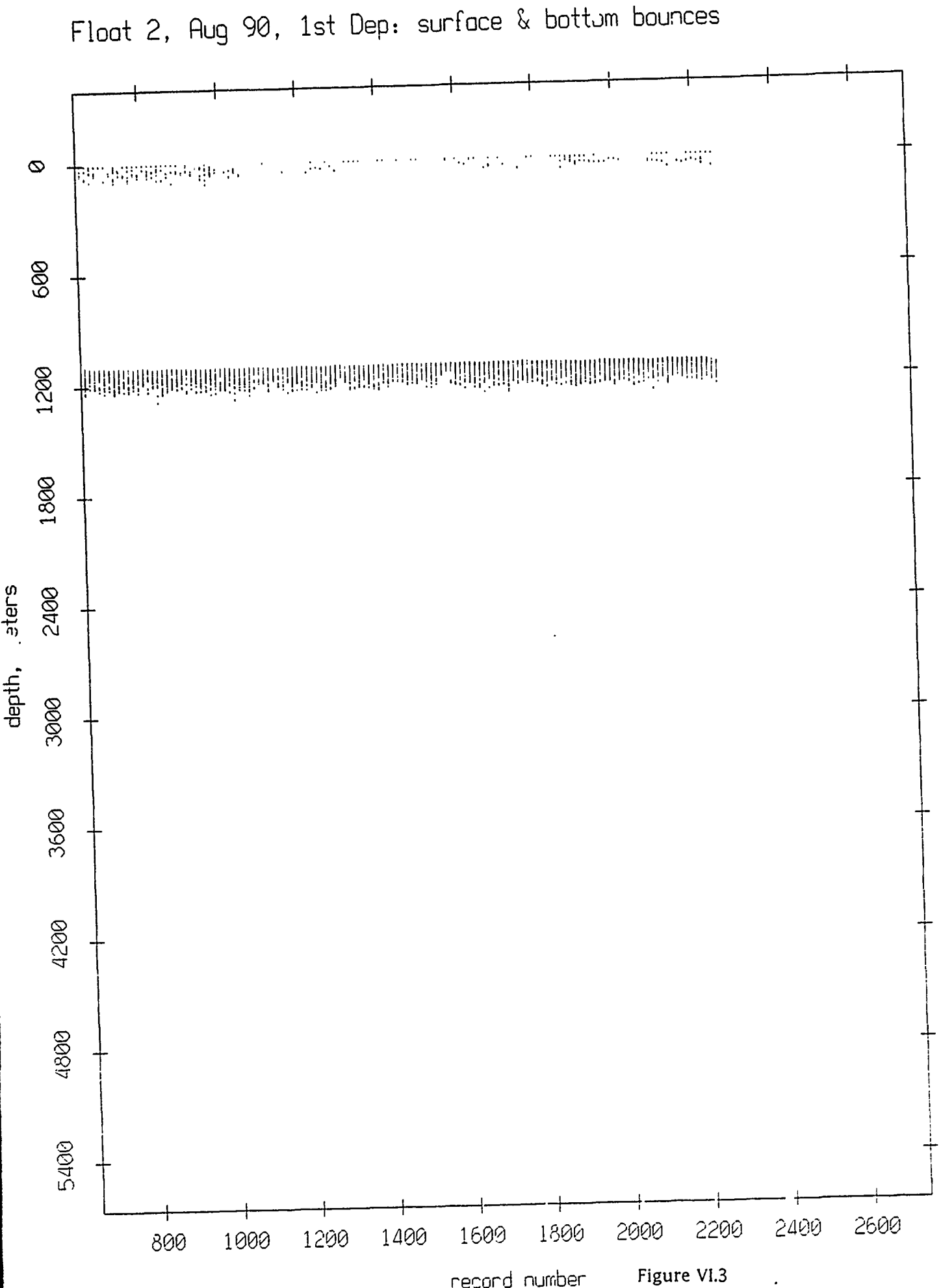
Float 2, Aug 90, 1st Dep: surface & bottom bounces
depth, meters
0
600
1200
1800
2400
3000
3600
4200
4800
5400
800
1000
1200
1400
1600
1800
2000
2200
2400
2600
record number

Figure VI.3

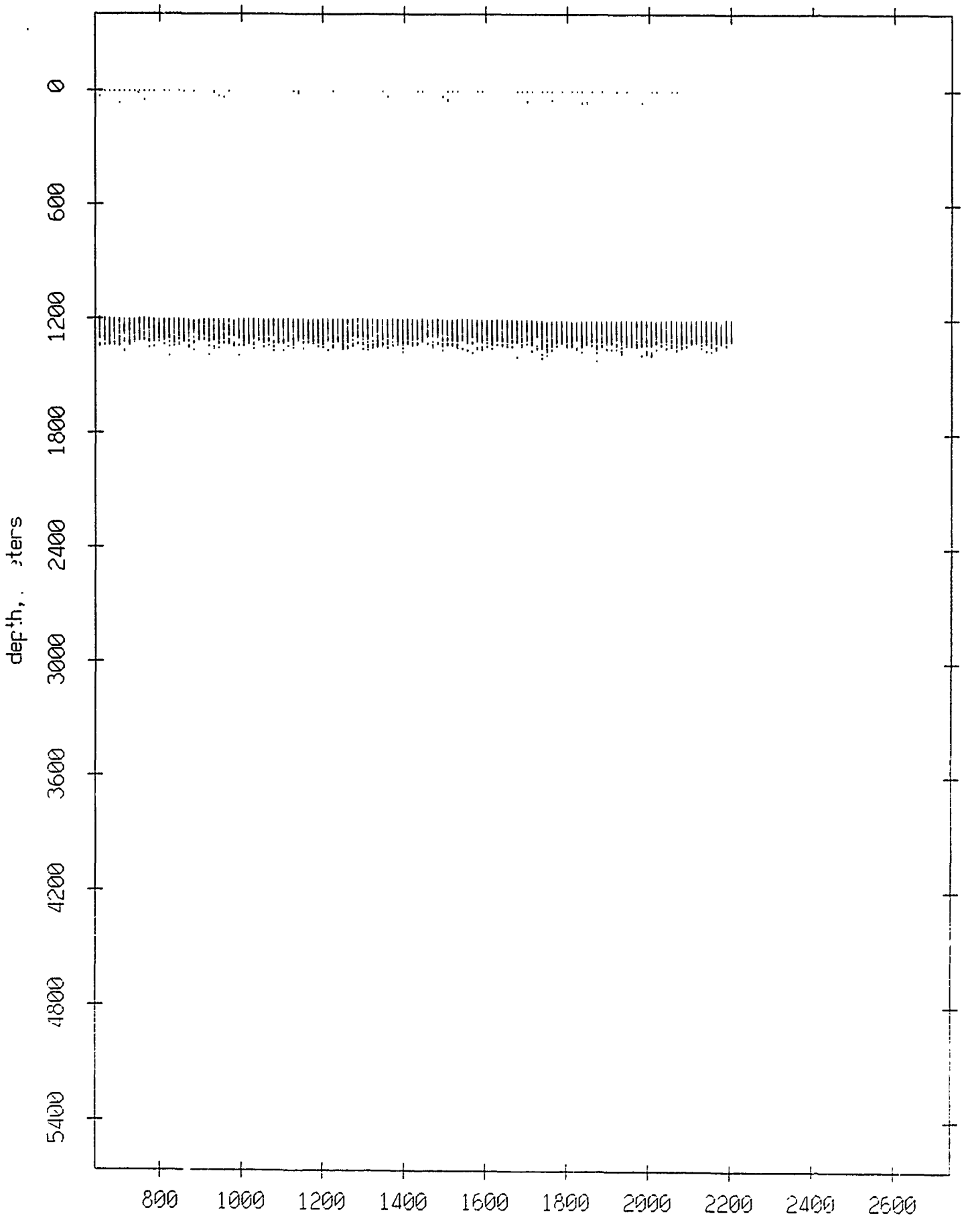
Float 3, Aug 90, 1st Dep: surface & bottom bounces
0
600
1200
1800
2400
3000
3600
4200
4800
5400
depth, meters
800
1000
1200
1400
1600
1800
2000
2200
2400
2600
record number

Figure VI.4

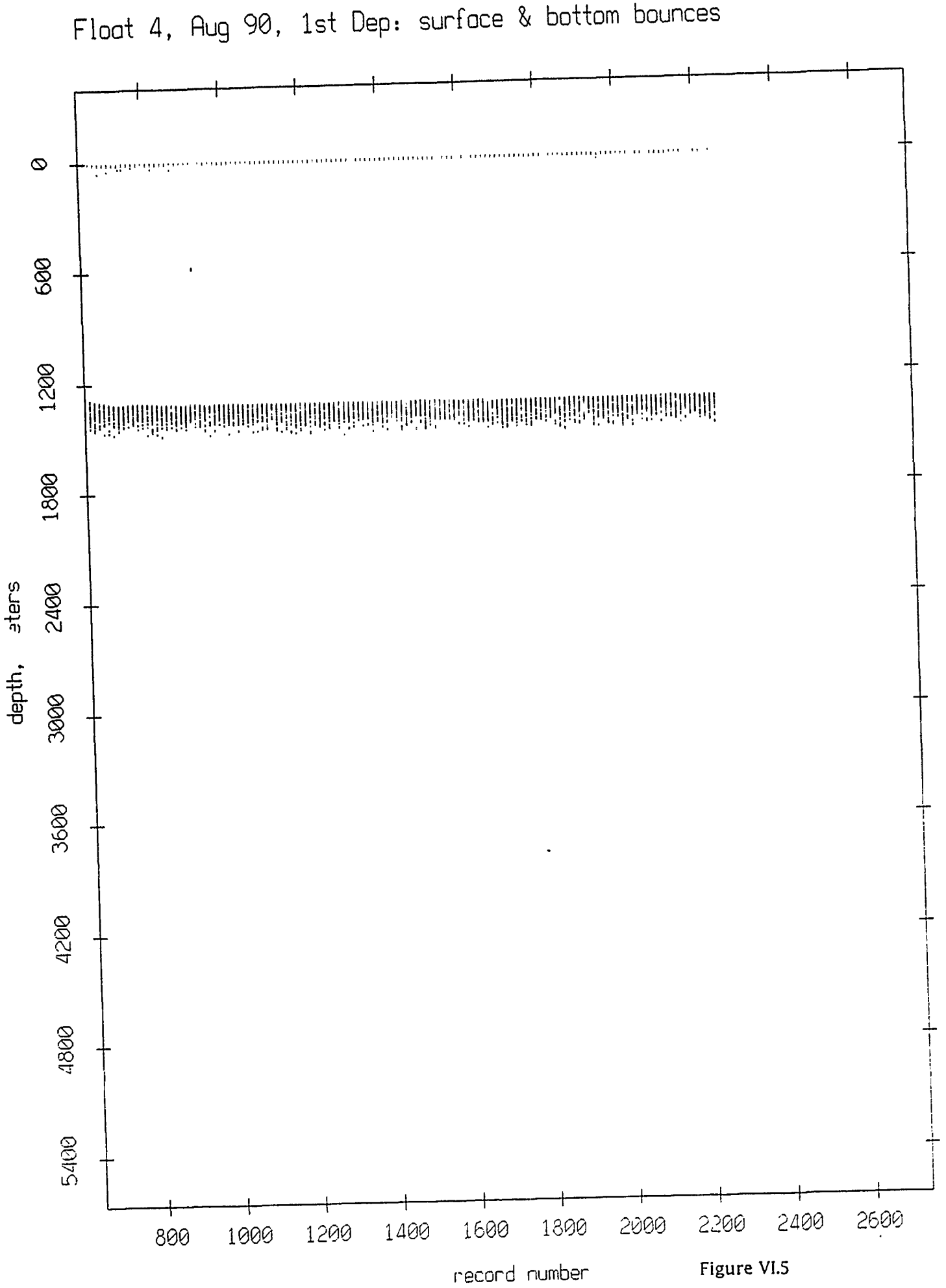
Float 4, Aug 90, 1st Dep: surface & bottom bounces
depth, meters
0
600
1200
1800
2400
3000
3600
4200
4800
5400
800
1000
1200
1400
1600
1800
2000
2200
2400
2600
record number

Figure VI.5

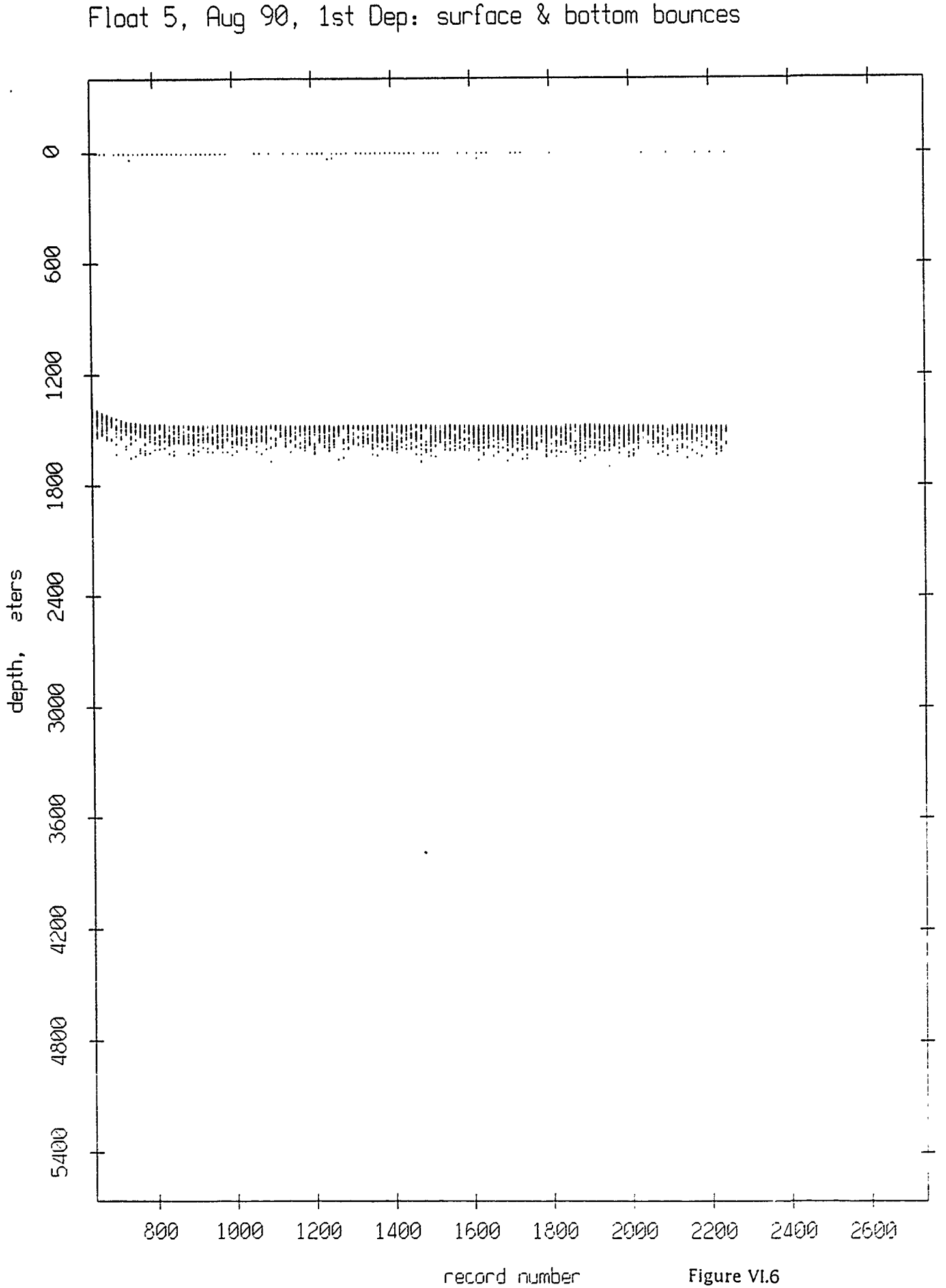
Float 5, Aug 90, 1st Dep: surface & bottom bounces
depth, meters
0
600
1200
1800
2400
3000
3600
4200
4800
5400
800
1000
1200
1400
1600
1800
2000
2200
2400
2600
record number

Figure VI.6

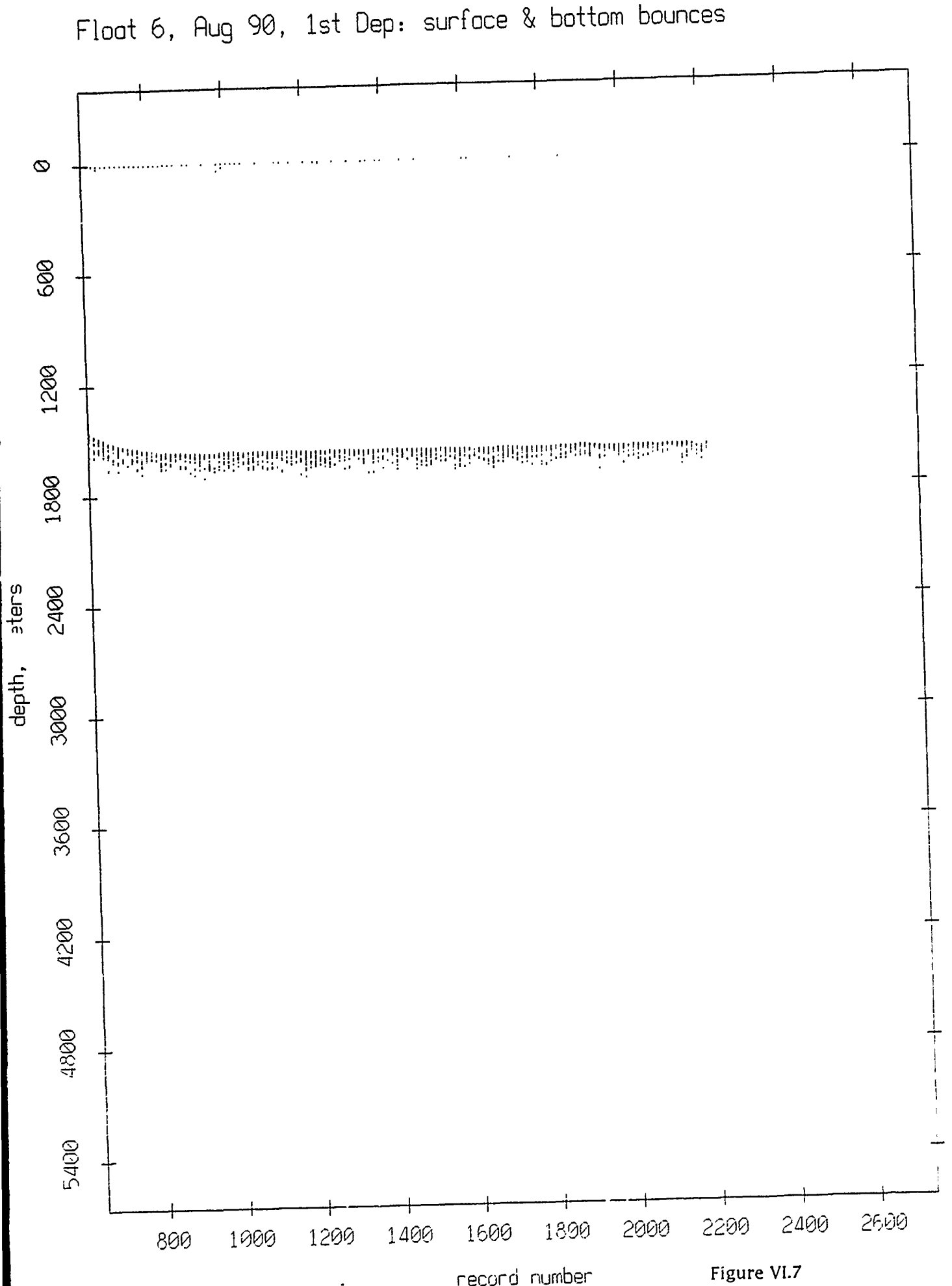
Float 6, Aug 90, 1st Dep: surface & bottom bounces
depth, eters
0
600
1200
1800
2400
3000
3600
4200
4800
5400
800
1000
1200
1400
1600
1800
2000
2200
2400
2600
record number

Figure VI.7

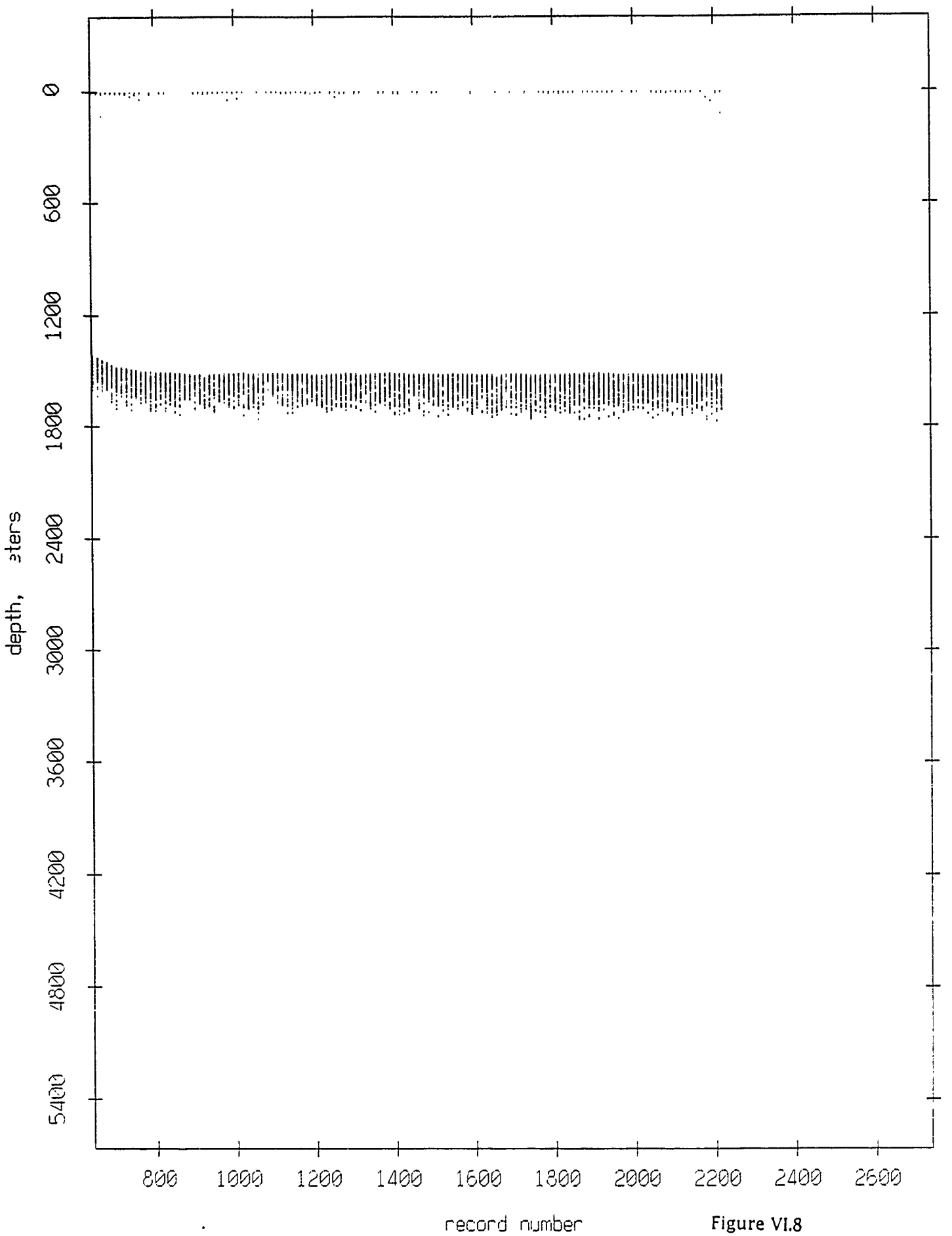
Float 7, Aug 90, 1st Dep: surface & bottom bounces
depth, meters
0
600
1200
1800
2400
3000
3600
4200
4800
5400
800
1000
1200
1400
1600
1800
2000
2200
2400
2600
record number

Figure VI.8

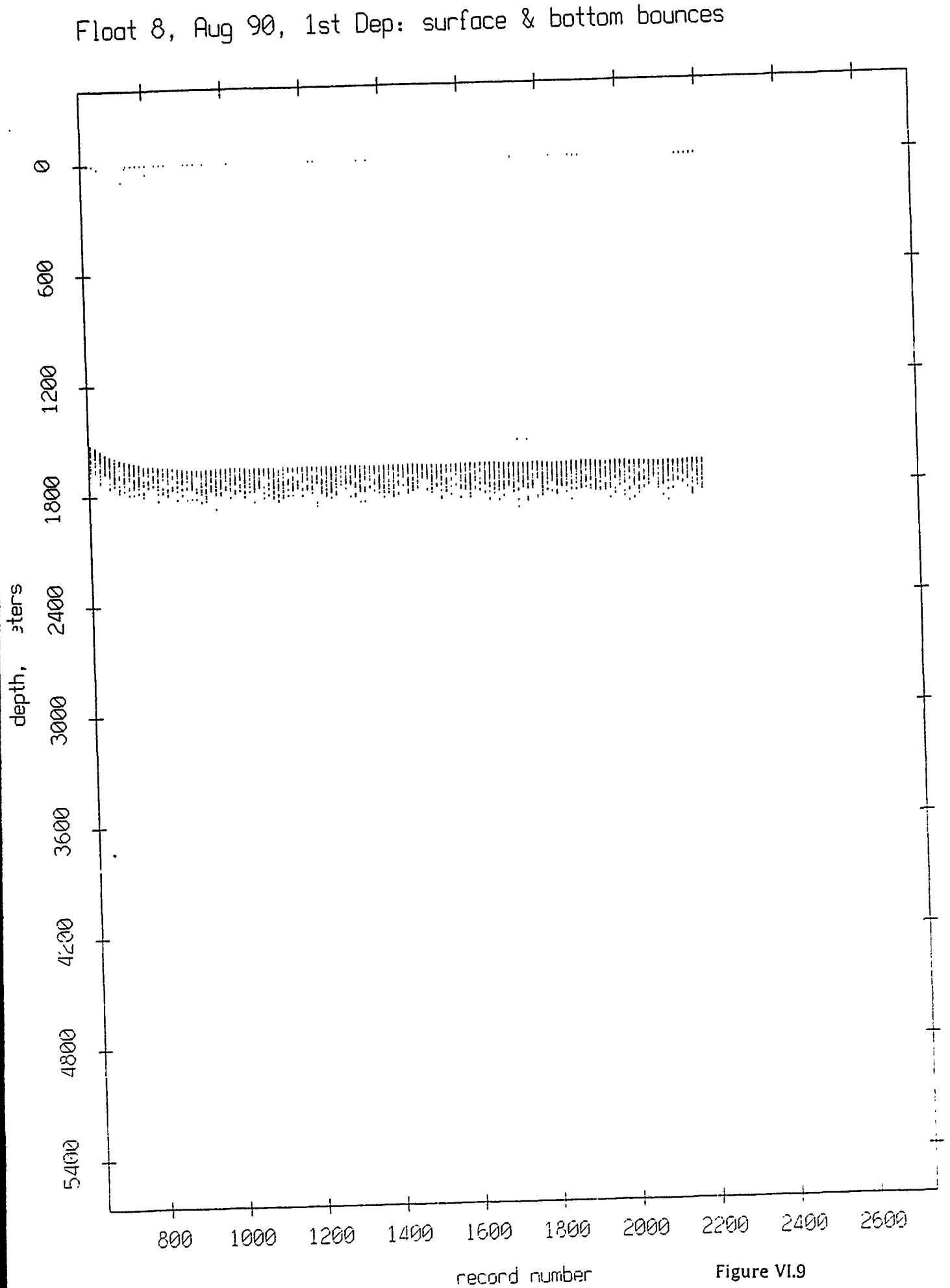
Float 8, Aug 90, 1st Dep: surface & bottom bounces
depth, meters
0
600
1200
1800
2400
3000
3600
4200
4800
5400
800
1000
1200
1400
1600
1800
2000
2200
2400
2600
record number

Figure VI.9

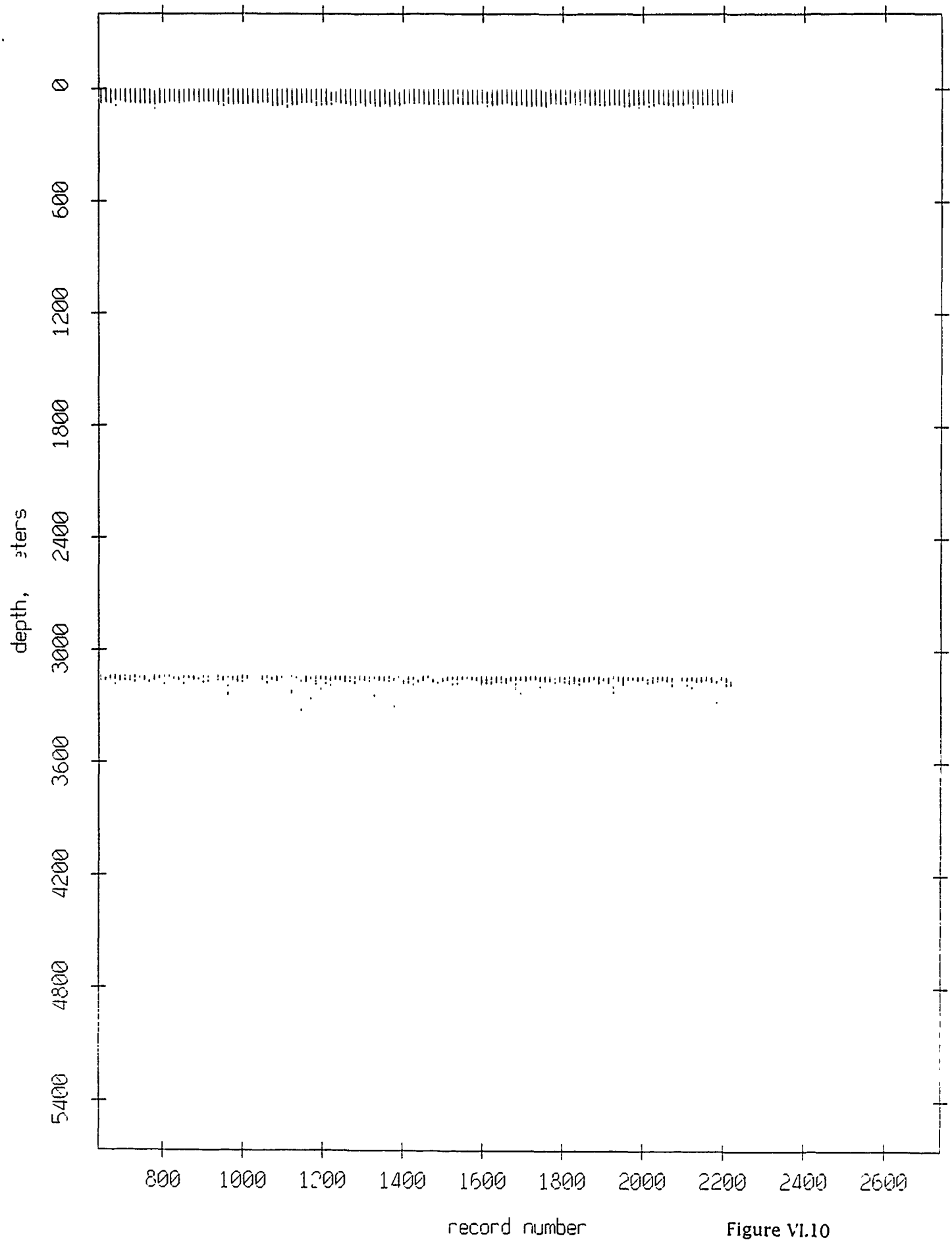
Float 9, Aug 90, 1st Dep: surface & bottom bounces
depth, meters
0
600
1200
1800
2400
3000
3600
4200
4800
5400
800
1000
1200
1400
1600
1800
2000
2200
2400
2600
record number

Figure VI.10

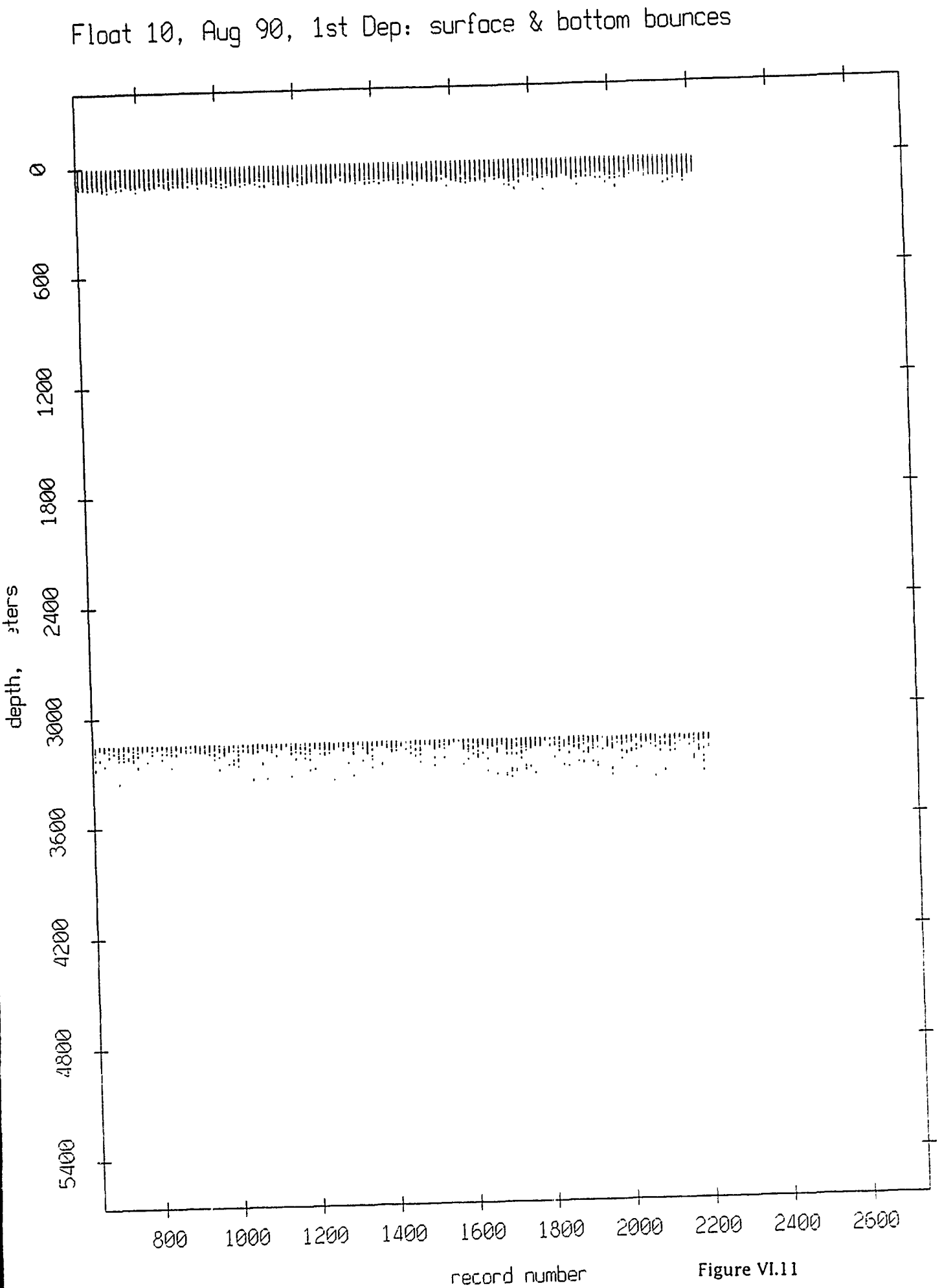
Float 10, Aug 90, 1st Dep: surface & bottom bounces
depth, meters
0
600
1200
1800
2400
3000
3600
4200
4800
5400
800
1000
1200
1400
1600
1800
2000
2200
2400
2600
record number

Figure VI.11

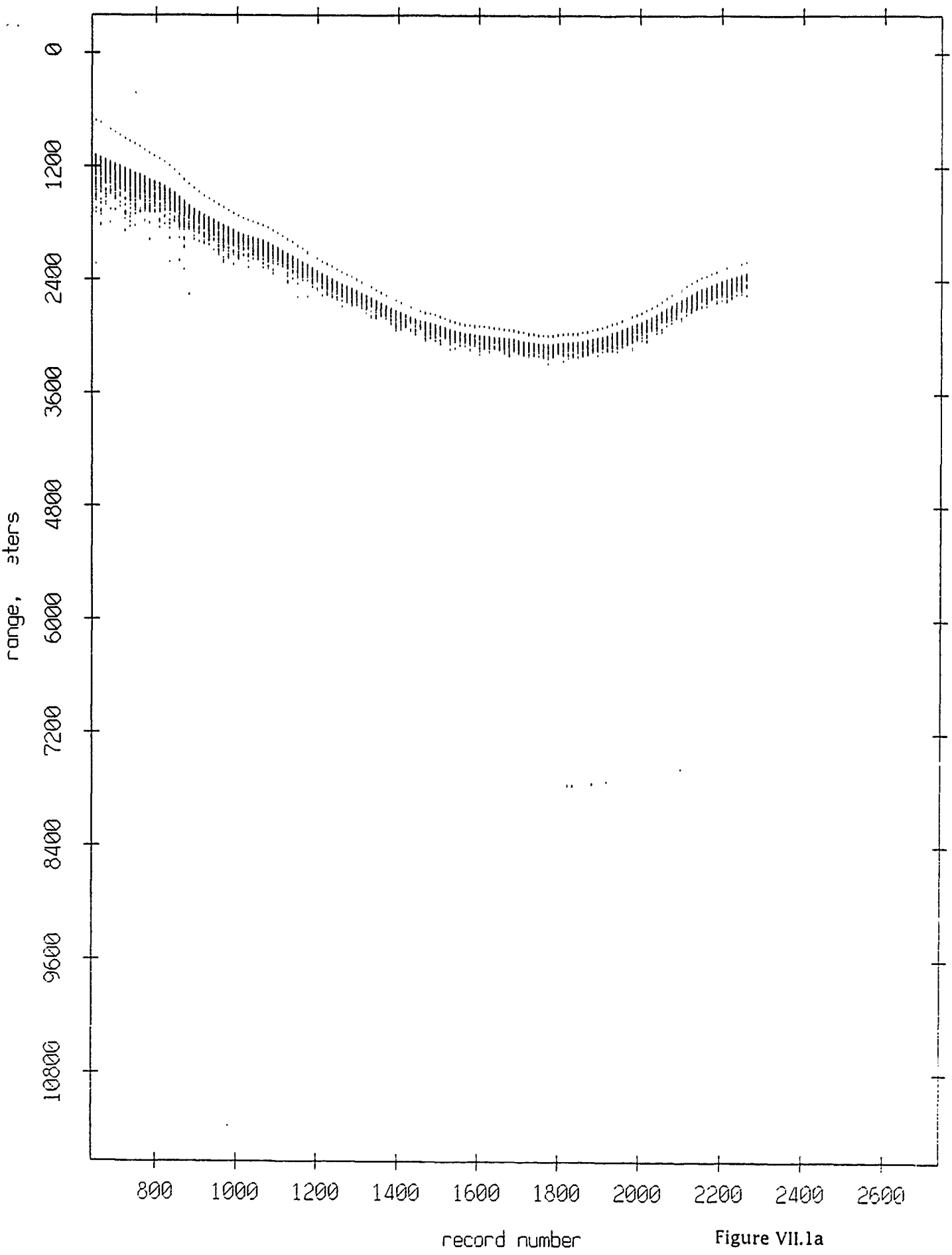

Figure VII.1a

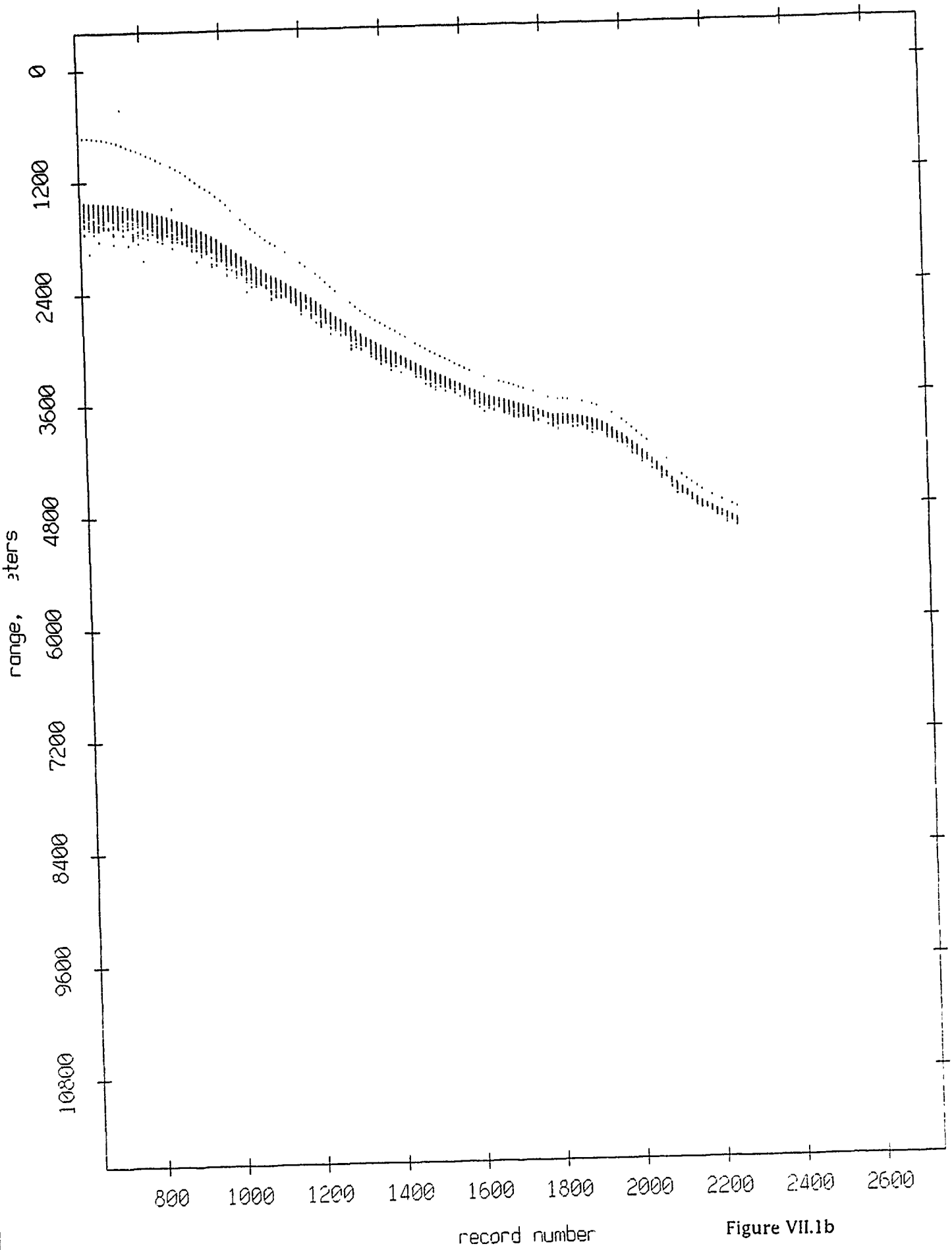

Figure VII.1b

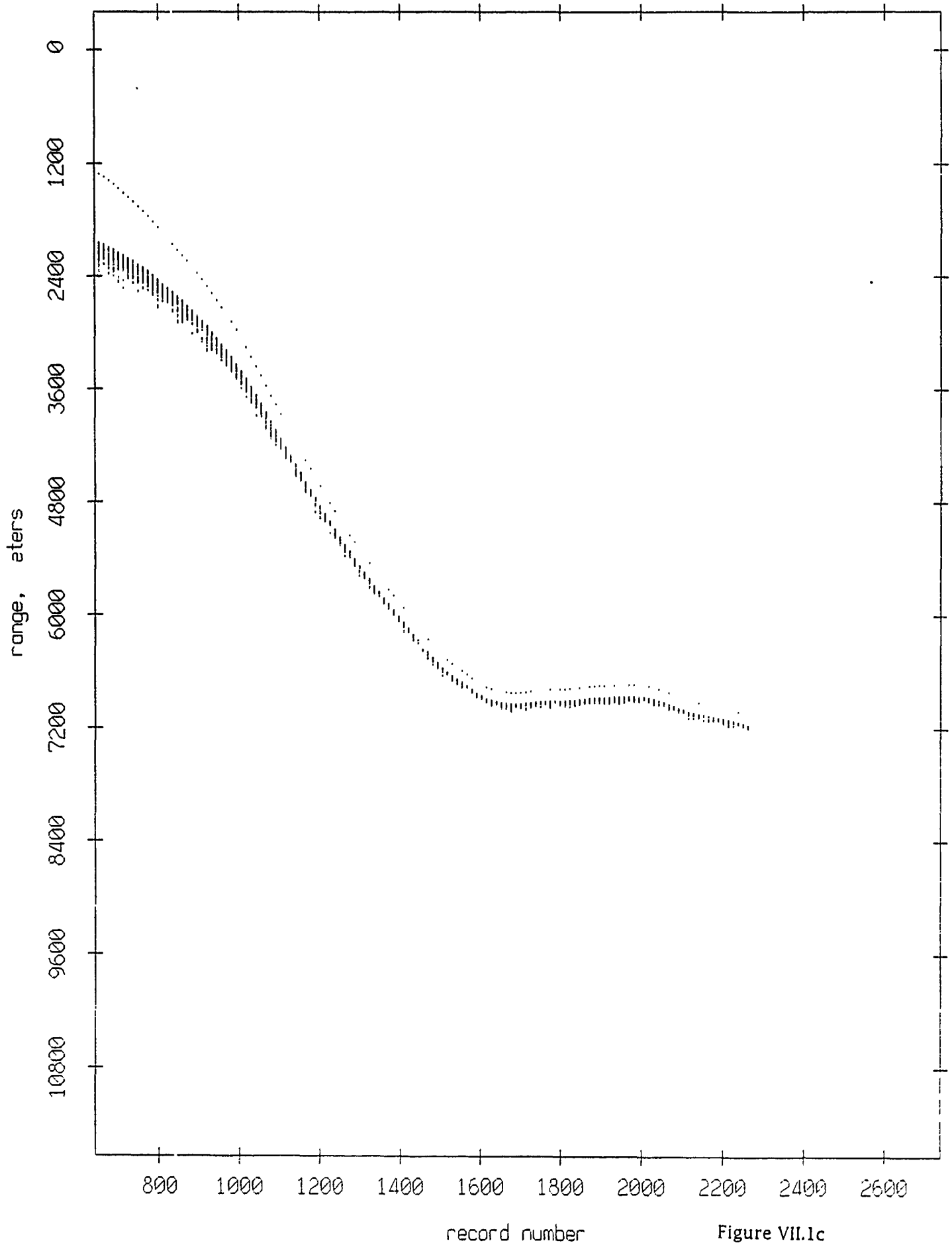

Figure VII.1c

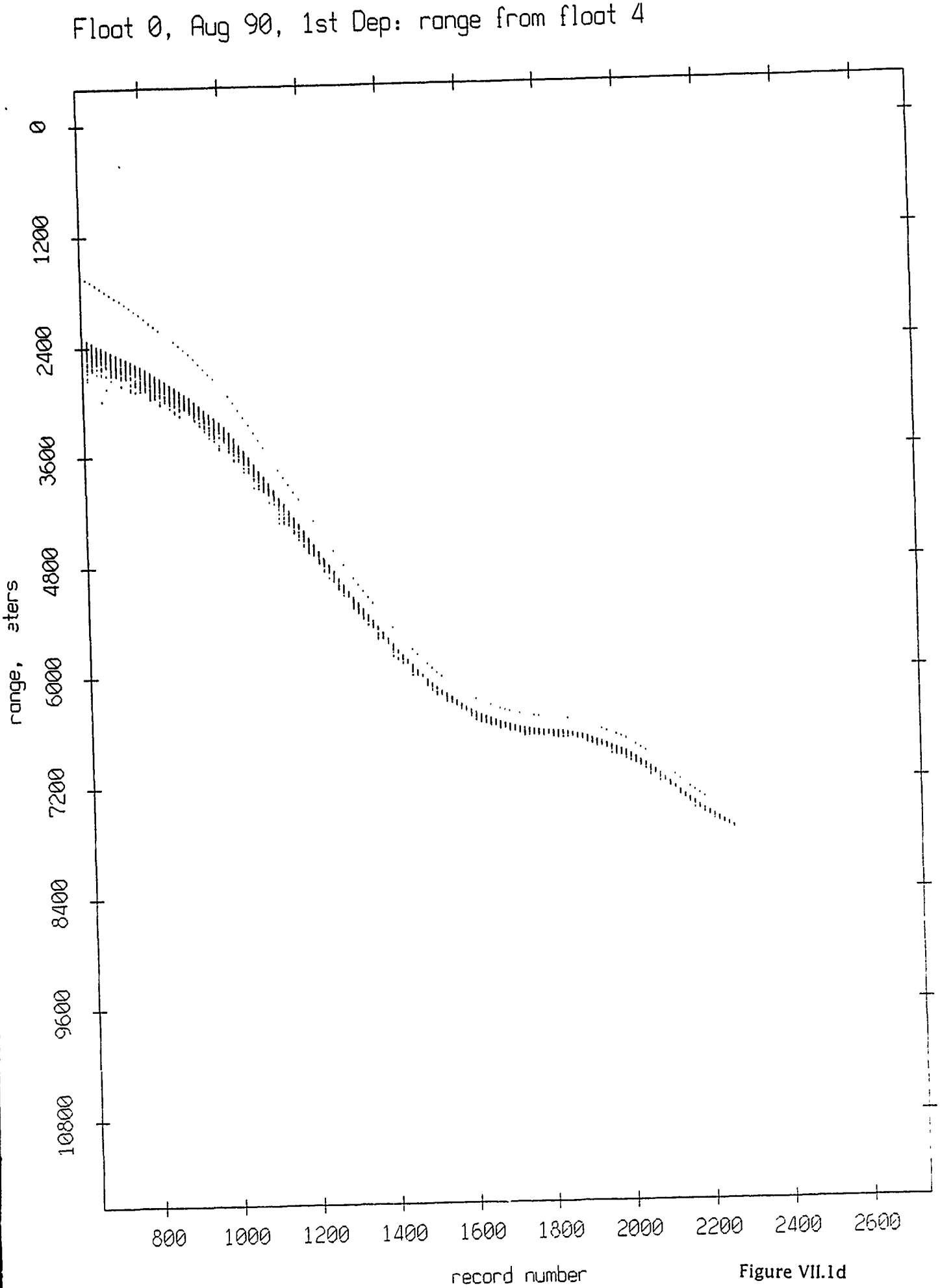

Figure VII.1d

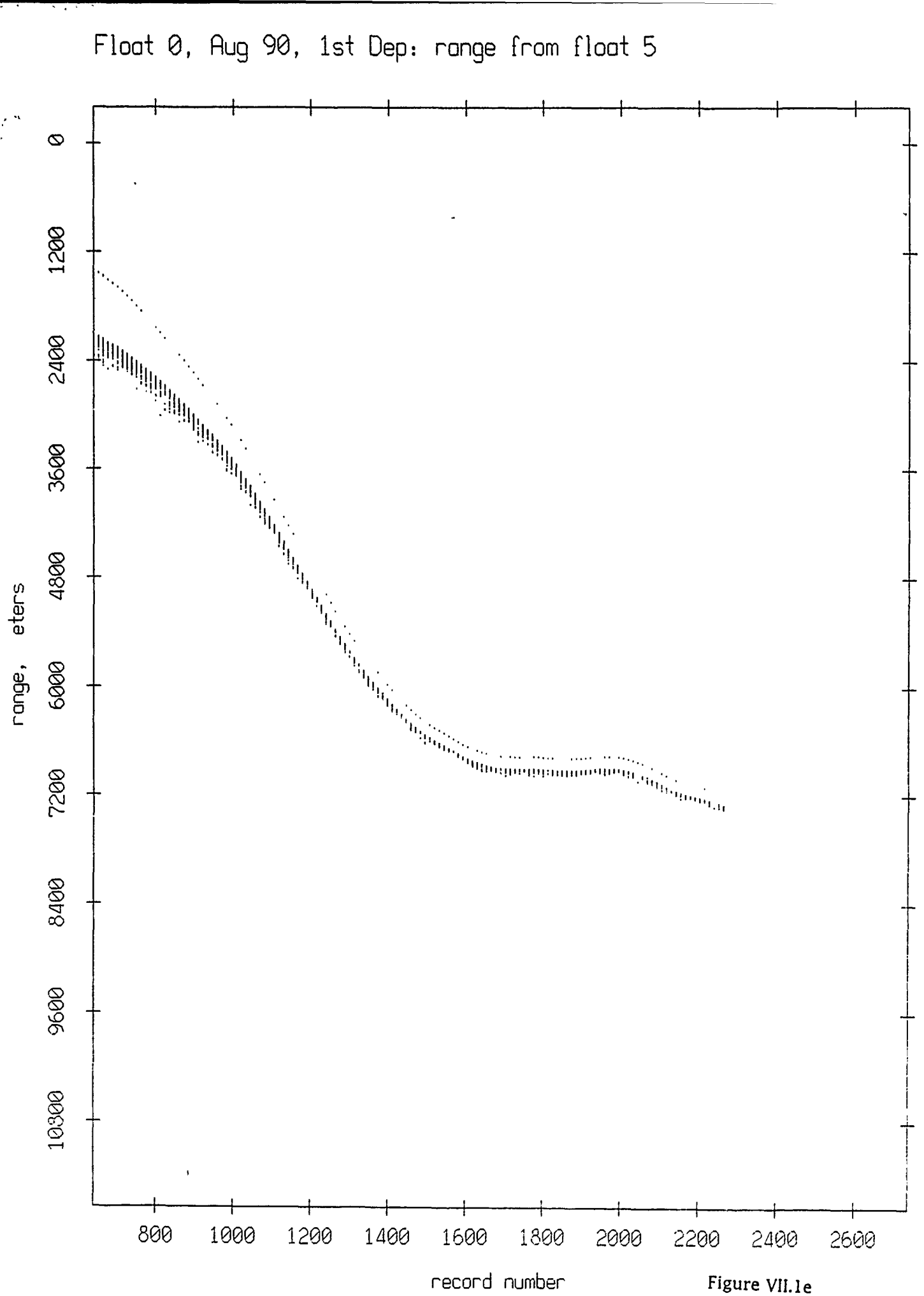

Figure VII.1e

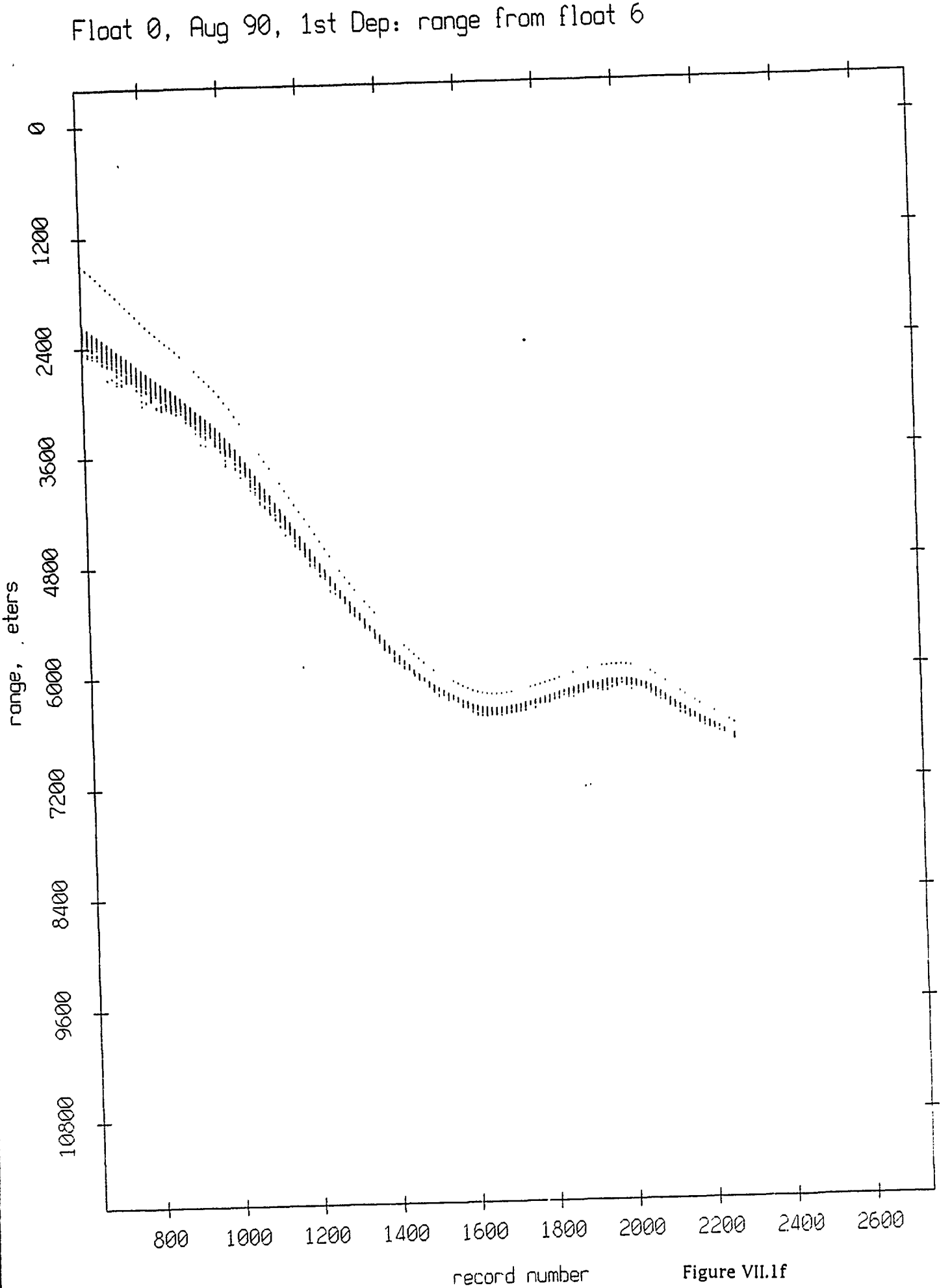

Figure VII.1f

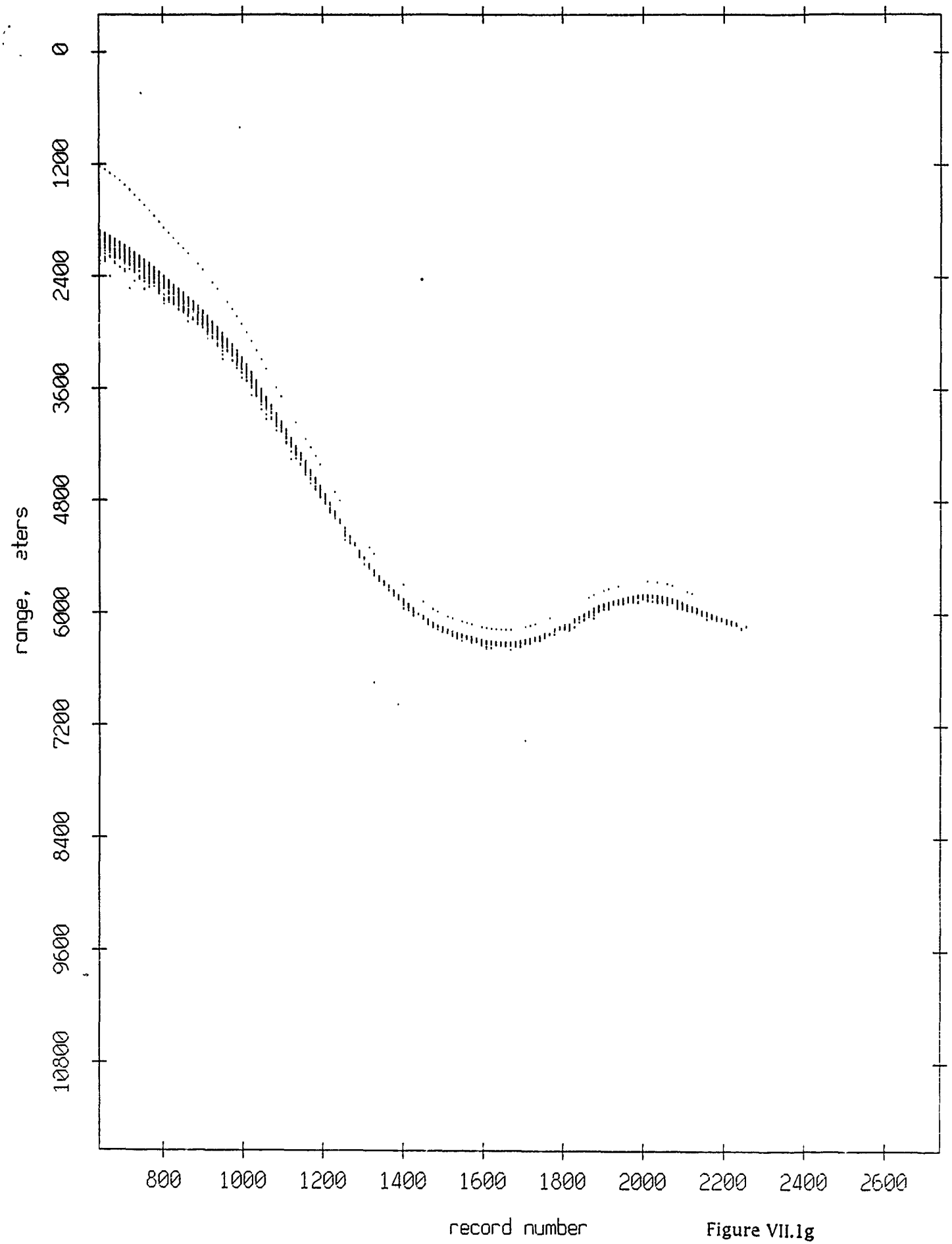

Figure VII.1g

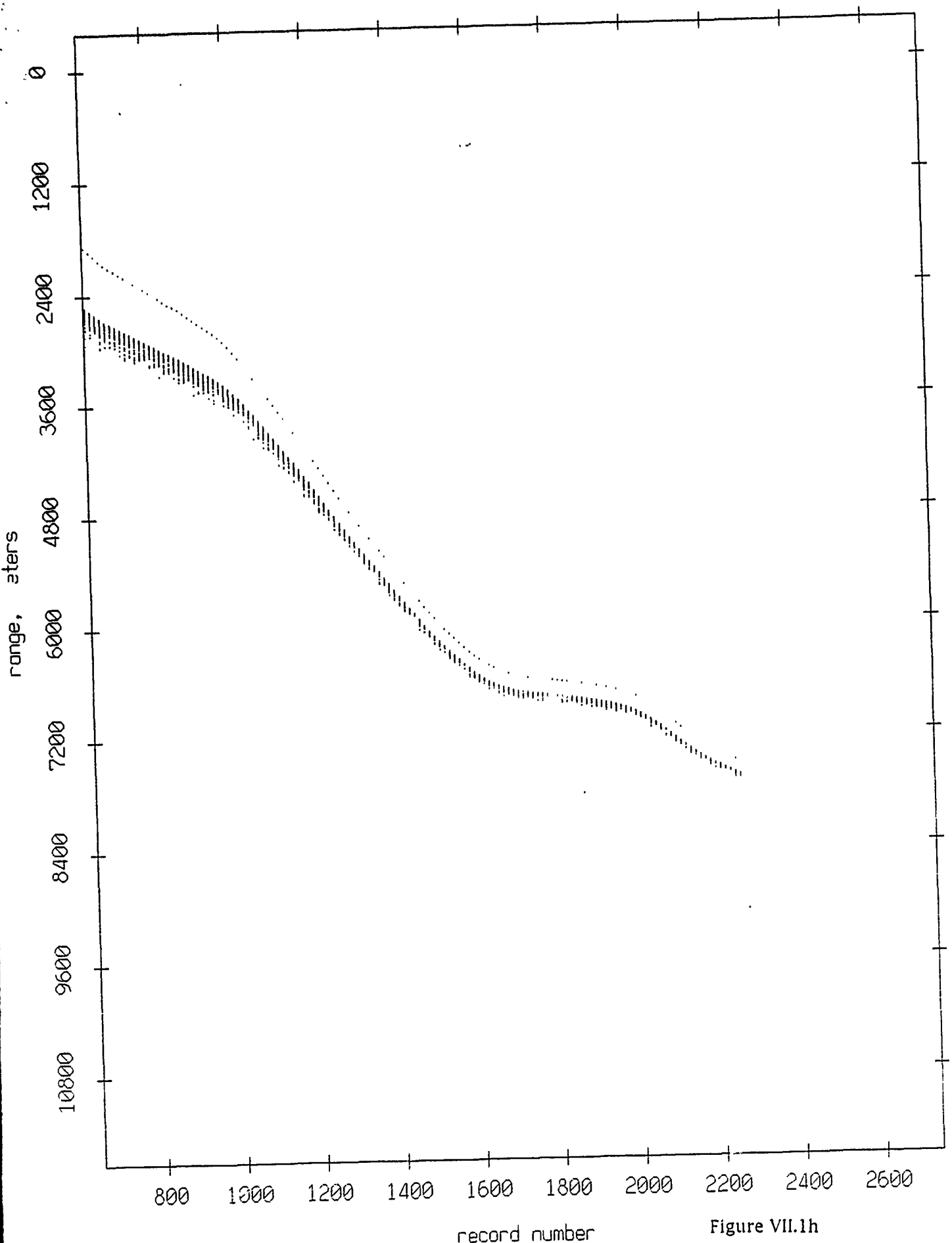

Figure VII.1h

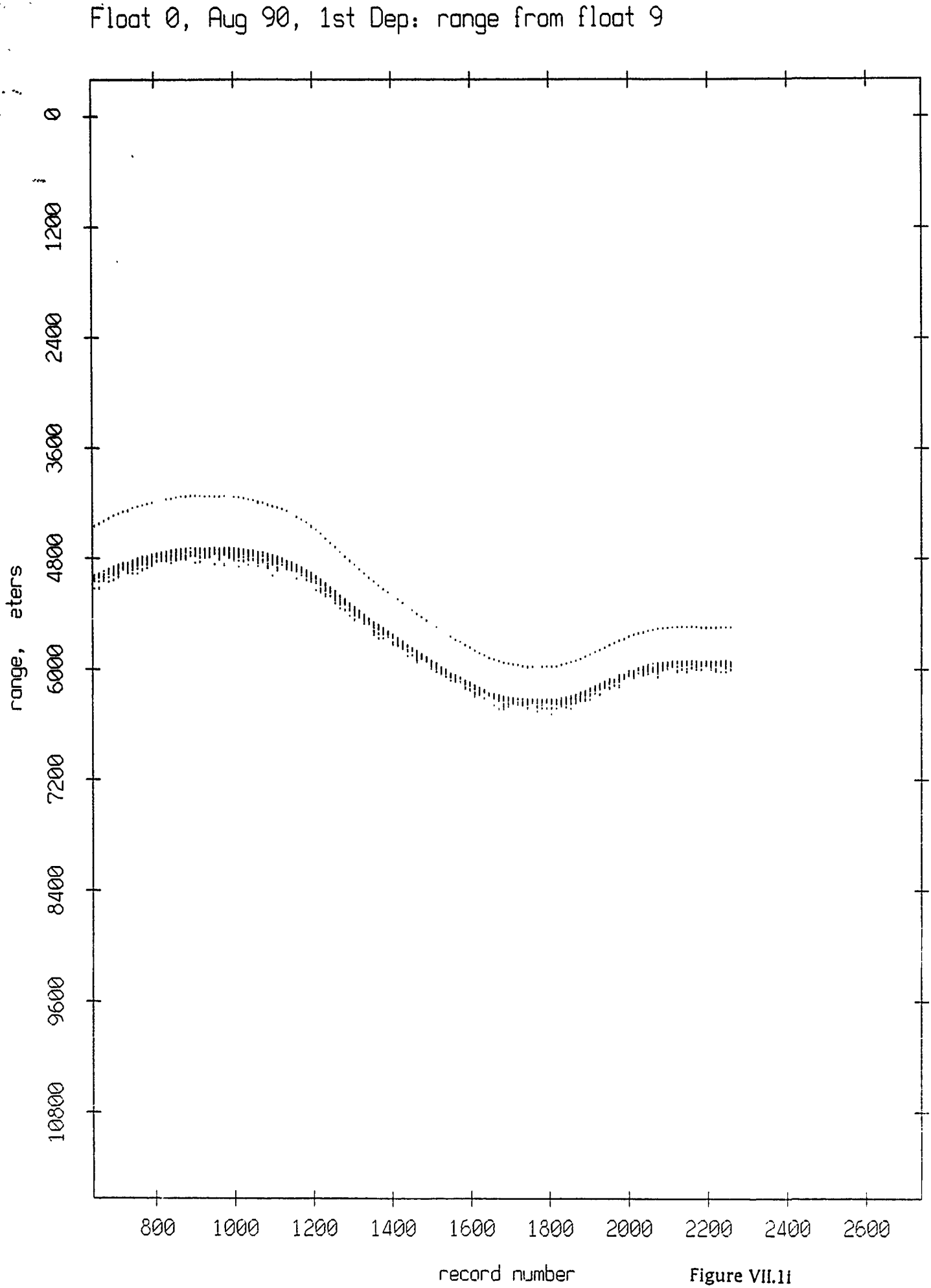

Figure VII.1i

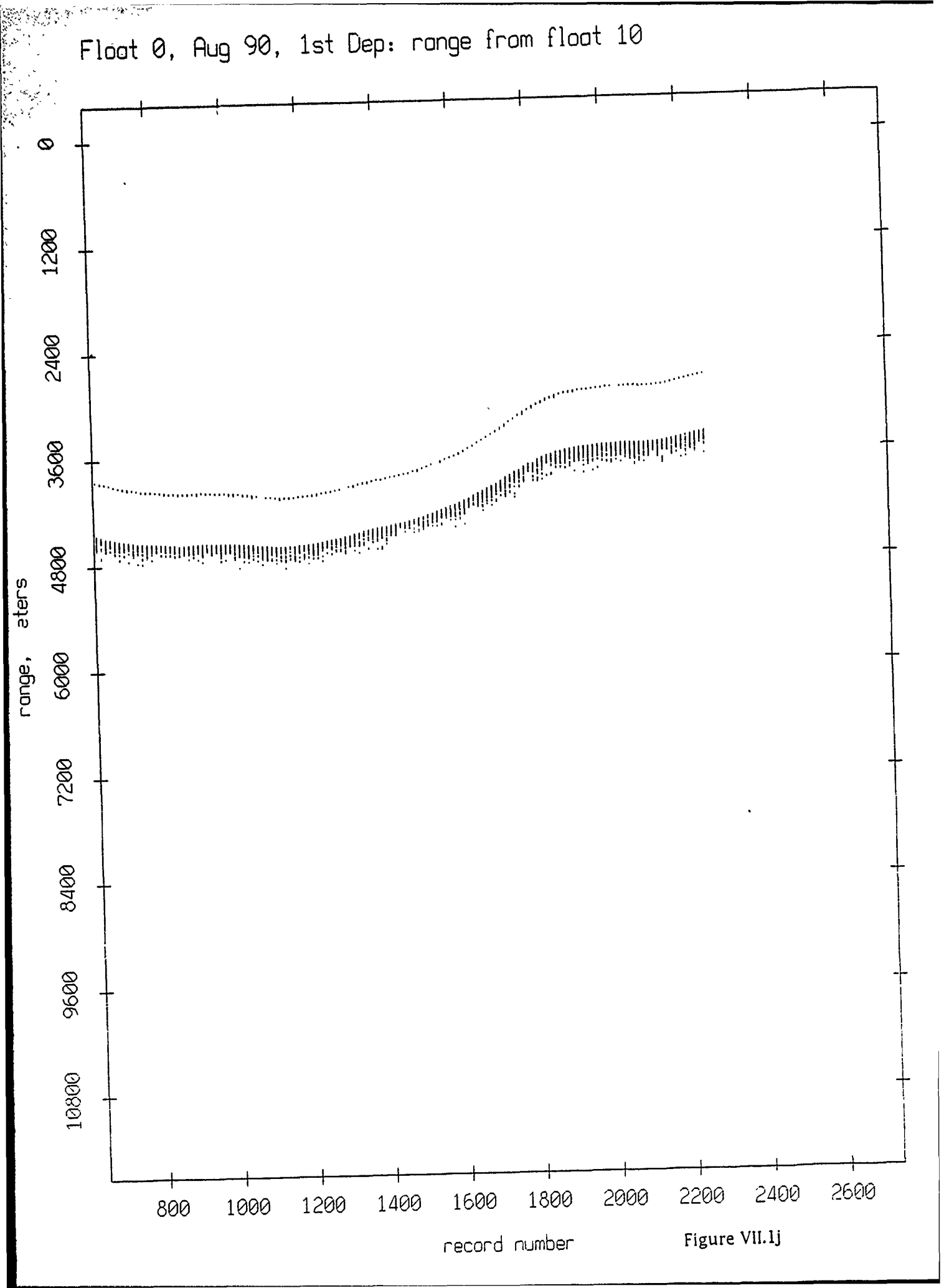

Figure VII.1j

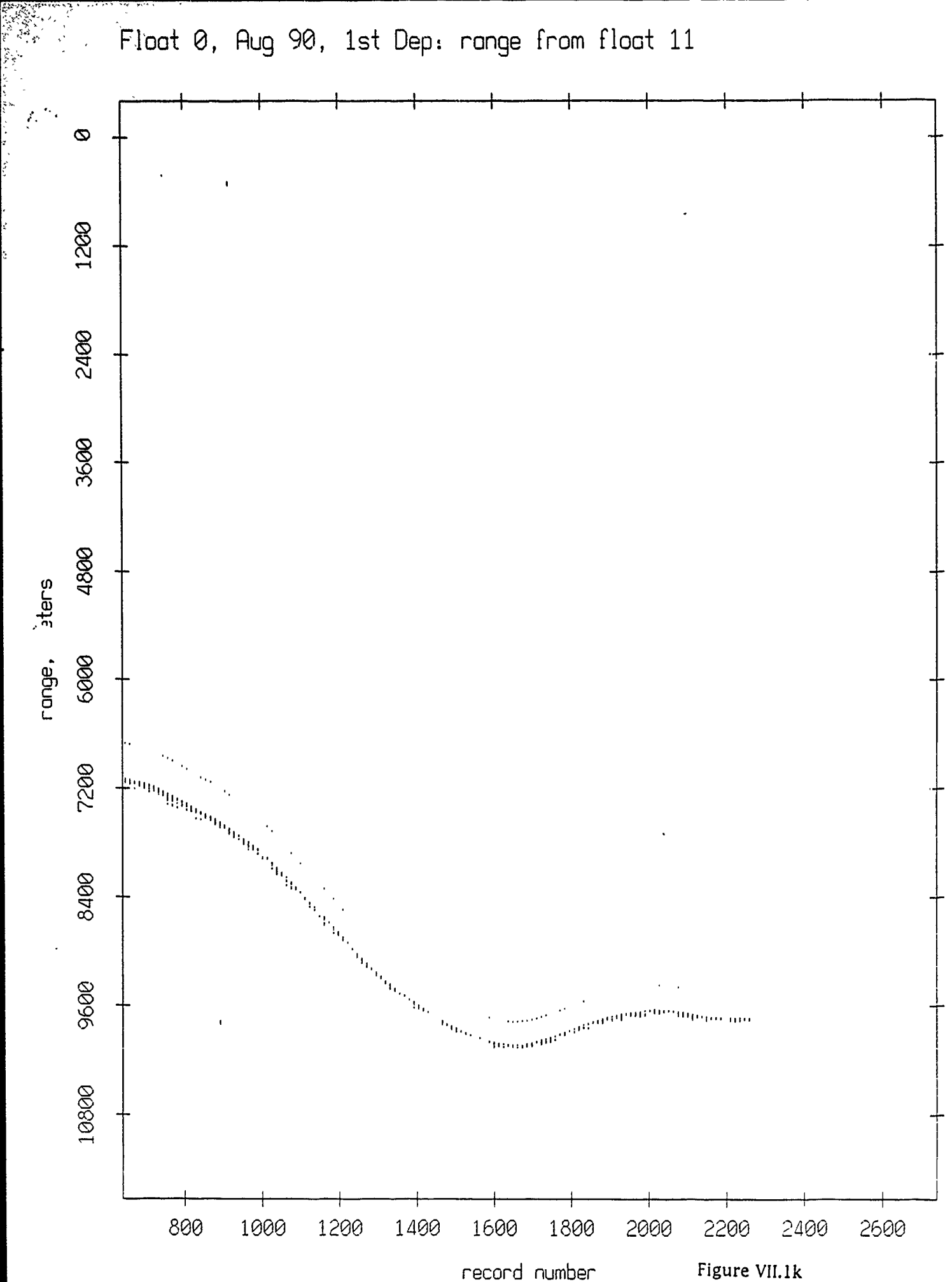

Figure VII.1k

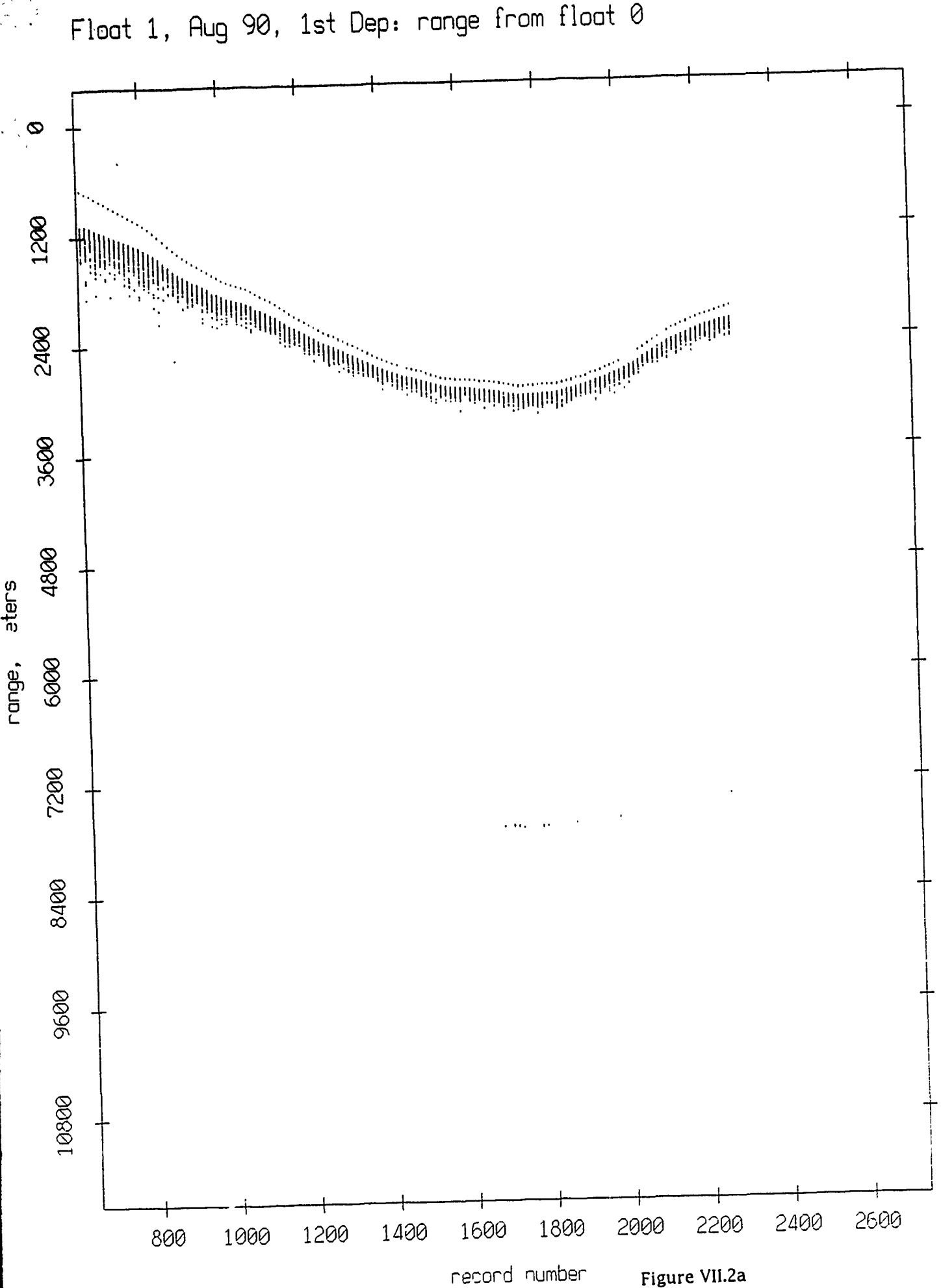

Figure VII.2a

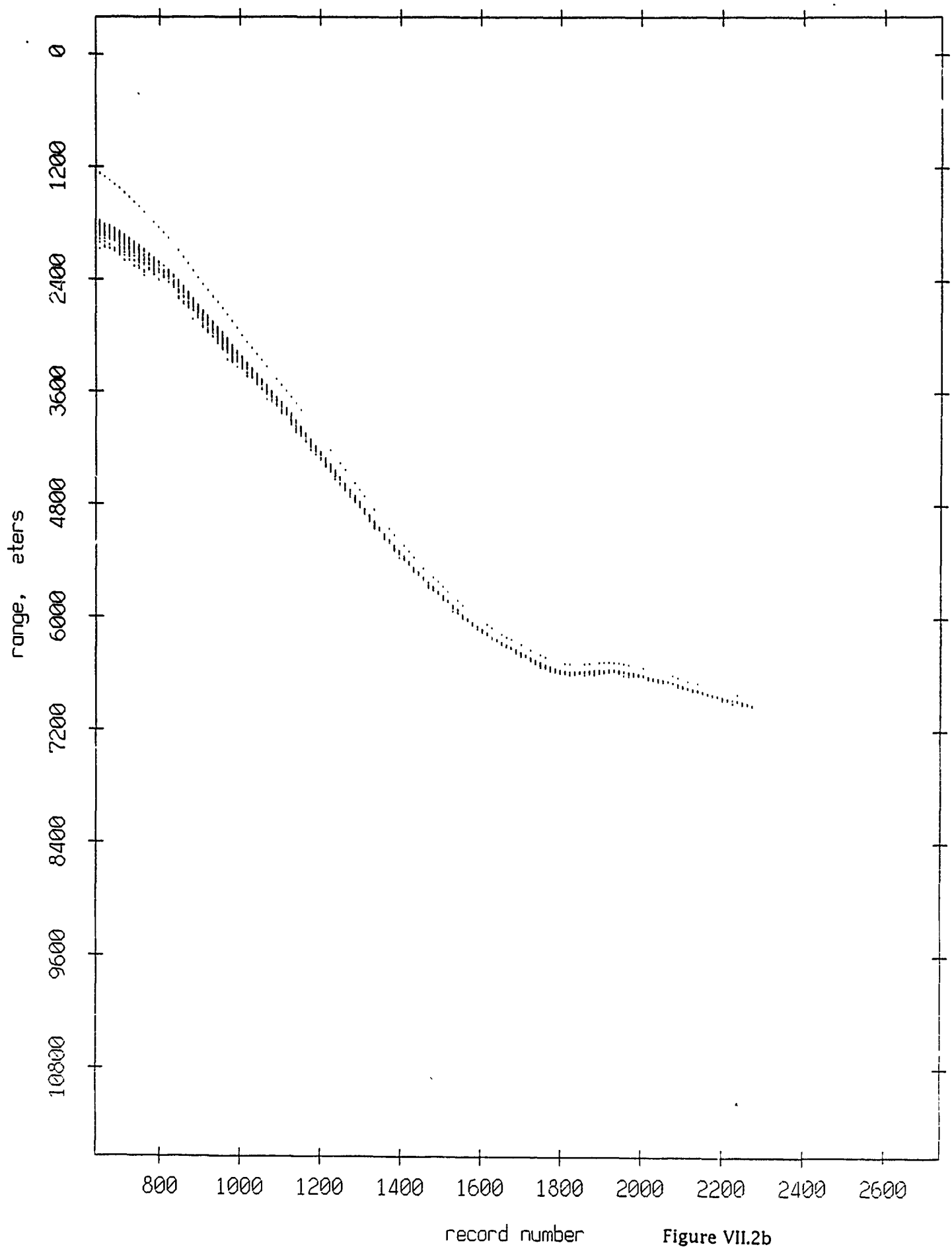

Figure VII.2b

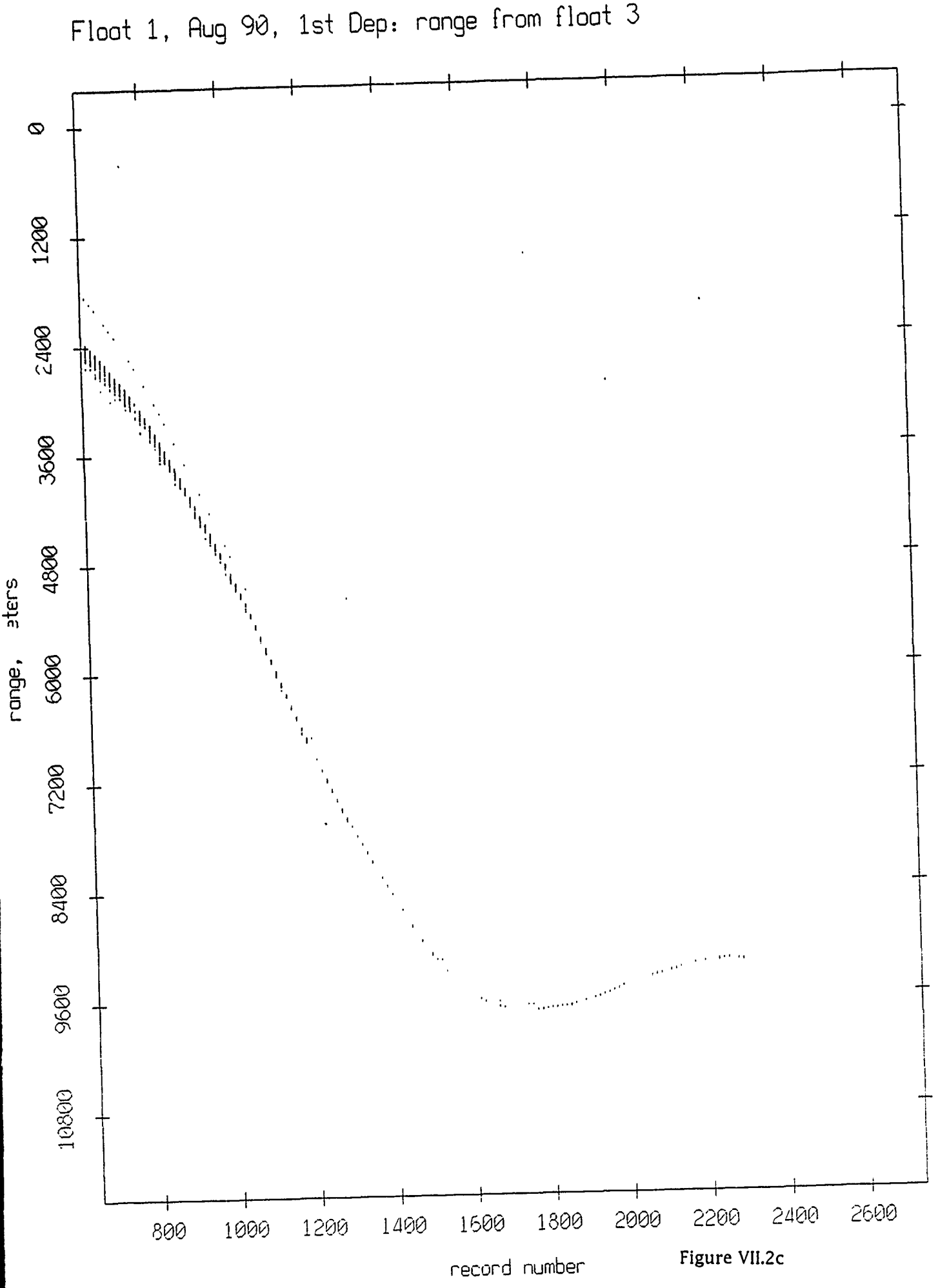

Figure VII.2c

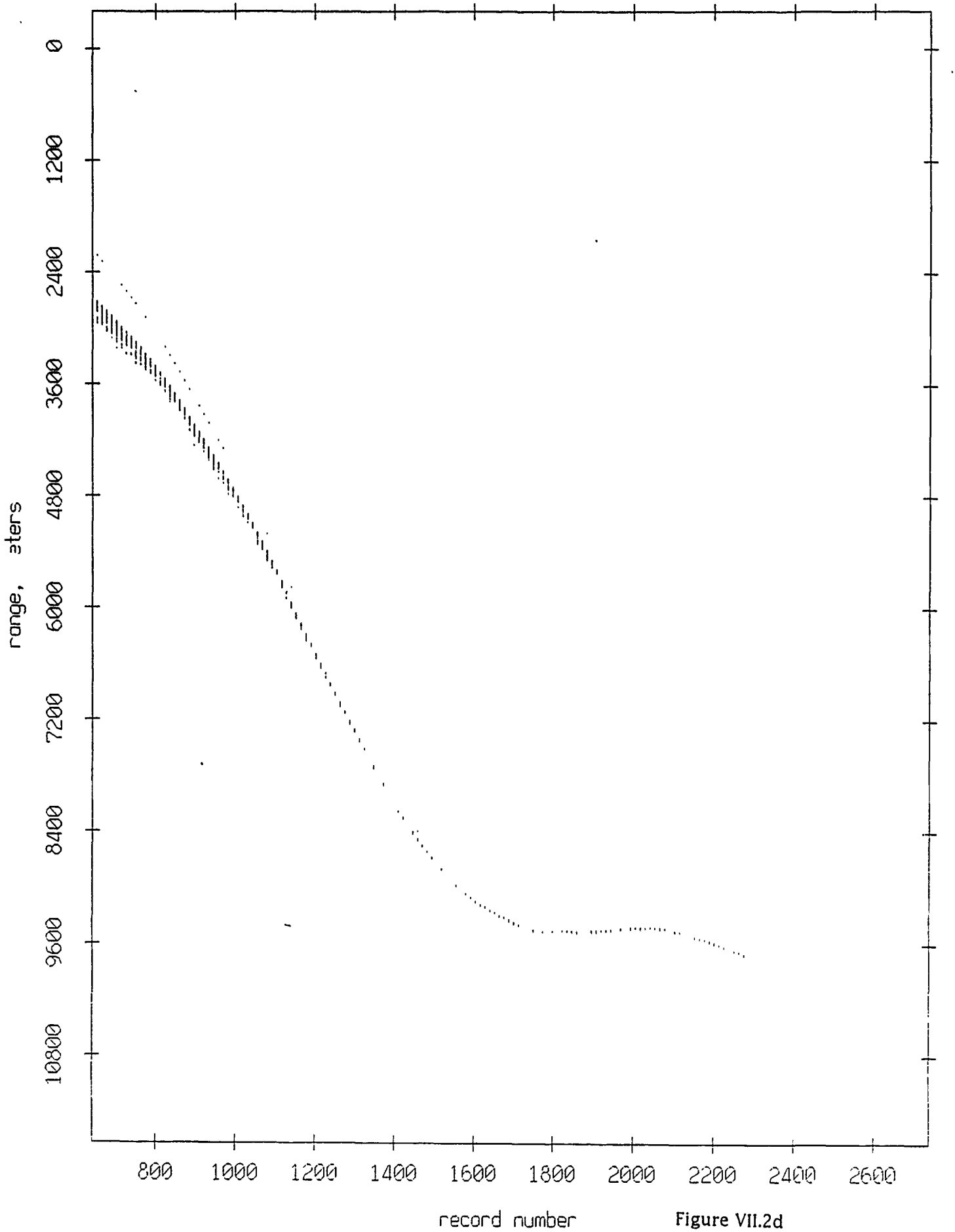

Figure VII.2d

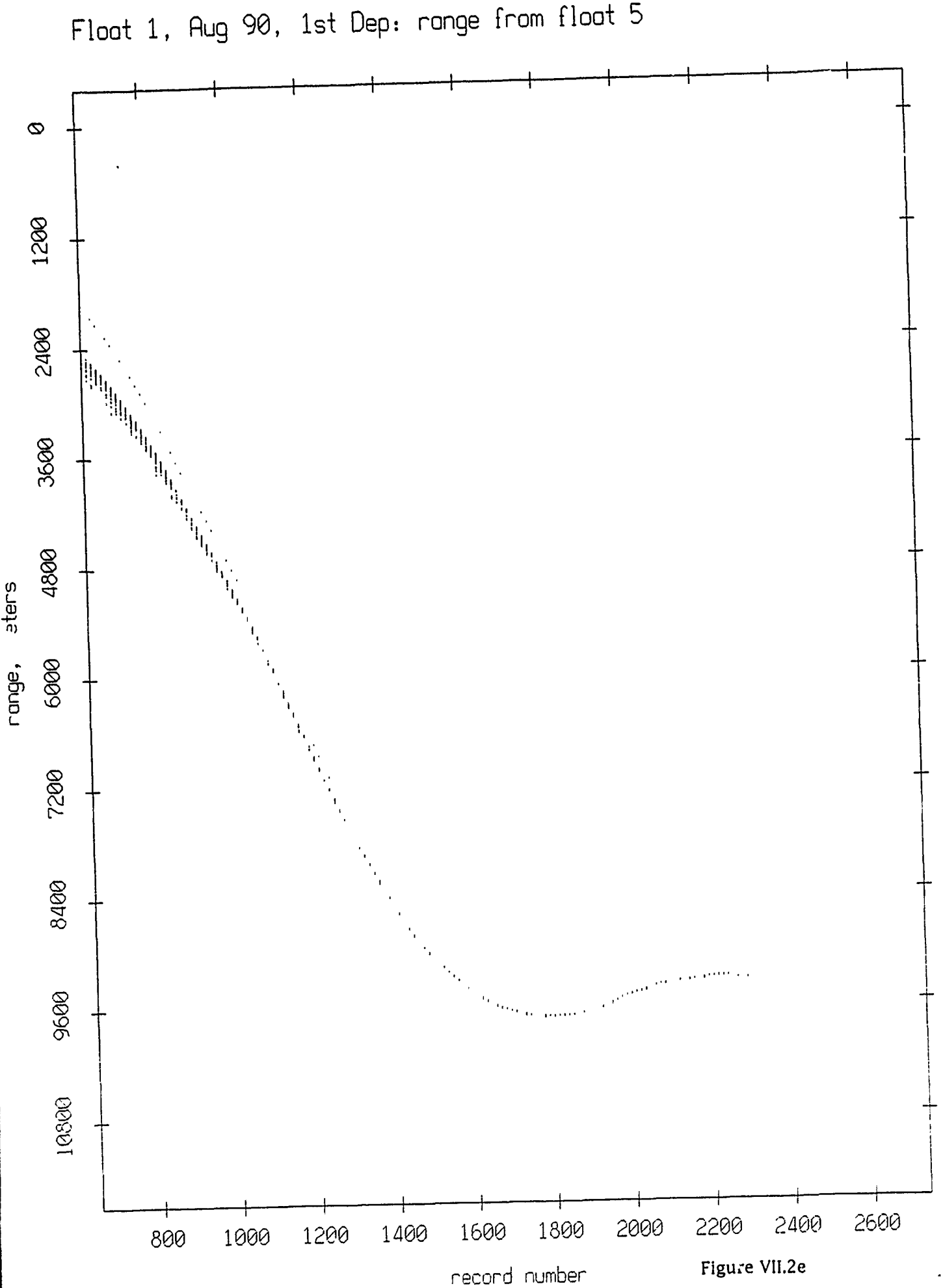

Figure VII.2e

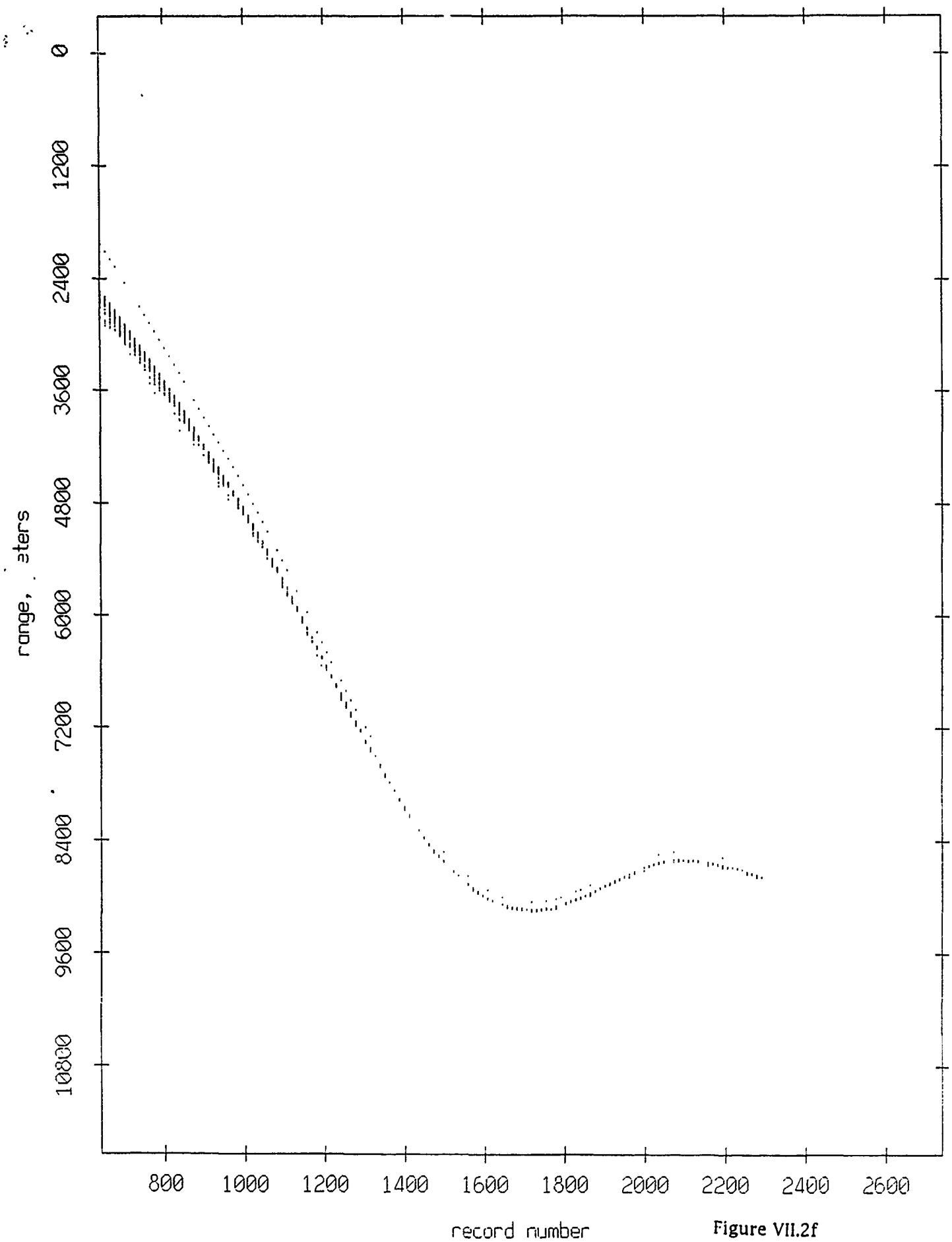

Figure VII.2f

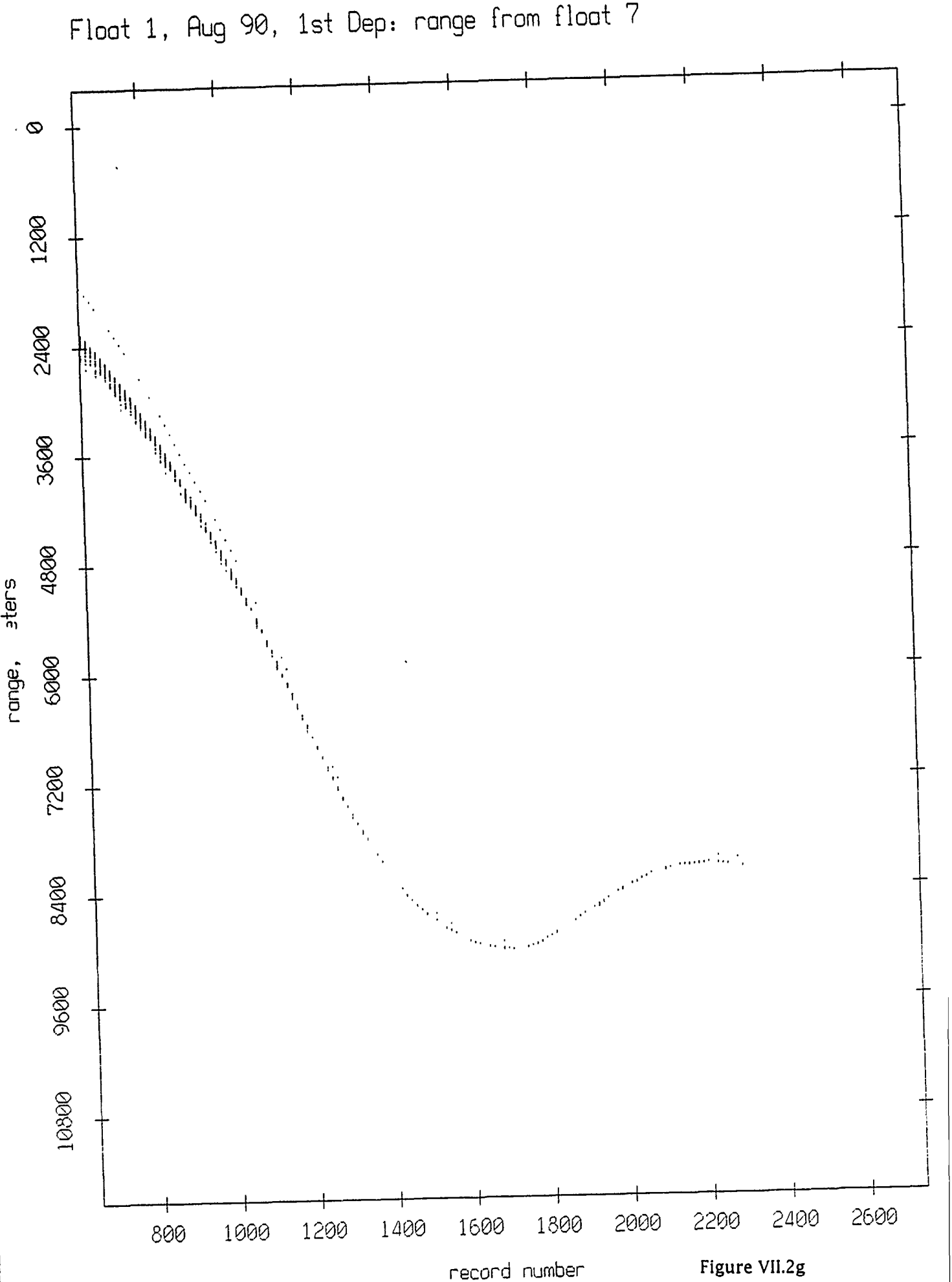

Figure VII.2g

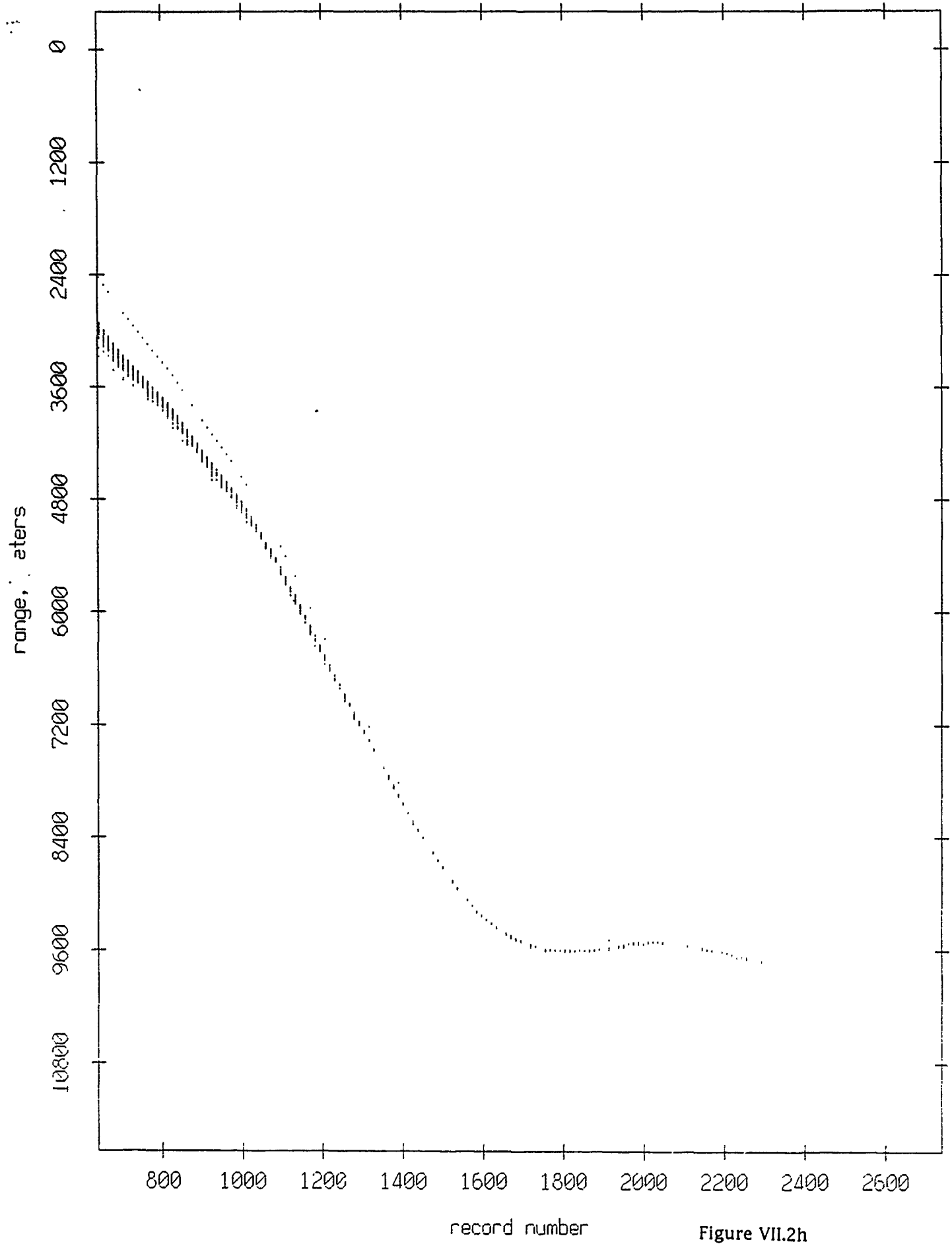

Figure VII.2h

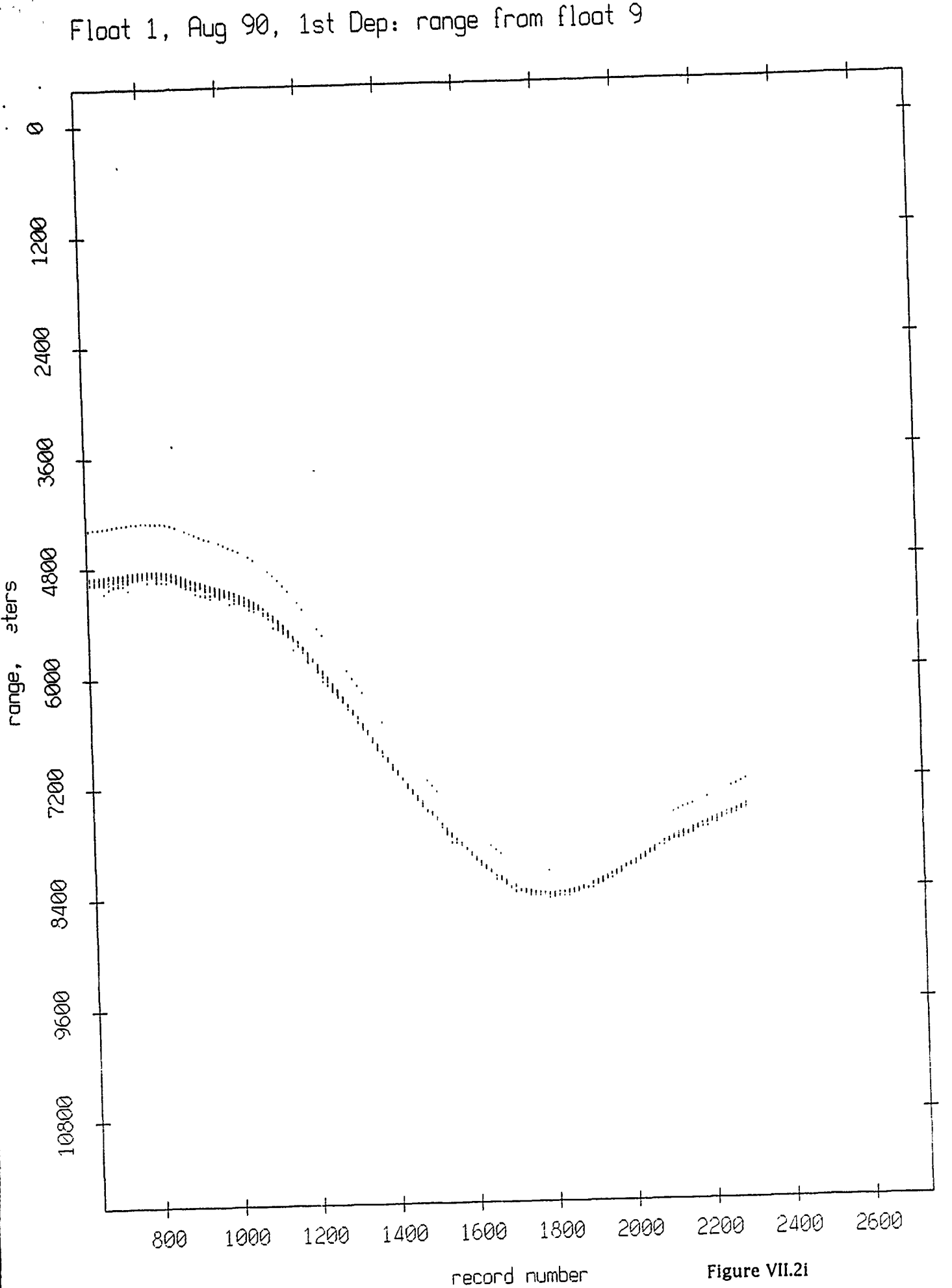

Figure VII.2i

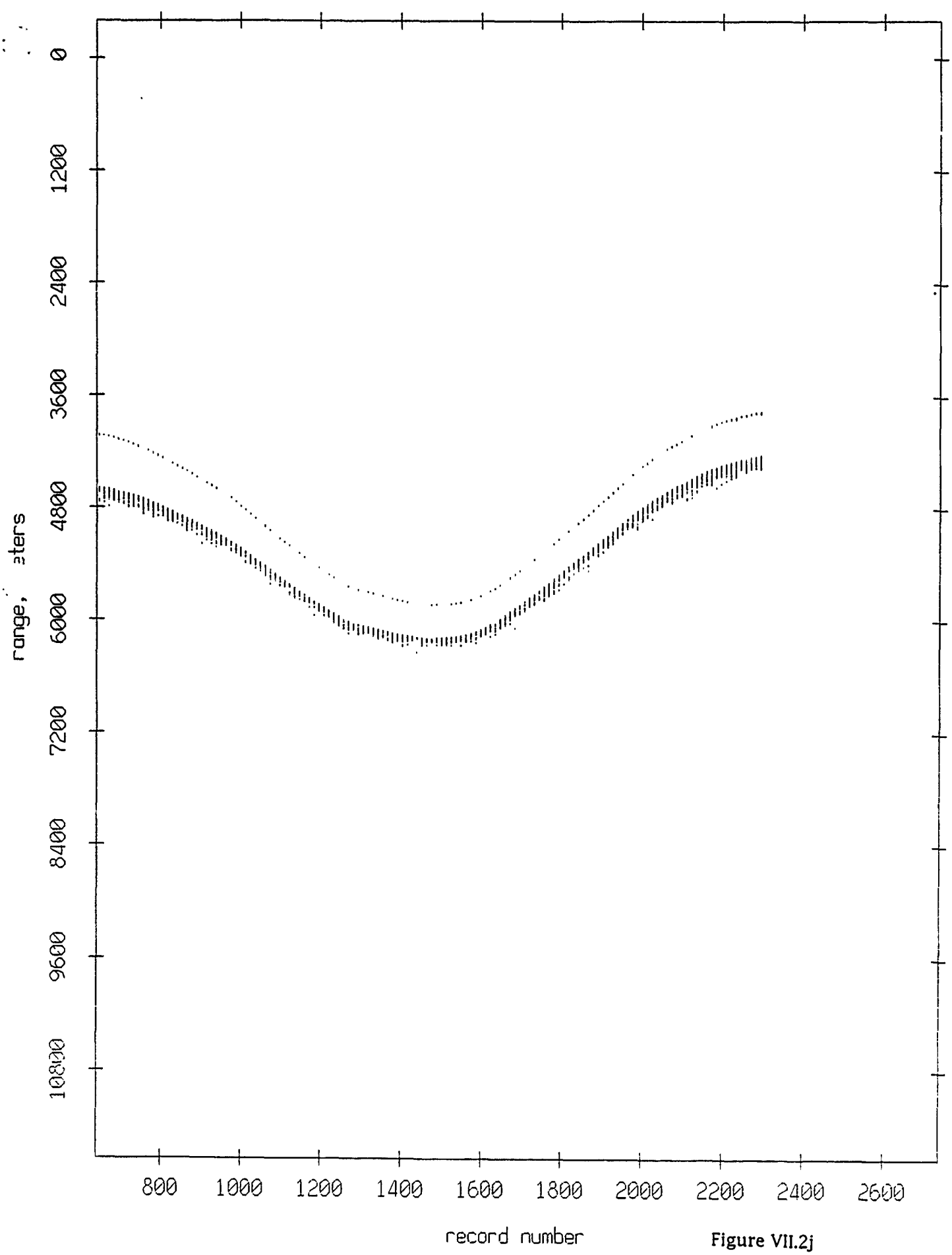

Figure VII.2j

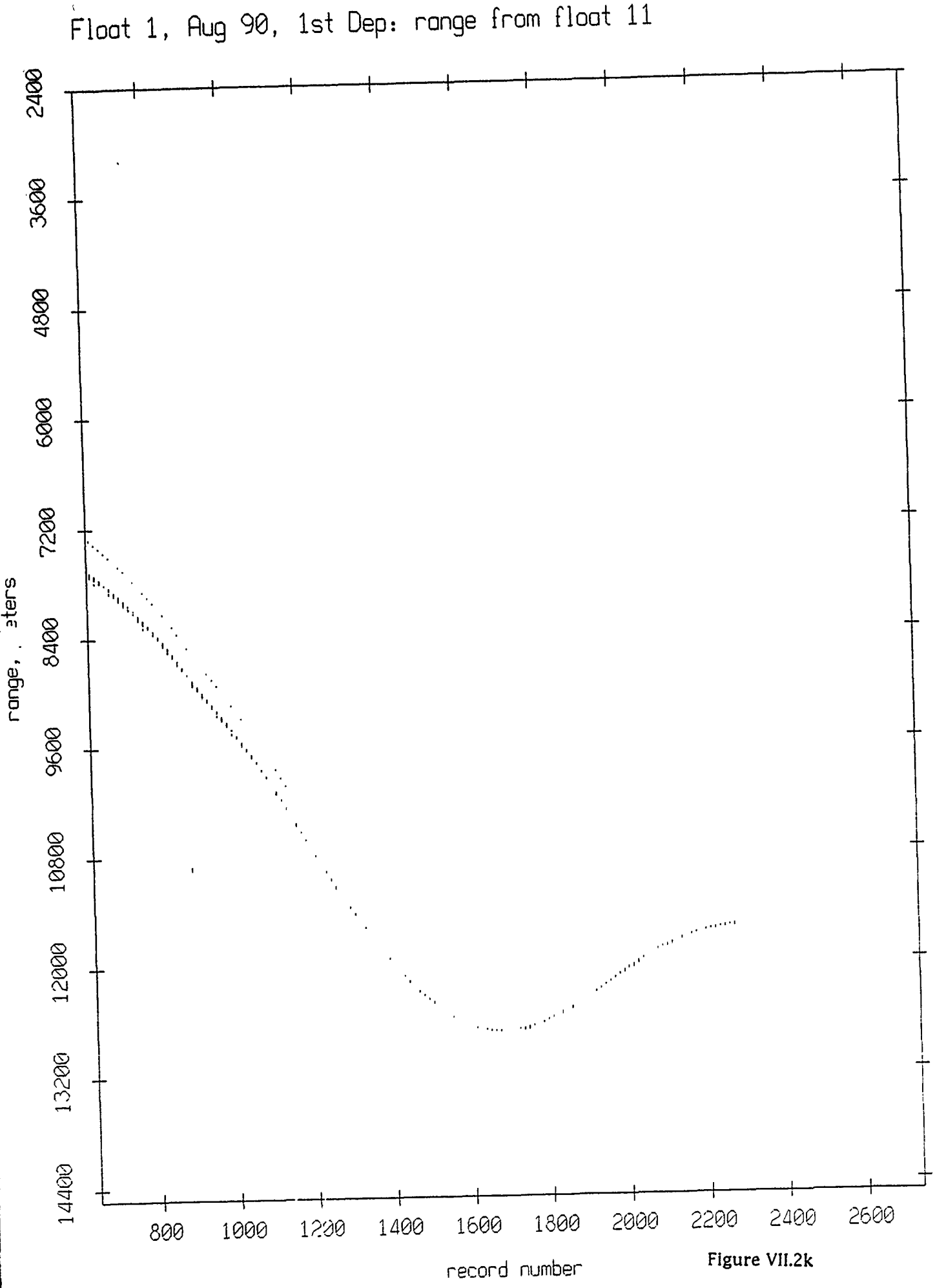

Figure VII.2k

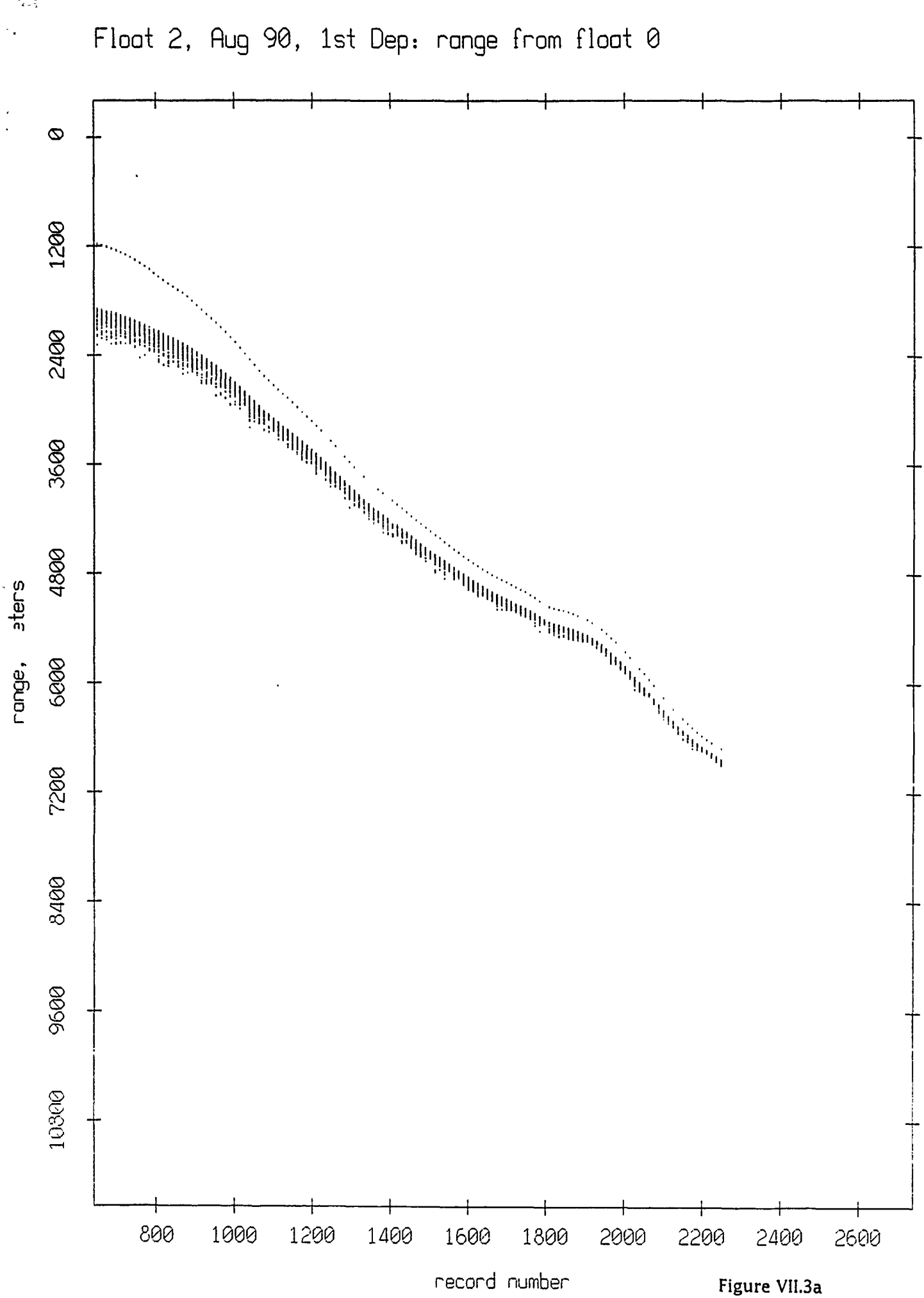

Figure VII.3a

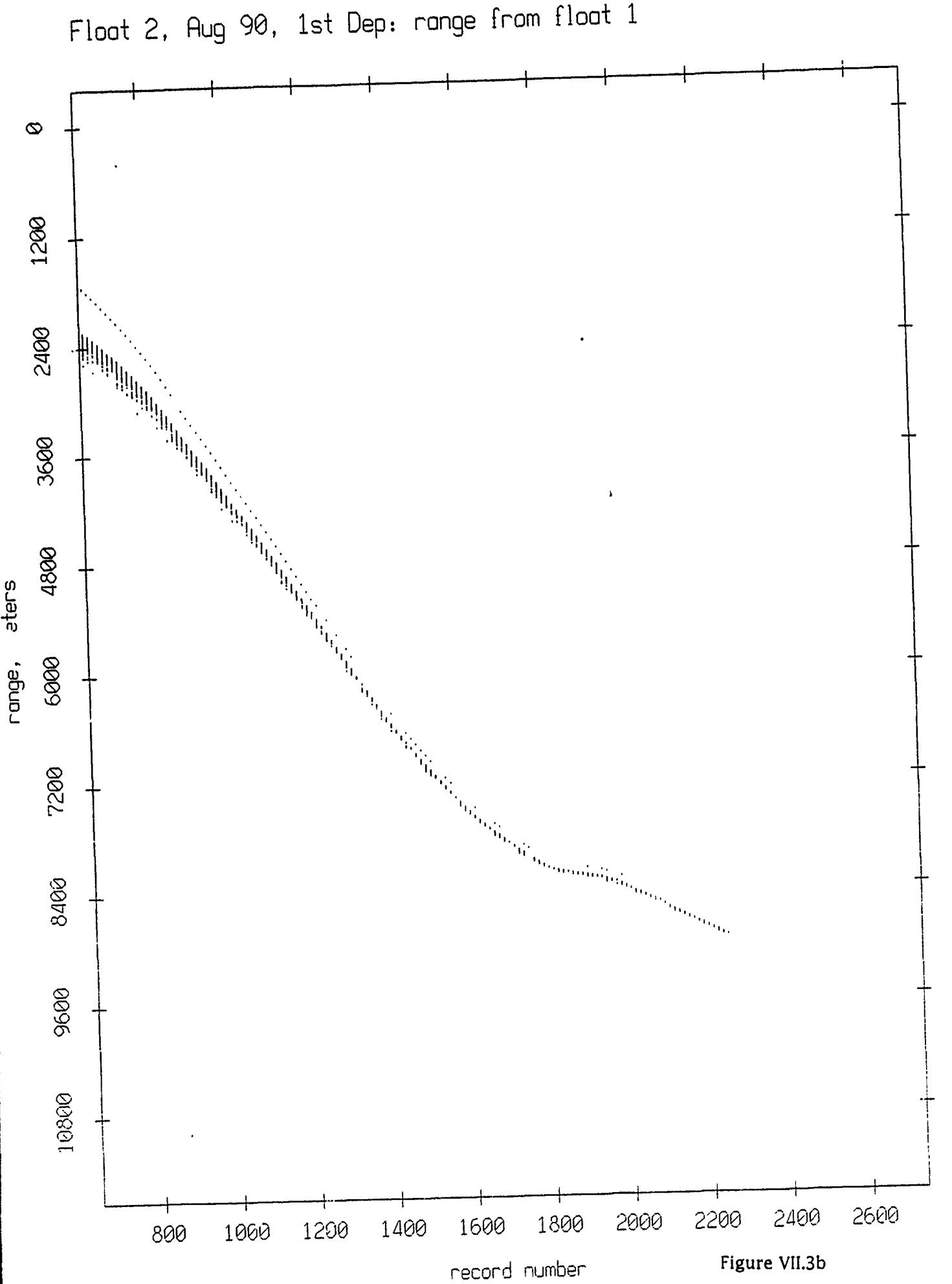

Figure VII.3b

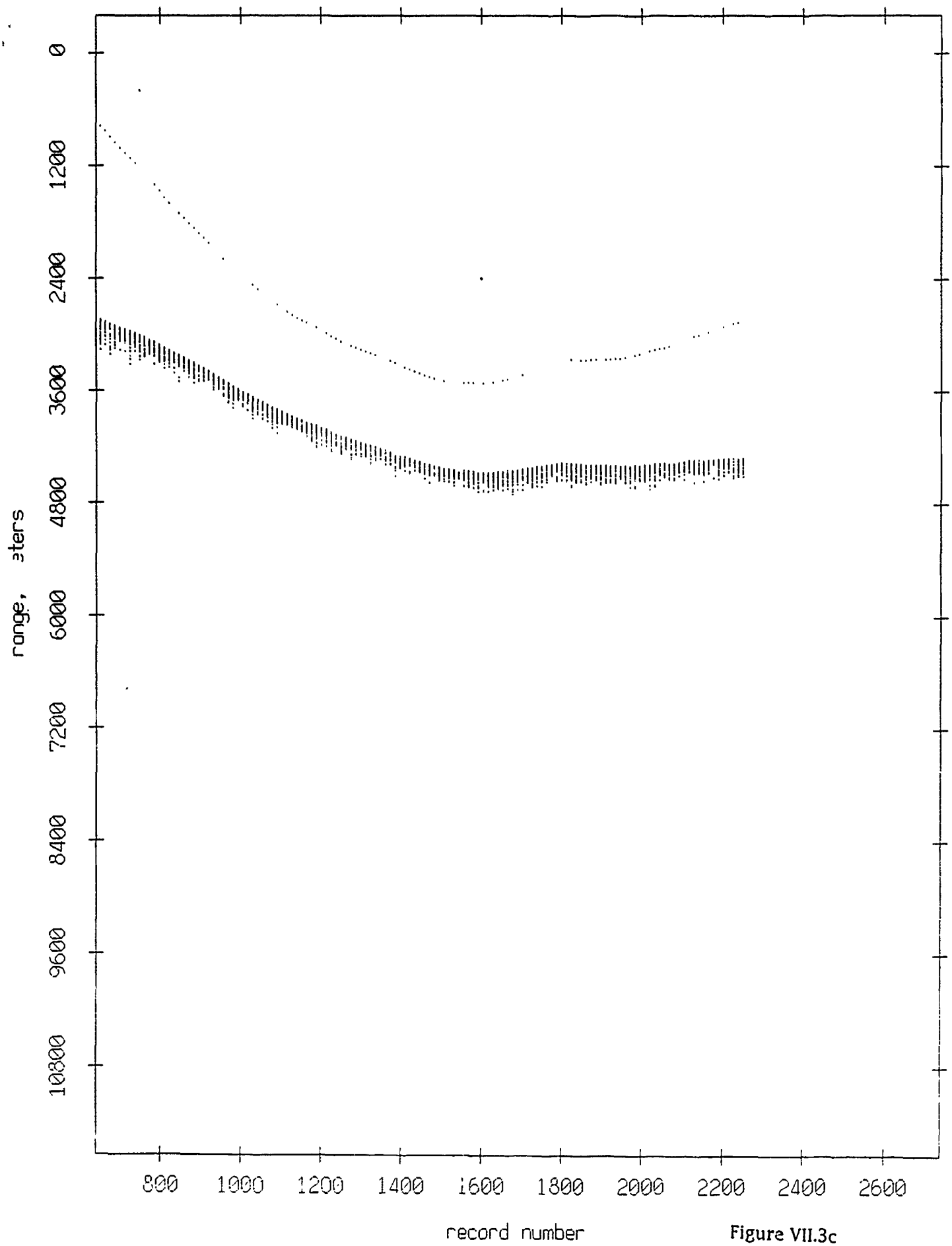

Figure VII.3c

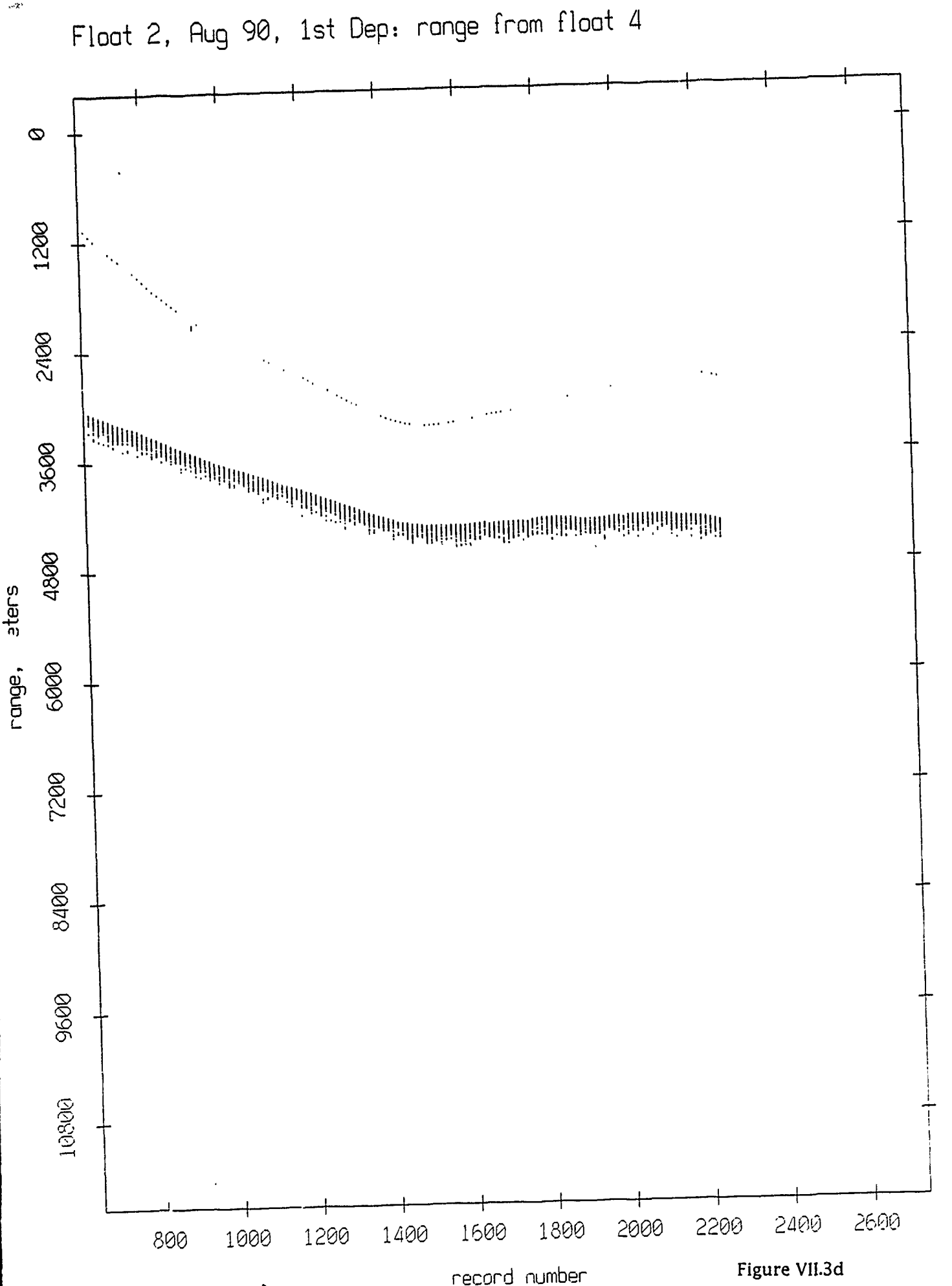

Figure VII.3d

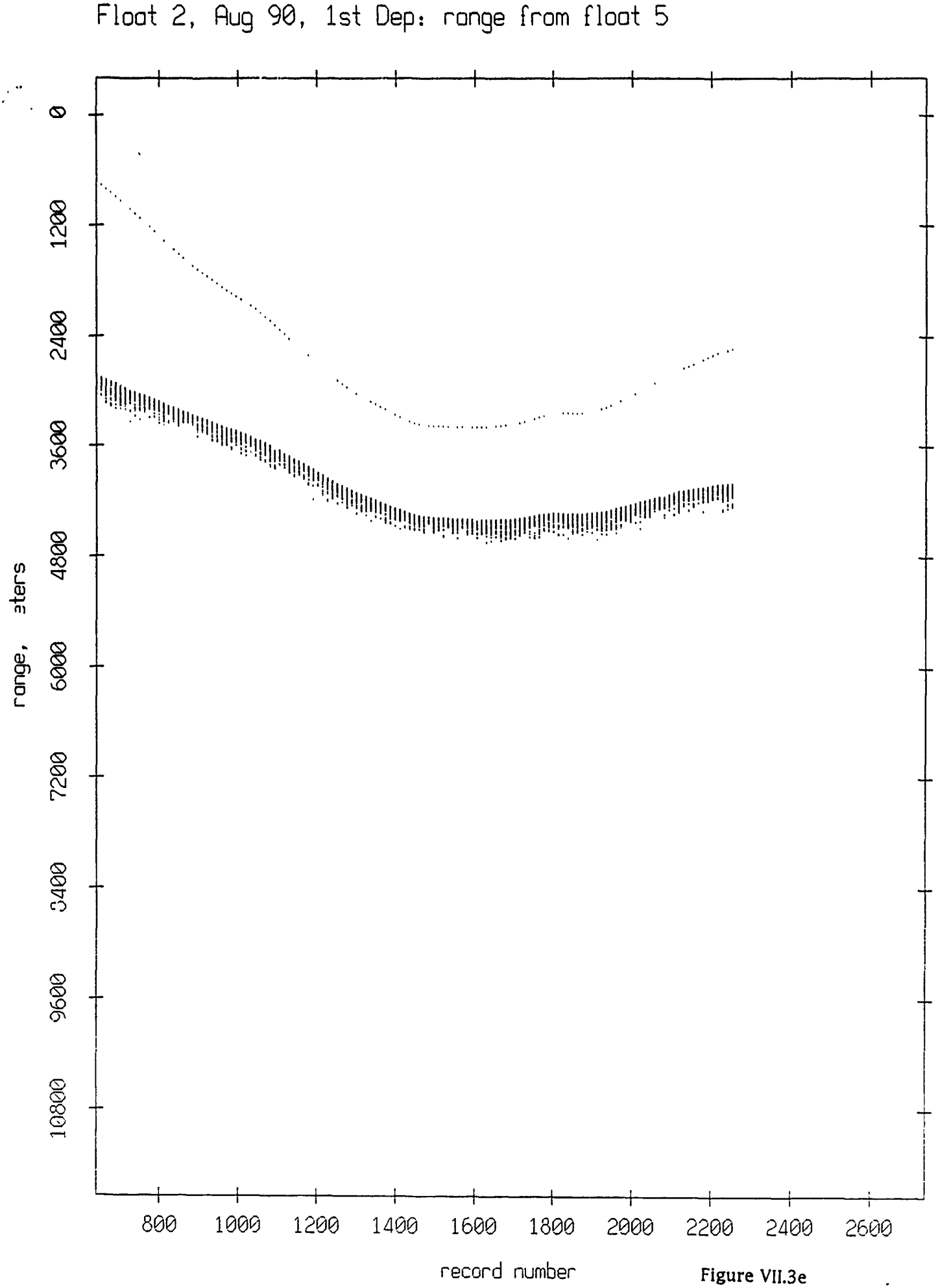

Figure VII.3e

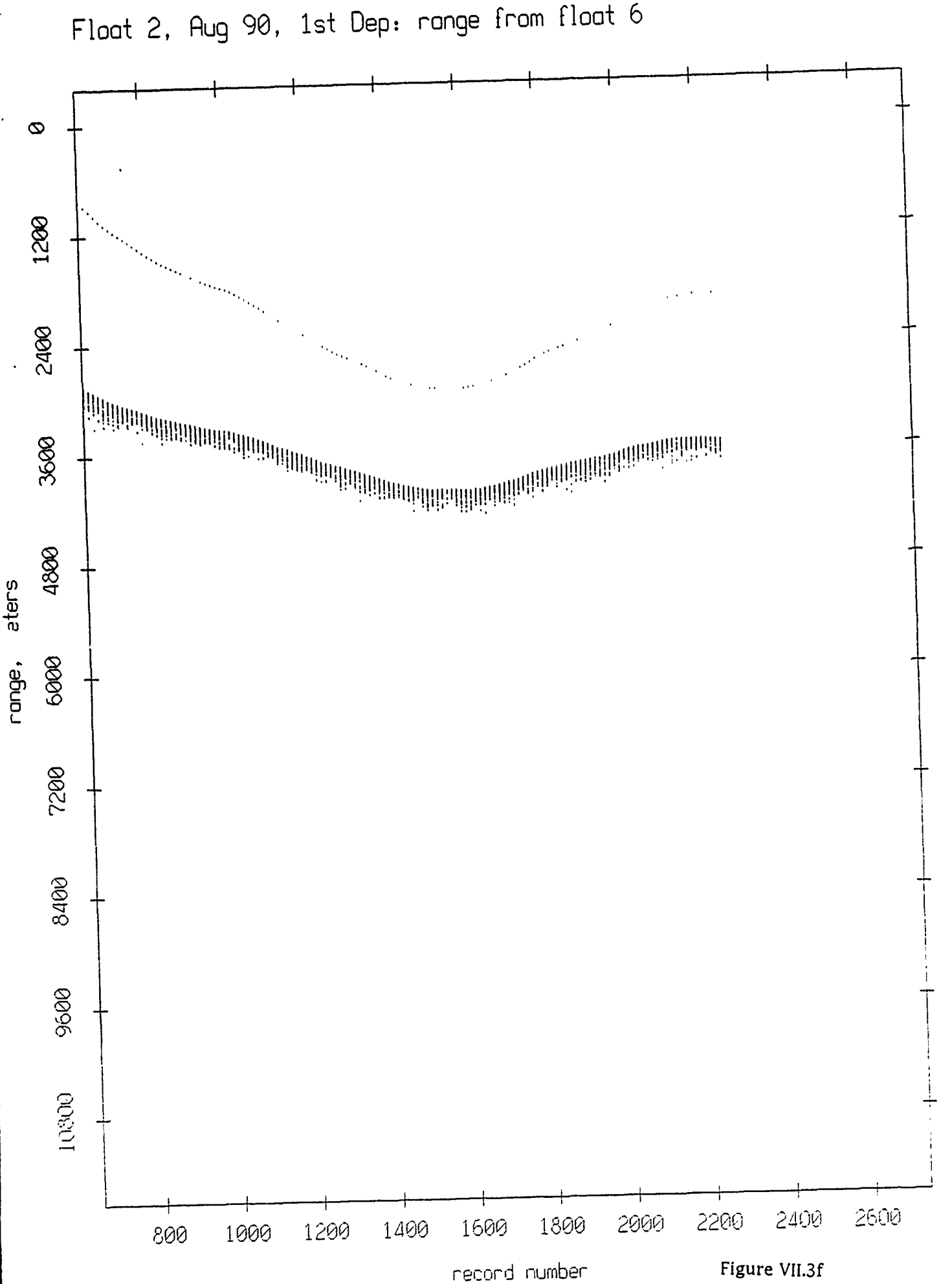

Figure VII.3f

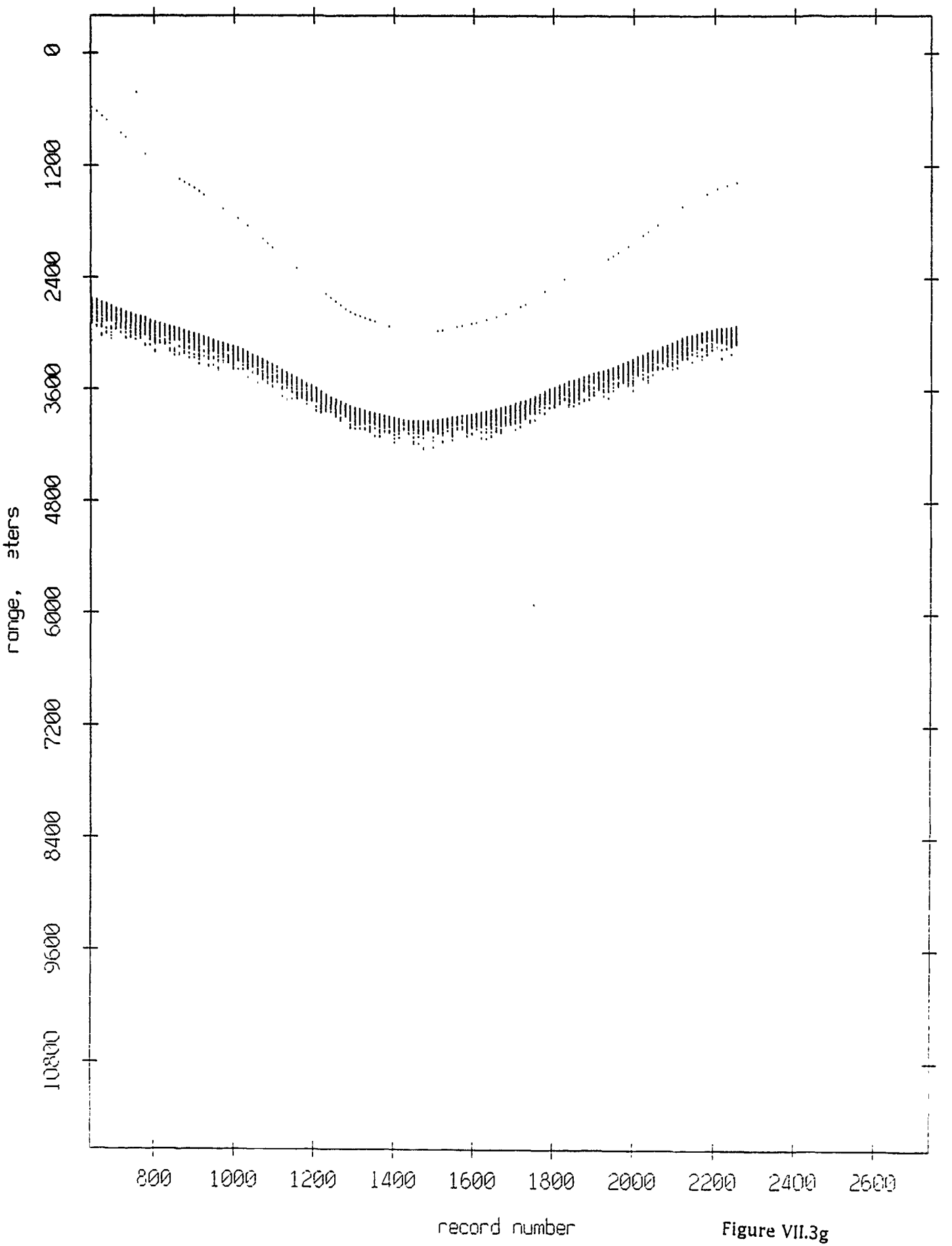

Figure VII.3g

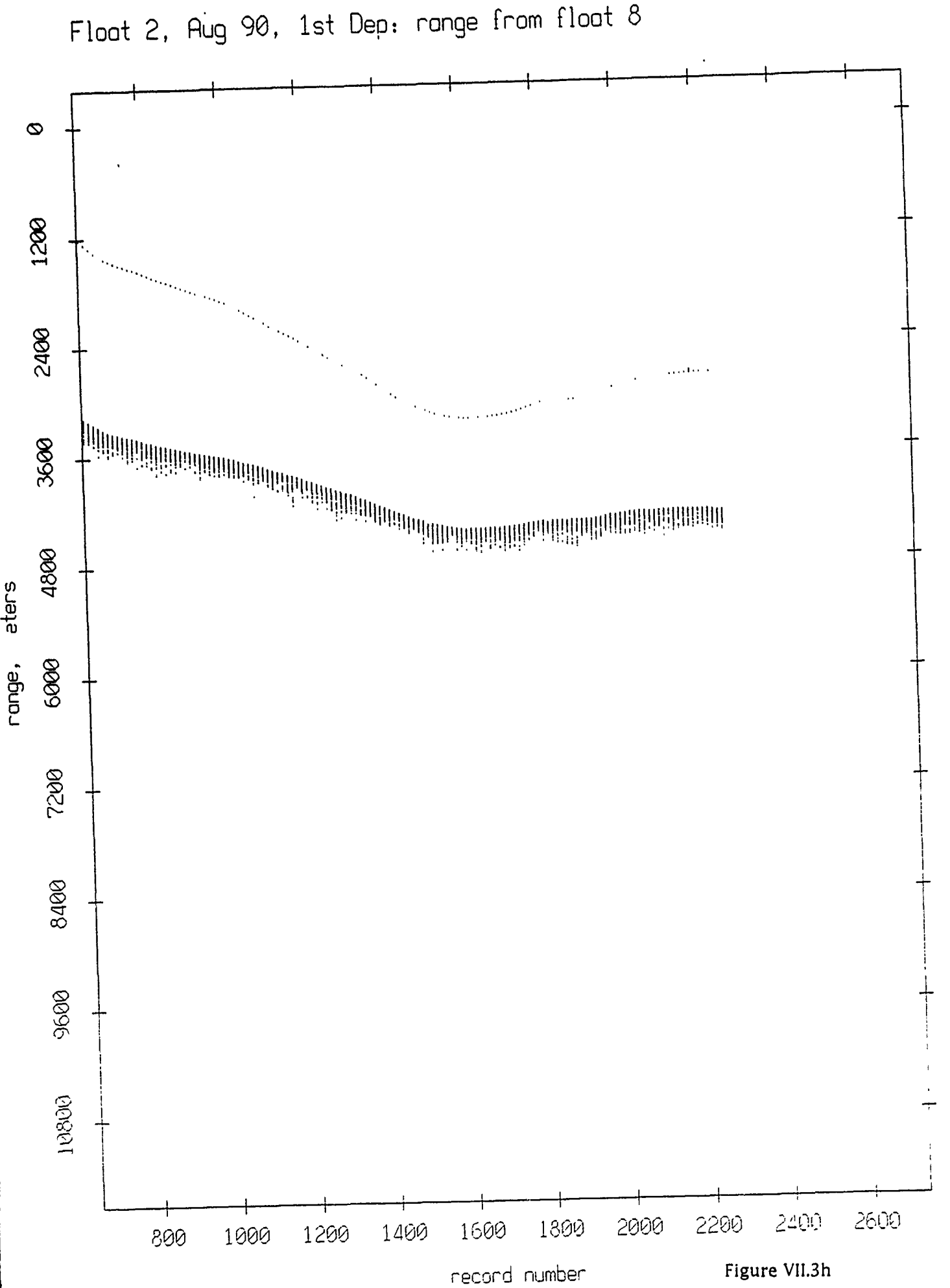

Figure VII.3h

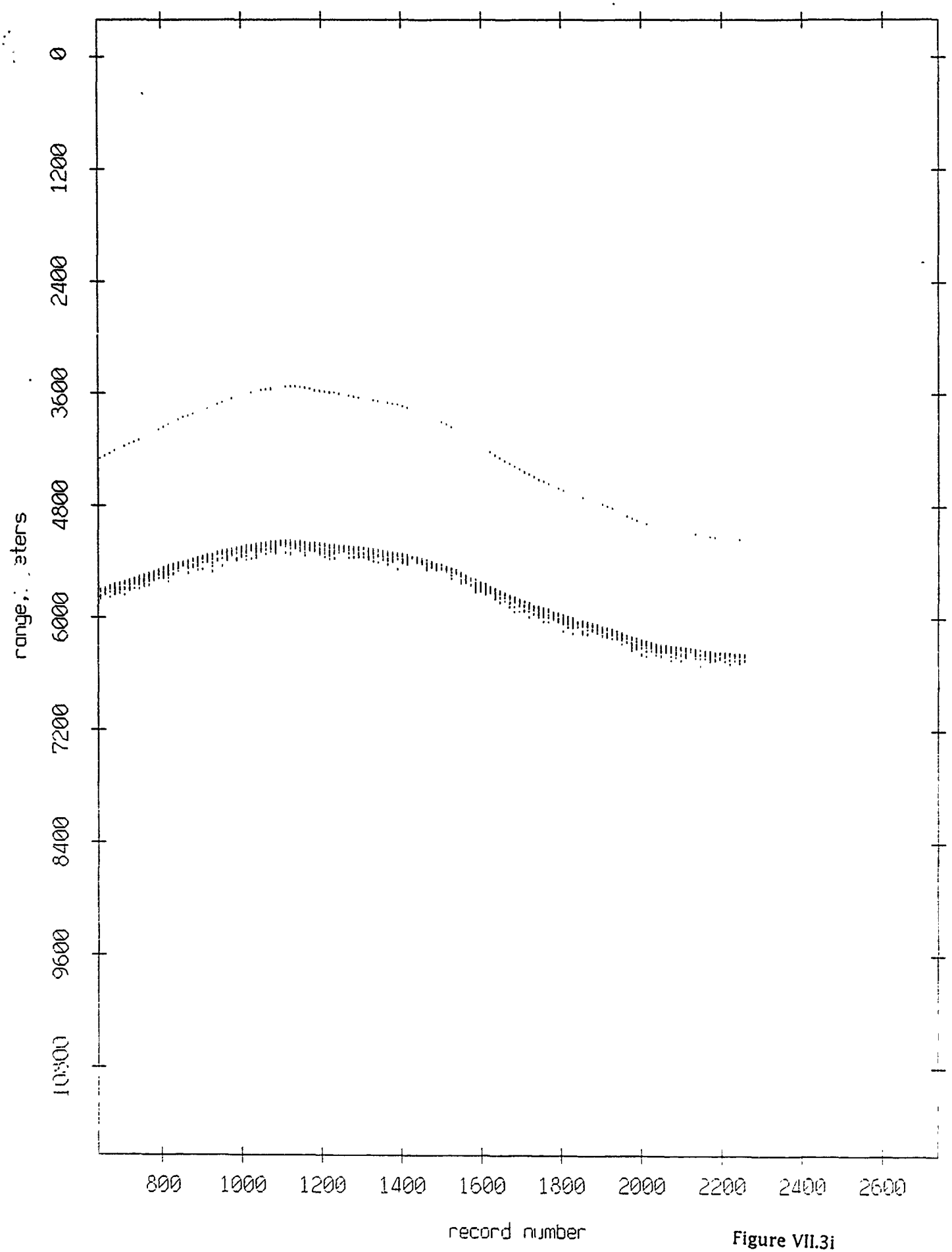

Figure VII.3i

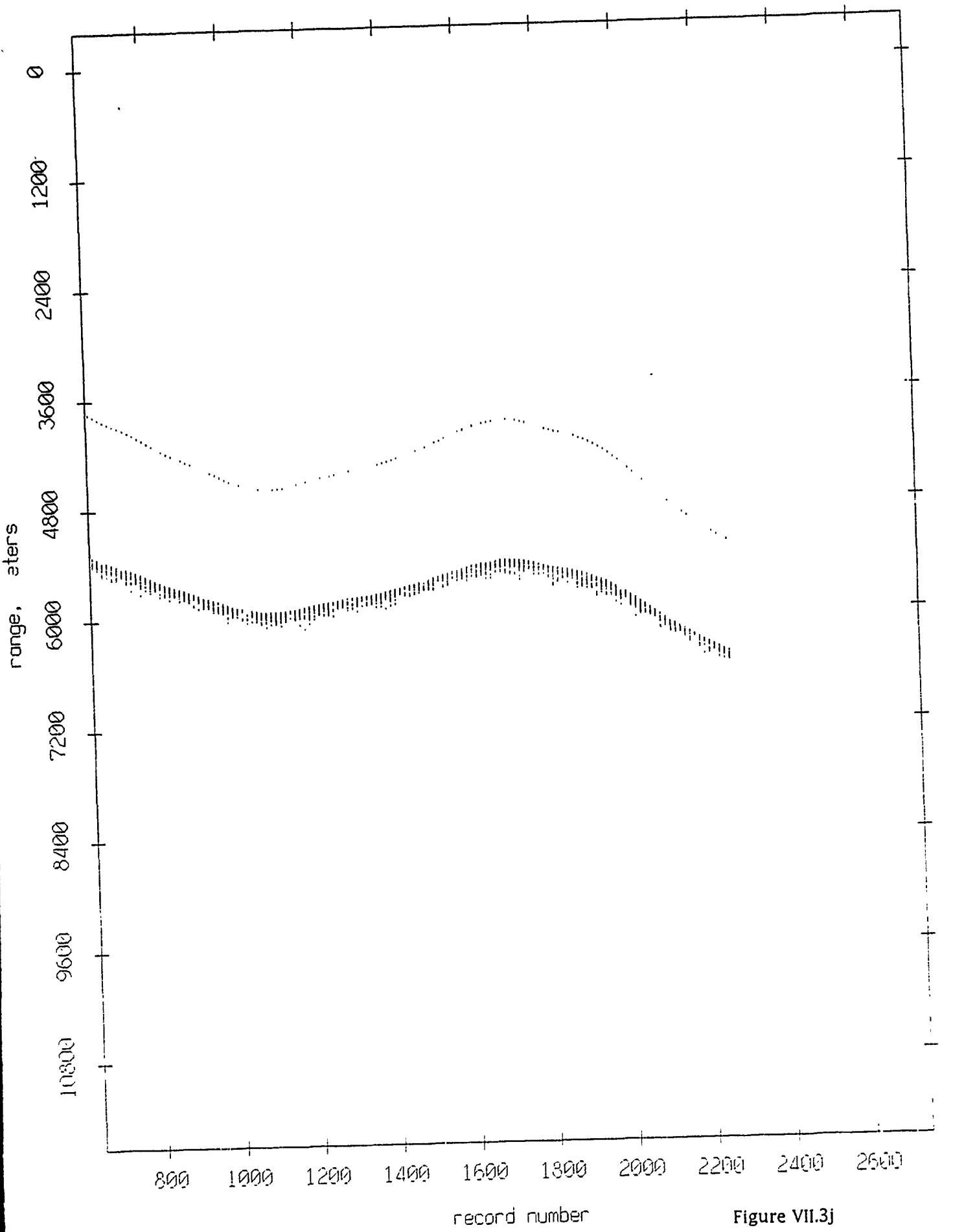

Figure VII.3j

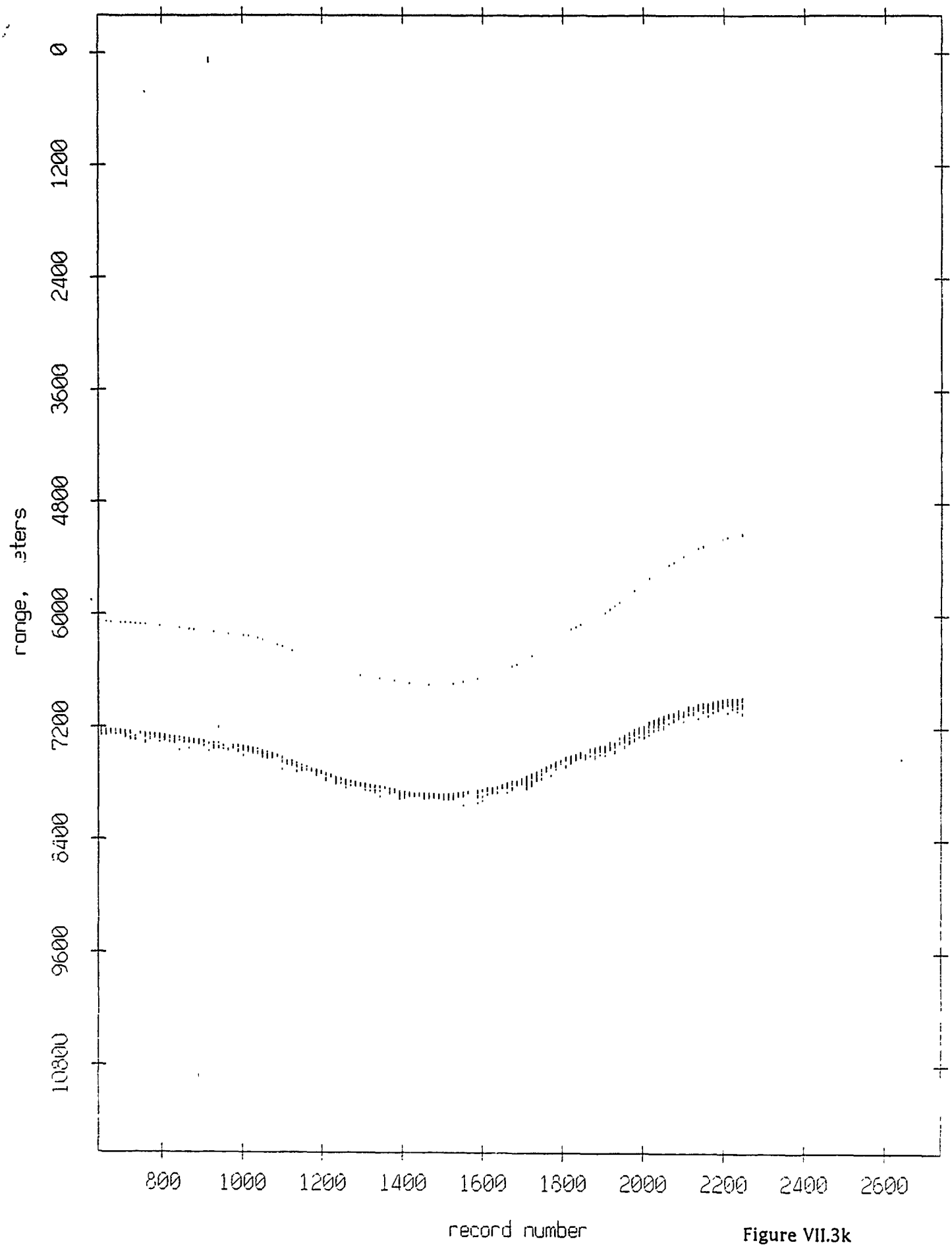

Figure VII.3k

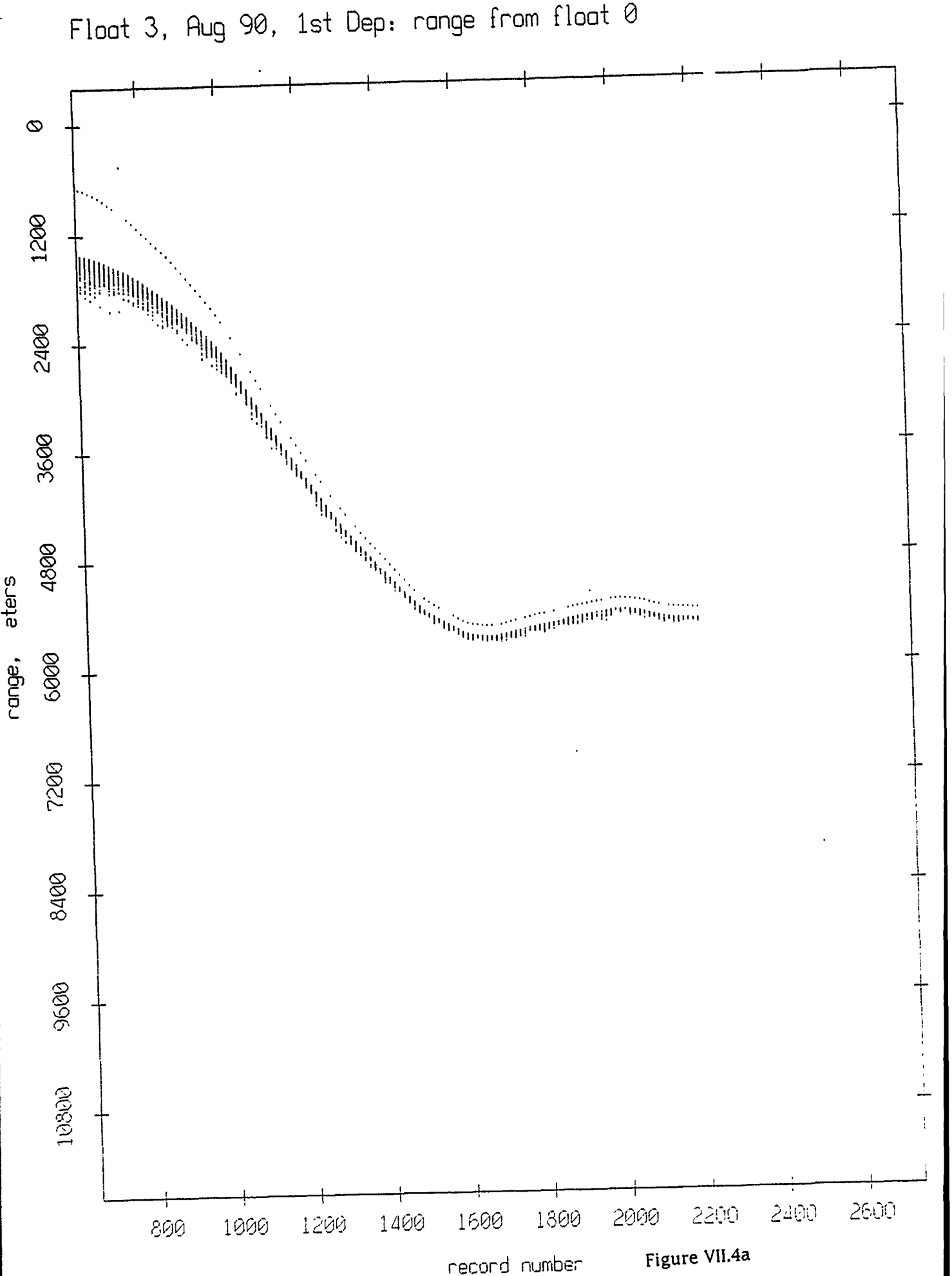

Figure VII.4a

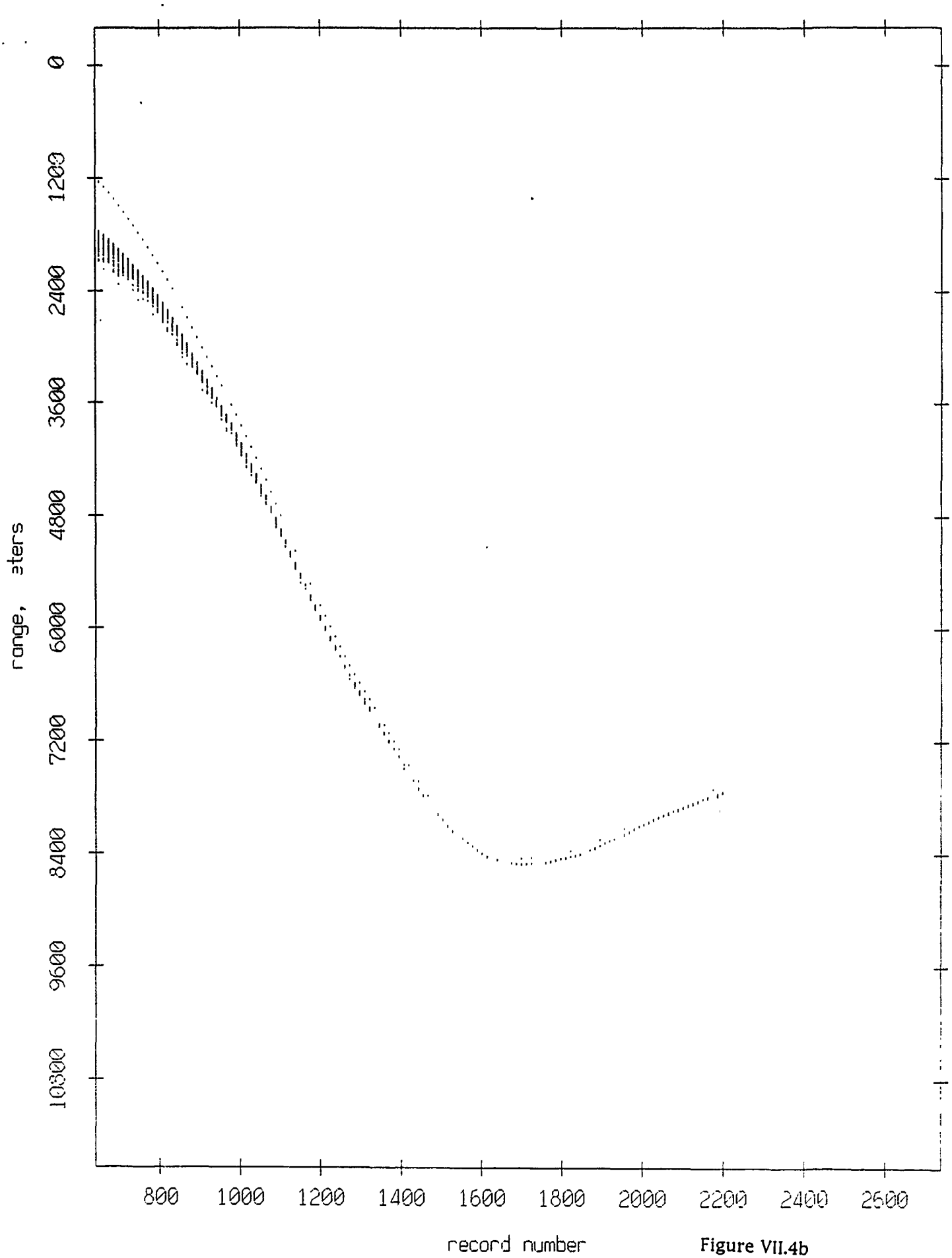

Figure VII.4b

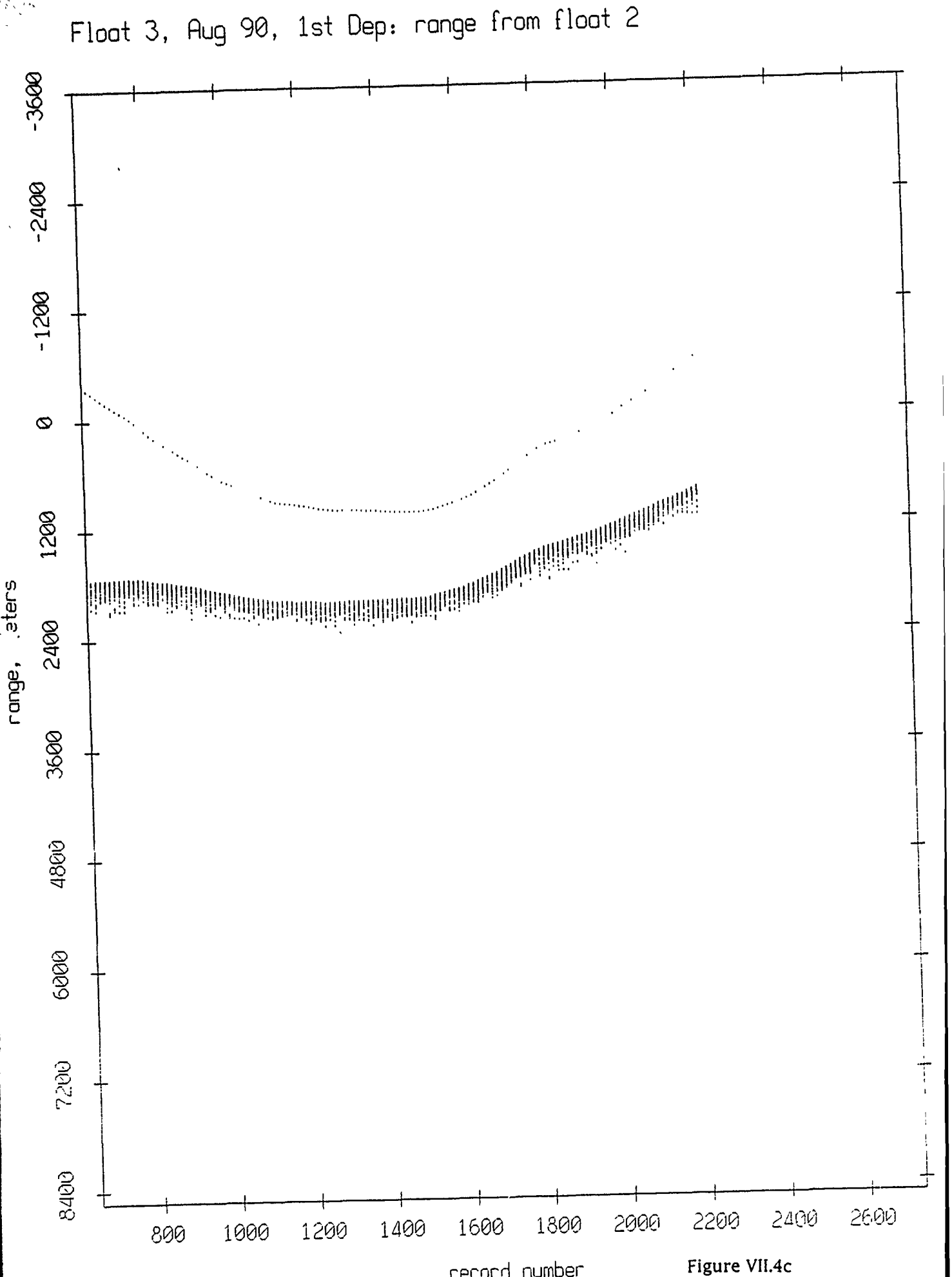

Figure VII.4c

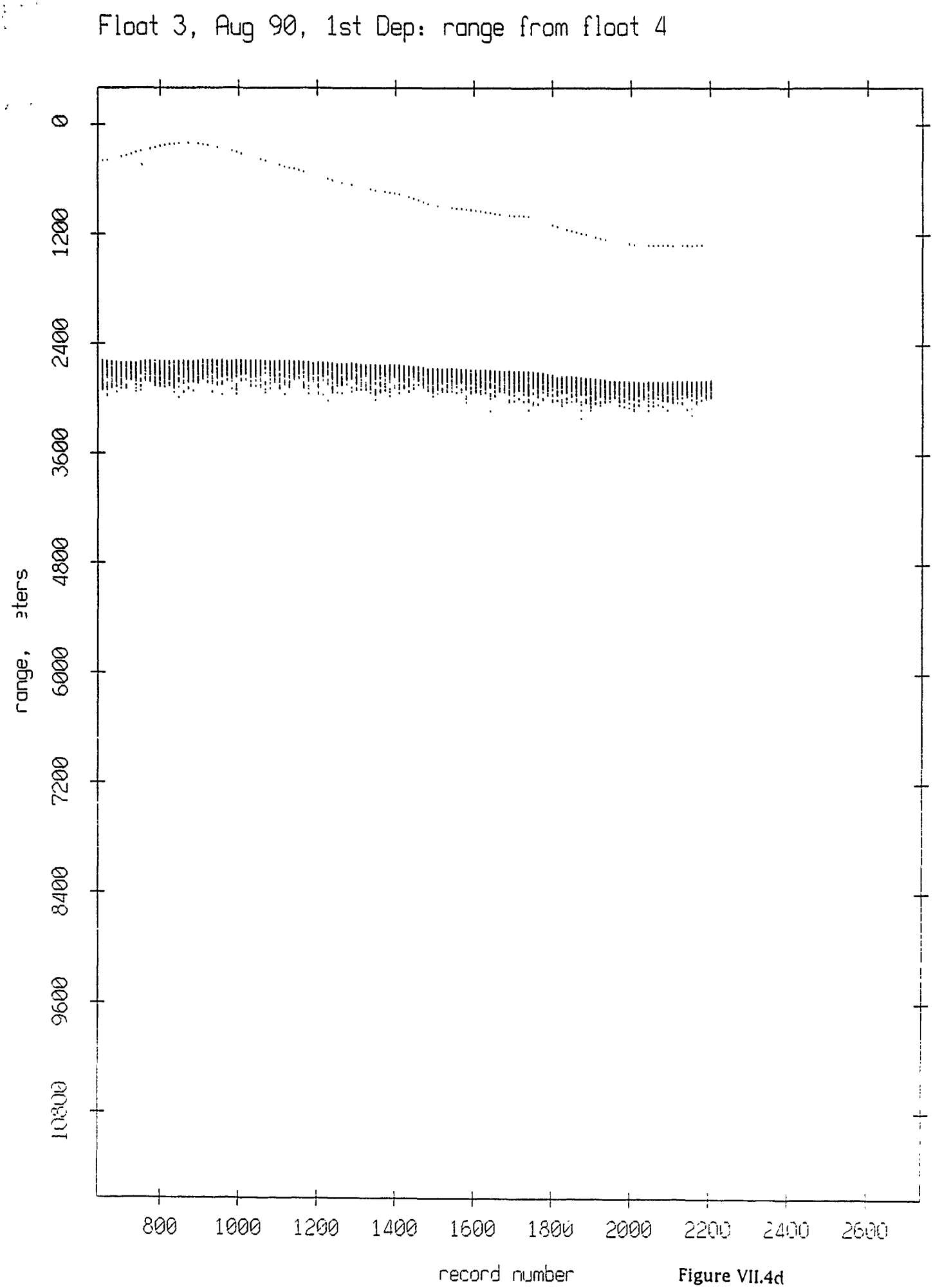

Figure VII.4d

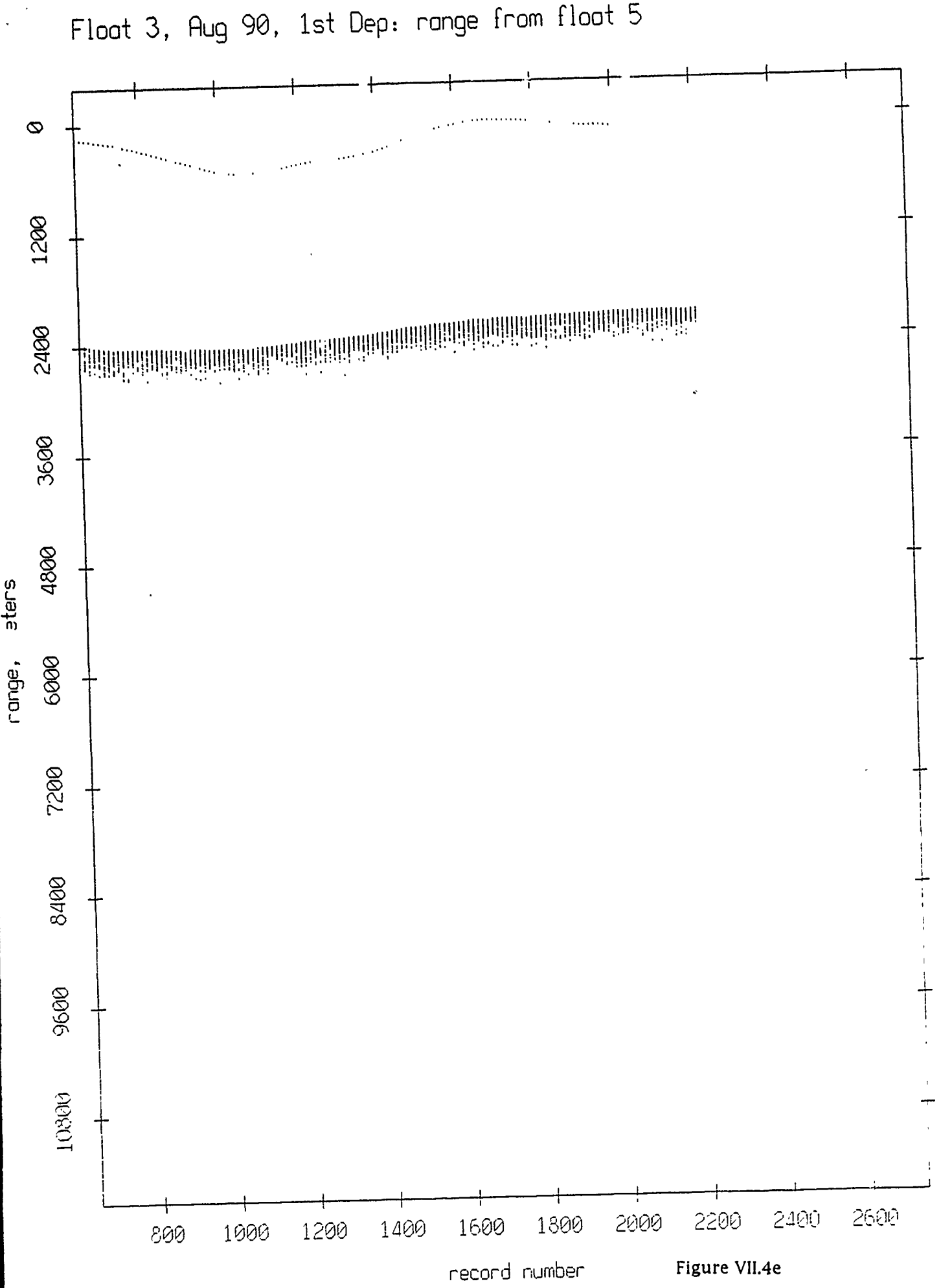

Figure VII.4e

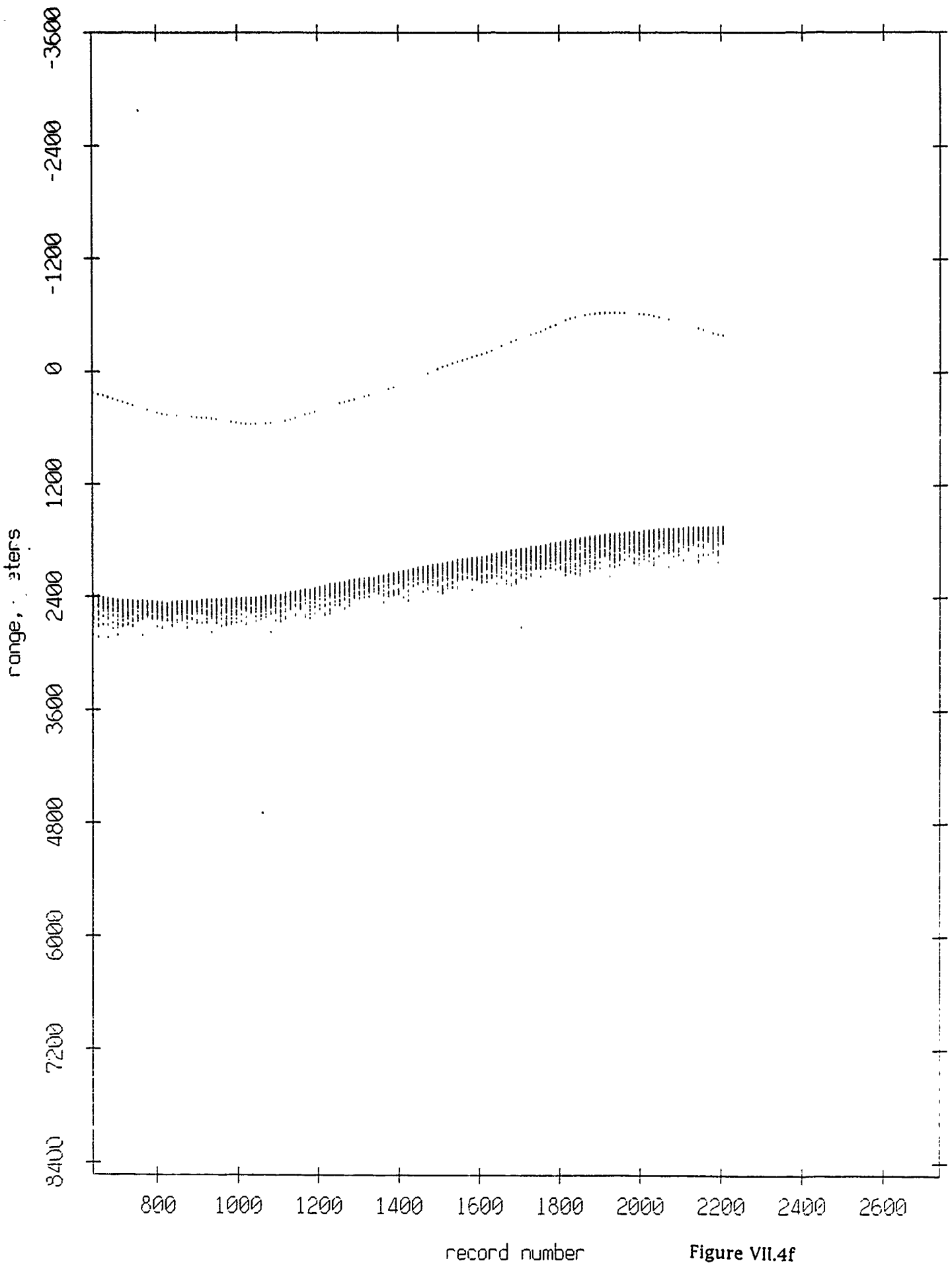

Figure VII.4f

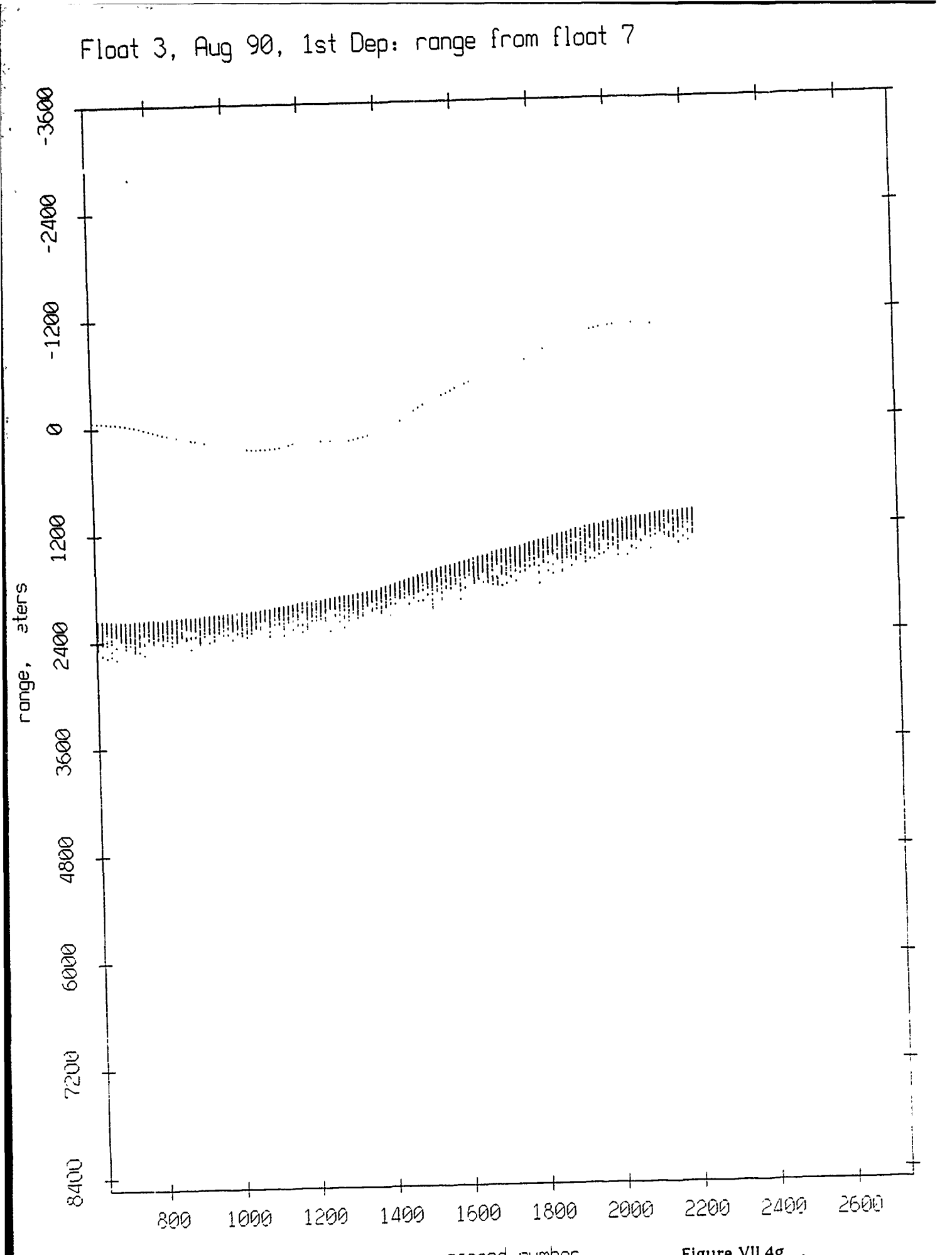

Figure VII.4g

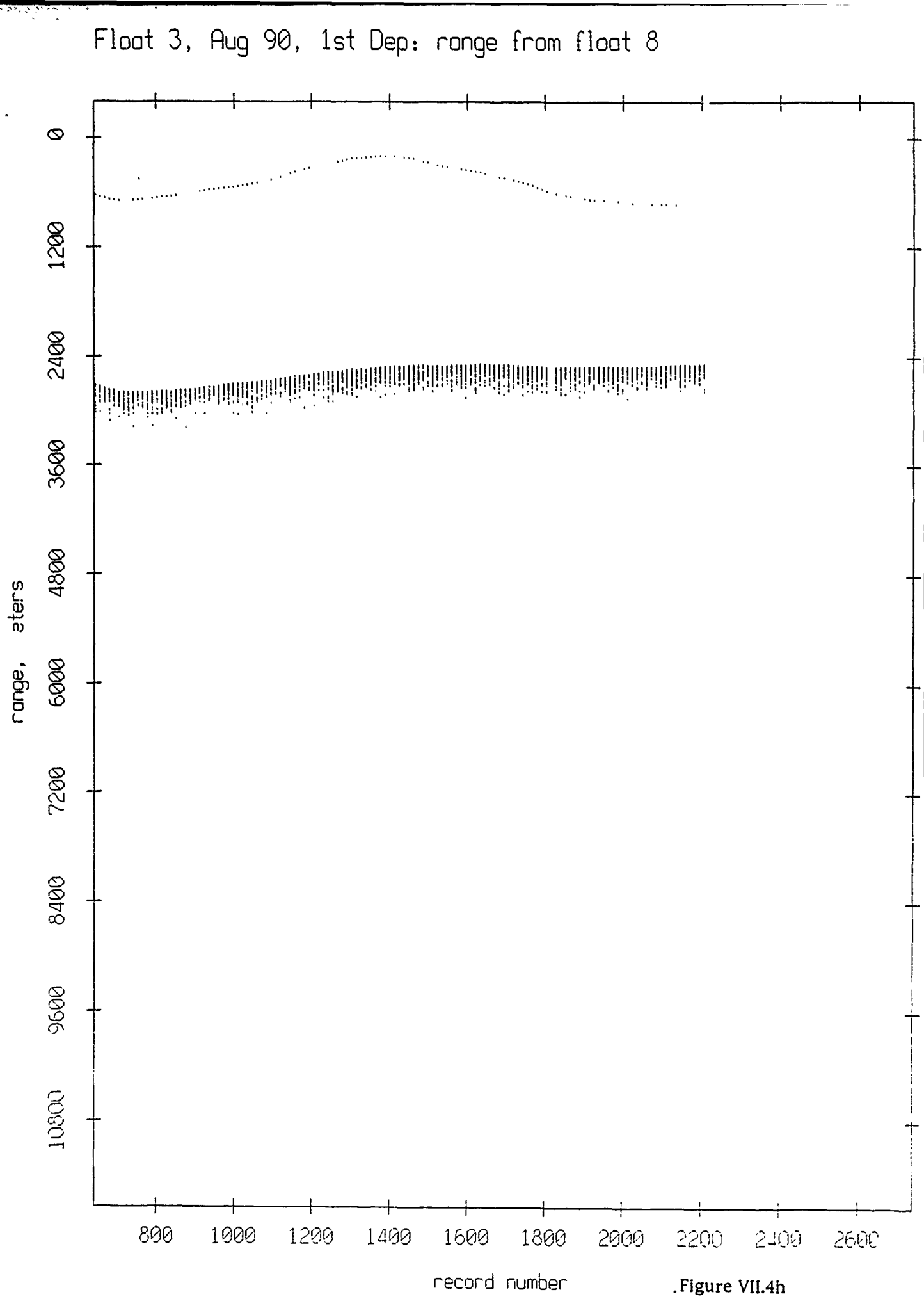

.Figure VII.4h

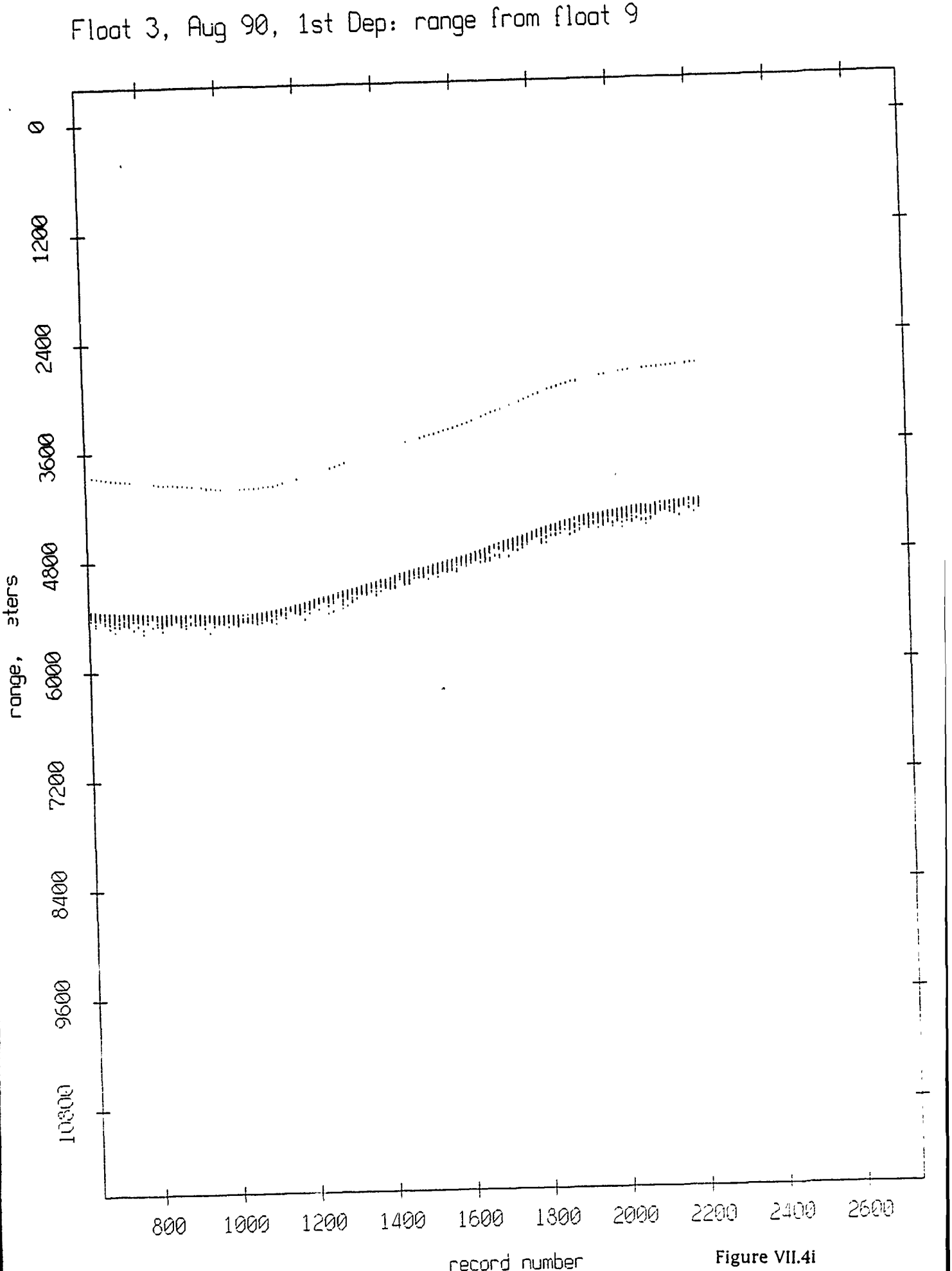

Figure VII.4i

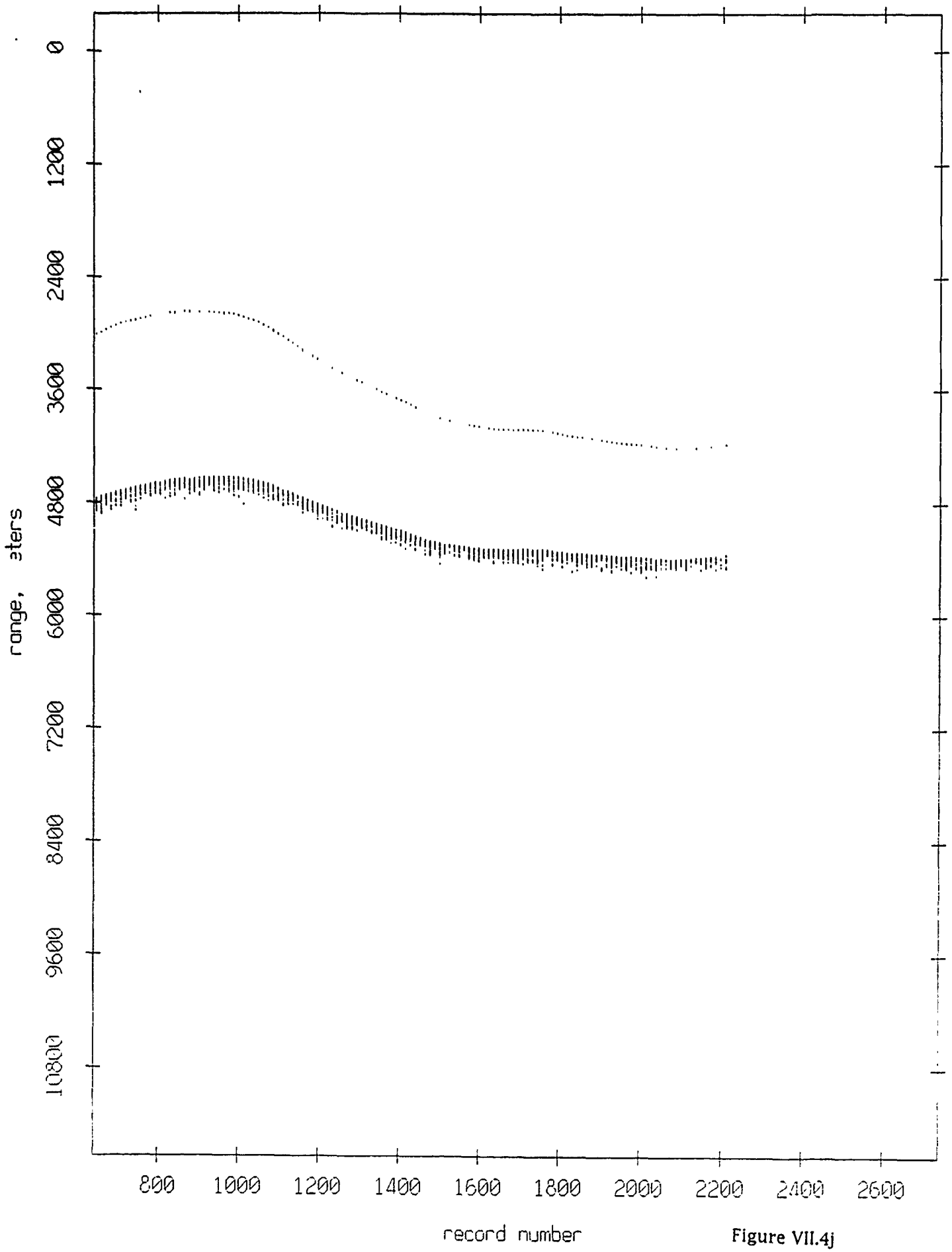

Figure VII.4j

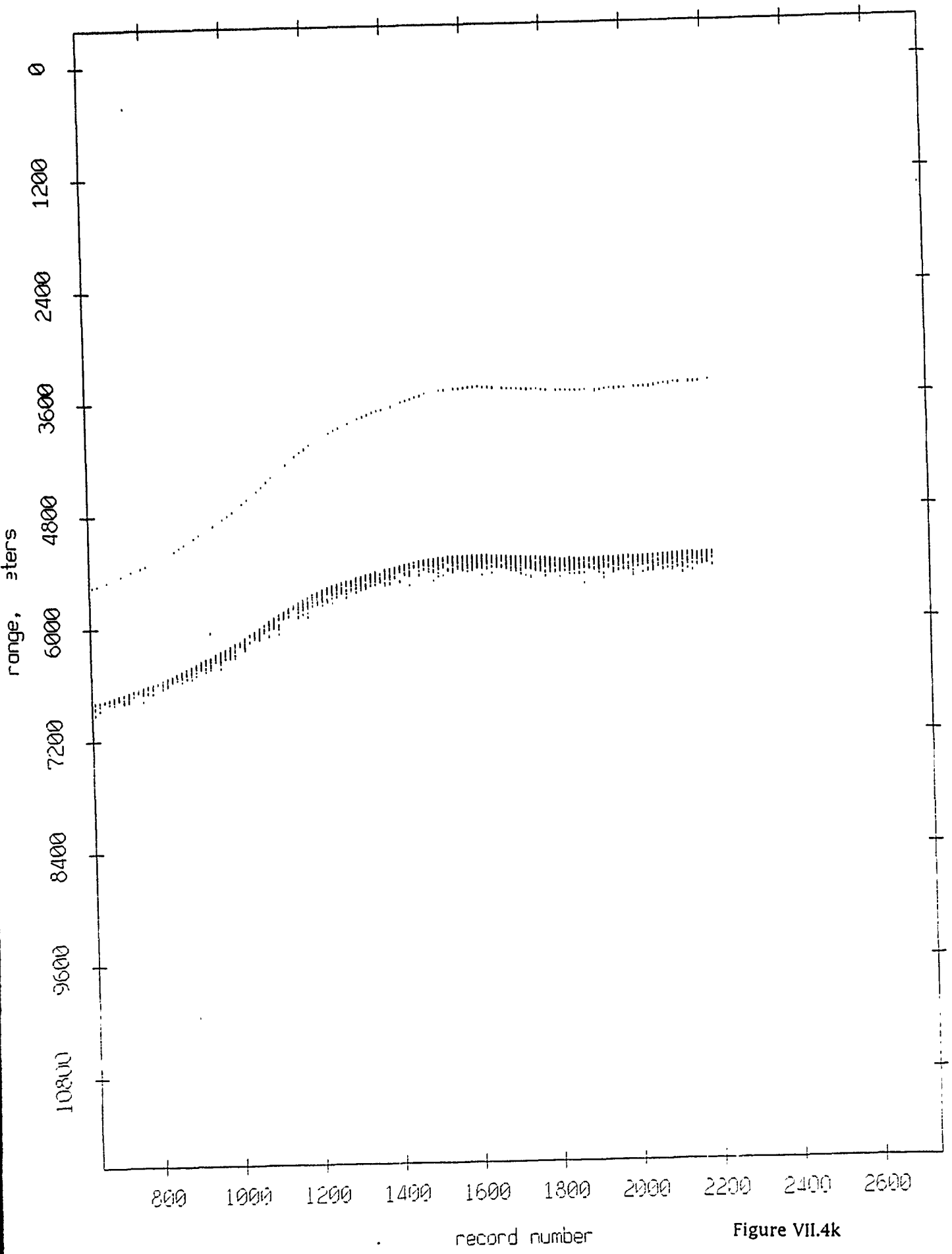

Figure VII.4k

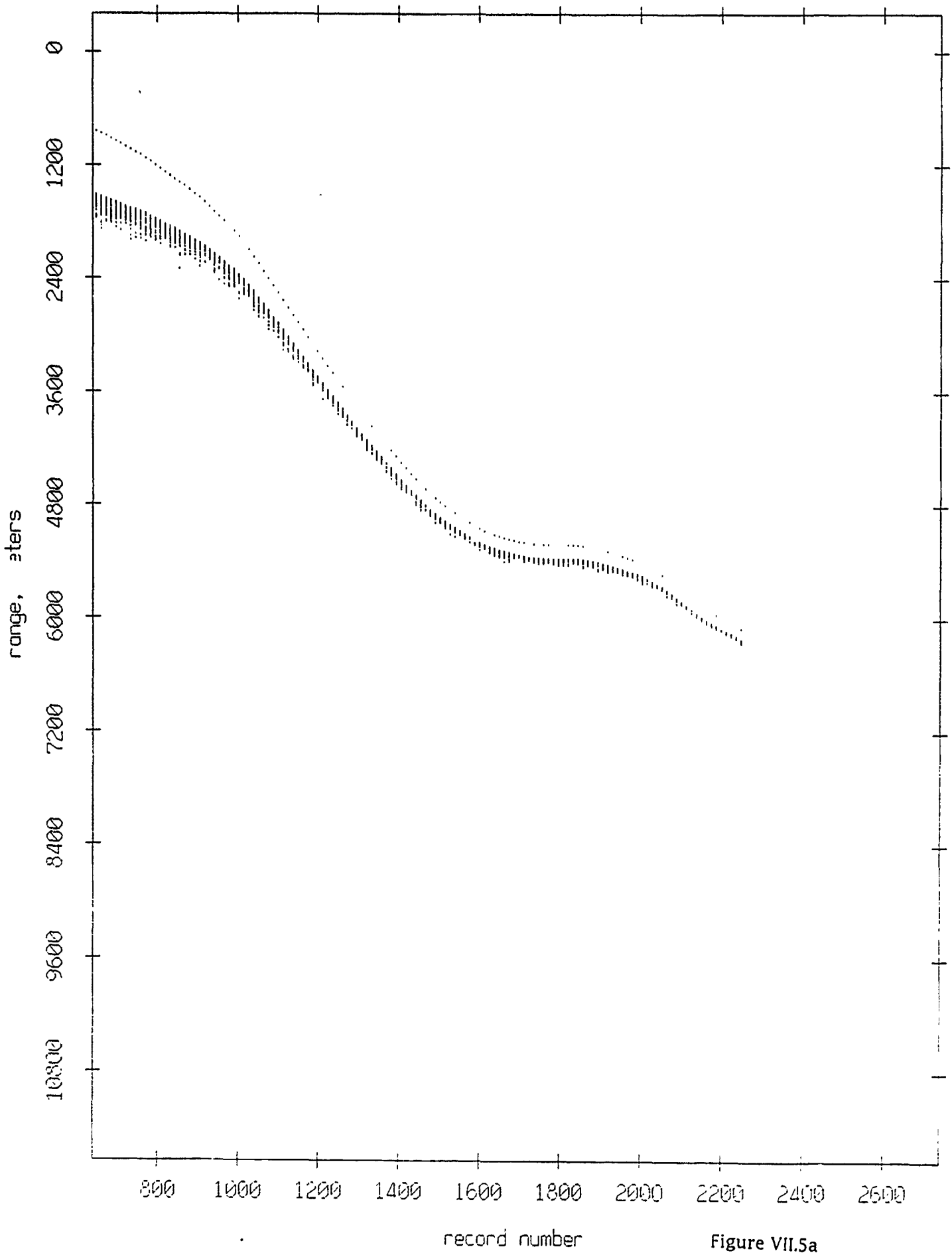

Figure VII.5a

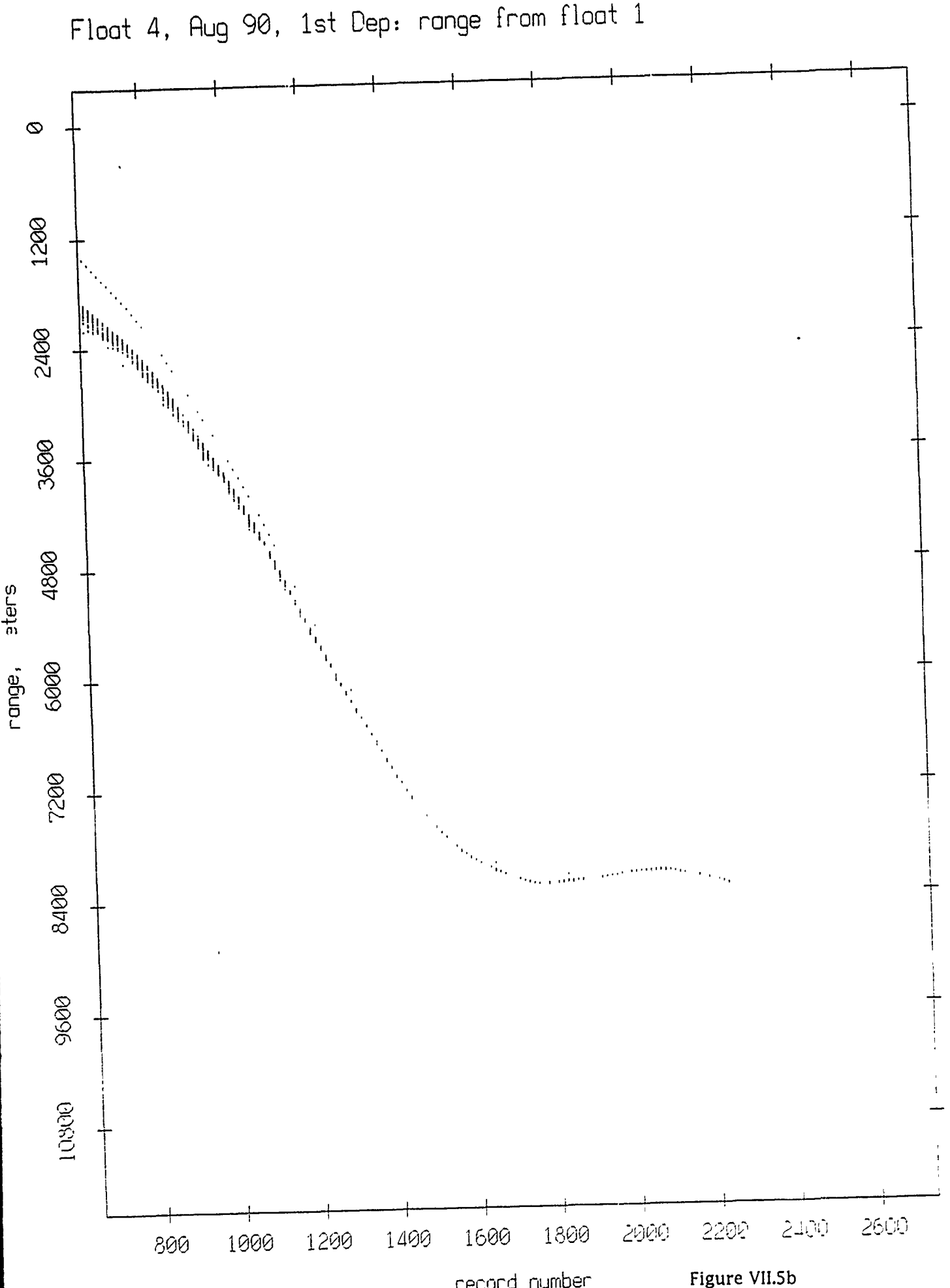

Figure VII.5b

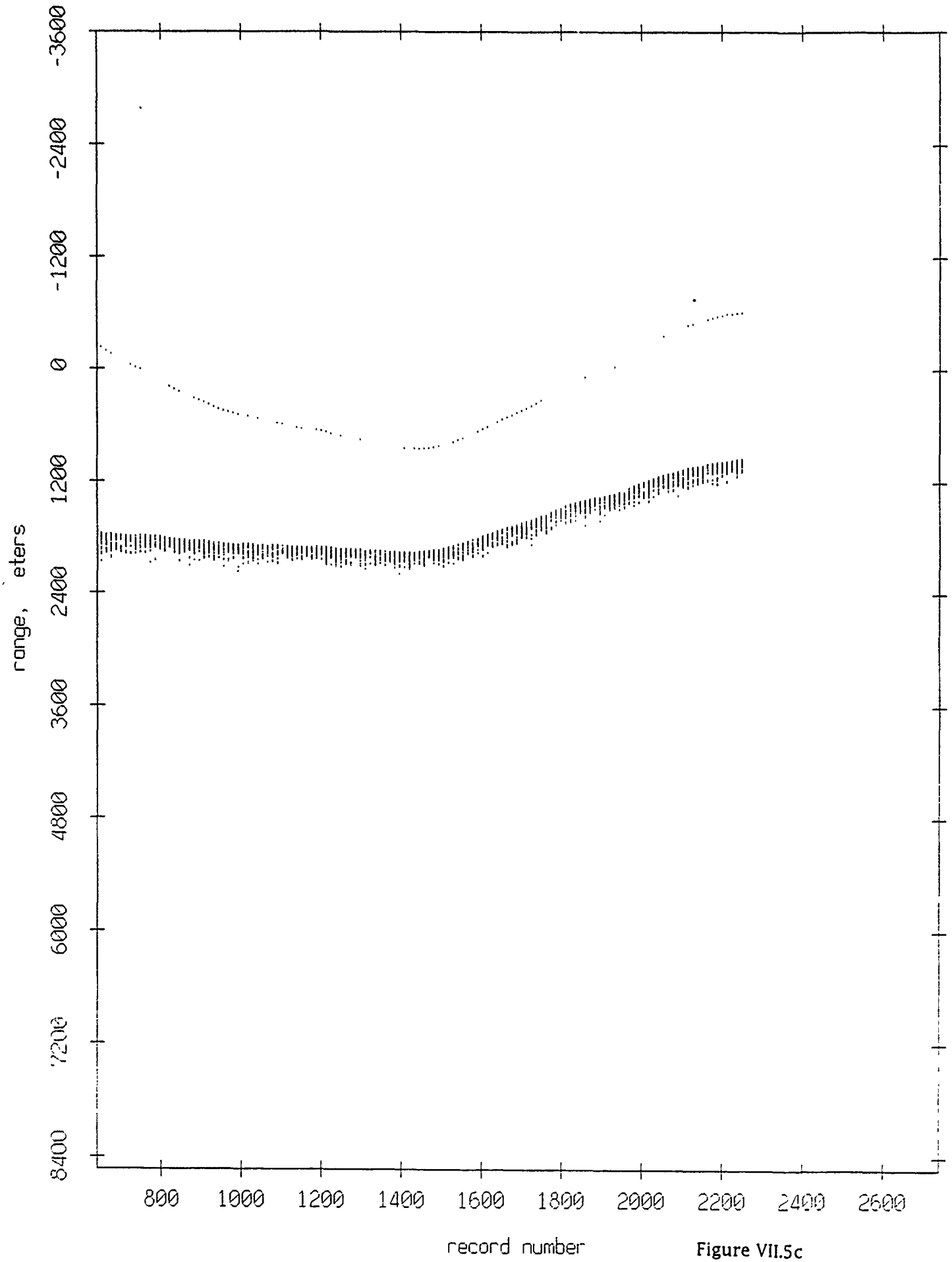

Figure VII.5c

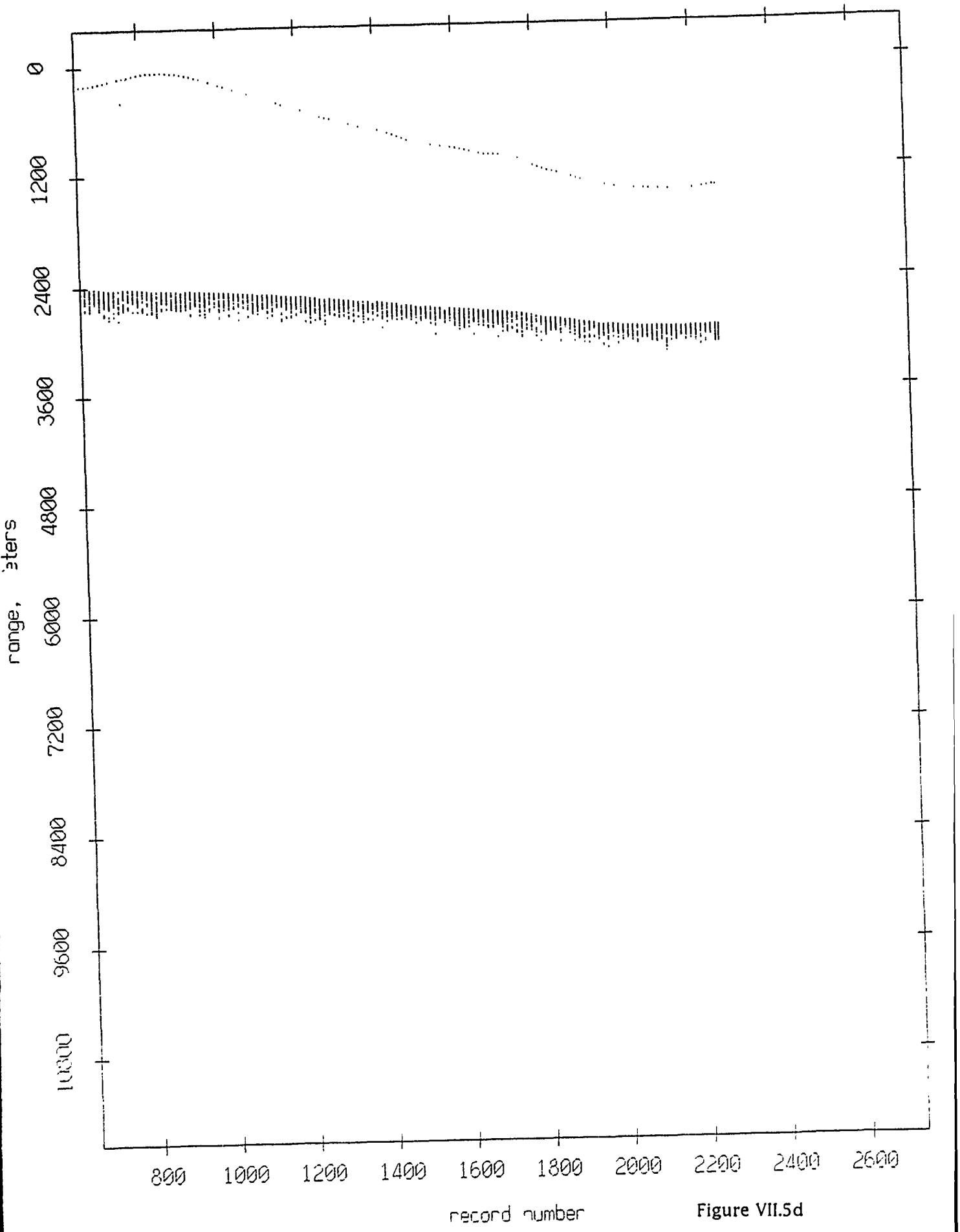

Figure VII.5d

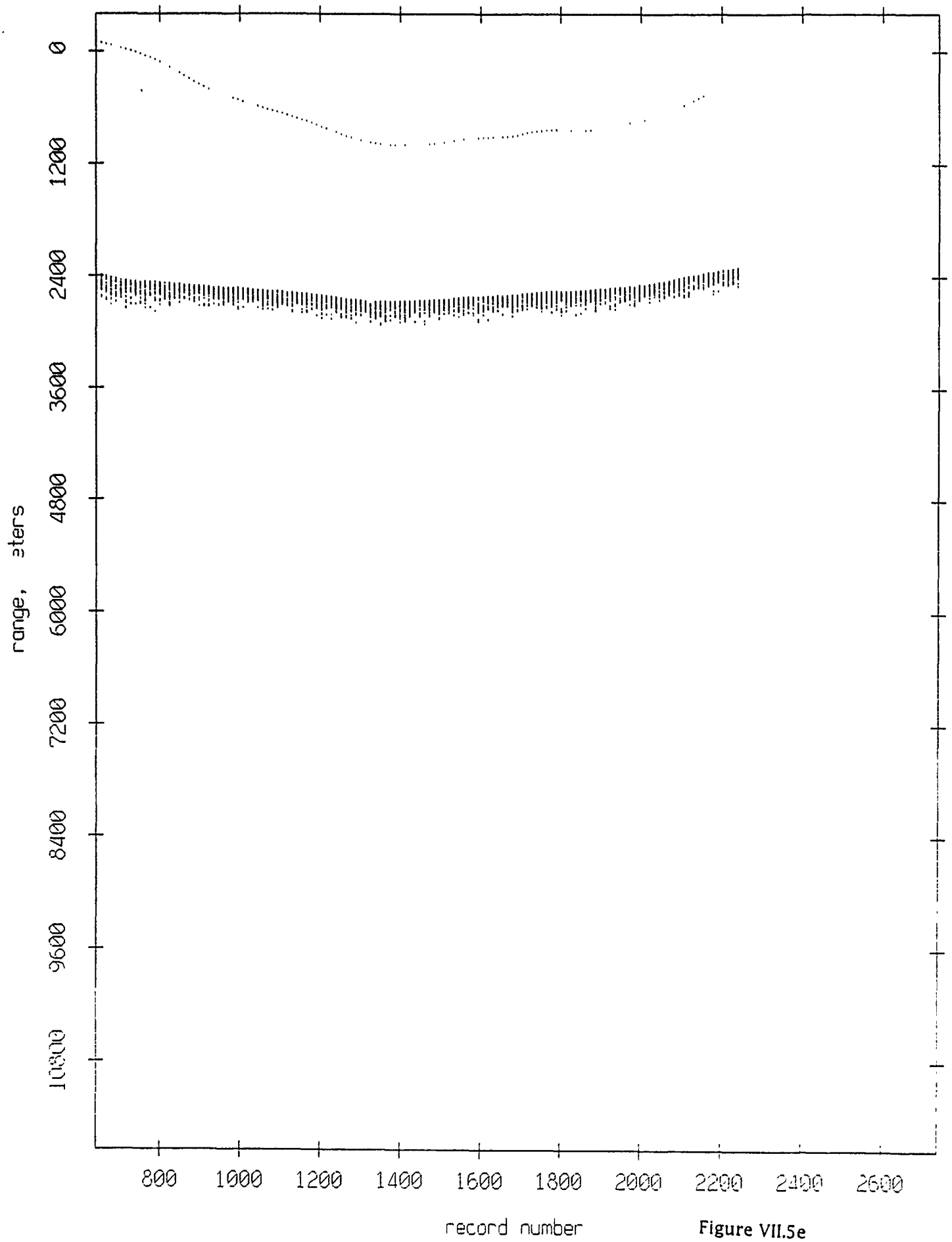

Figure VII.5e

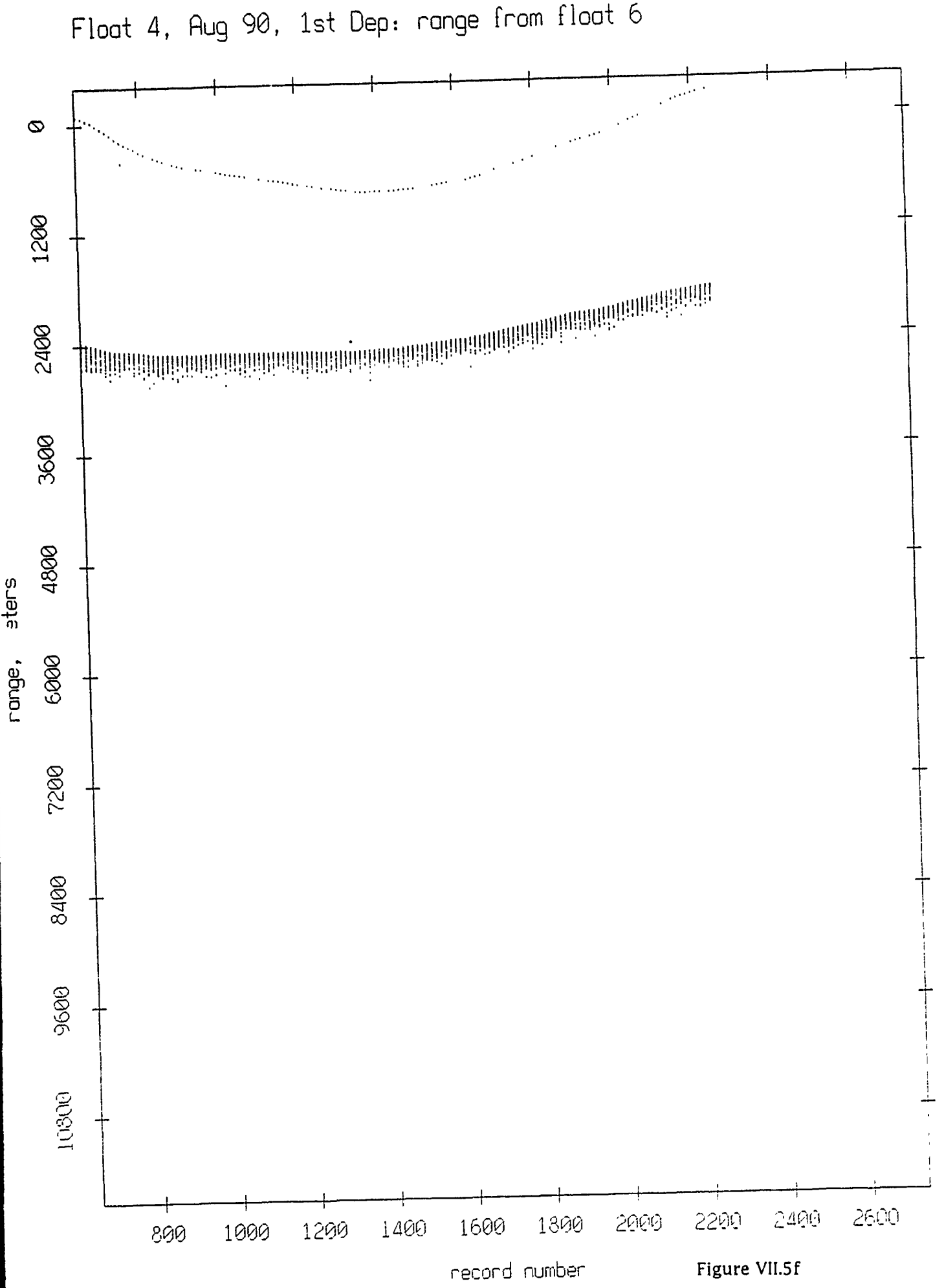

Figure VII.5f

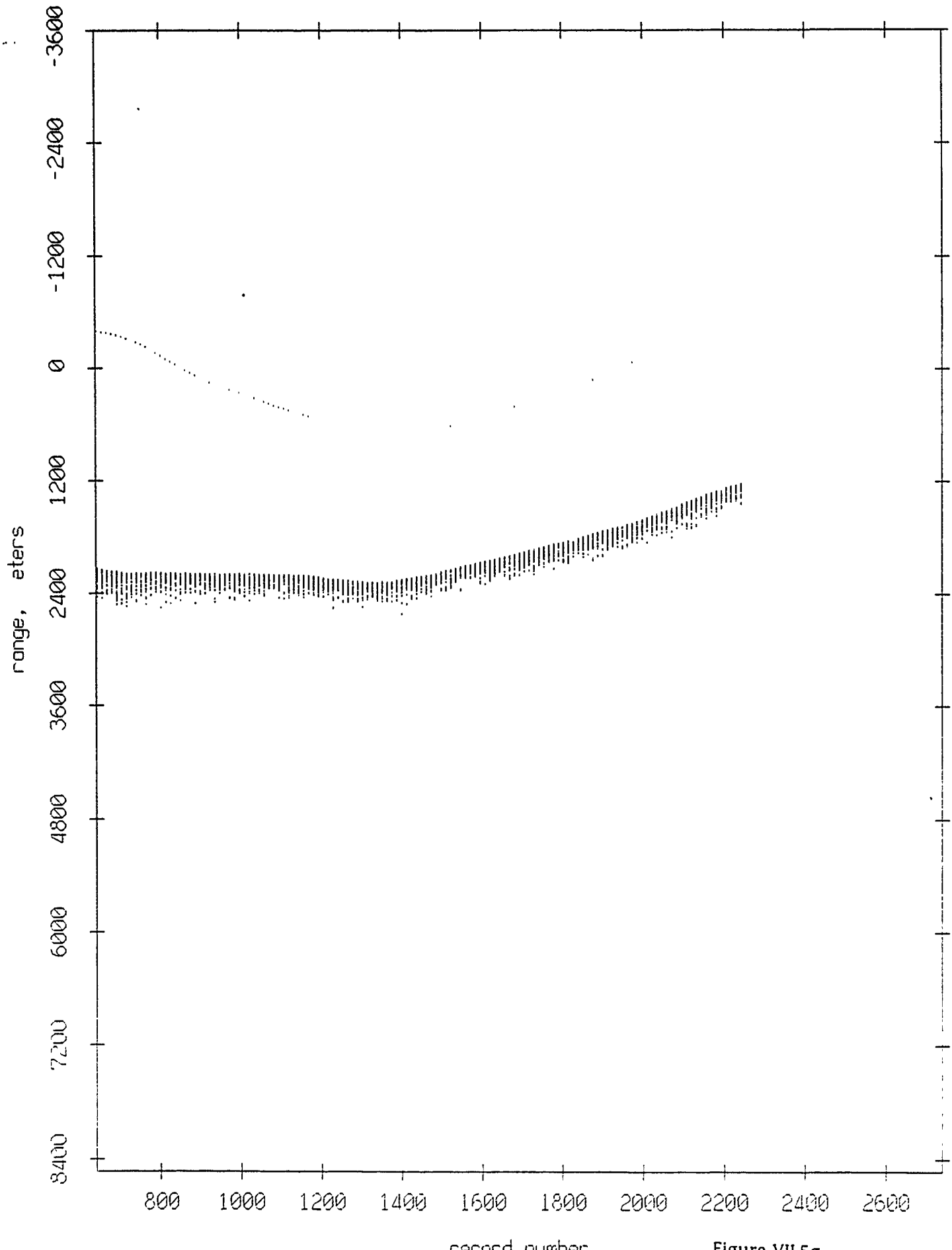

Figure VII.5g

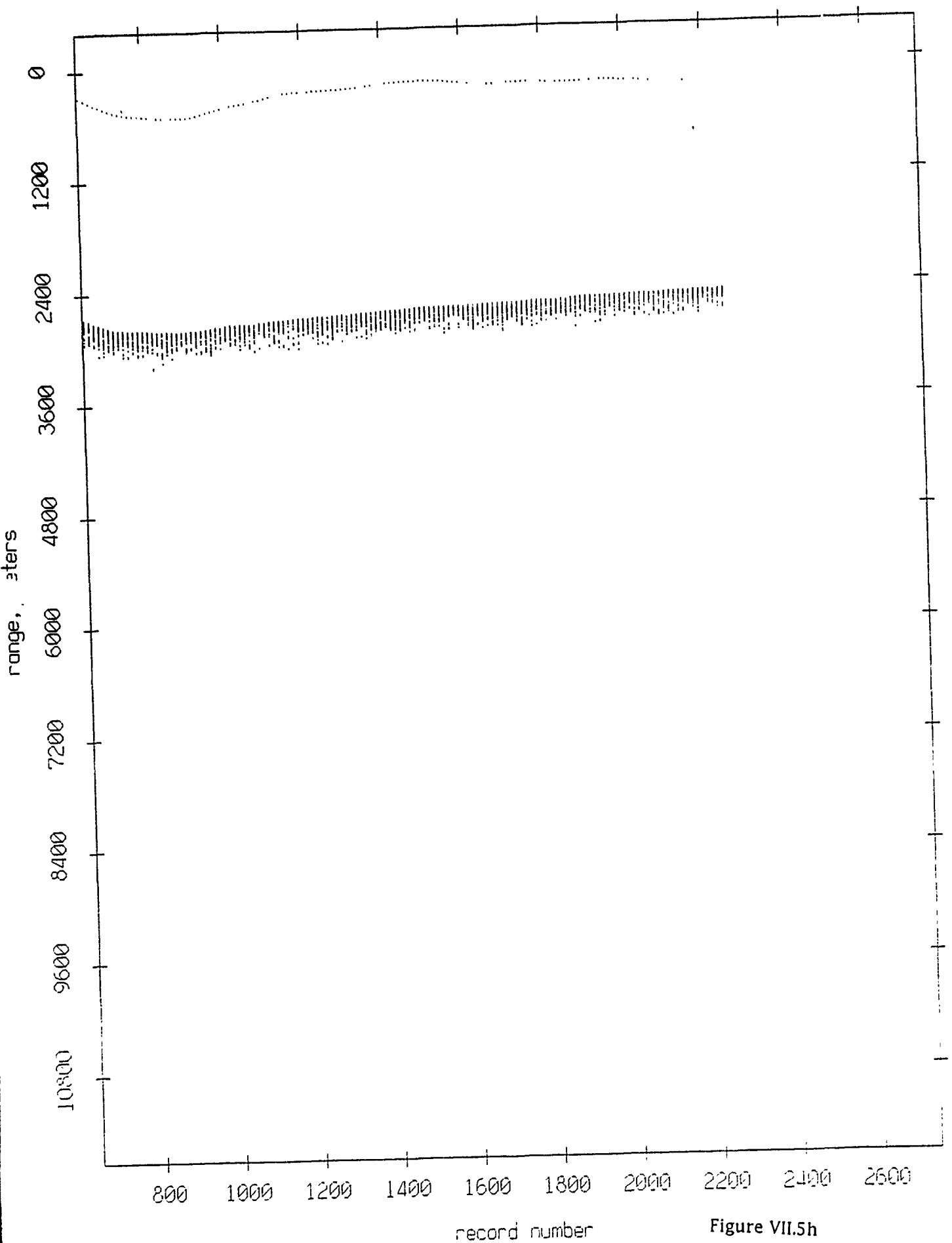

Figure VII.5h

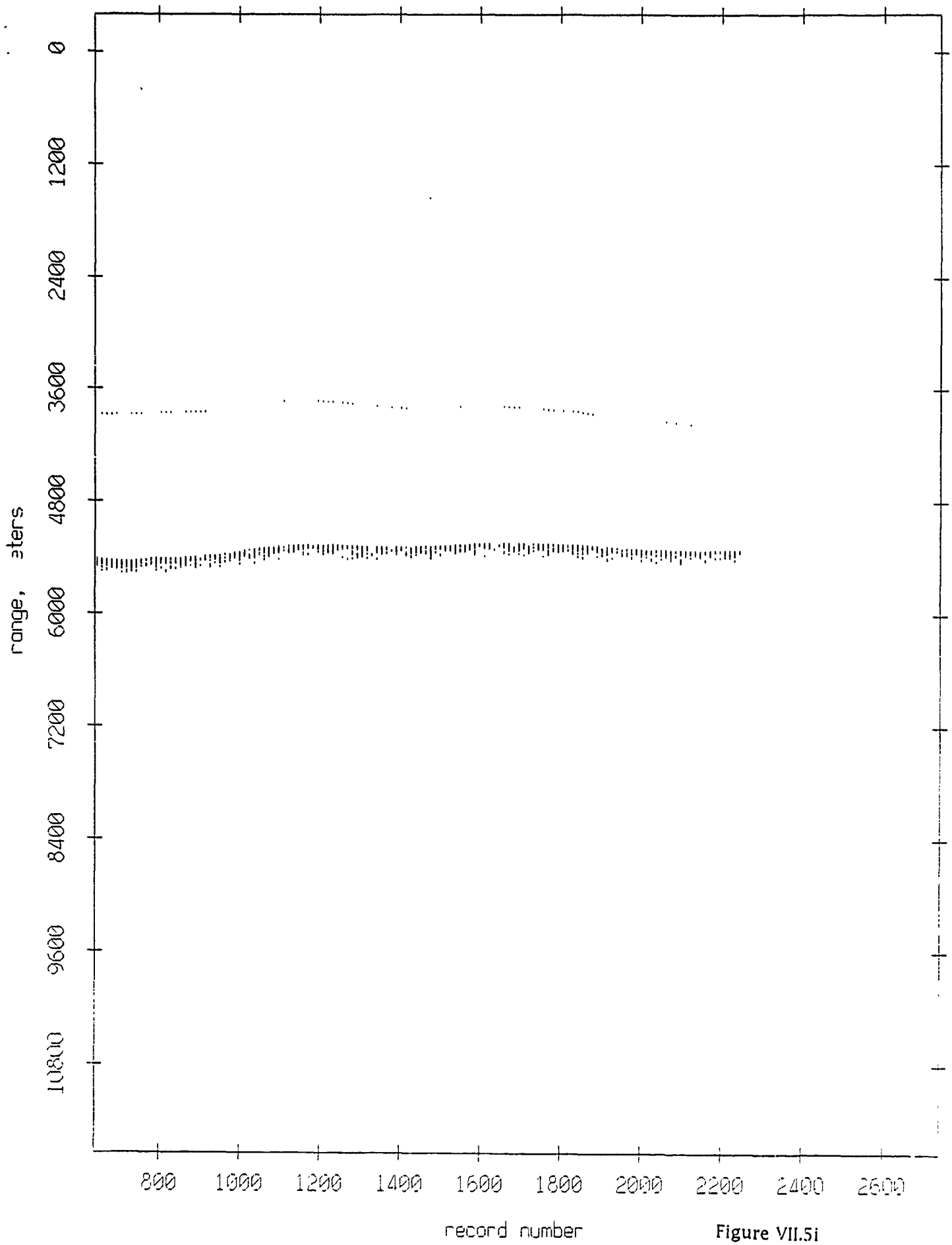

Figure VII.5i

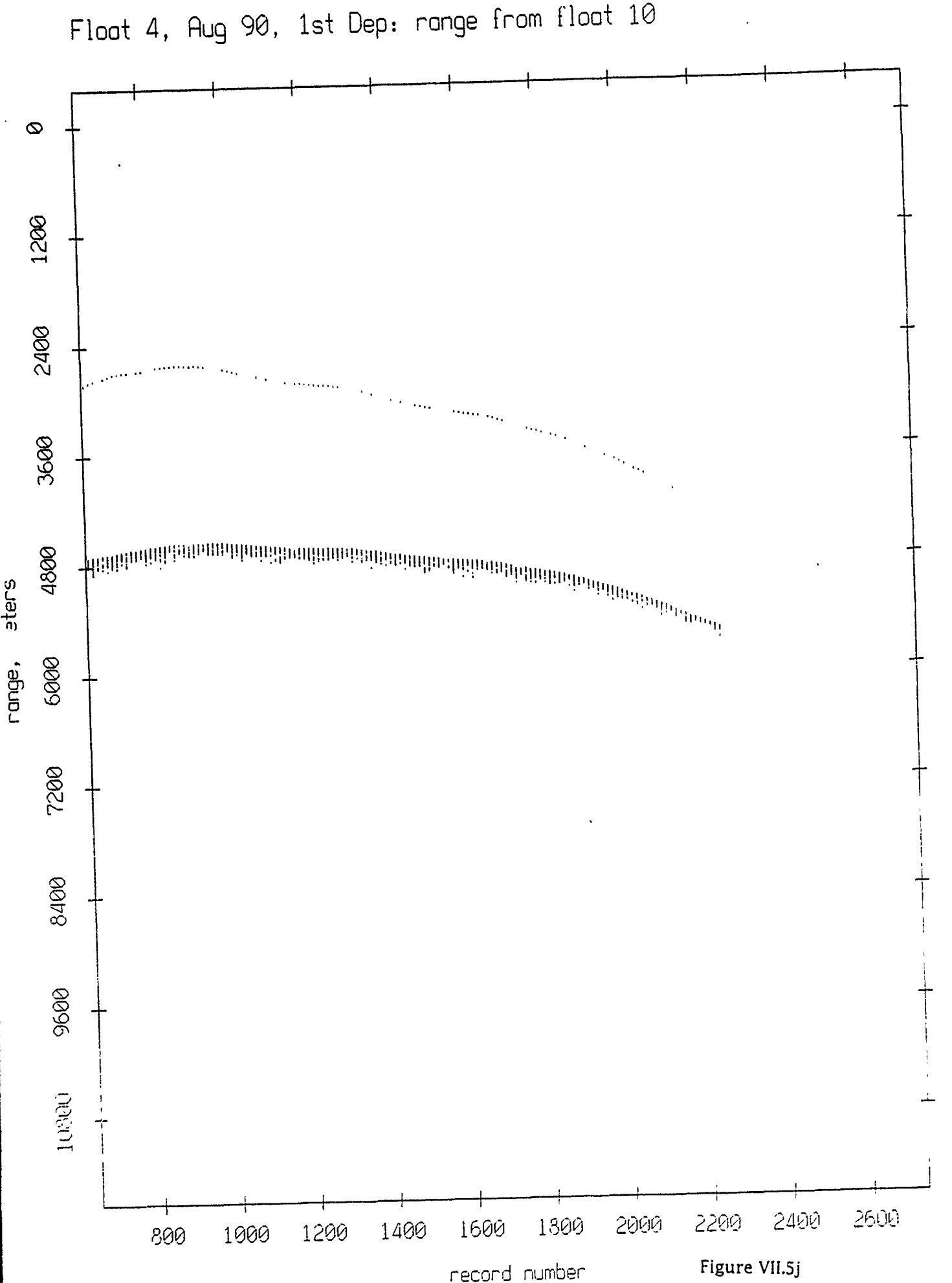

Figure VII.5j

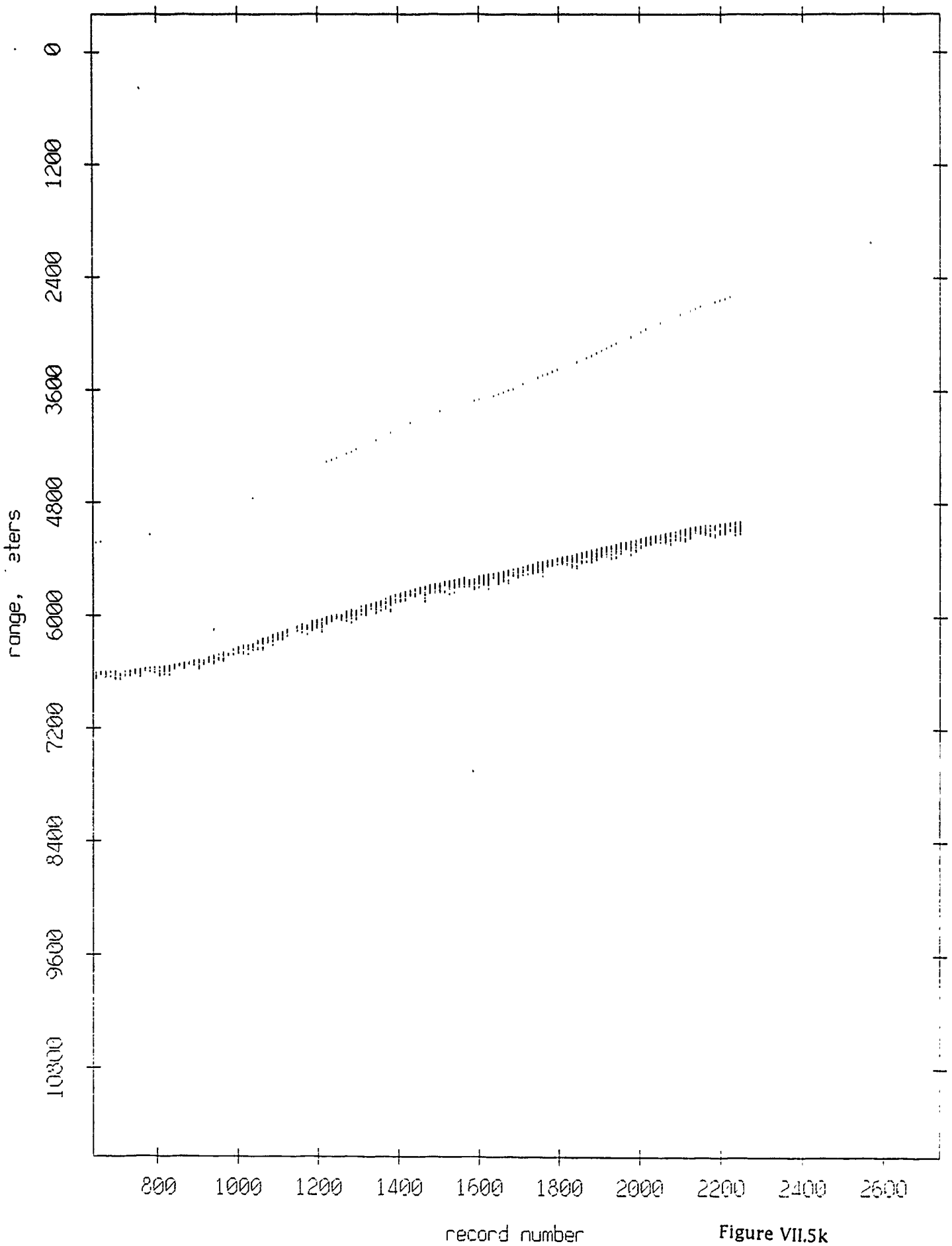

Figure VII.5k

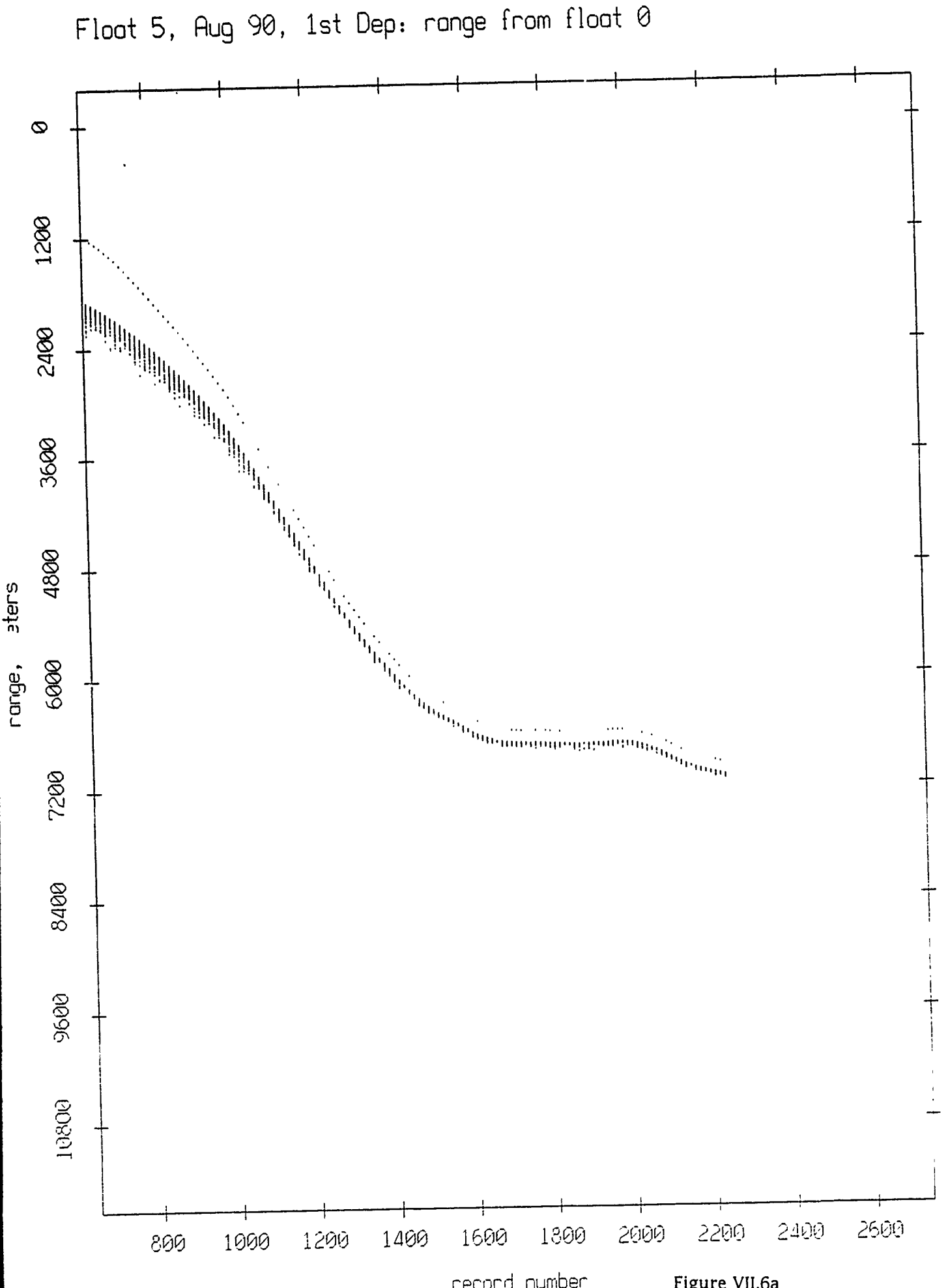

Figure VII.6a

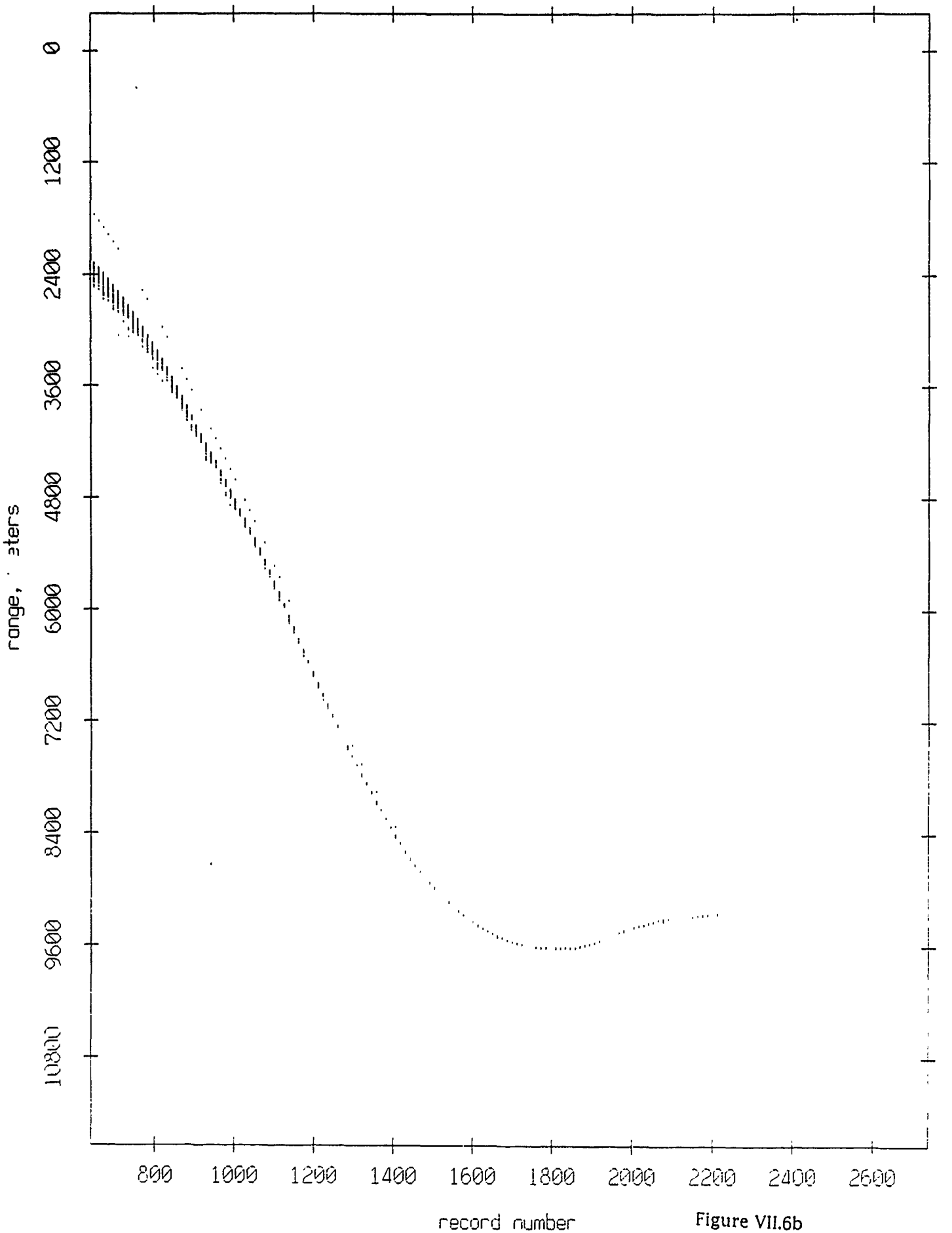

Figure VII.6b

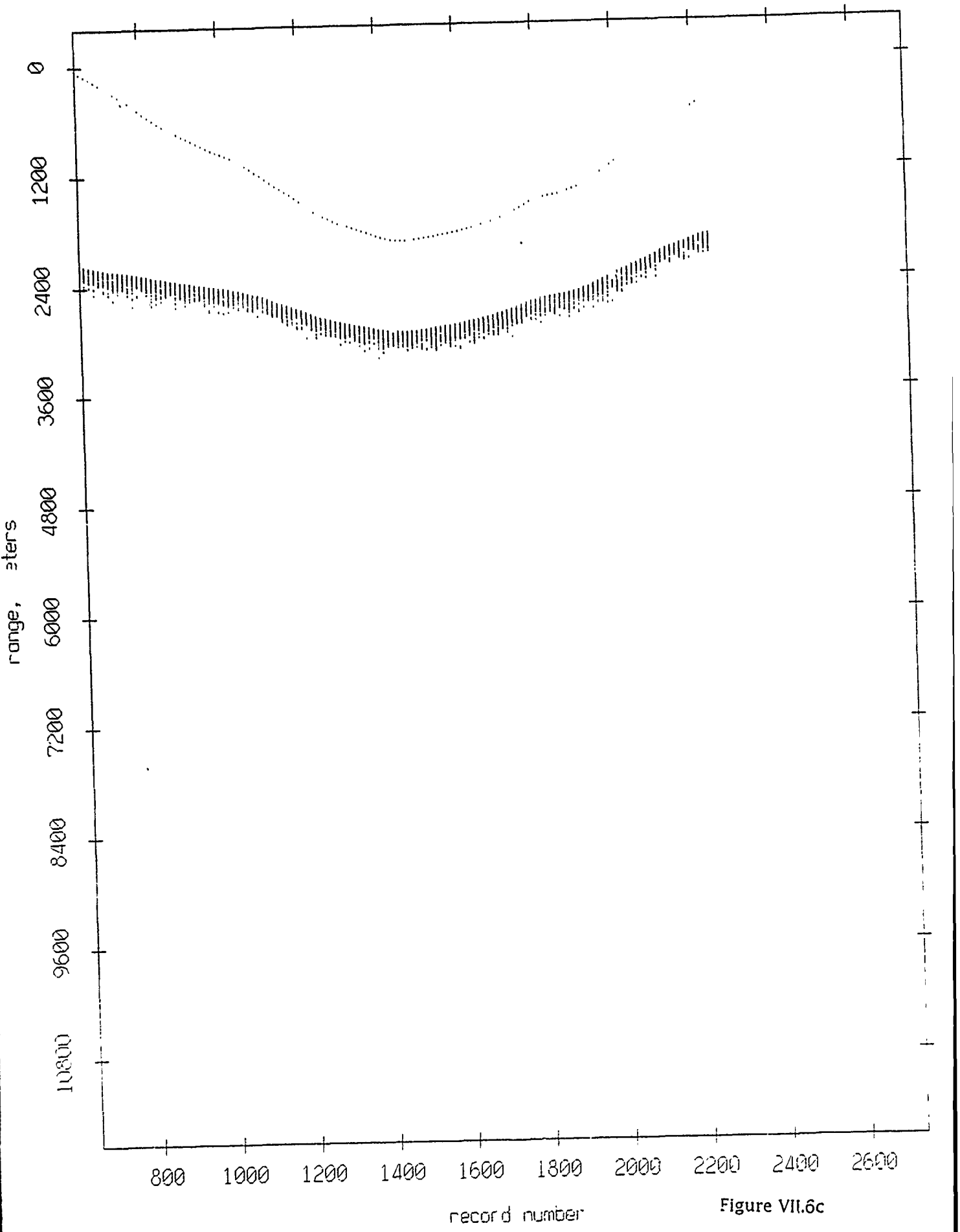

Figure VII.6c

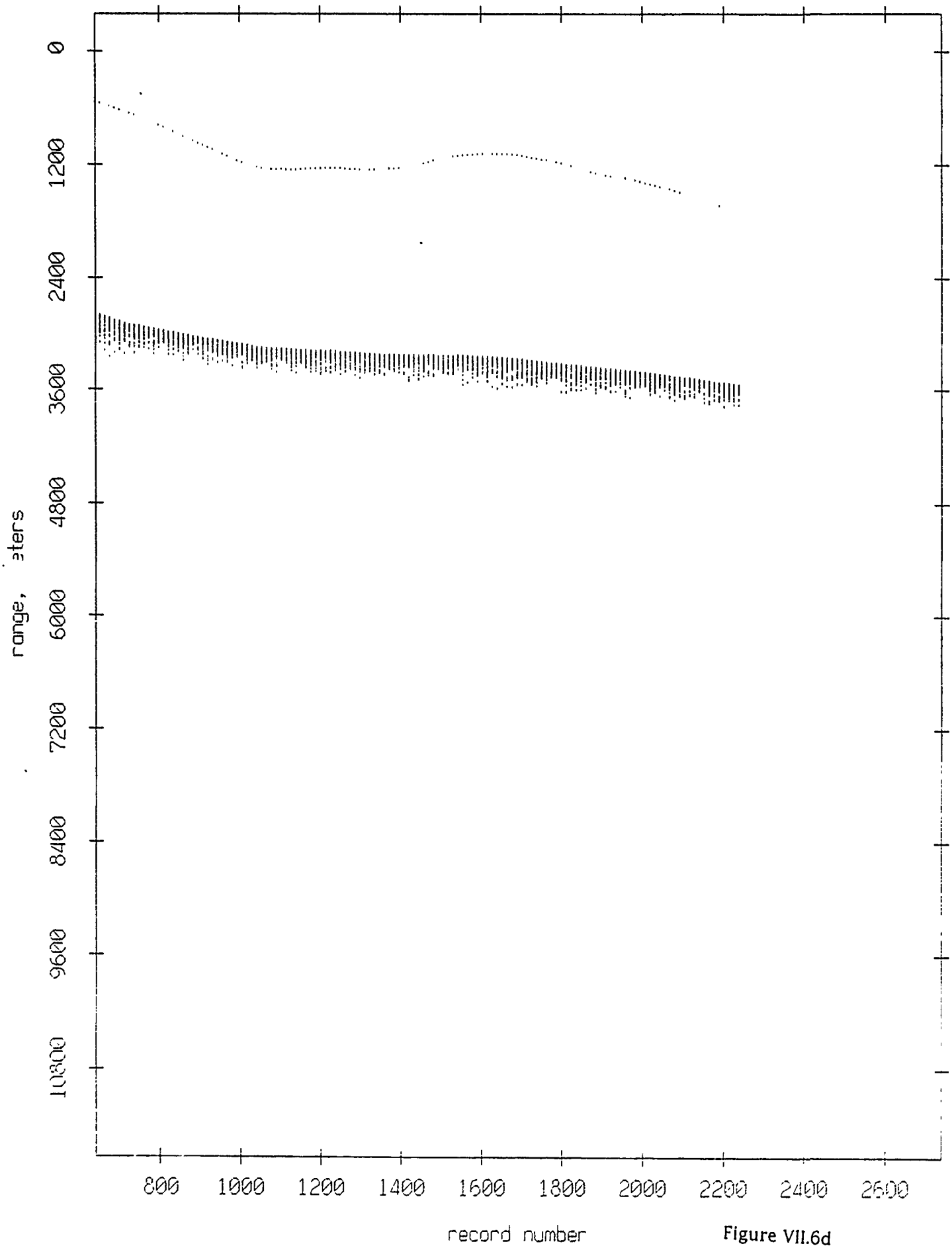

Figure VII.6d

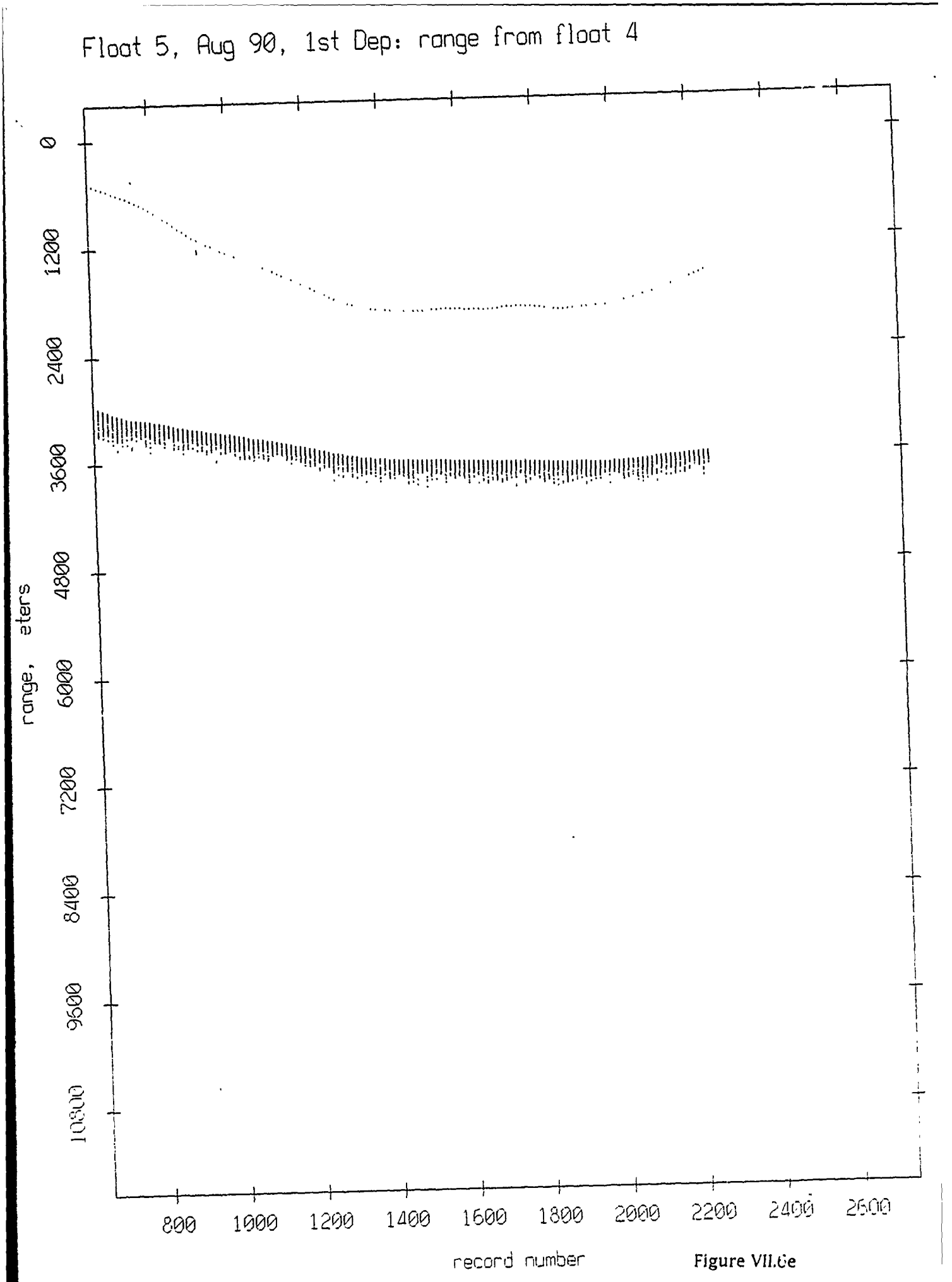

Figure VII.6e

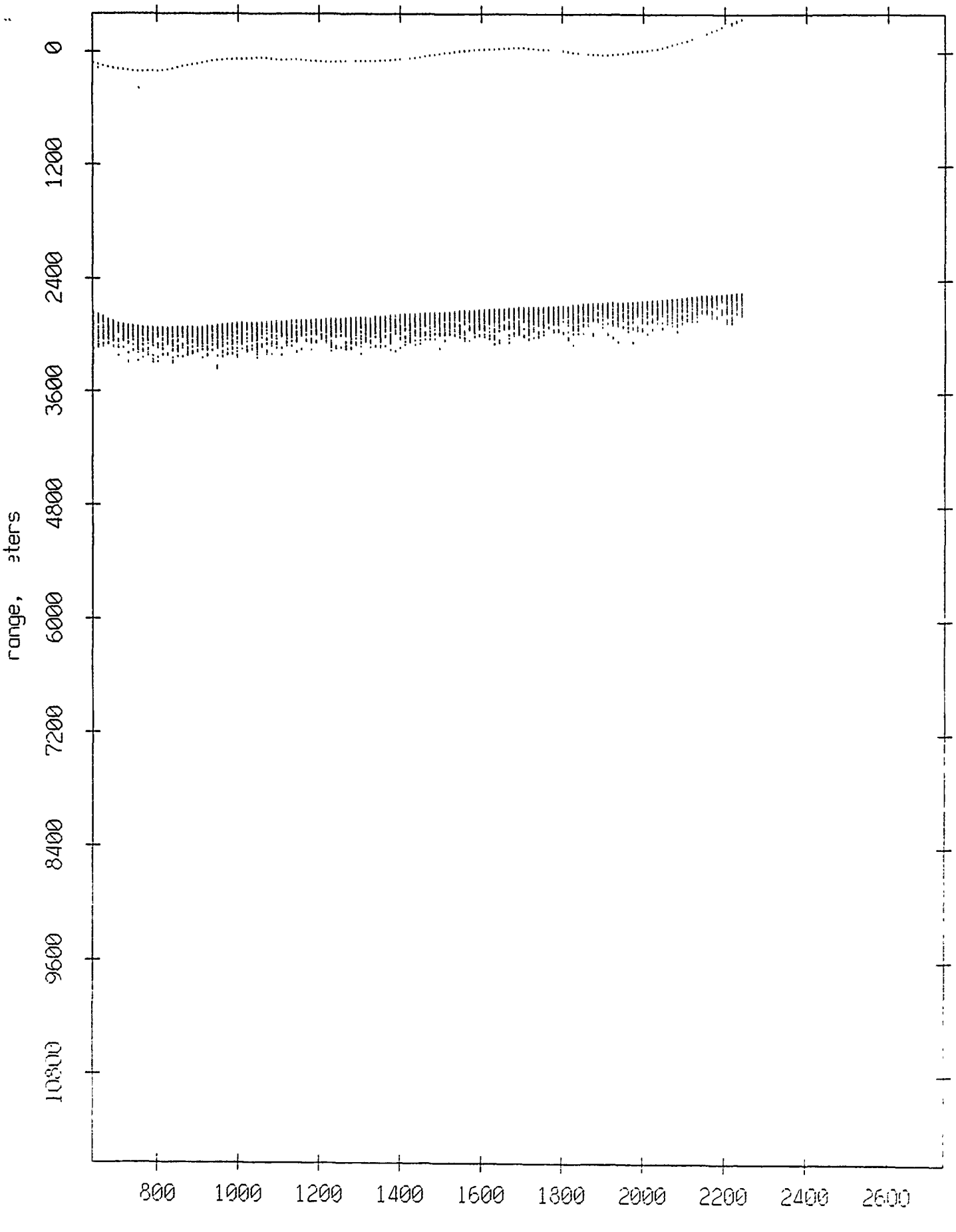

Figure VII.6f

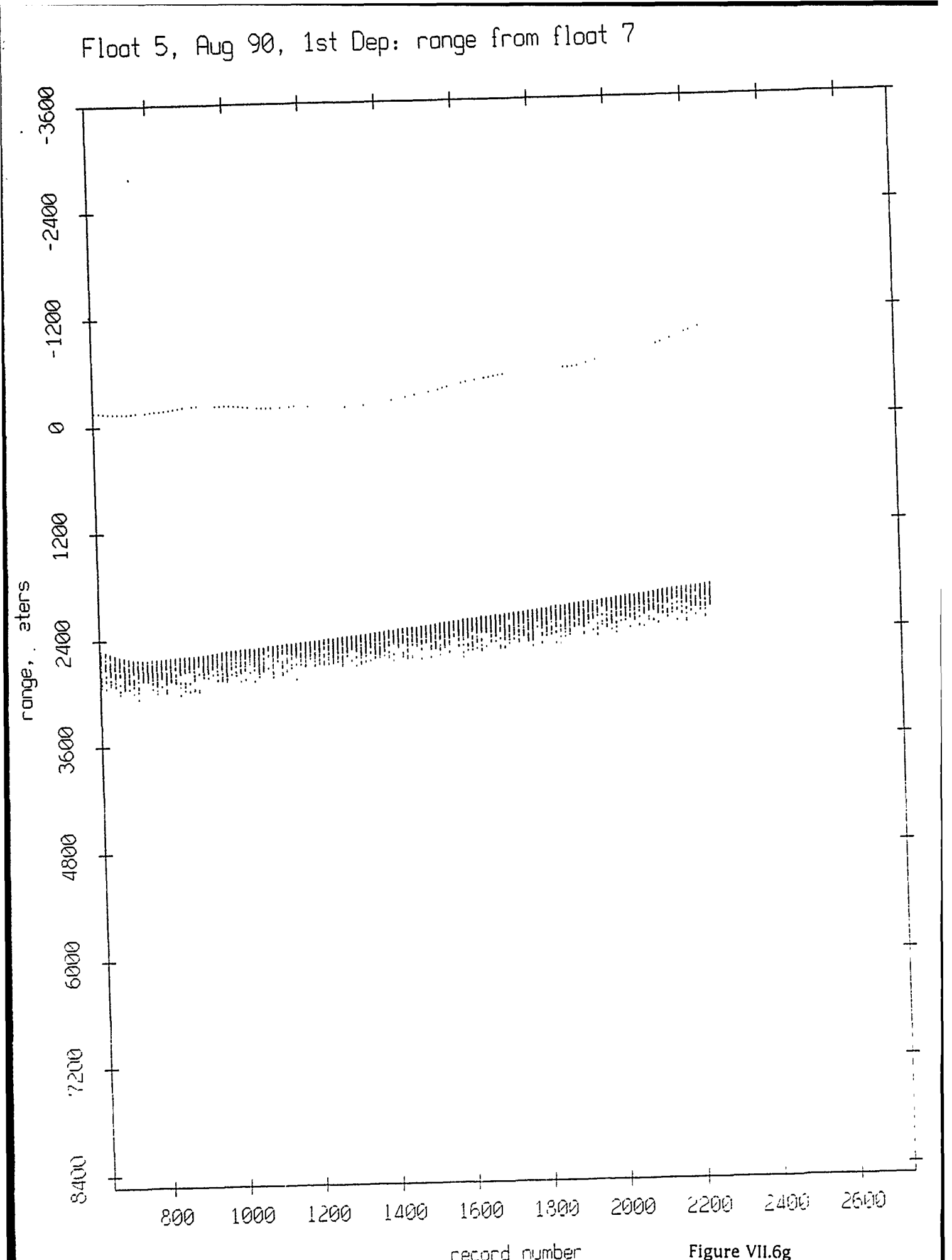

Figure VII.6g

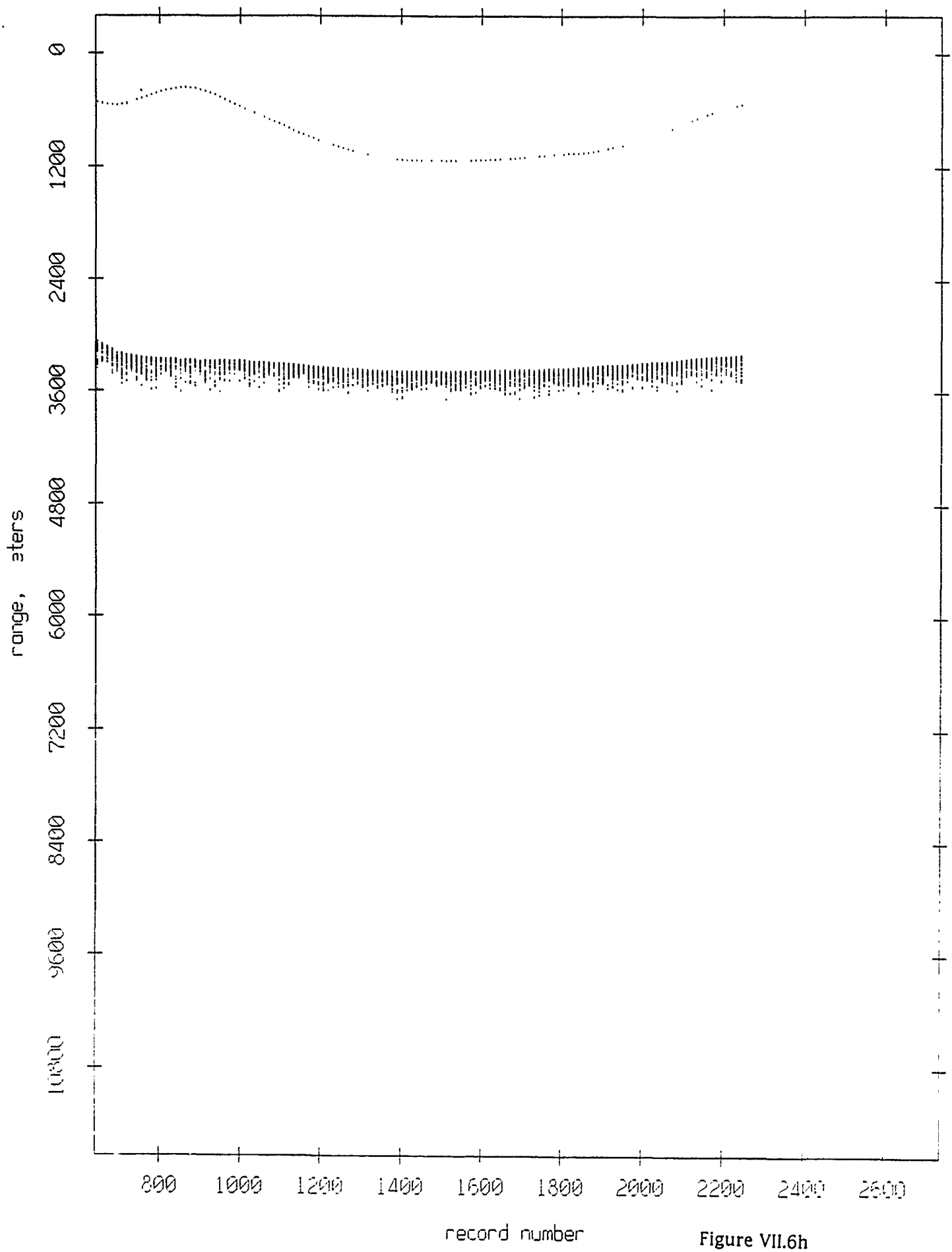

Figure VII.6h

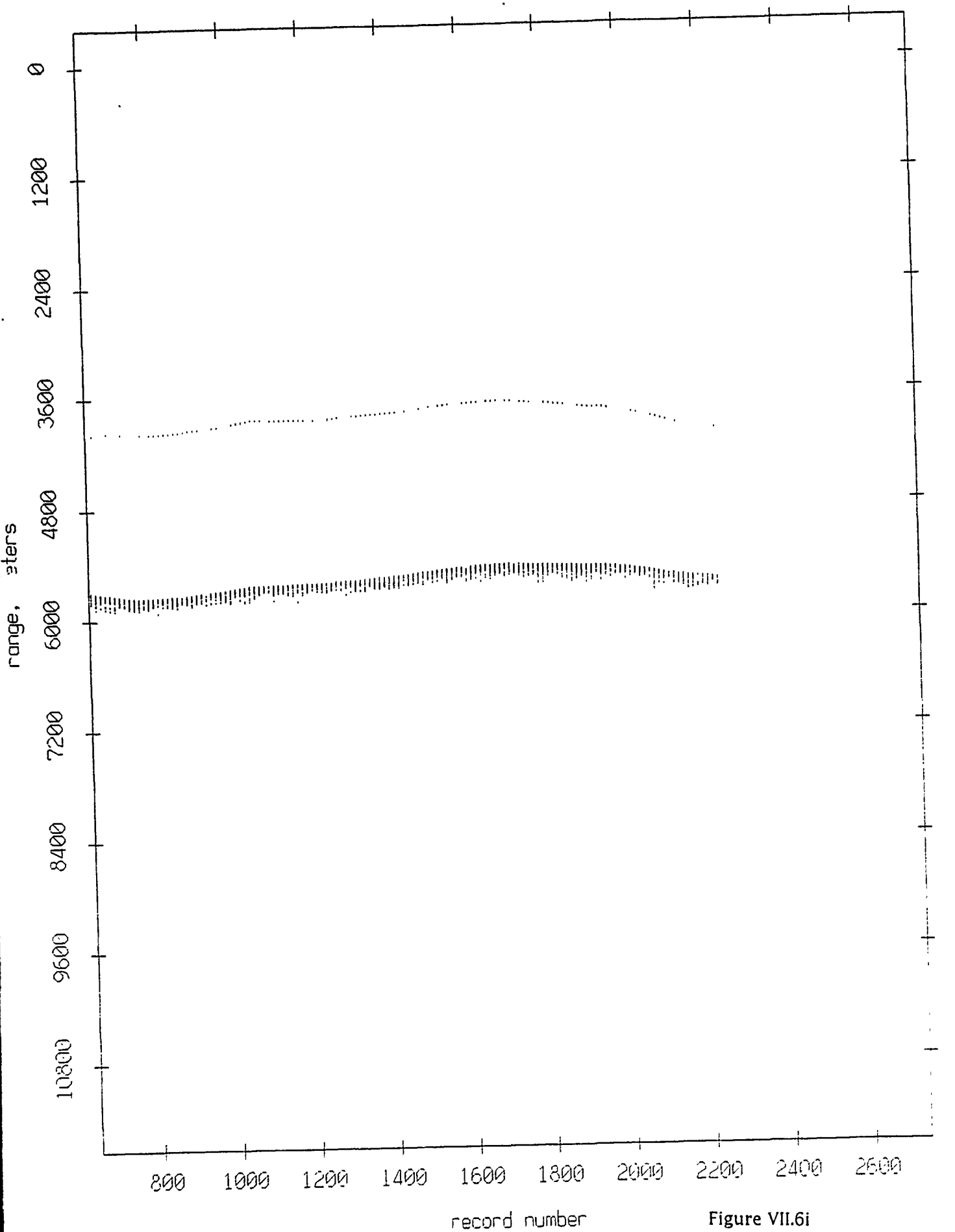

Figure VII.6i

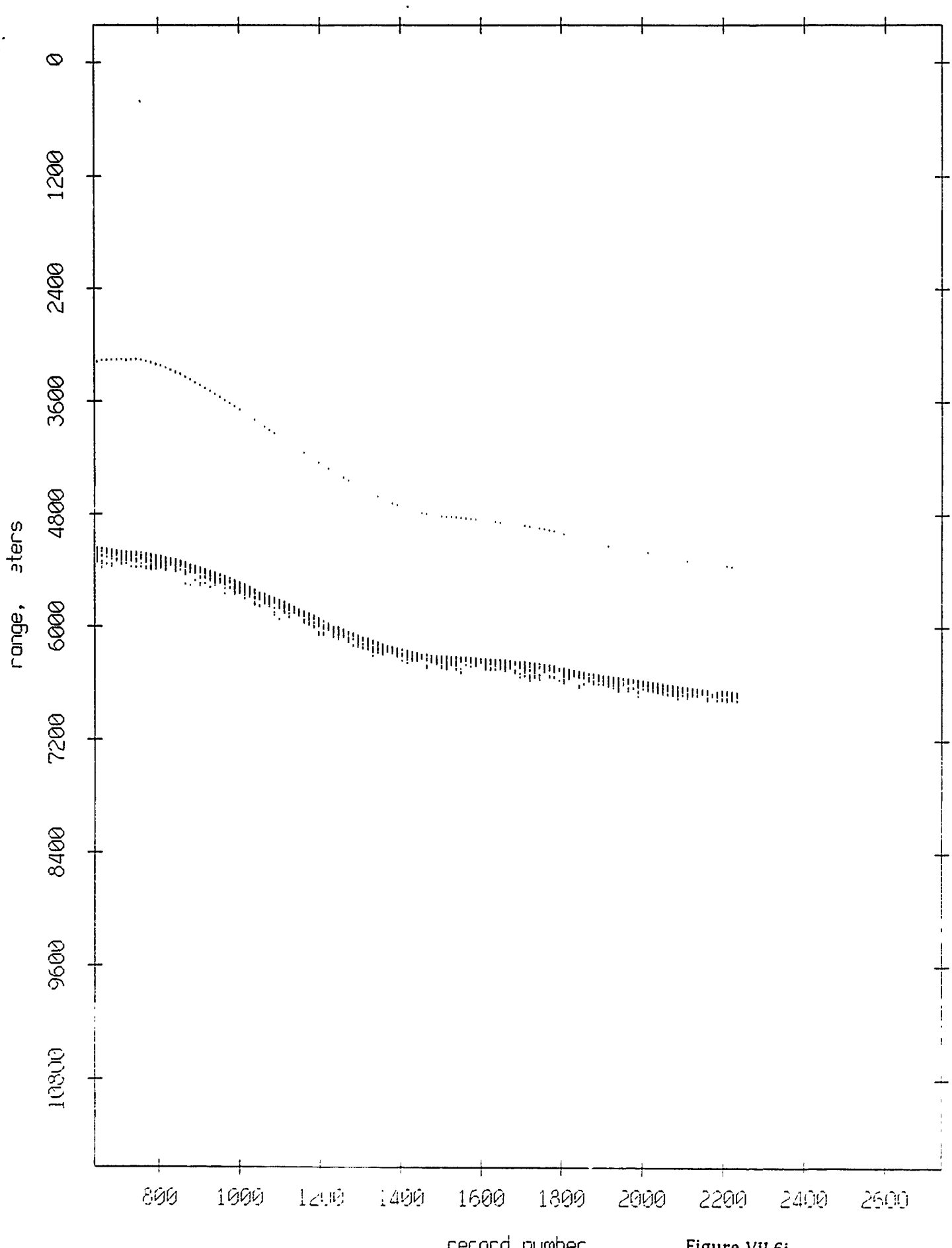

Figure VII.6j

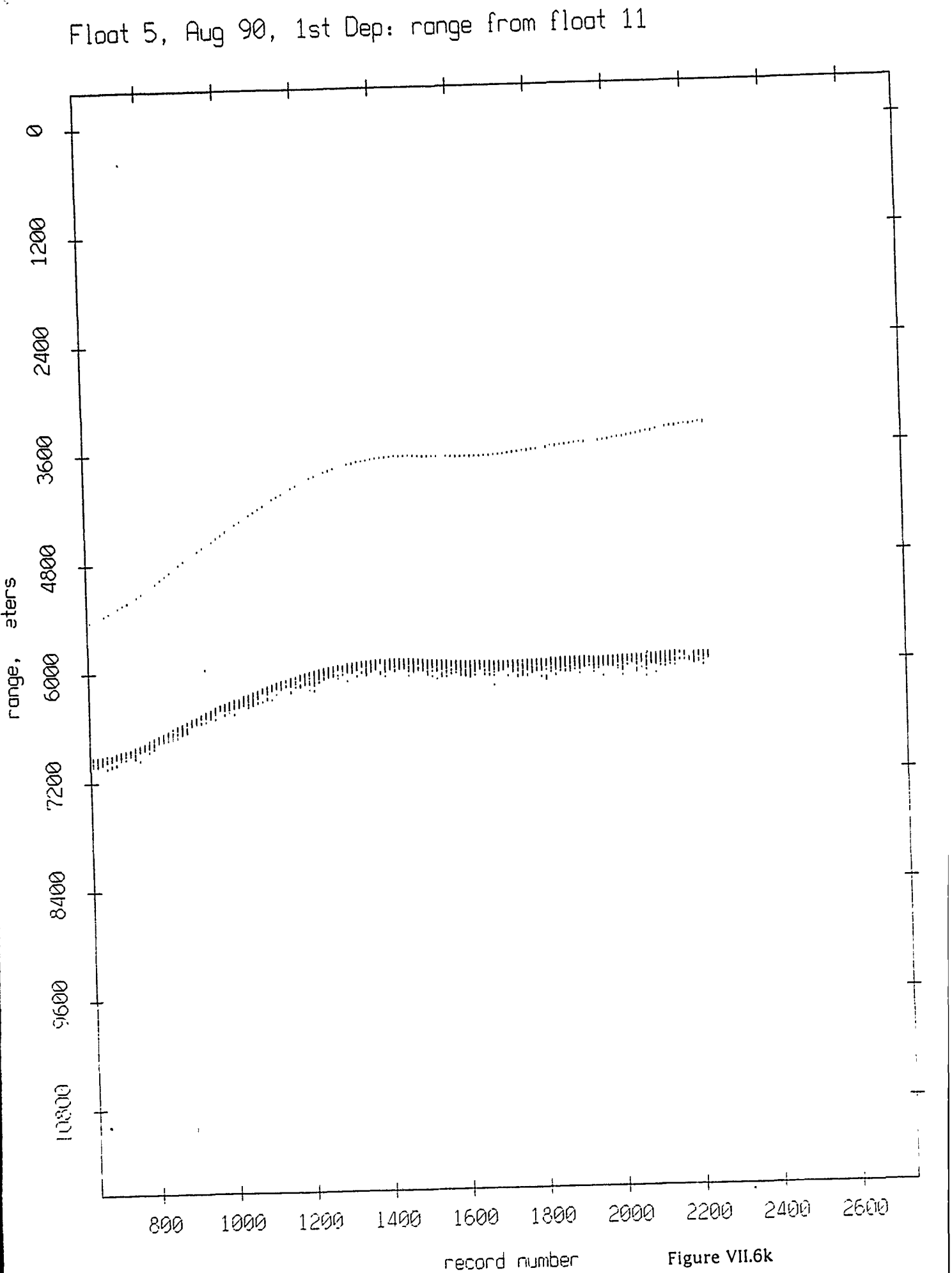

Figure VII.6k

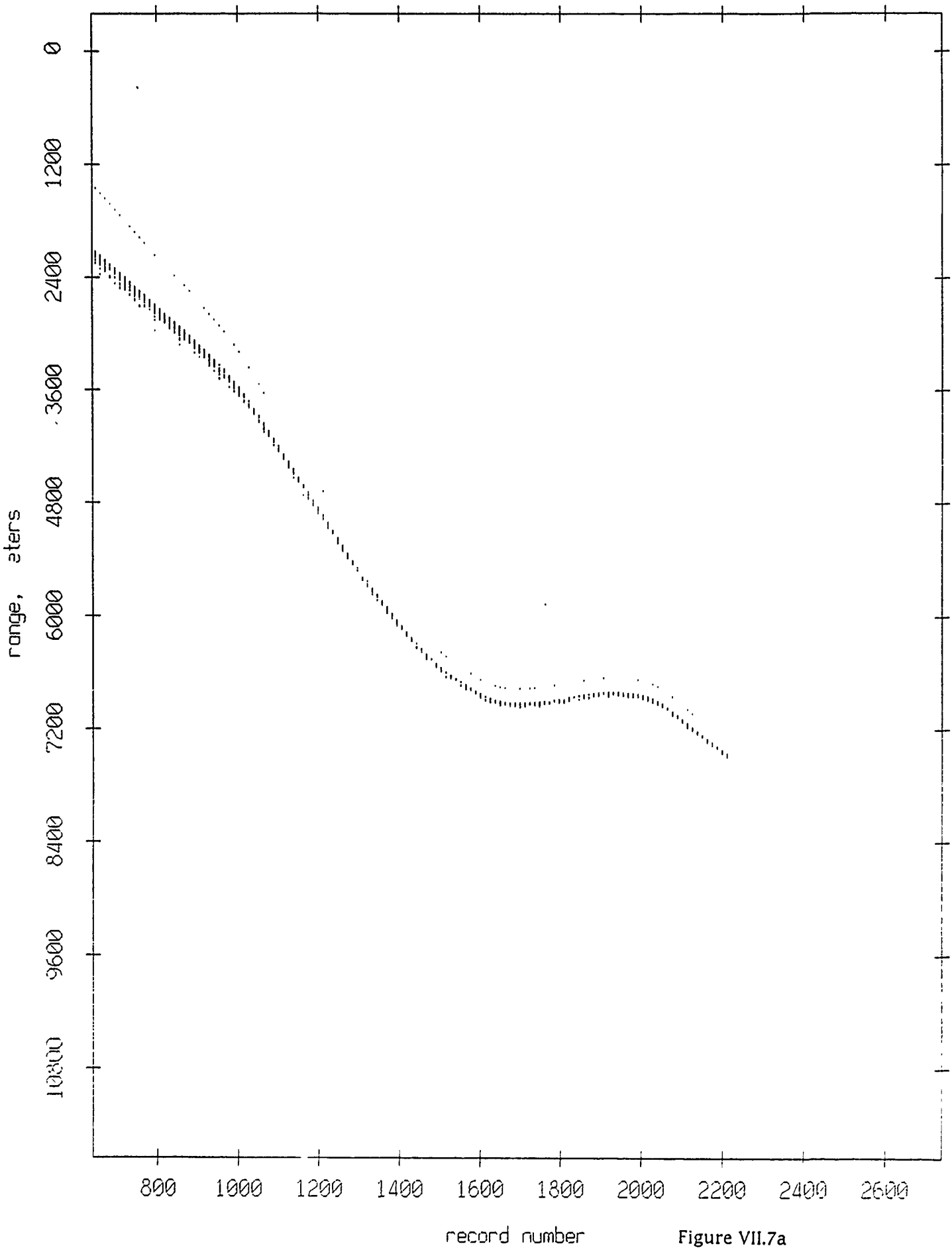

Figure VII.7a

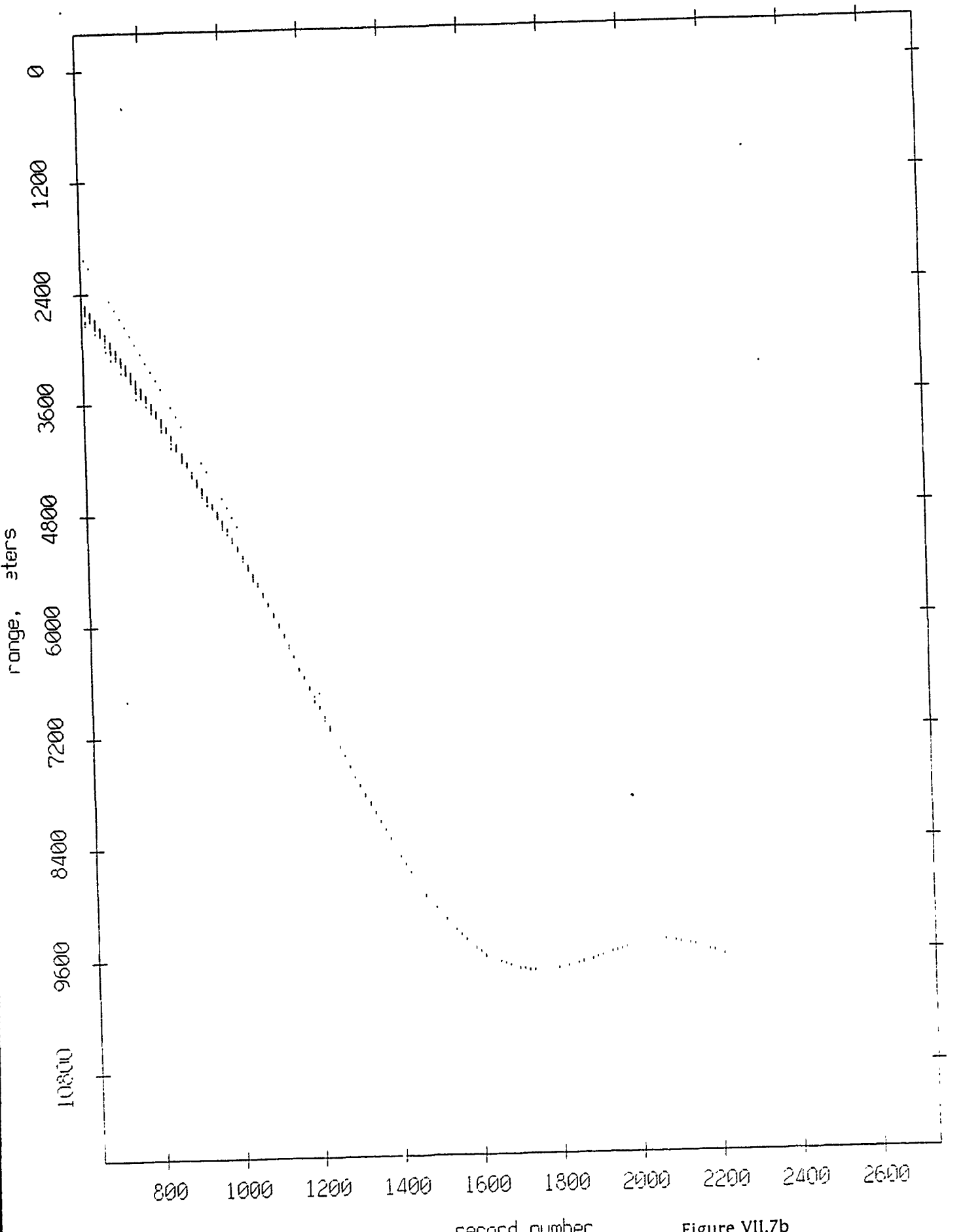

Figure VII.7b

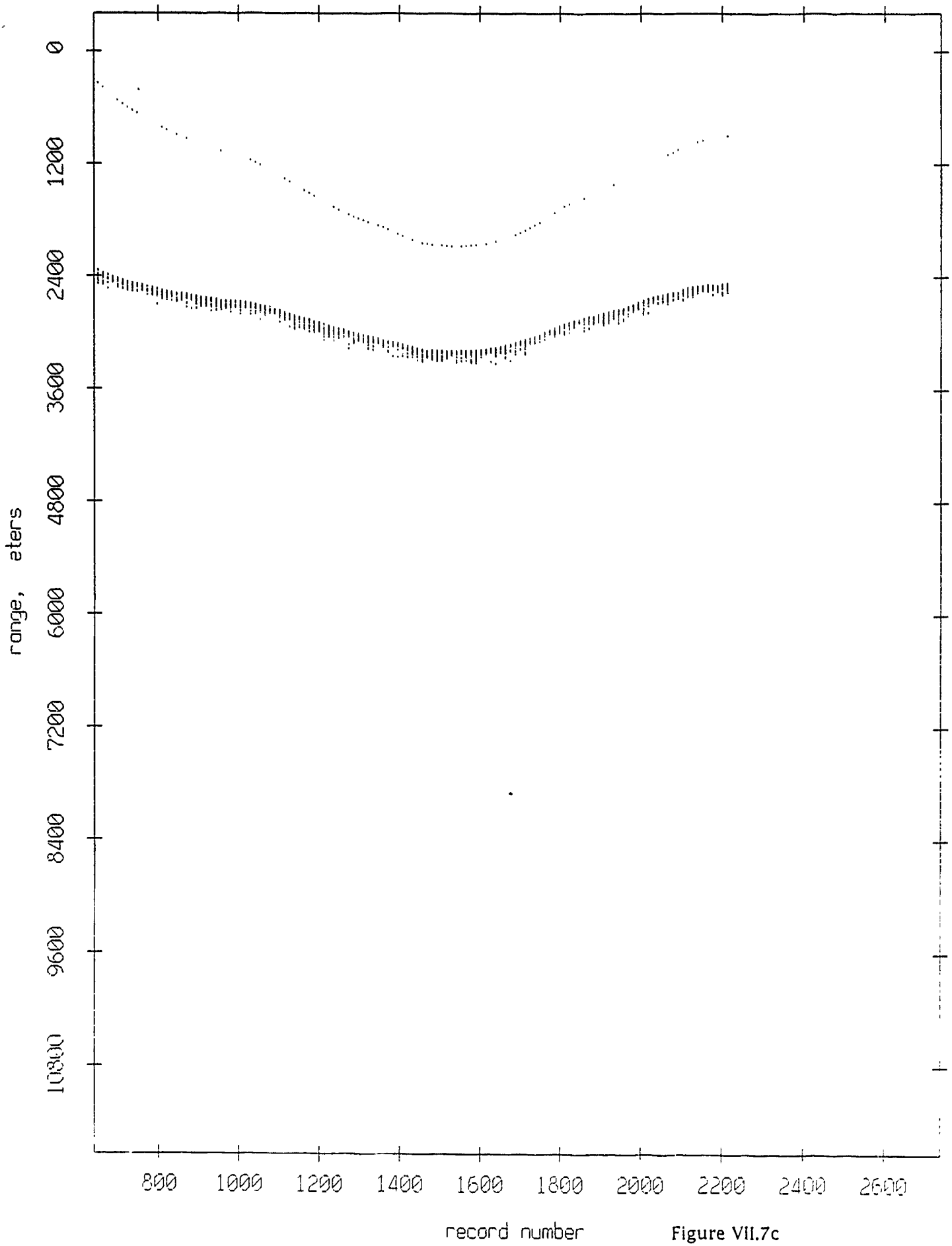

Figure VII.7c

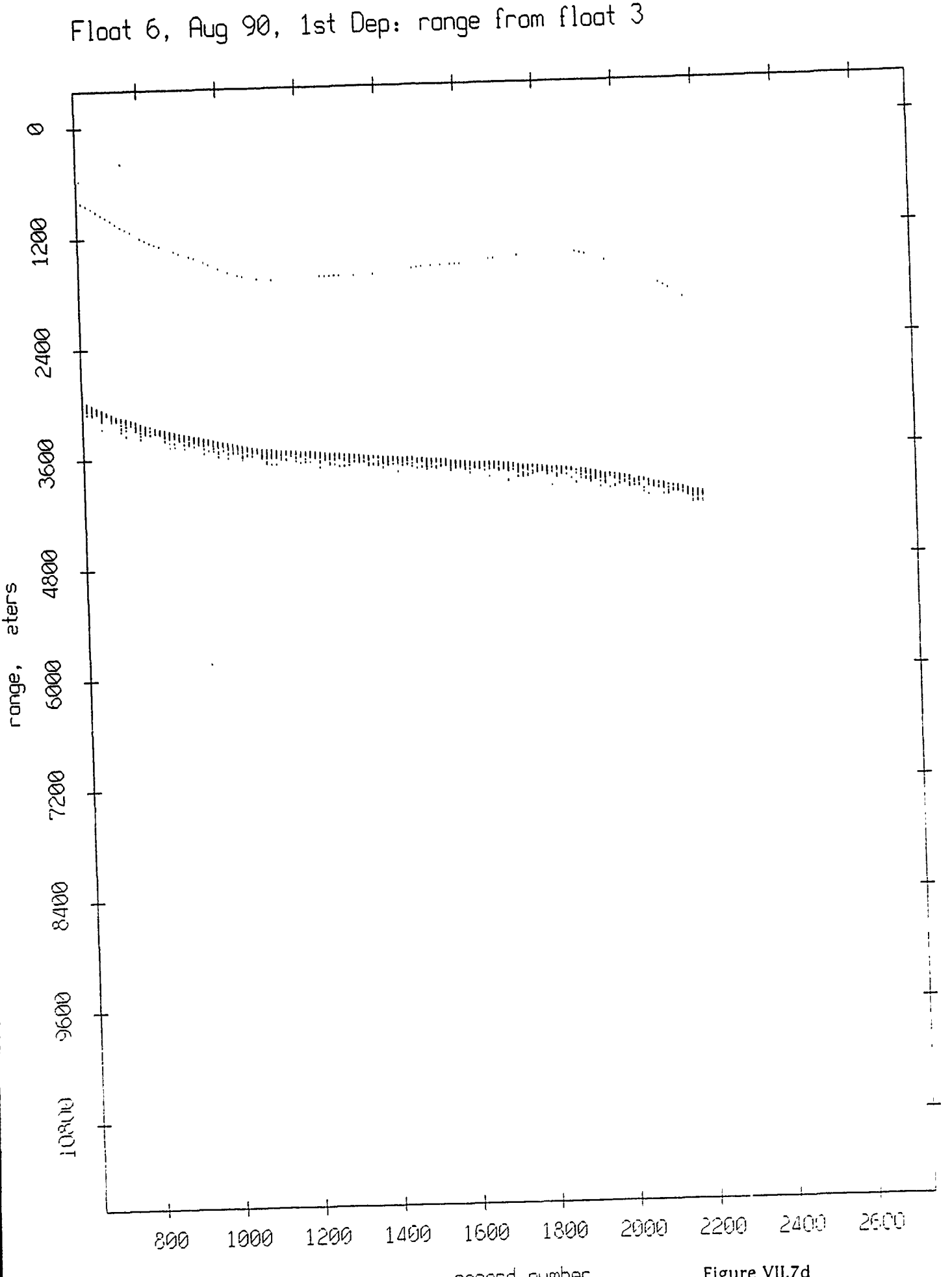

Figure VII.7d

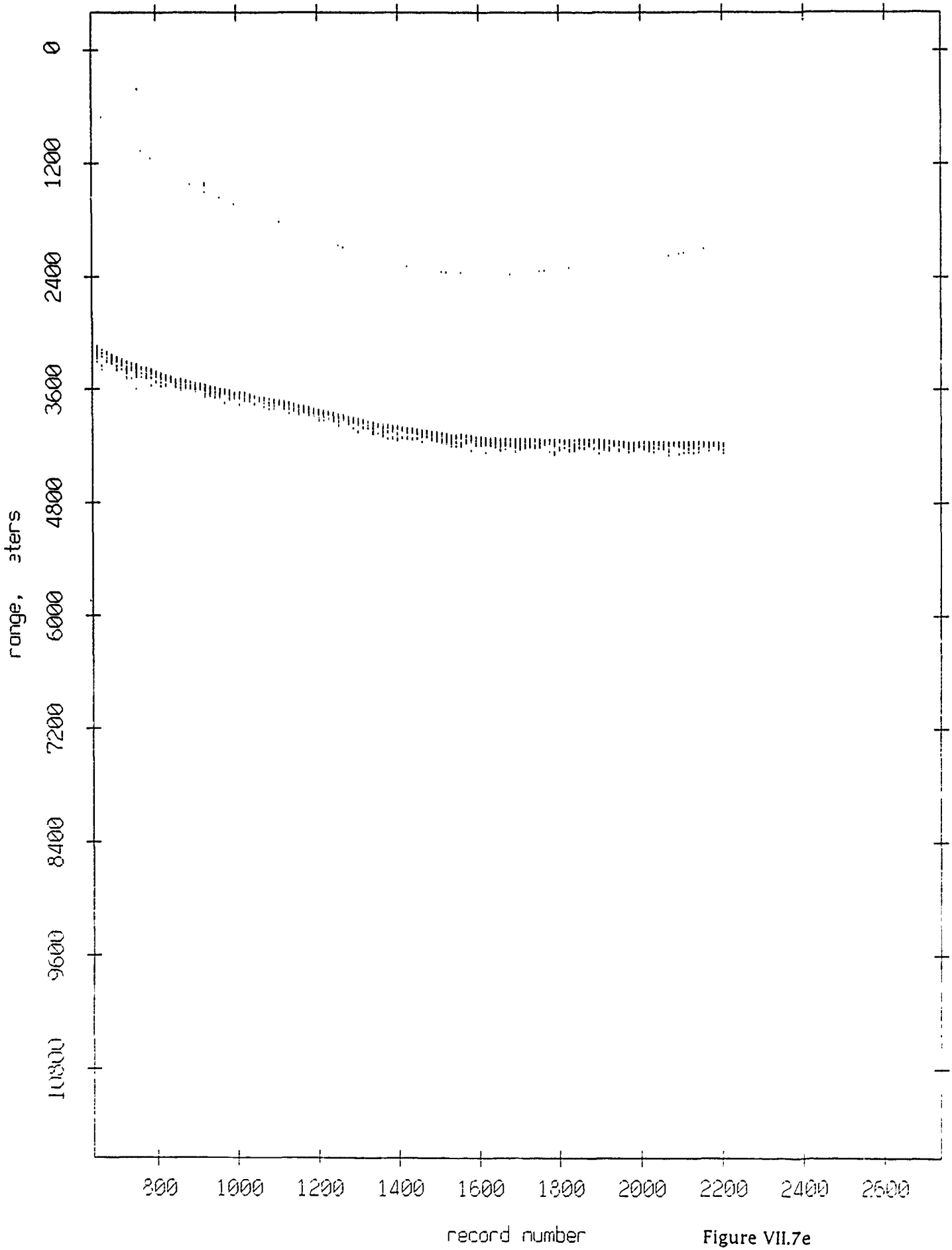

Figure VII.7e

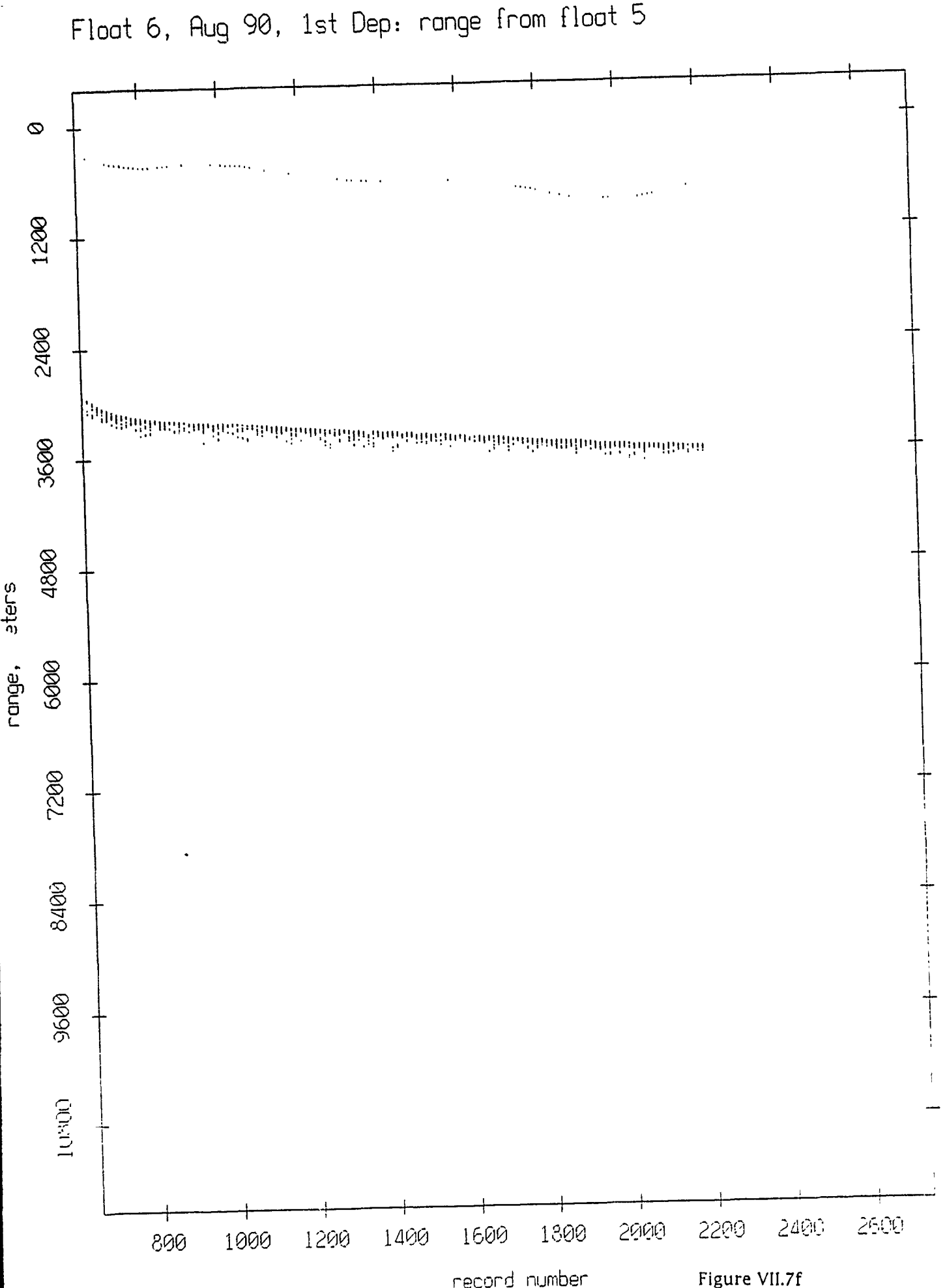

Figure VII.7f

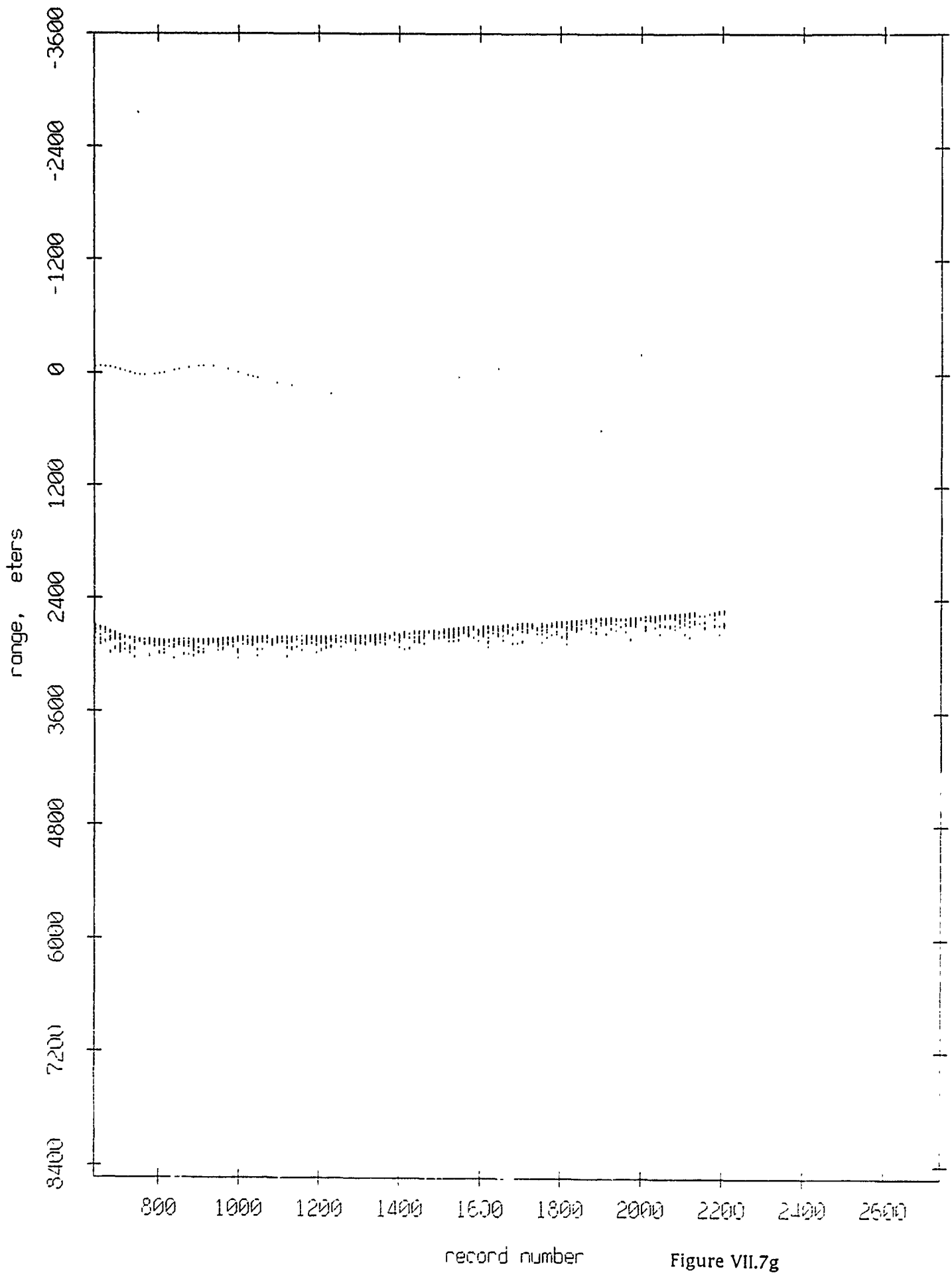

Figure VII.7g

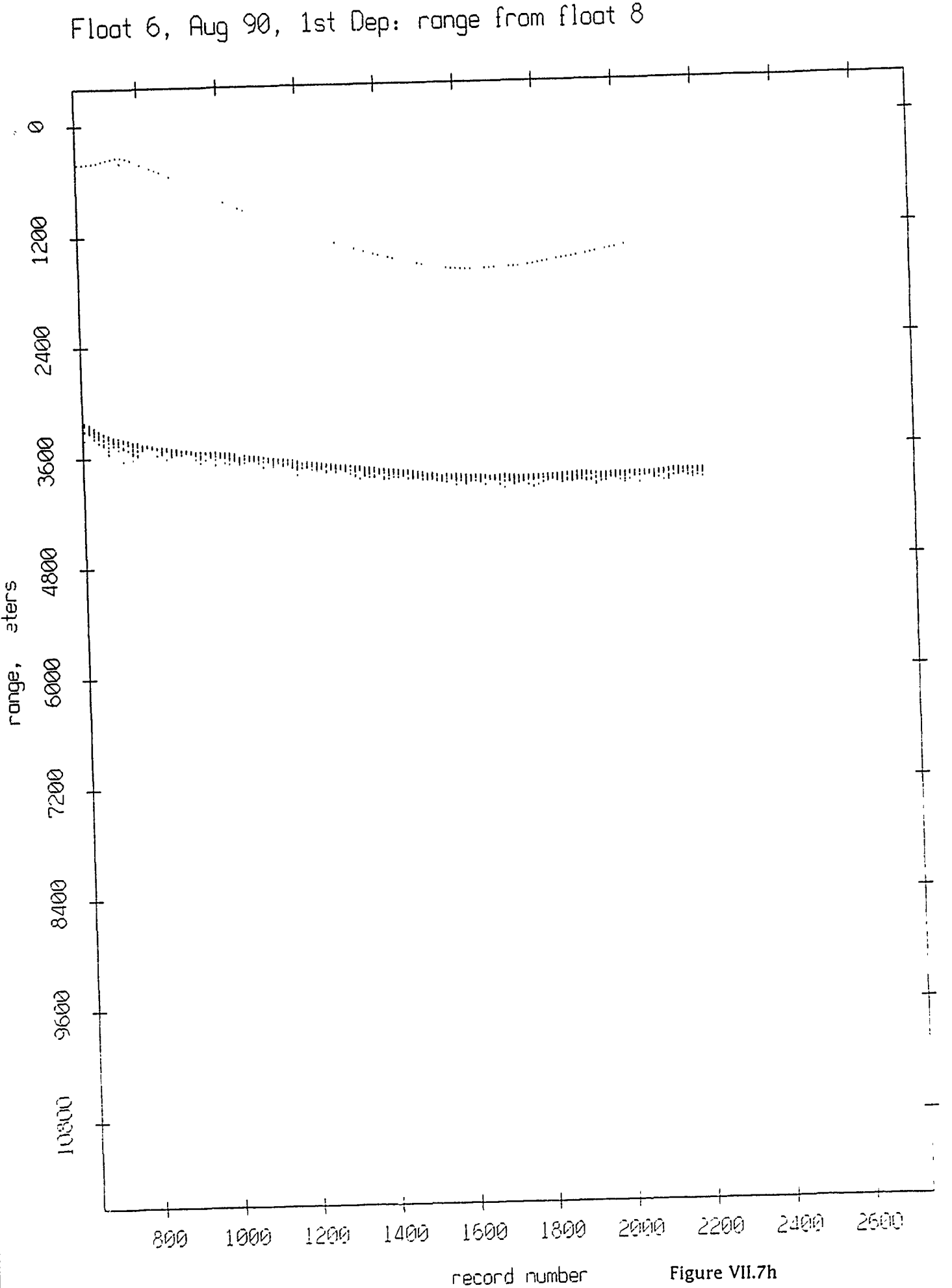

Figure VII.7h

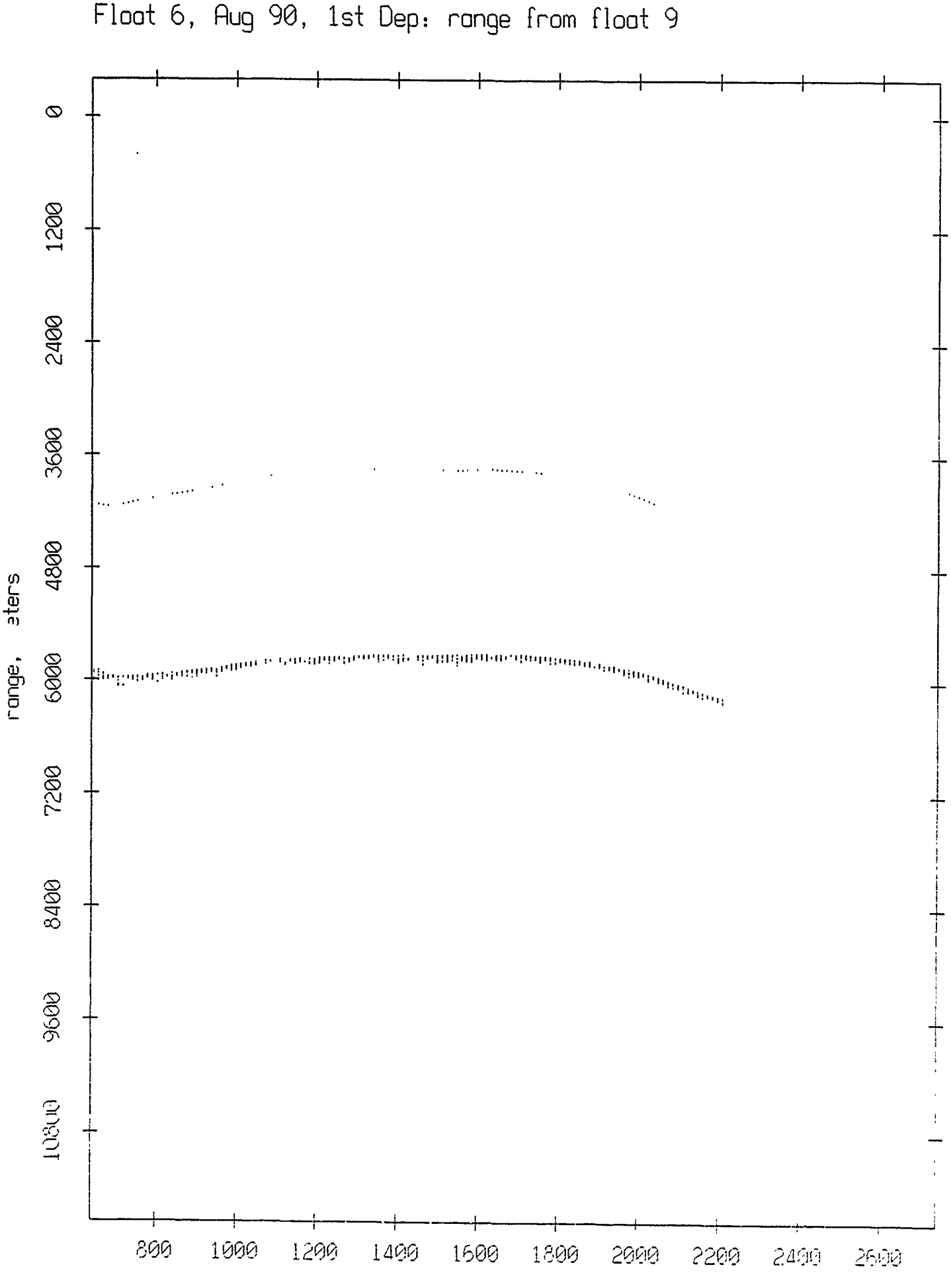

Figure VII.7i

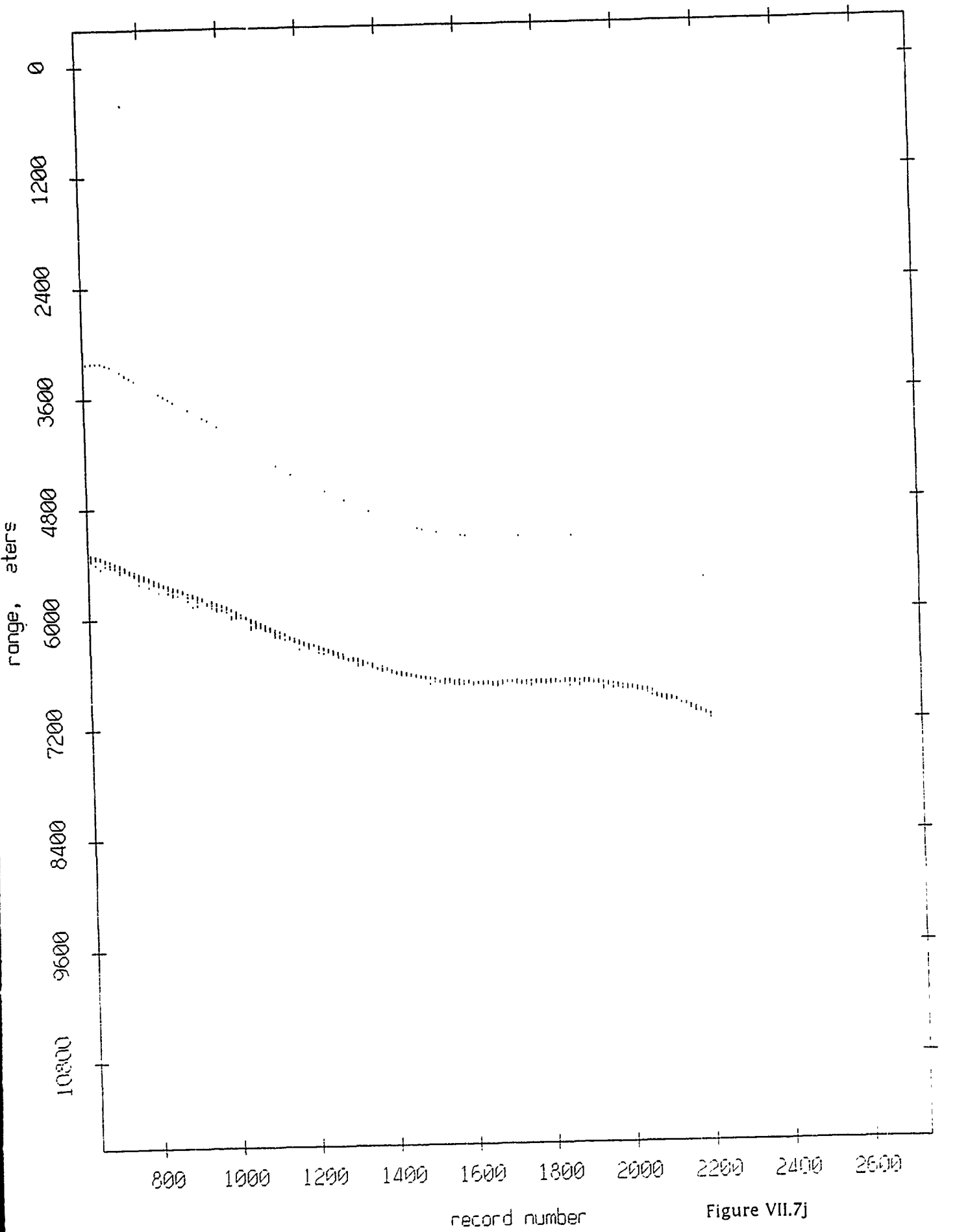

Figure VII.7j

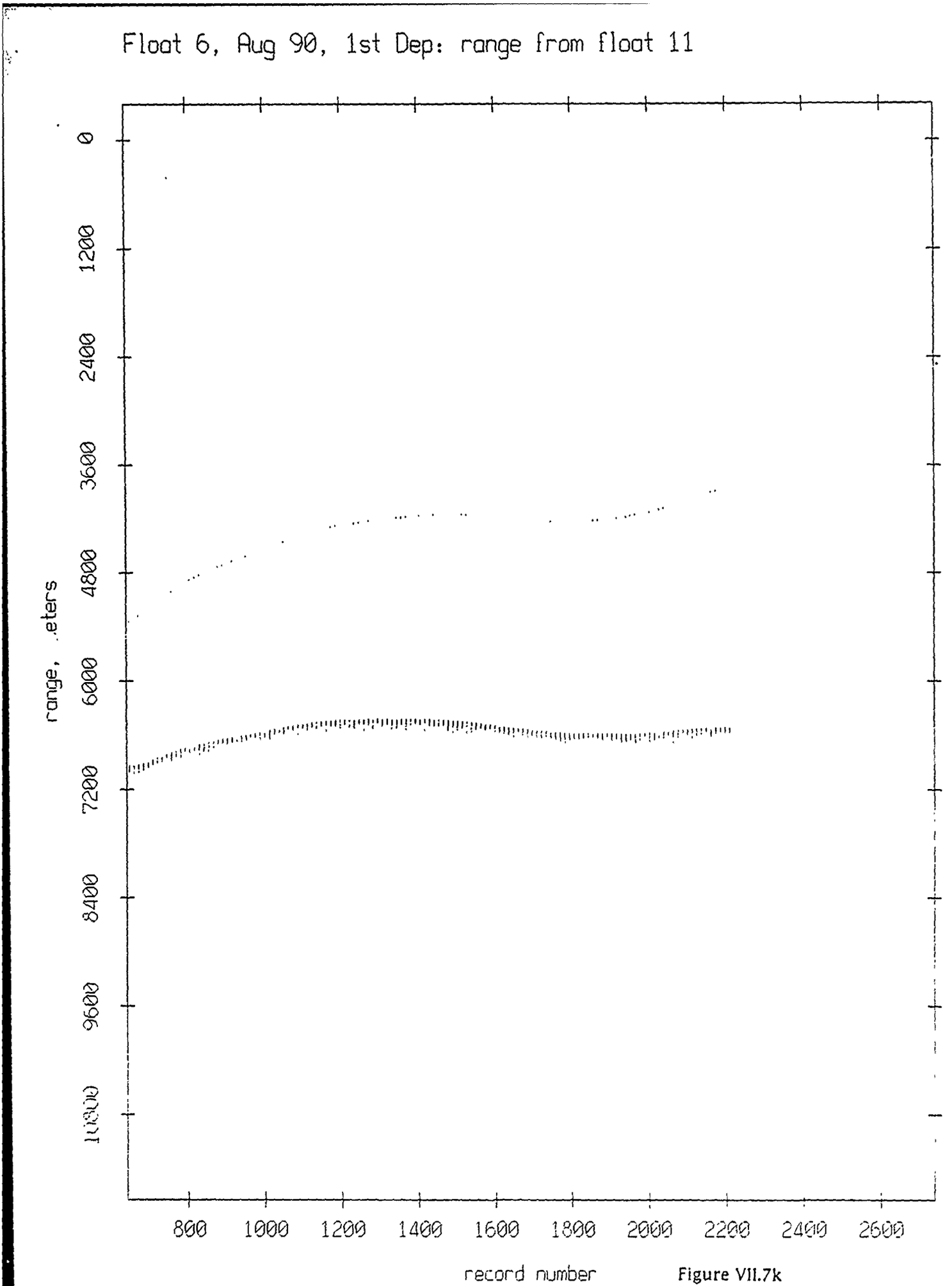

Figure VII.7k

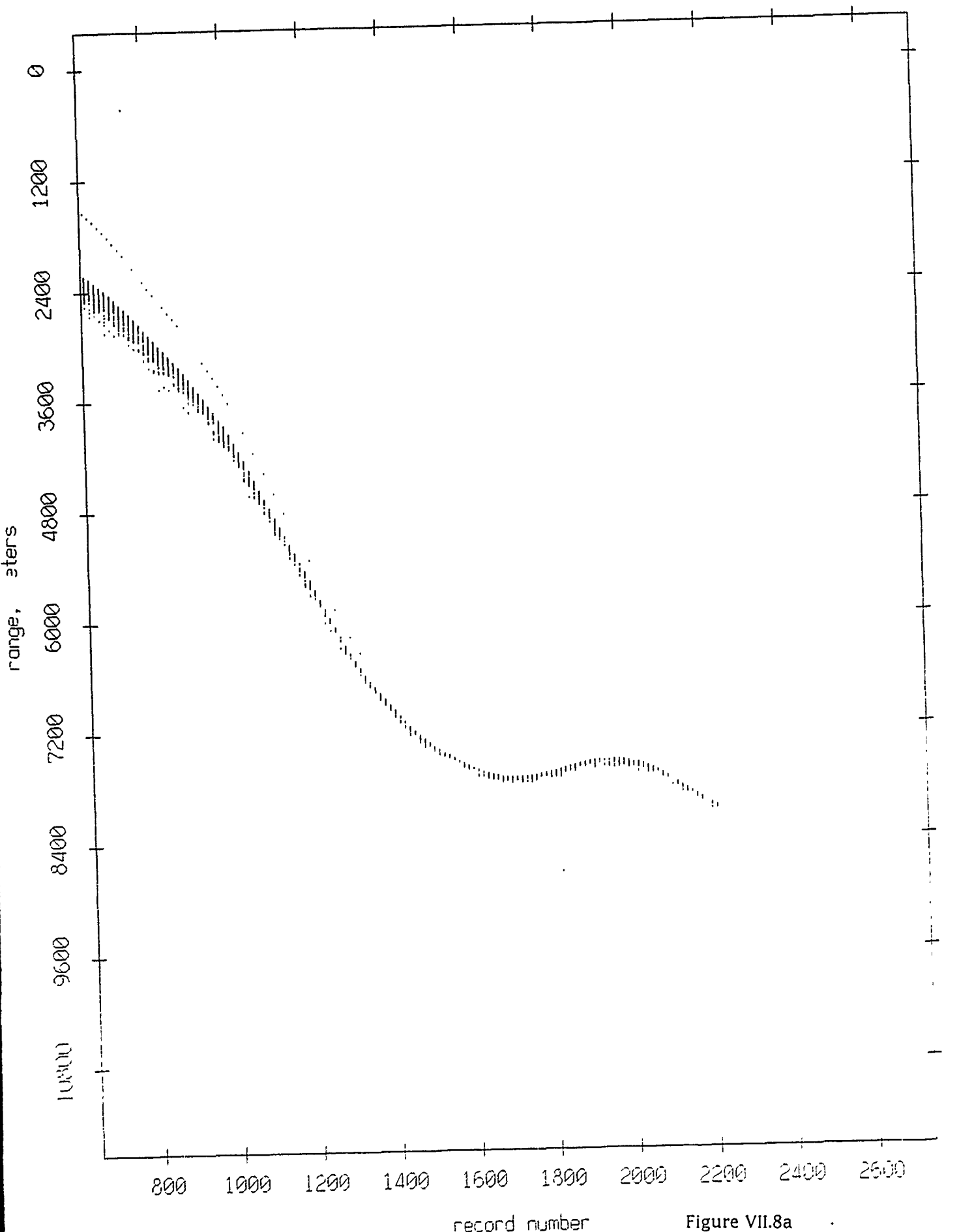

Figure VII.8a

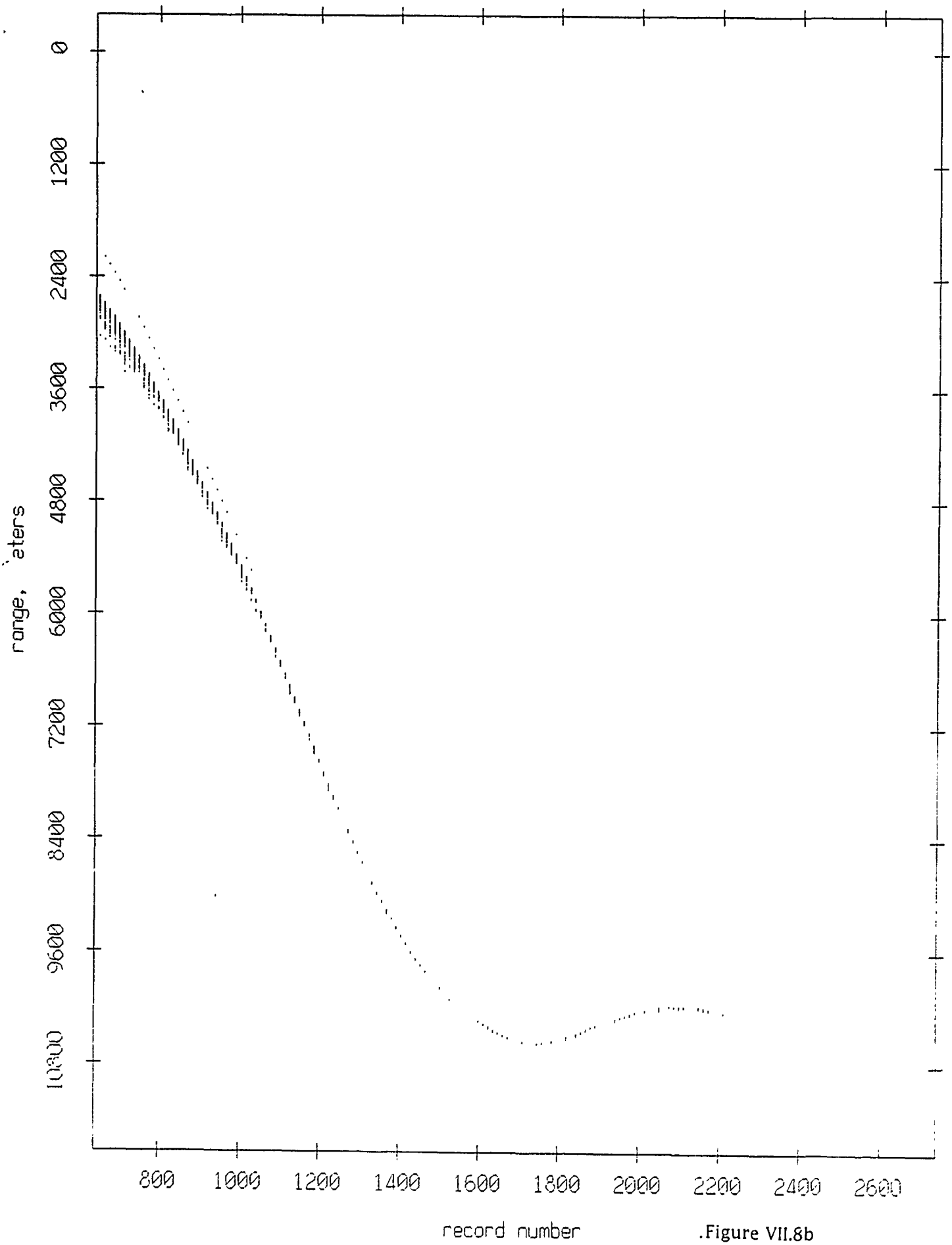

.Figure VII.8b

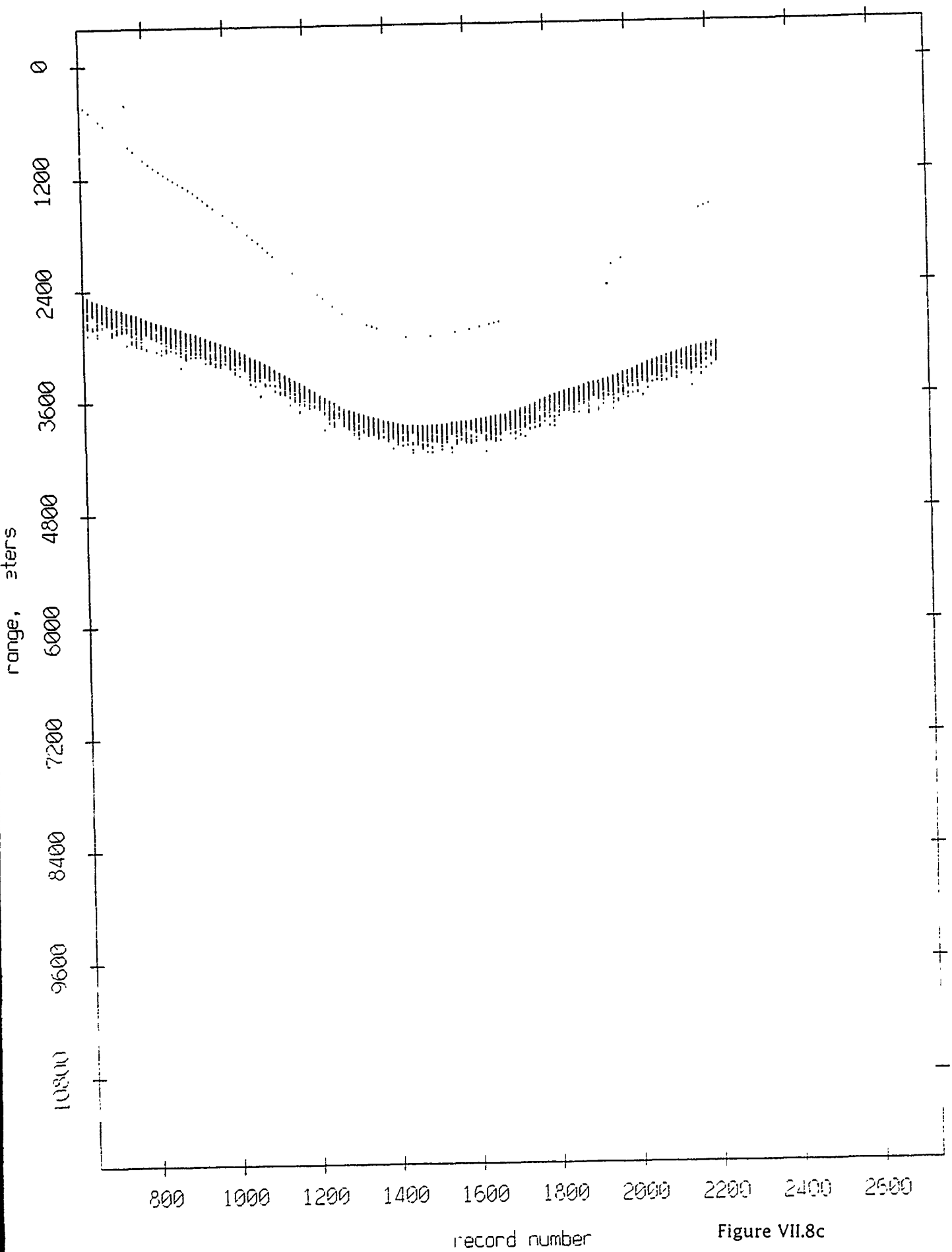

Figure VII.8c

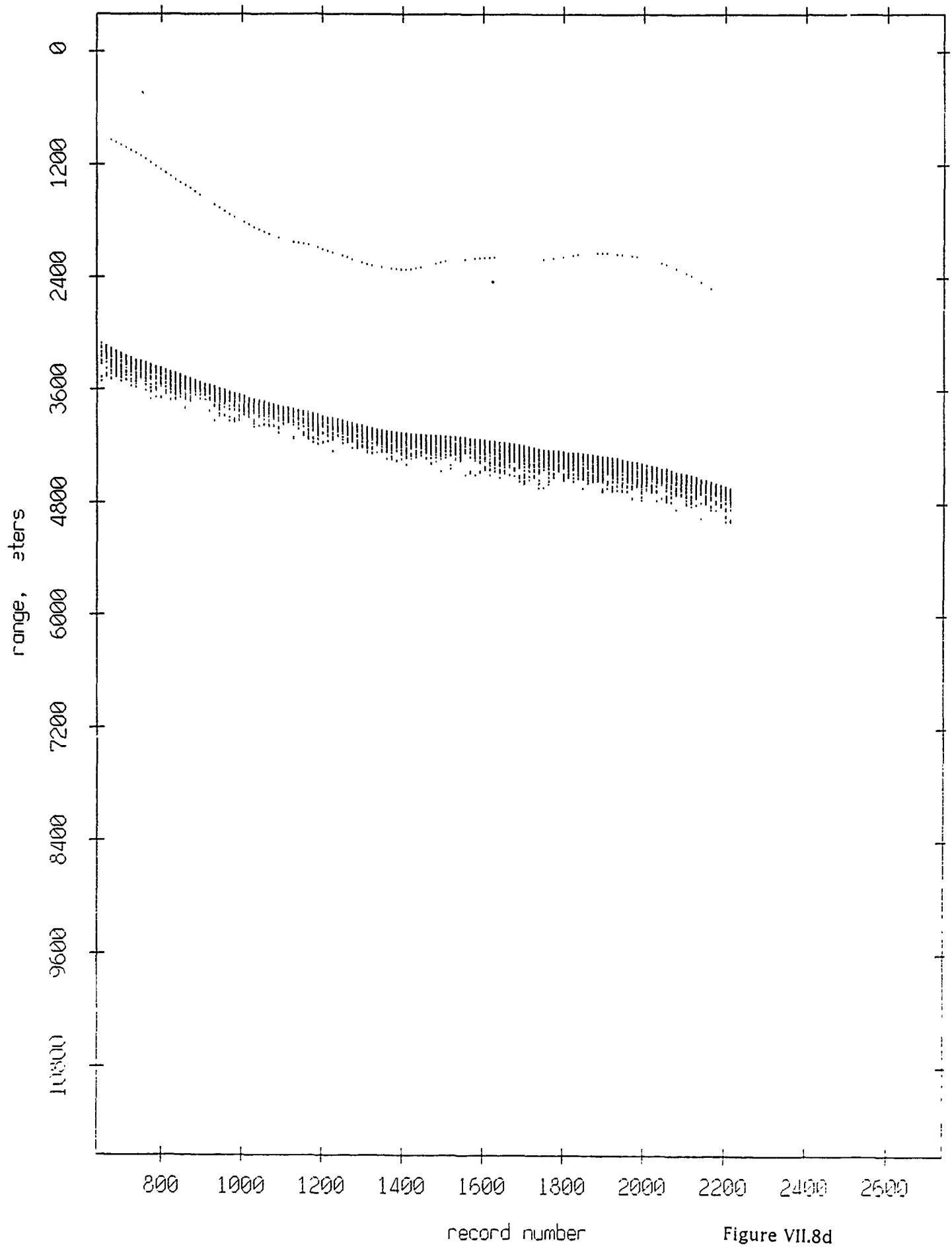

Figure VII.8d

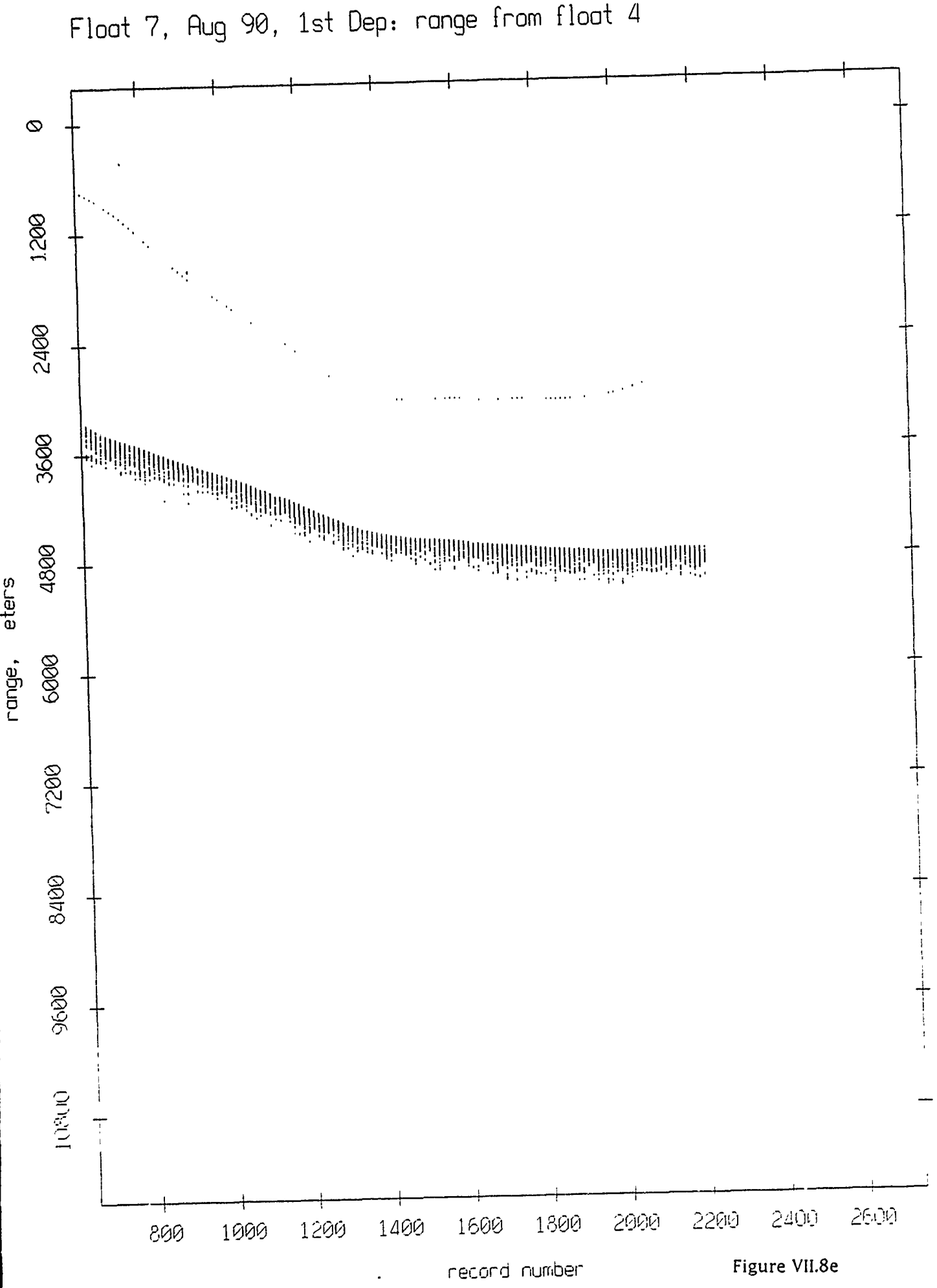

Figure VII.8e

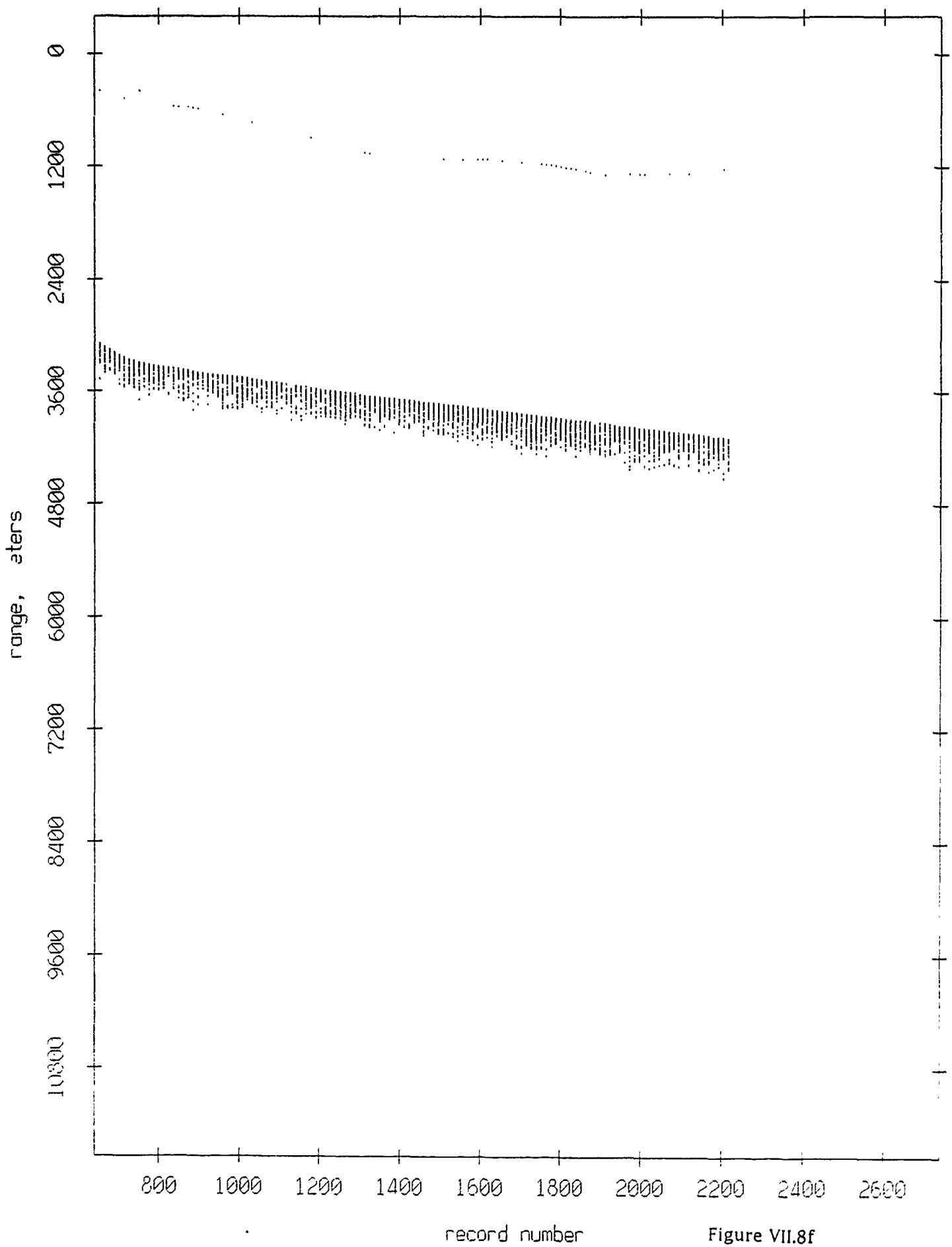

Figure VII.8f

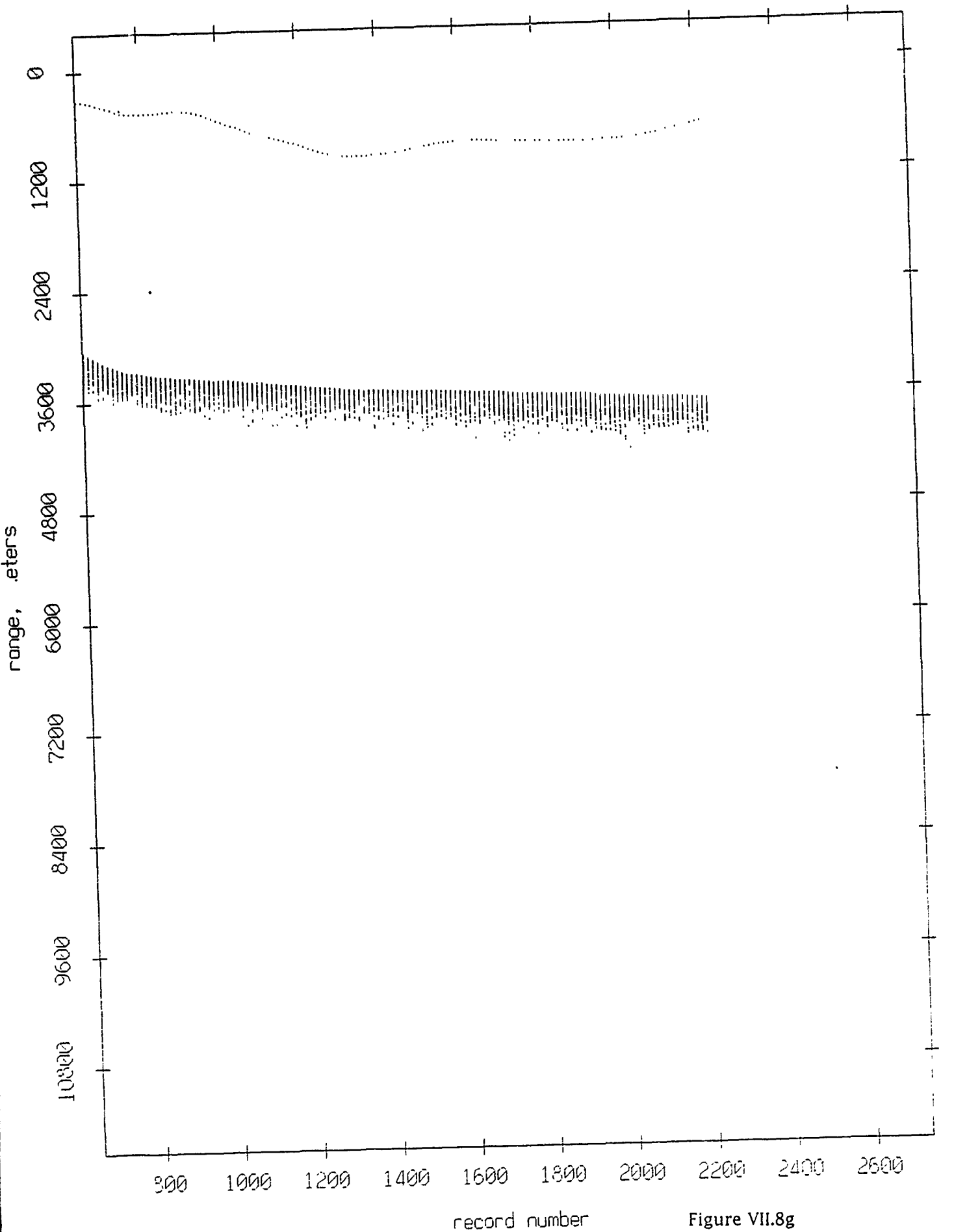

Figure VII.8g

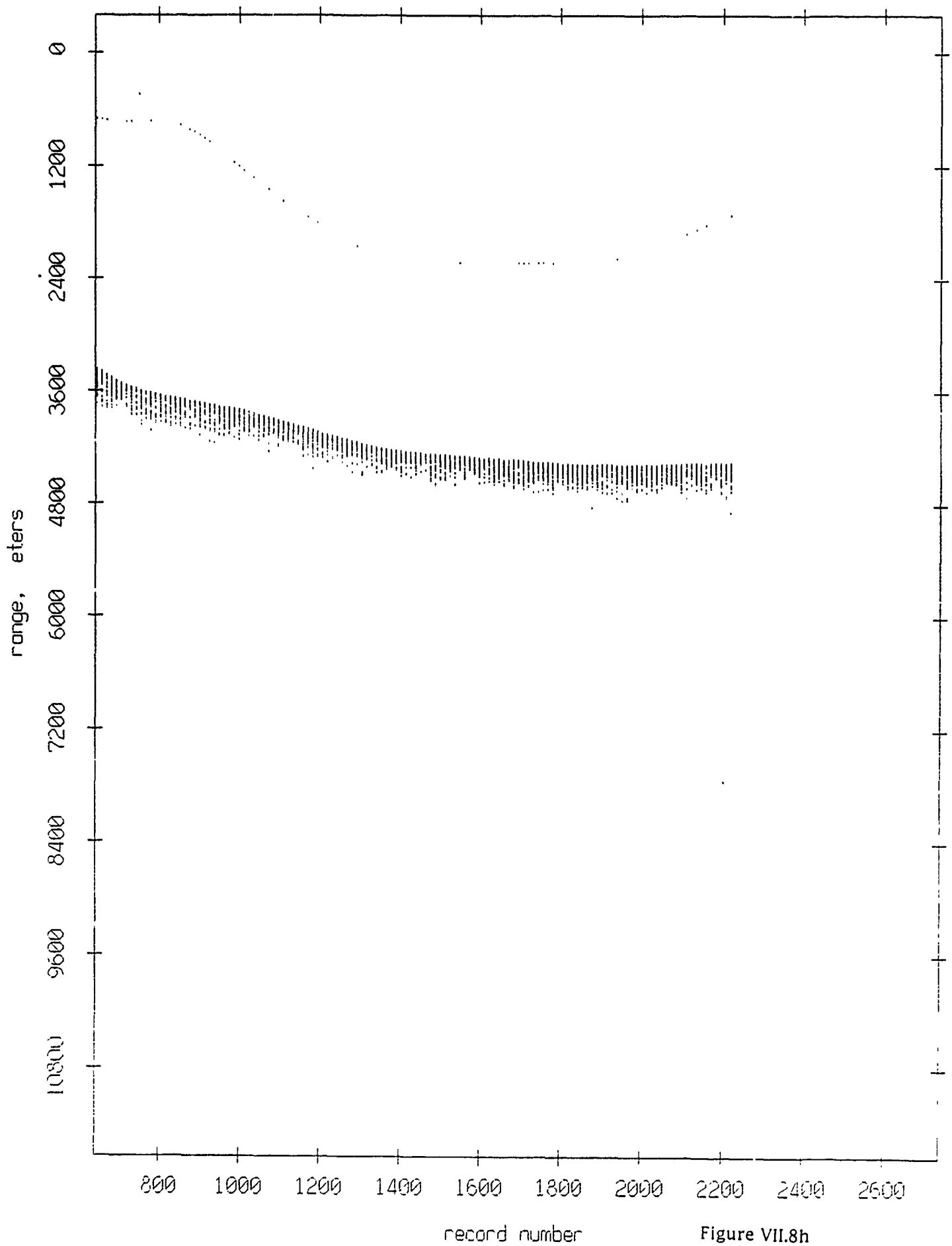

Figure VII.8h

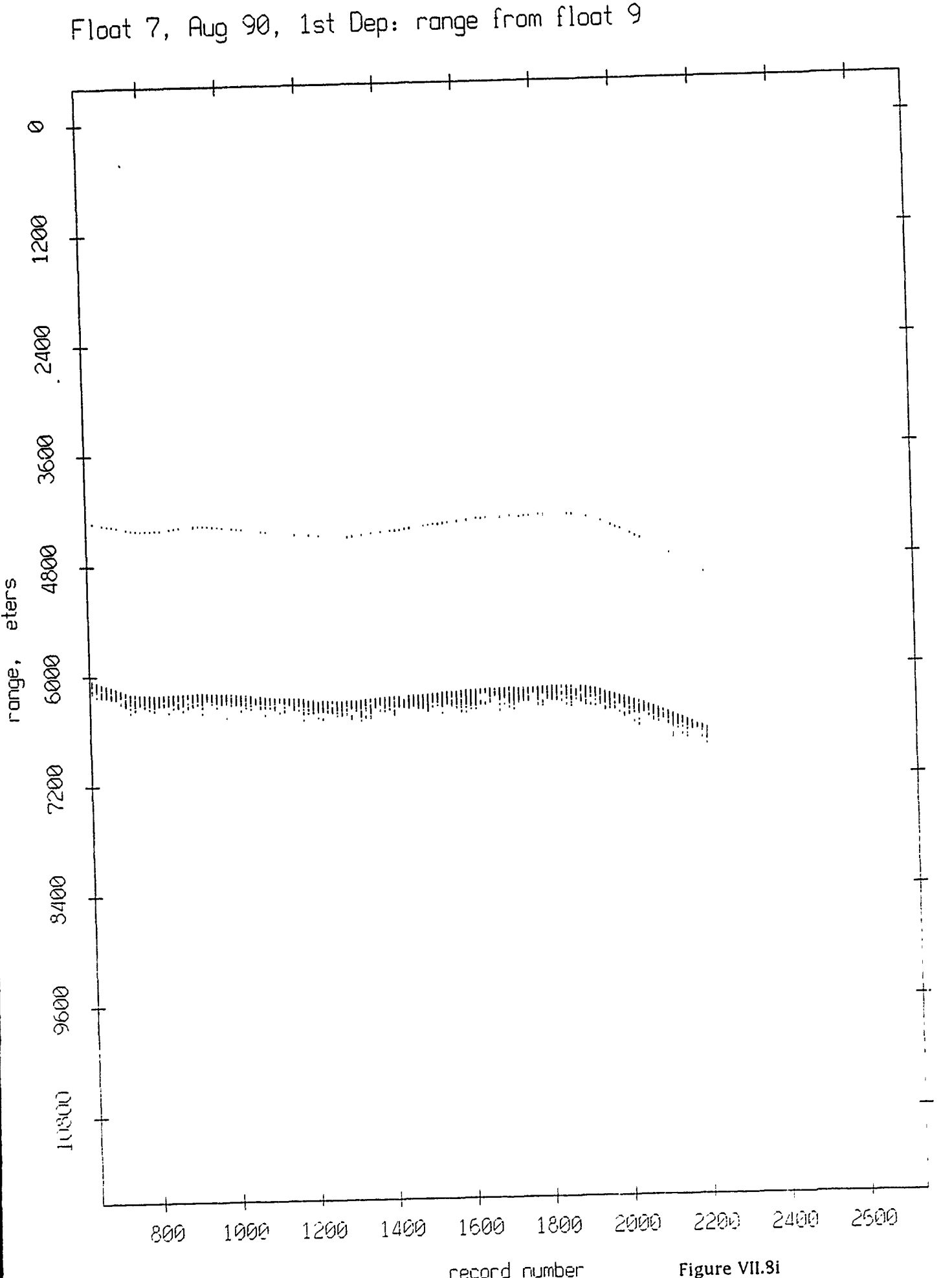

Figure VII.8i

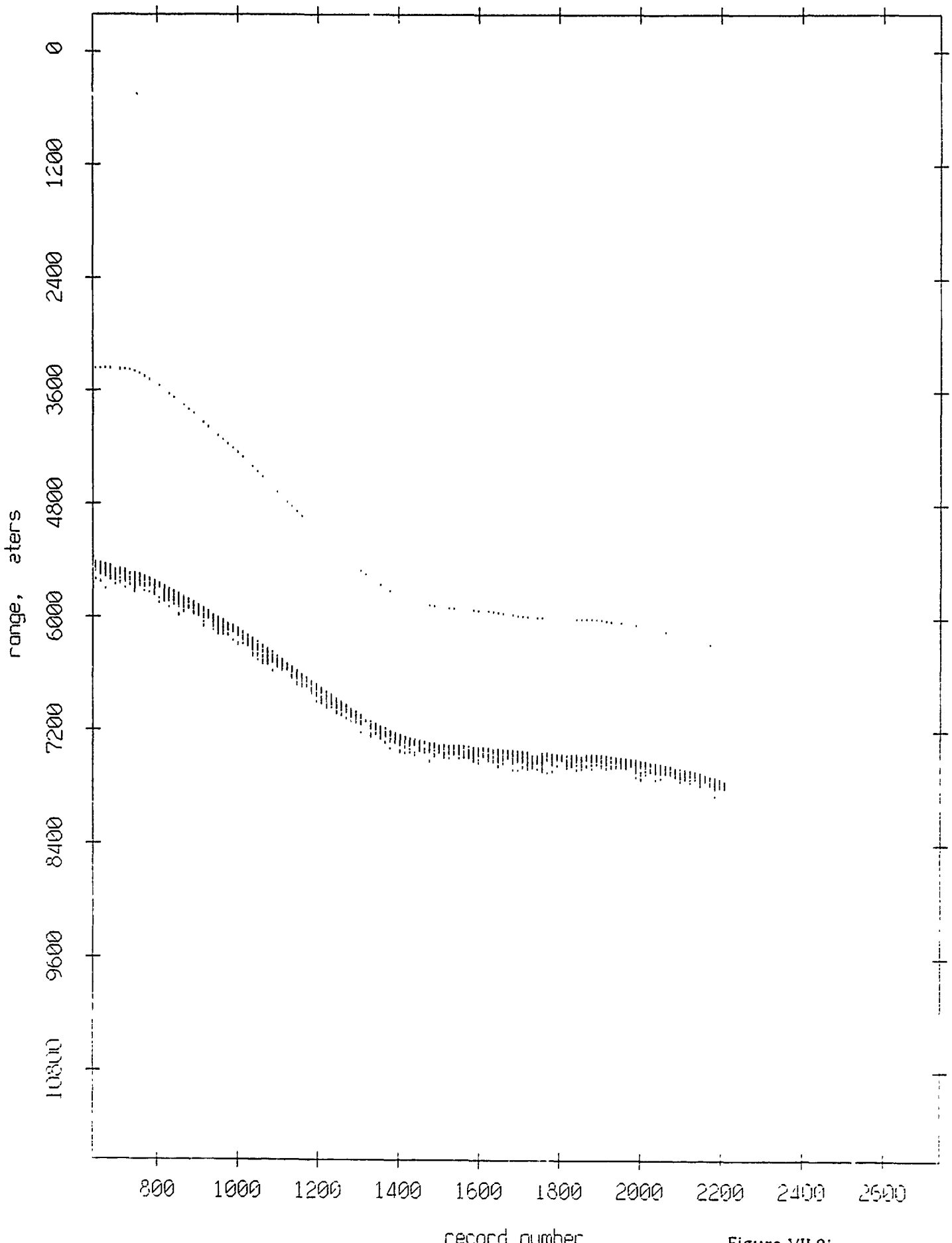

Figure VII.8j

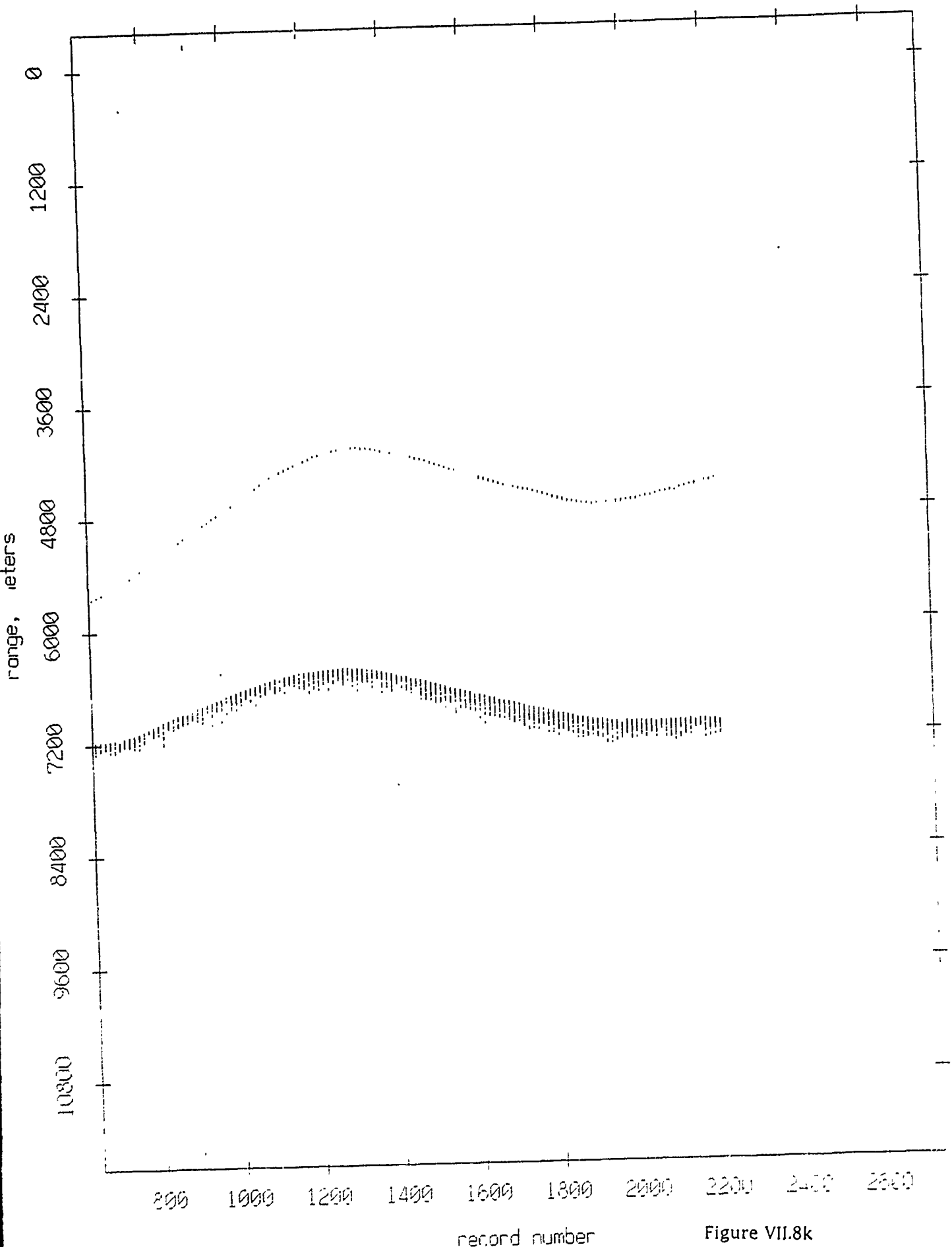

Figure VII.8k

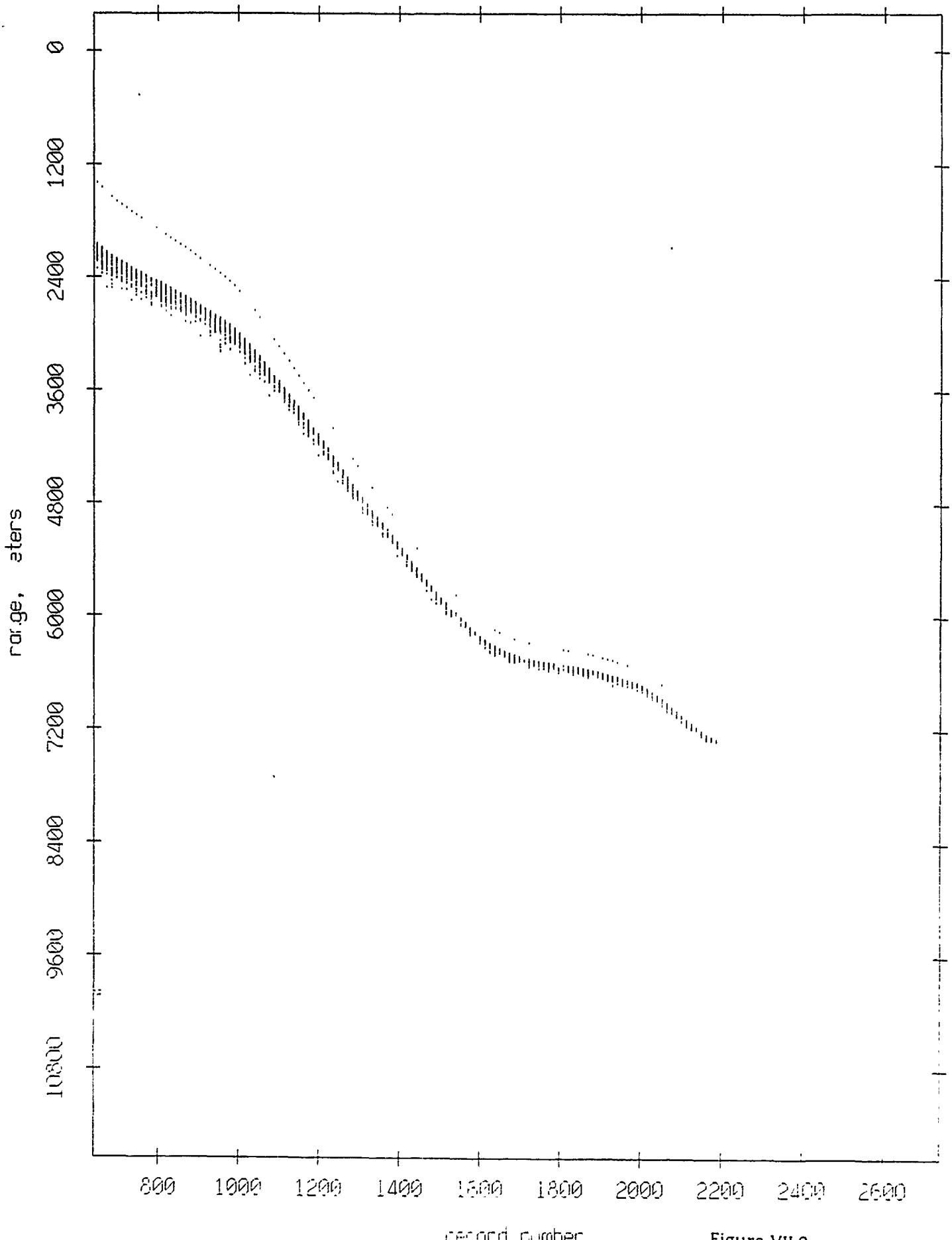

Figure VII.9a

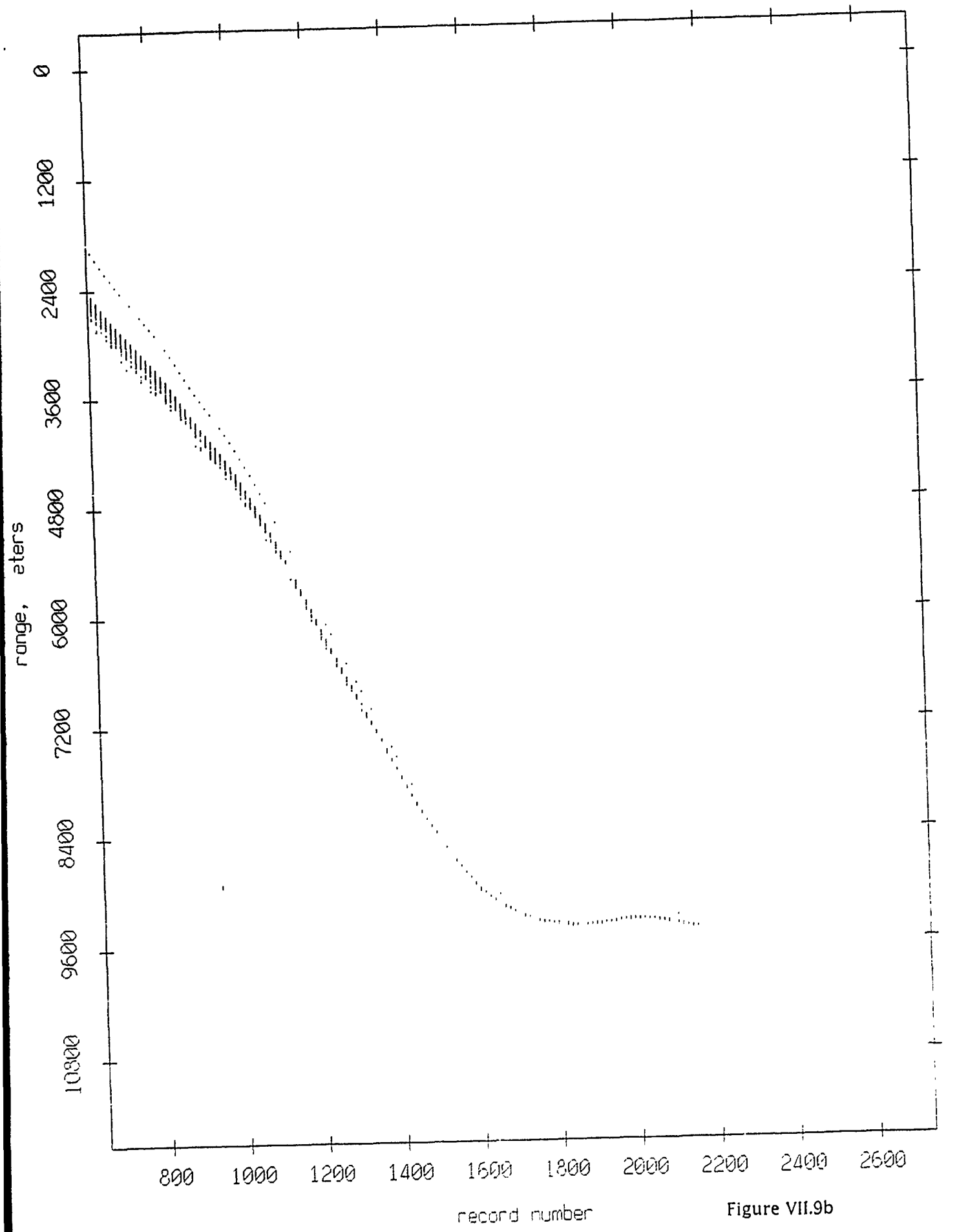

Figure VII.9b

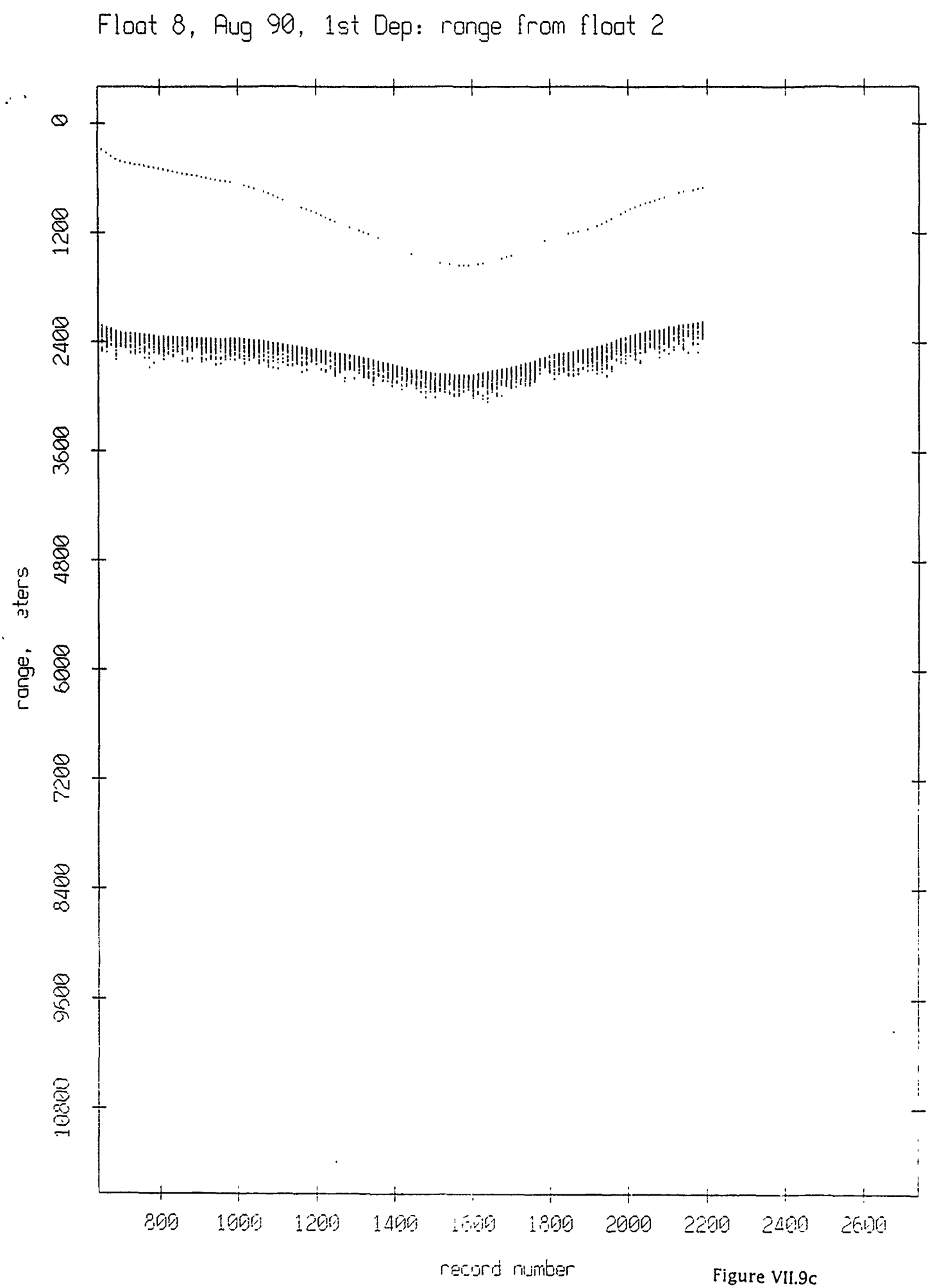

Figure VII.9c

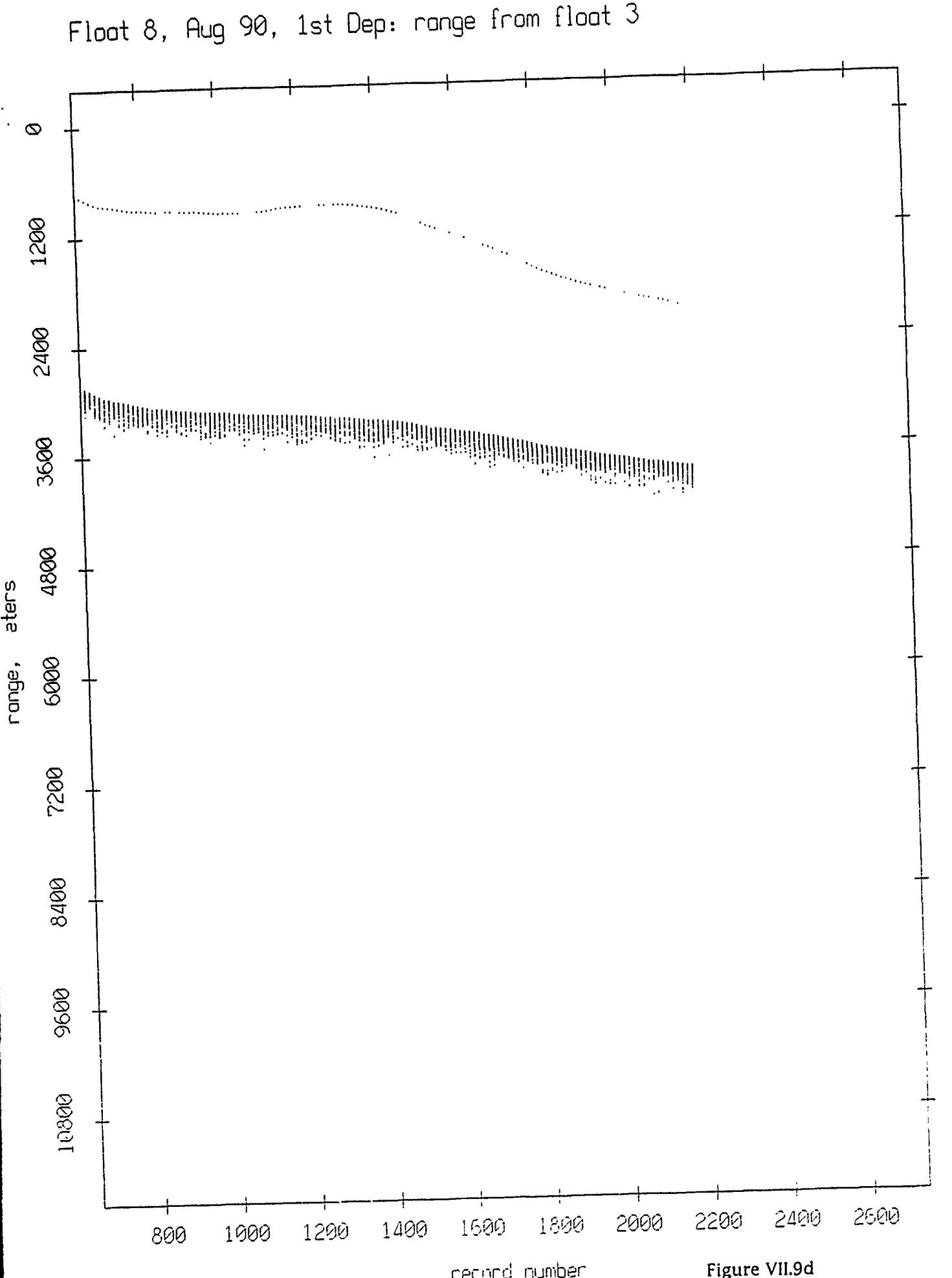

Figure VII.9d

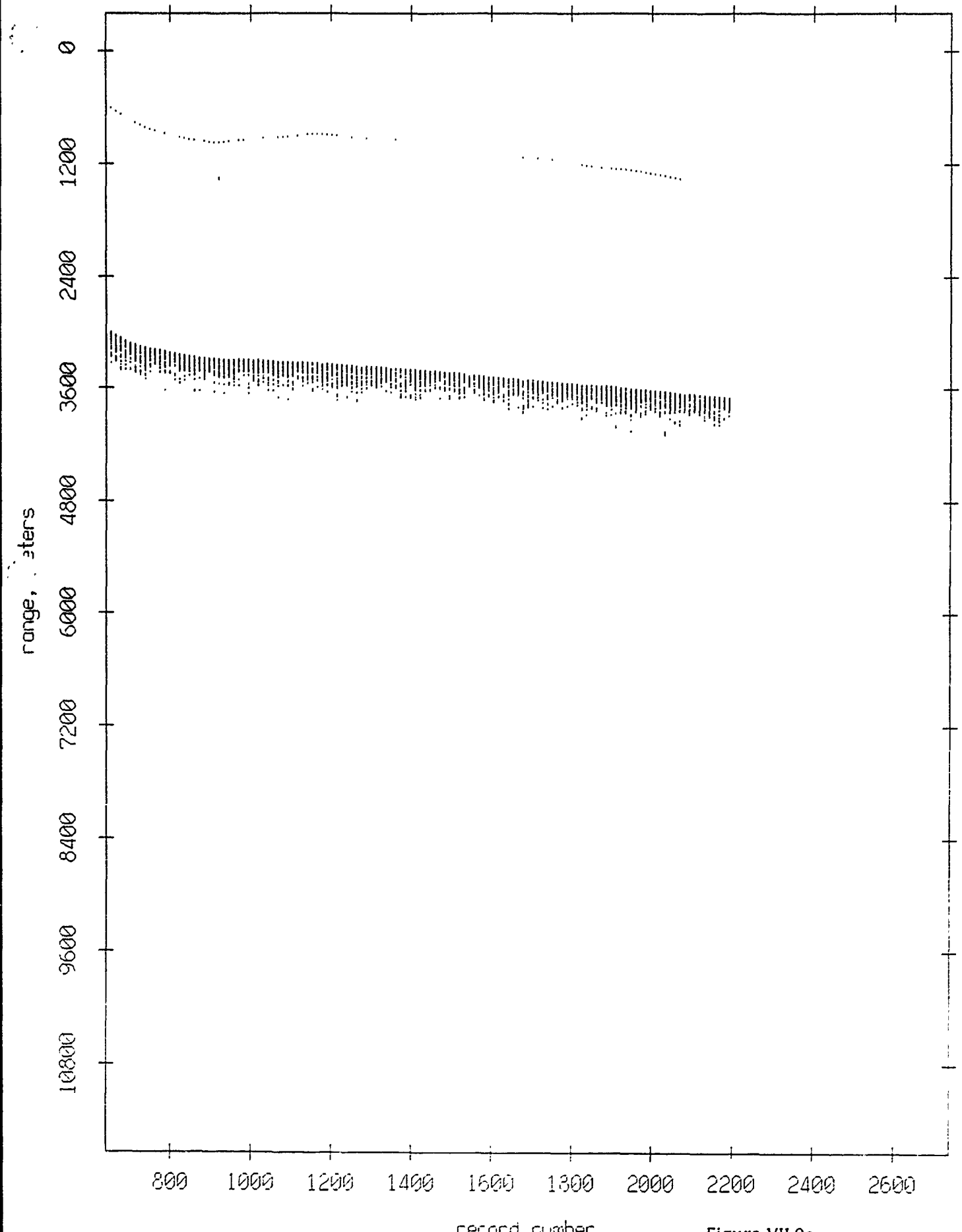

Figure VII.9e

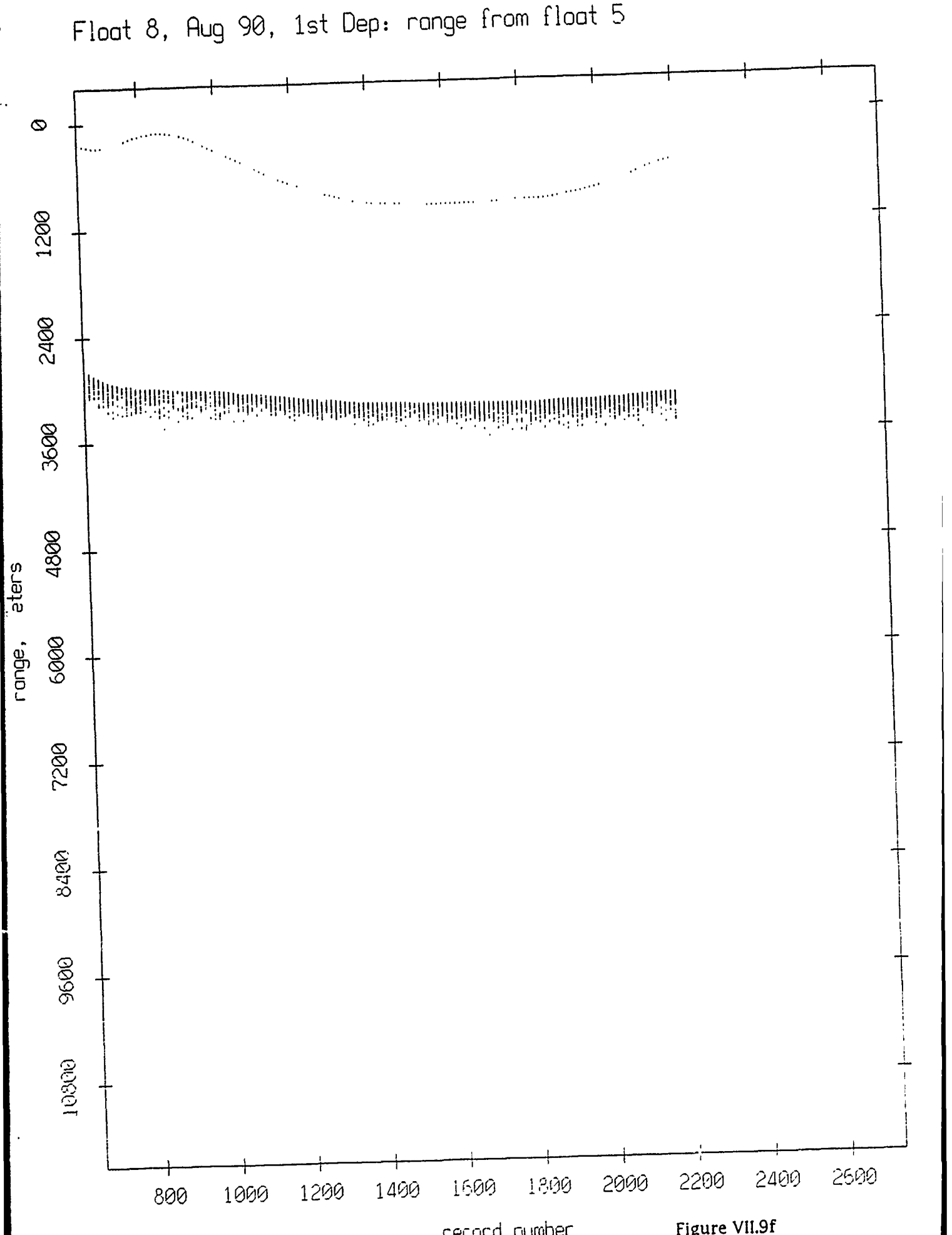

Figure VII.9f

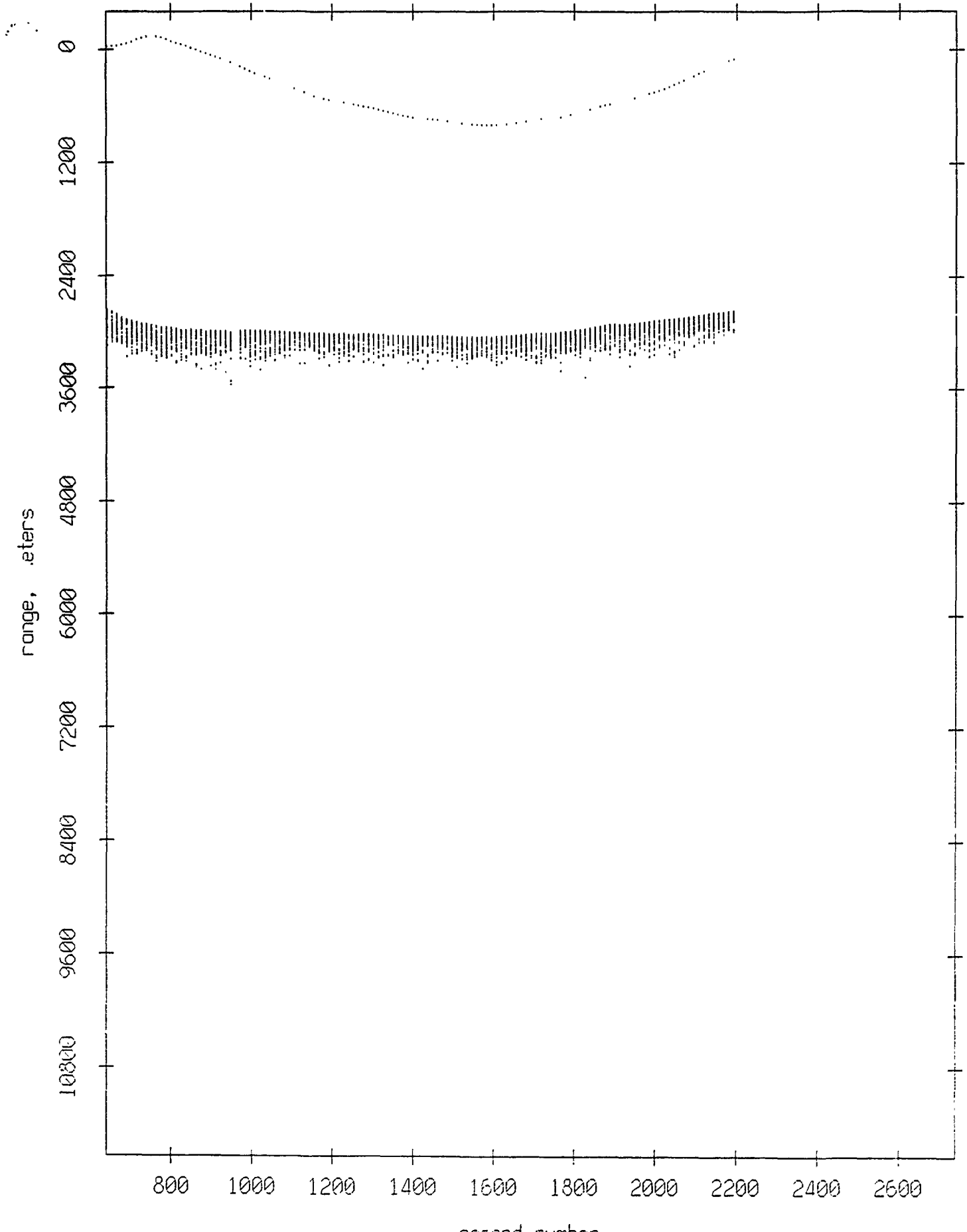

Figure VII.9g

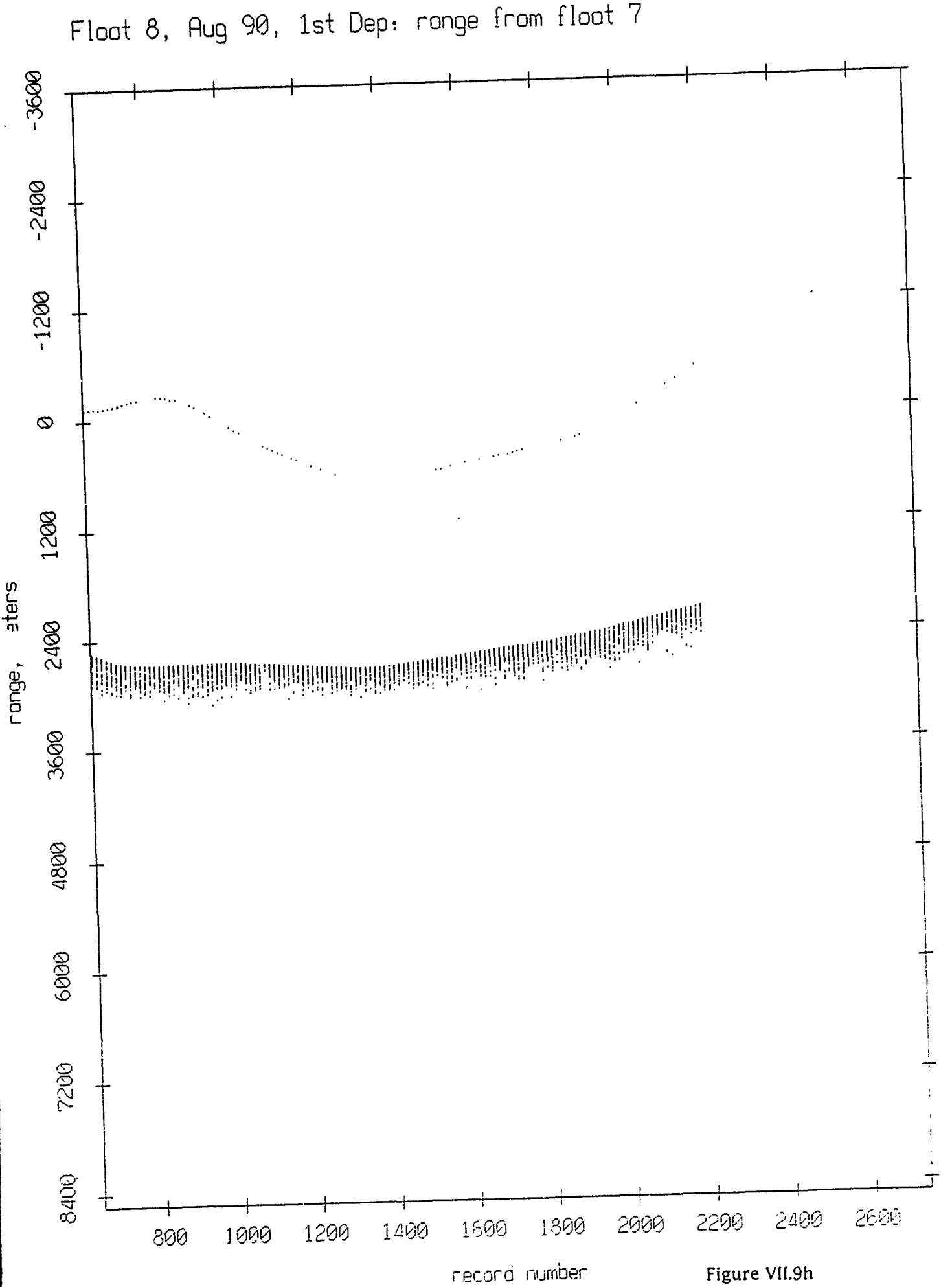

Figure VII.9h

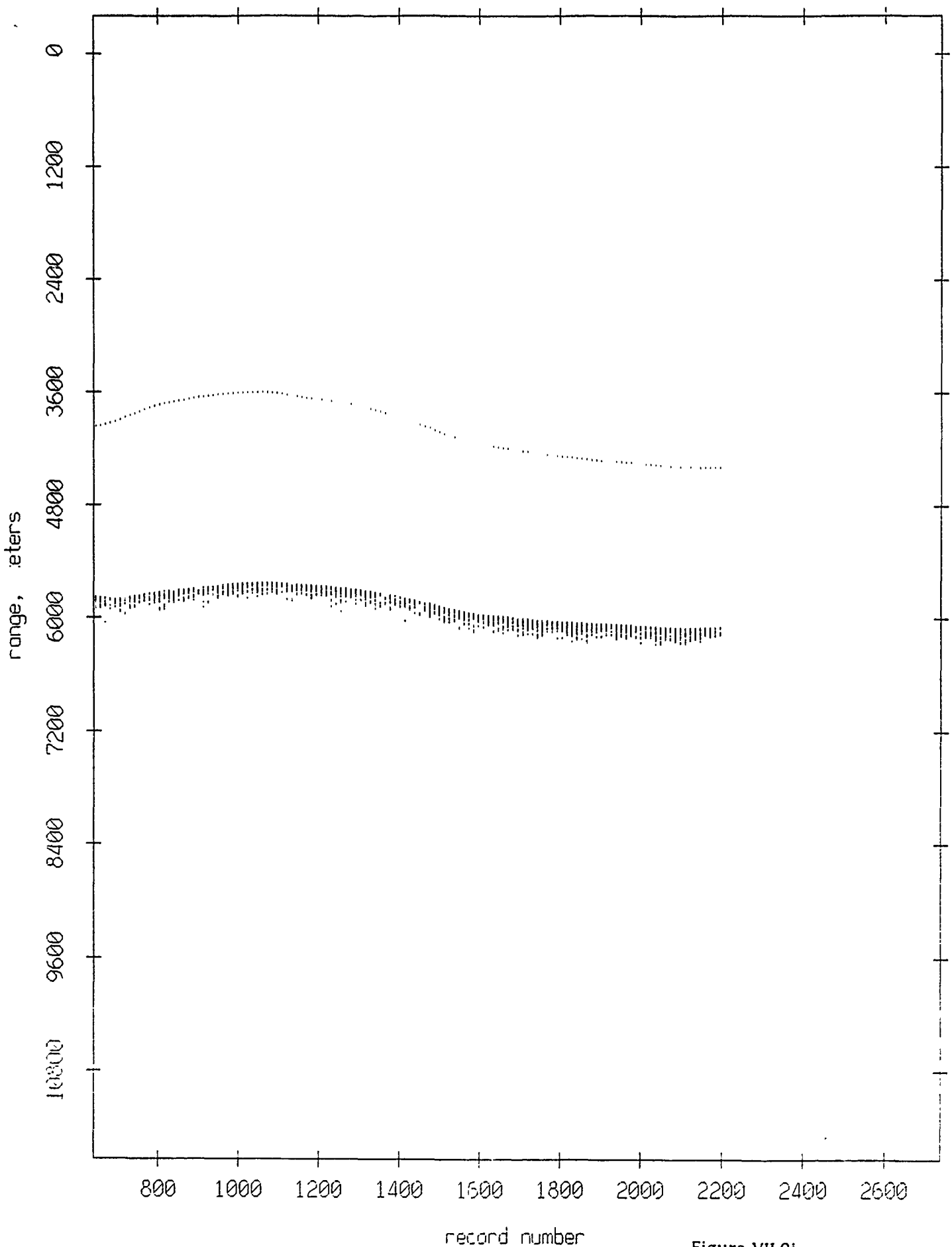

Figure VII.9i

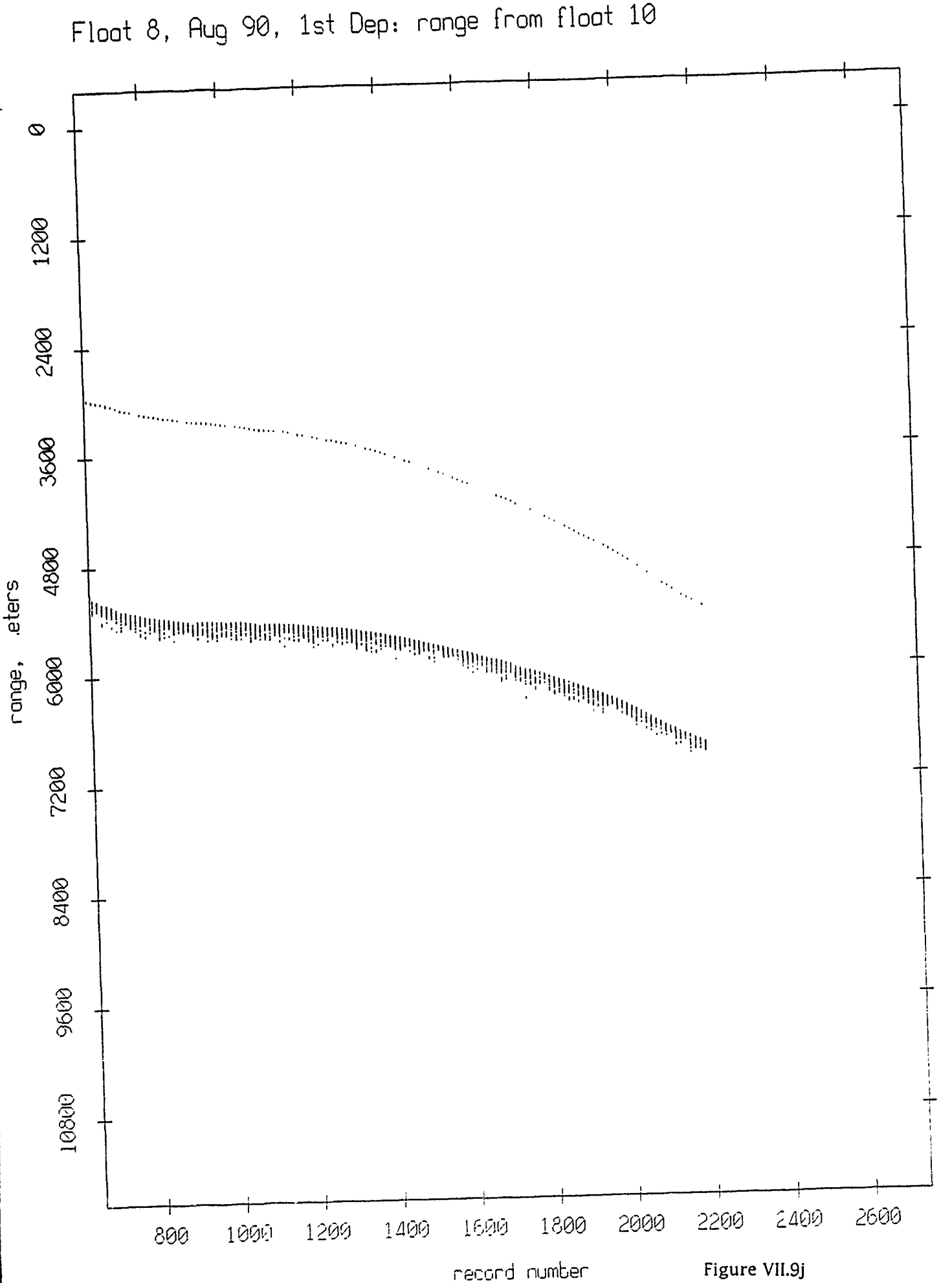

Figure VII.9j

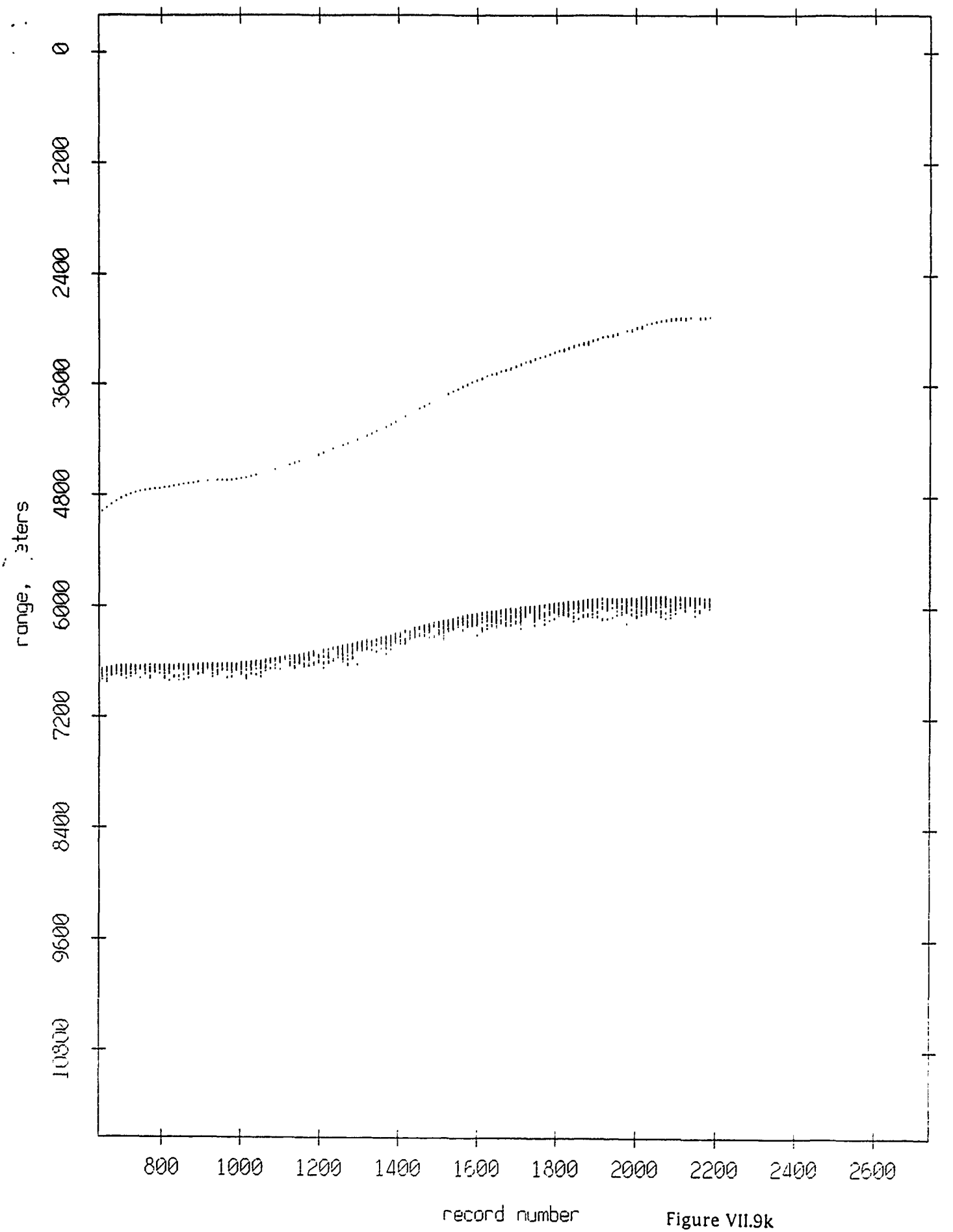

Figure VII.9k

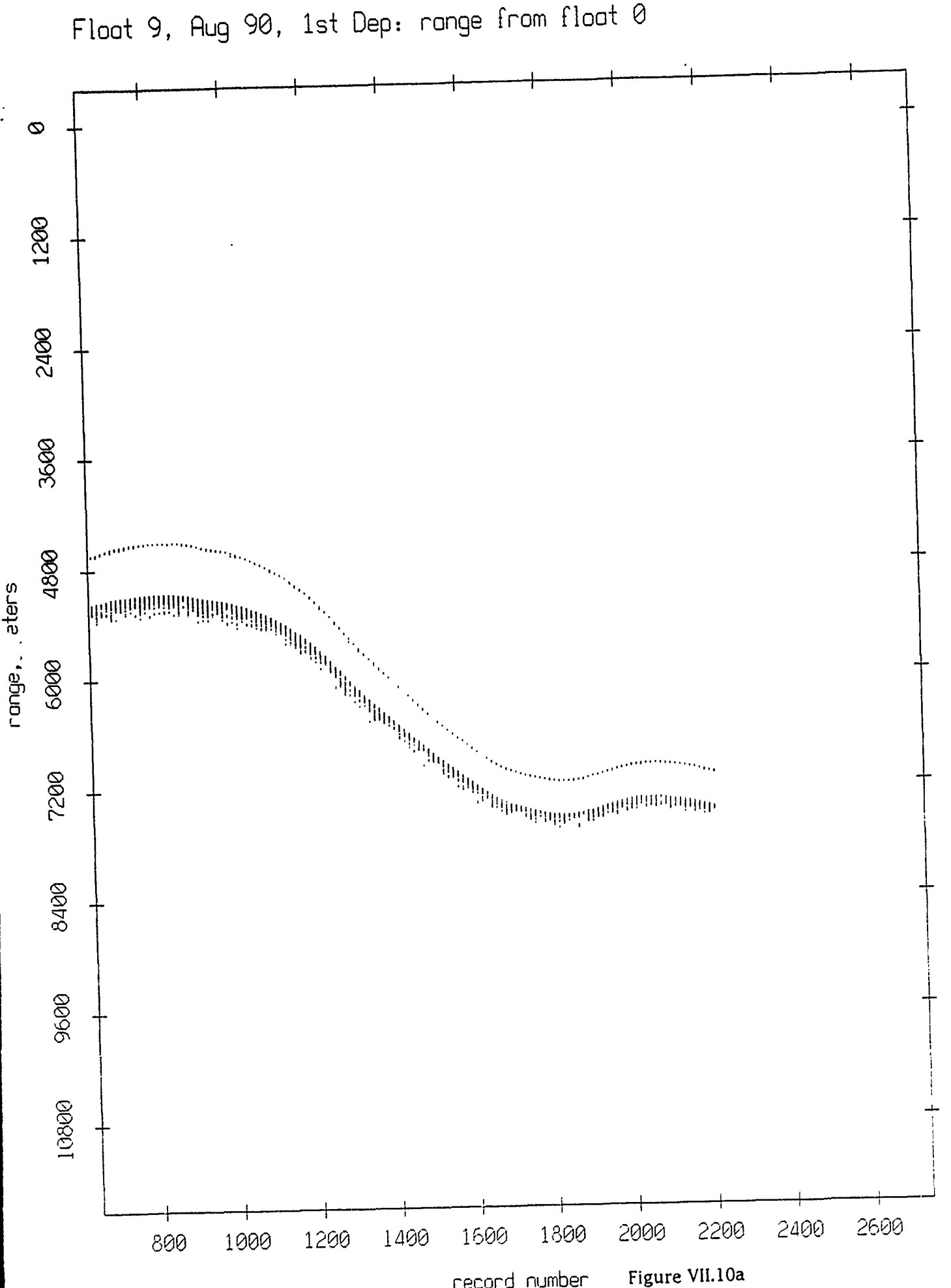

Figure VII.10a

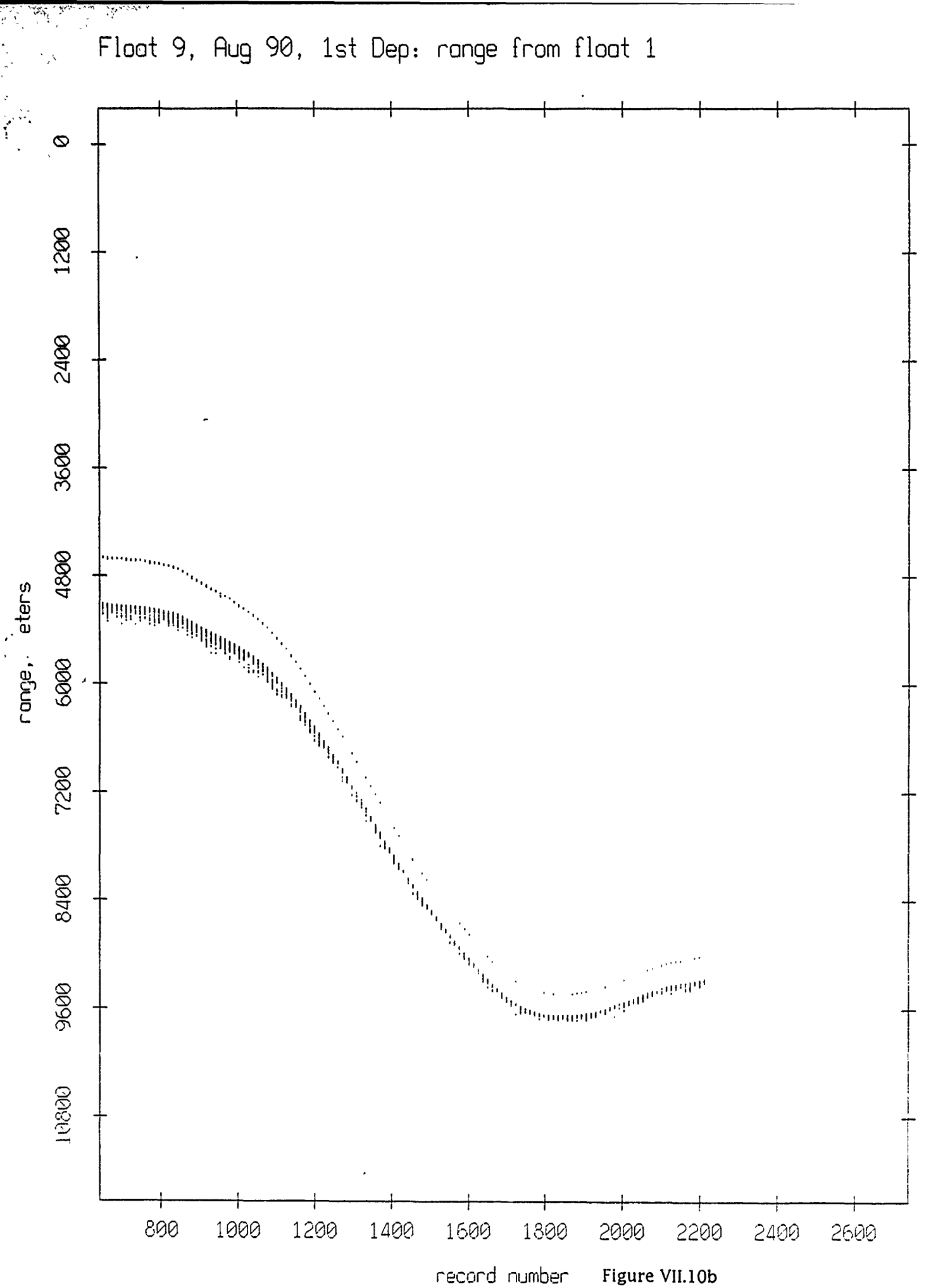

Figure VII.10b

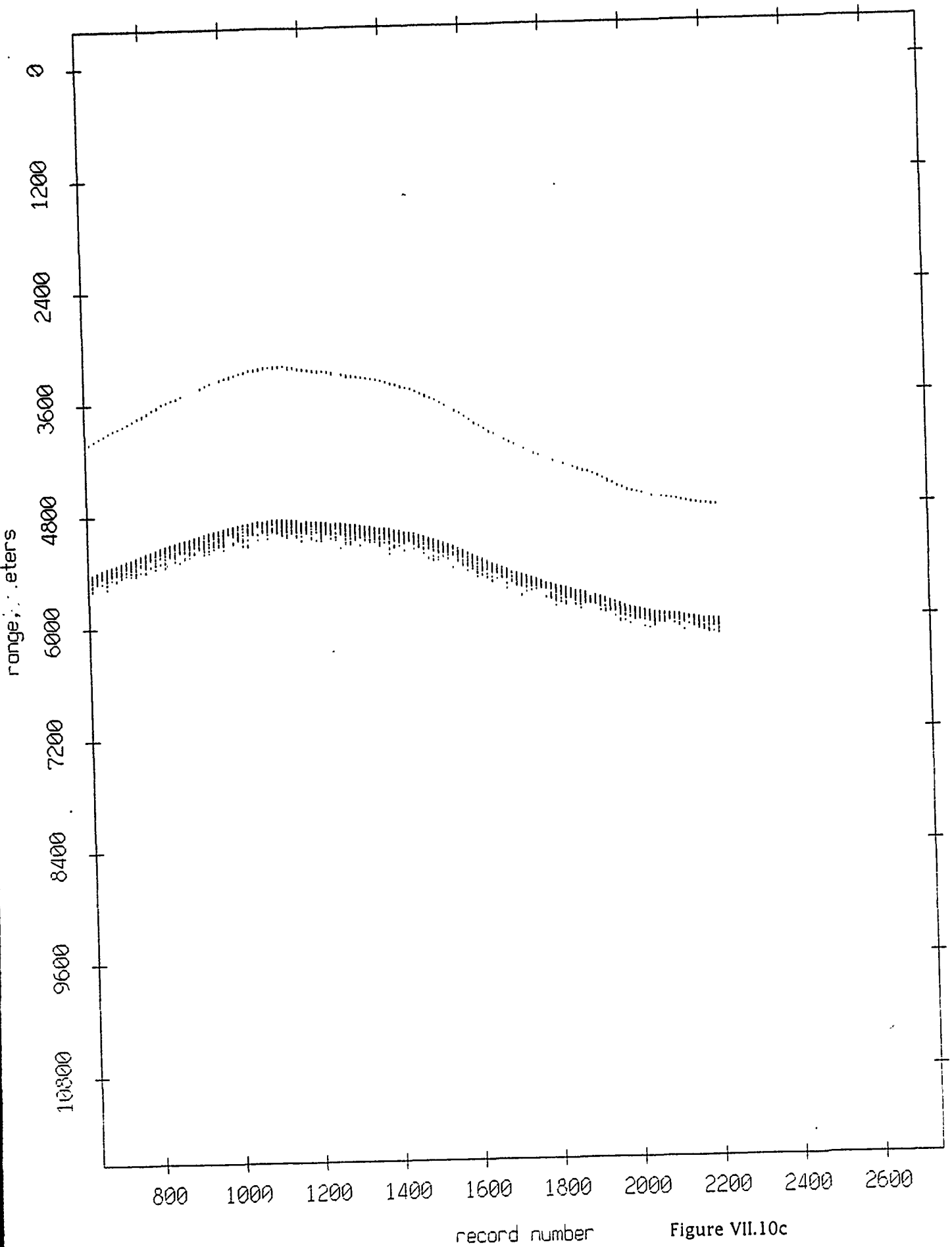

Figure VII.10c

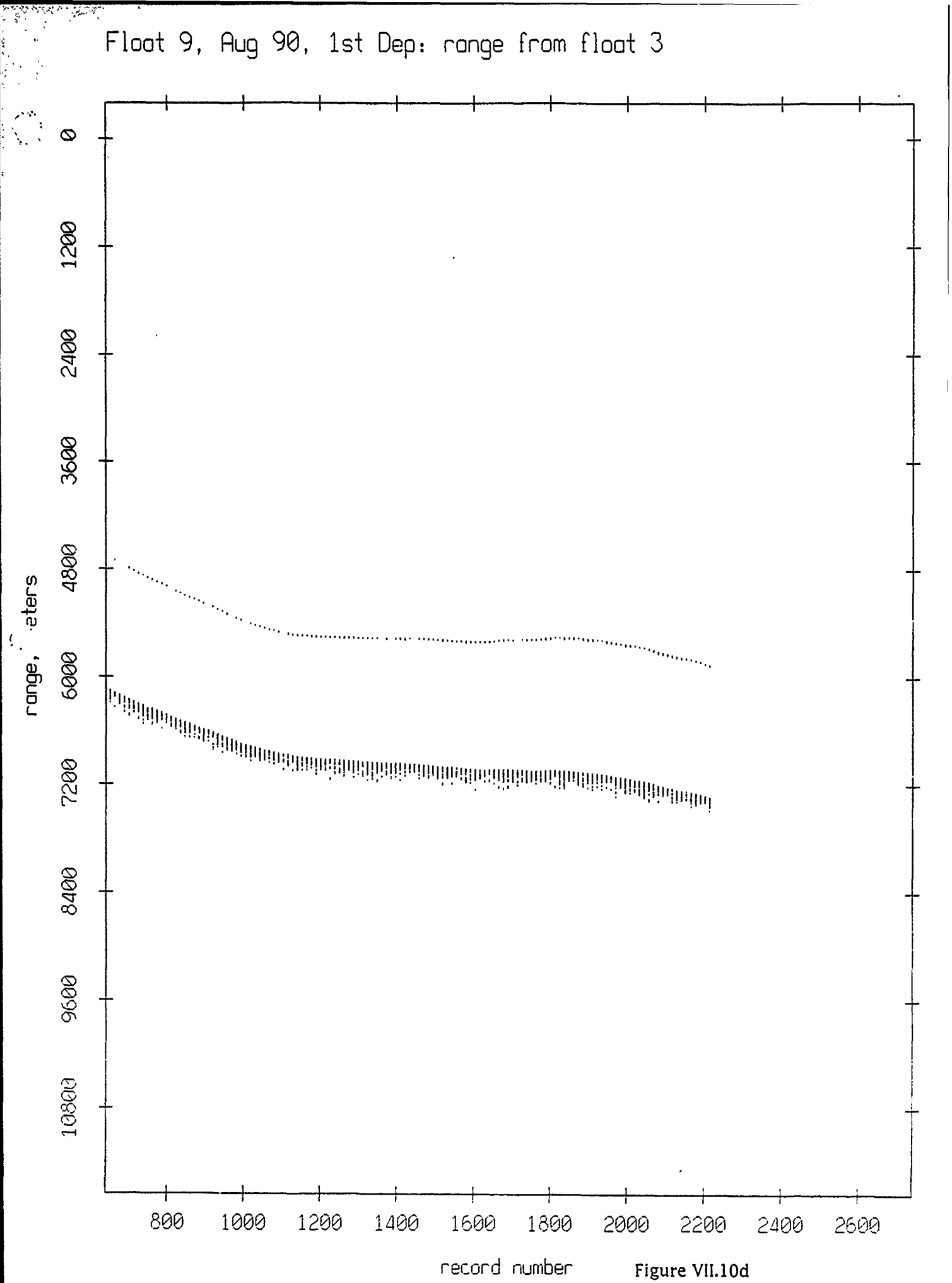

Figure VII.10d

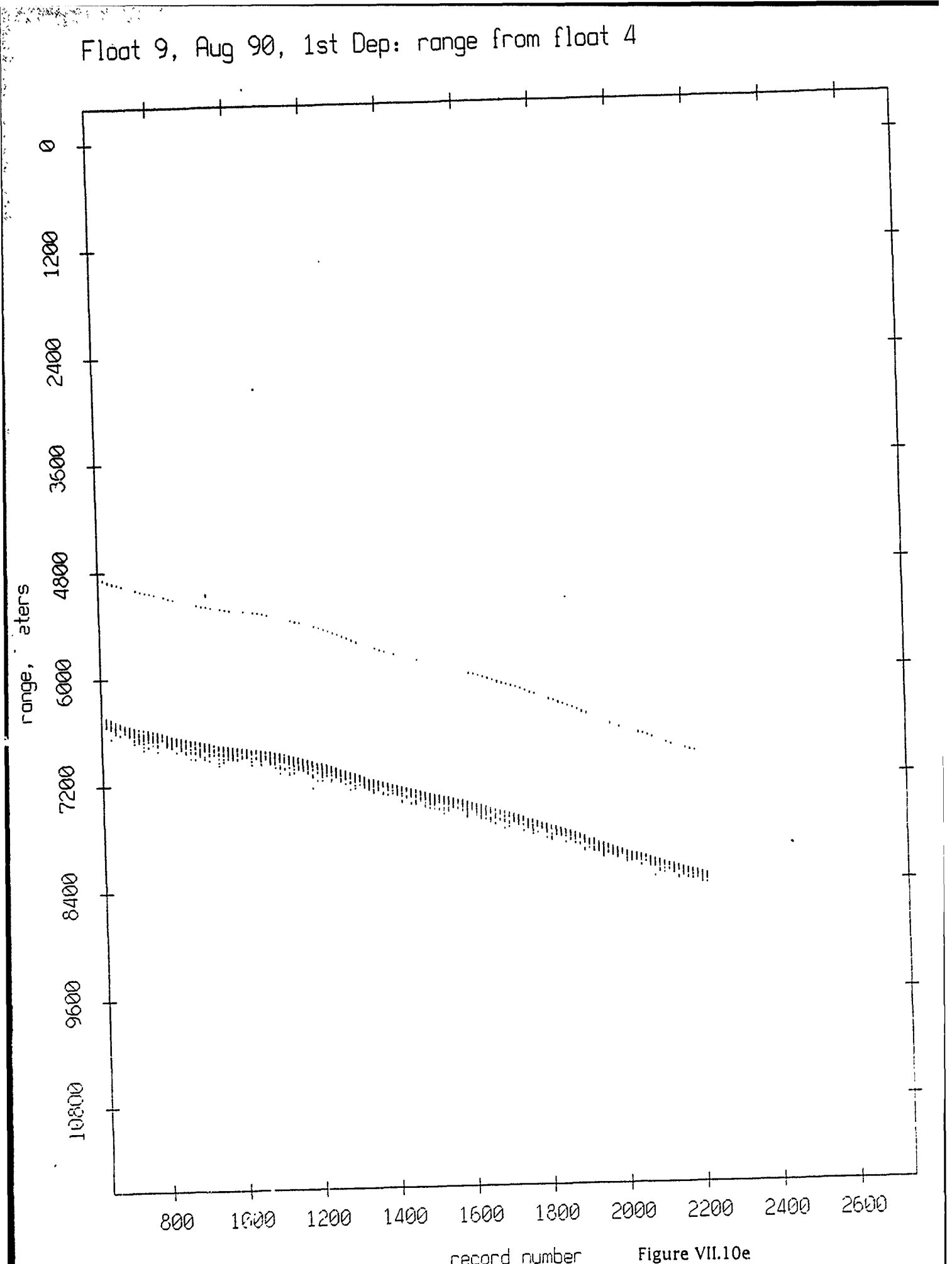

Figure VII.10e

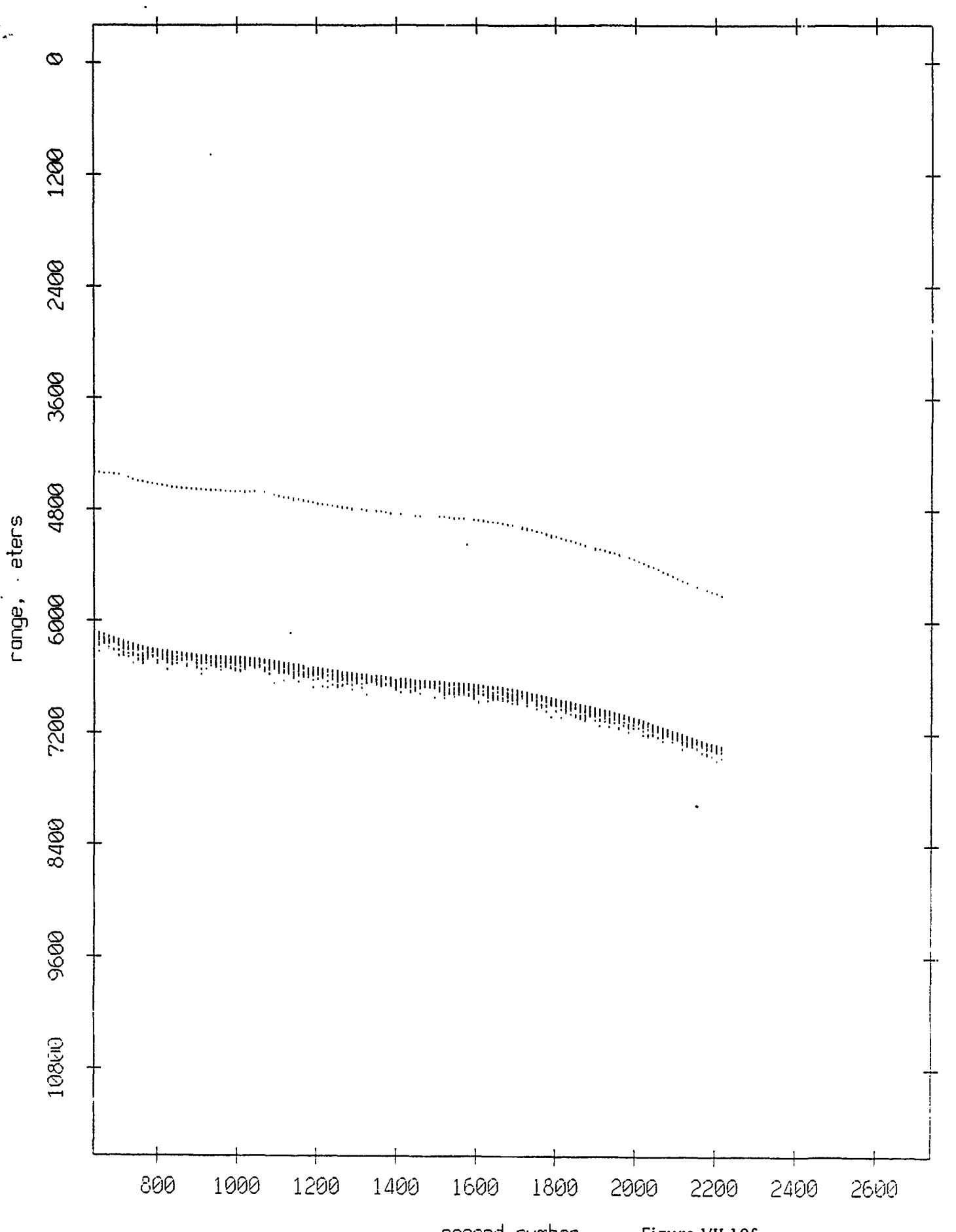

Figure VII.10f

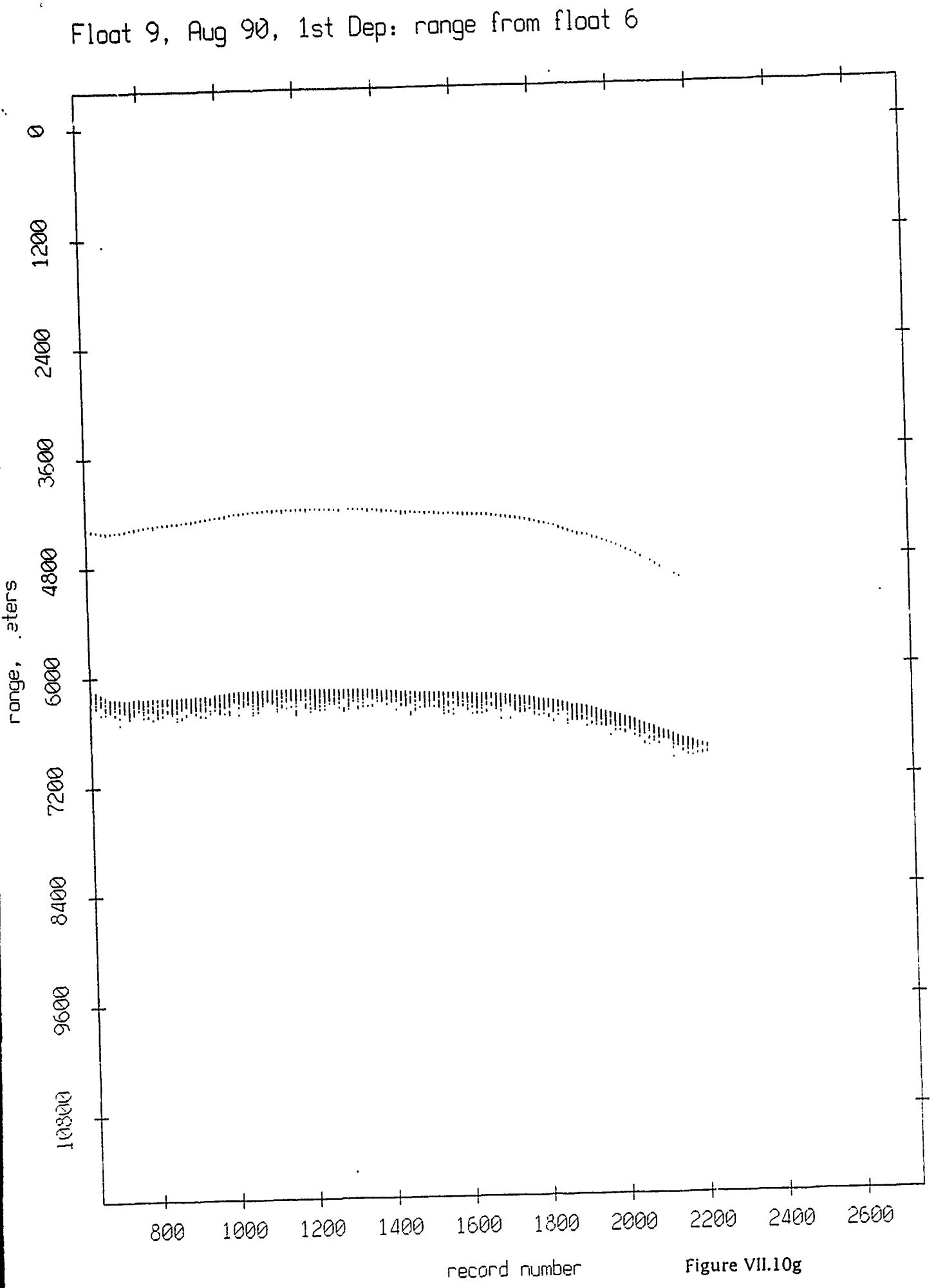

Figure VII.10g

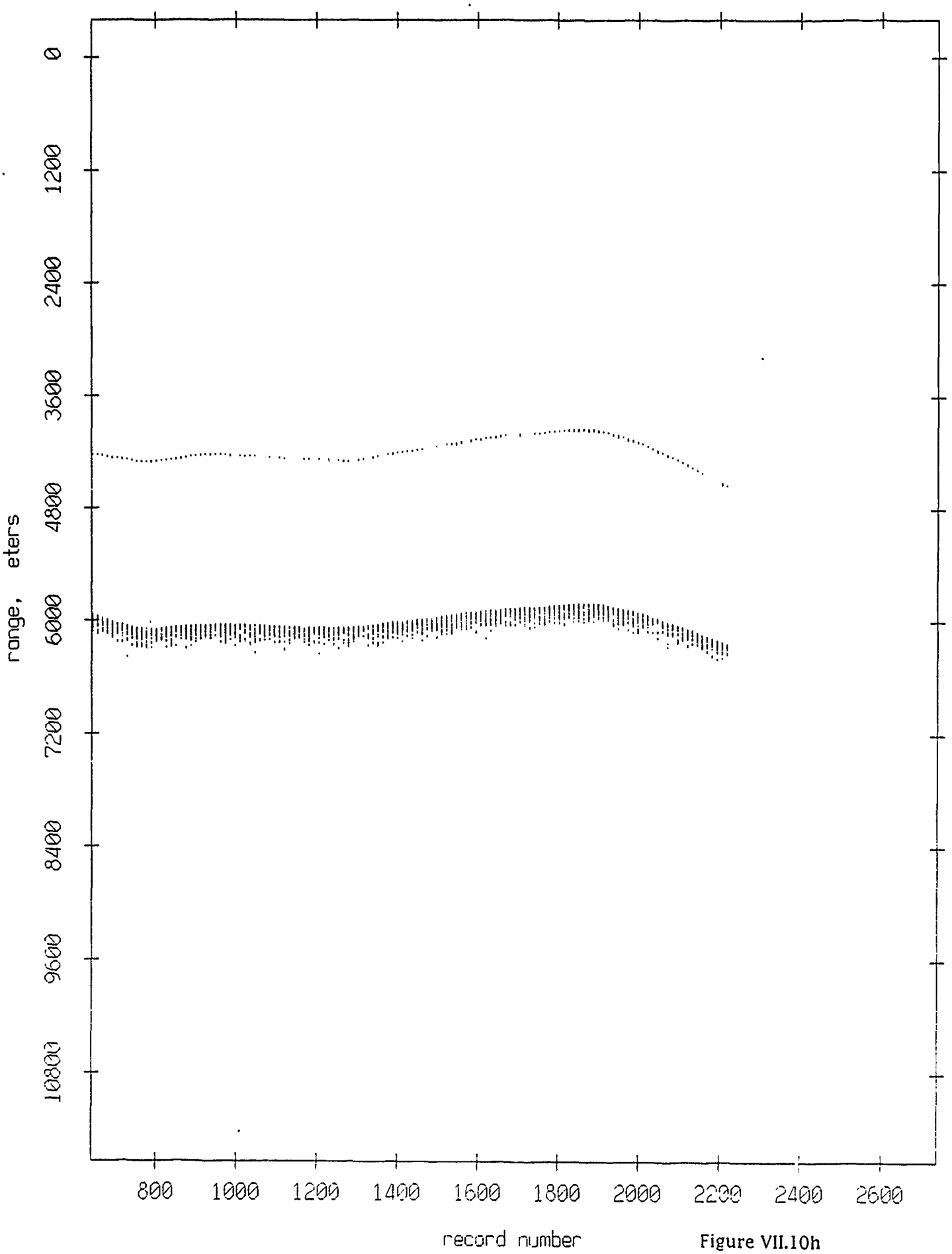

Figure VII.10h

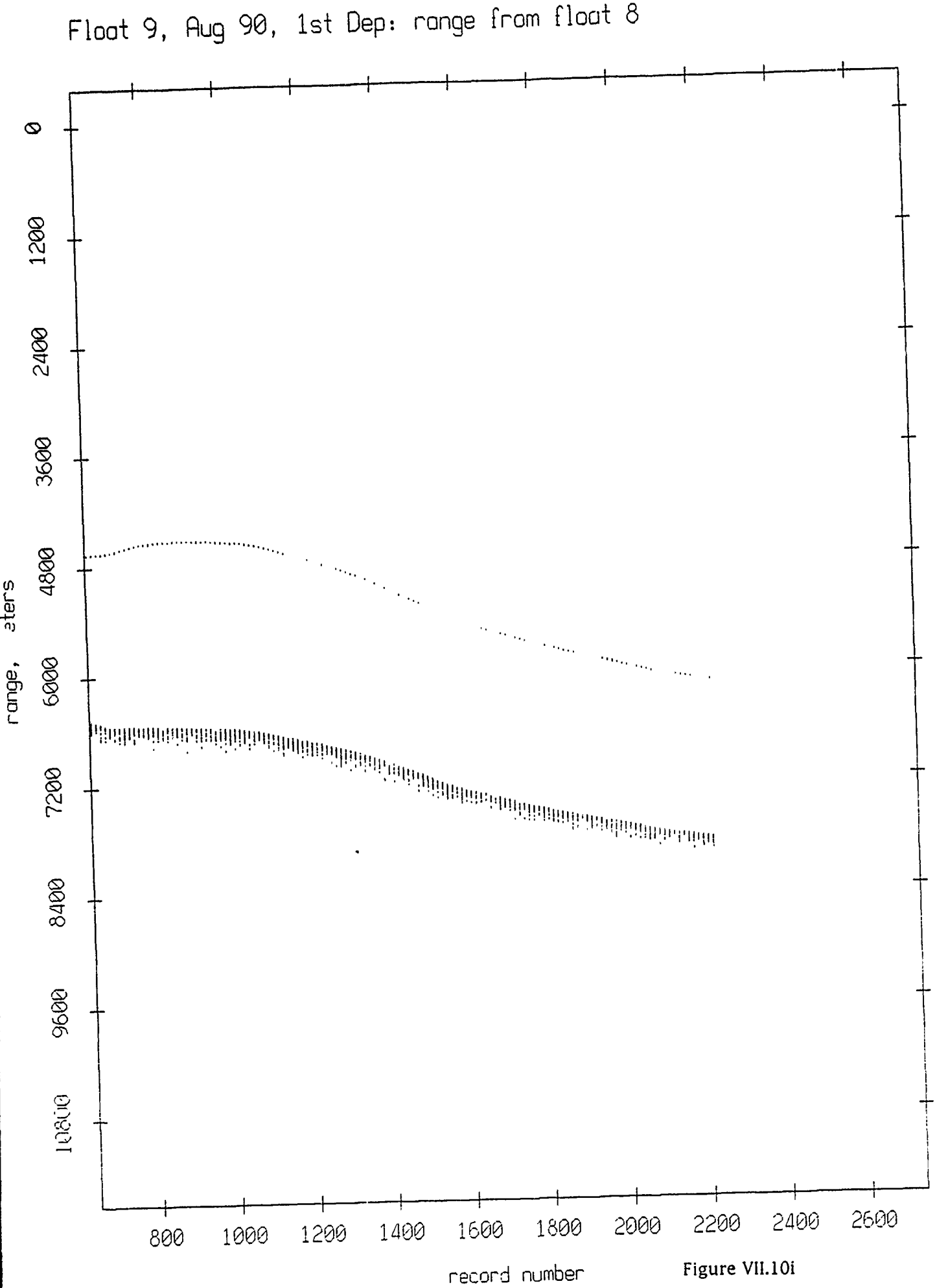

Figure VII.10i

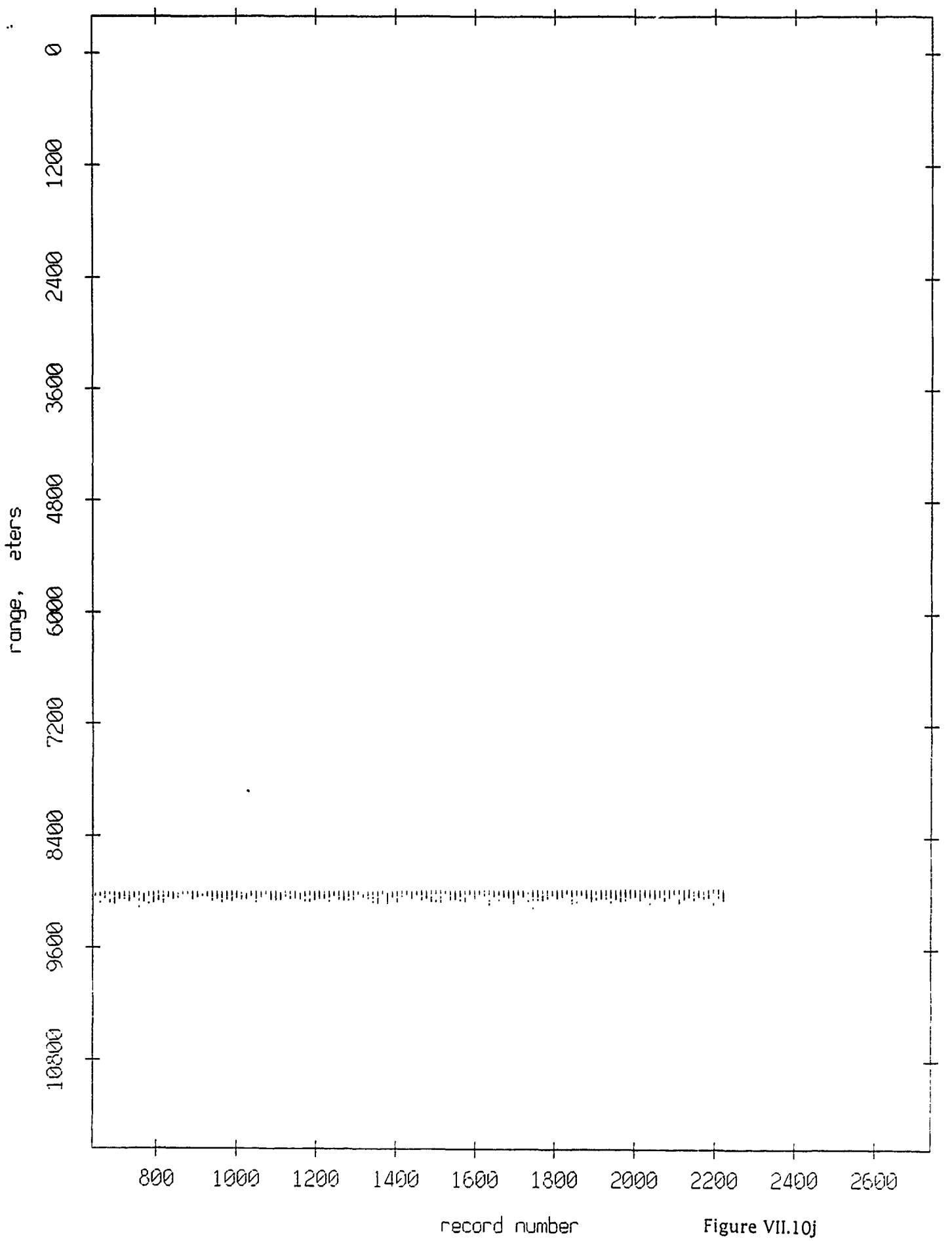

Figure VII.10j

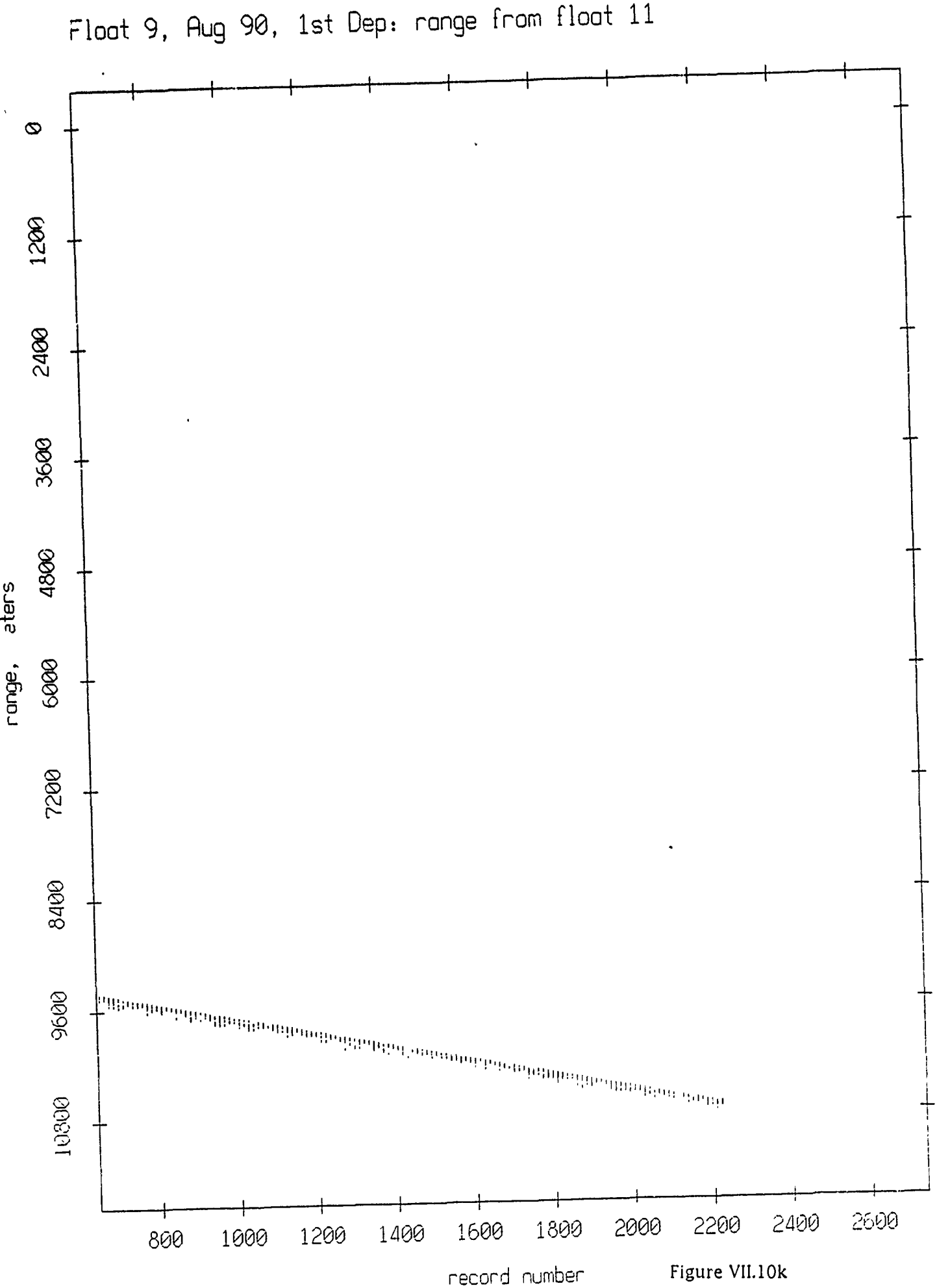

Figure VII.10k

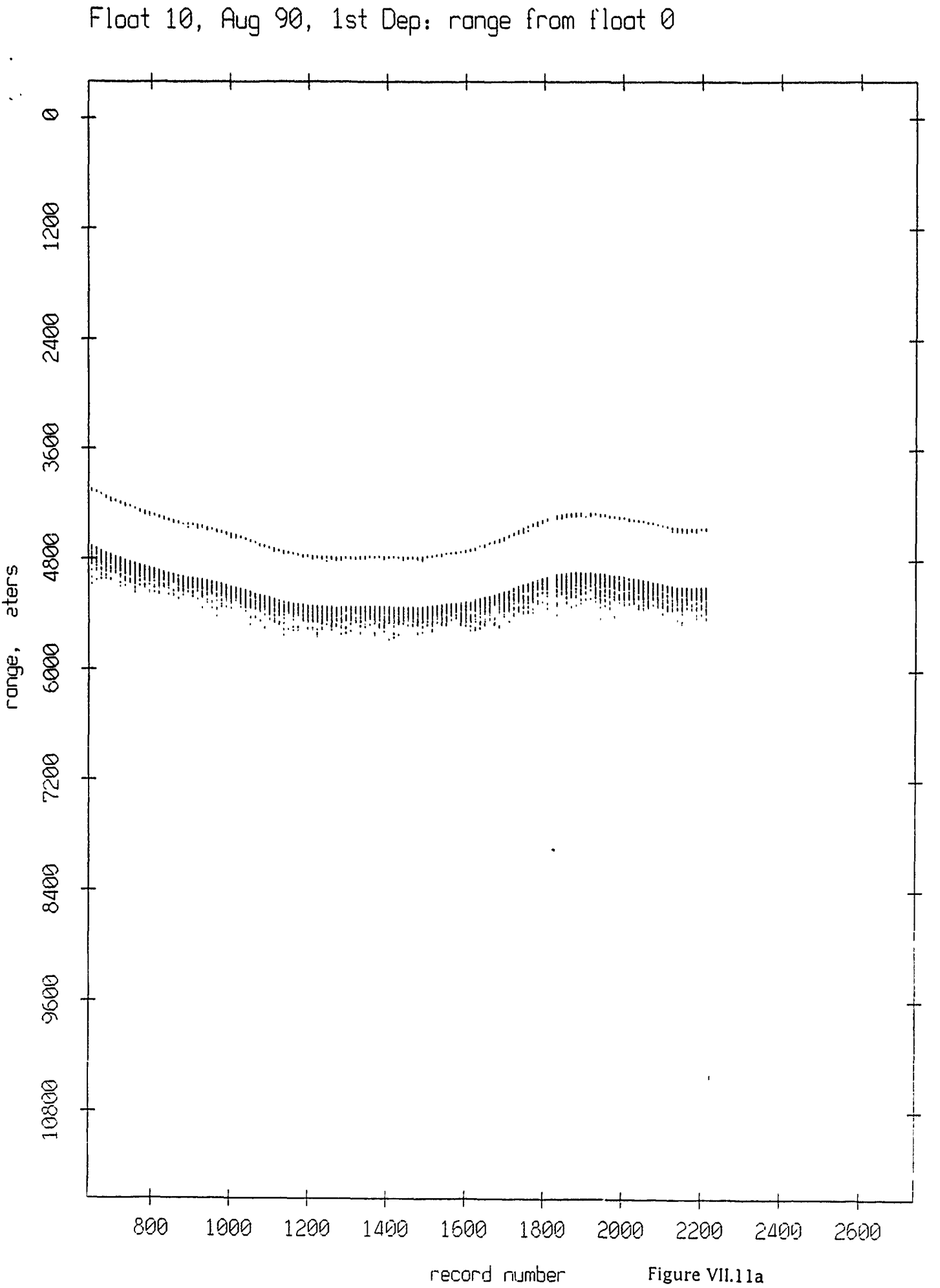

Figure VII.11a

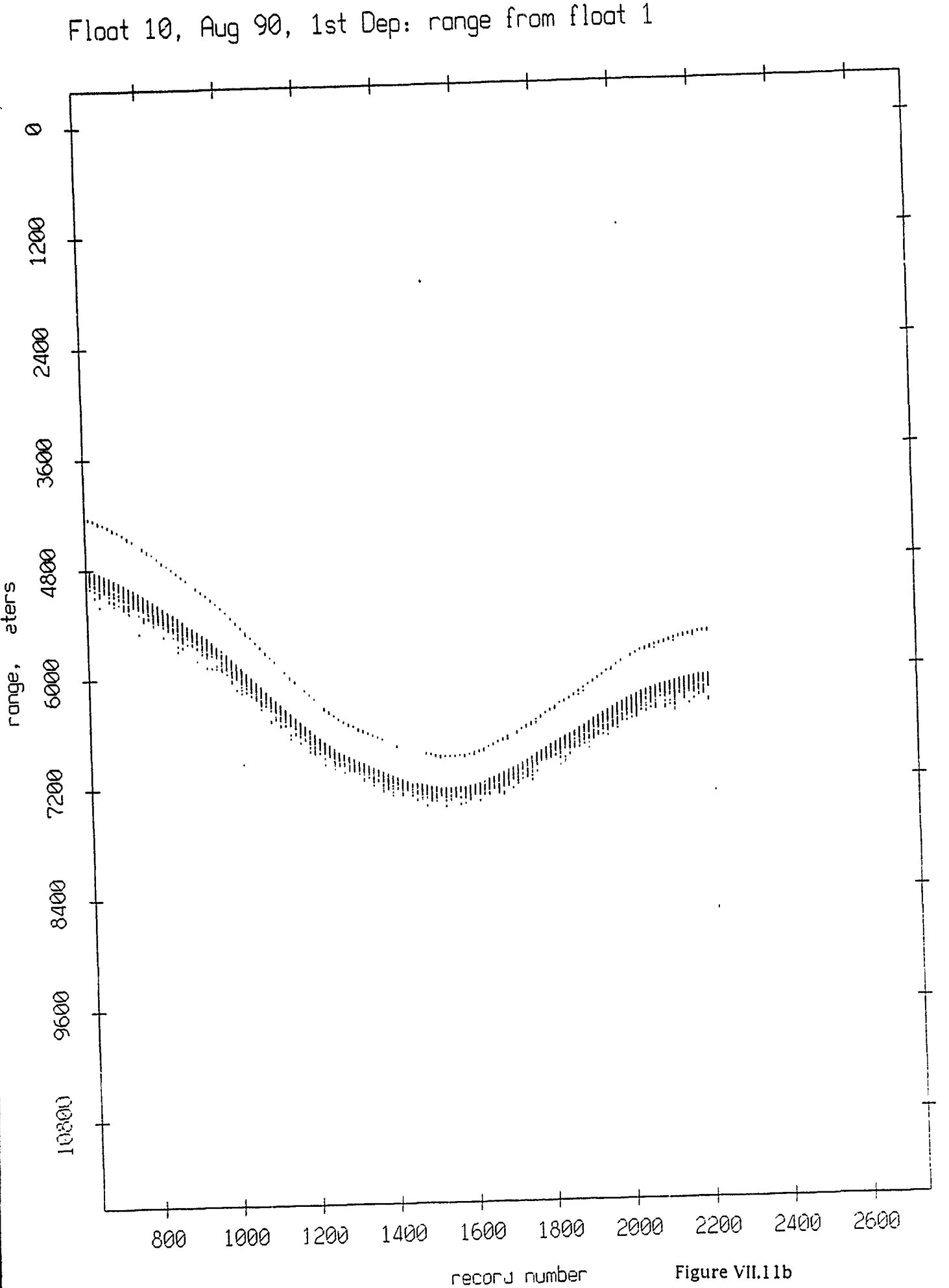

Figure VII.11b

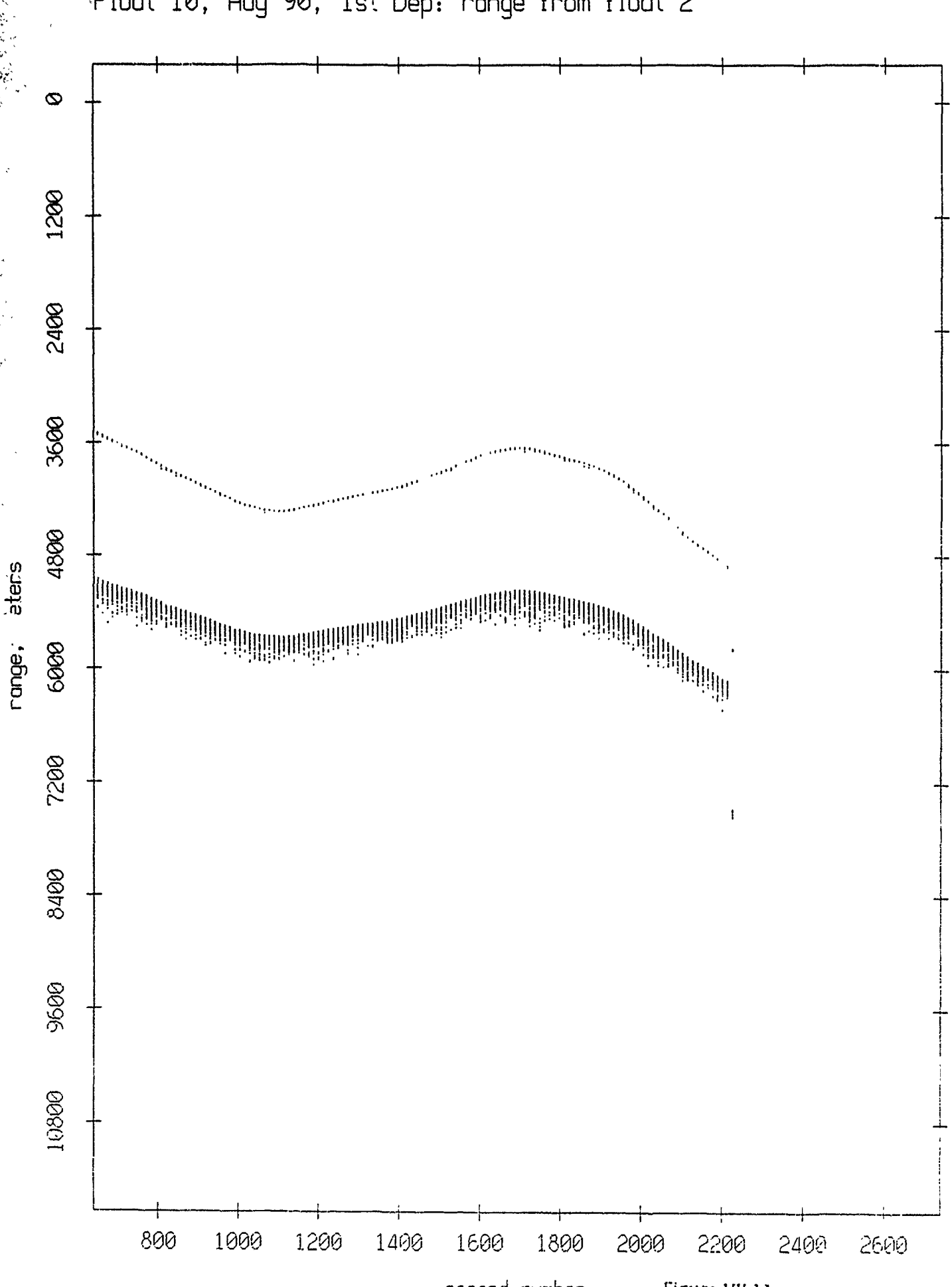

Figure VII.11c

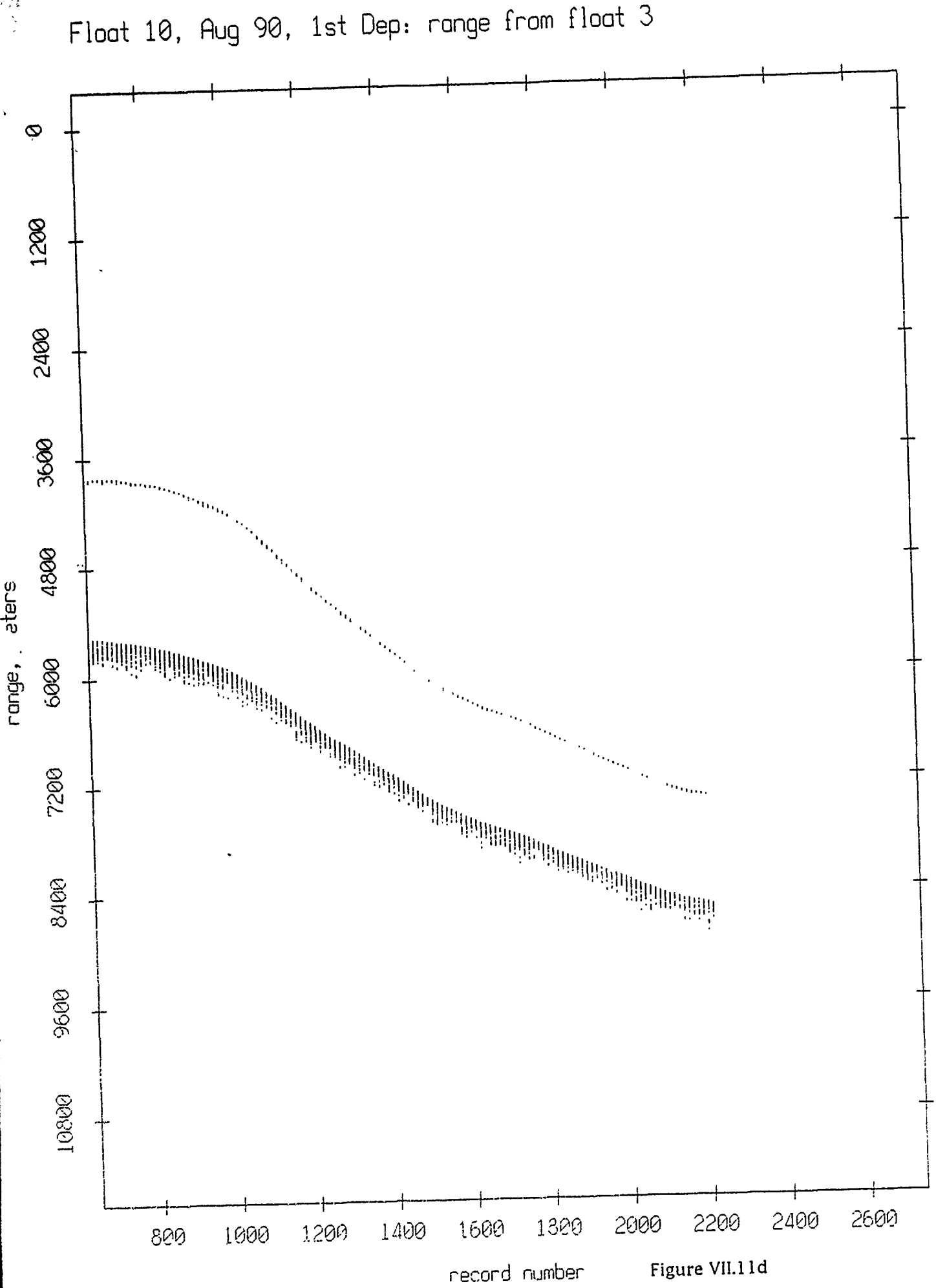

Figure VII.11d

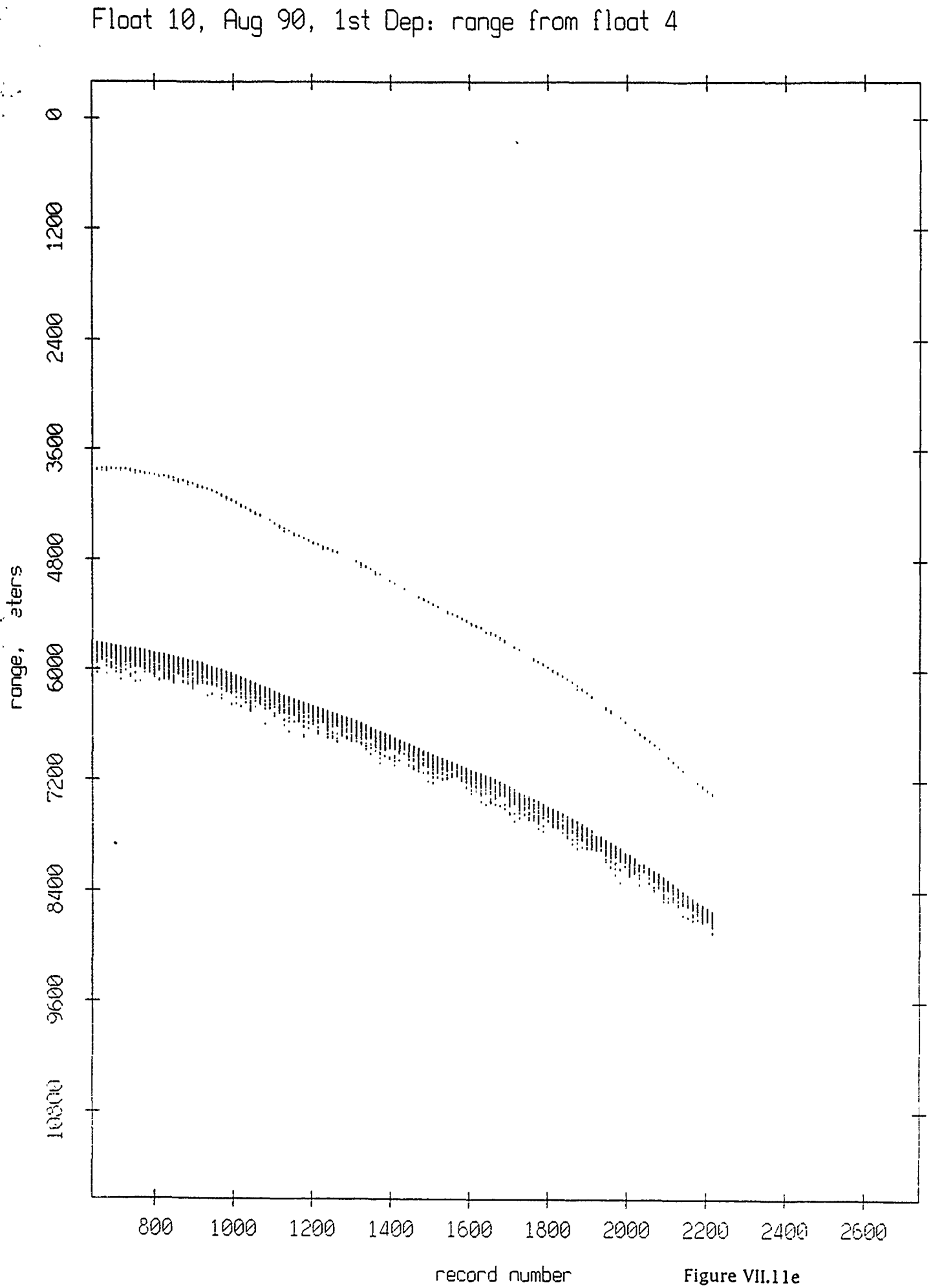

Figure VII.11e

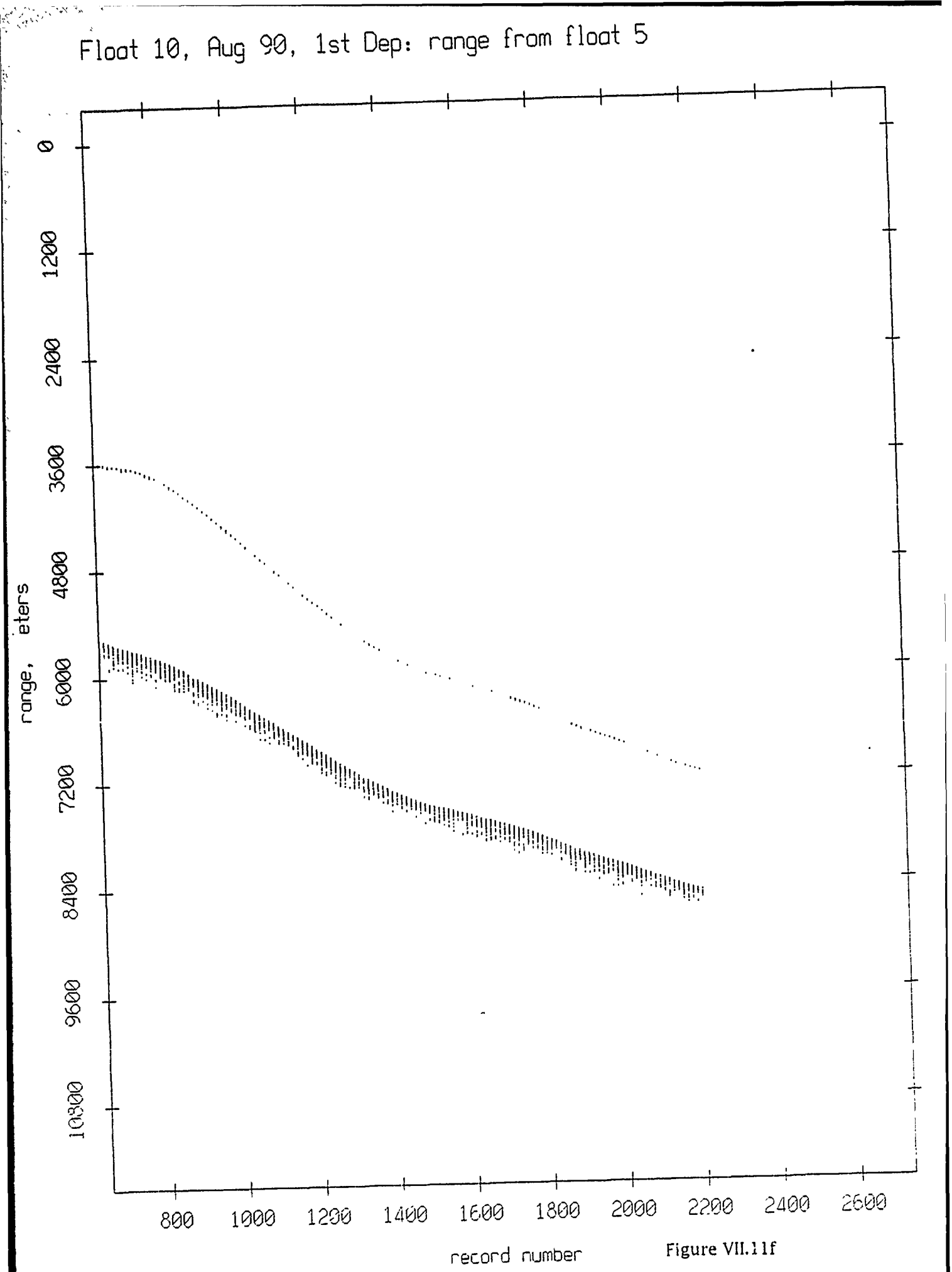

Figure VII.11f

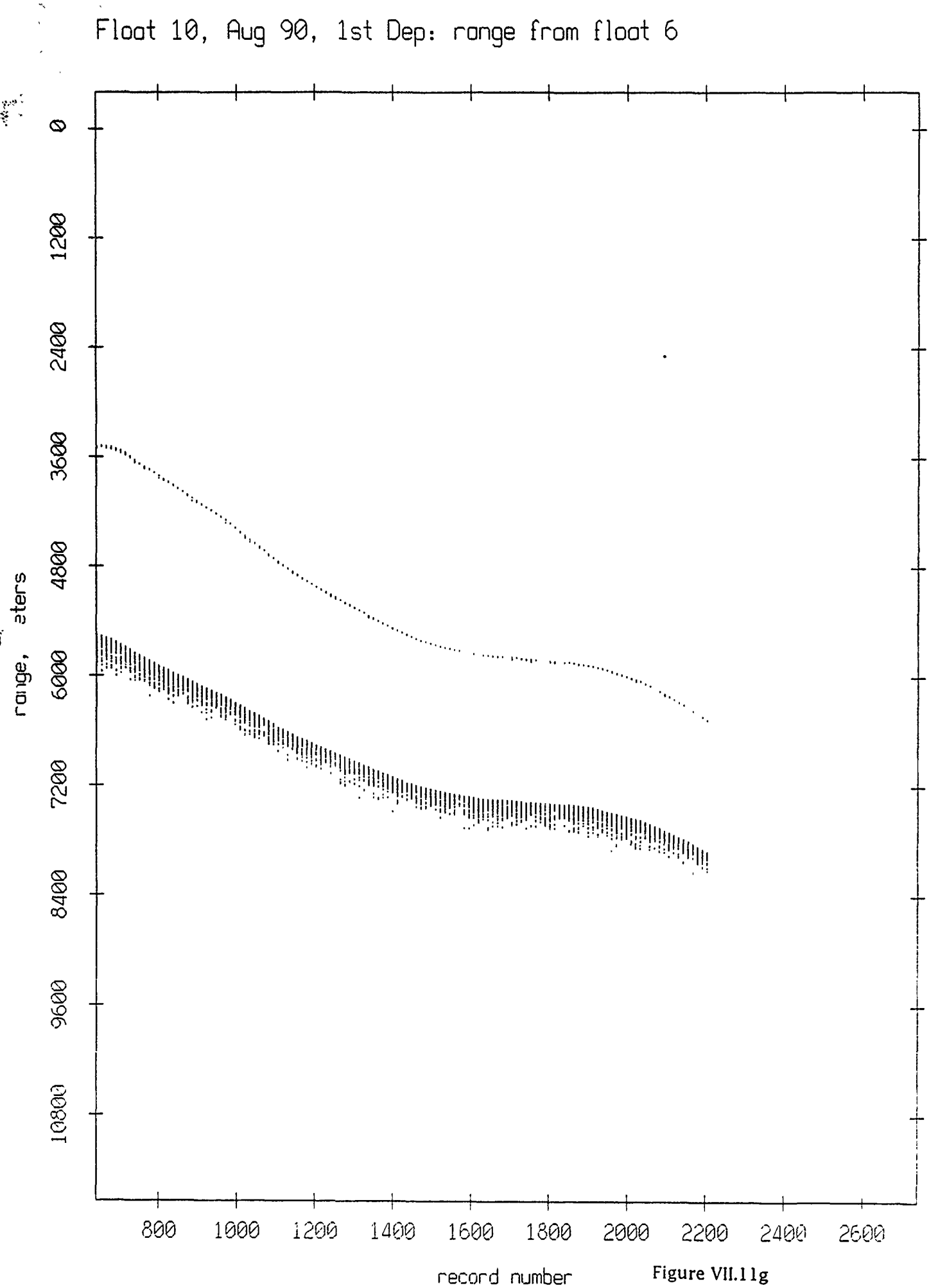

Figure VII.11g

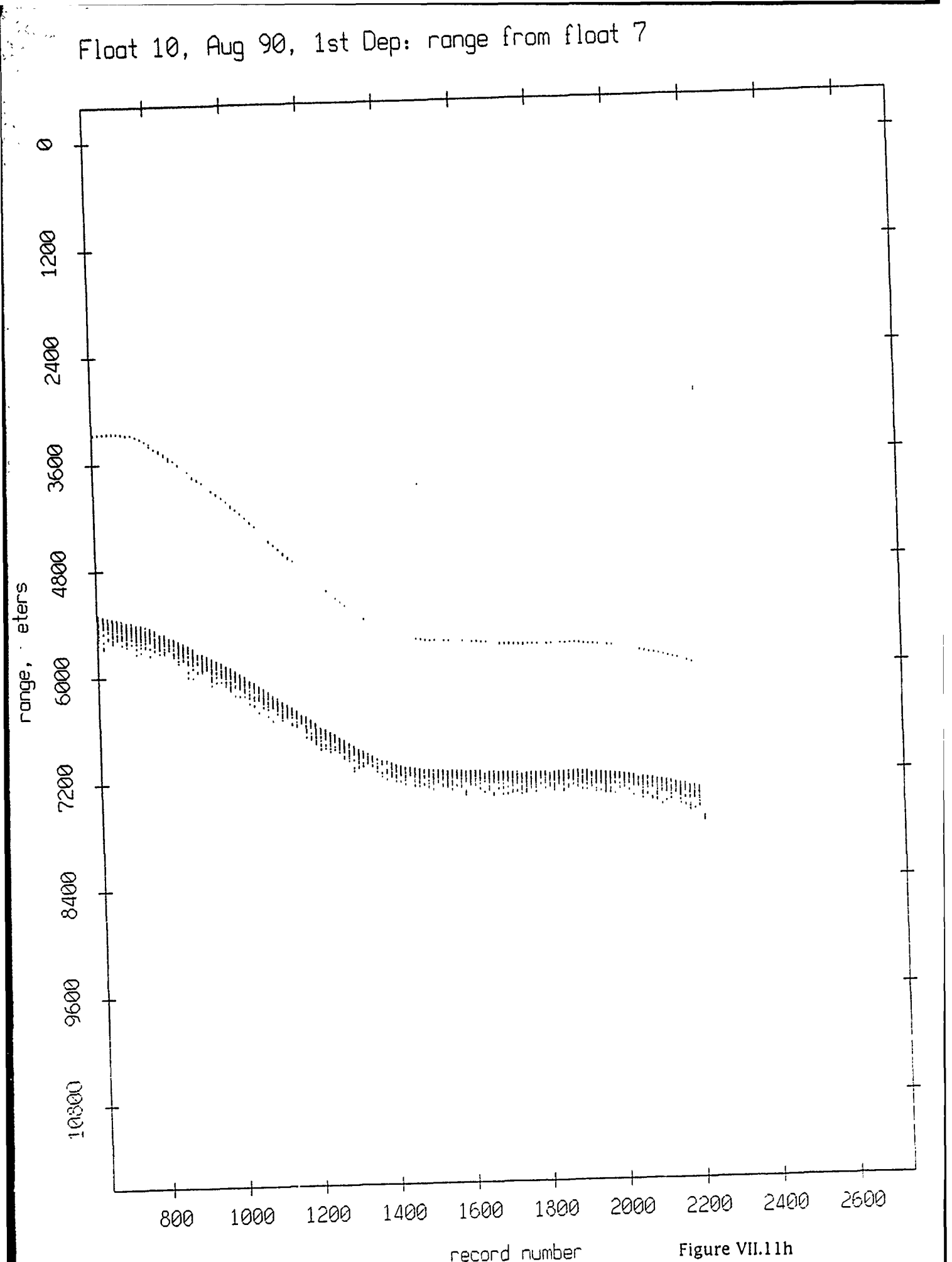

Figure VII.11h

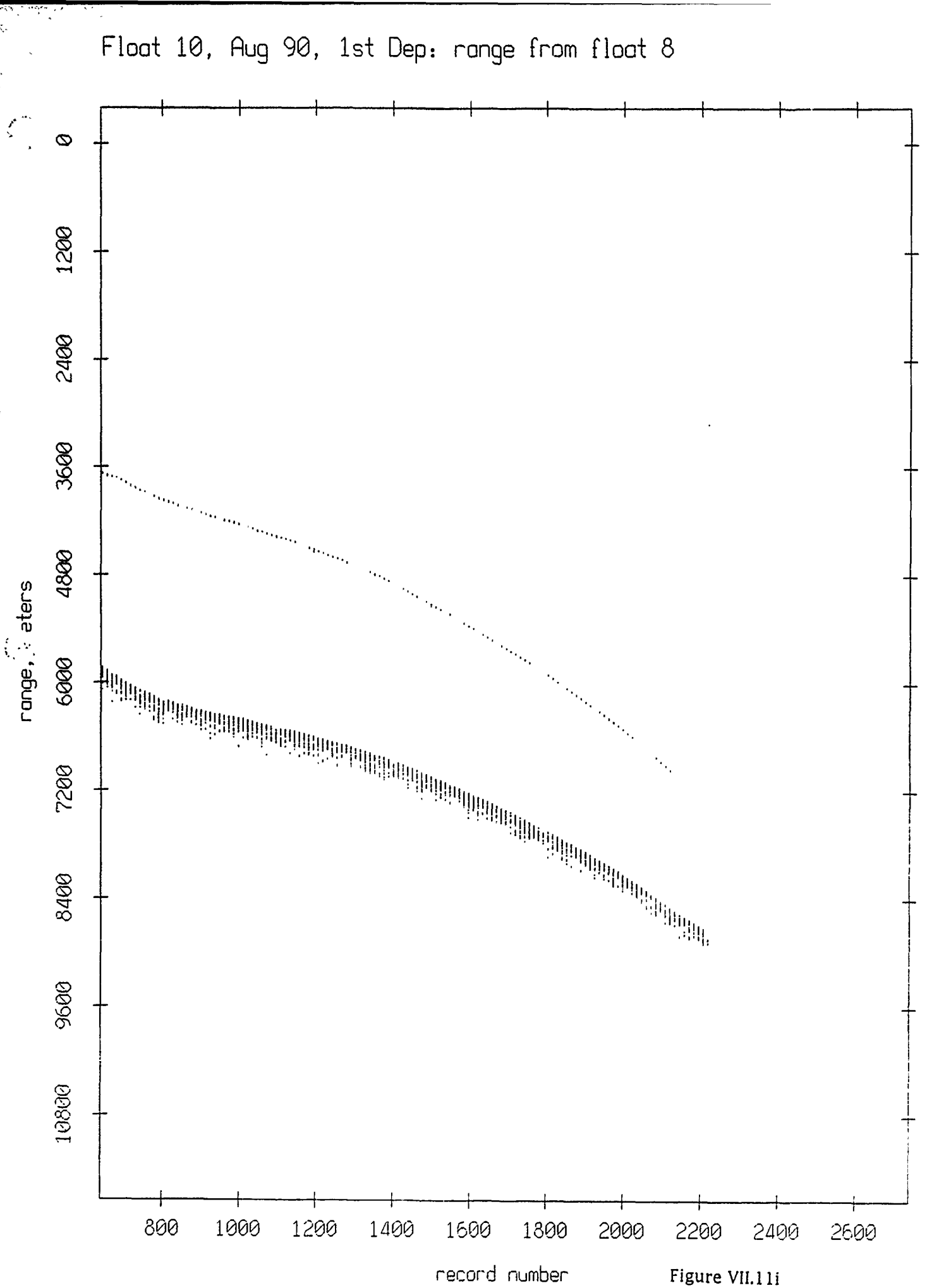

Figure VII.11i

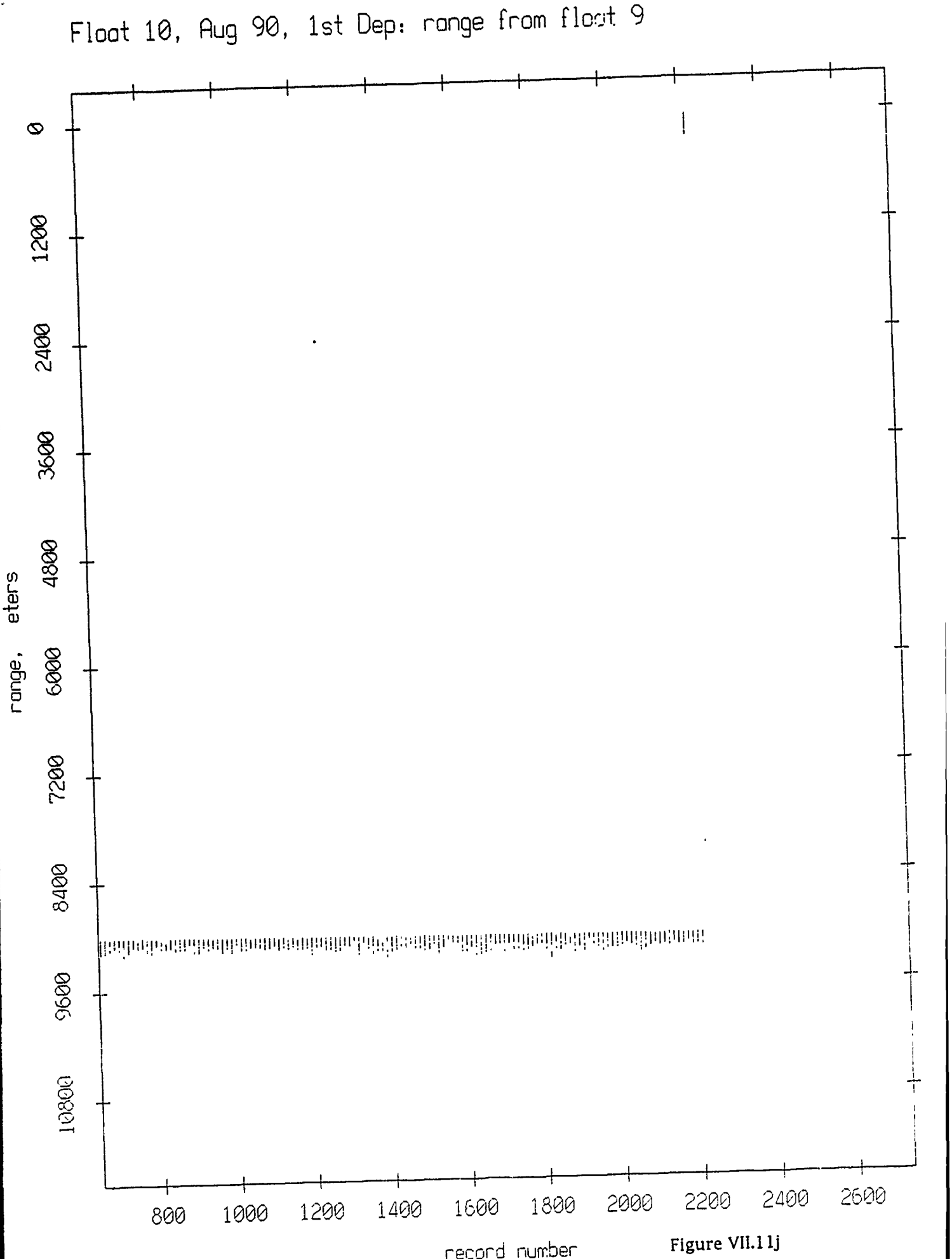

Figure VII.11j

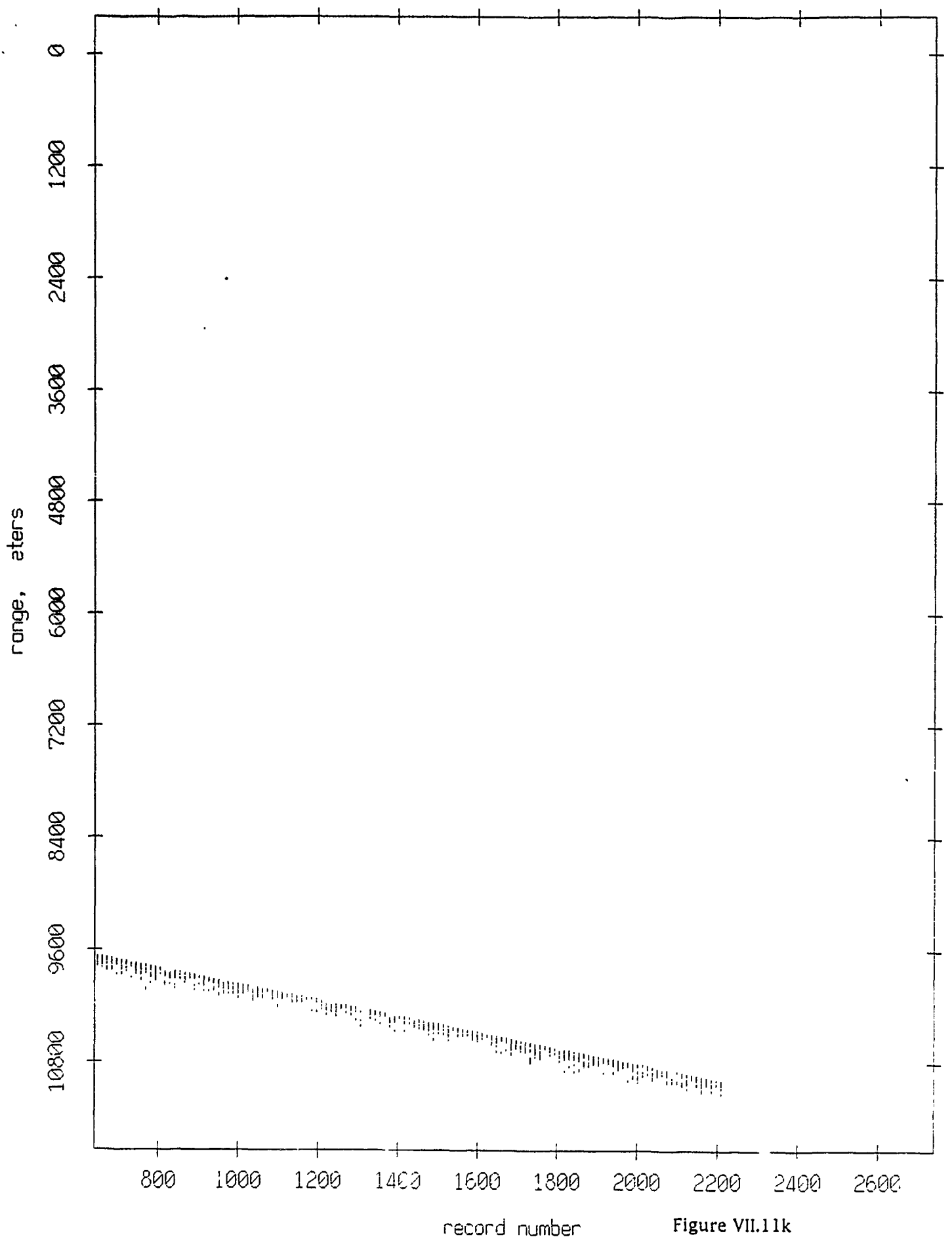

Figure VII.11k

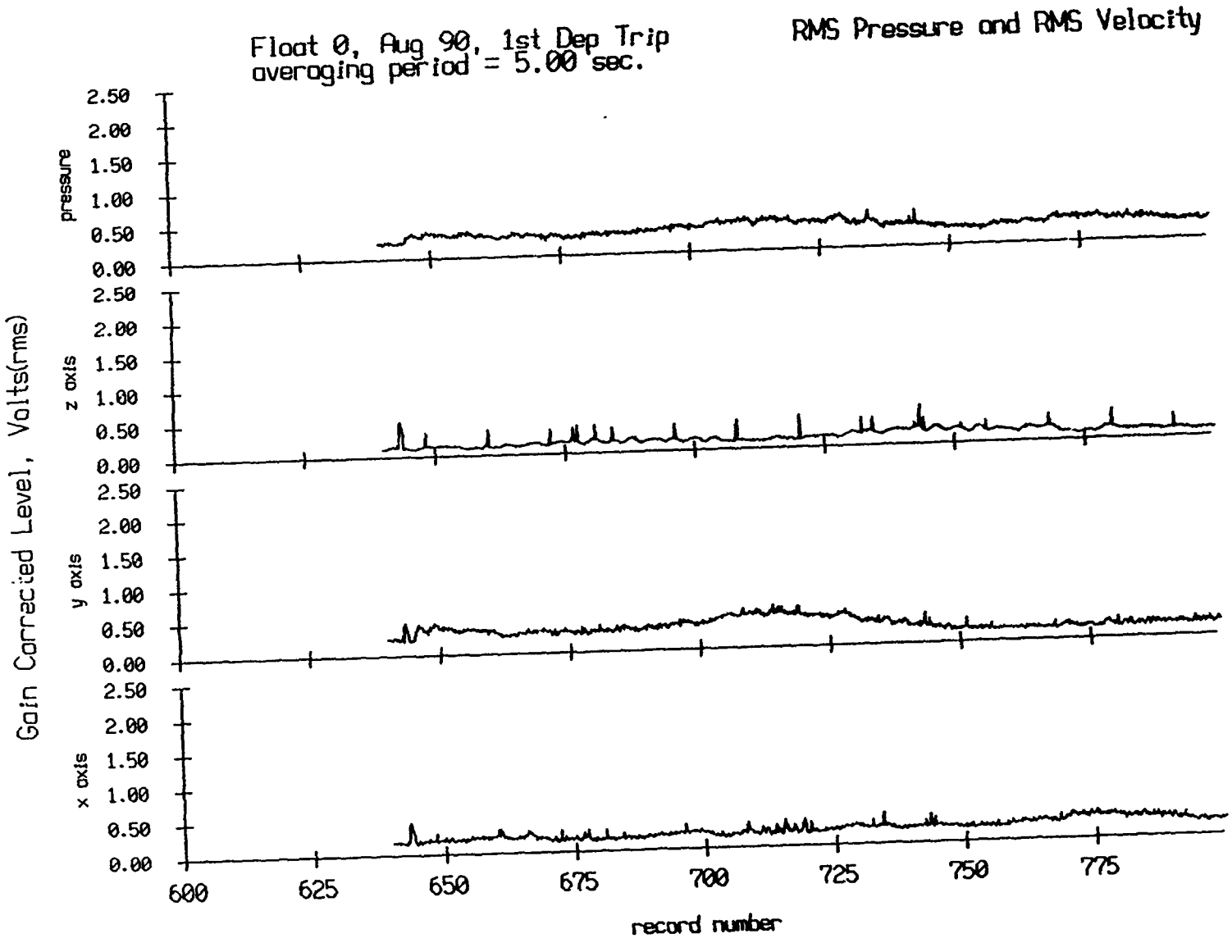

Figure VIII.1a

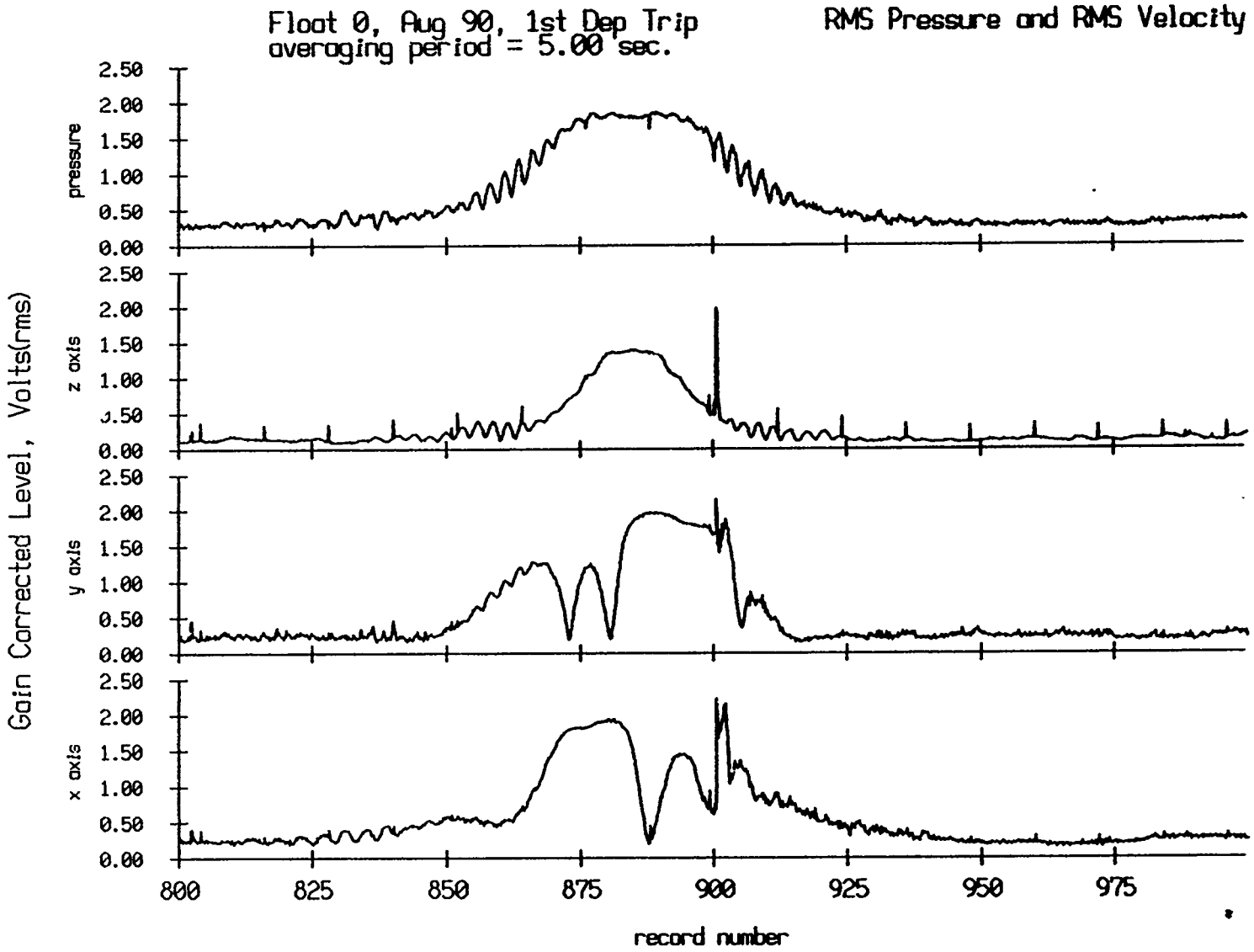

Figure VIII.1b

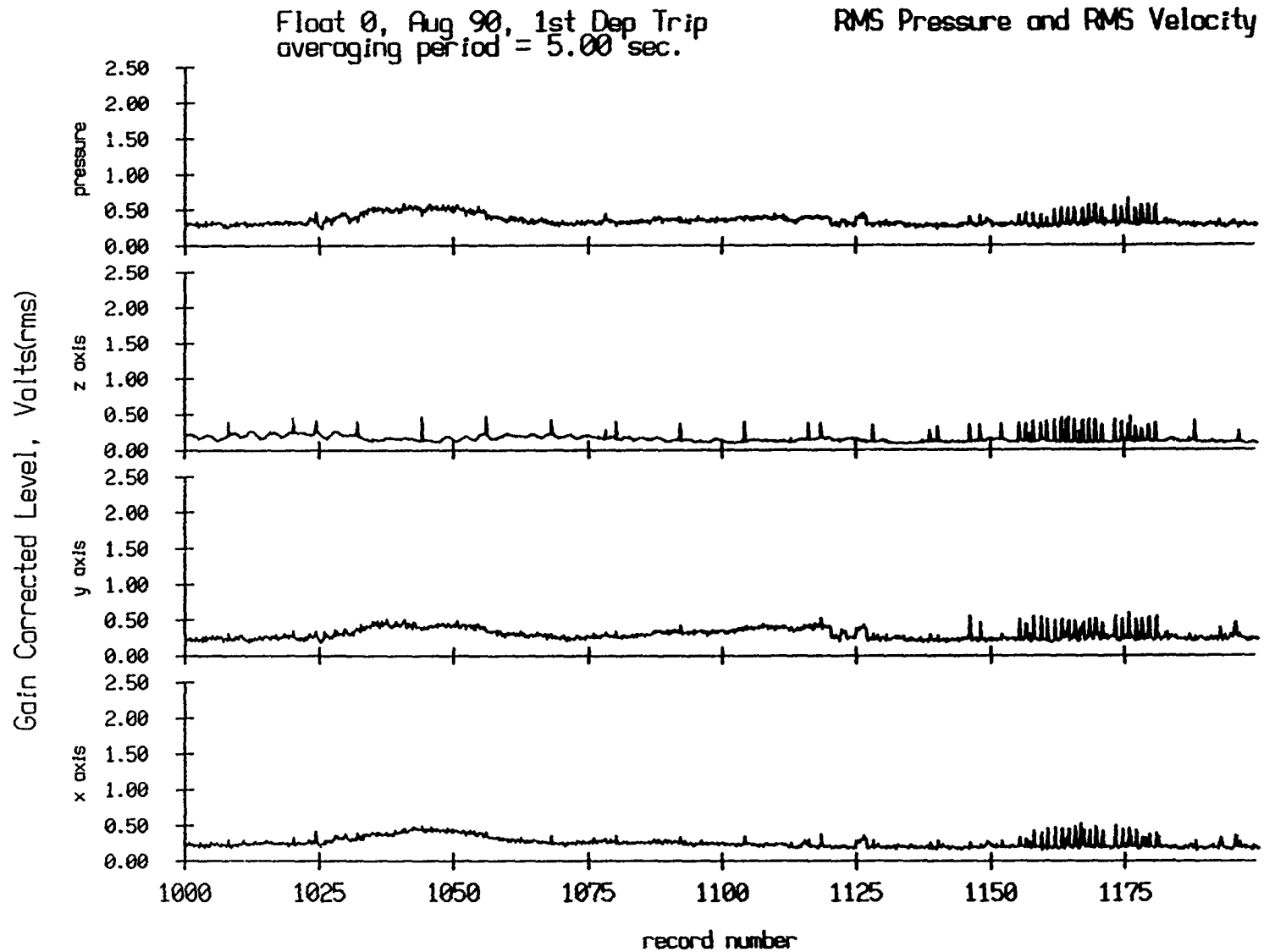

Figure VIII.1c

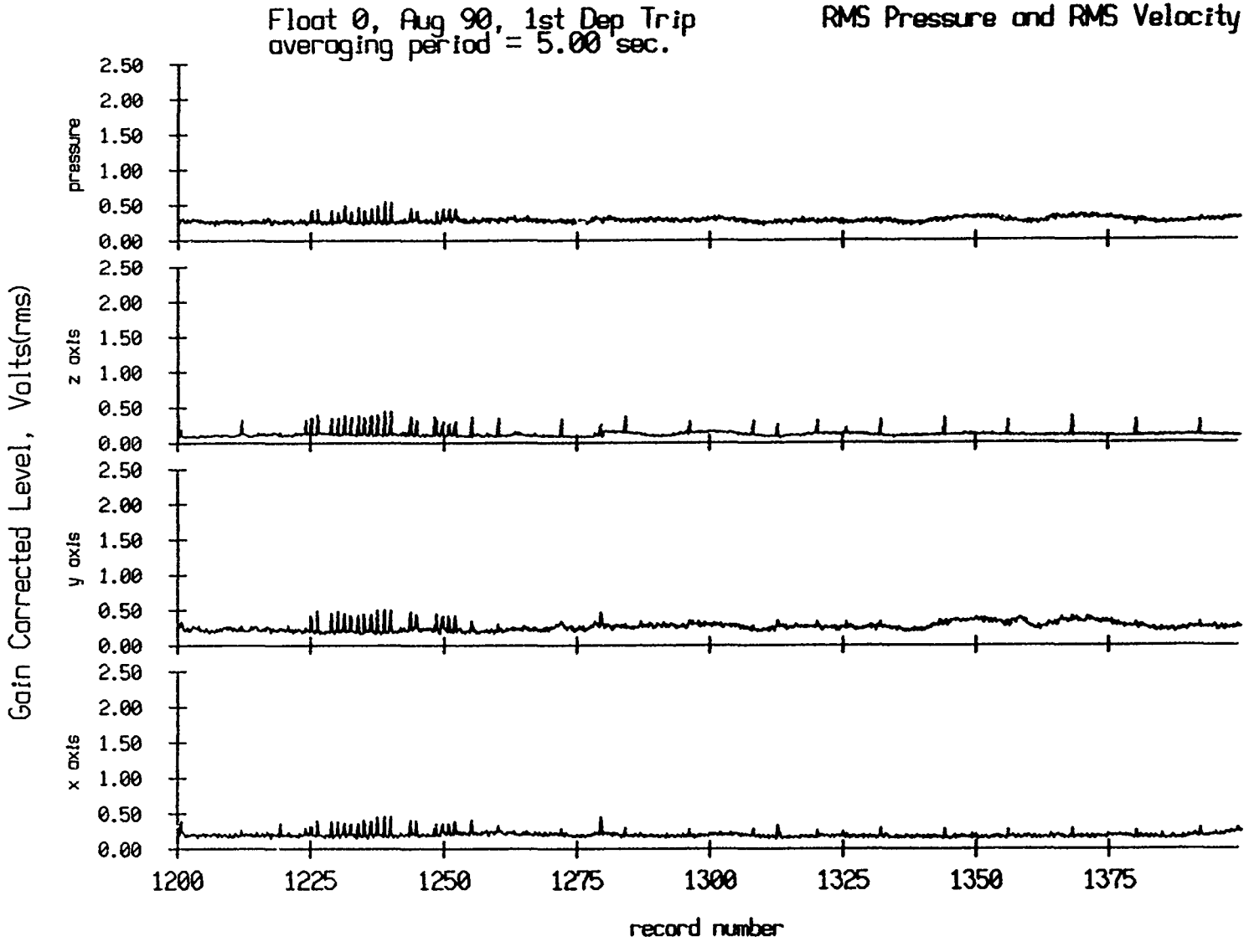

Figure VIII.1d

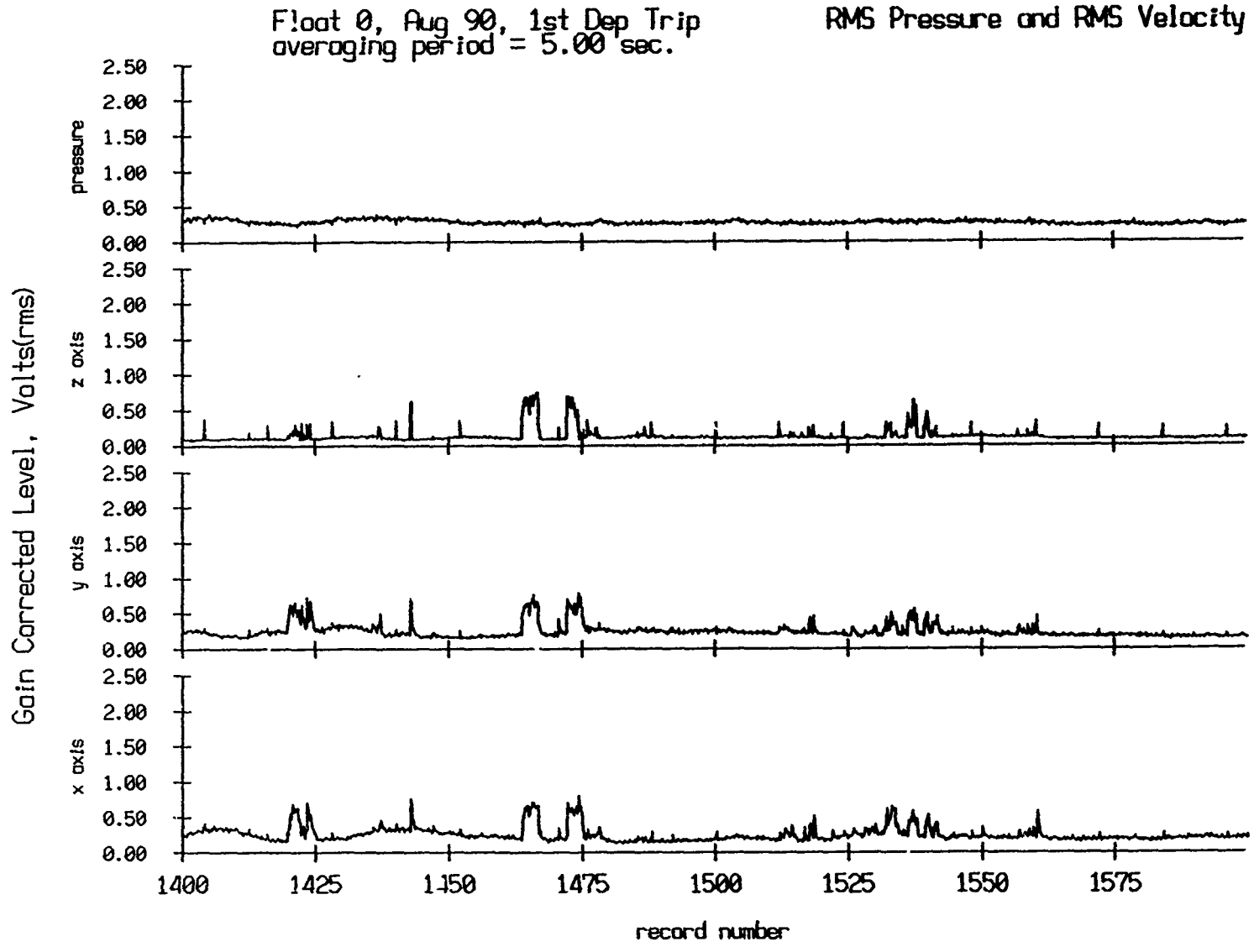

Figure VIII.1e

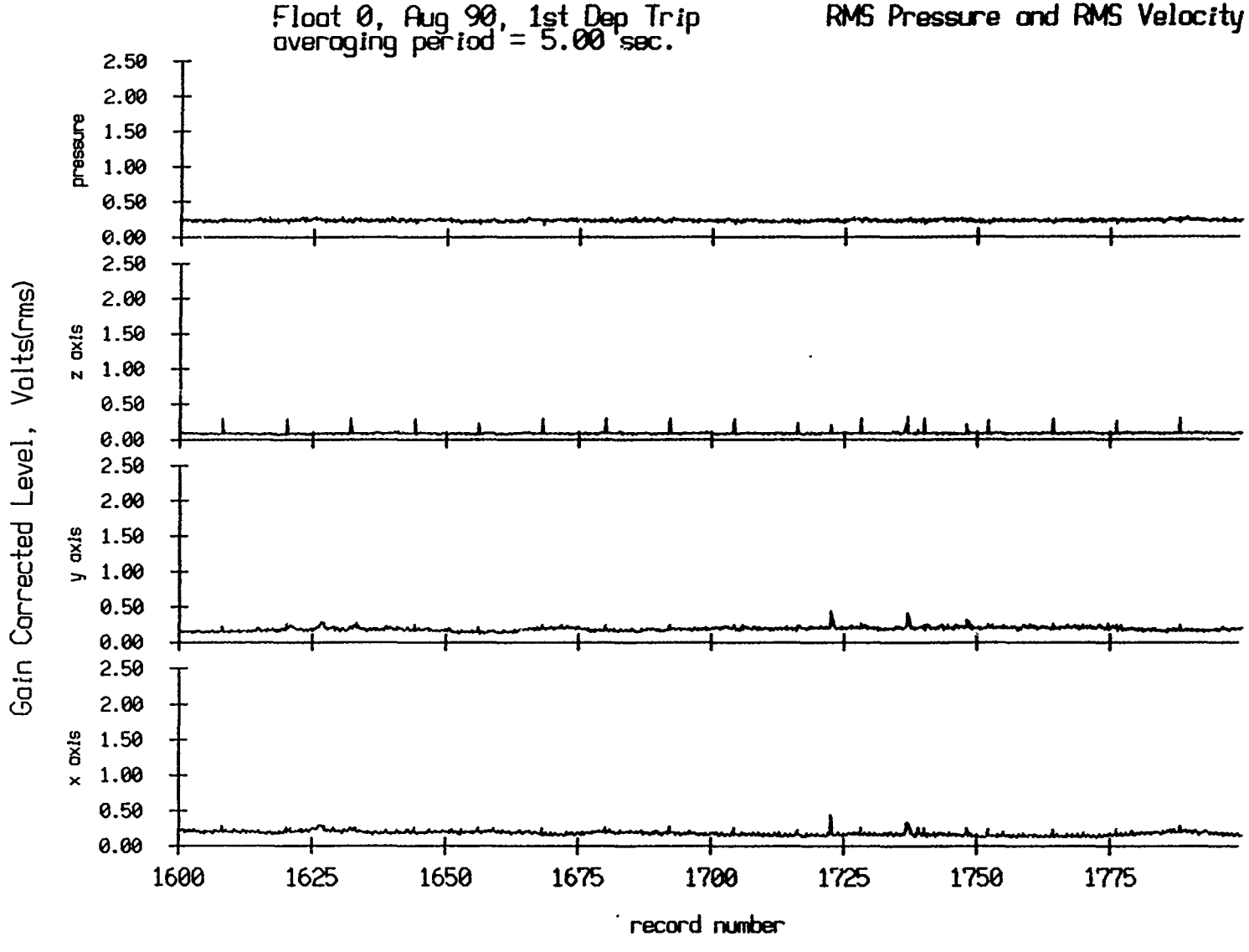

Figure VIII.1f

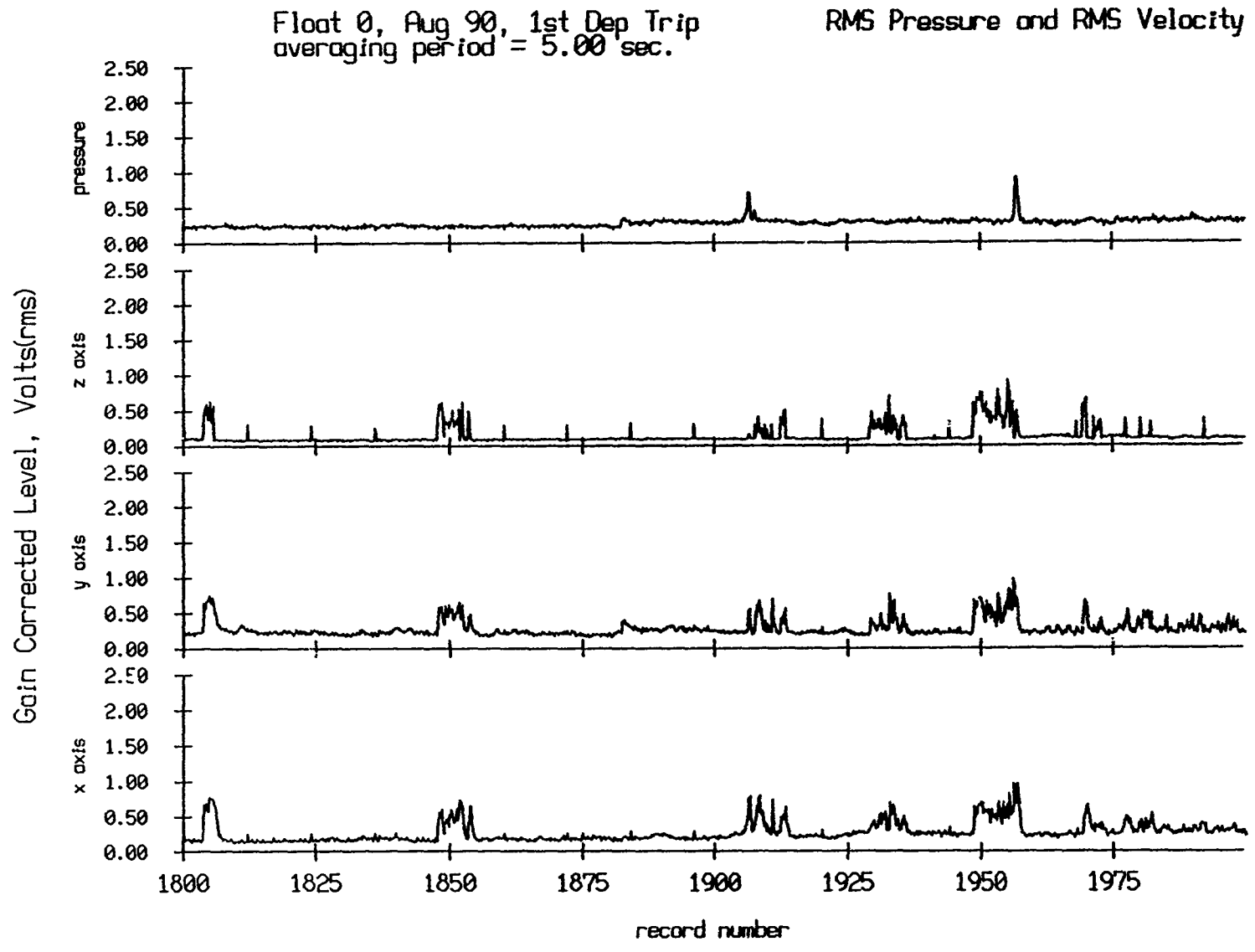

Figure VIII.1g

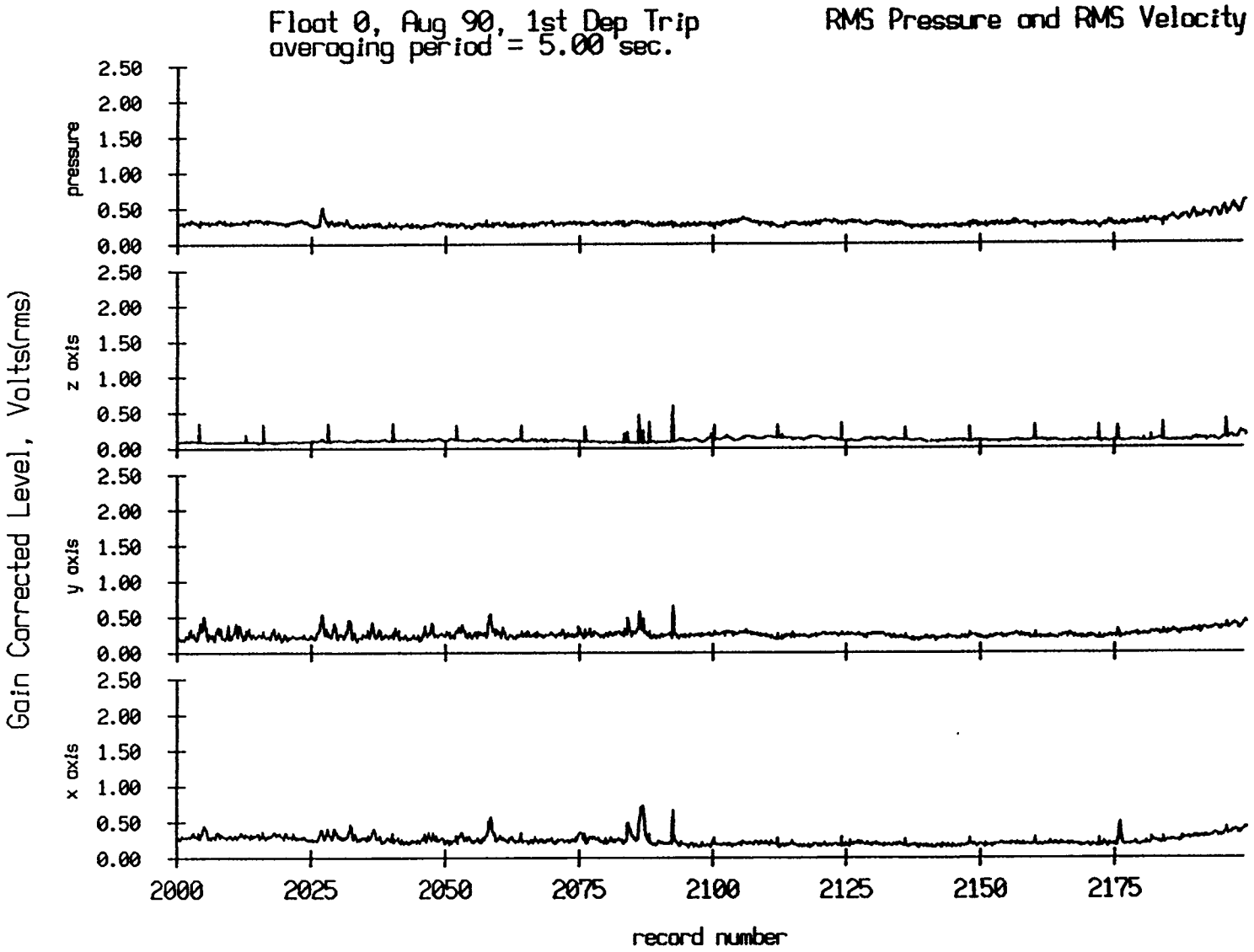

Figure VIII.1h

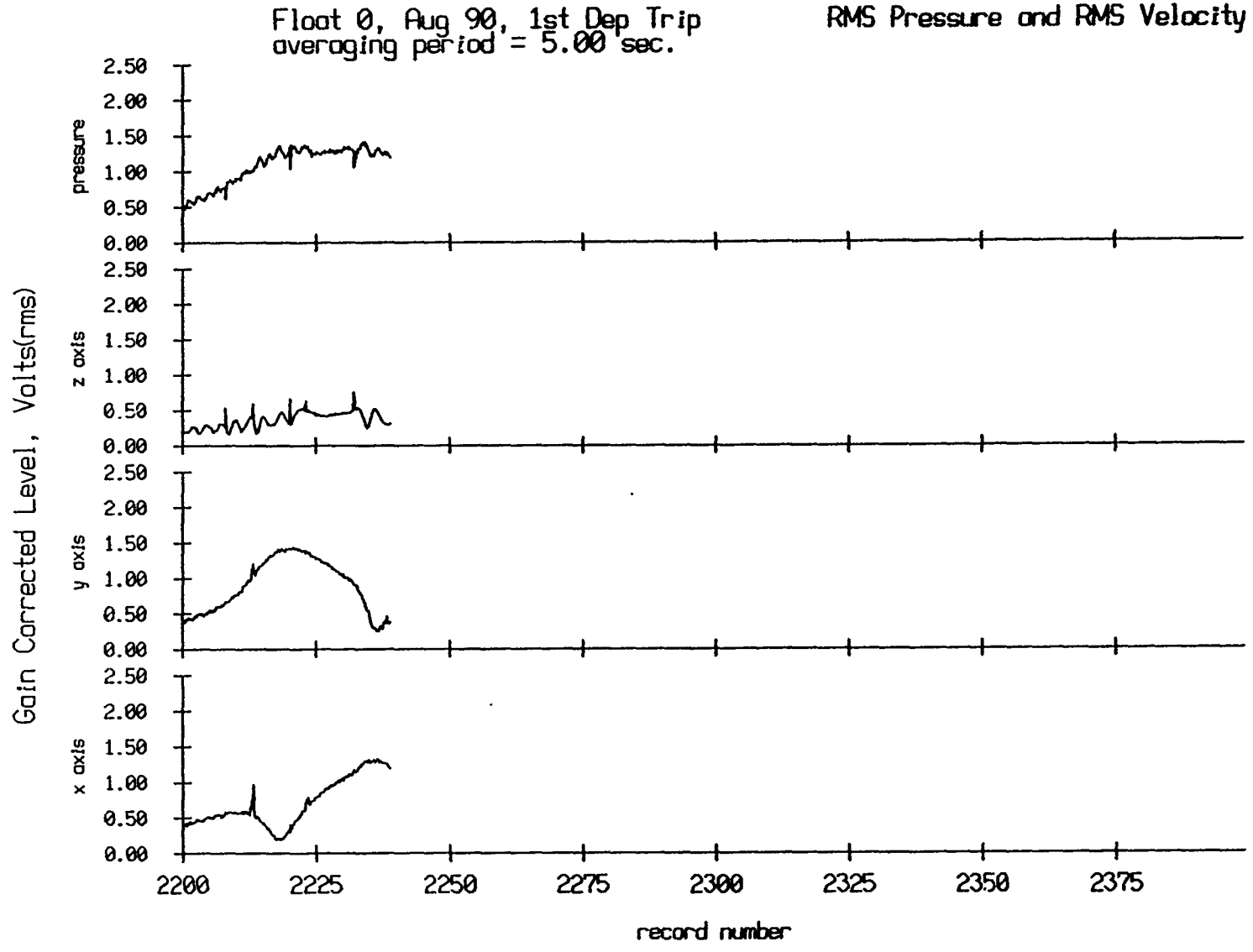

Figure VIII.11

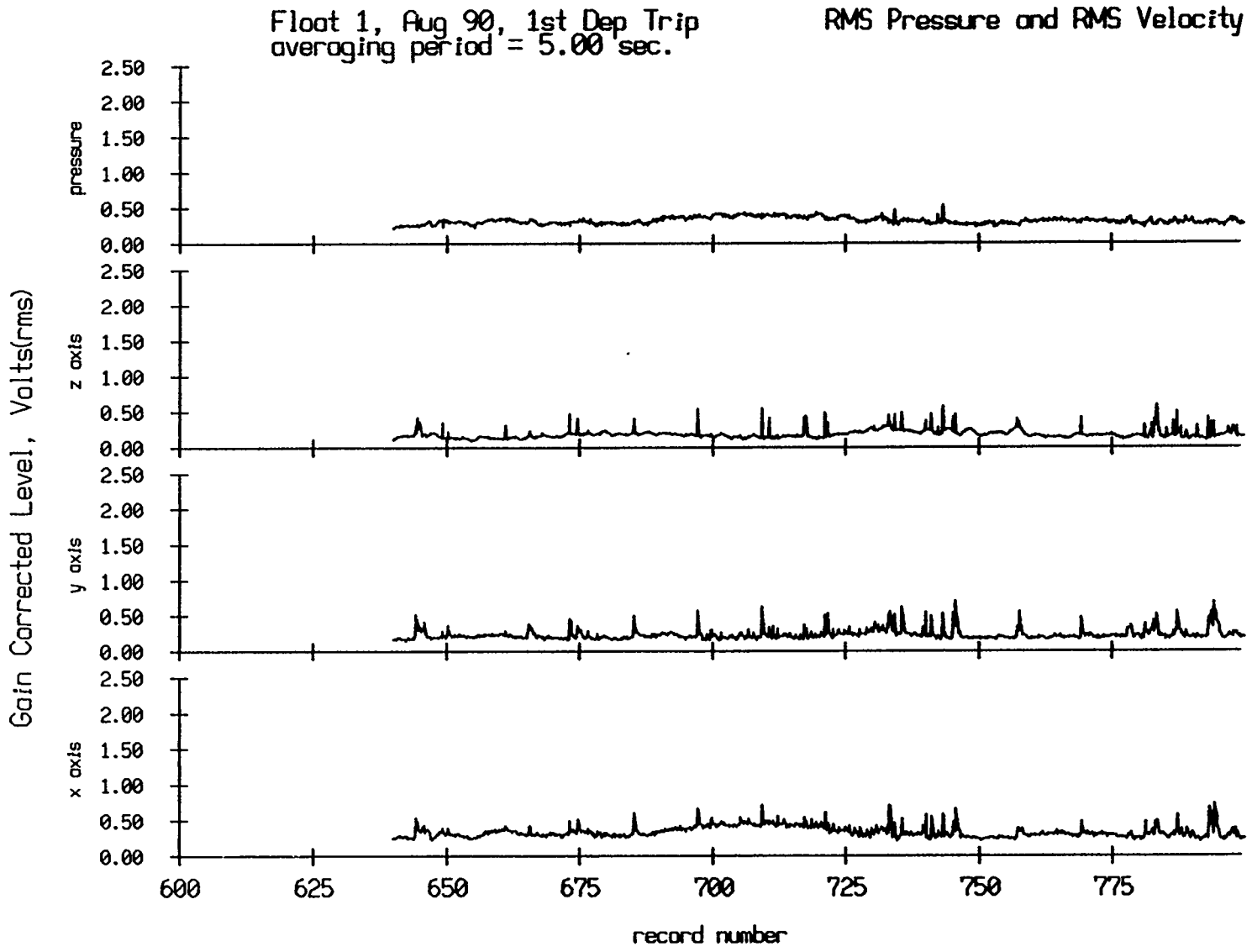

Figure VIII.2a

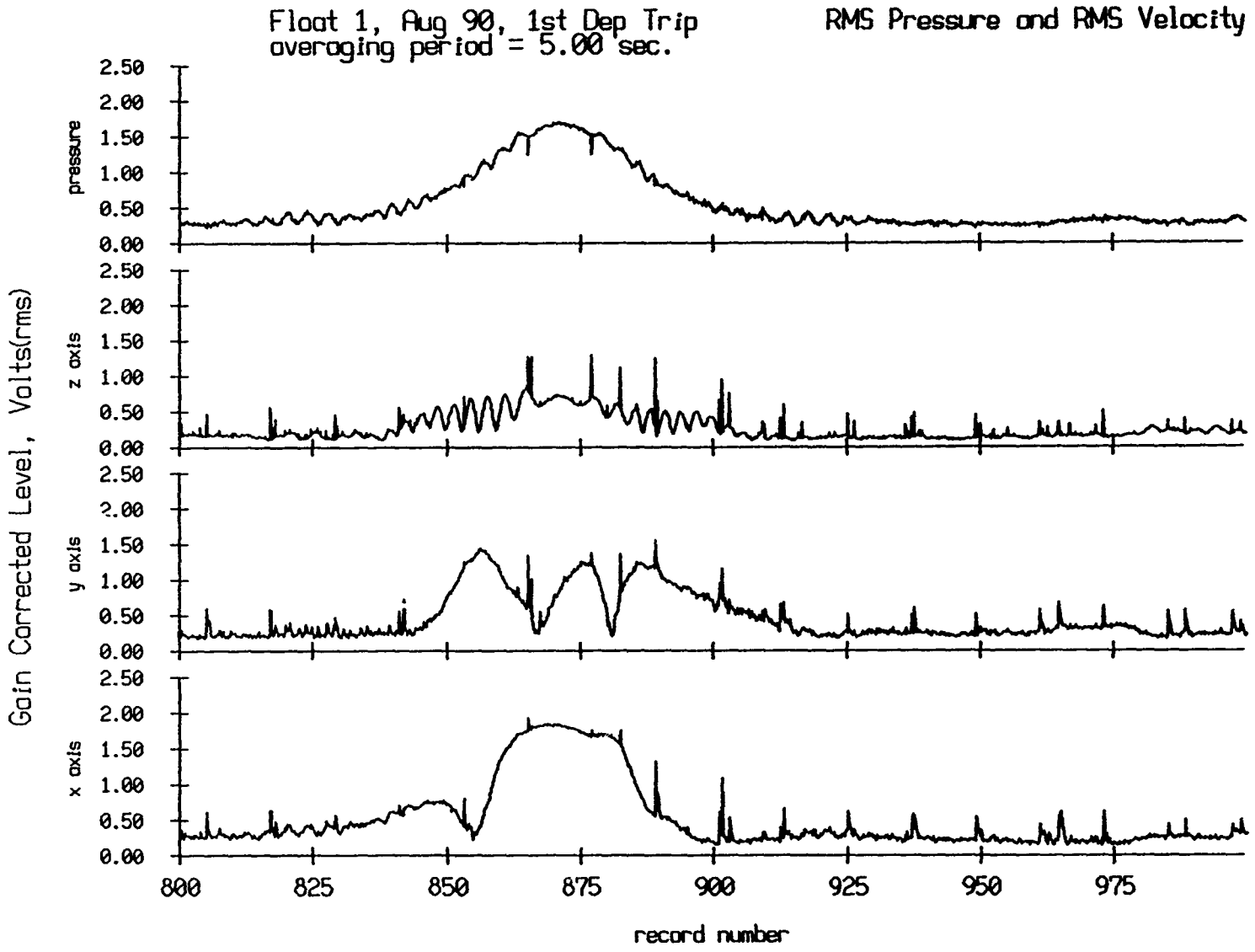

Figure VIII.2b

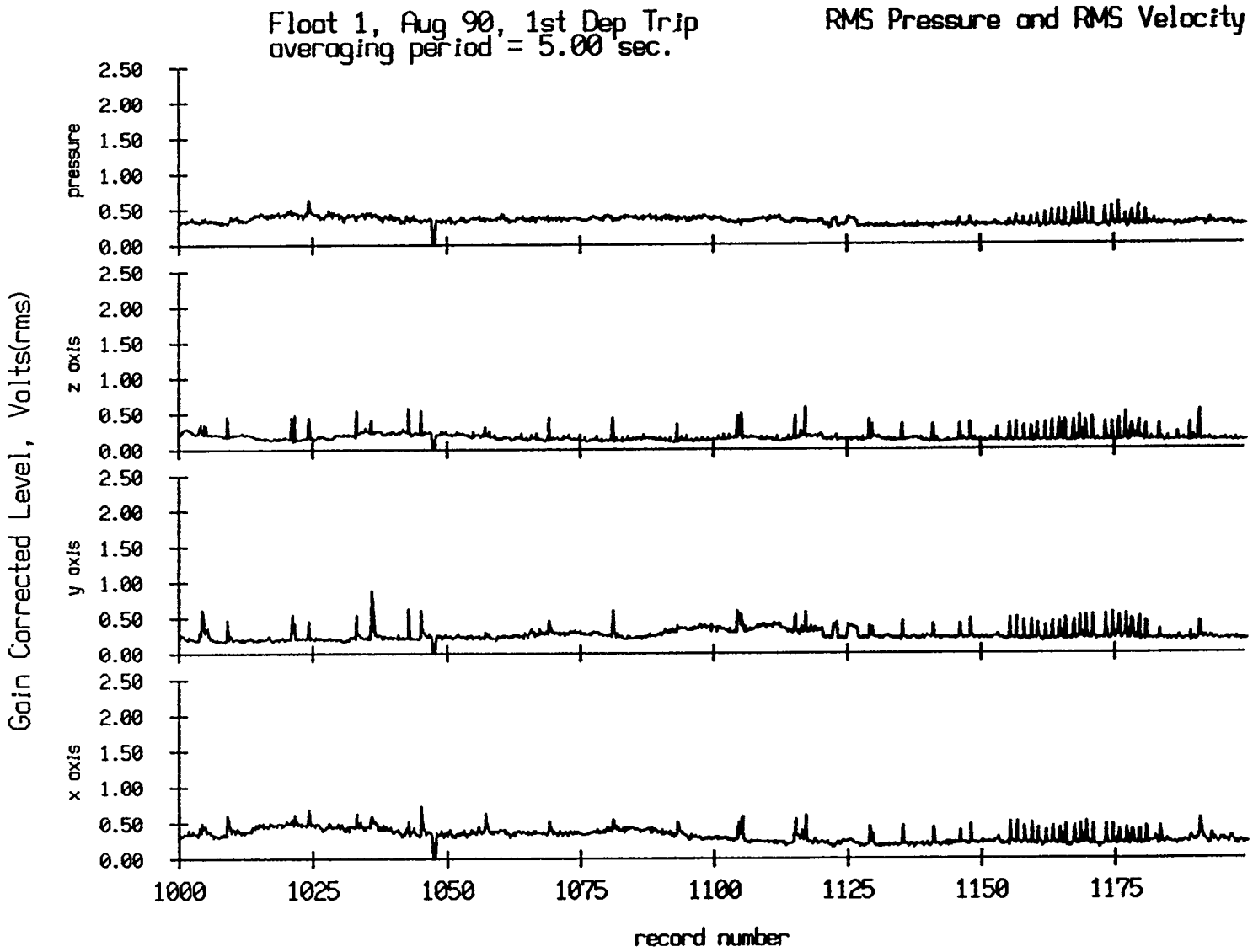

Figure VIII.2c

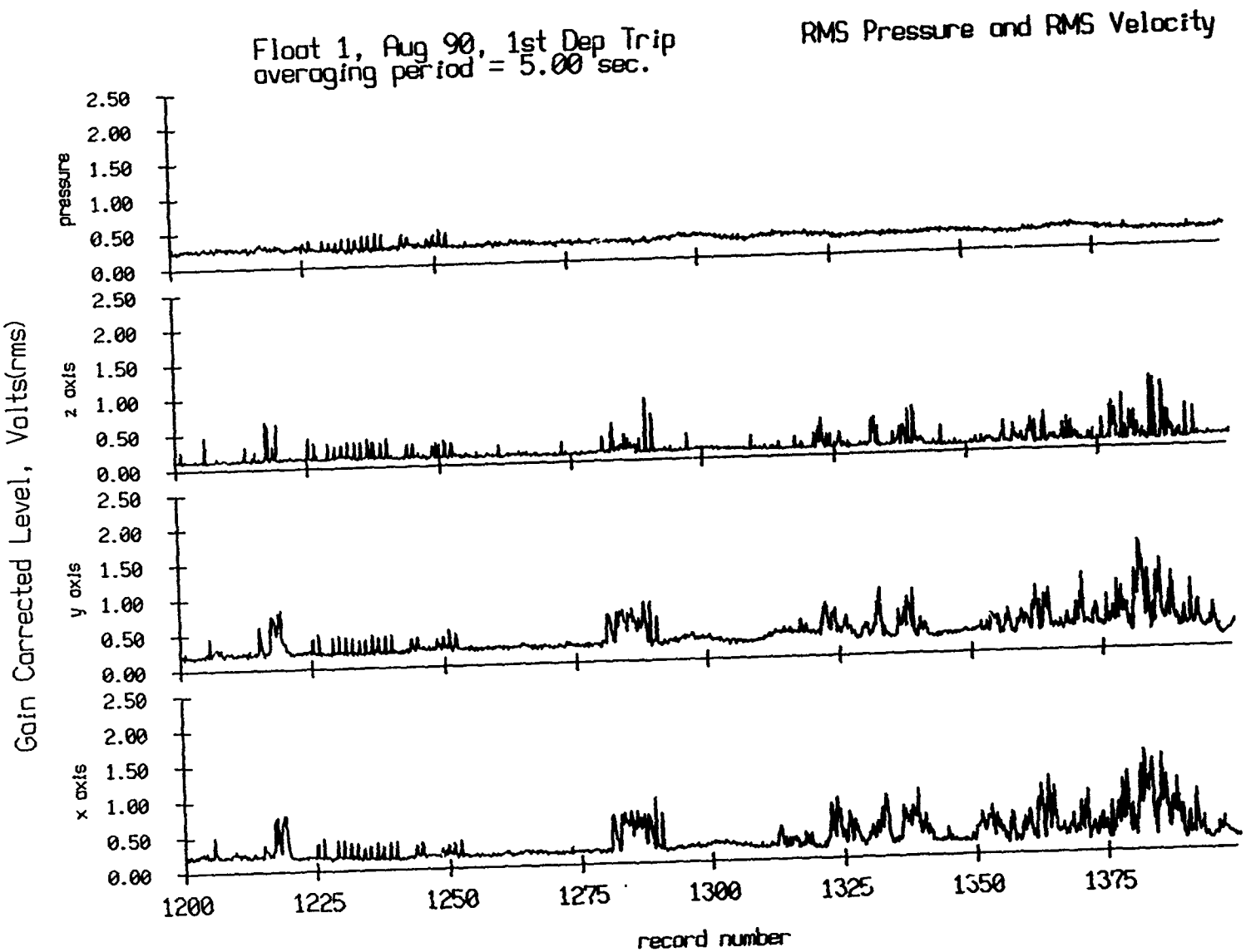

Figure VIII.2d

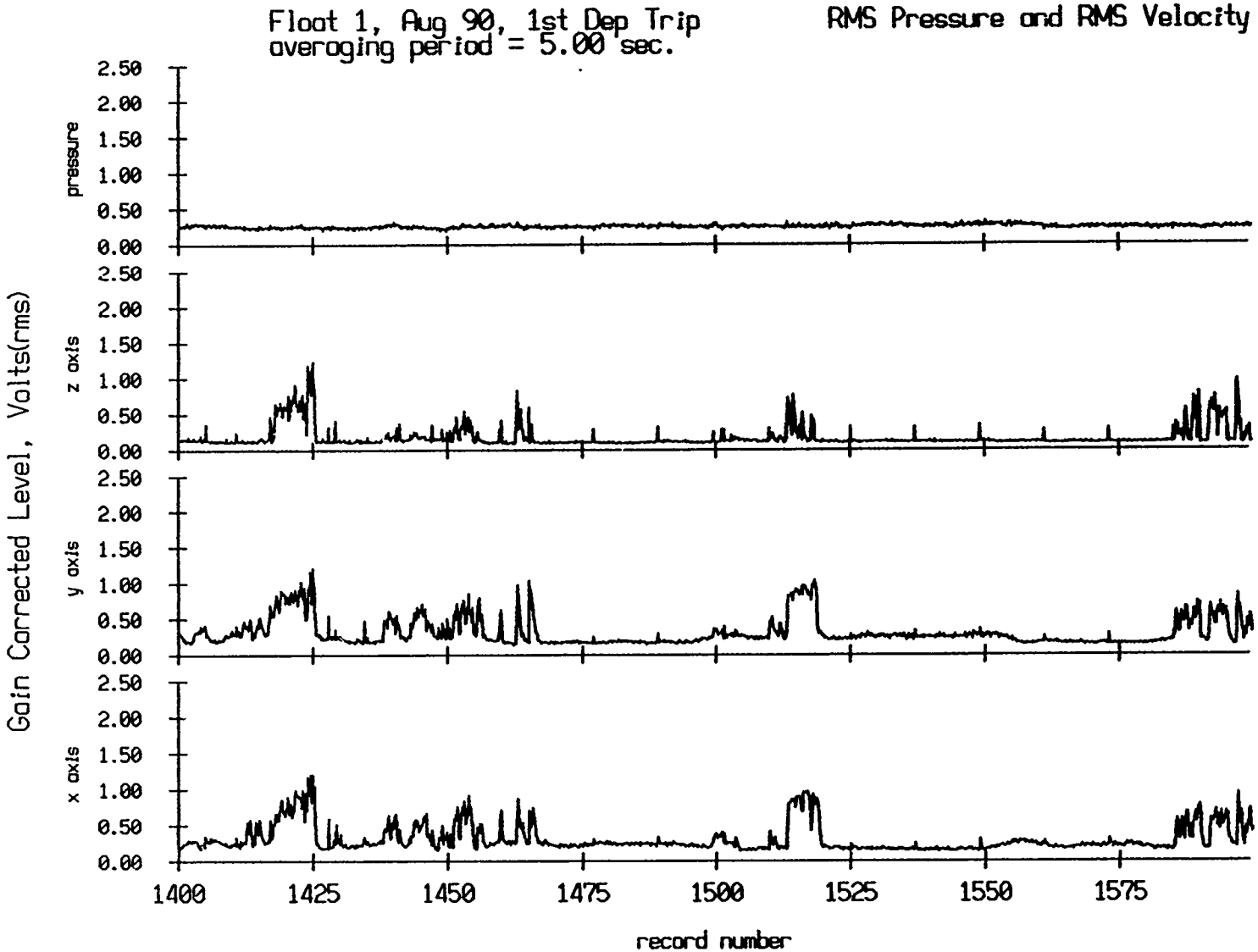

Figure VIII.2e

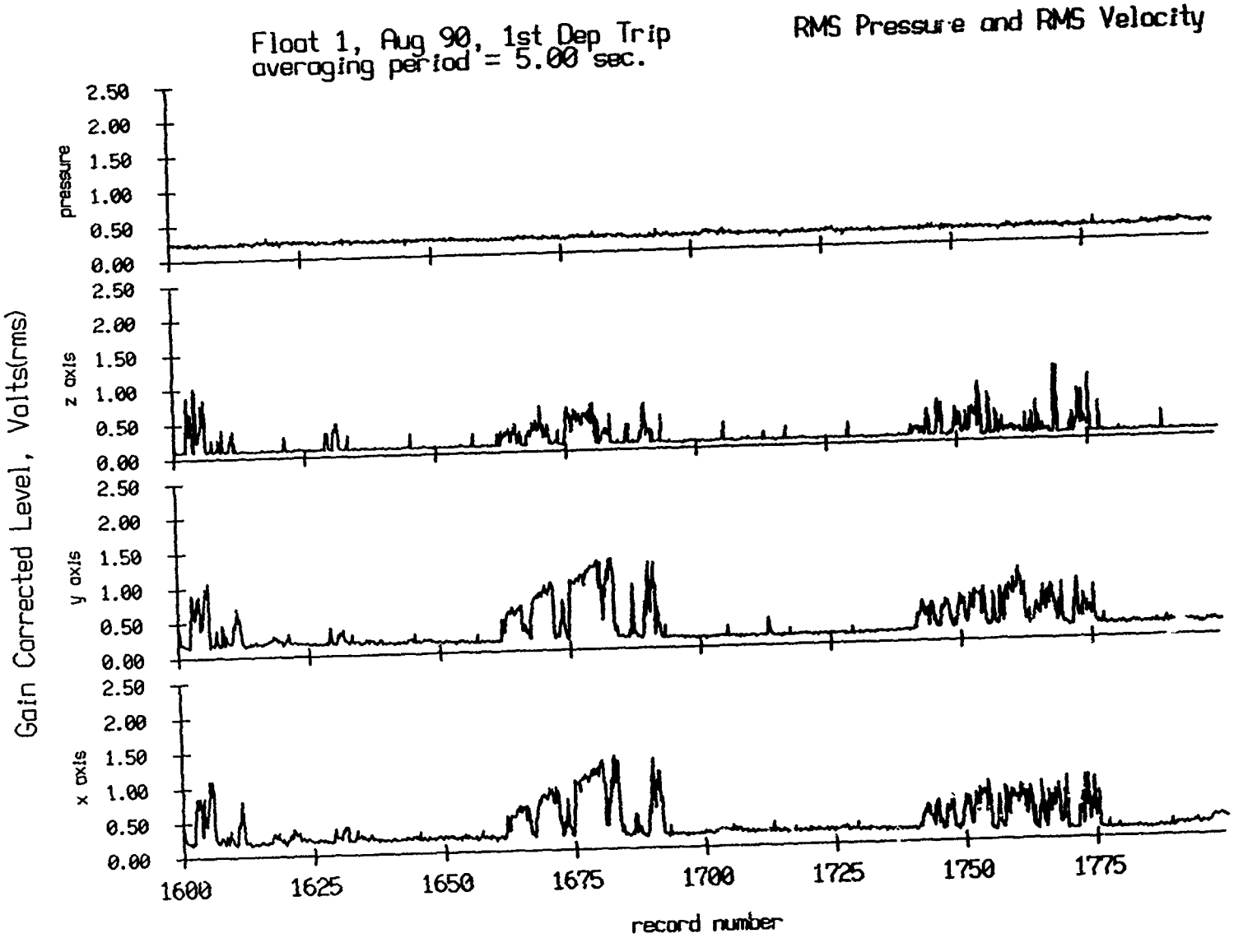

Figure VIII.2f

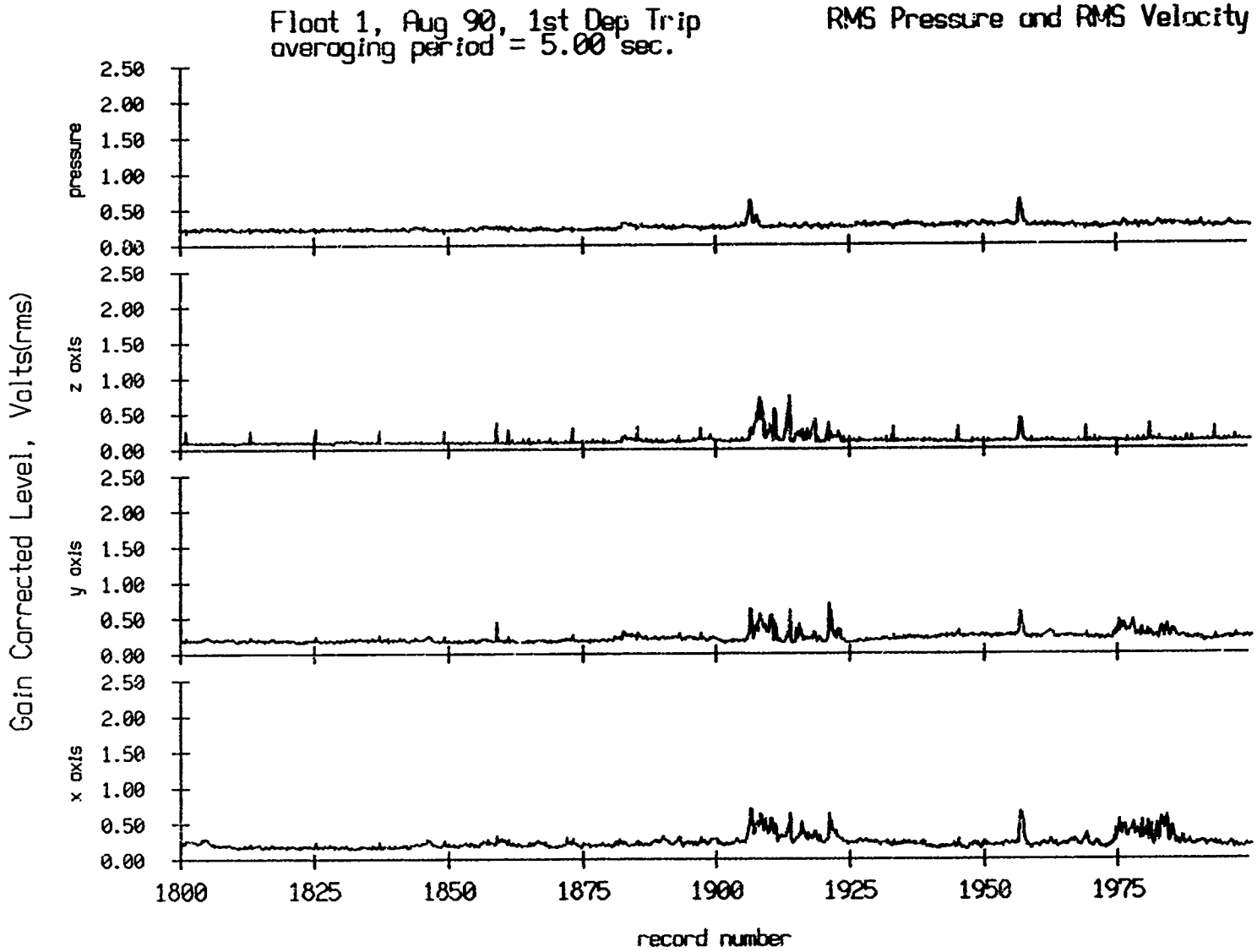

Figure VIII.2g

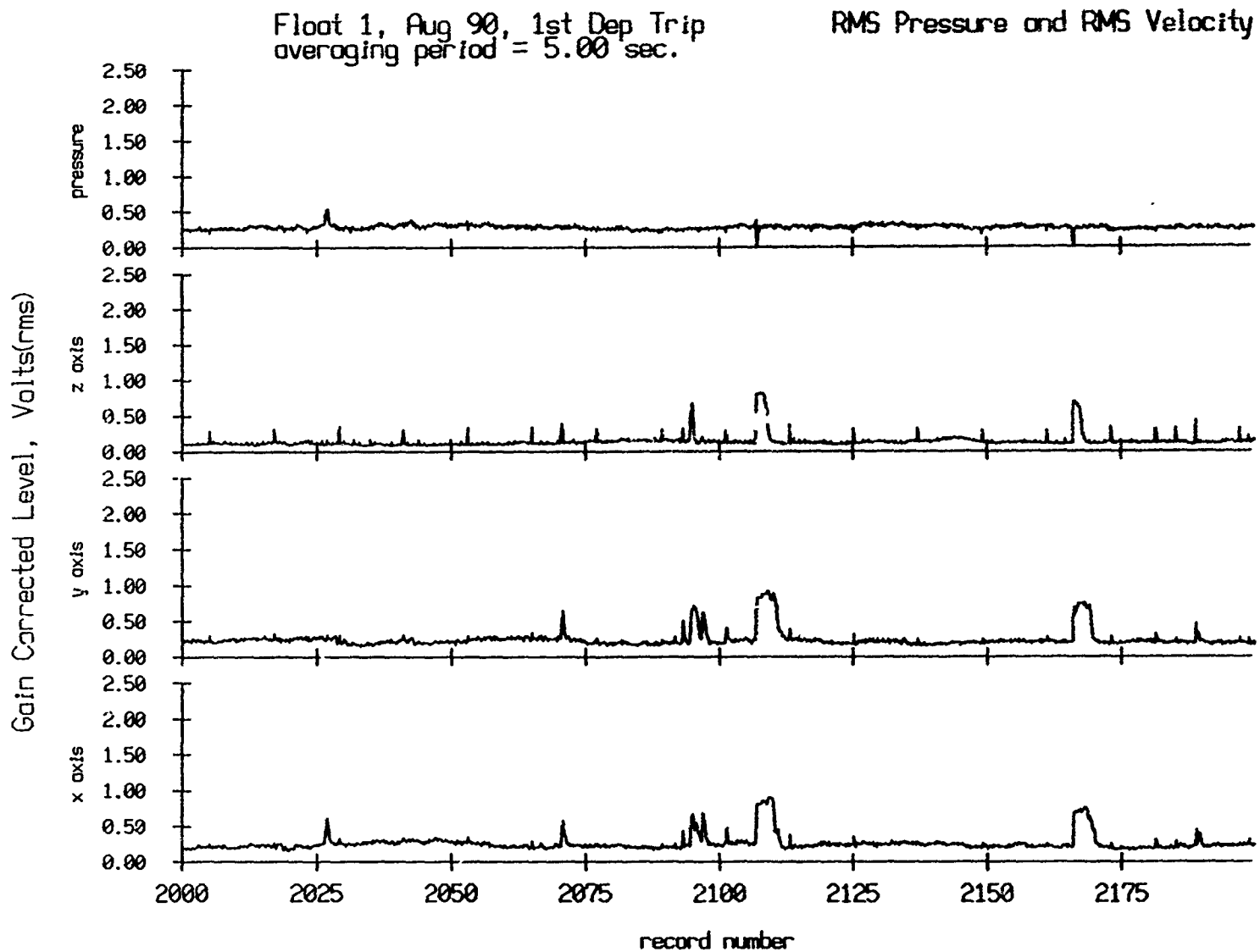

Figure VIII.2h

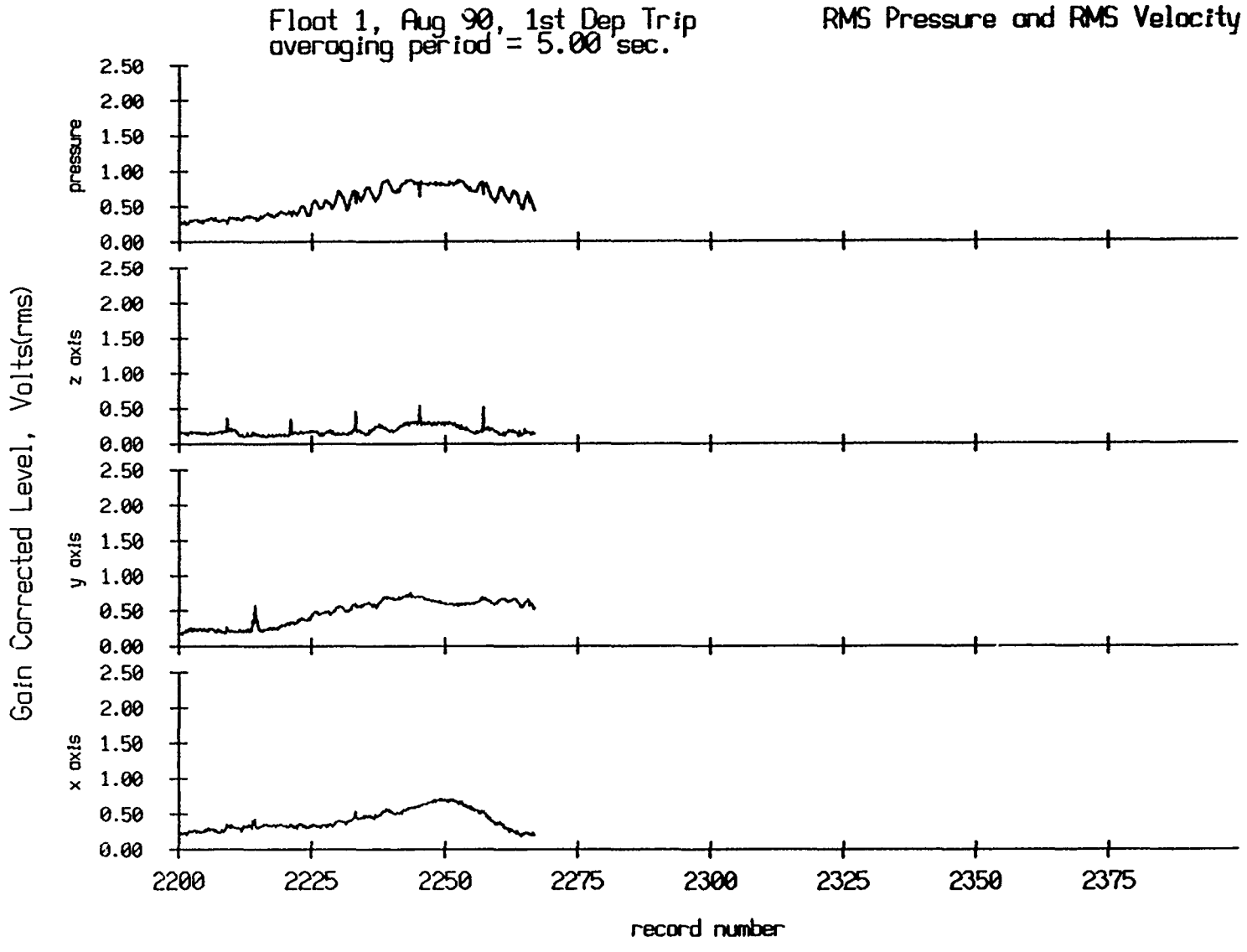

Figure VIII.2i

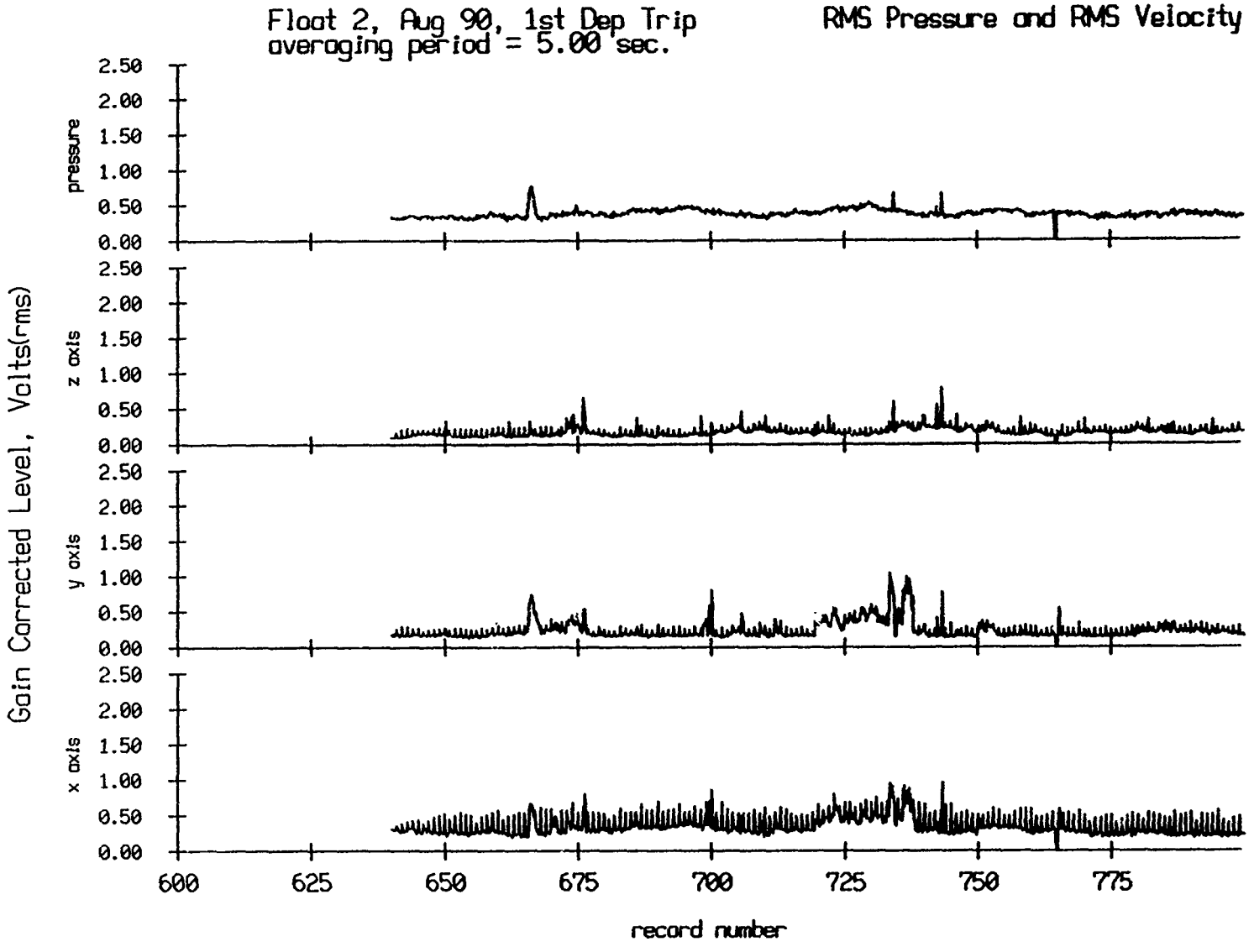

Figure VIII.3a

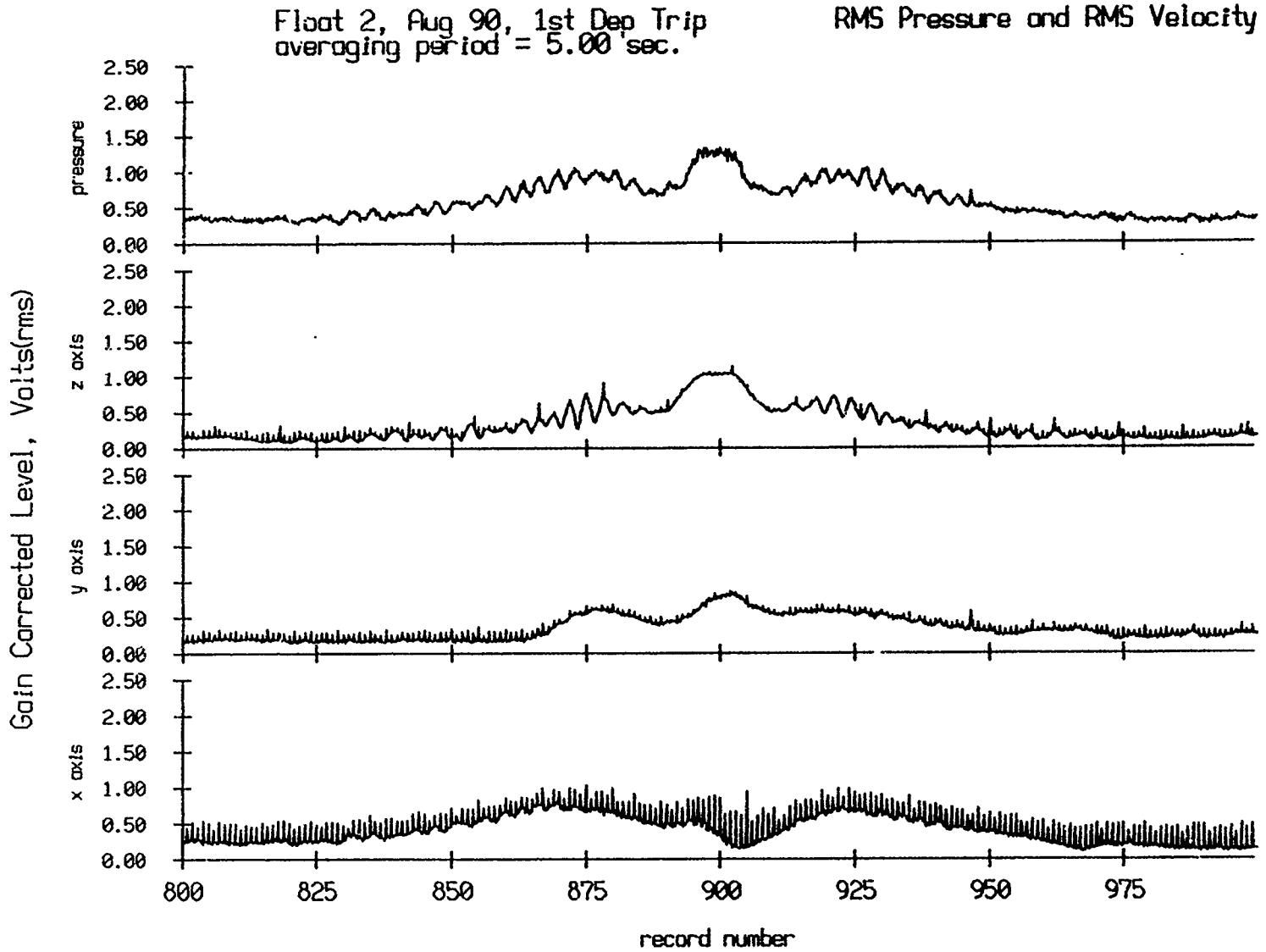

Figure VIII.3b

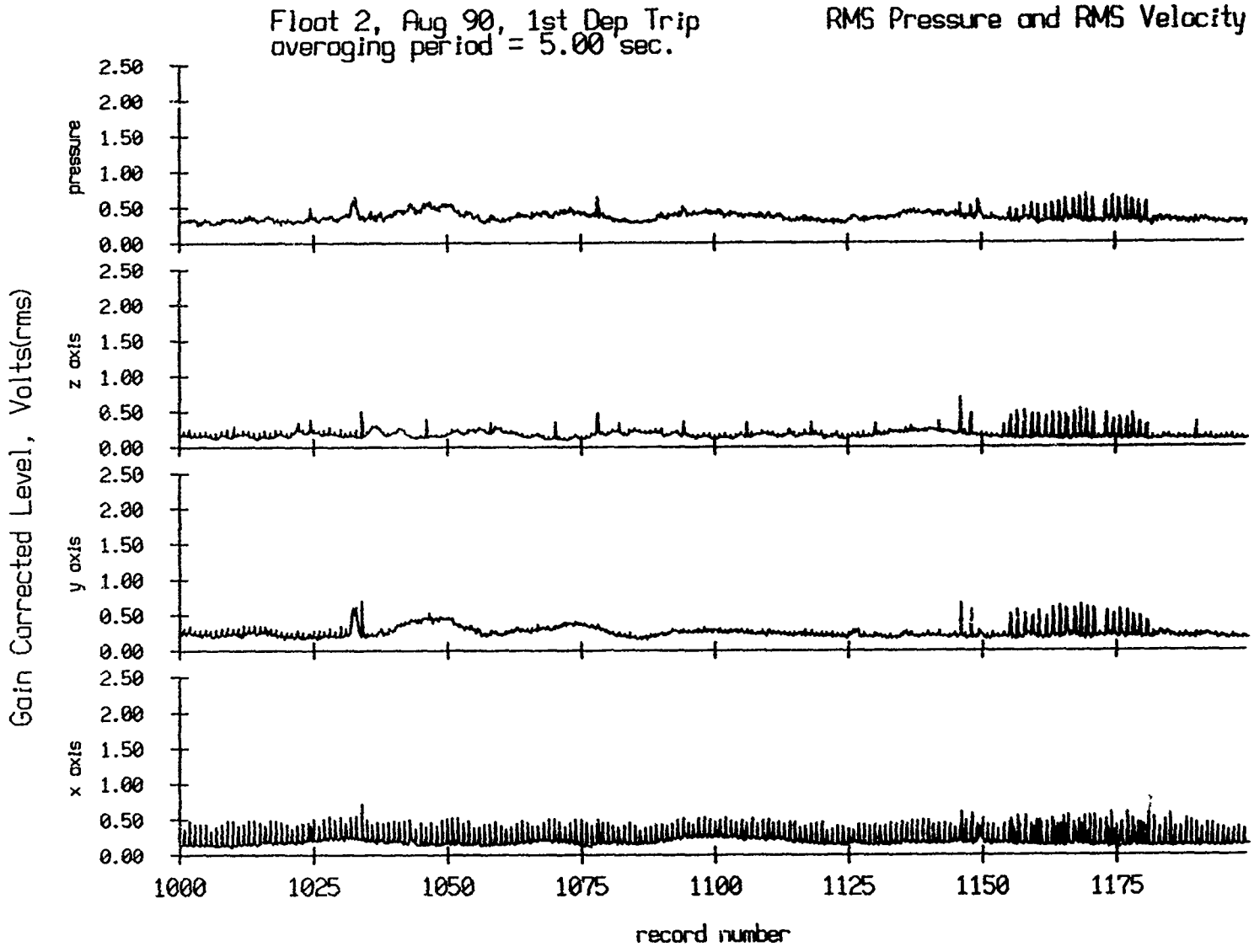

Figure VIII.3c

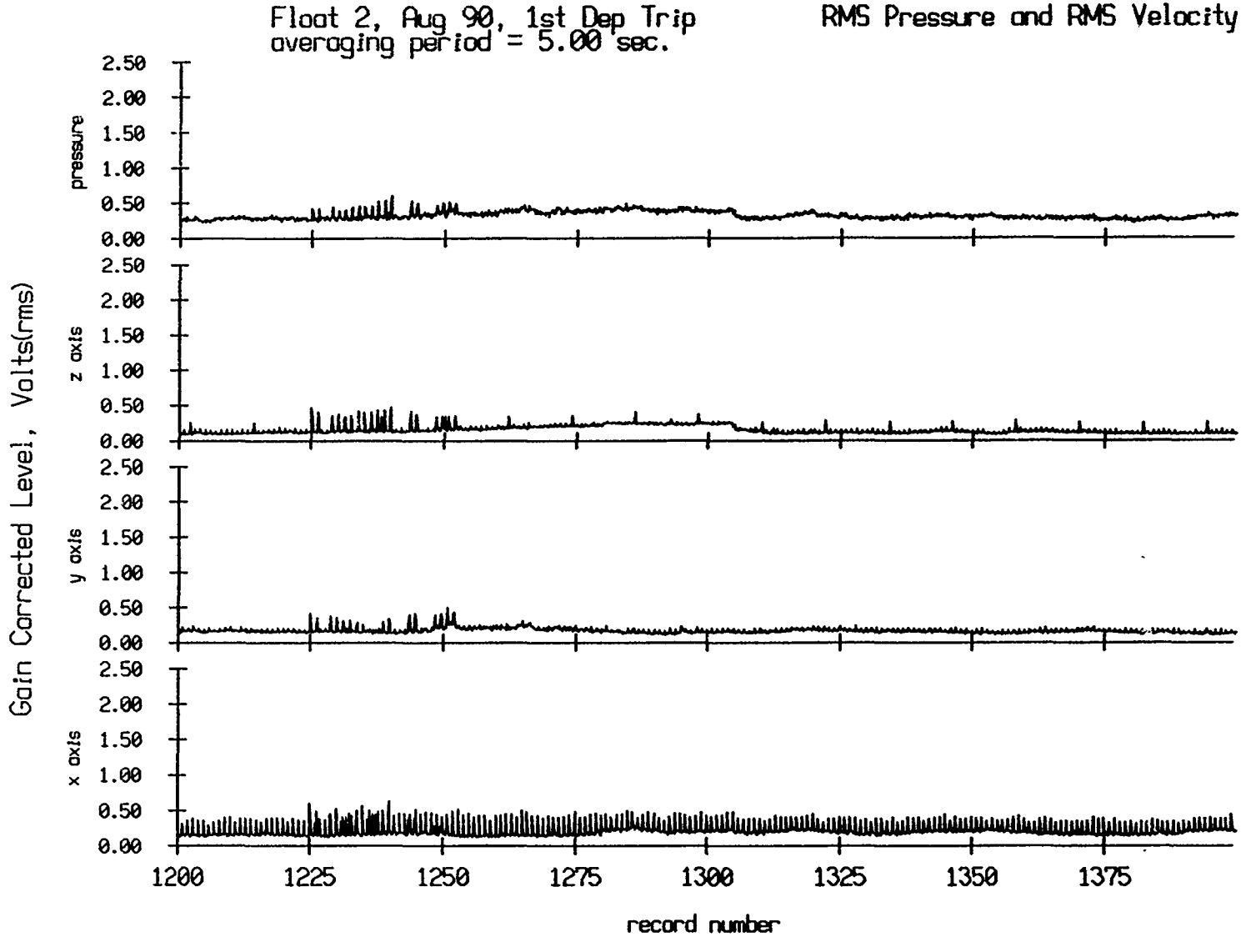

Figure VIII.3d

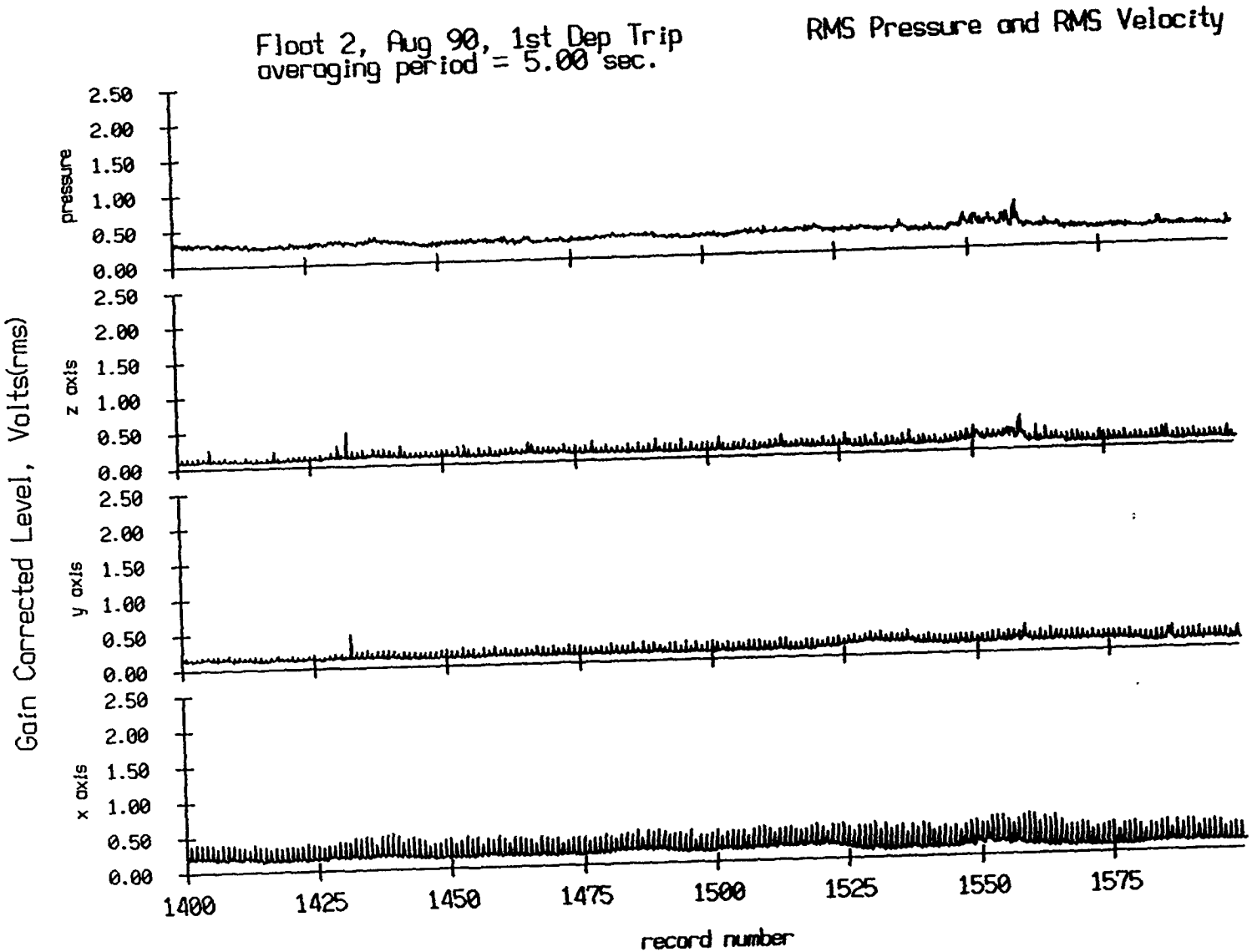

Figure VIII.3e

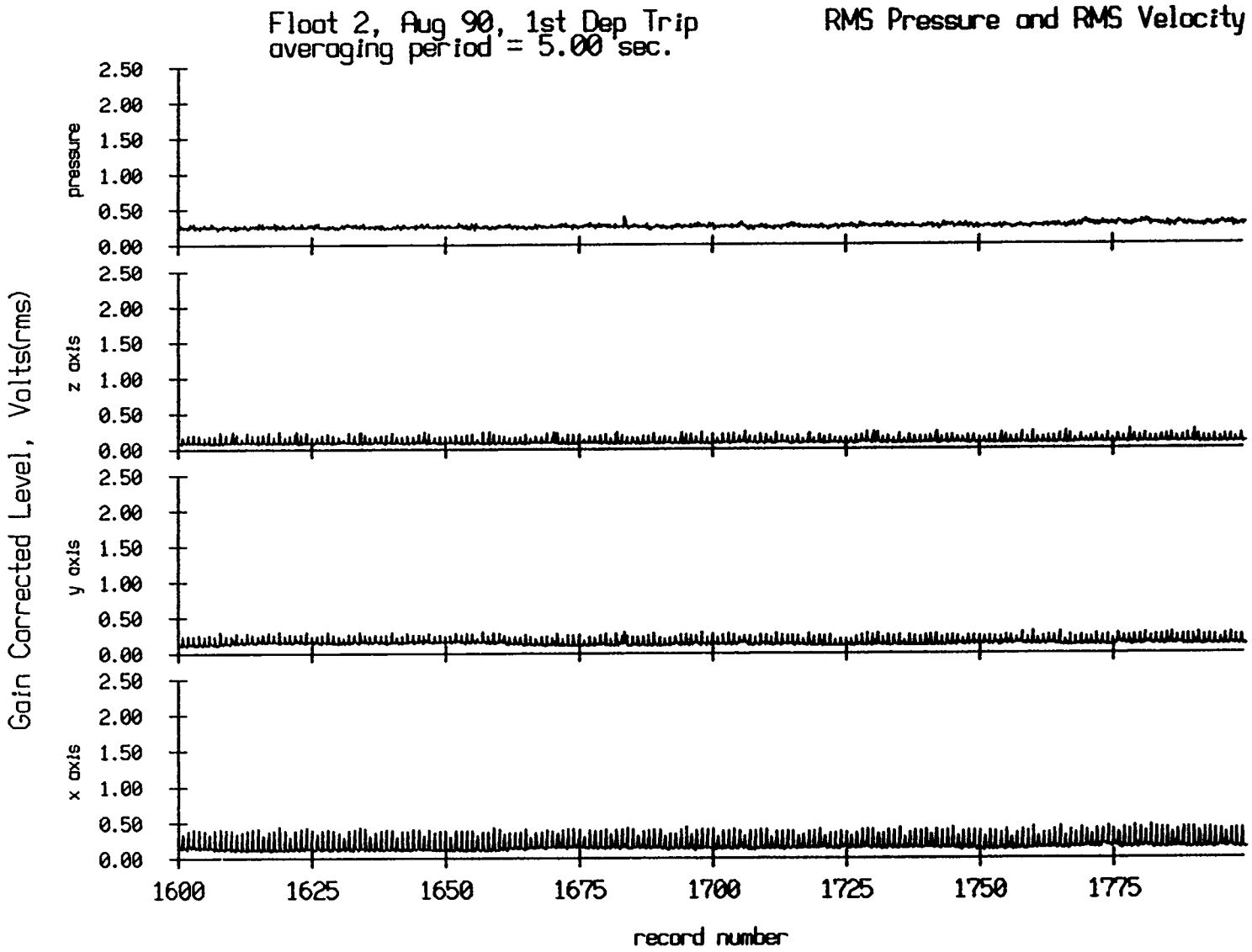

Figure VIII.3f

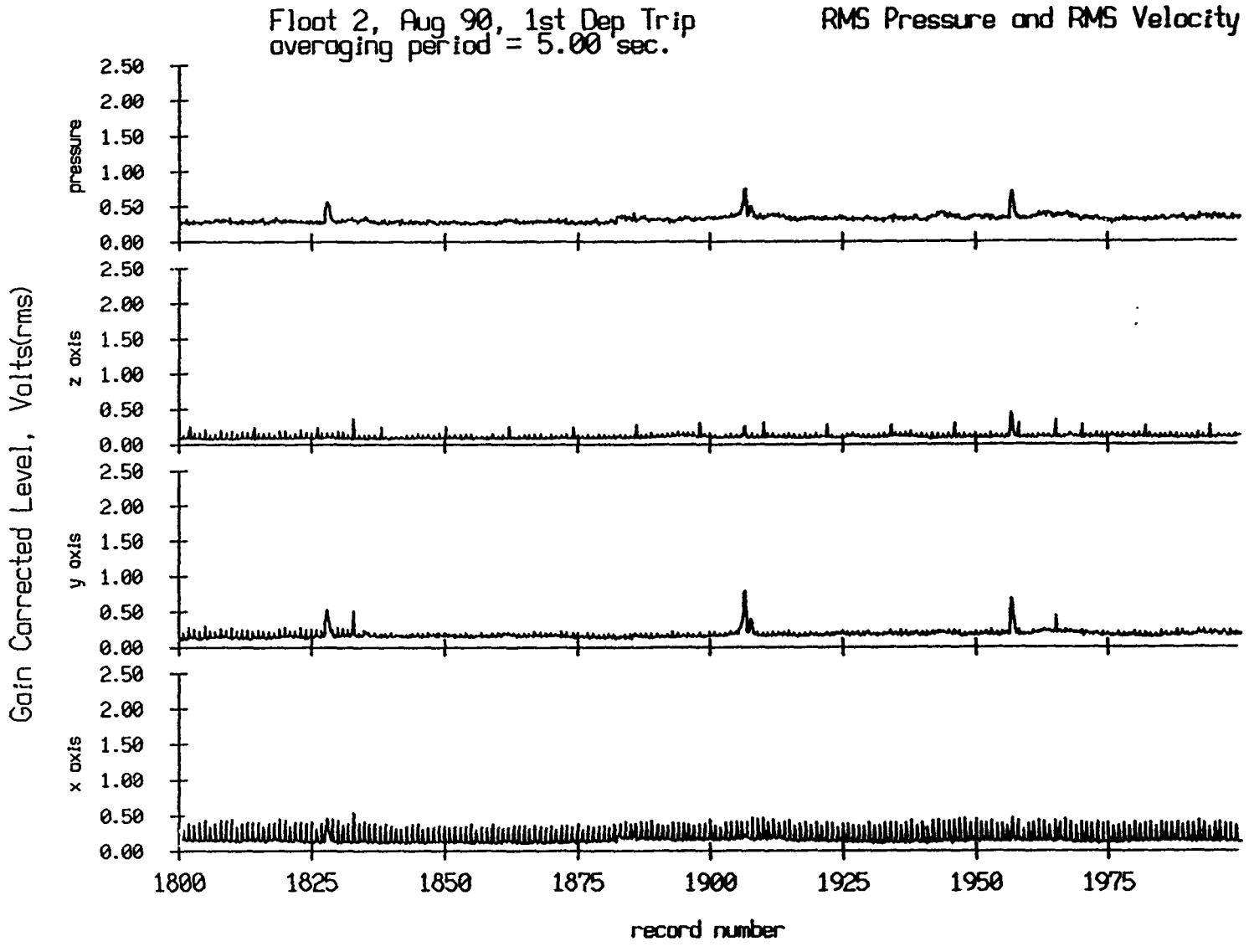

Figure VIII.3B

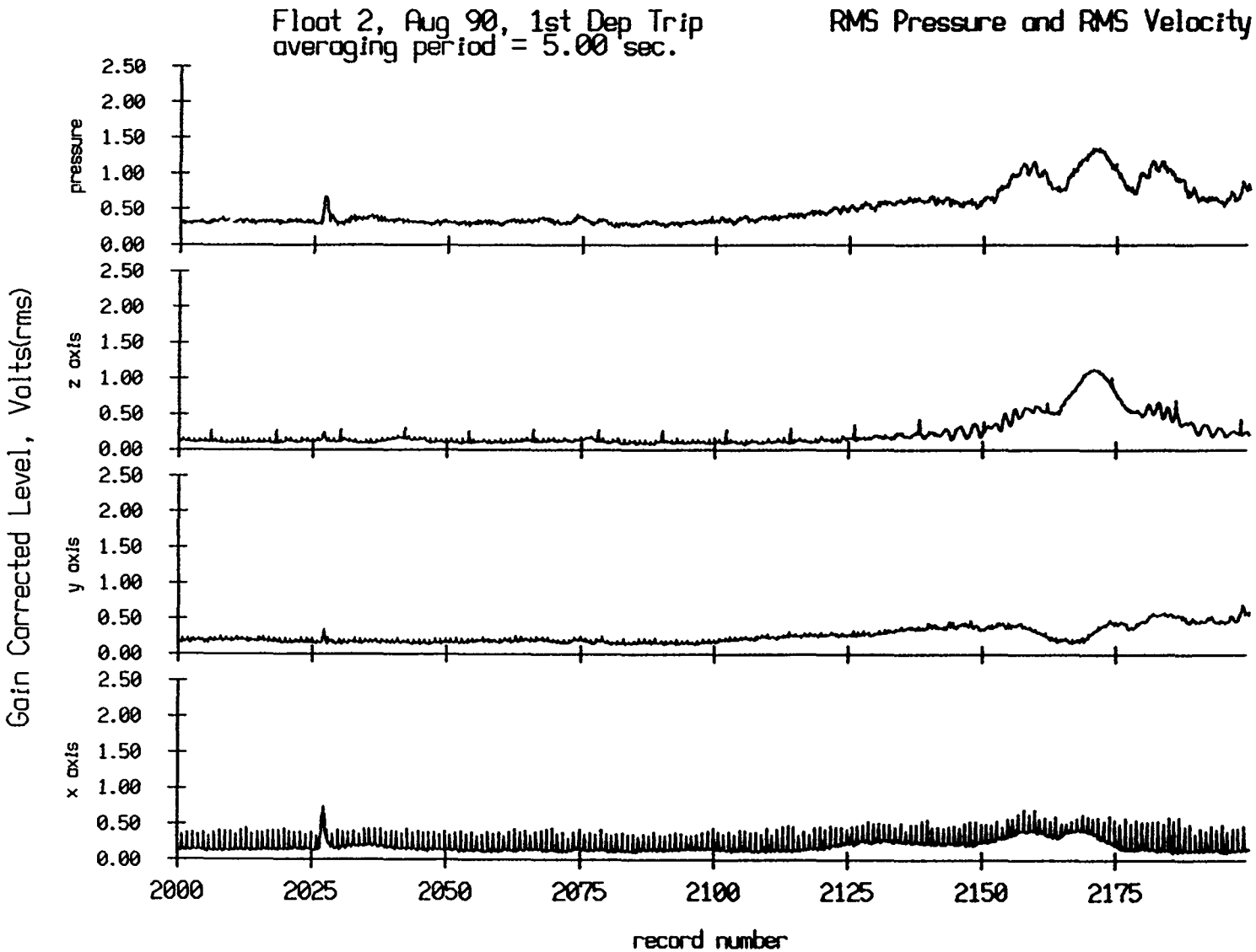

Figure VIII.3h

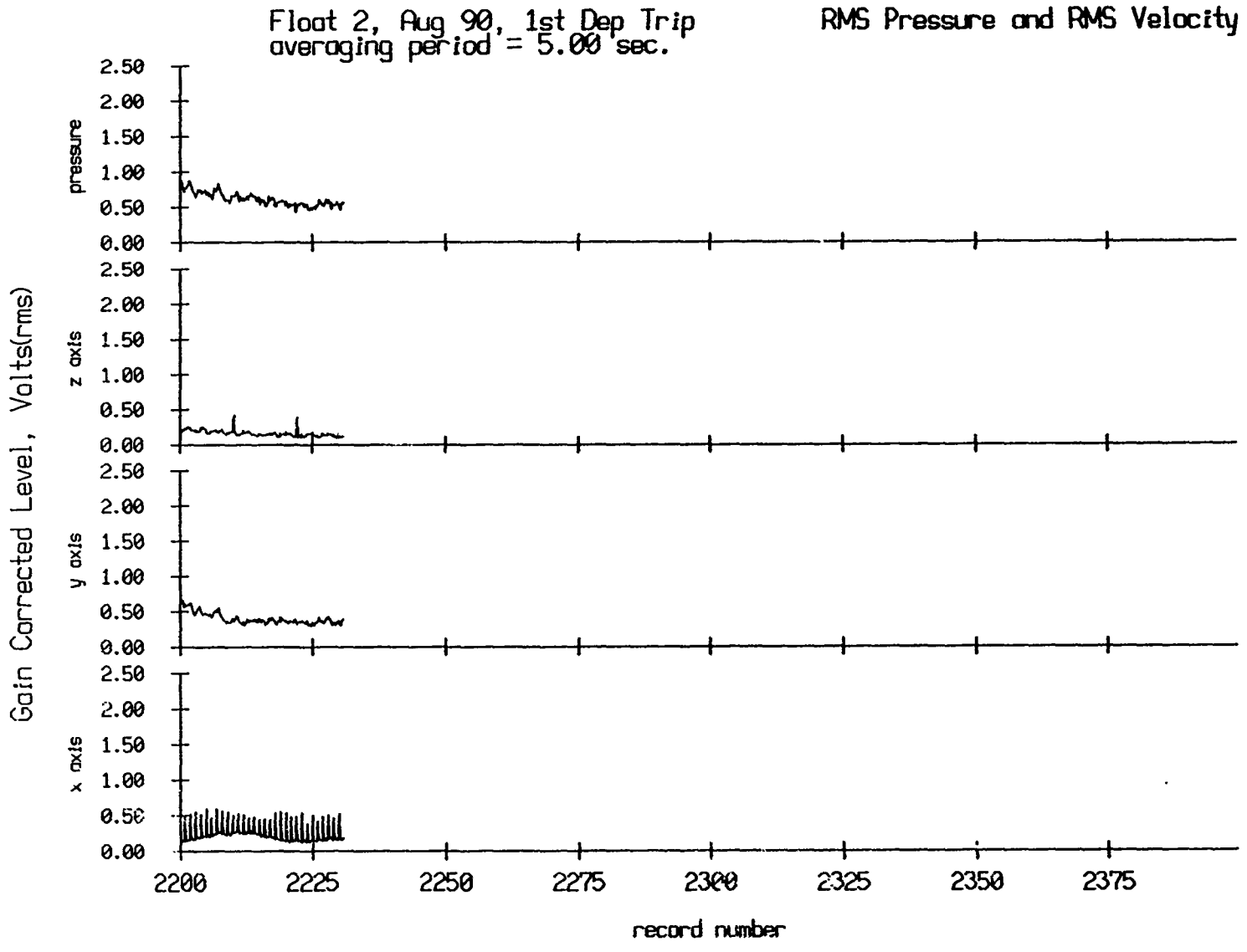

Figure VIII.3i

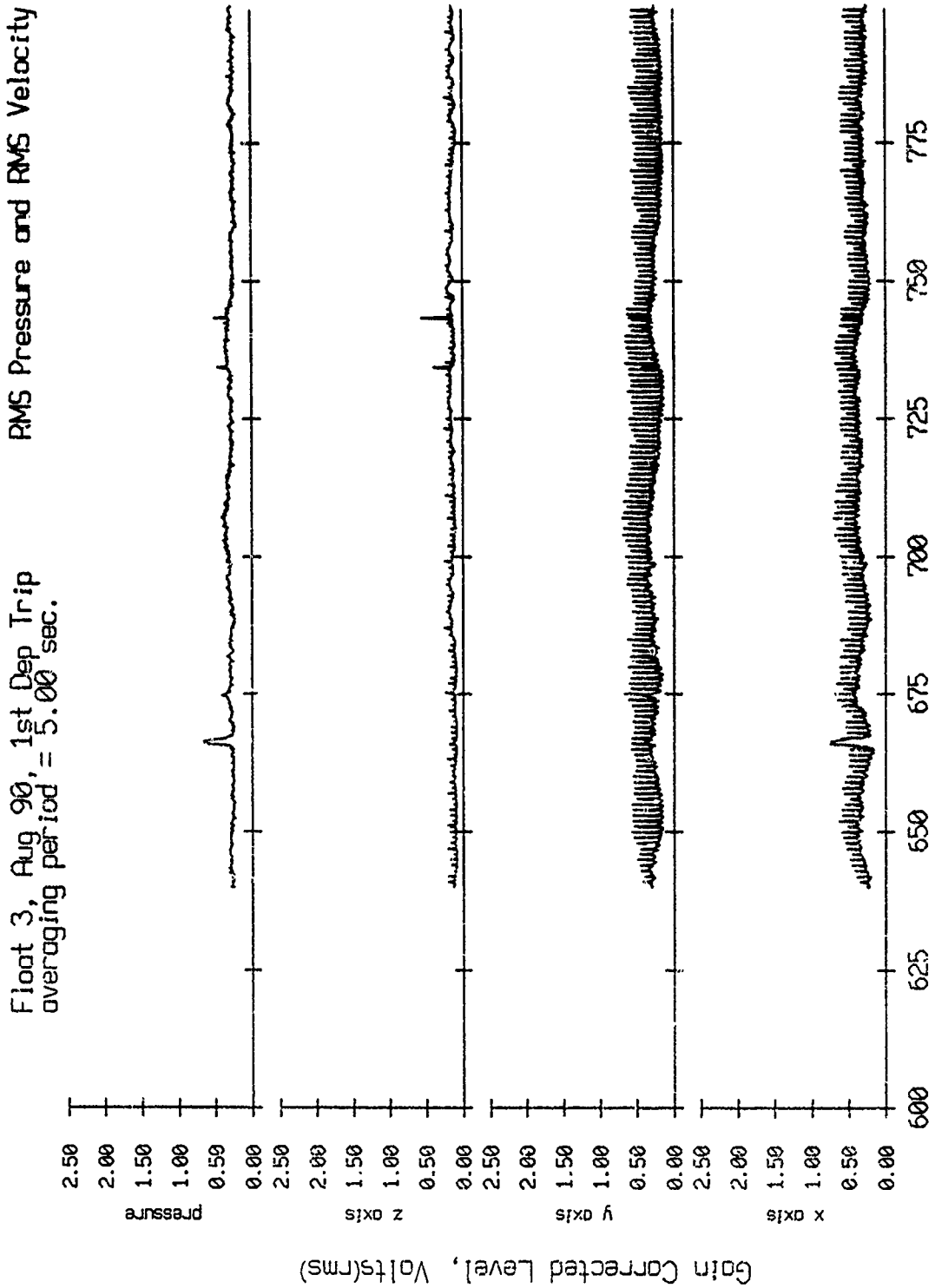

Figure VIII.4a

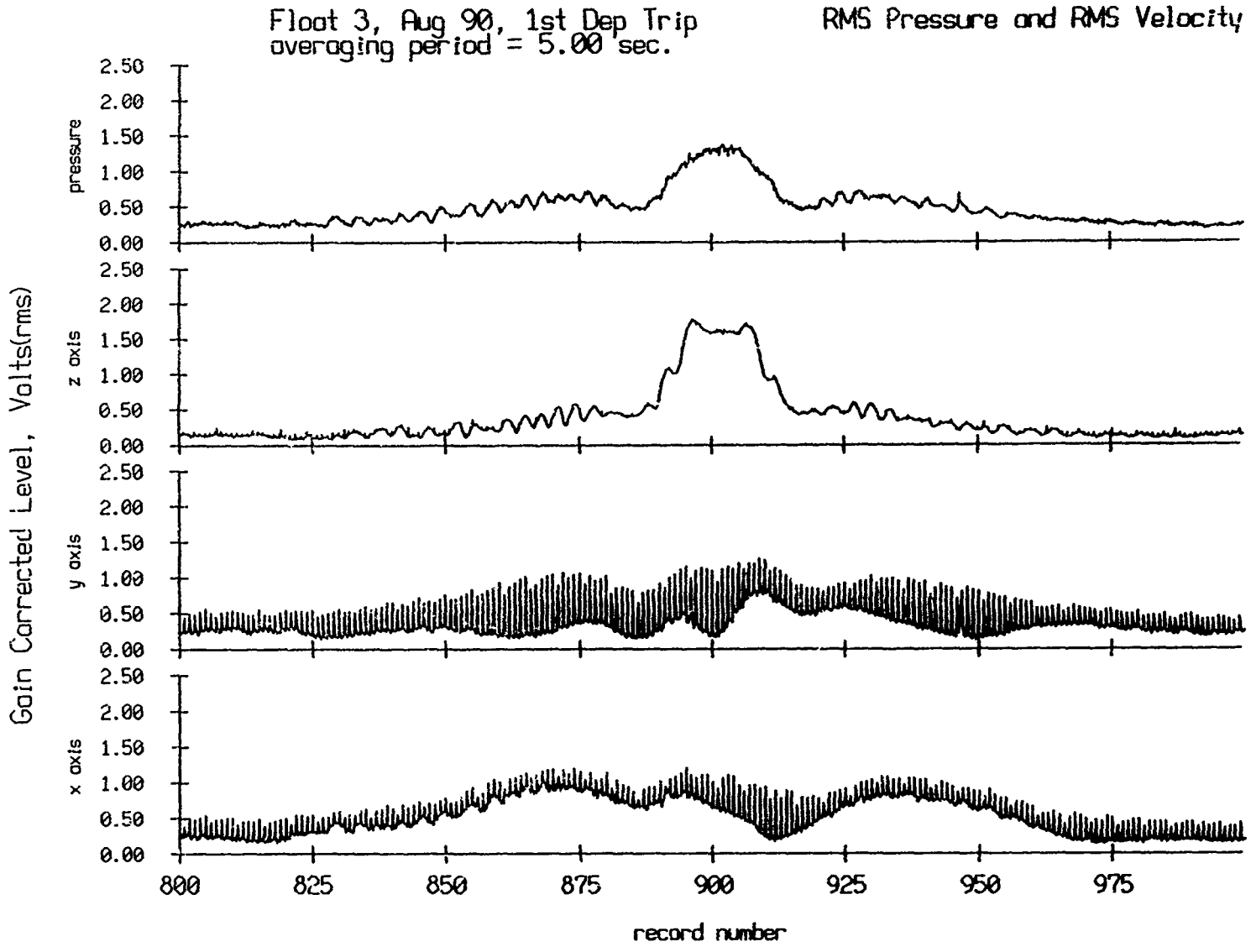

Figure VIII.4b

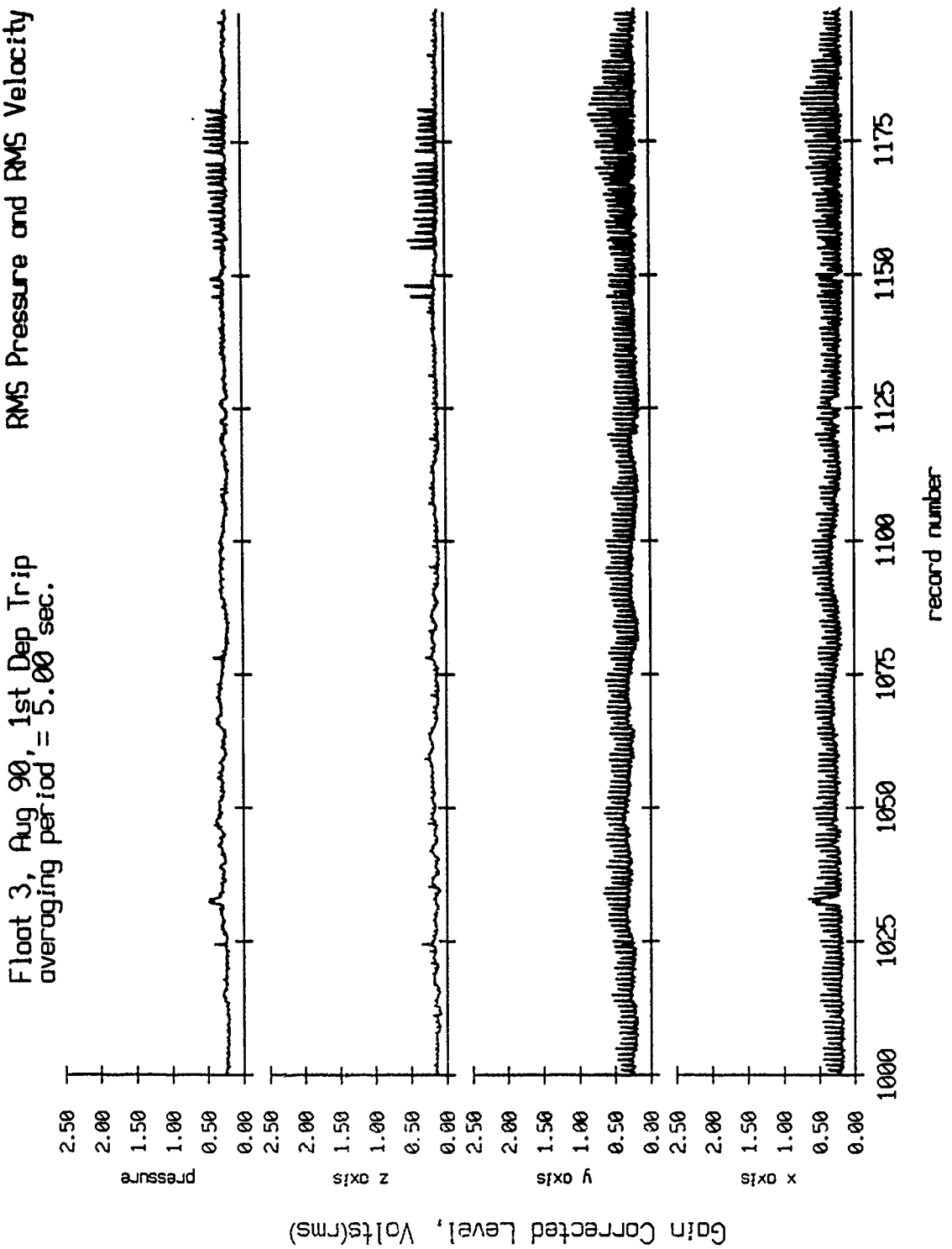

Figure VIII.4c

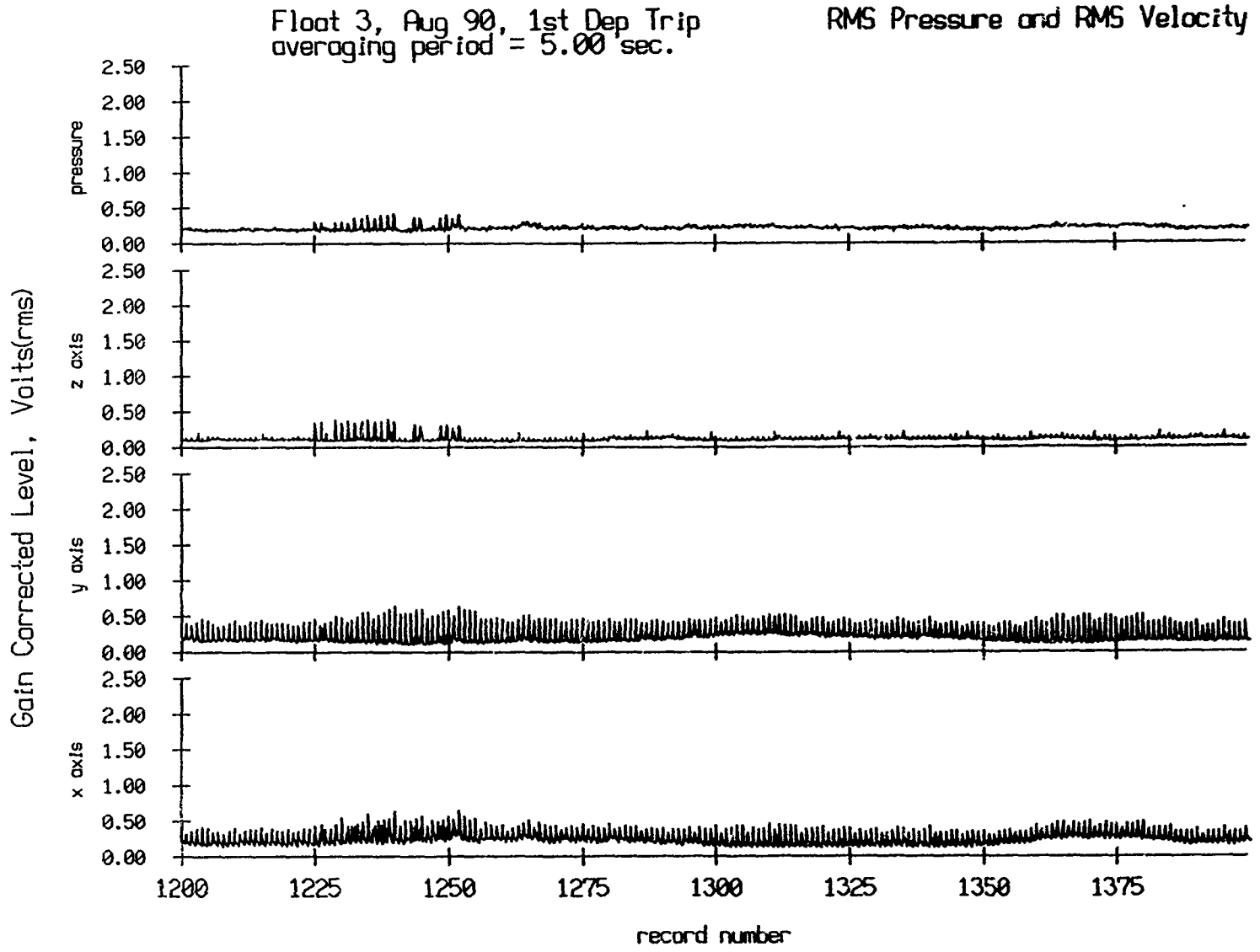

Figure VIII.4d

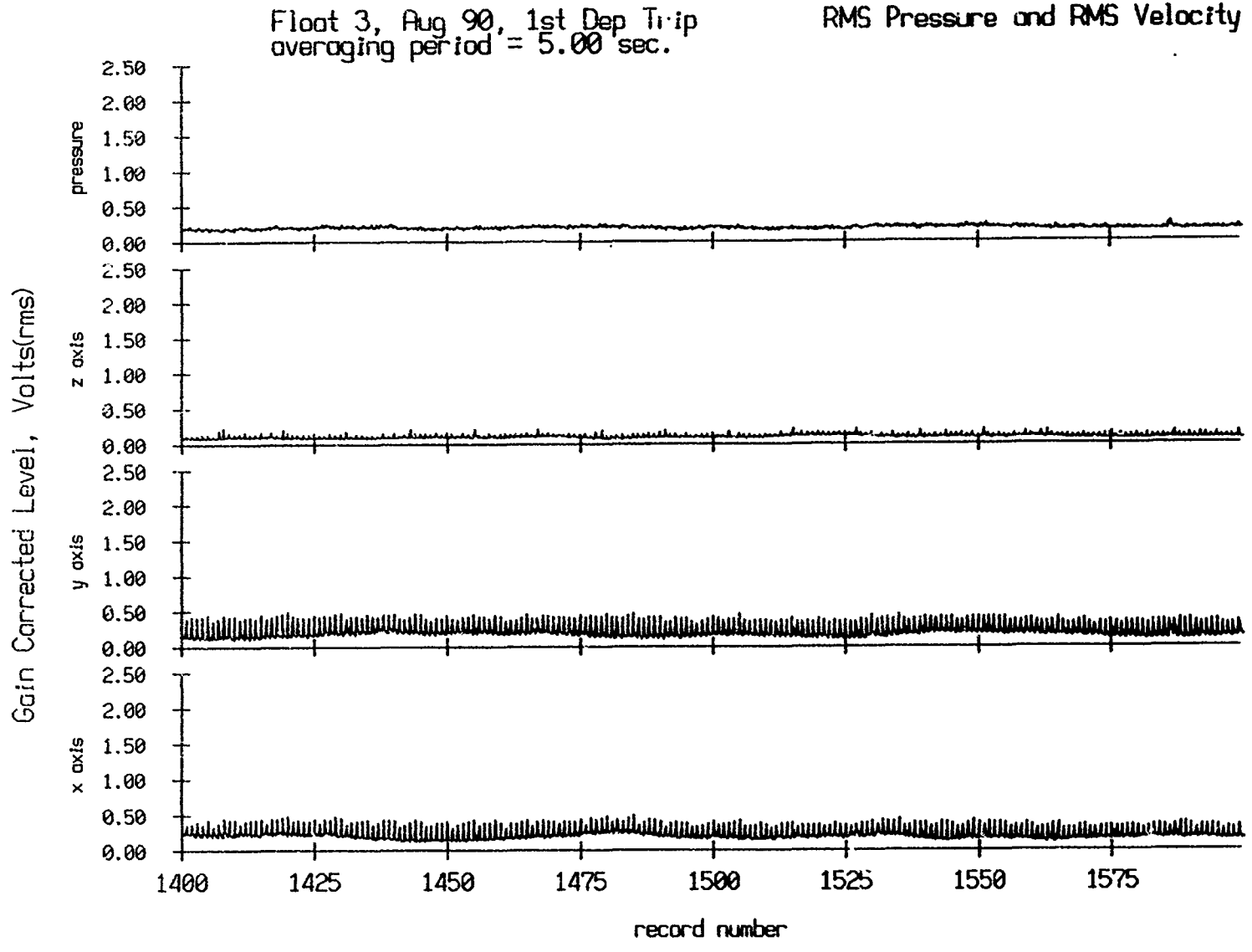

Figure VIII.4e

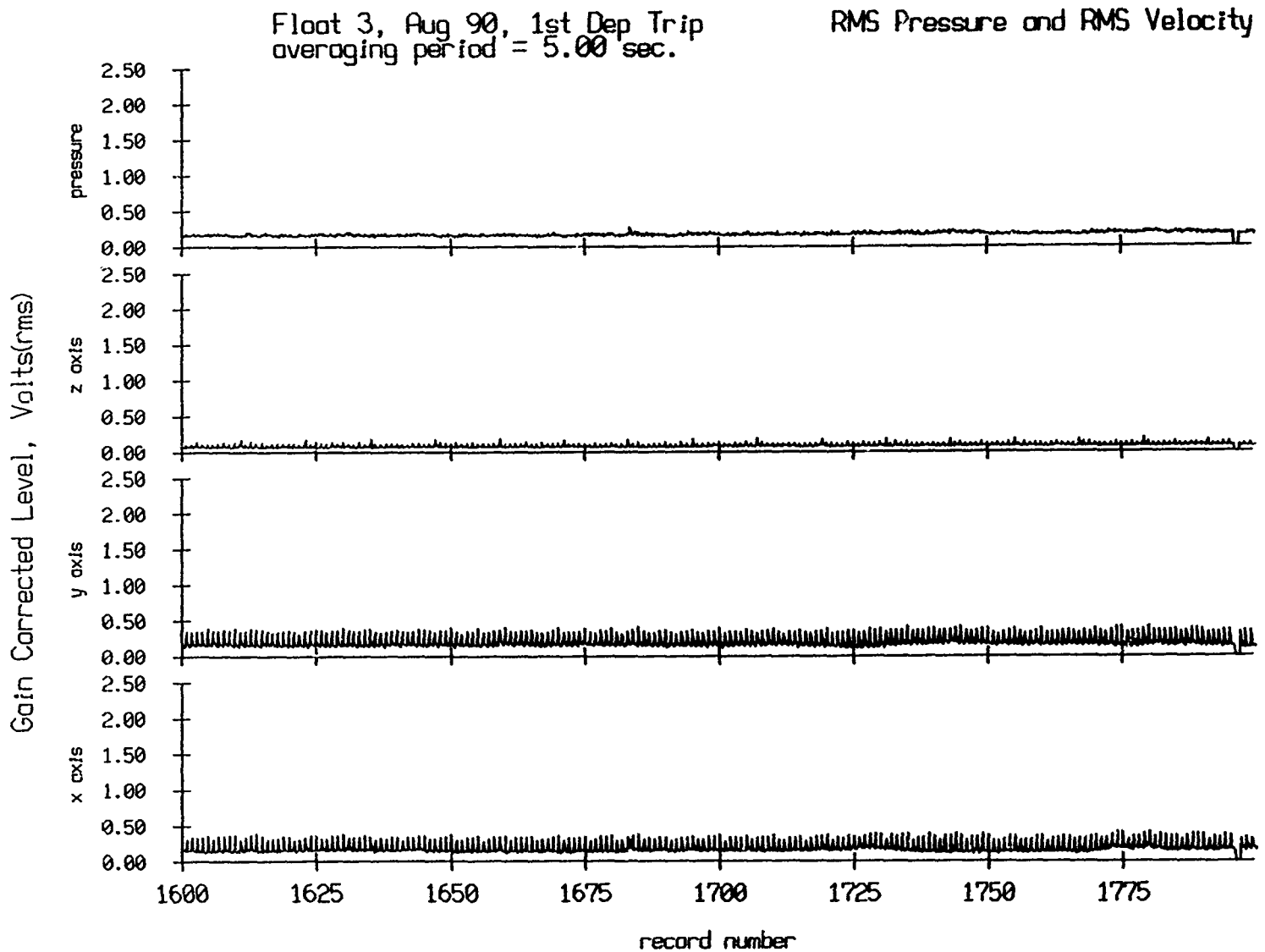

Figure VIII.4f

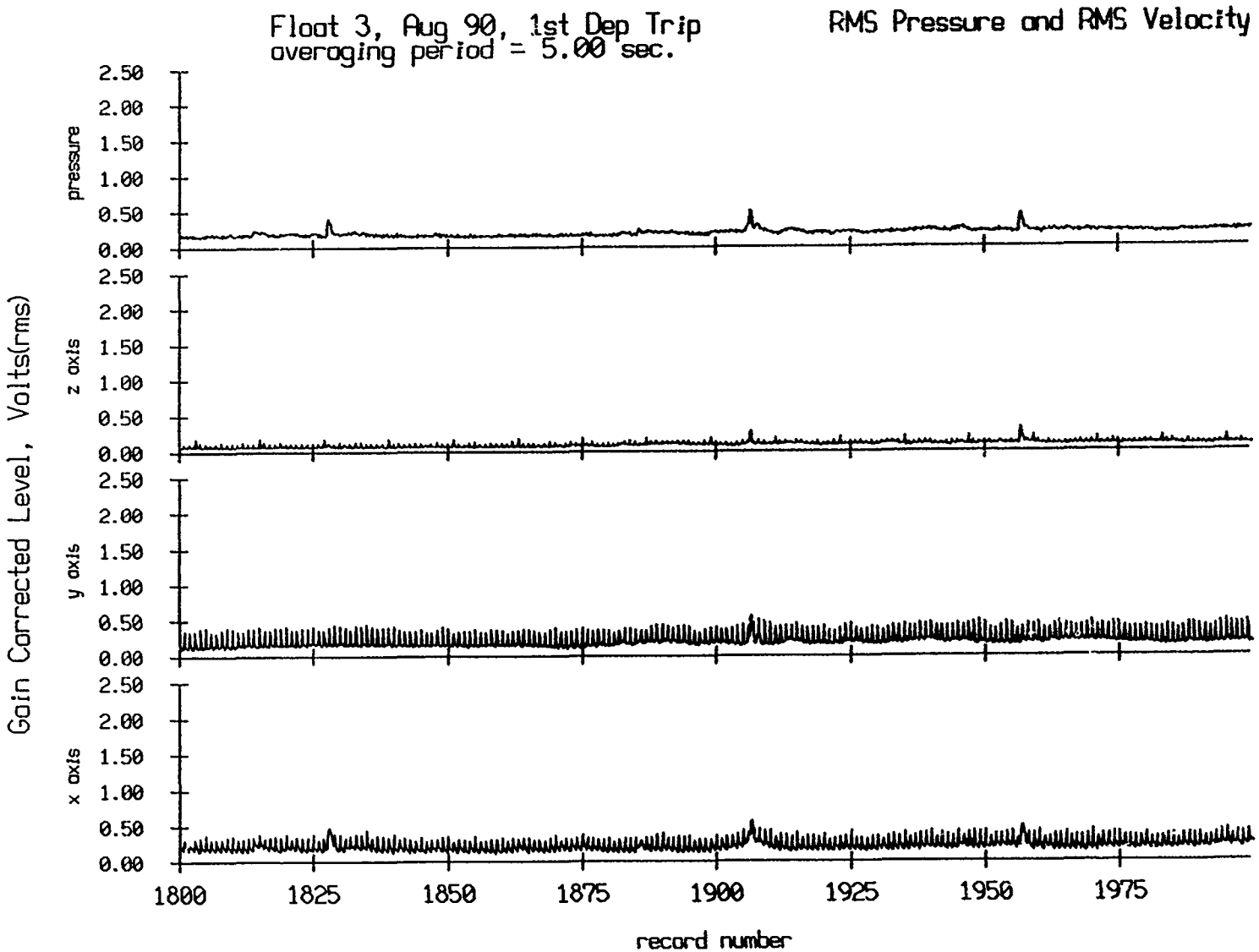

Figure VIII.48

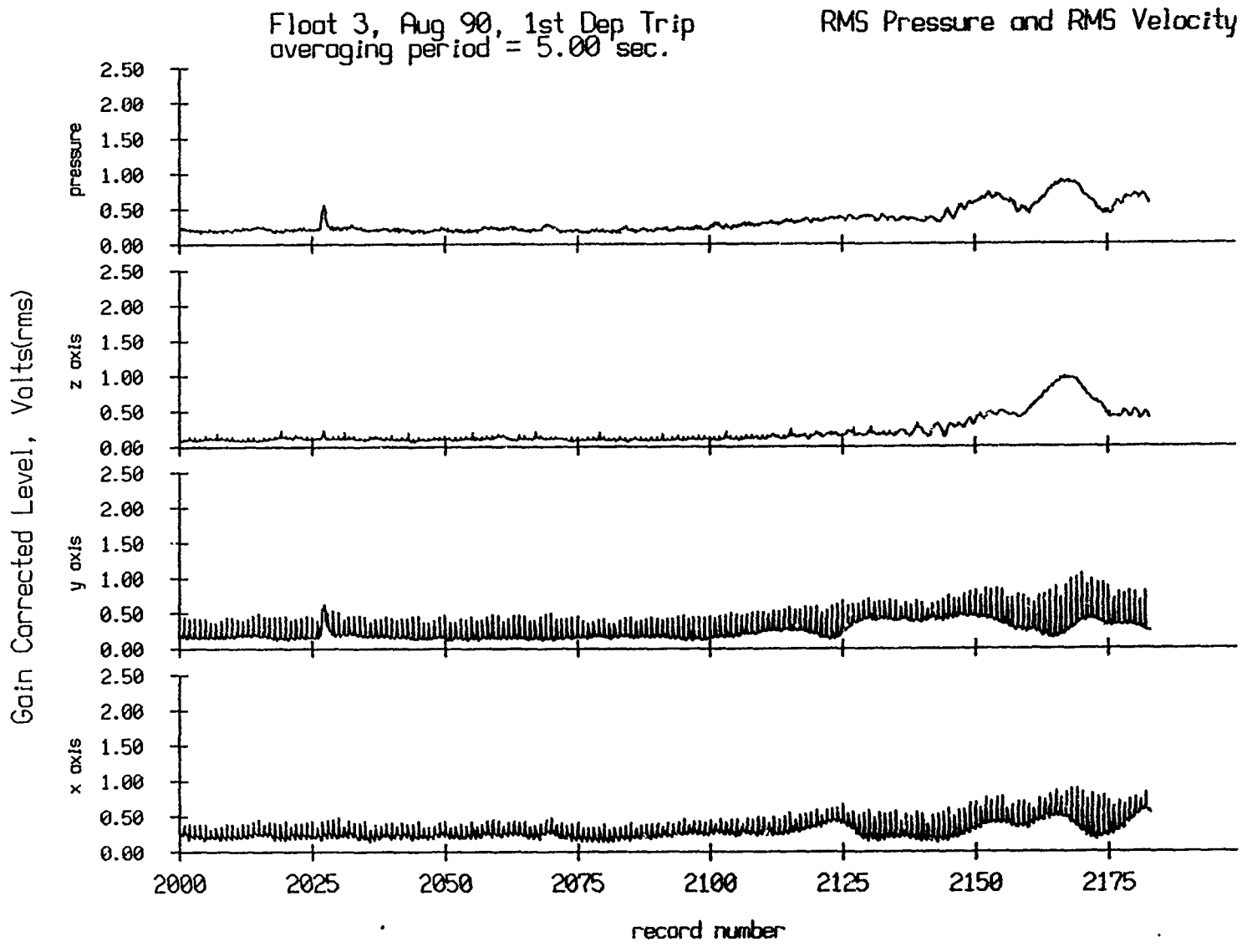

Figure VIII.4h

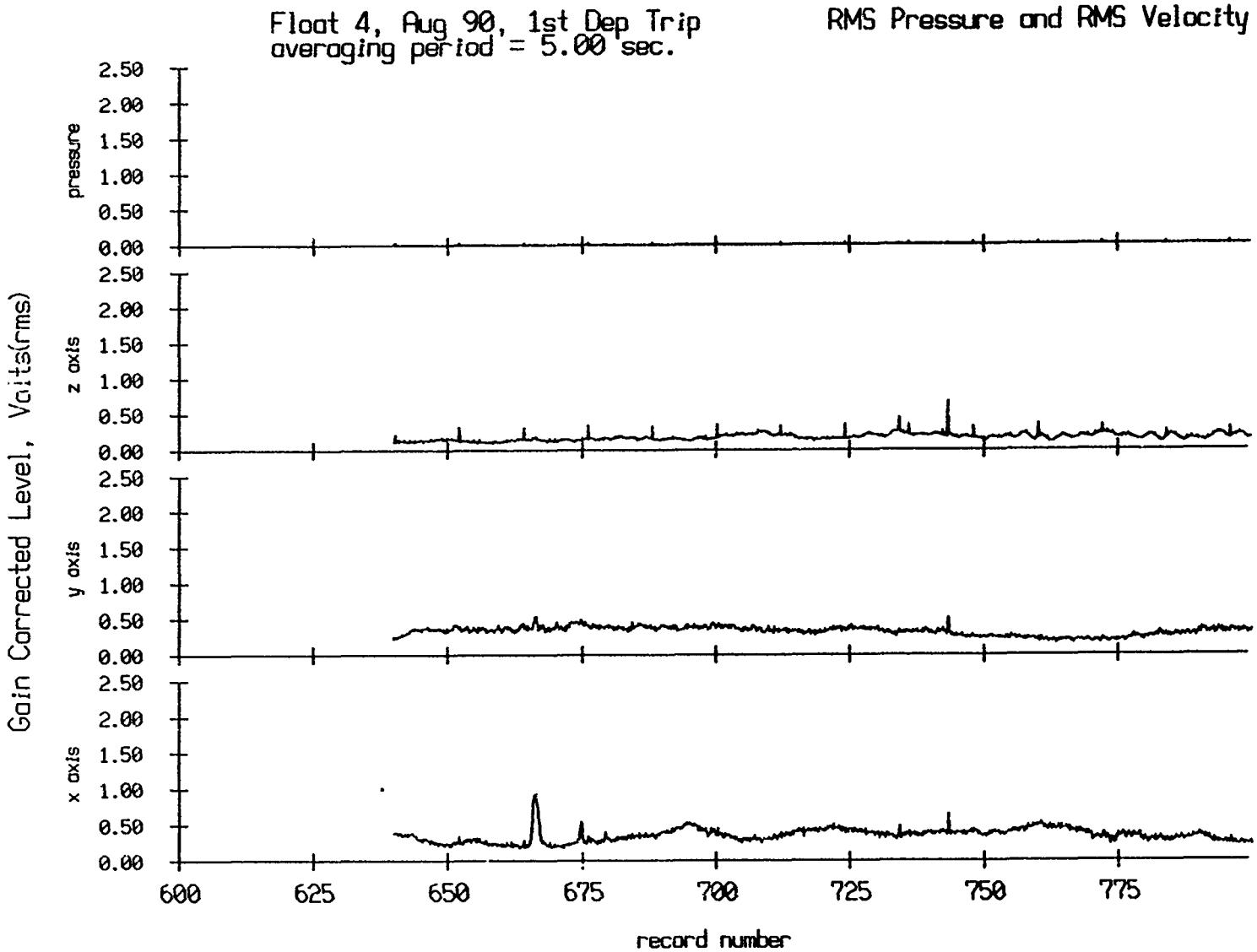

Figure VIII.5a

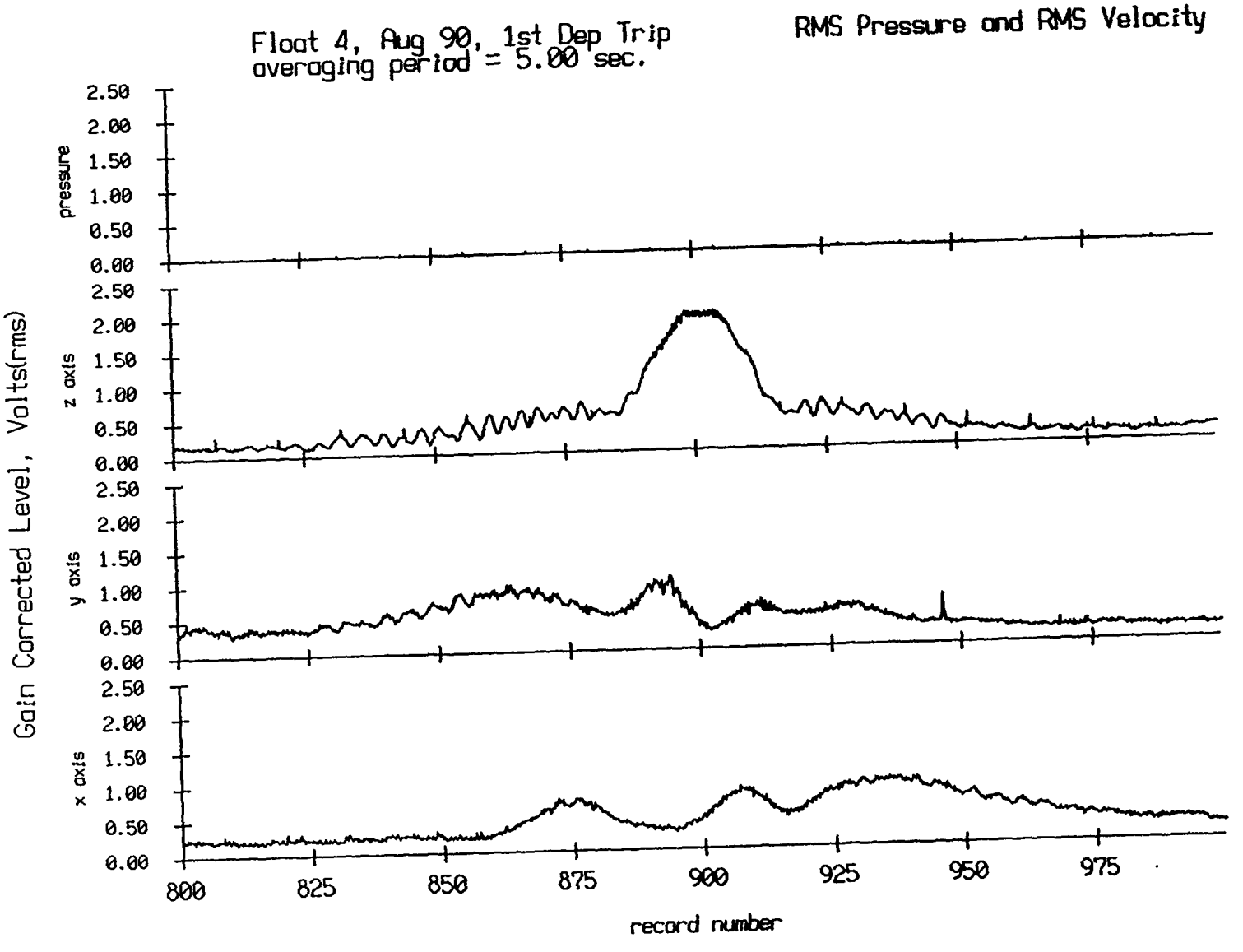

Figure VIII.5b

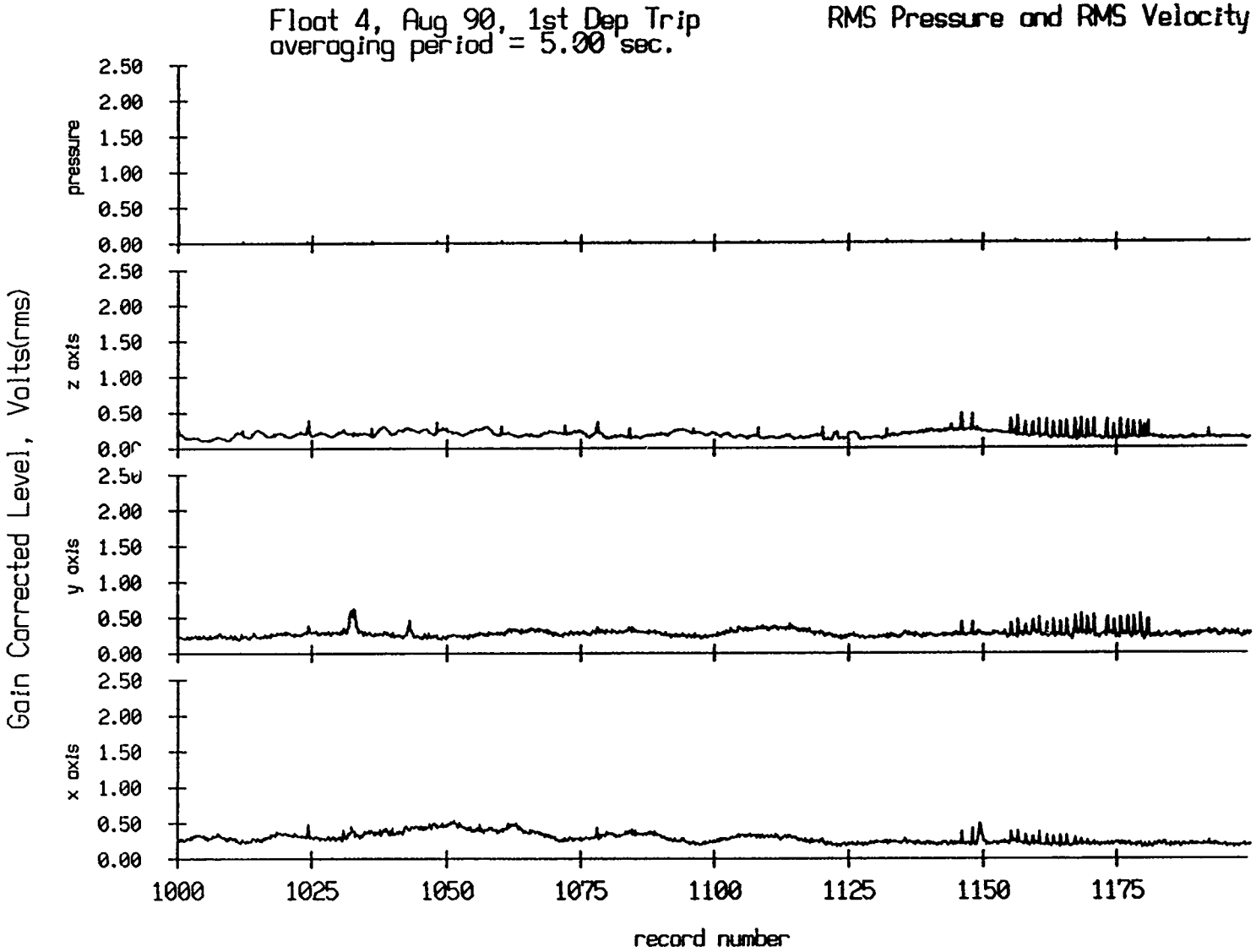

Figure VIII.5c

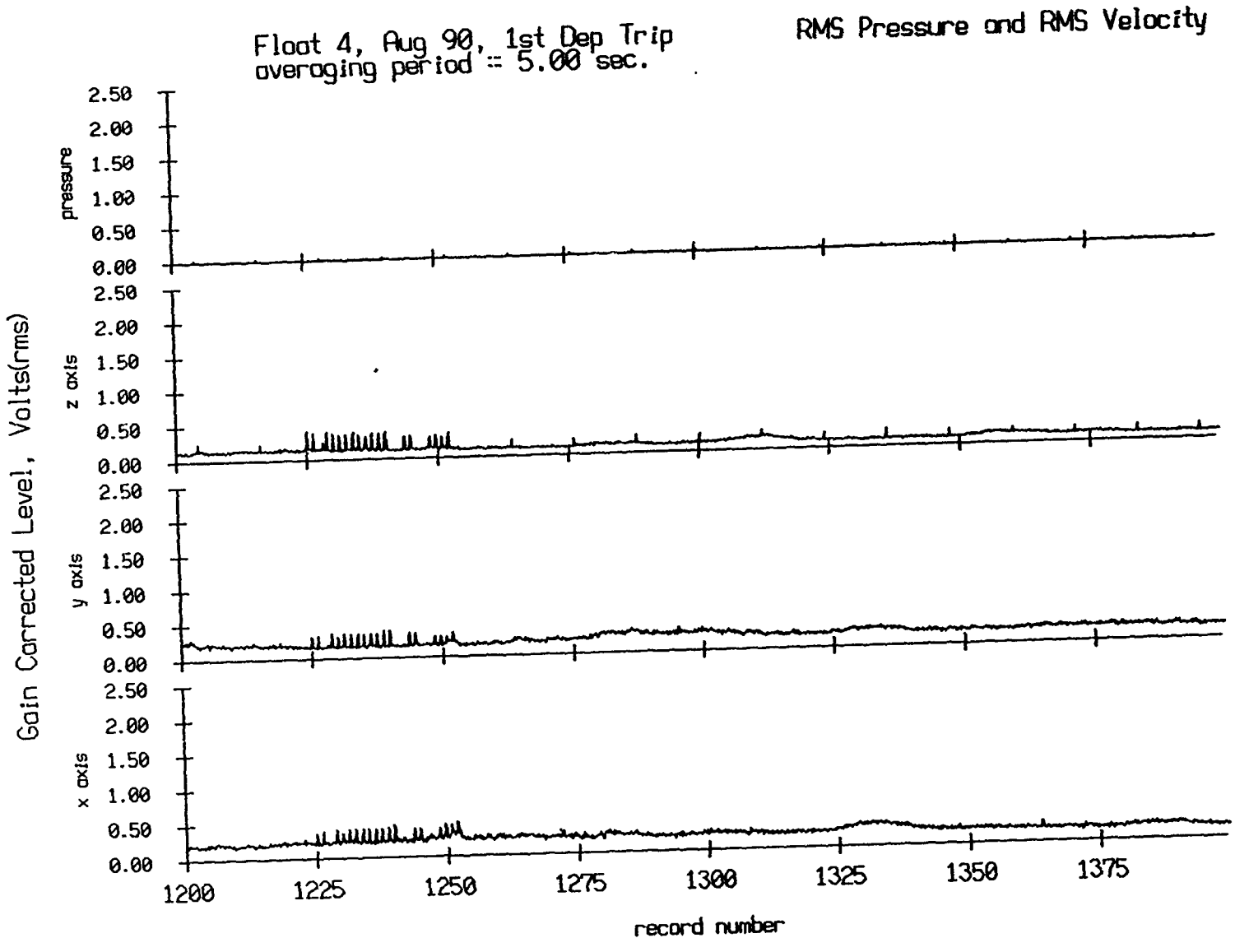

Figure VIII.5d

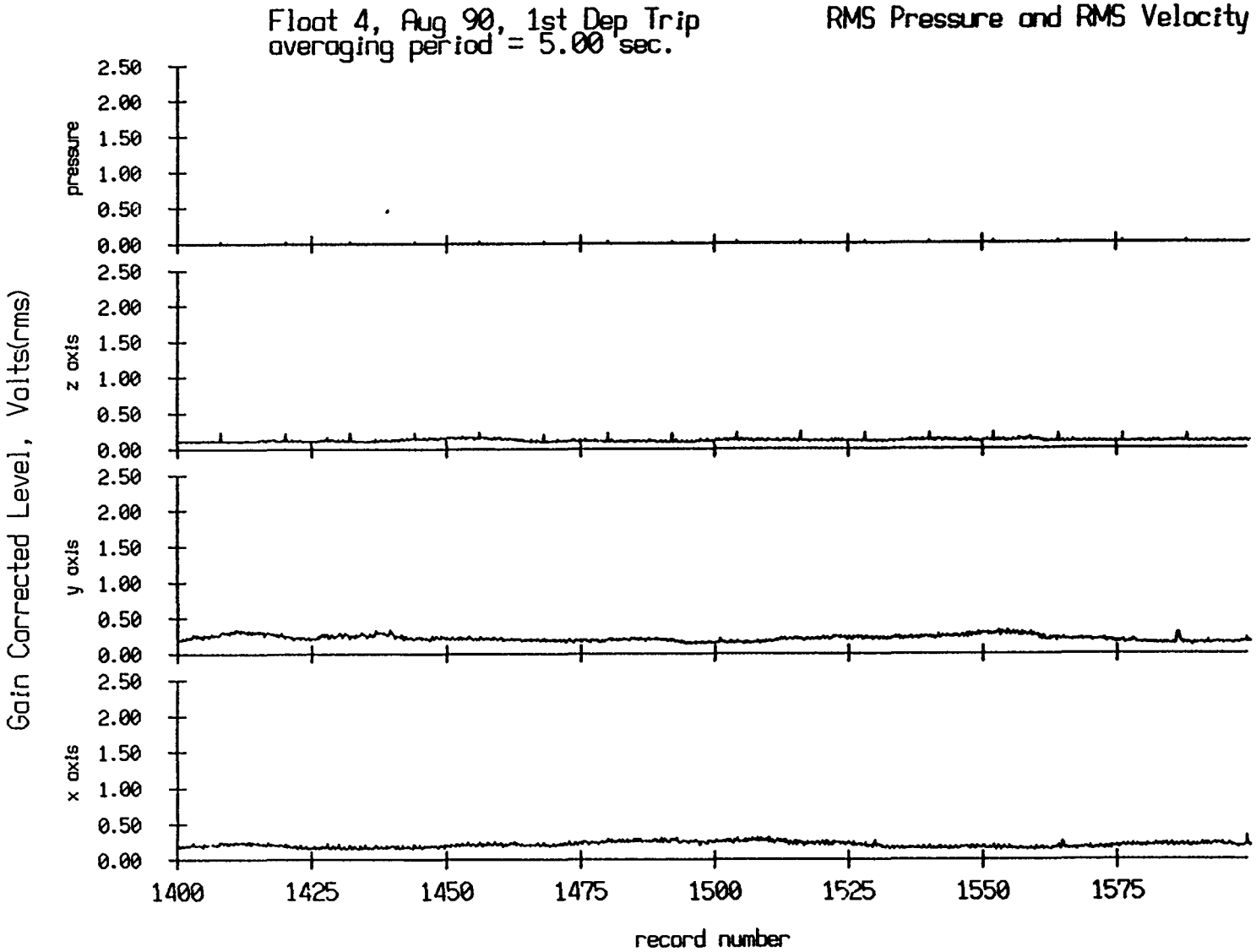

Figure VIII.5e

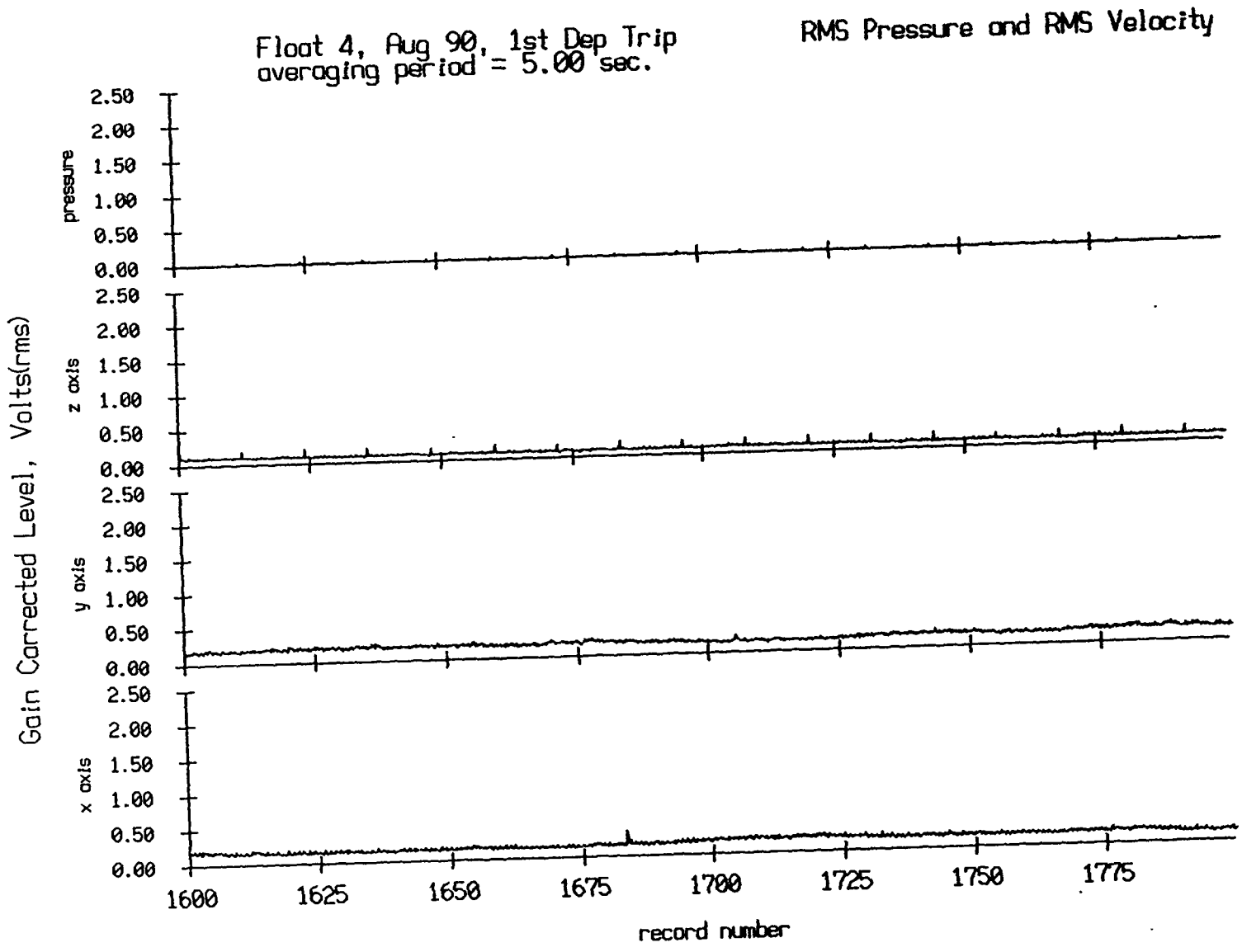

Figure VIII.5f

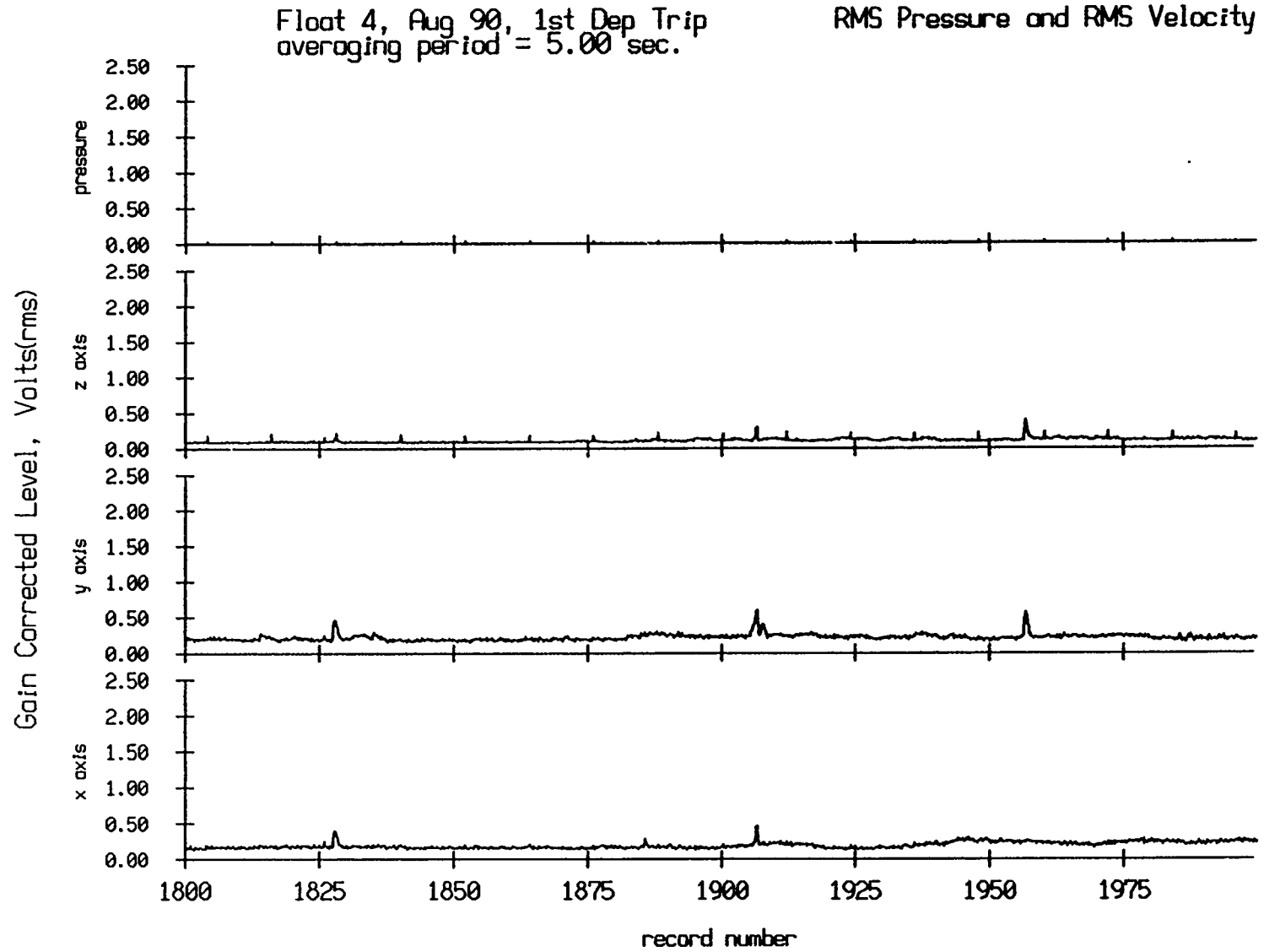

Figure VIII.5B

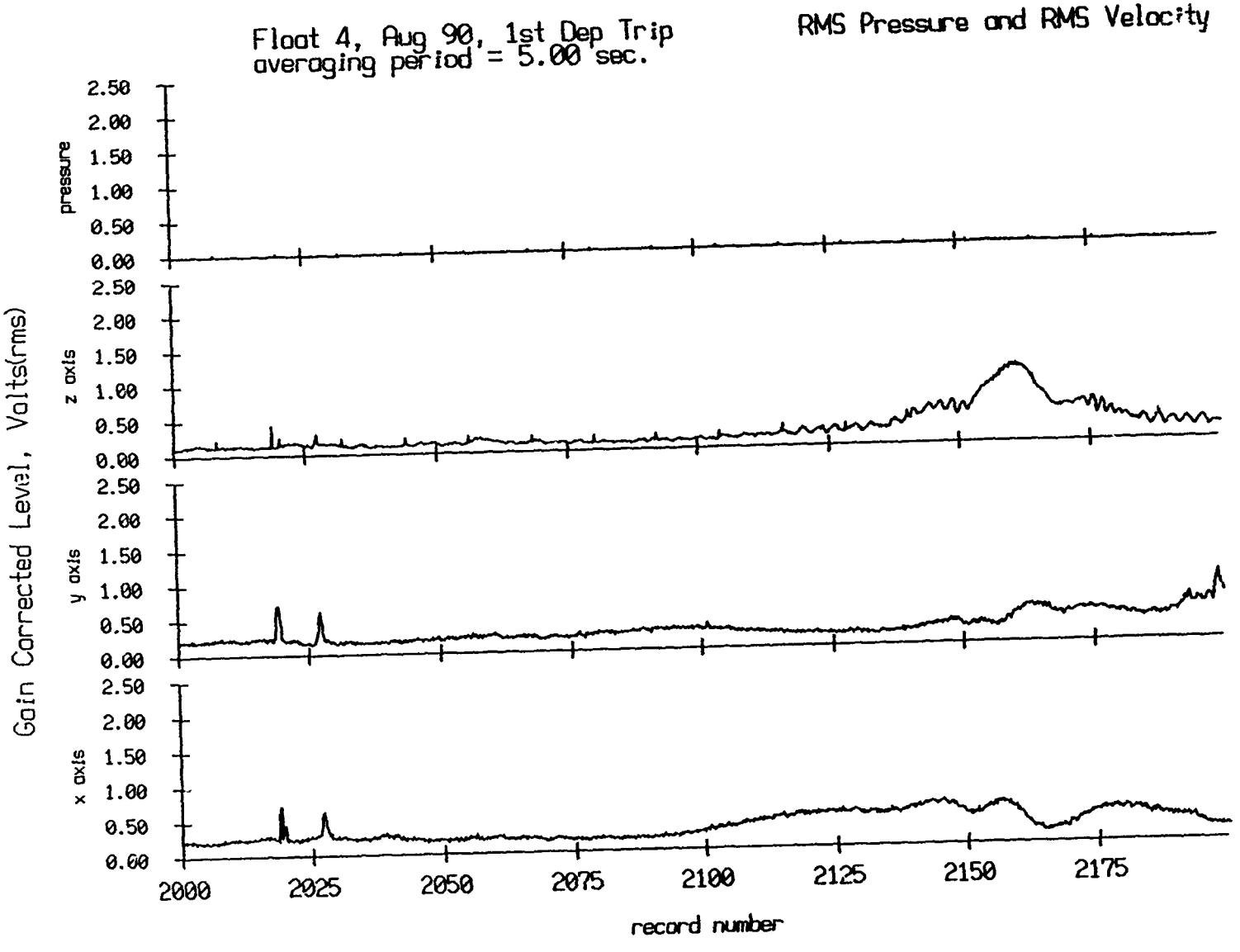

Figure VIII.5h

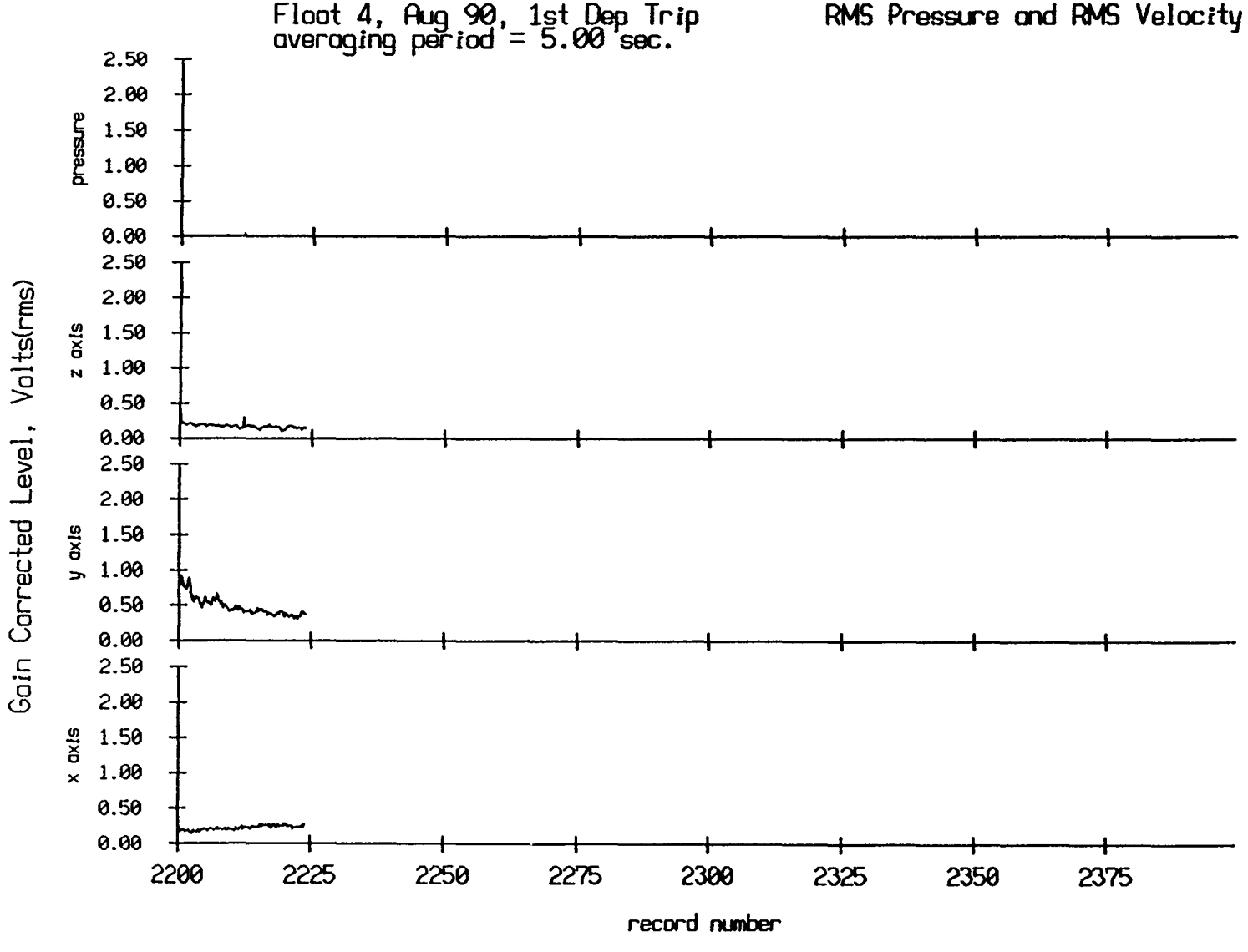

Figure VIII.5i

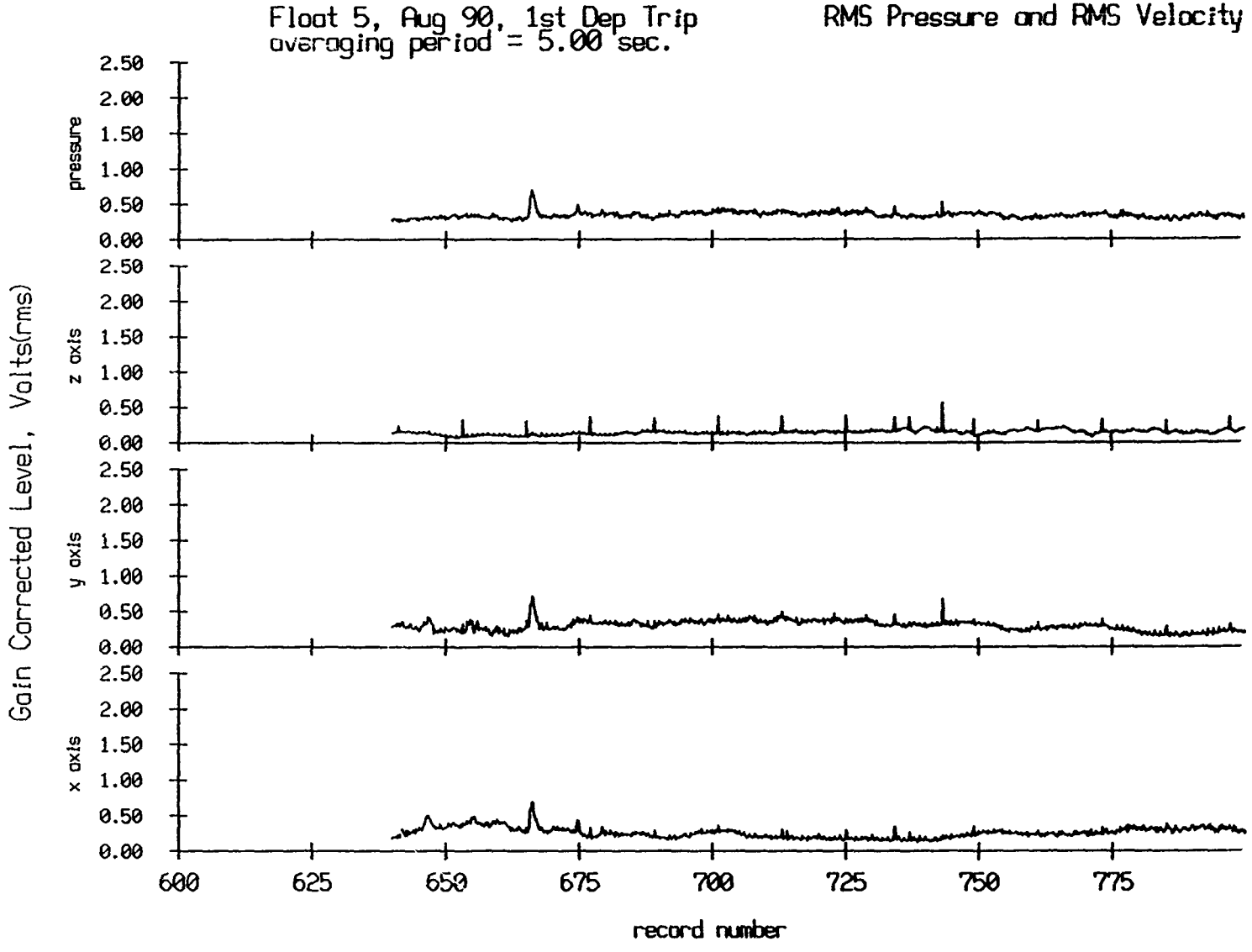

Figure VIII.6a

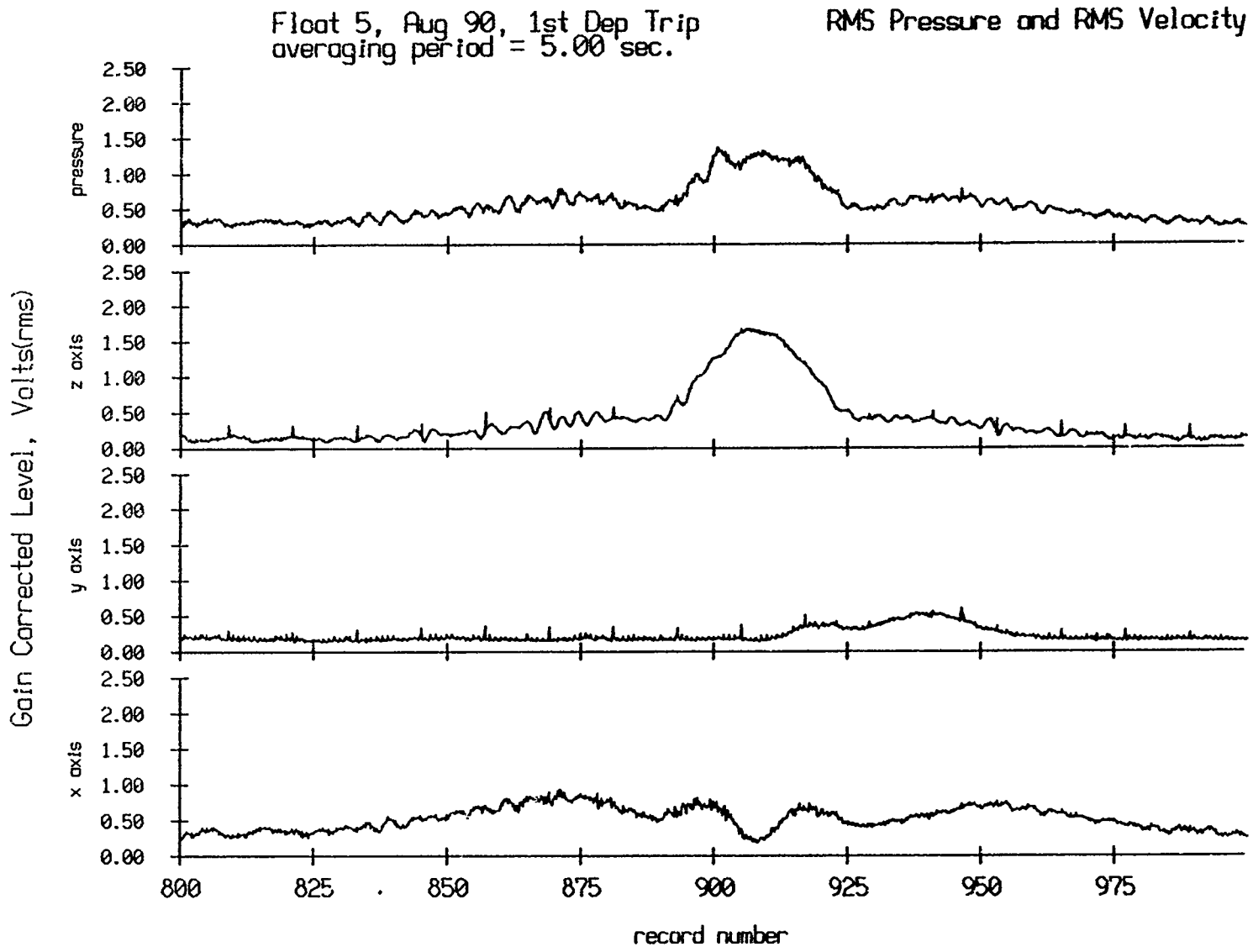

Figure VIII.6b

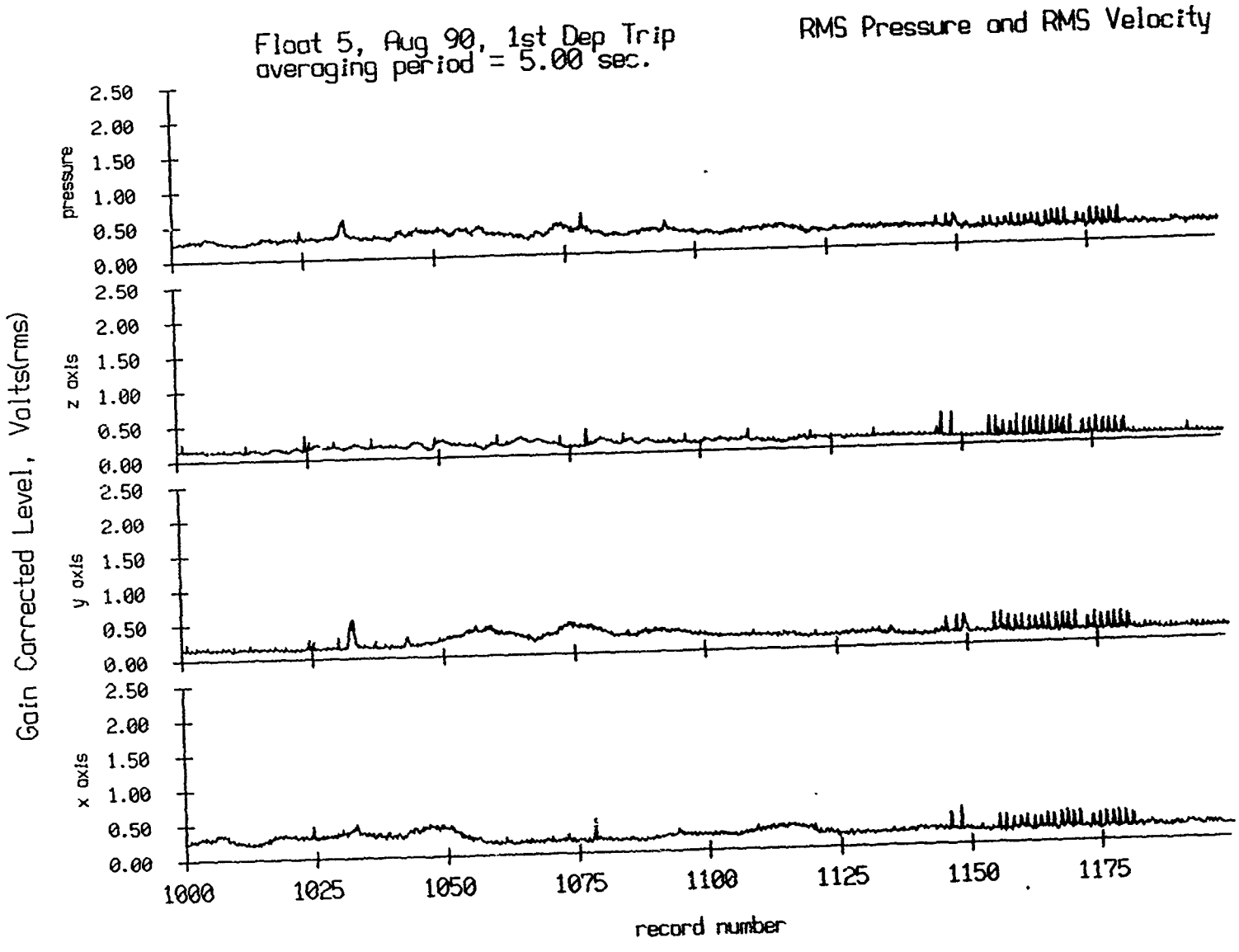

Figure VIII.6c

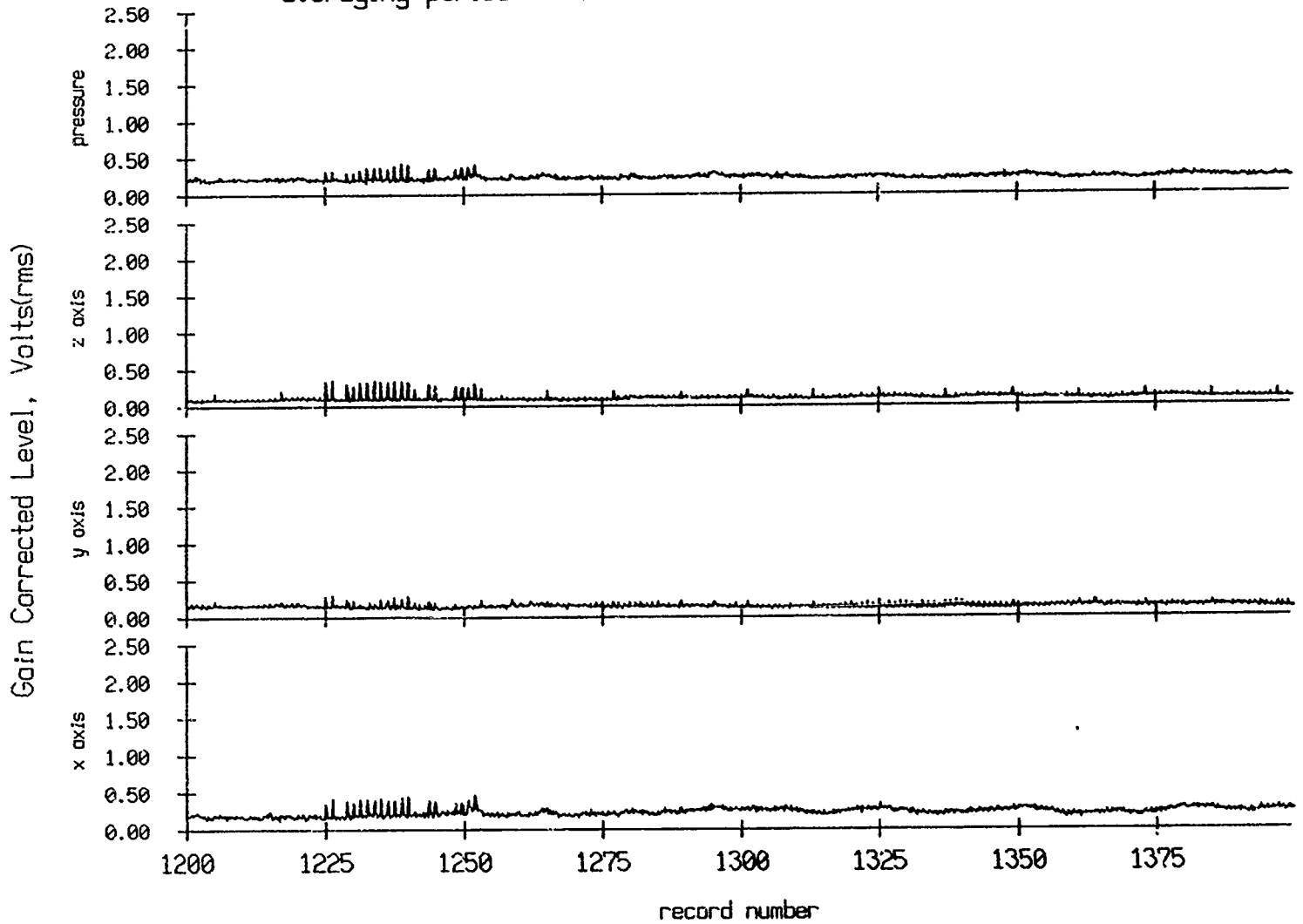

Figure VIII.6d

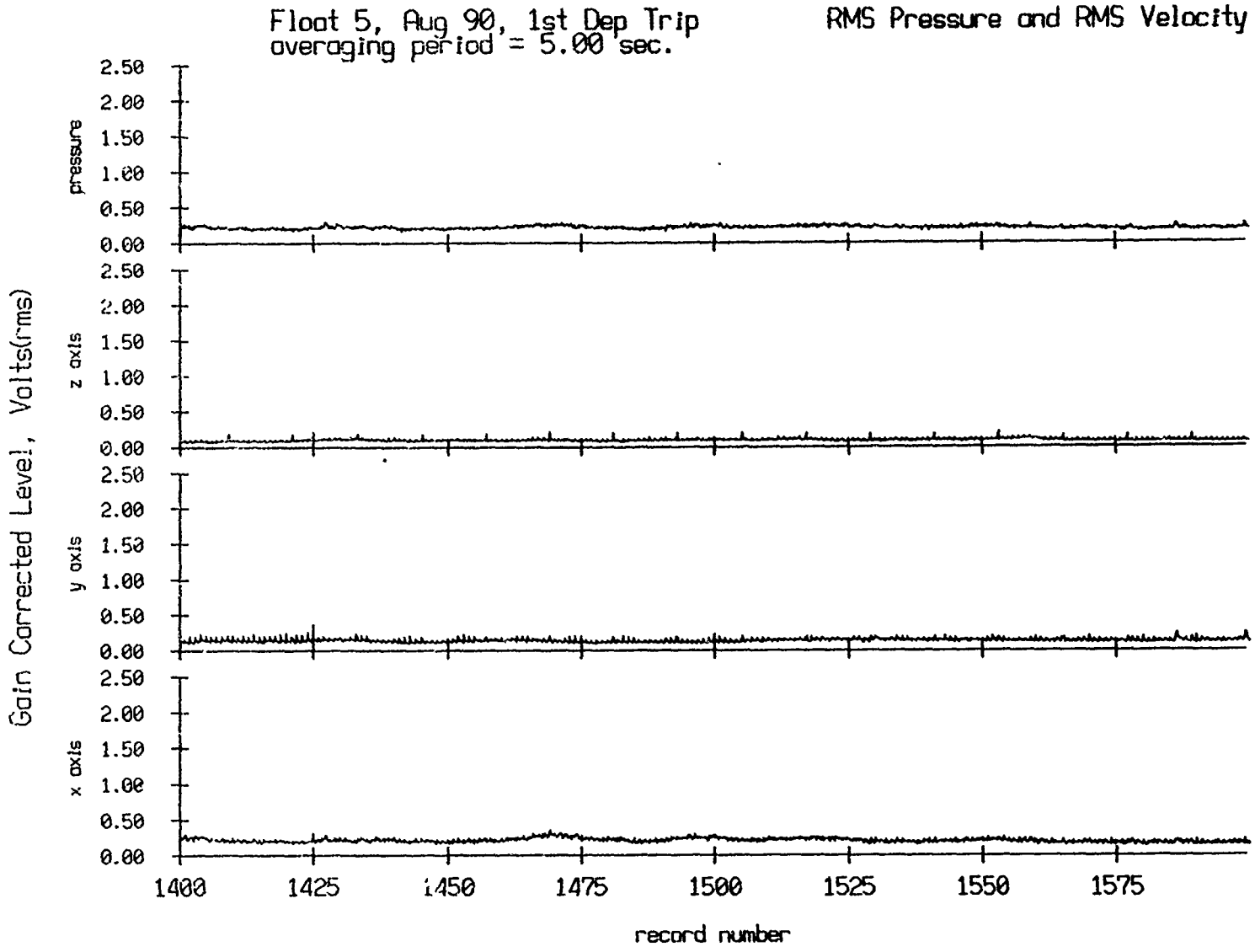

Figure VIII.6e

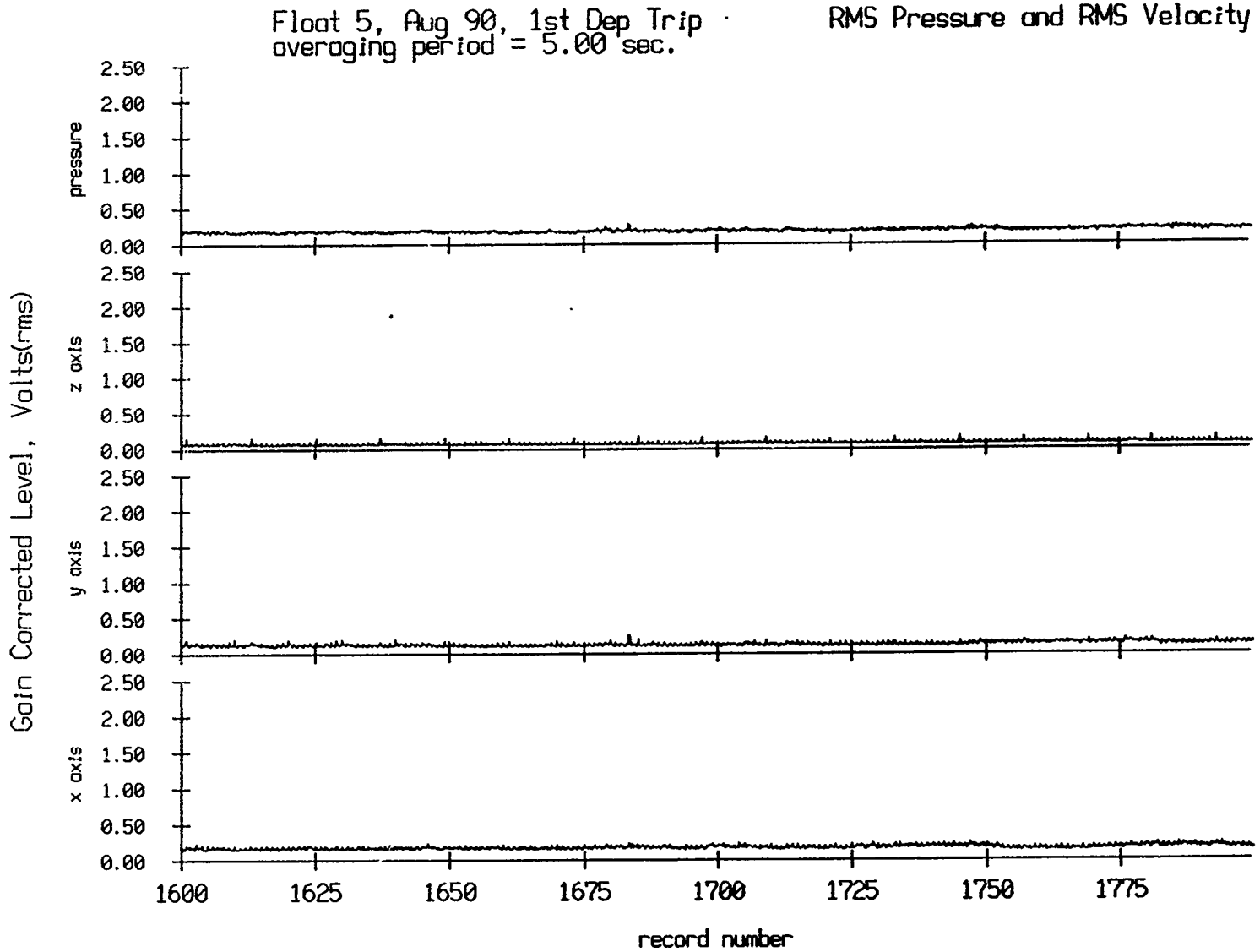

Figure VIII.6f

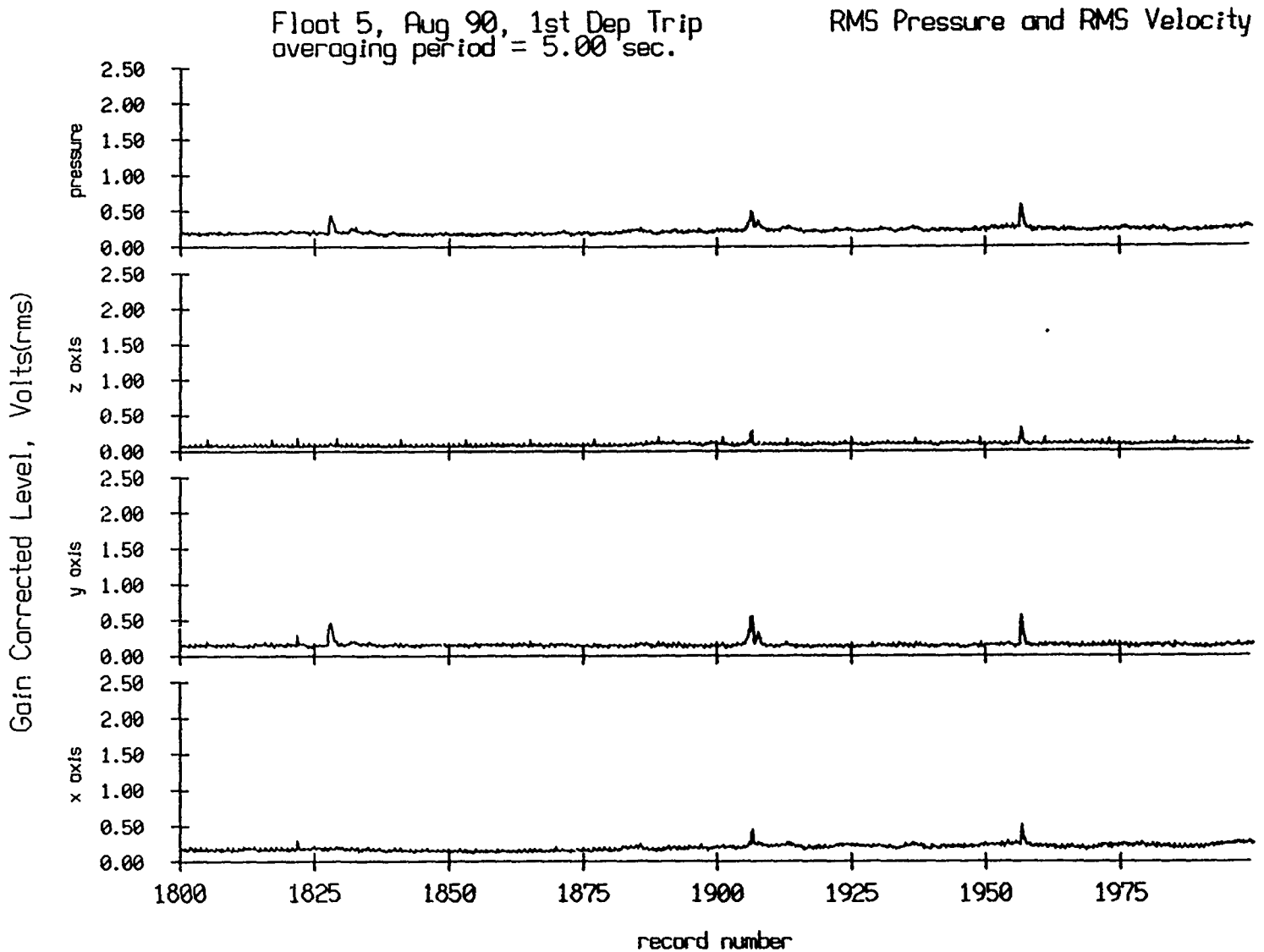

Figure VIII.6B

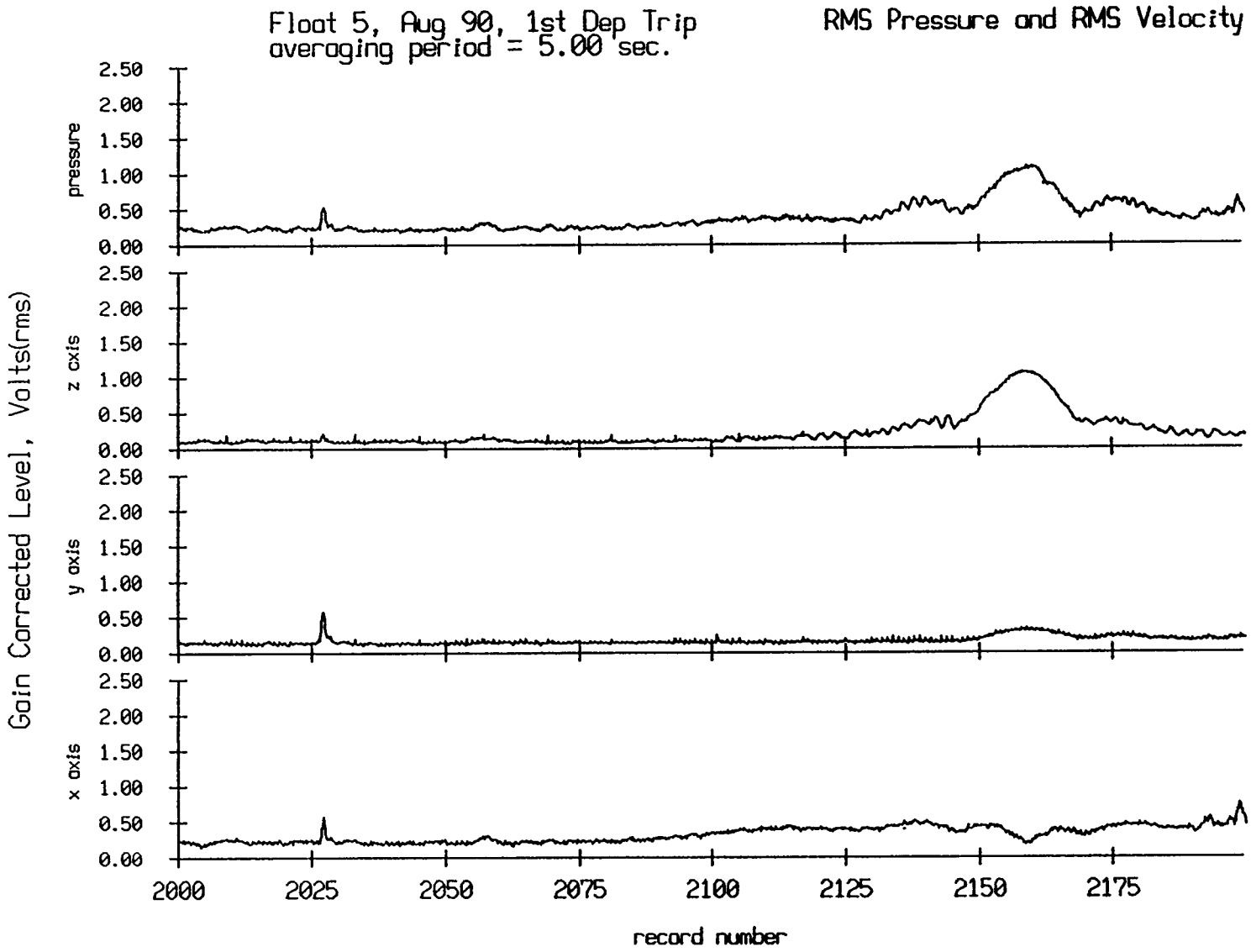

Figure VIII.6h

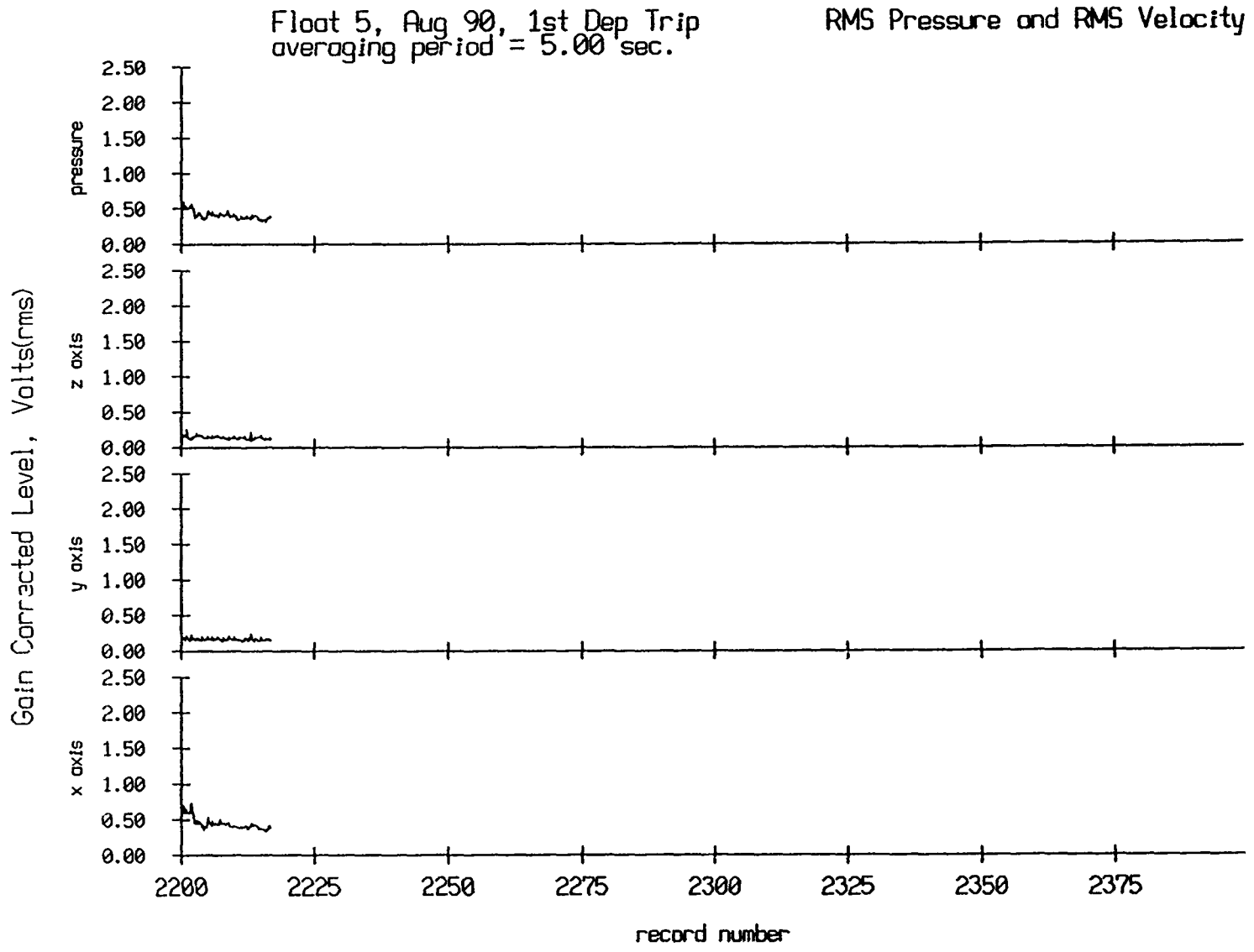

Figure VIII.6i

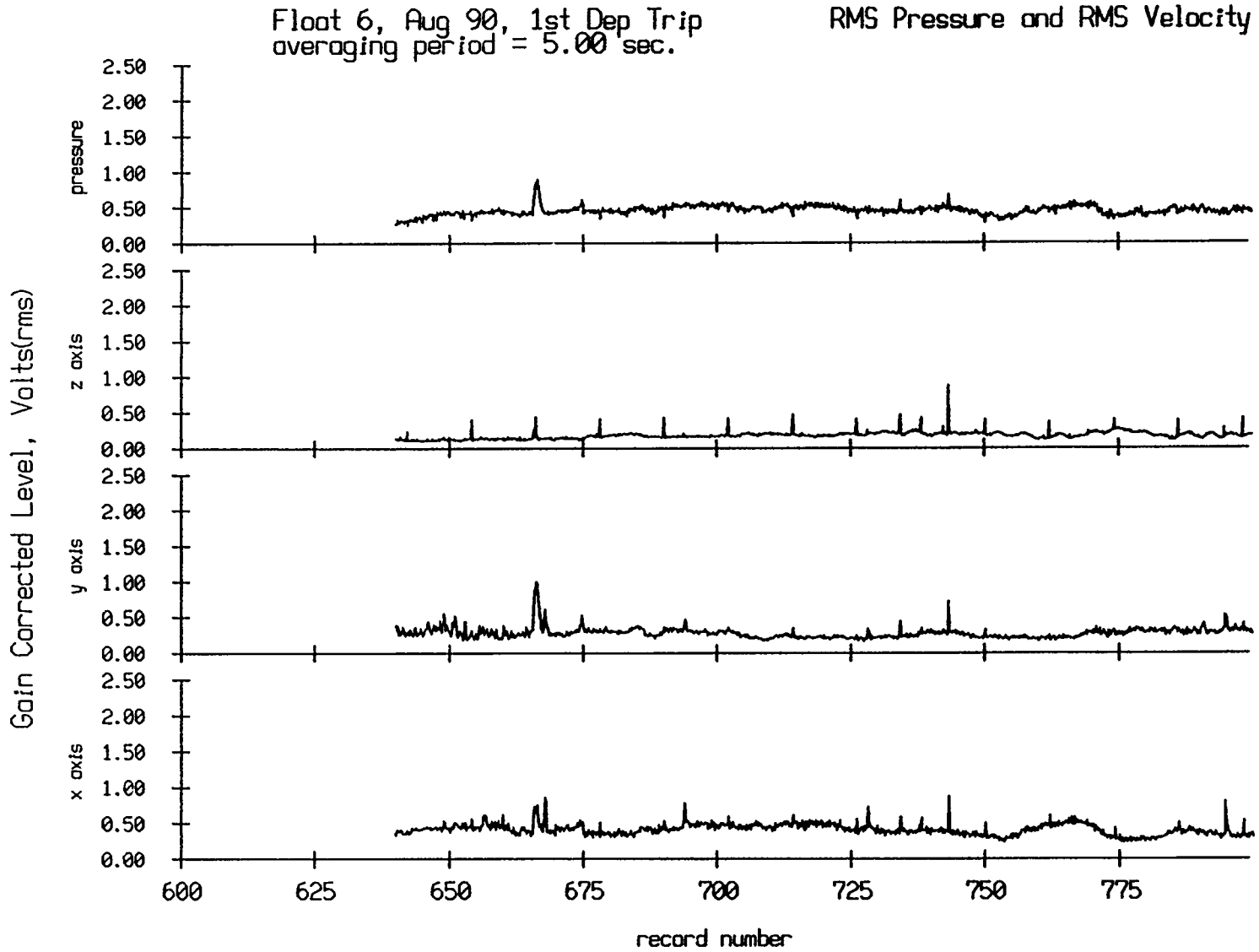

Figure VIII.7a

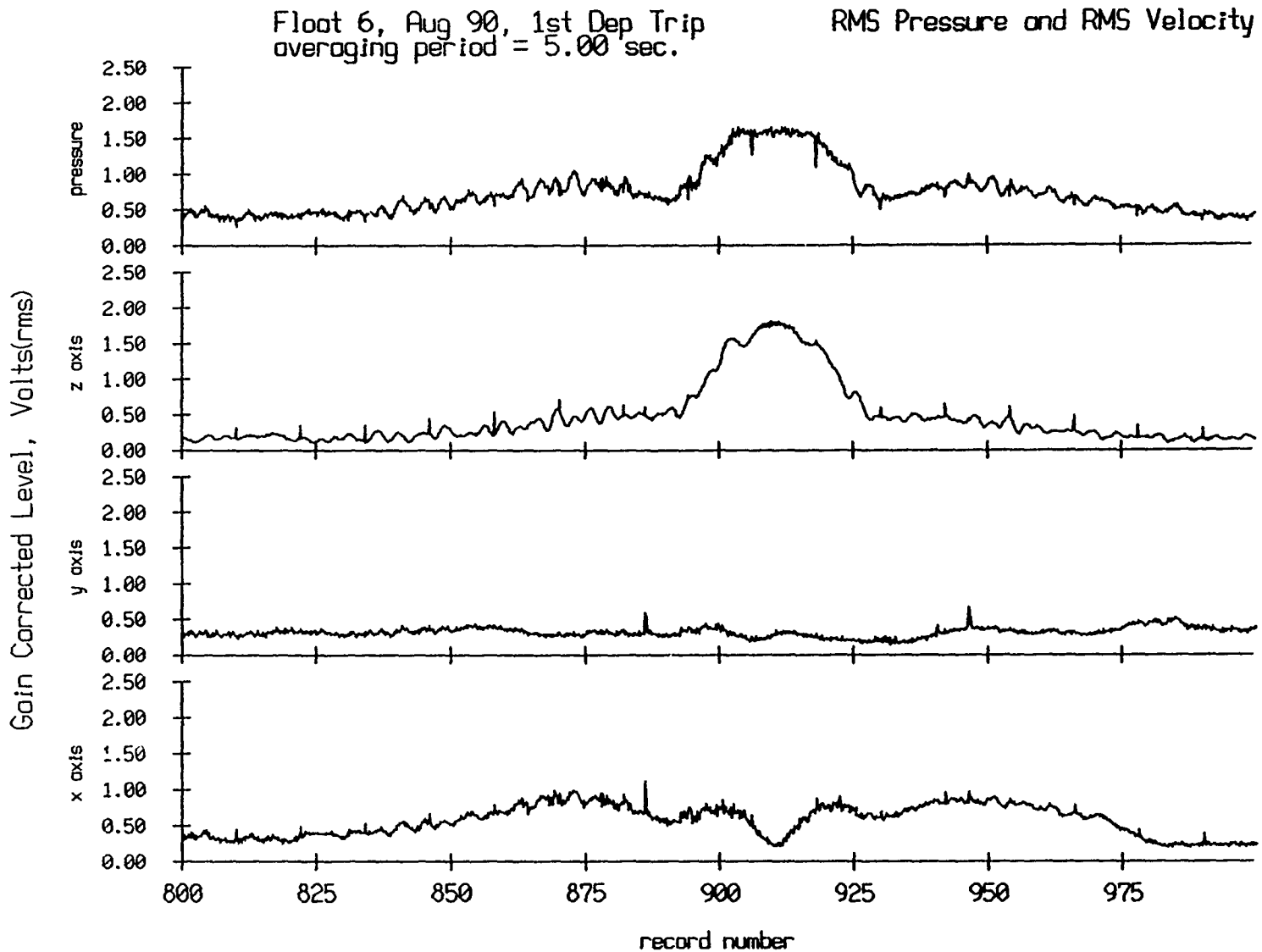

Figure VIII.7b

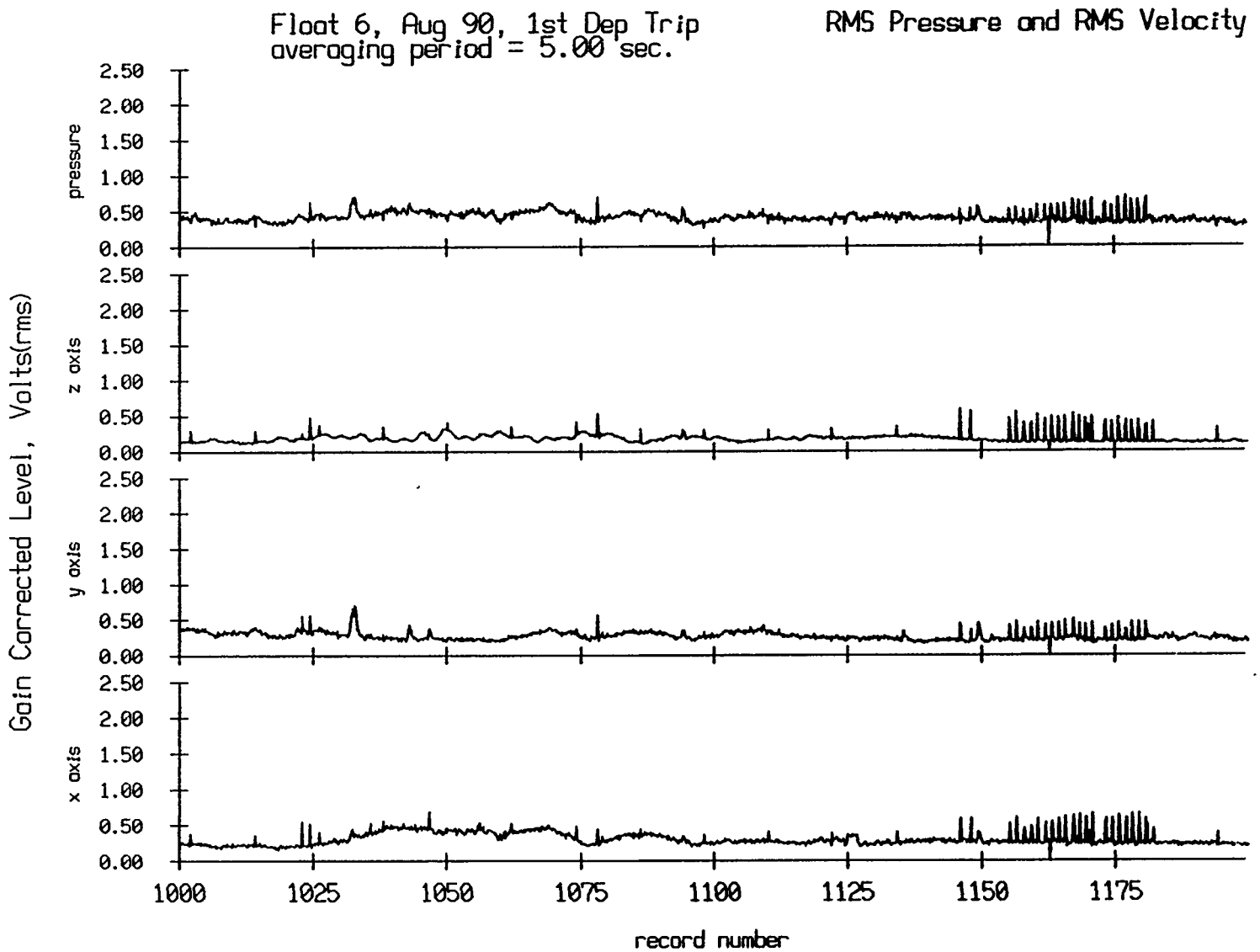

Figure VIII.7c

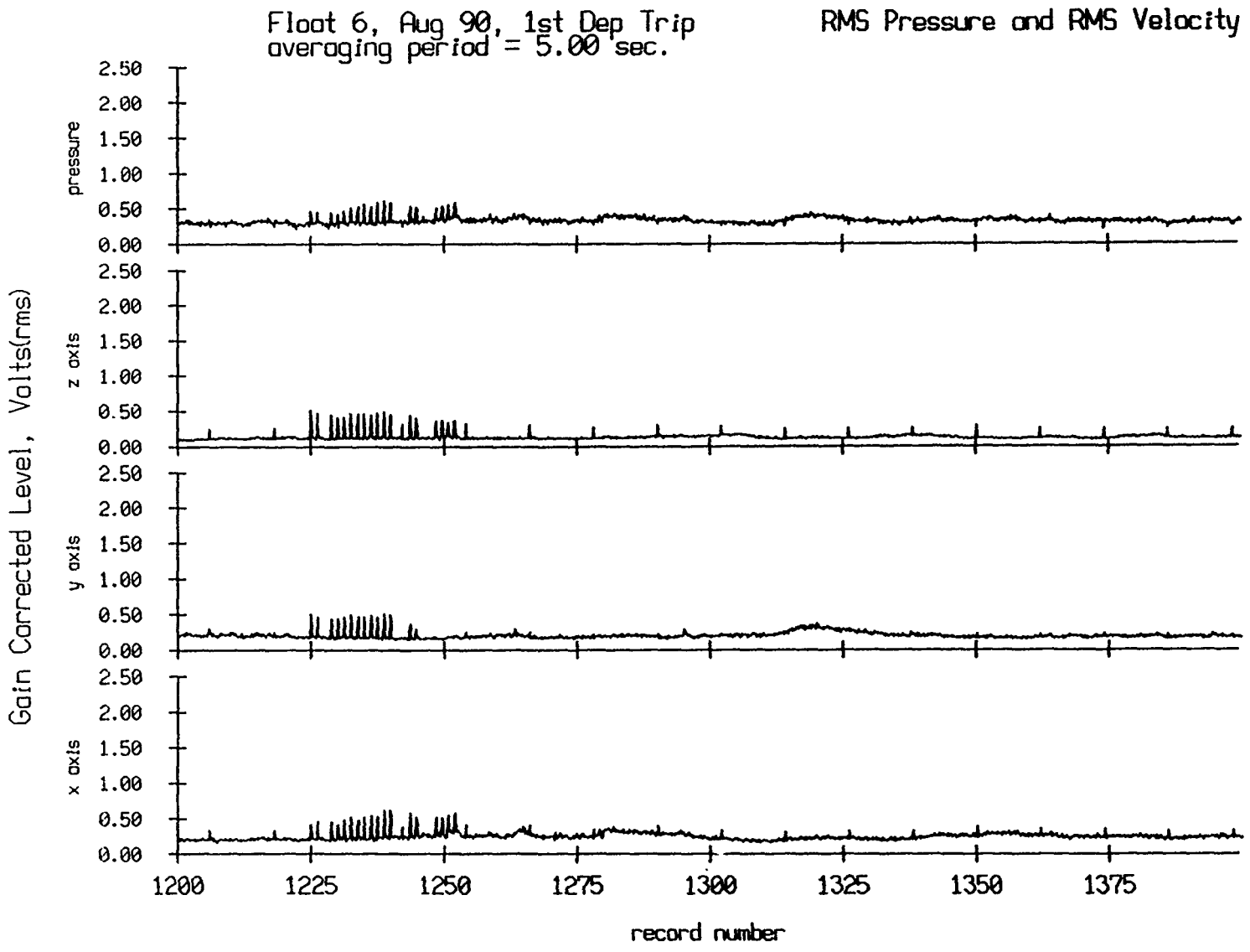

Figure VIII.7d

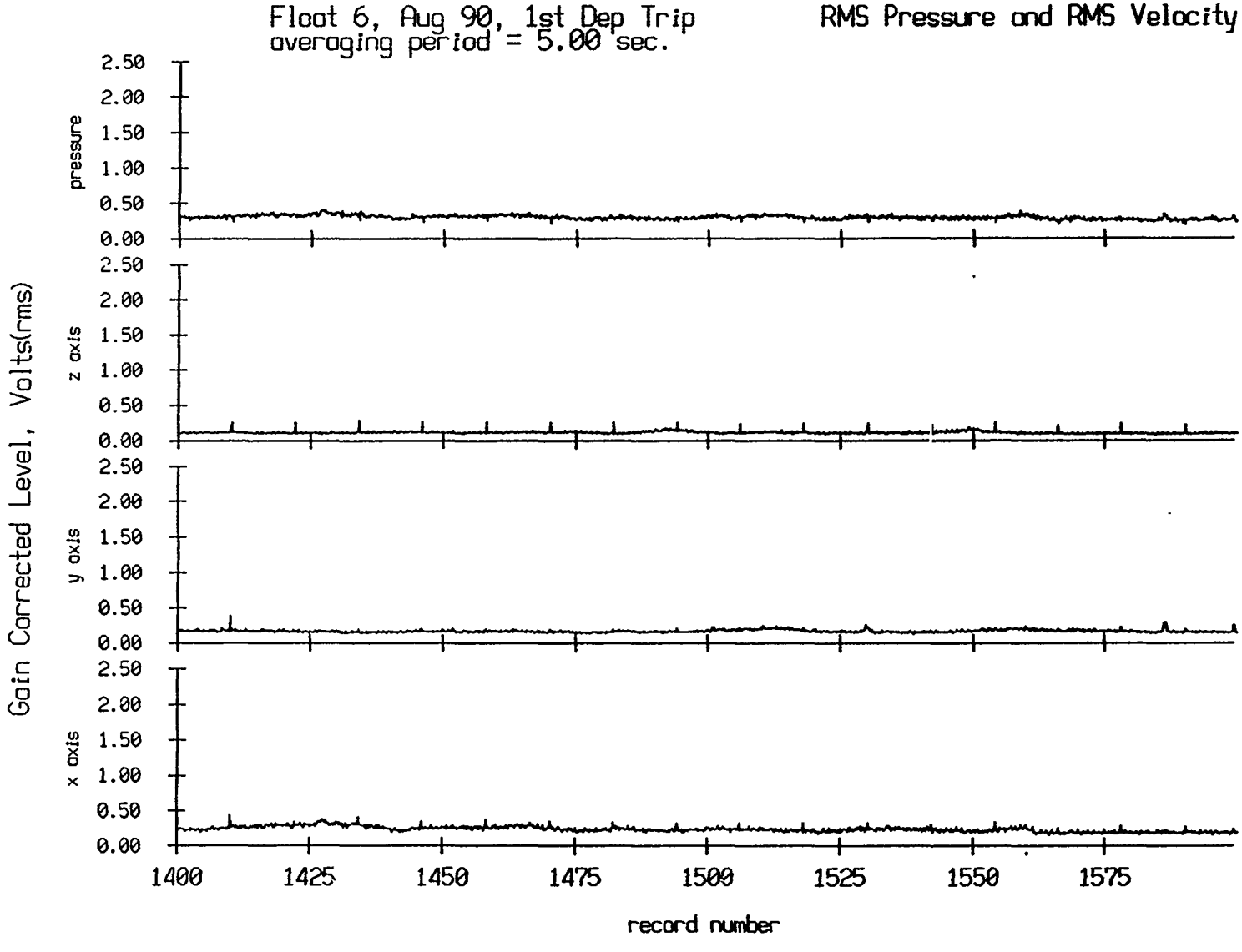

Figure VIII.7e

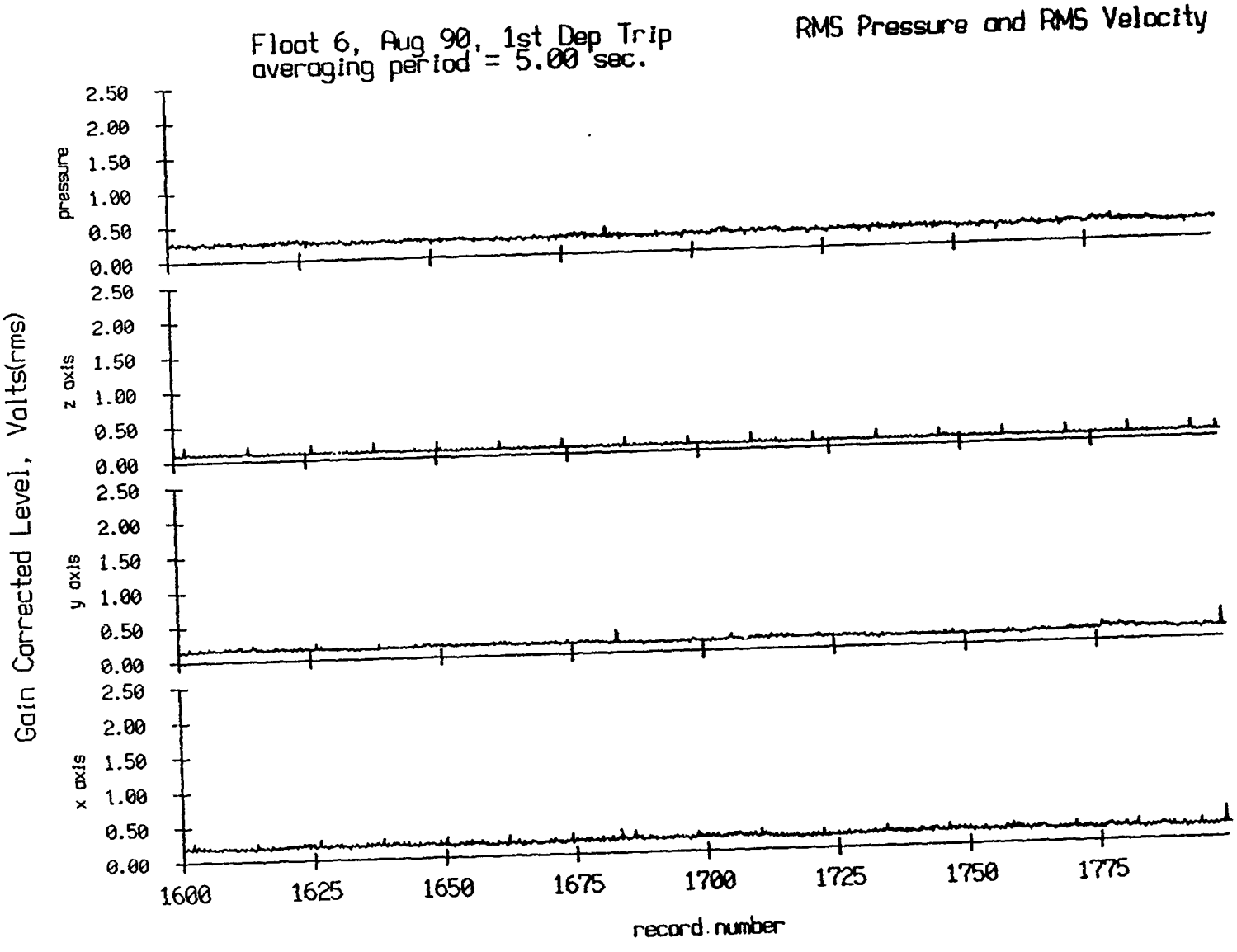

Figure VIII.7f

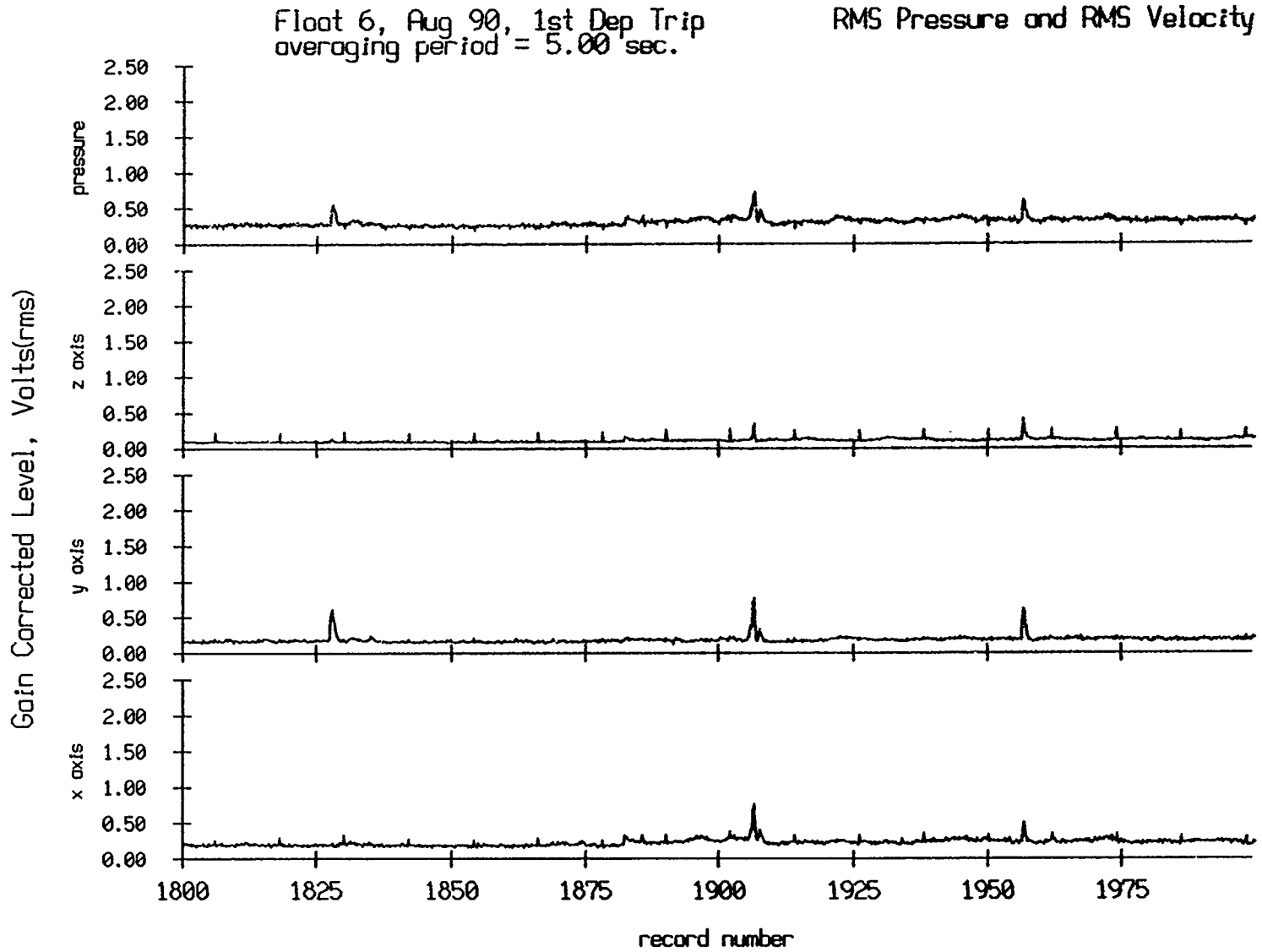

Figure VIII.7g

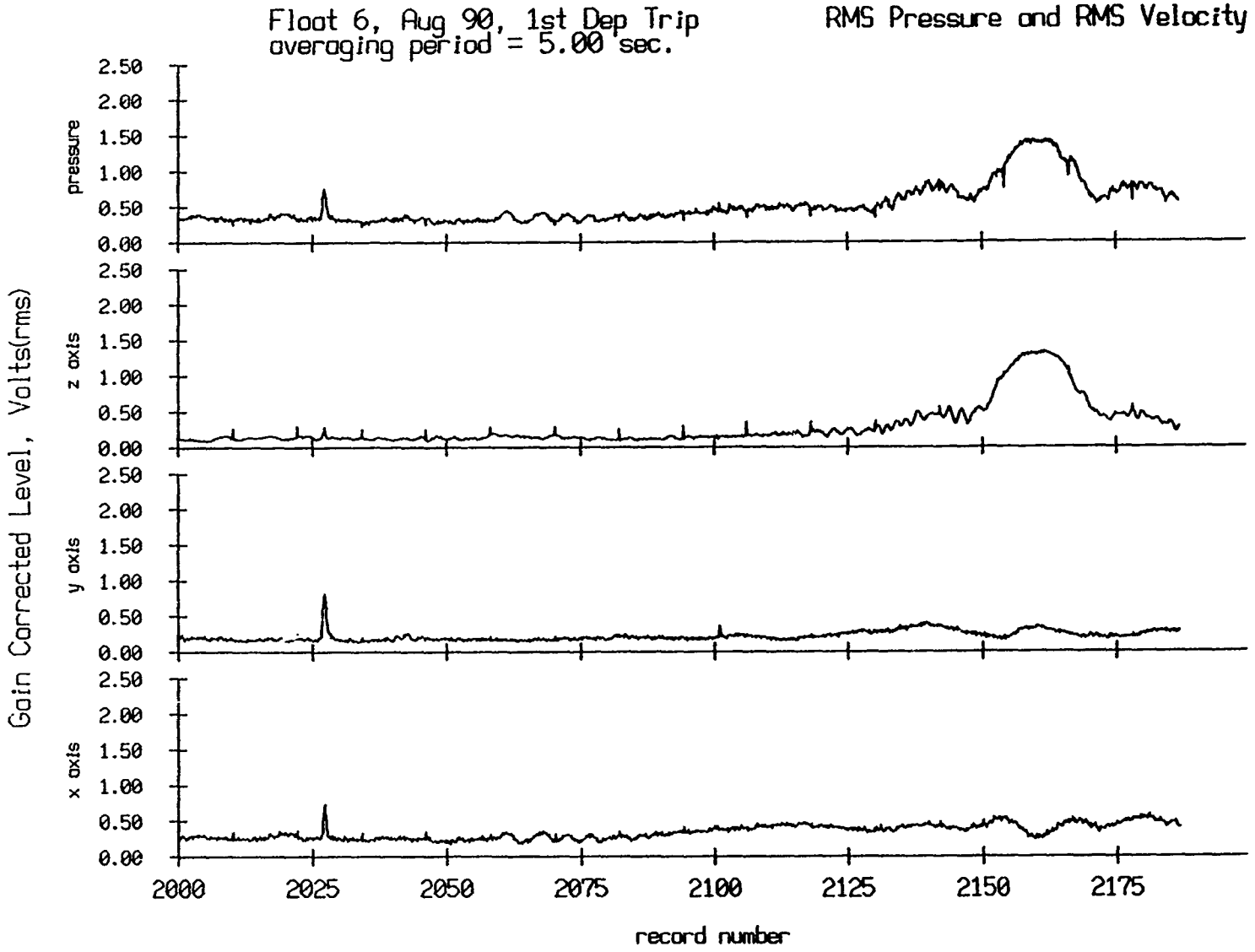

Figure VIII.7h

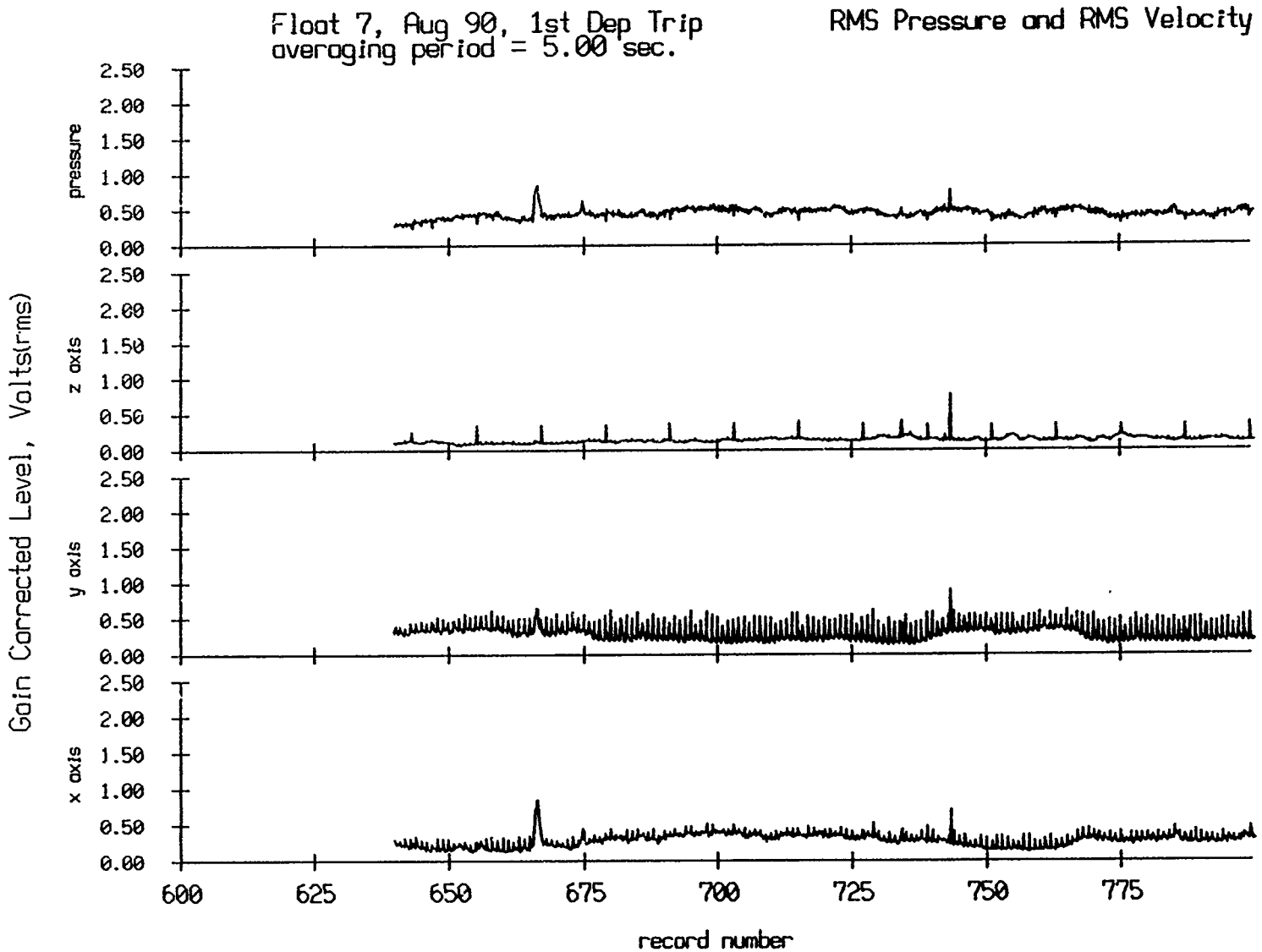

Figure VIII.3a

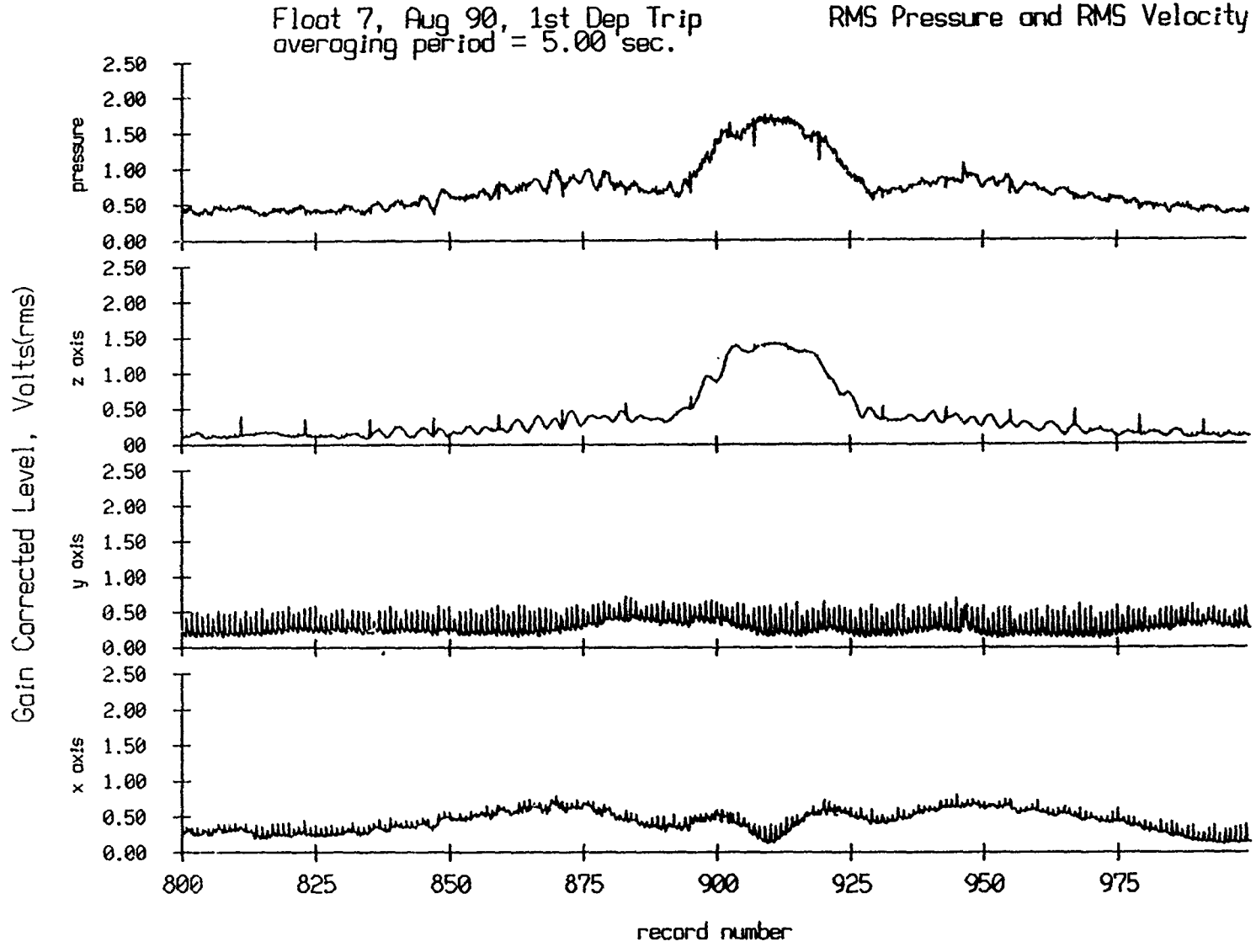

Figure VIII.8b

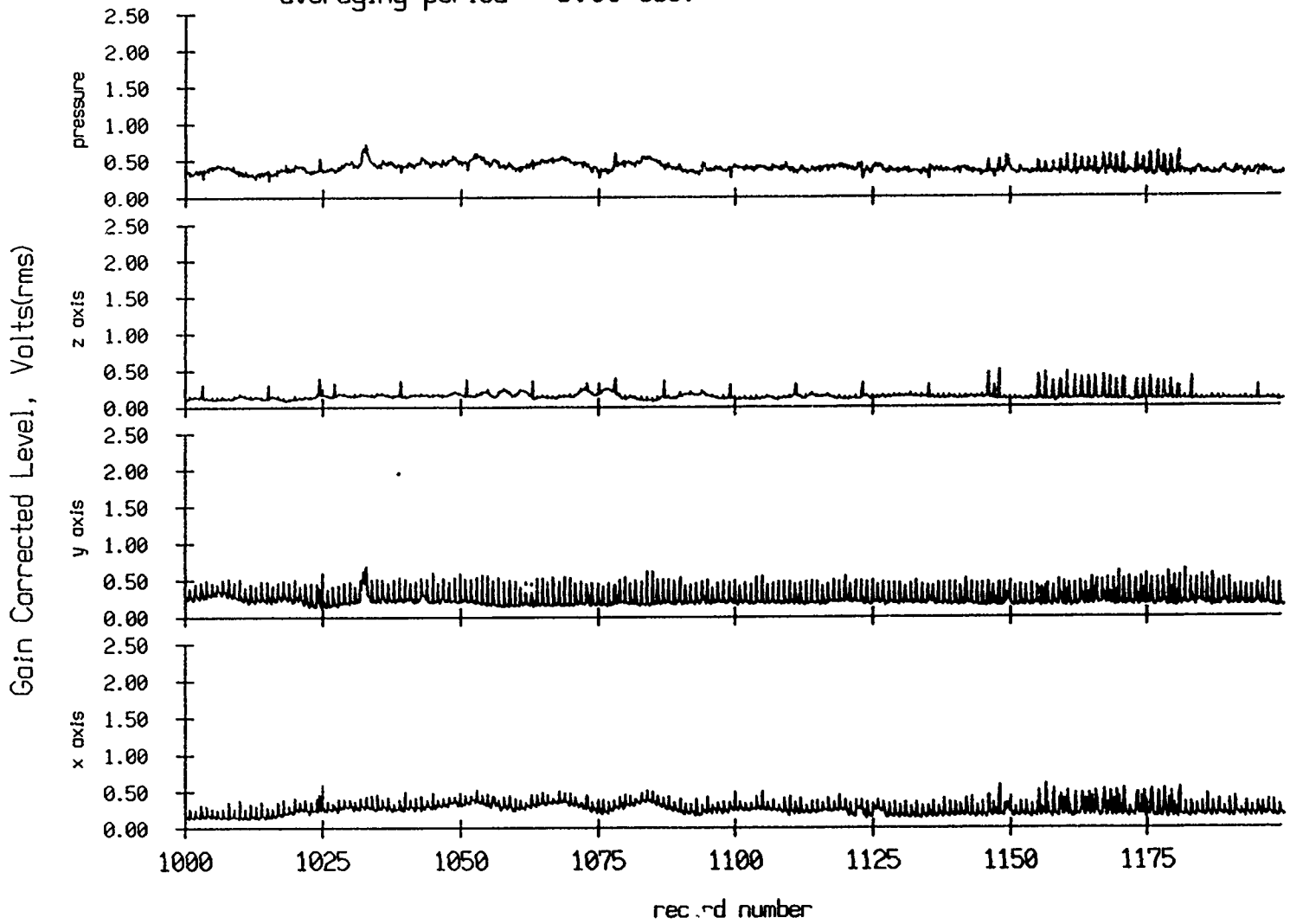

Figure VII.8c

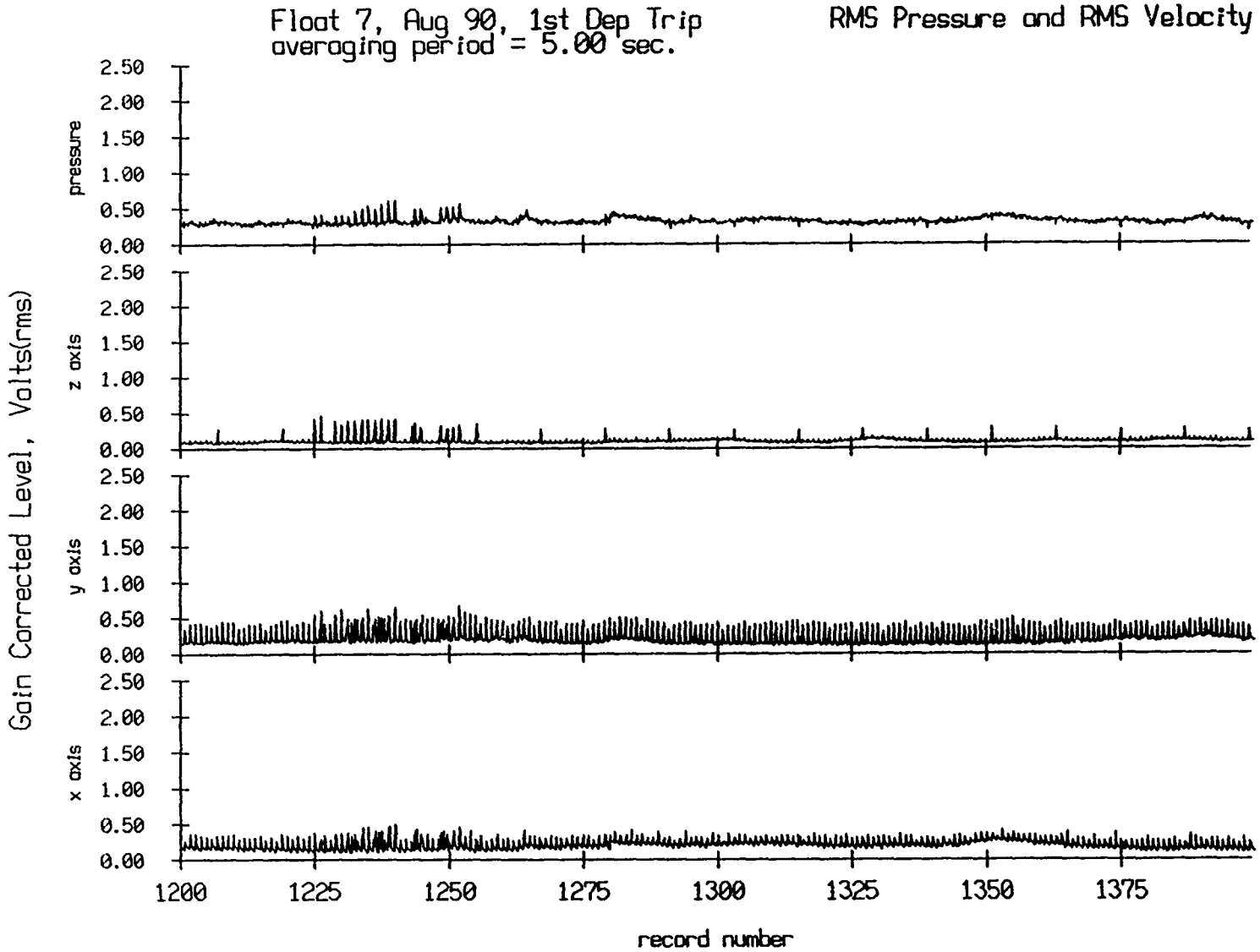

Figure VIII.8d

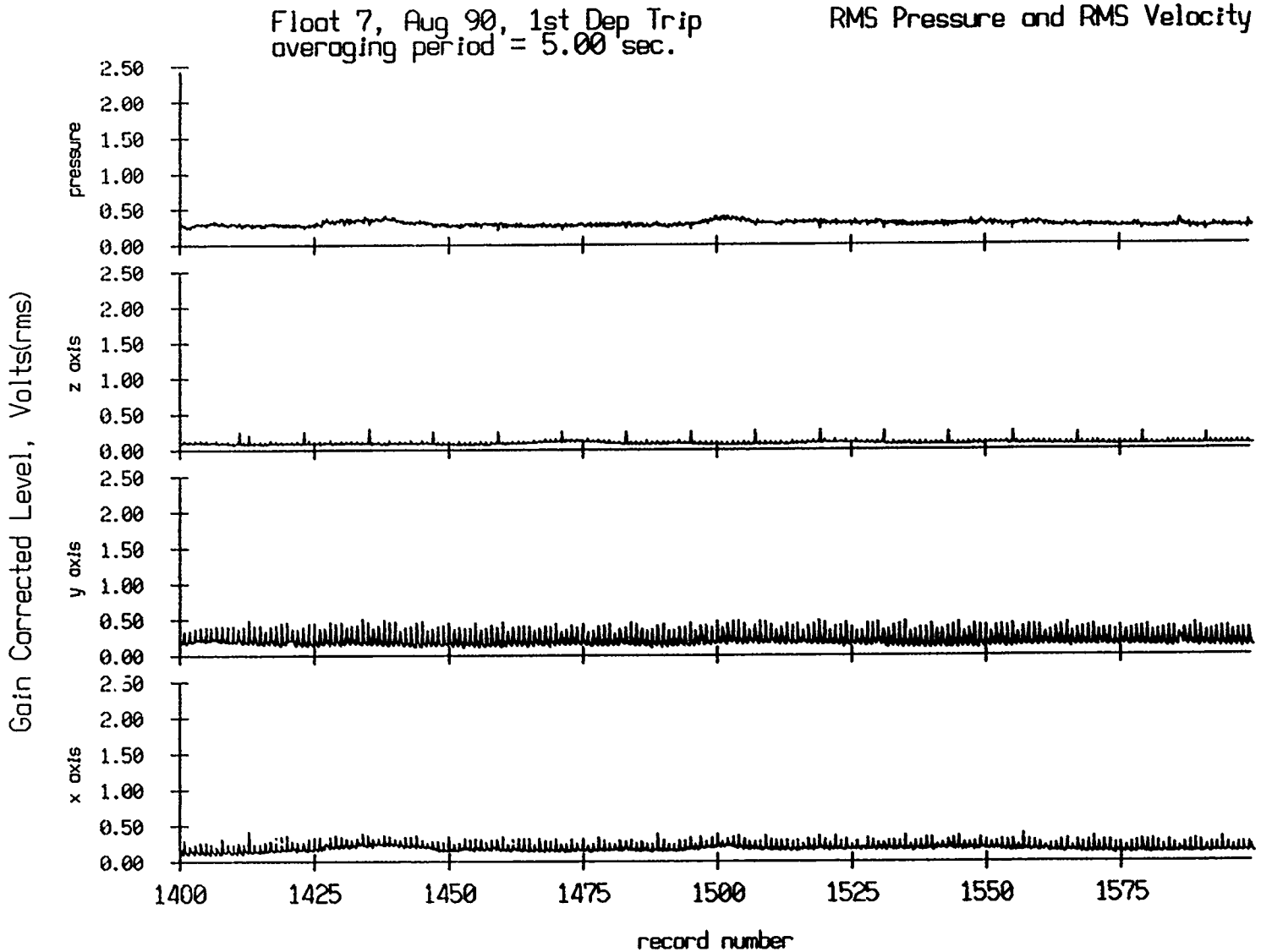

Figure VIII.8e

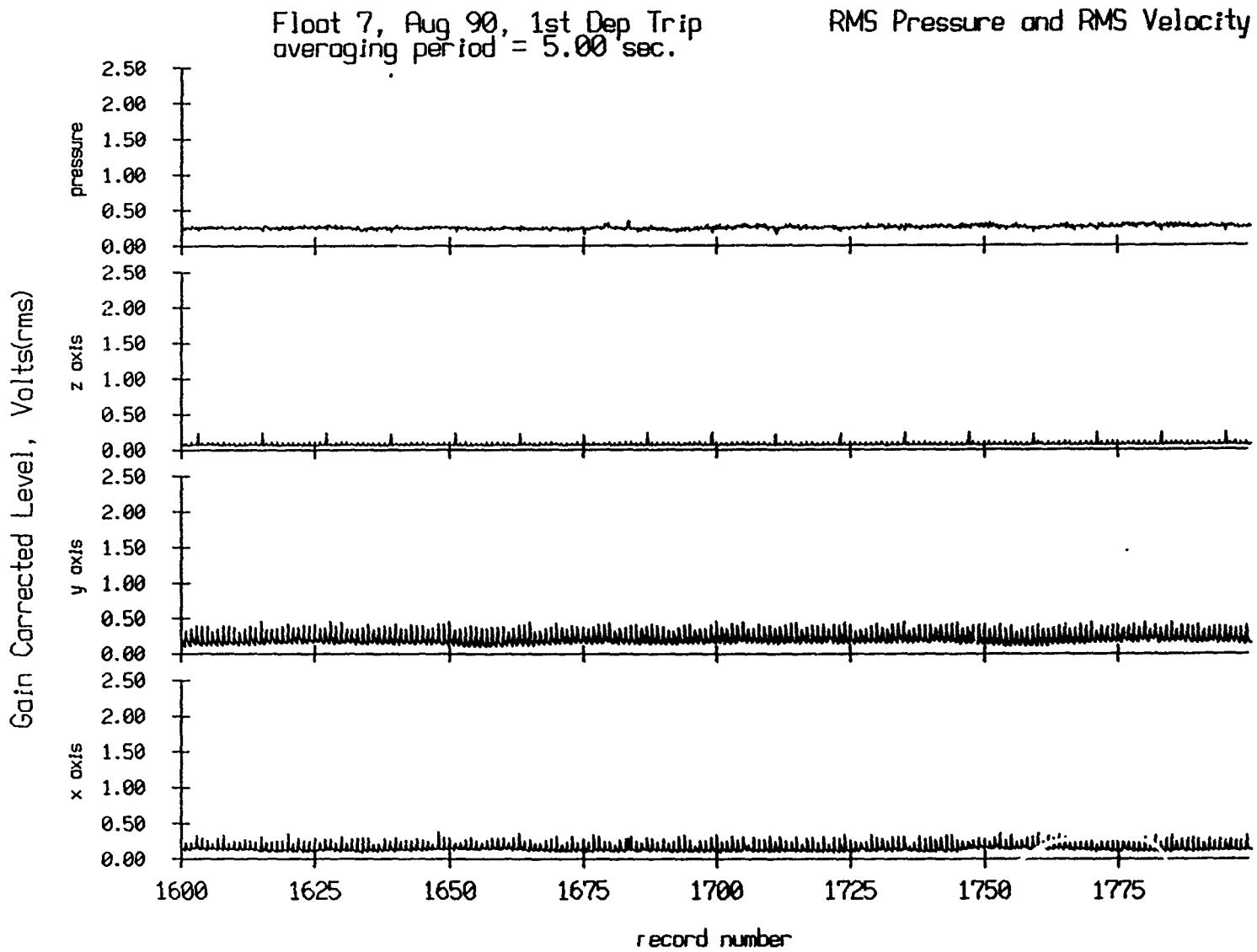

Figure VIII.8f

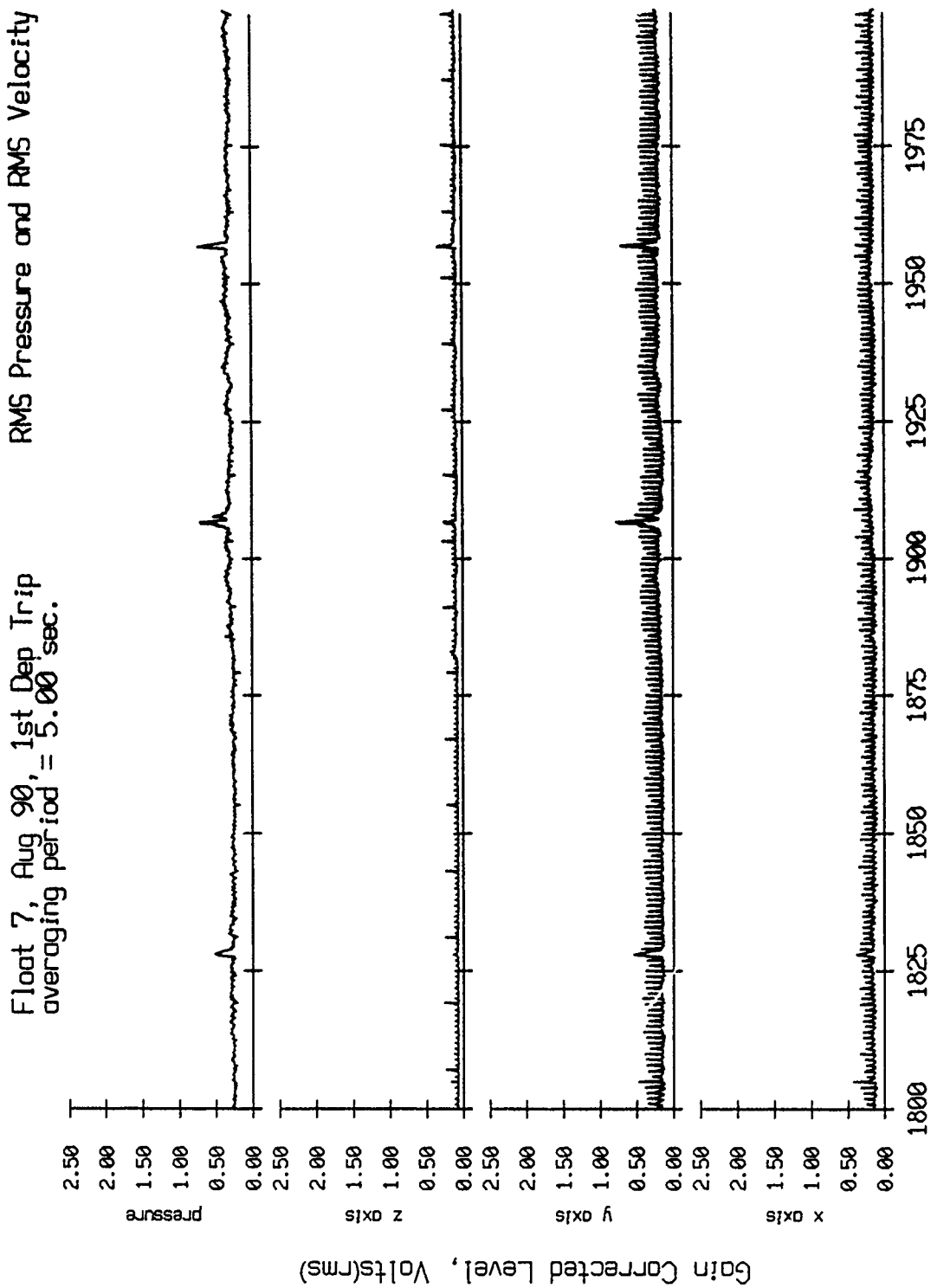

Figure VIII.8g

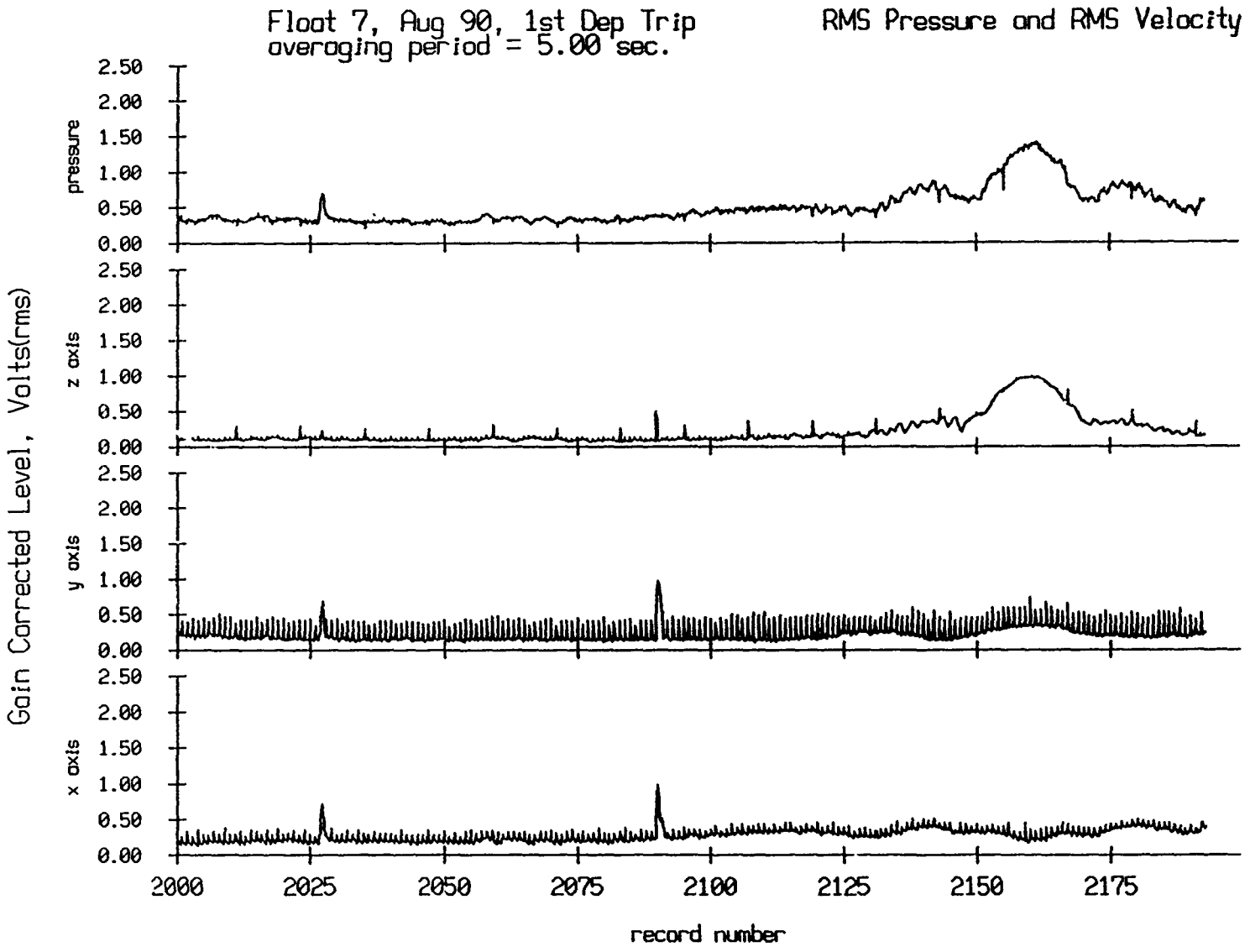

Figure VIII.8h

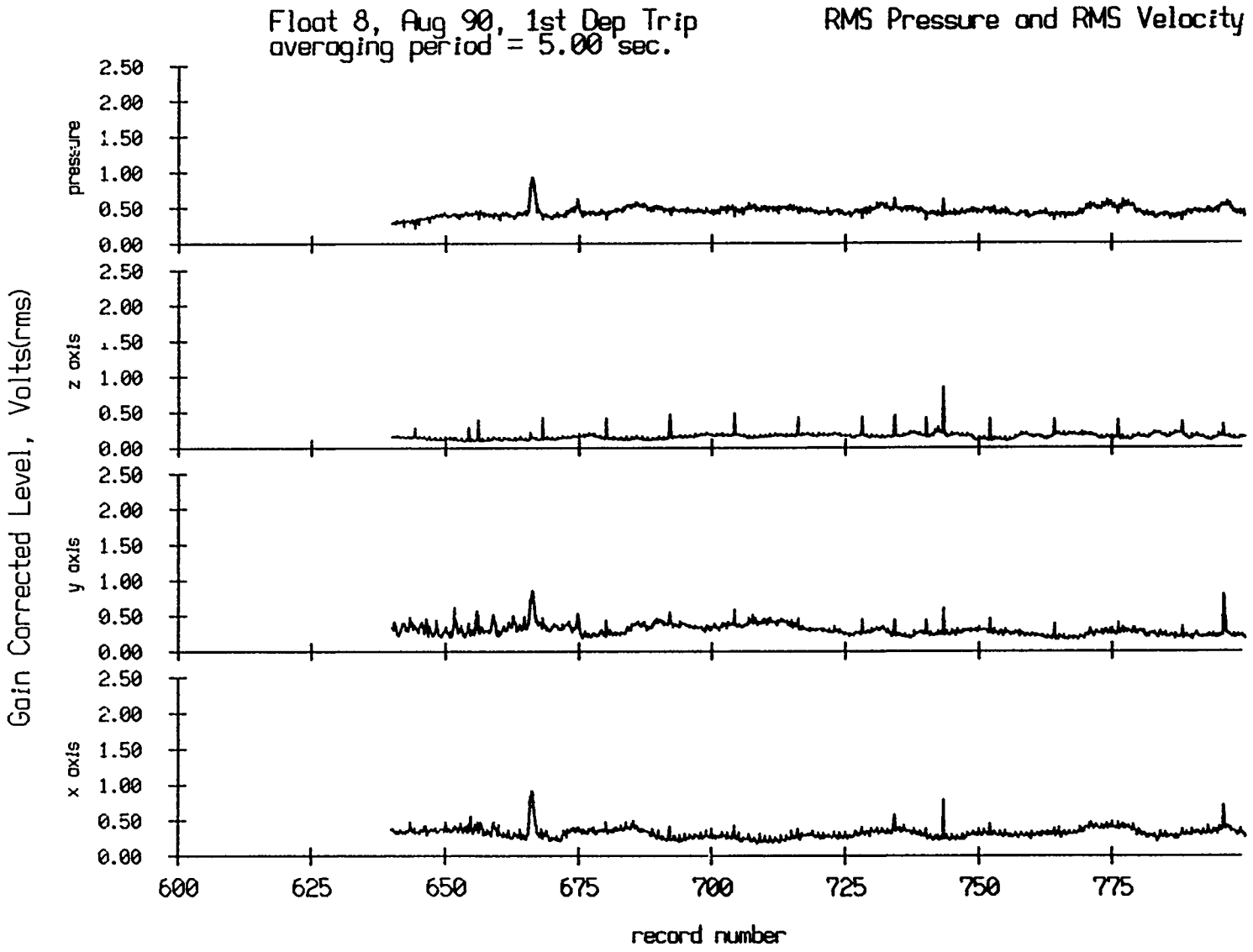

Figure VIII.9a

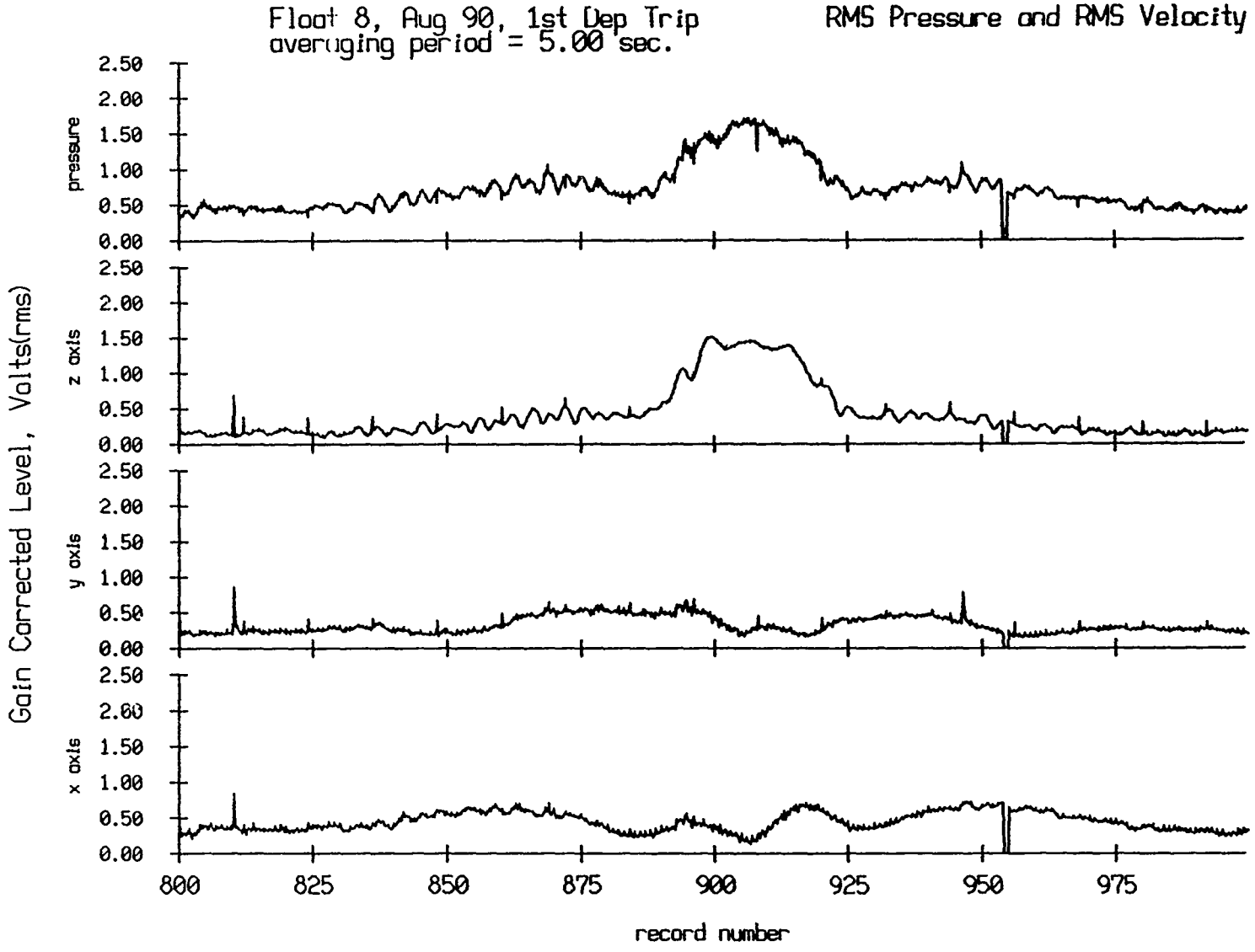

Figure VIII.9b

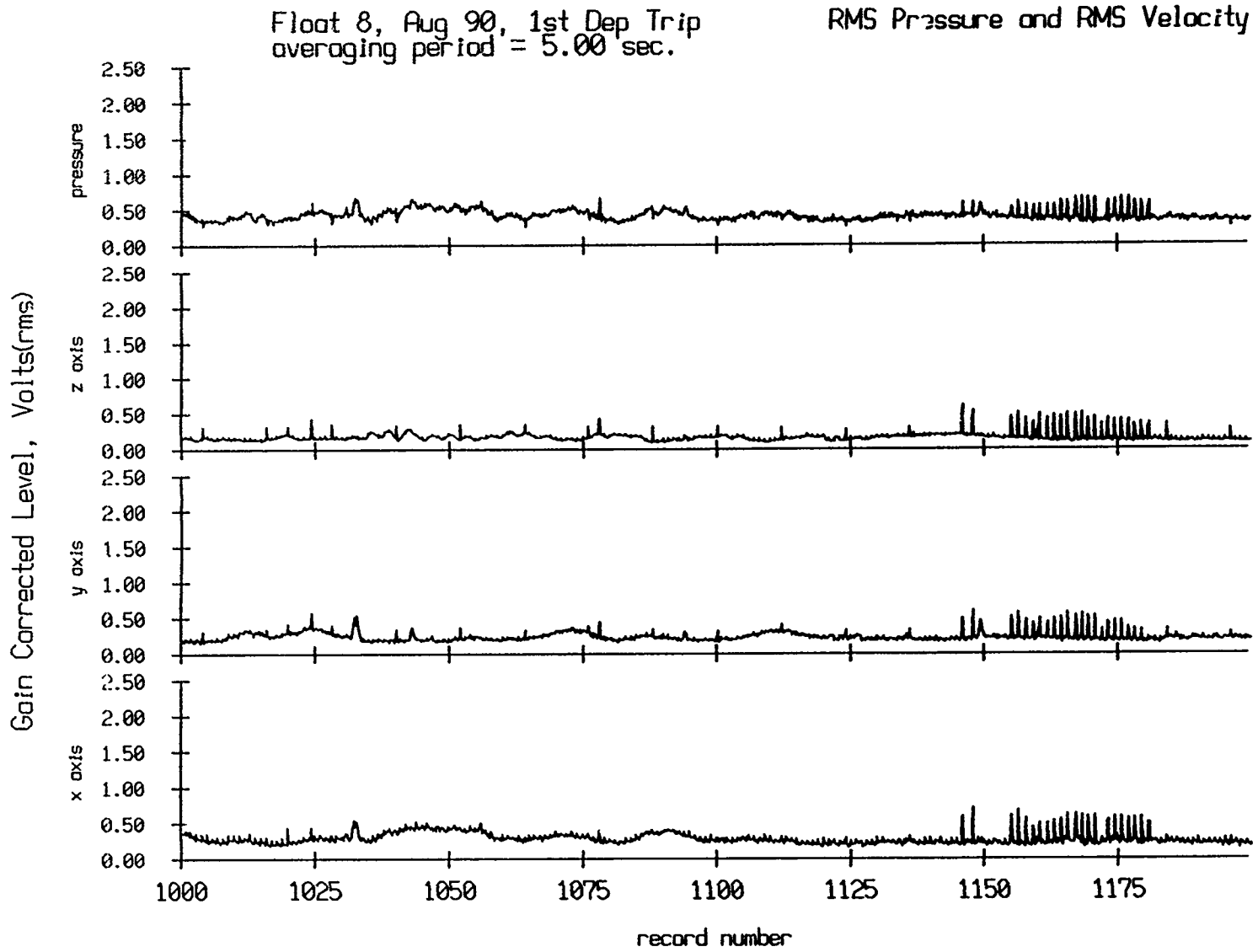

Figure VIII.9c

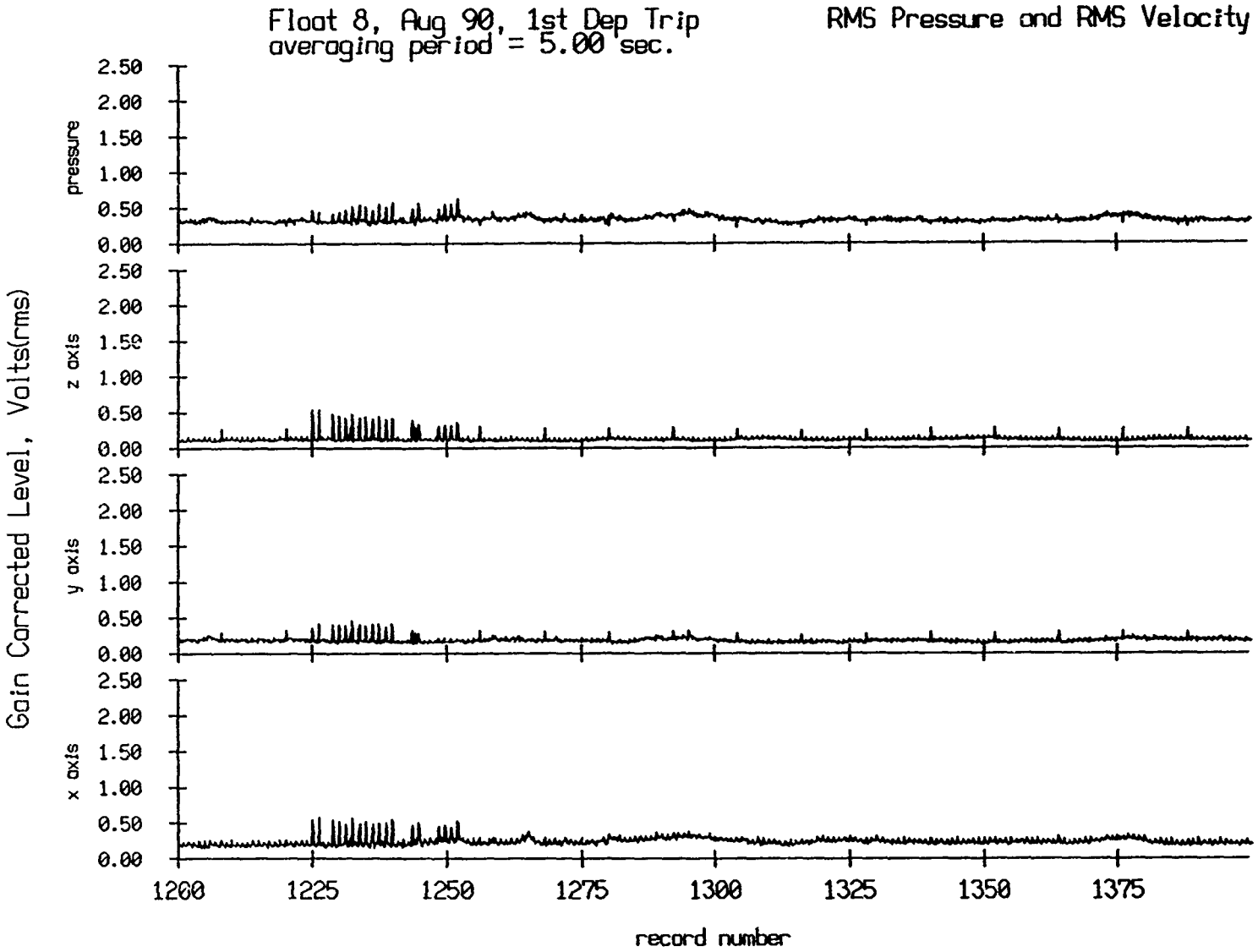

Figure VIII.9d

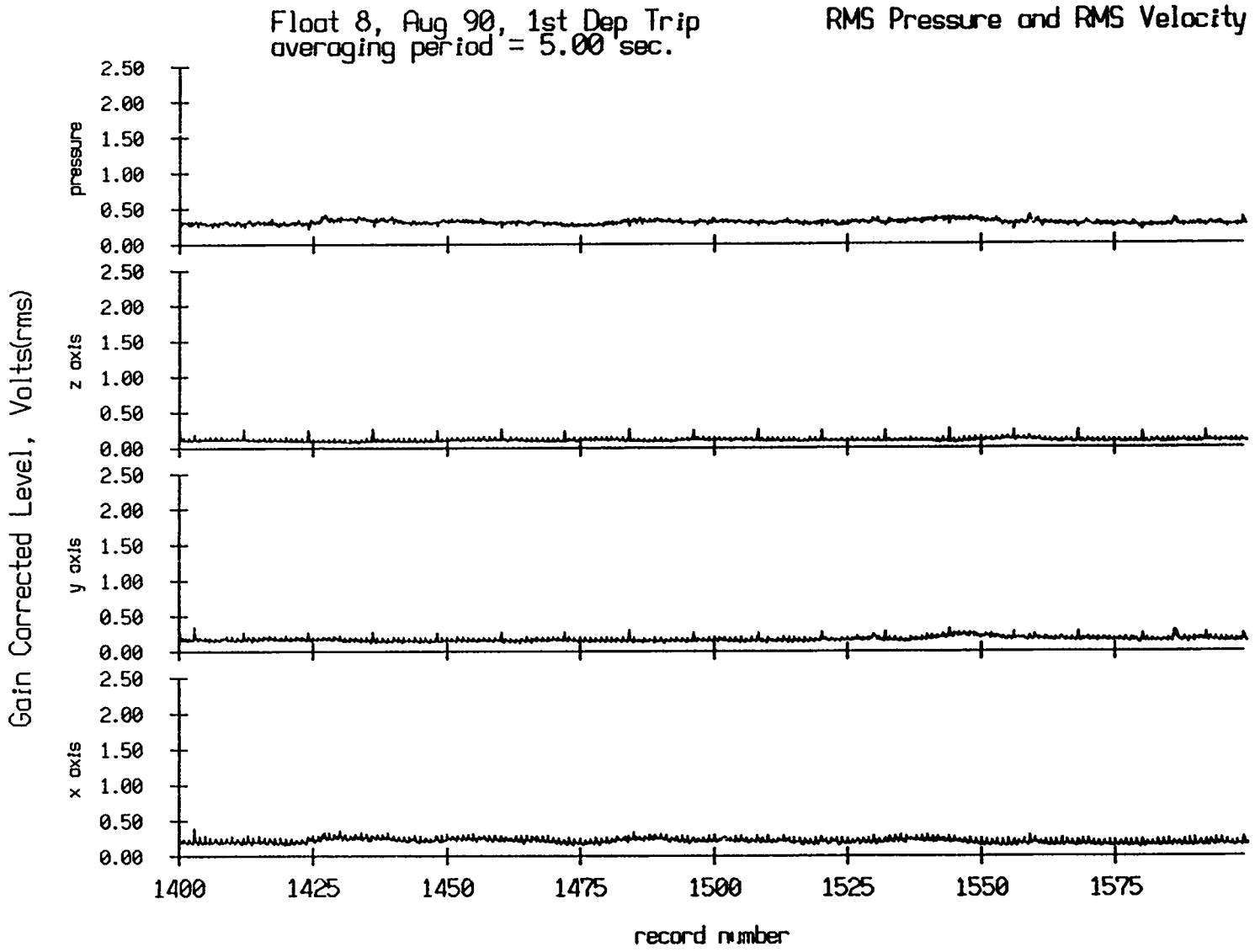

Figure VIII.9e

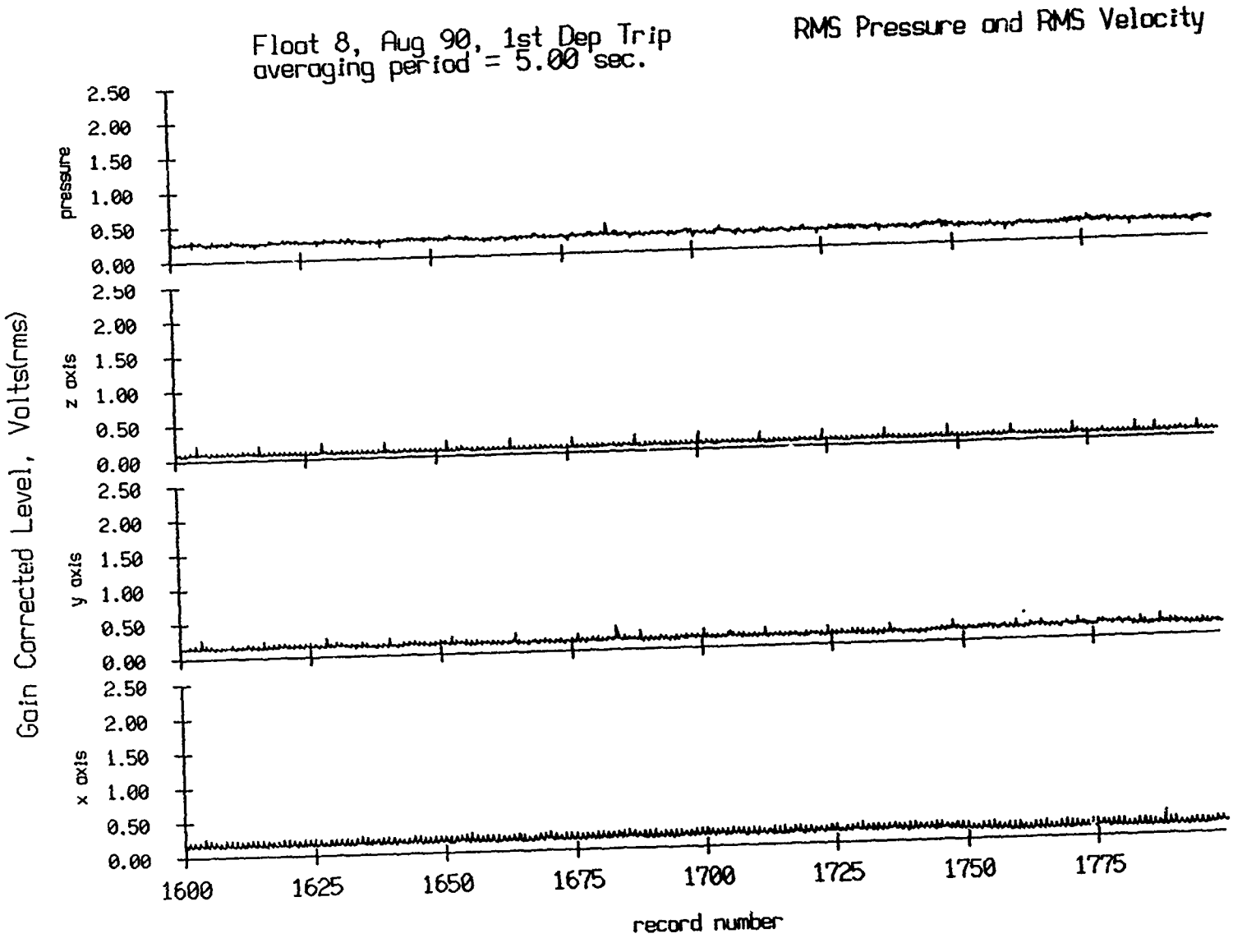

Figure VIII.9f

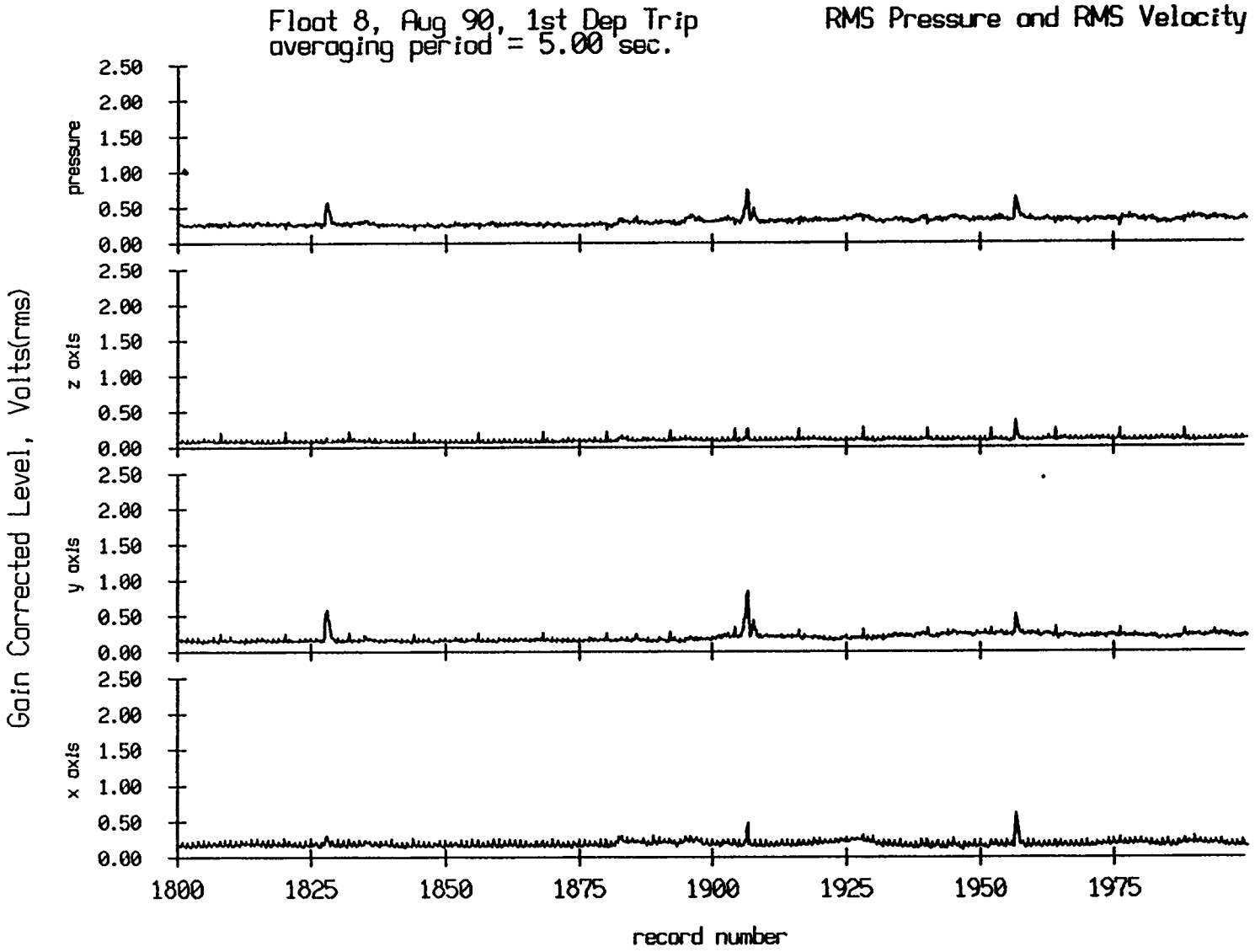

Figure VIII.9g

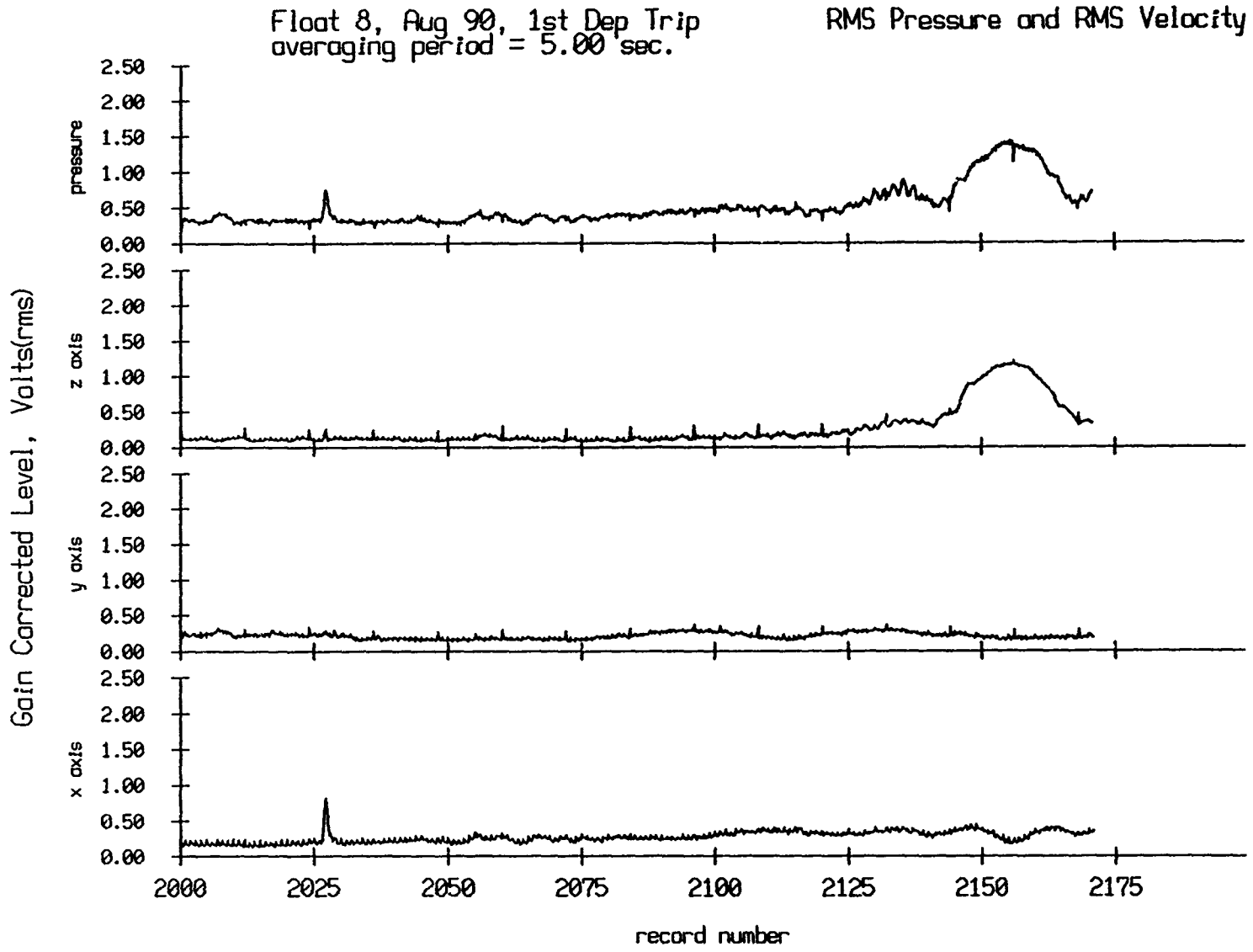

Figure VIII.9h

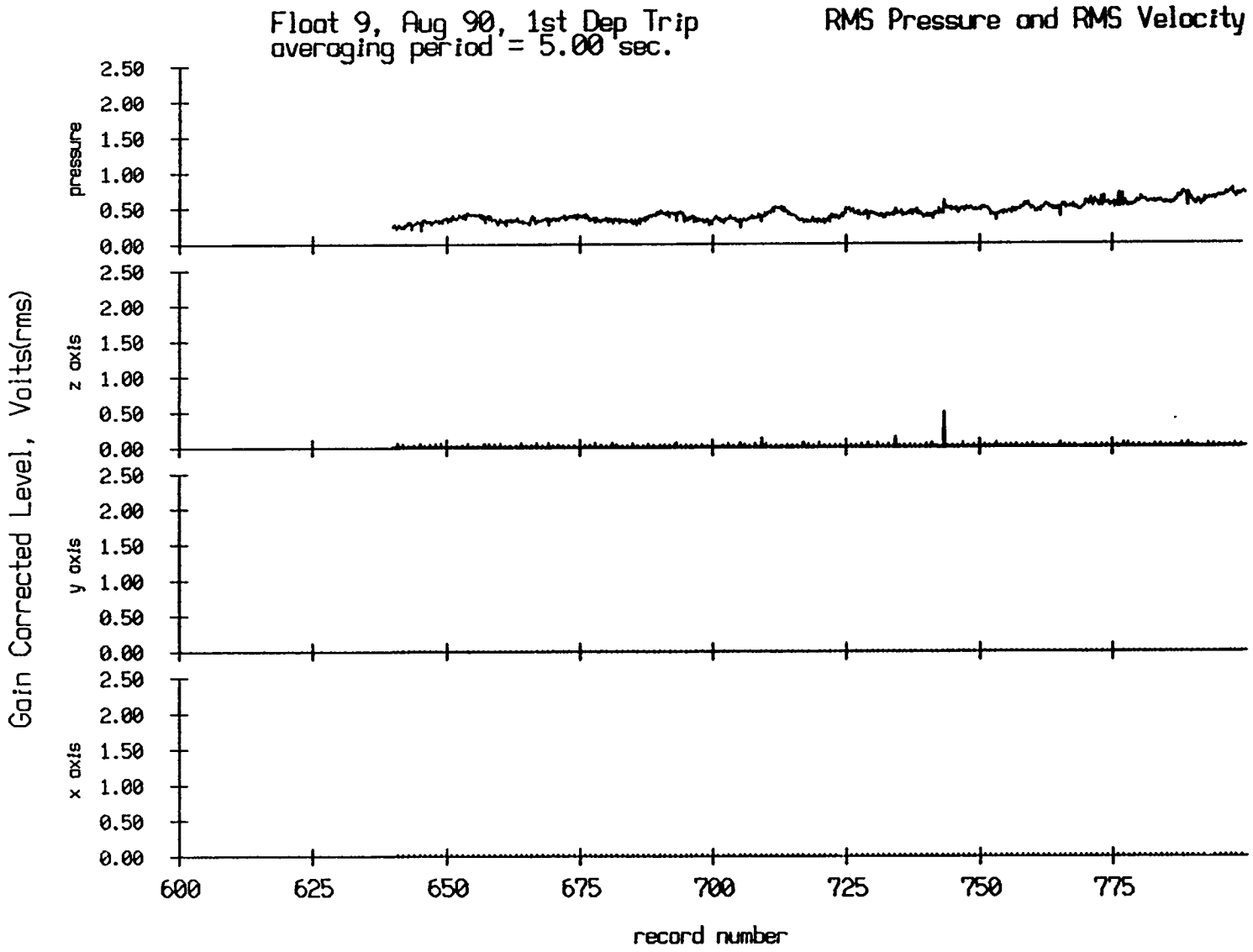

Figure VIII.10a

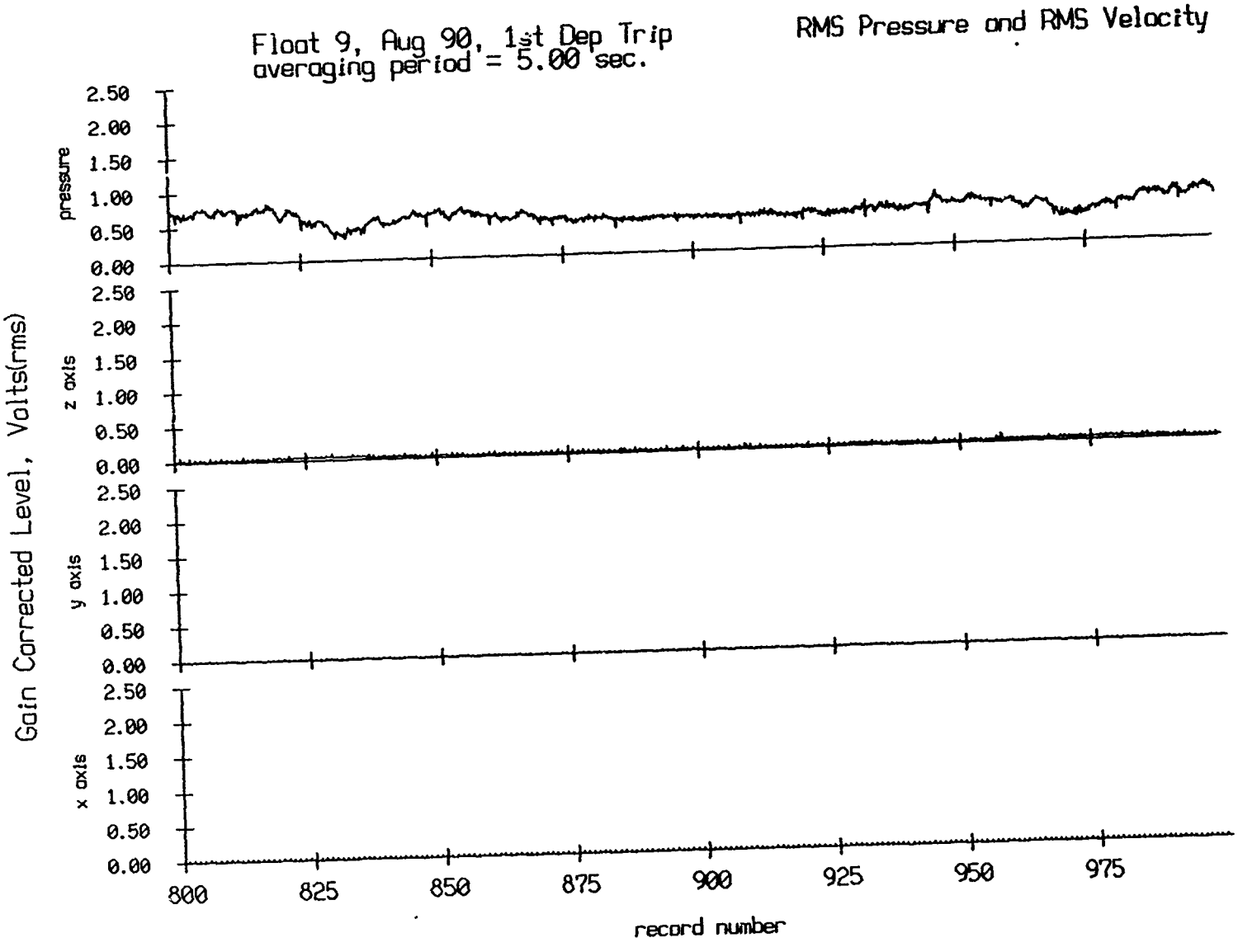

Figure VIII.10b

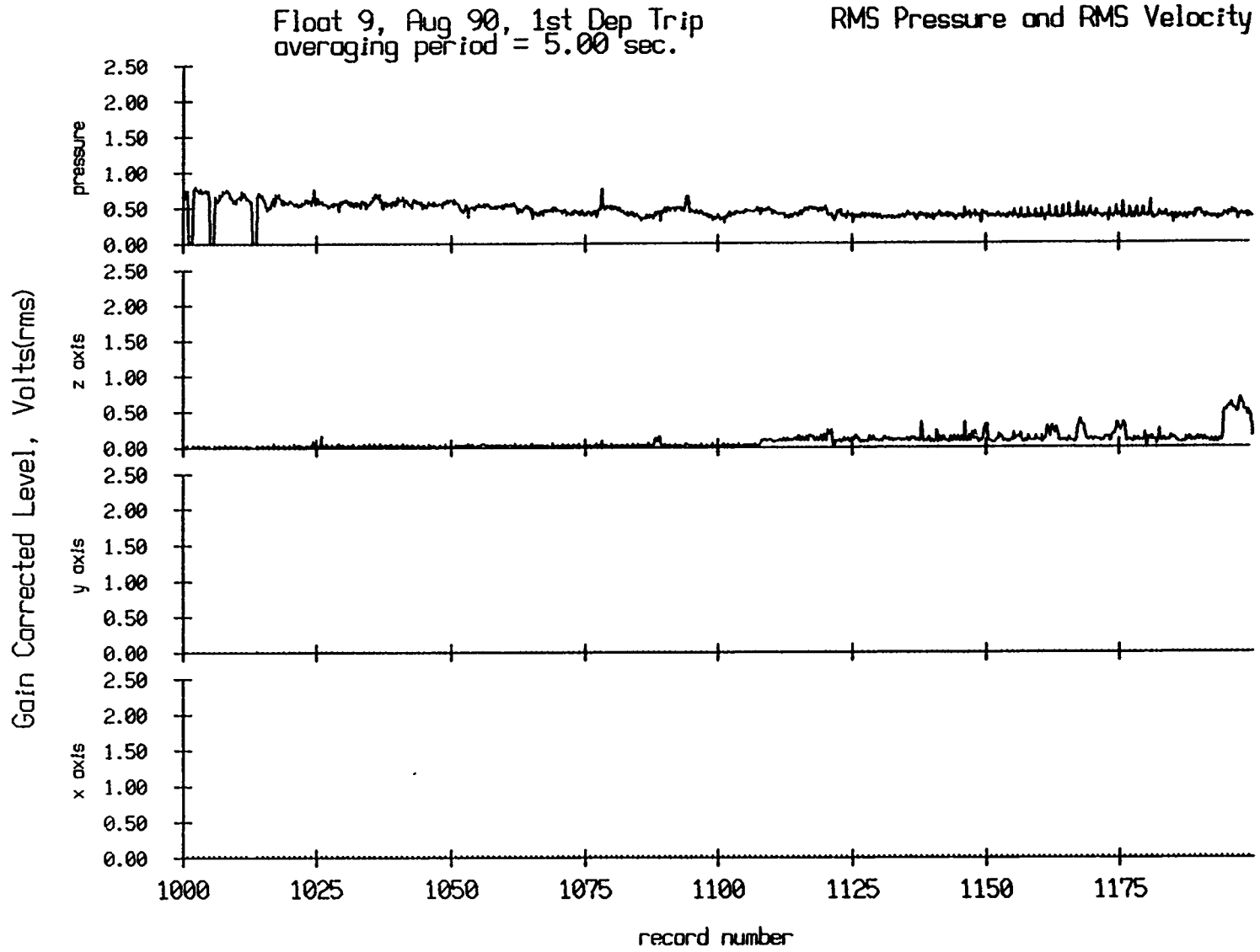

Figure VIII.10c

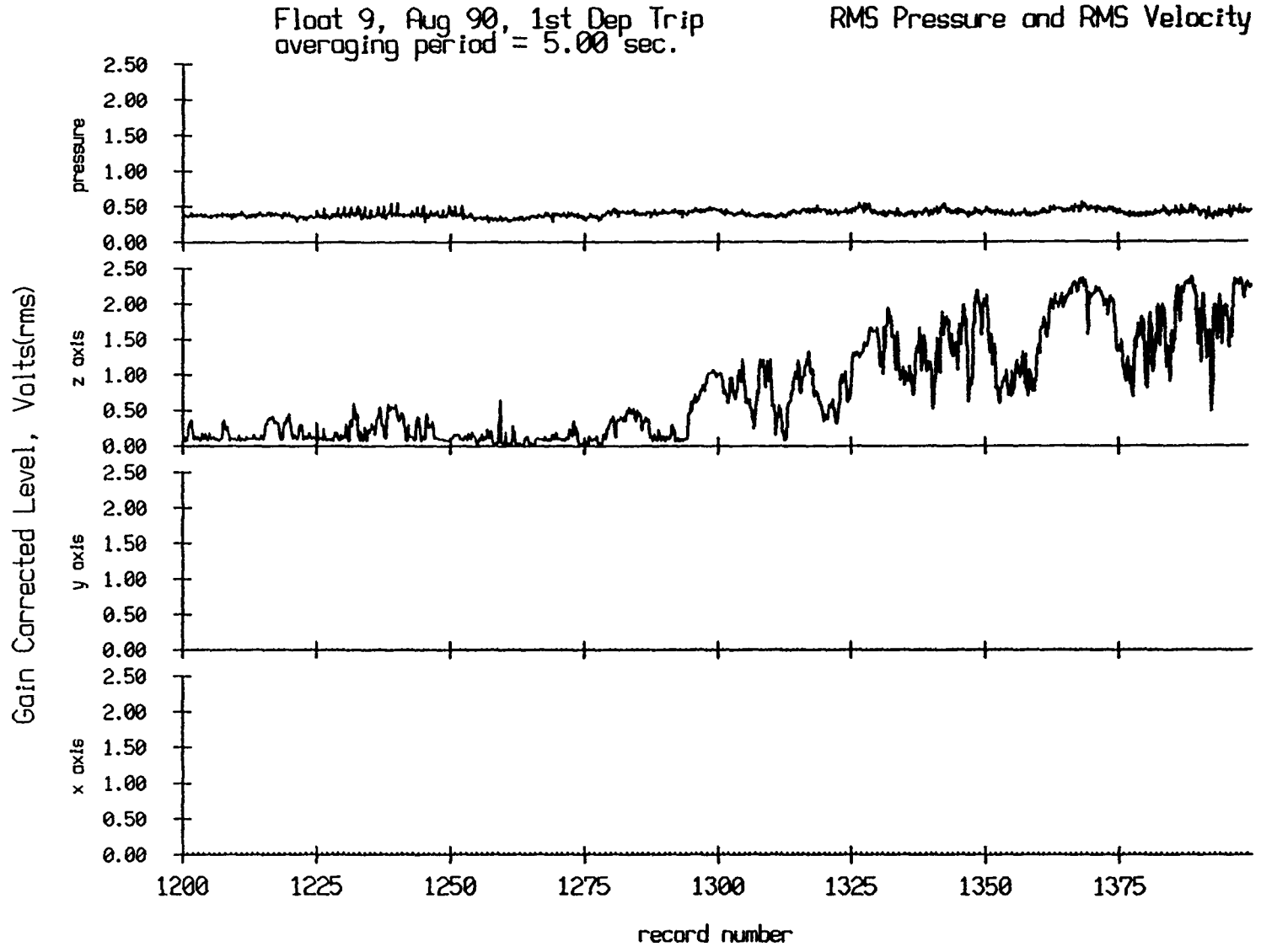

Figure VIII.10d

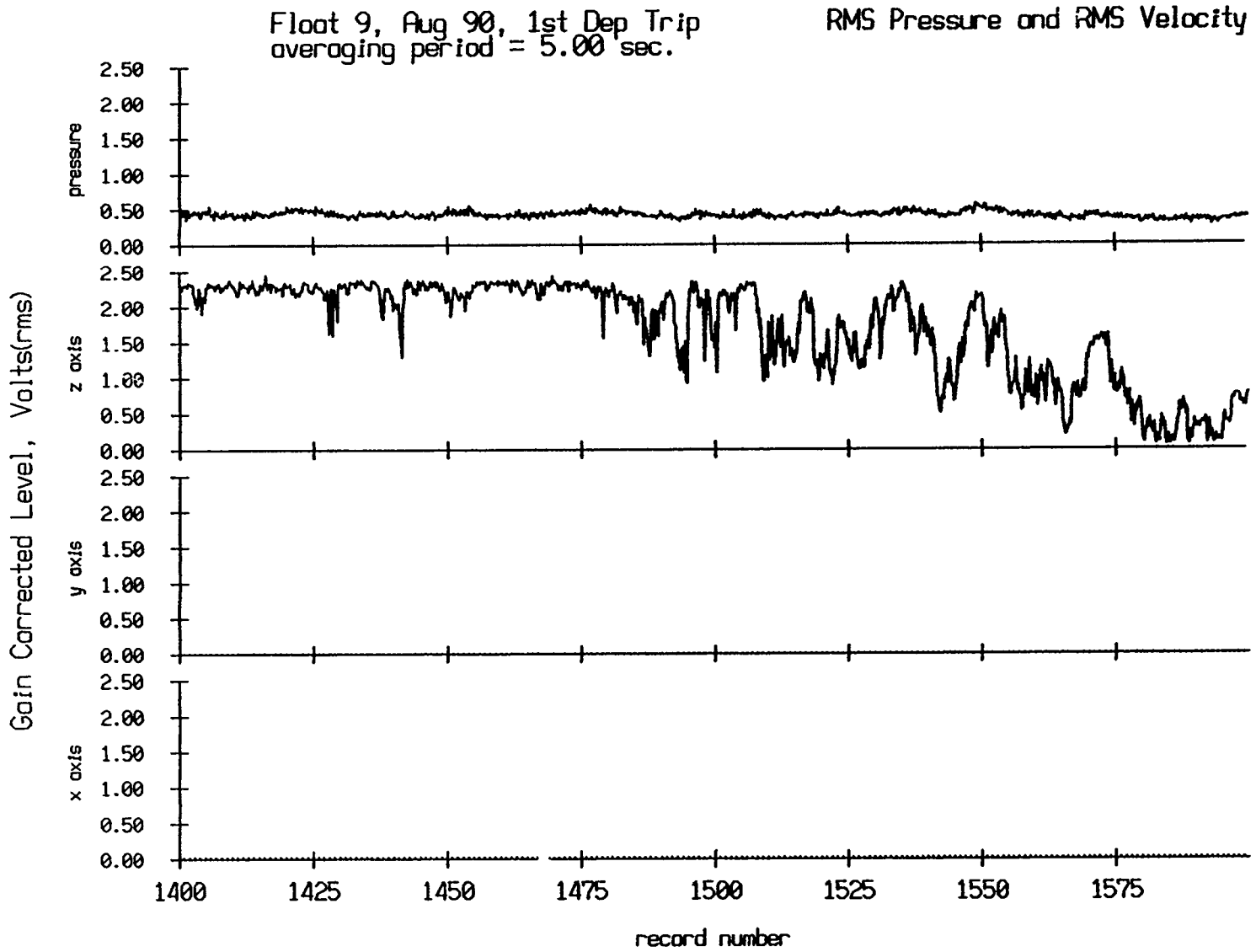

Figure VIII.10e

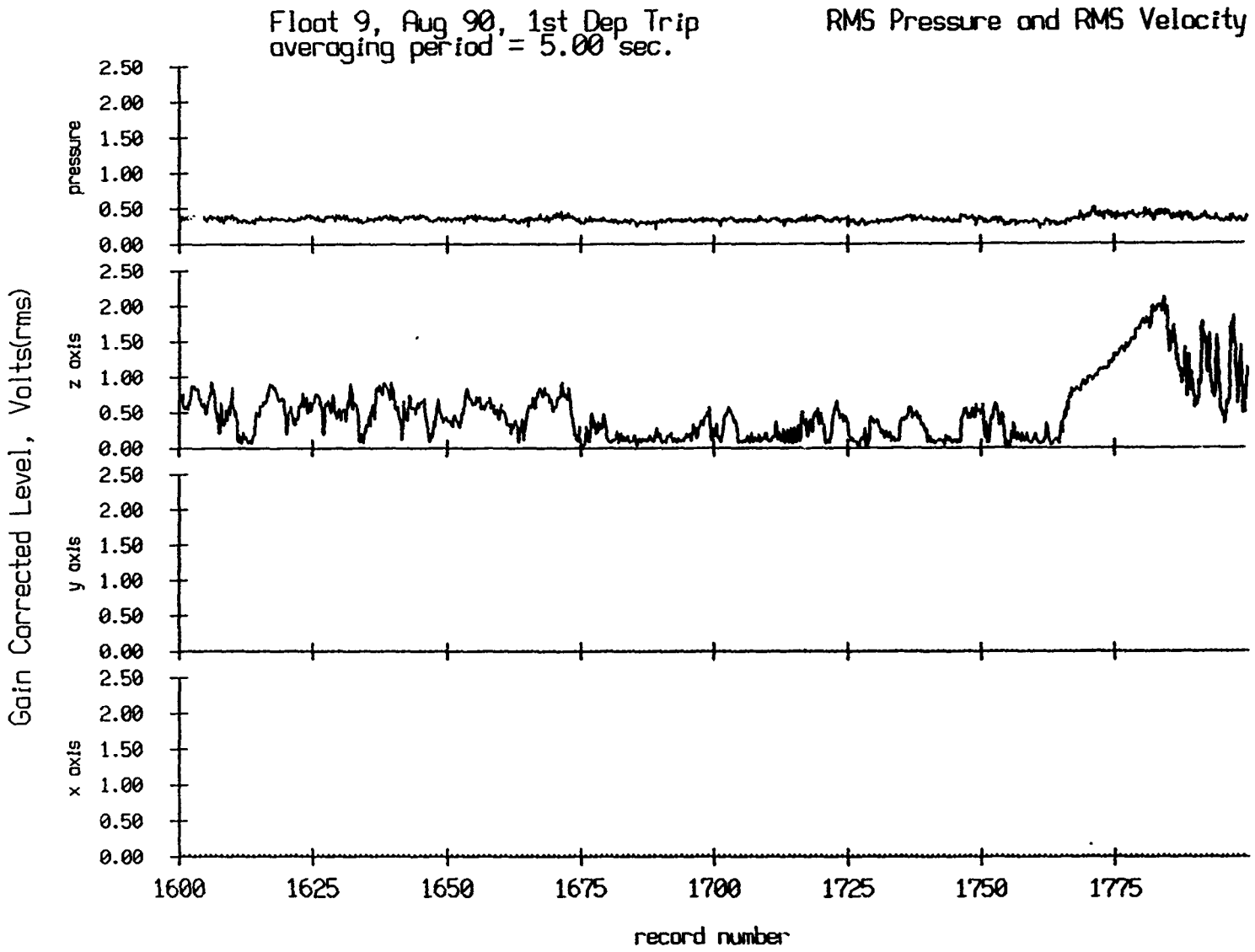

Figure VIII.10f

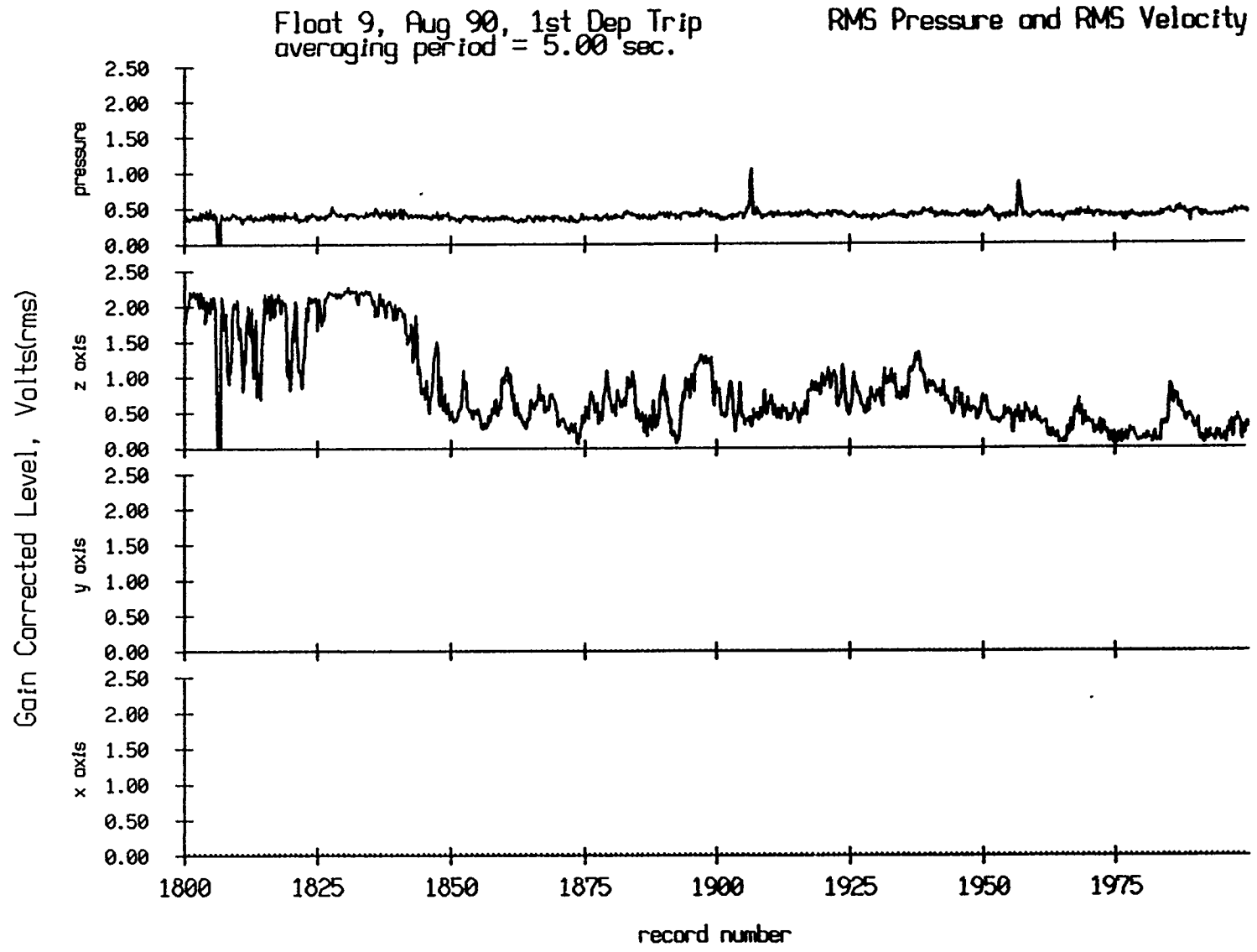

Figure VIII.10B

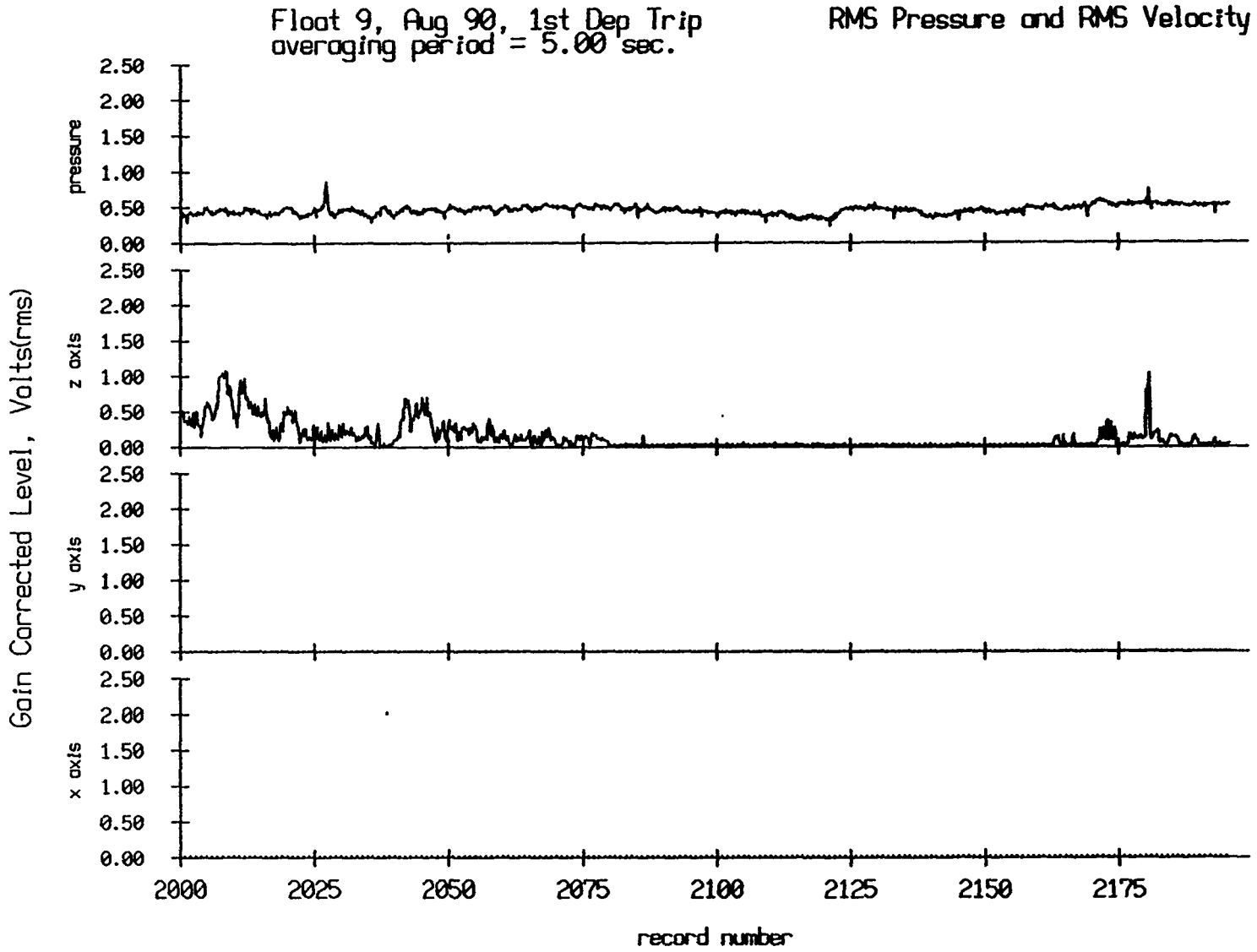

Figure VIII.10h

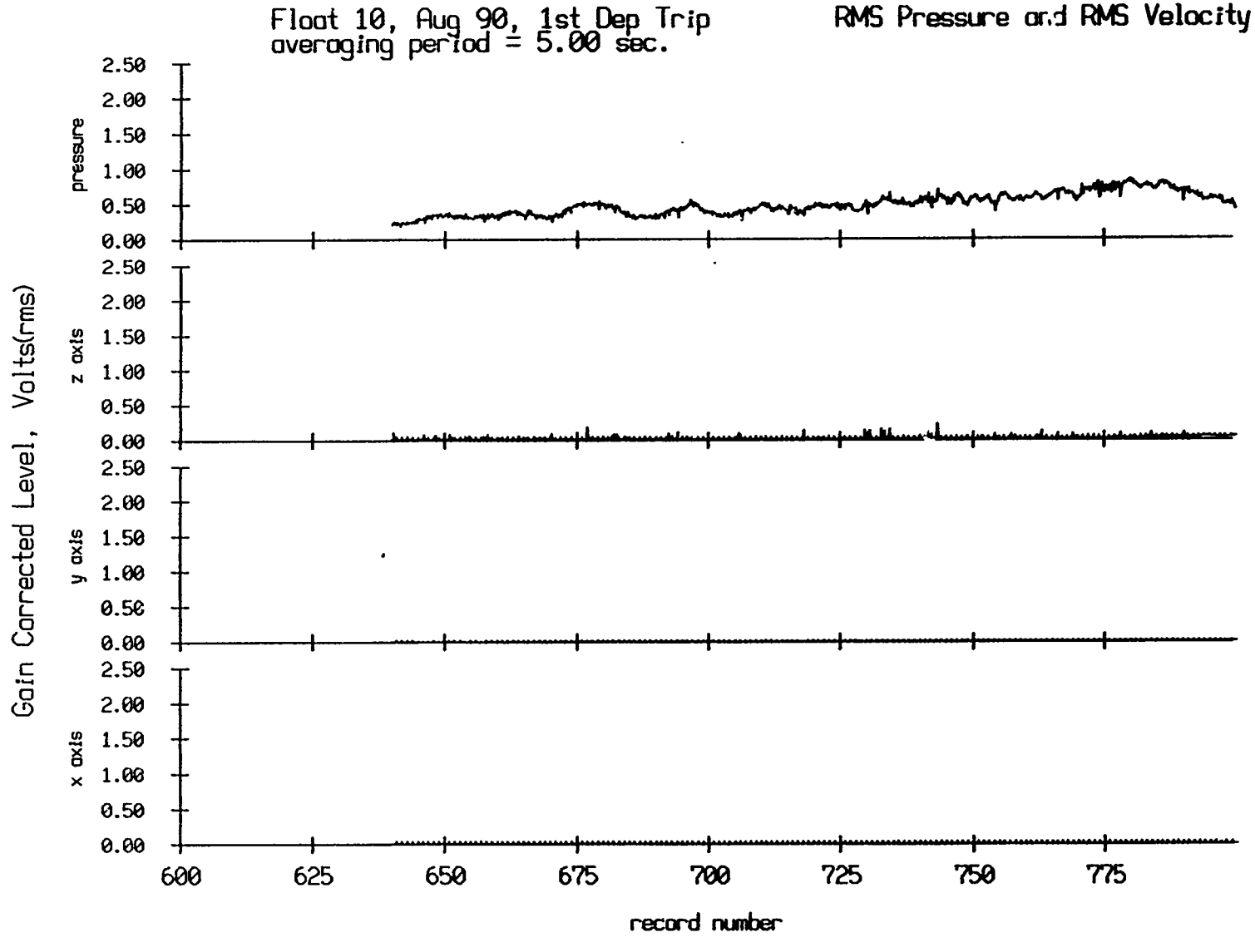

Figure VIII.11a

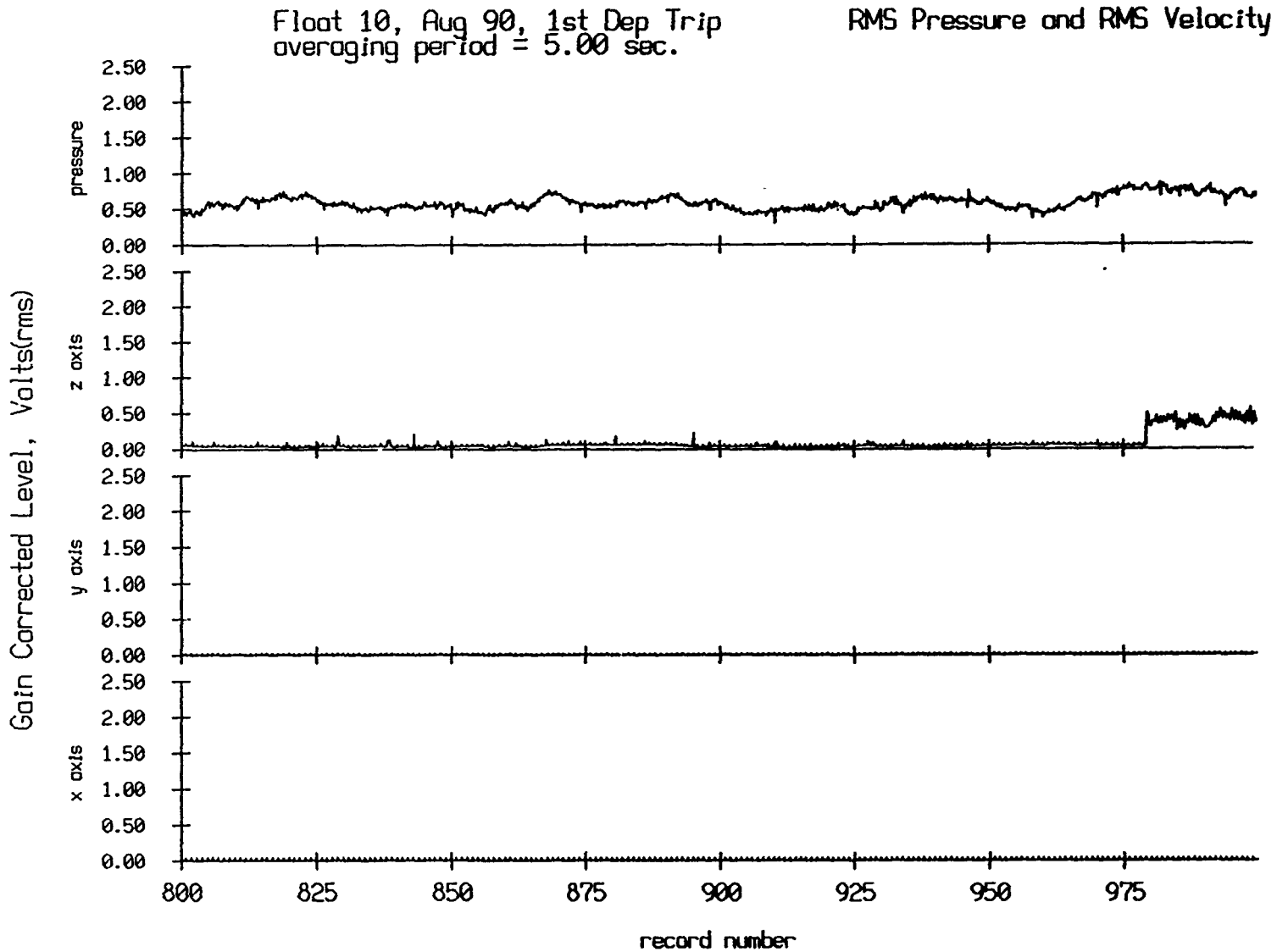

Figure VIII.11b

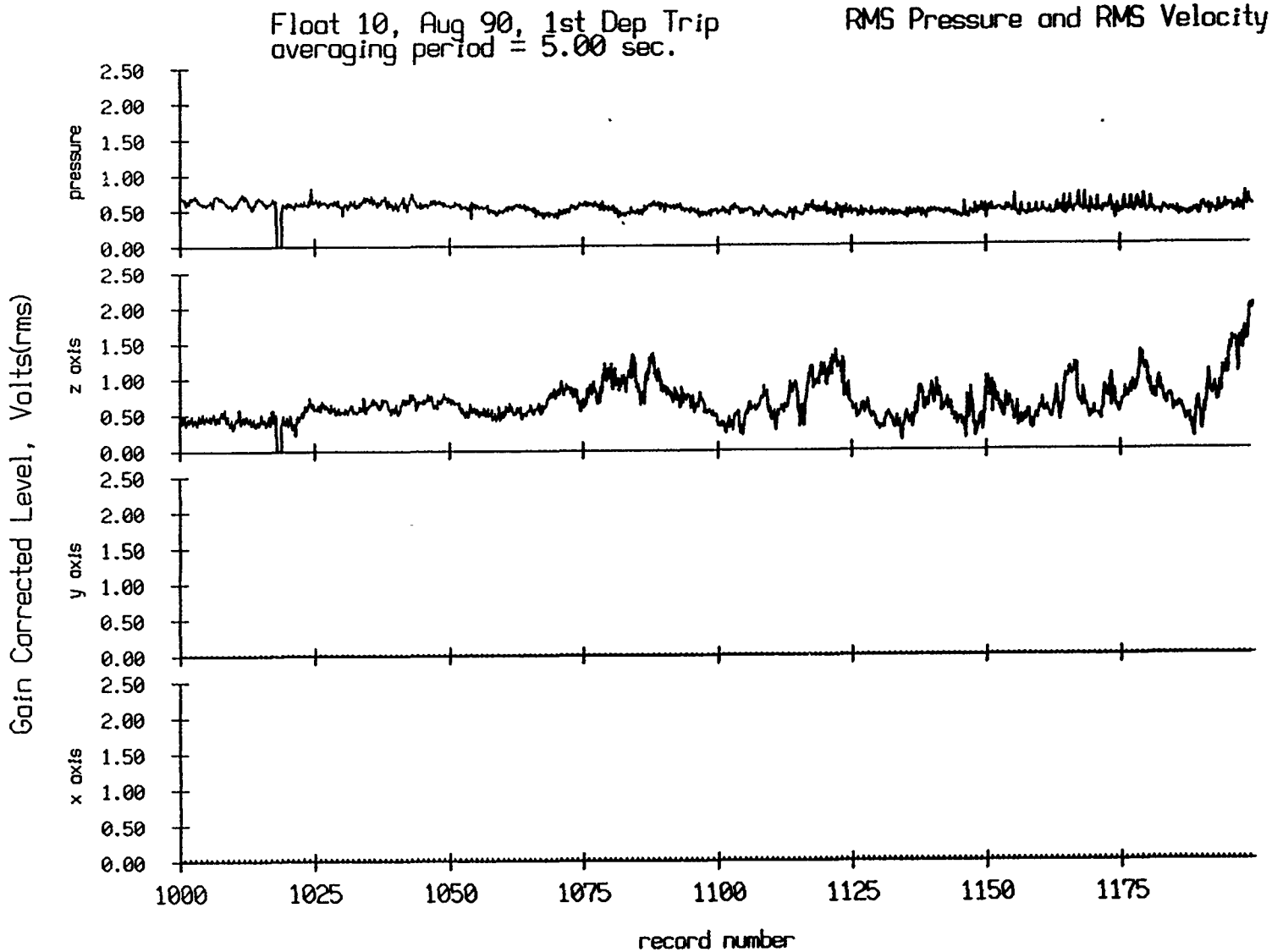

Figure VIII.11c

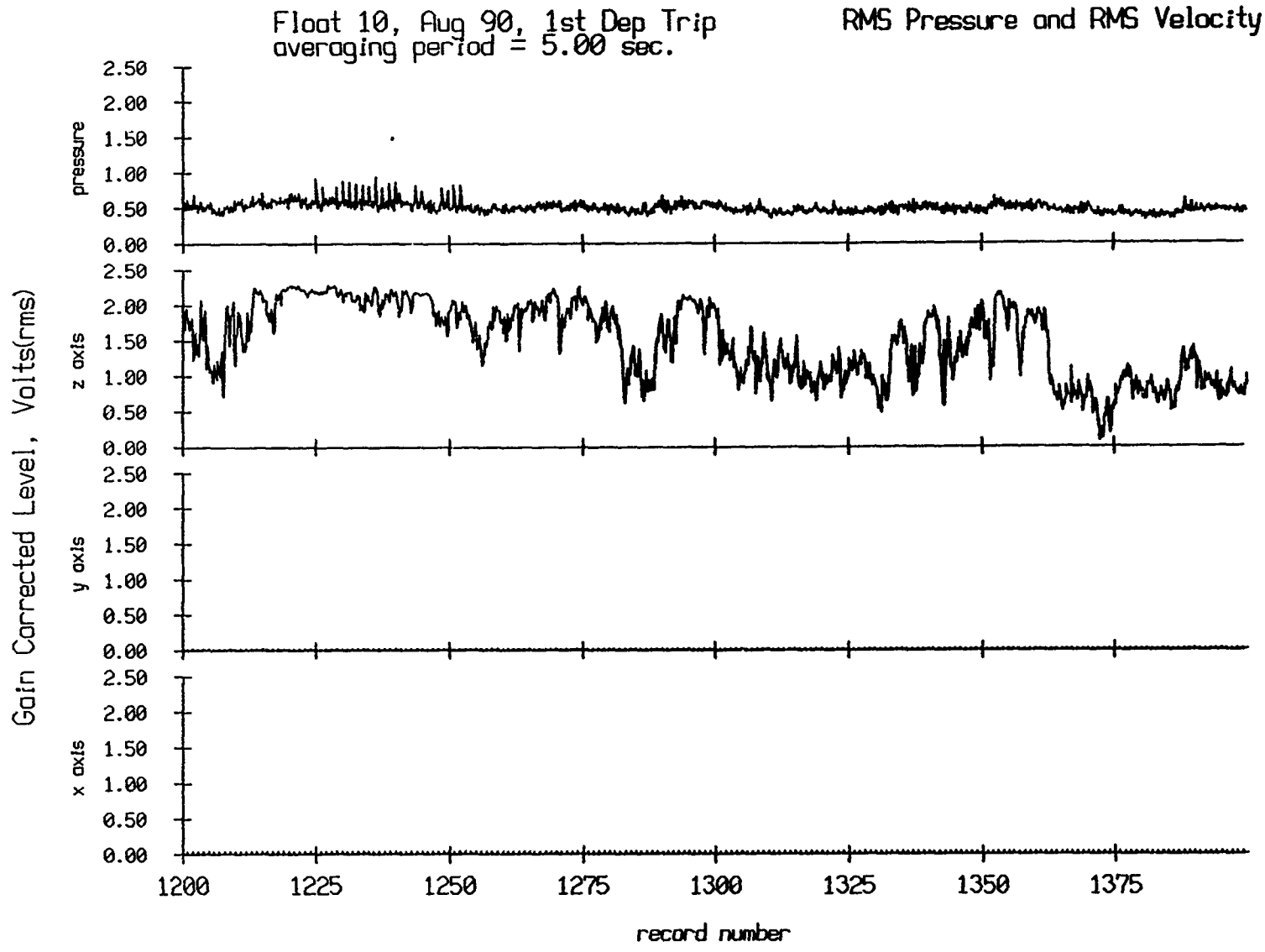

Figure VIII.11d

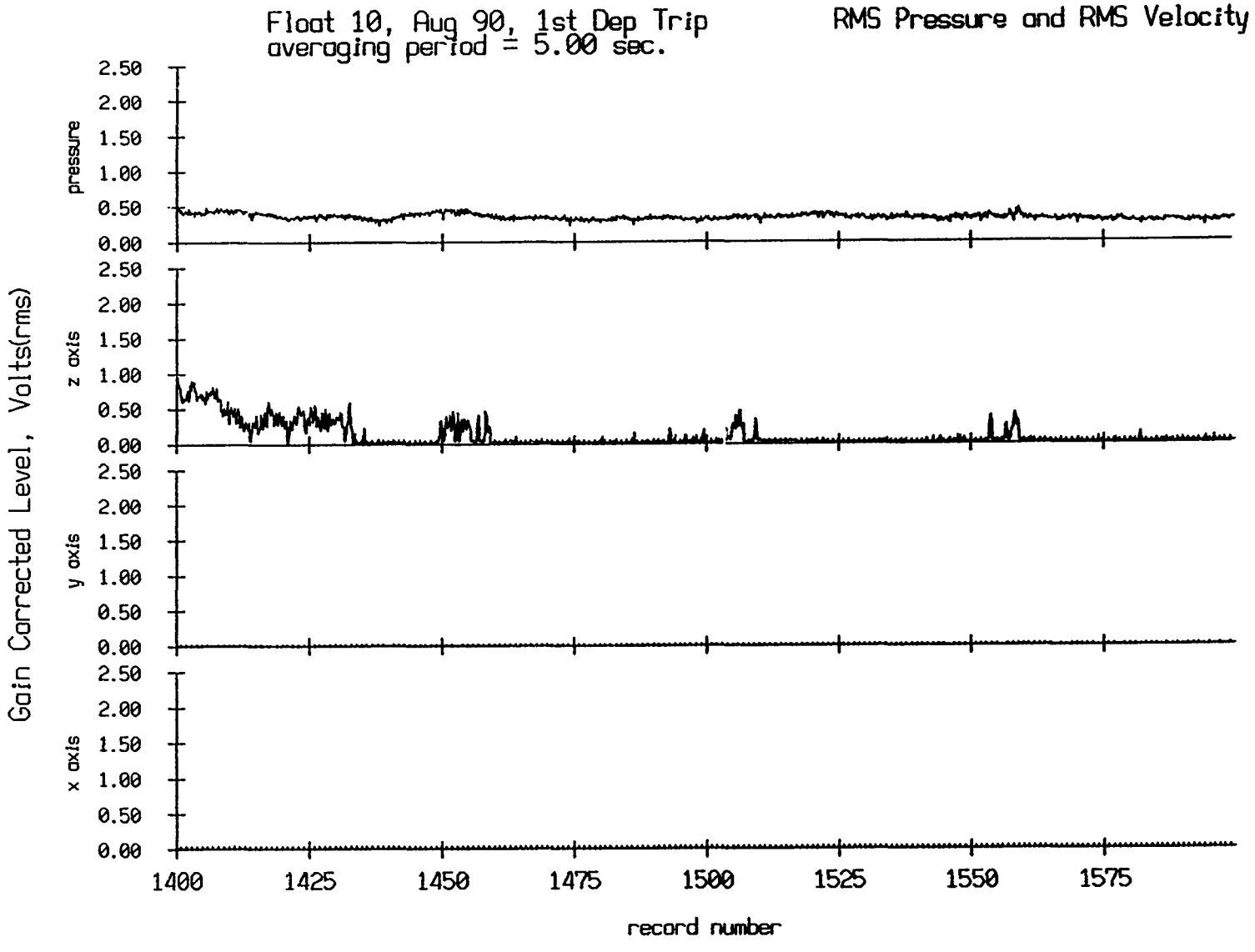

Figure VIII.11e

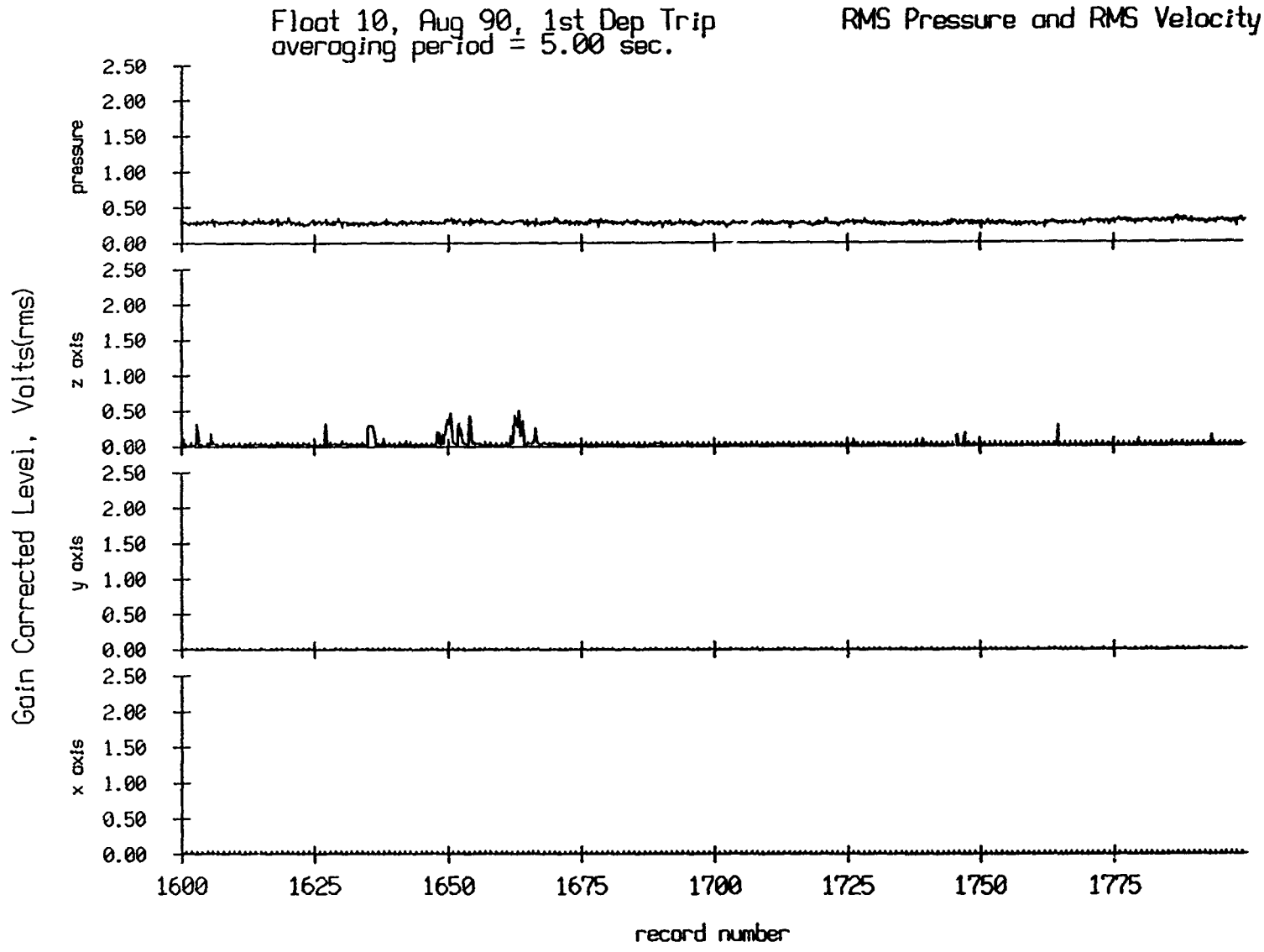

Figure VIII.11f

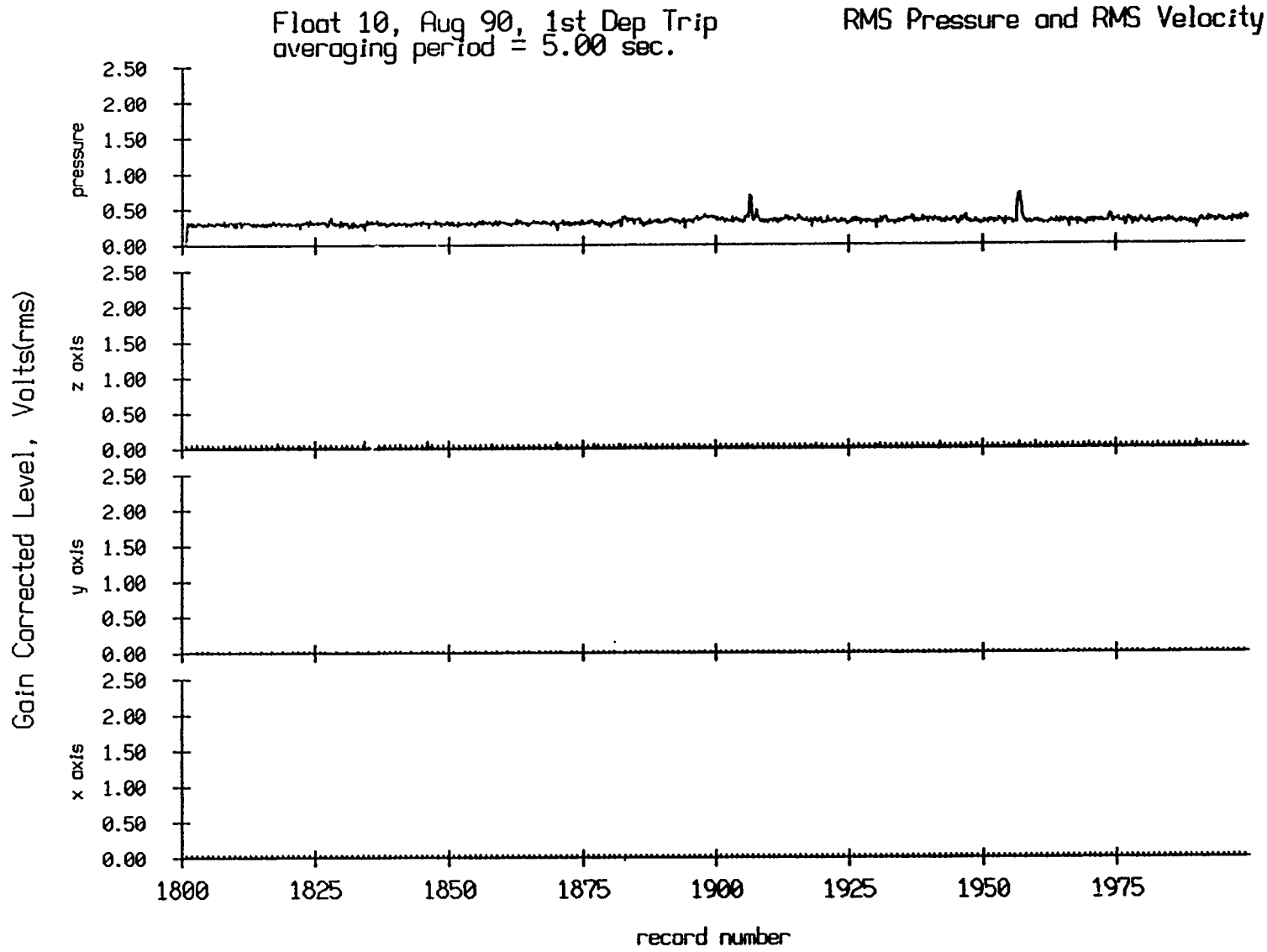

Figure VIII.11g

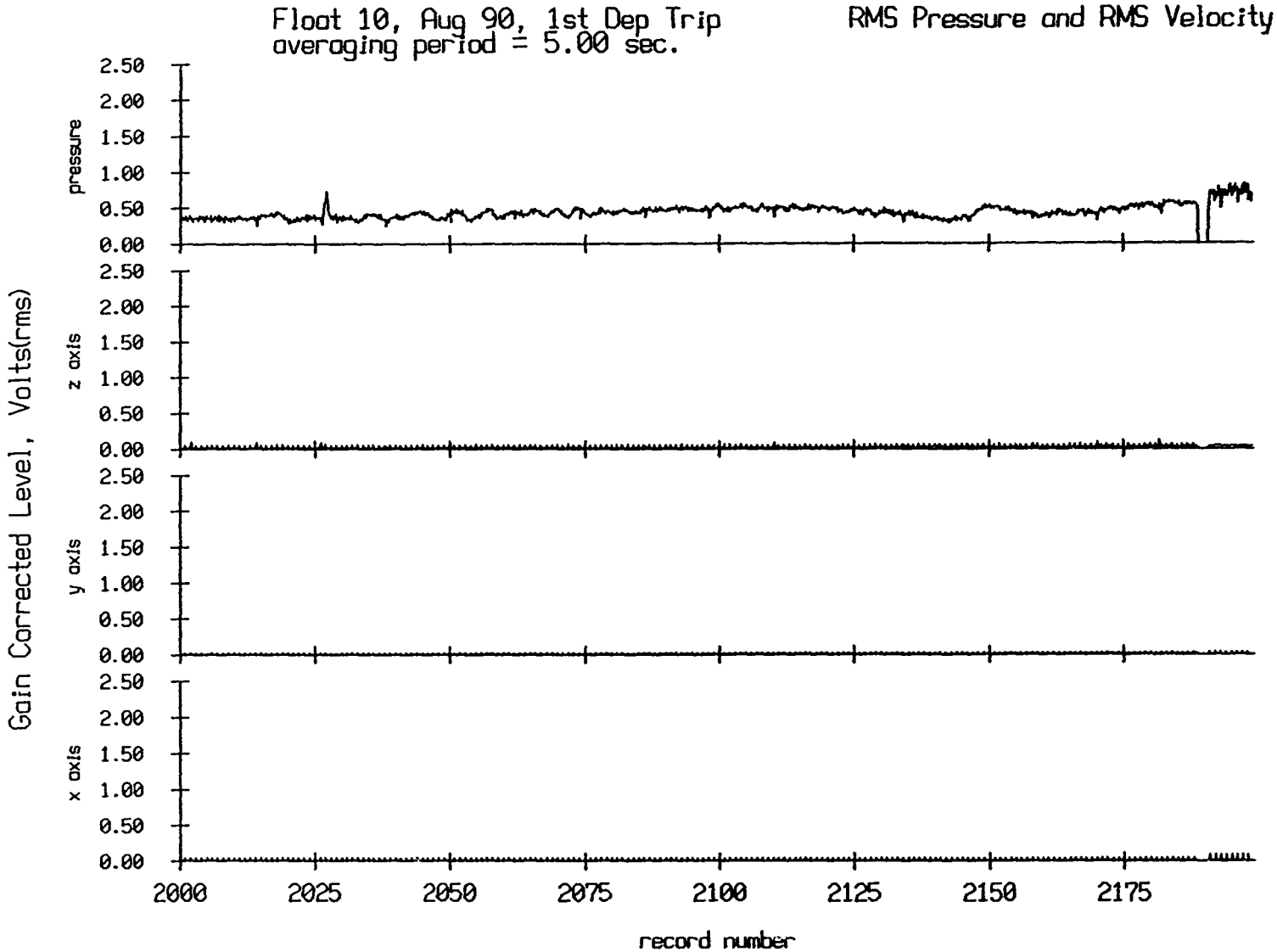

Figure VIII.11h

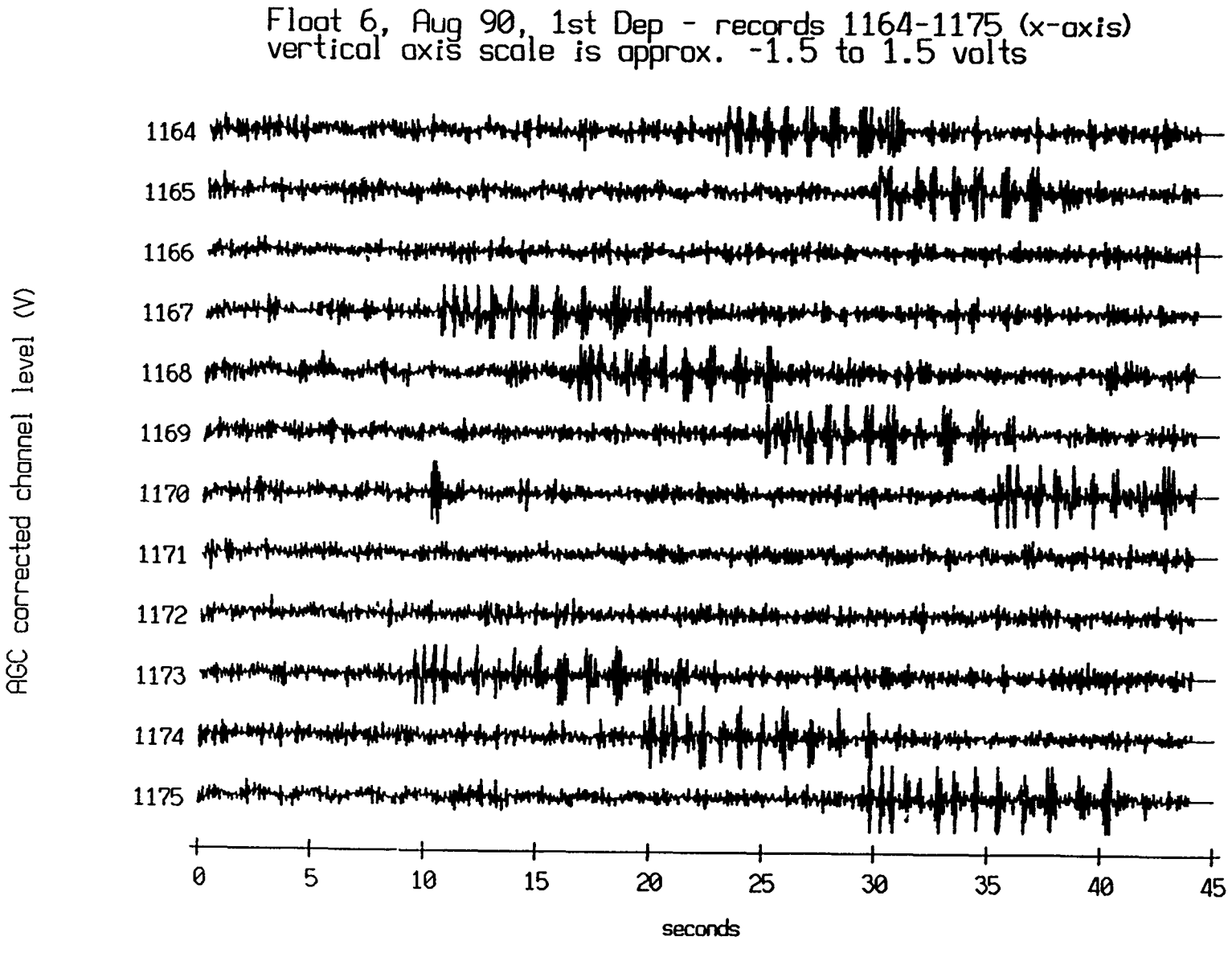
Float 6, Aug 90, 1st Dep - records 1164-1175 (x-axis)
vertical axis scale is approx. -1.5 to 1.5 volts
AGC corrected channel level (V)
1164
1165
1166
1167
1168
1169
1170
1171
1172
1173
1174
1175
0
5
10
15
20
25
30
35
40
45
seconds

Figure IX.1a

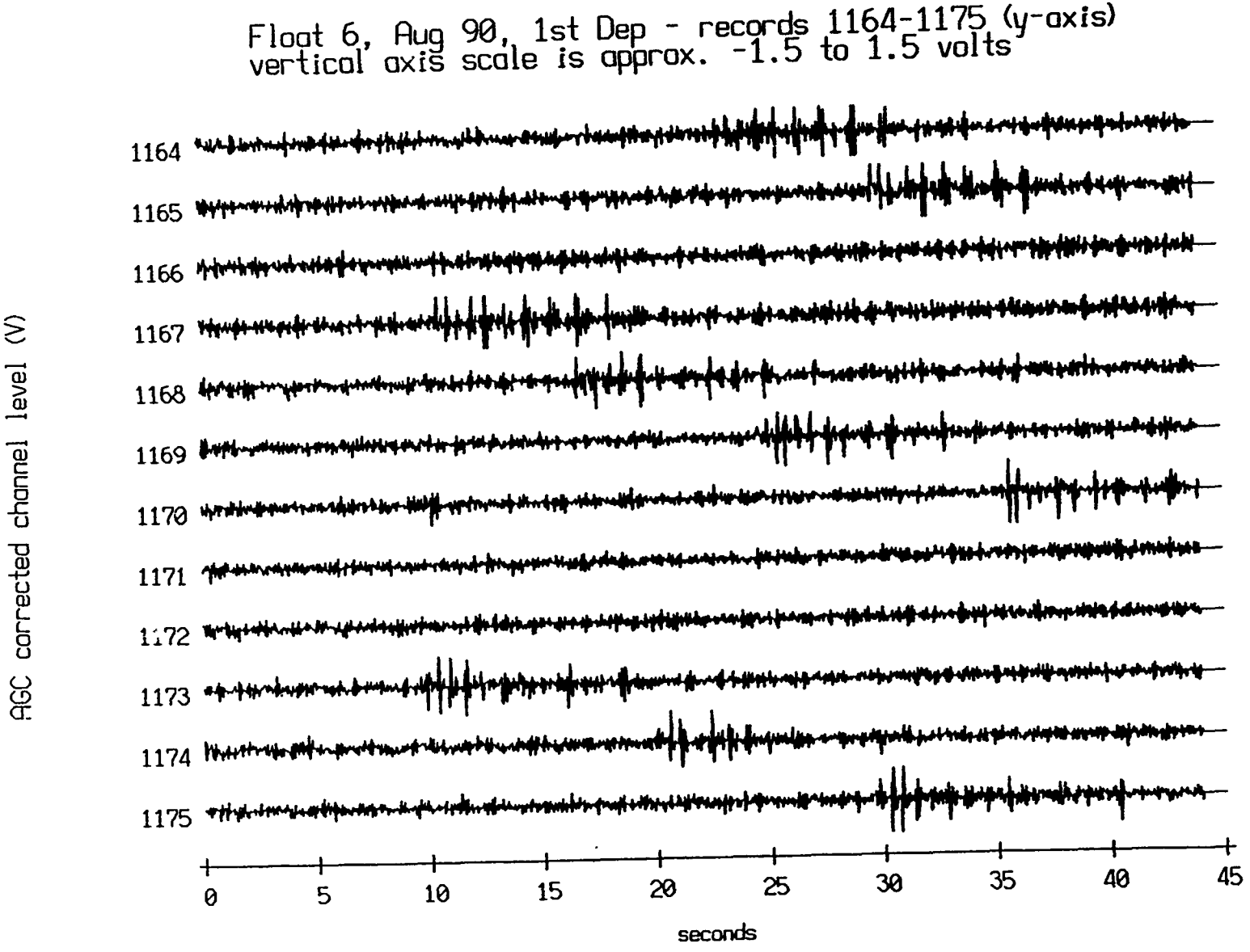
Float 6, Aug 90, 1st Dep - records 1164-1175 (y-axis)
vertical axis scale is approx. -1.5 to 1.5 volts
AGC corrected channel level (V)
1164
1165
1166
1167
1168
1169
1170
1171
1172
1173
1174
1175
0
5
10
15
20
25
30
35
40
45
seconds

Figure IX.1b

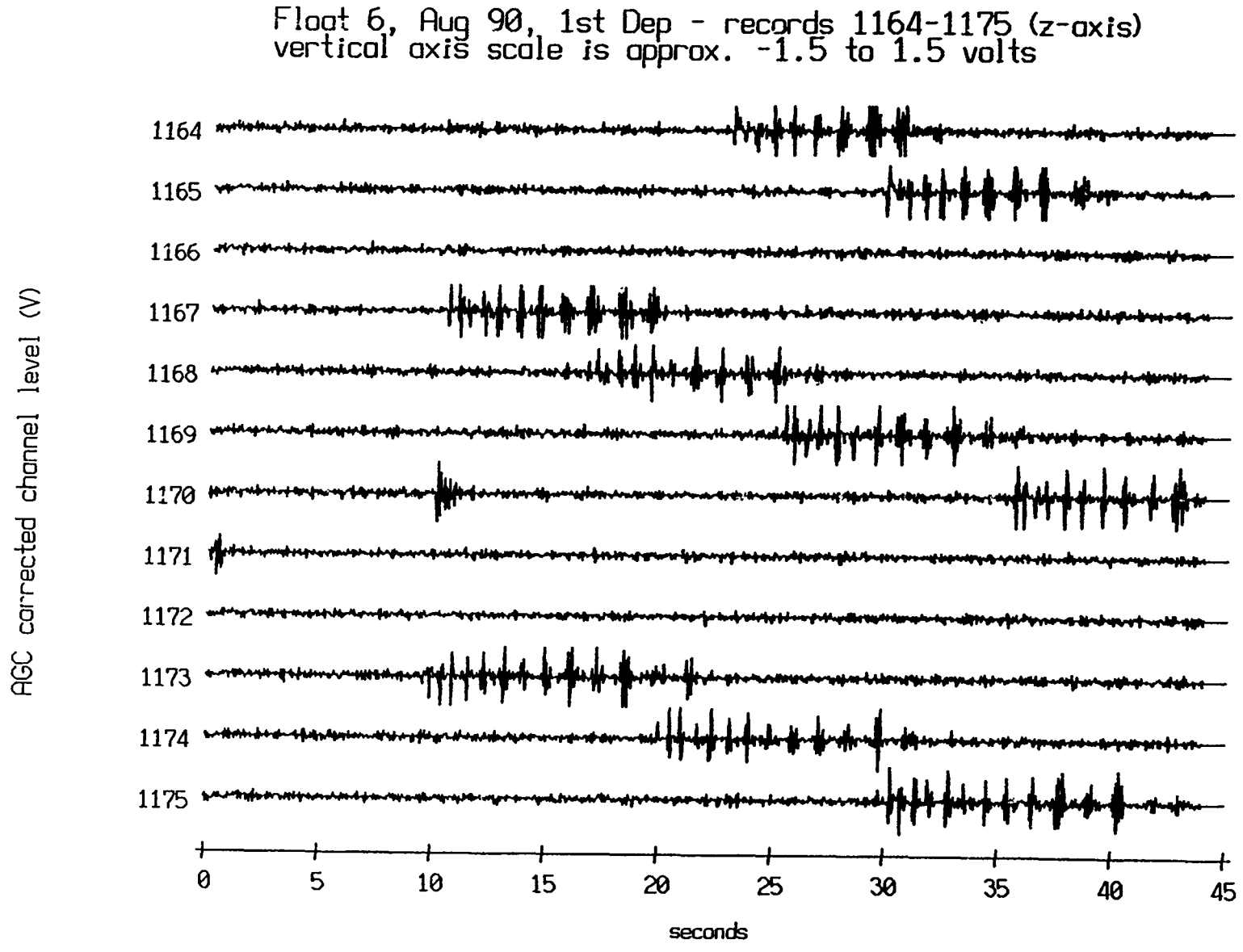
Float 6, Aug 90, 1st Dep - records 1164-1175 (z-axis)
vertical axis scale is approx. -1.5 to 1.5 volts
AGC corrected channel level (V)
1164
1165
1166
1167
1168
1169
1170
1171
1172
1173
1174
1175
0
5
10
15
20
25
30
35
40
45
seconds

Figure IX.1c

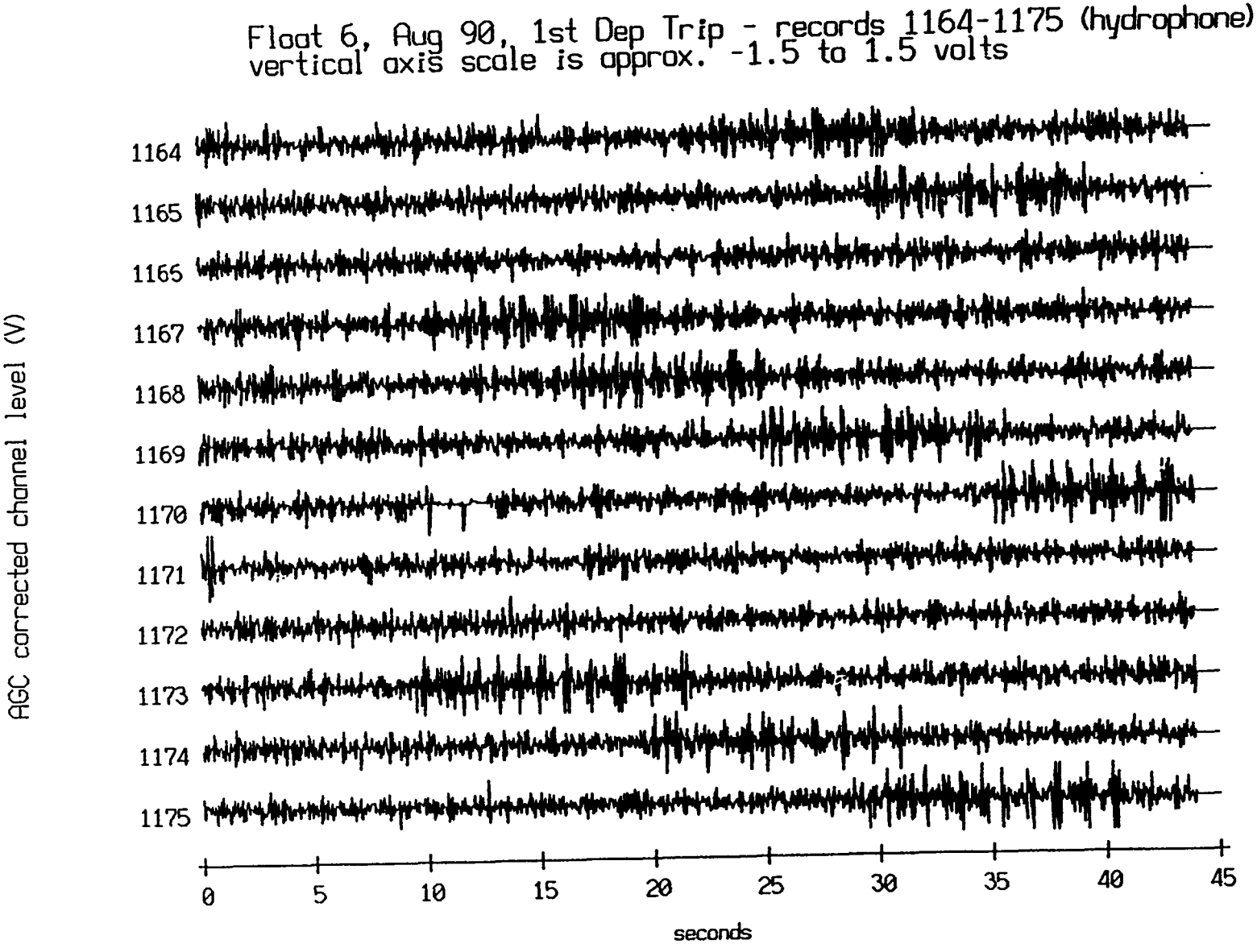
Float 6, Aug 90, 1st Dep Trip - records 1164-1175 (hydrophone)
vertical axis scale is approx. -1.5 to 1.5 volts
AGC corrected channel level (V)
1164
1165
1166
1167
1168
1169
1170
1171
1172
1173
1174
1175
0
5
10
15
20
25
30
35
40
45
seconds

Figure IX.1d

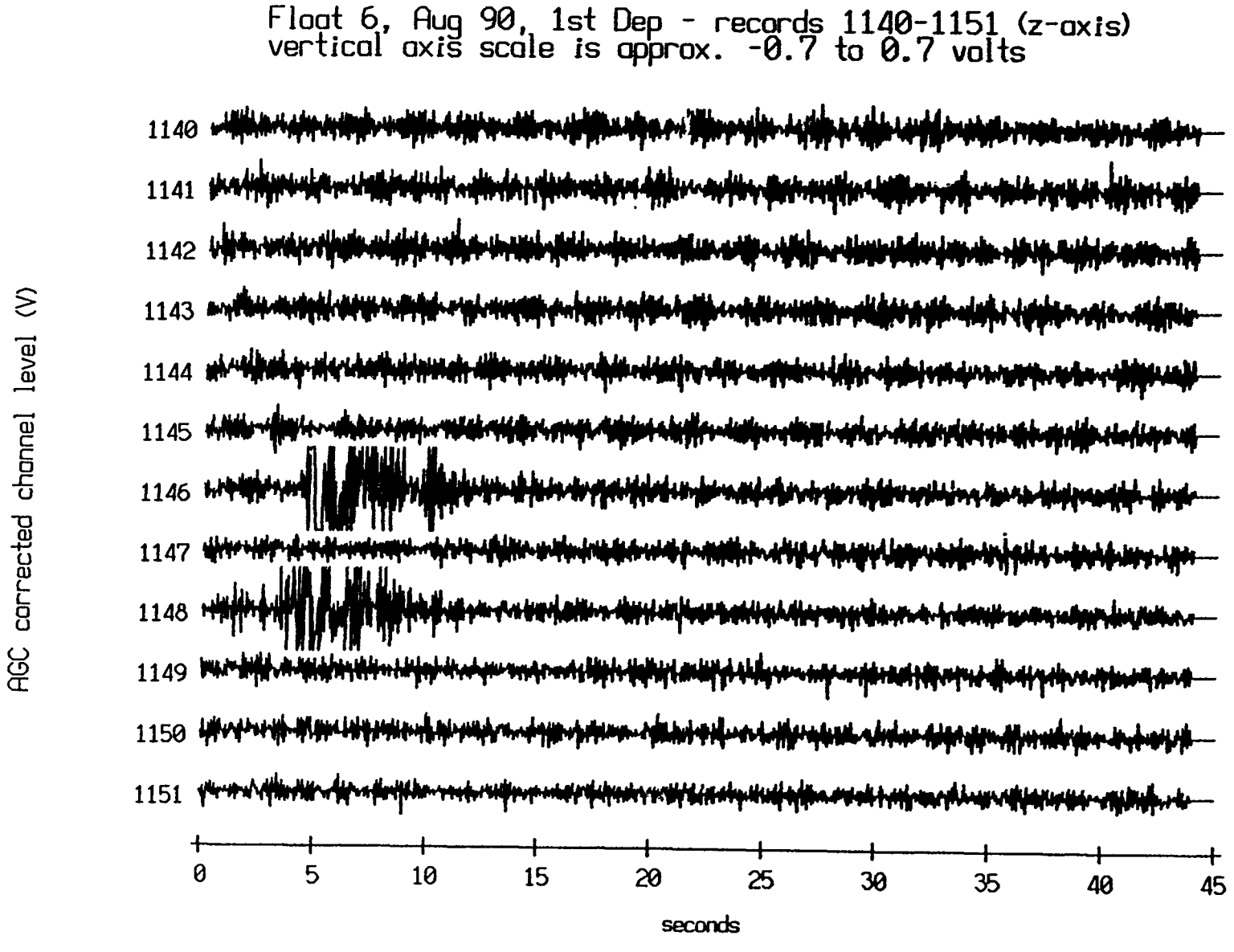
Float 6, Aug 90, 1st Dep - records 1140-1151 (z-axis)
vertical axis scale is approx. -0.7 to 0.7 volts
AGC corrected channel level (V)
1140
1141
1142
1143
1144
1145
1146
1147
1148
1149
1150
1151
0
5
10
15
20
25
30
35
40
45
seconds

Figure IX.2a

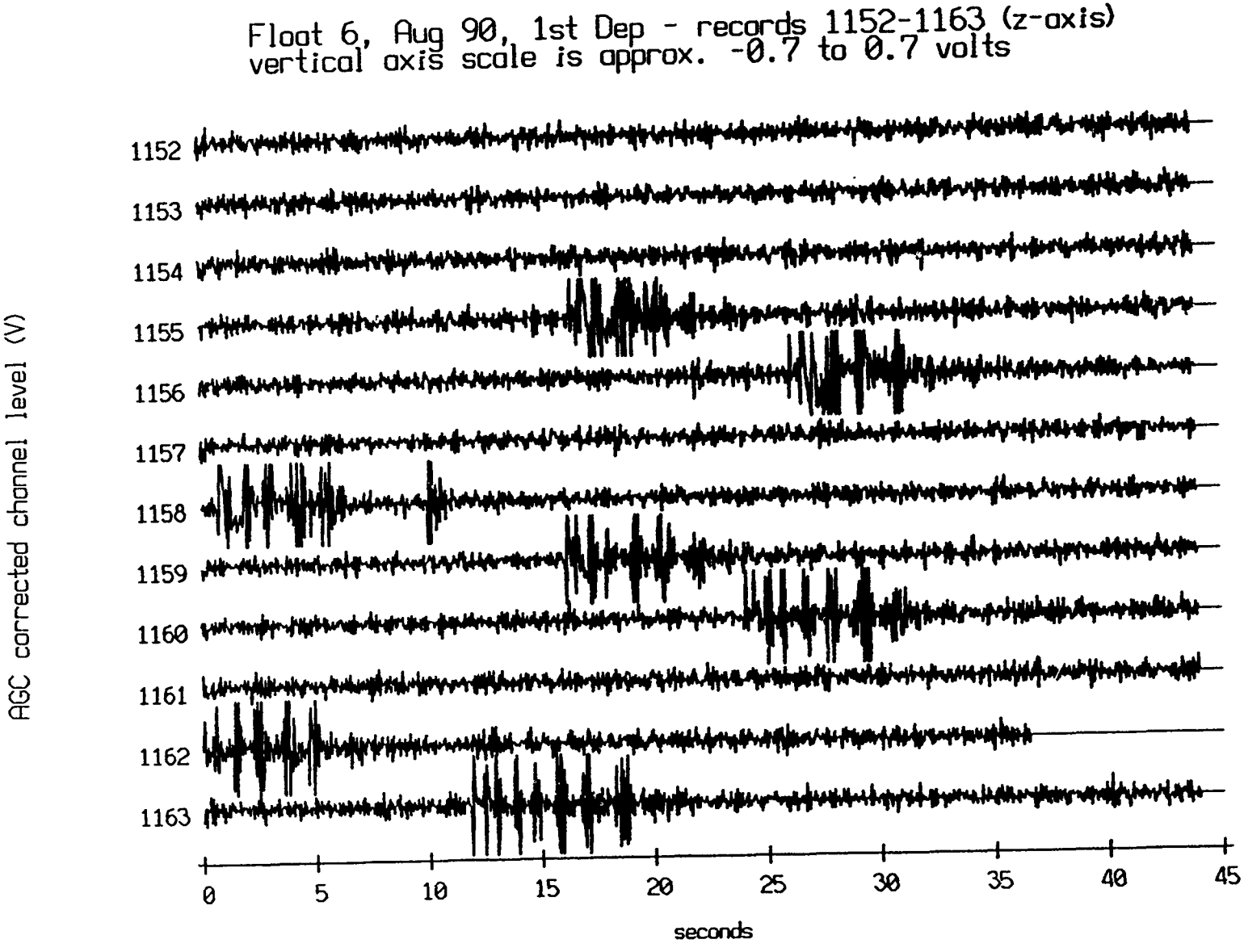
Float 6, Aug 90, 1st Dep - records 1152-1163 (z-axis)
vertical axis scale is approx. -0.7 to 0.7 volts
AGC corrected channel level (V)
1152
1153
1154
1155
1156
1157
1158
1159
1160
1161
1162
1163
0
5
10
15
20
25
30
35
40
45
seconds

Figure IX.2b

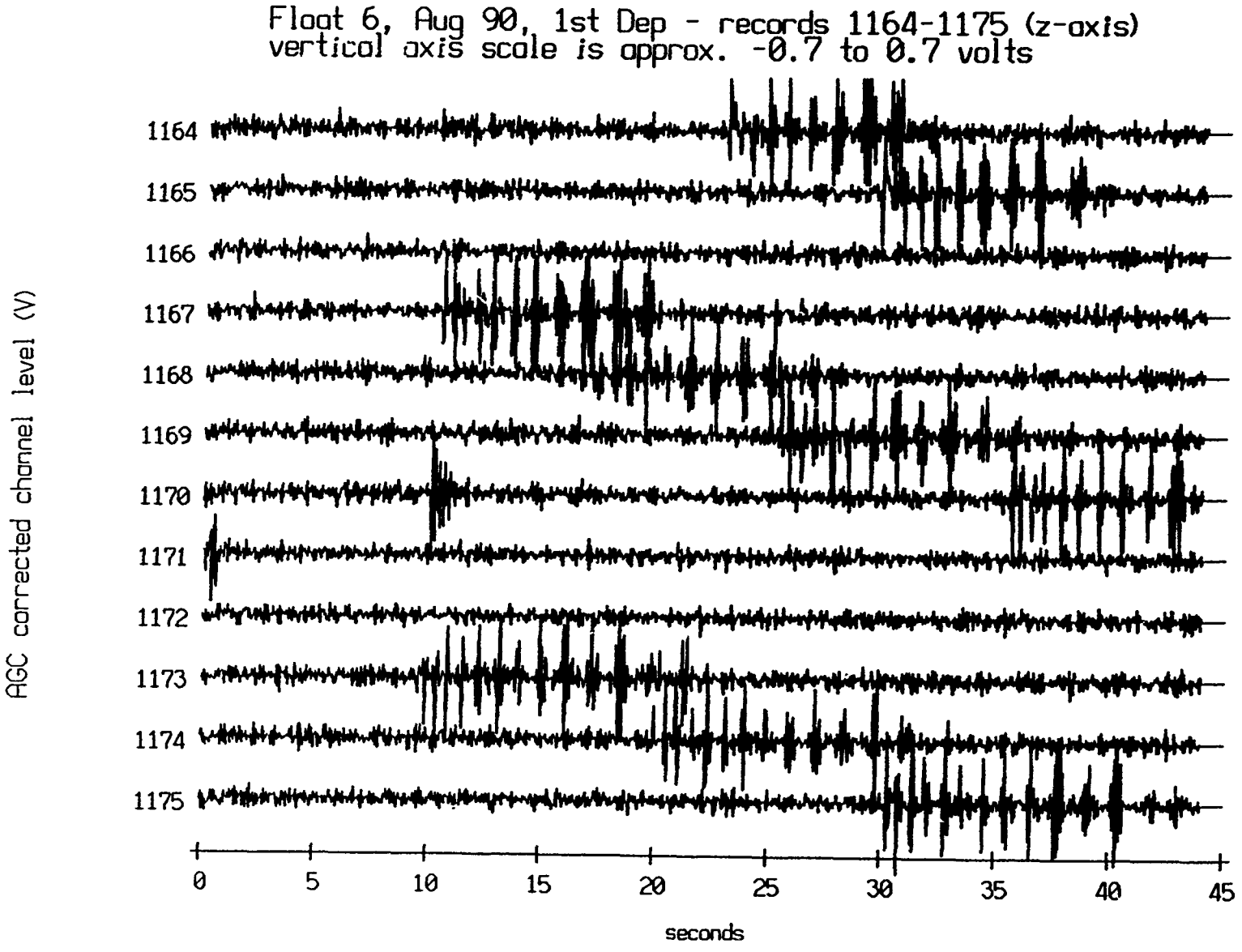
Float 6, Aug 90, 1st Dep - records 1164-1175 (z-axis)
vertical axis scale is approx. -0.7 to 0.7 volts
AGC corrected channel level (V)
1164
1165
1166
1167
1168
1169
1170
1171
1172
1173
1174
1175
0
5
10
15
20
25
30
35
40
45
seconds

Figure IX.2c

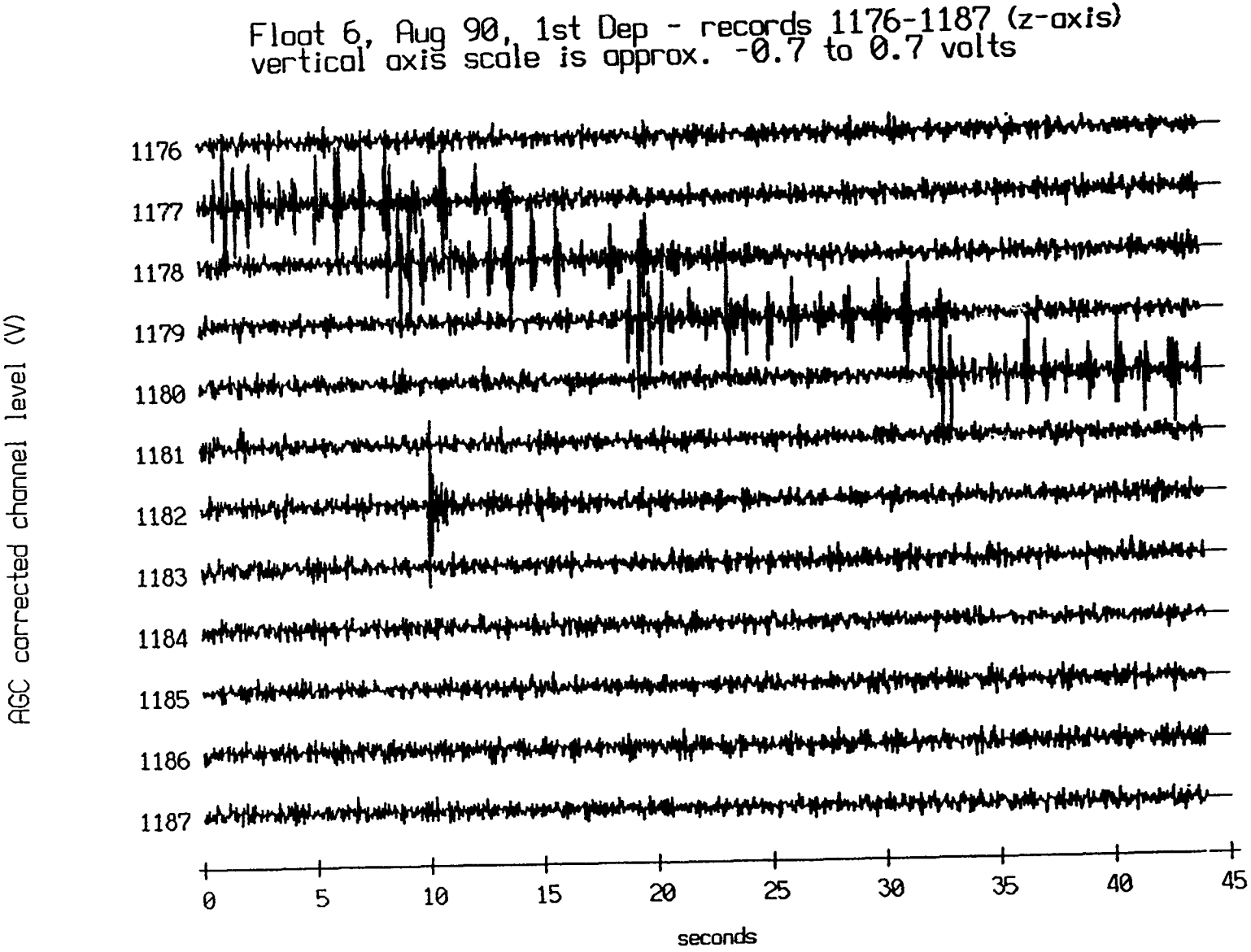
Float 6, Aug 90, 1st Dep - records 1176-1187 (z-axis)
vertical axis scale is approx. -0.7 to 0.7 volts
AGC corrected channel level (V)
1176
1177
1178
1179
1180
1181
1182
1183
1184
1185
1186
1187
0
5
10
15
20
25
30
35
40
45
seconds

Figure IX.2d

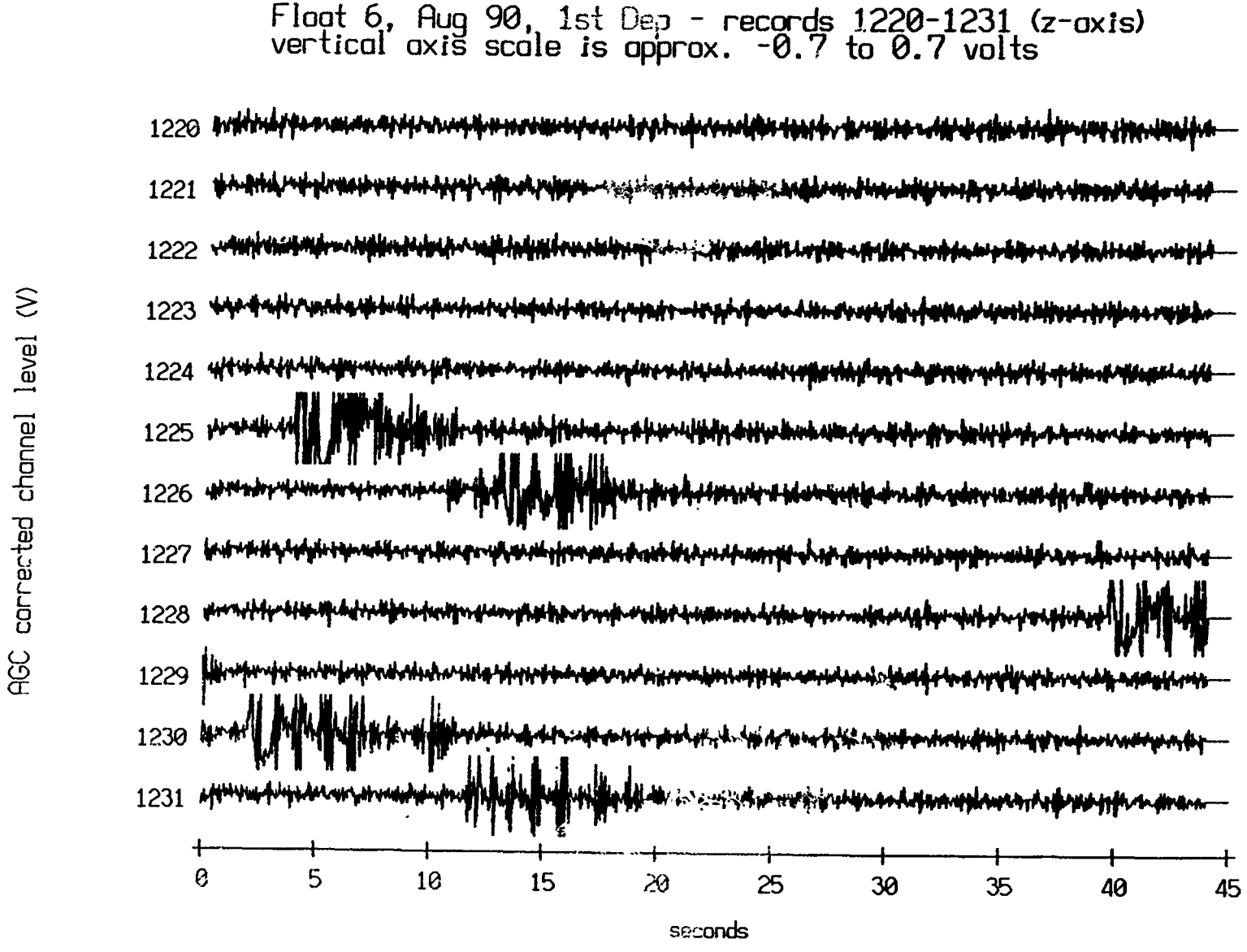
Float 6, Aug 90, 1st Dep - records 1220-1231 (z-axis)
vertical axis scale is approx. -0.7 to 0.7 volts
AGC corrected channel level (V)
1220
1221
1222
1223
1224
1225
1226
1227
1228
1229
1230
1231
0
5
10
15
20
25
30
35
40
45
seconds

Figure IX.3a

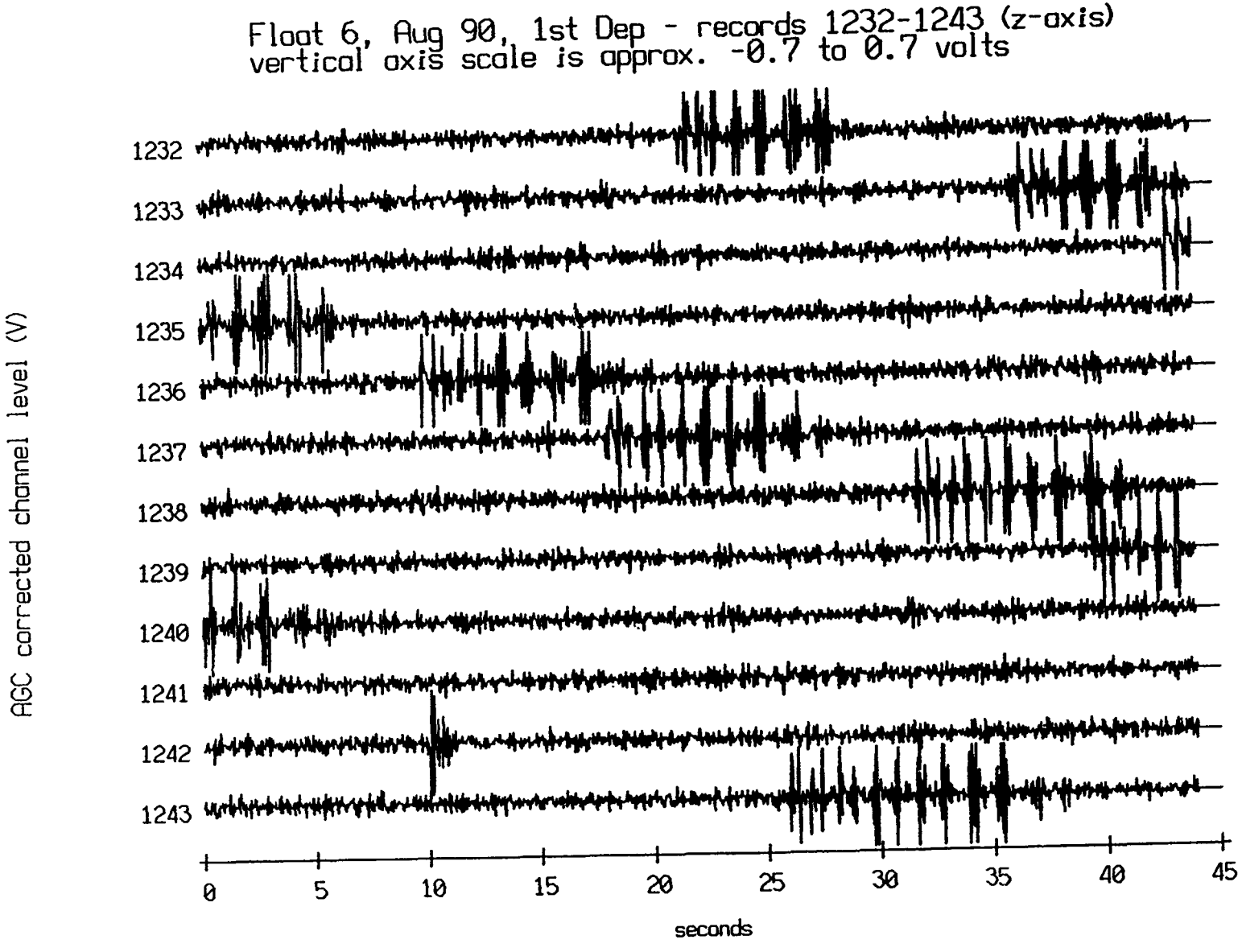
Float 6, Aug 90, 1st Dep - records 1232-1243 (z-axis)
vertical axis scale is approx. -0.7 to 0.7 volts
1232
1233
1234
1235
1236
1237
1238
1239
1240
1241
1242
1243
0
5
10
15
20
25
30
35
40
45
seconds
AGC corrected channel level (V)

Figure IX.3b

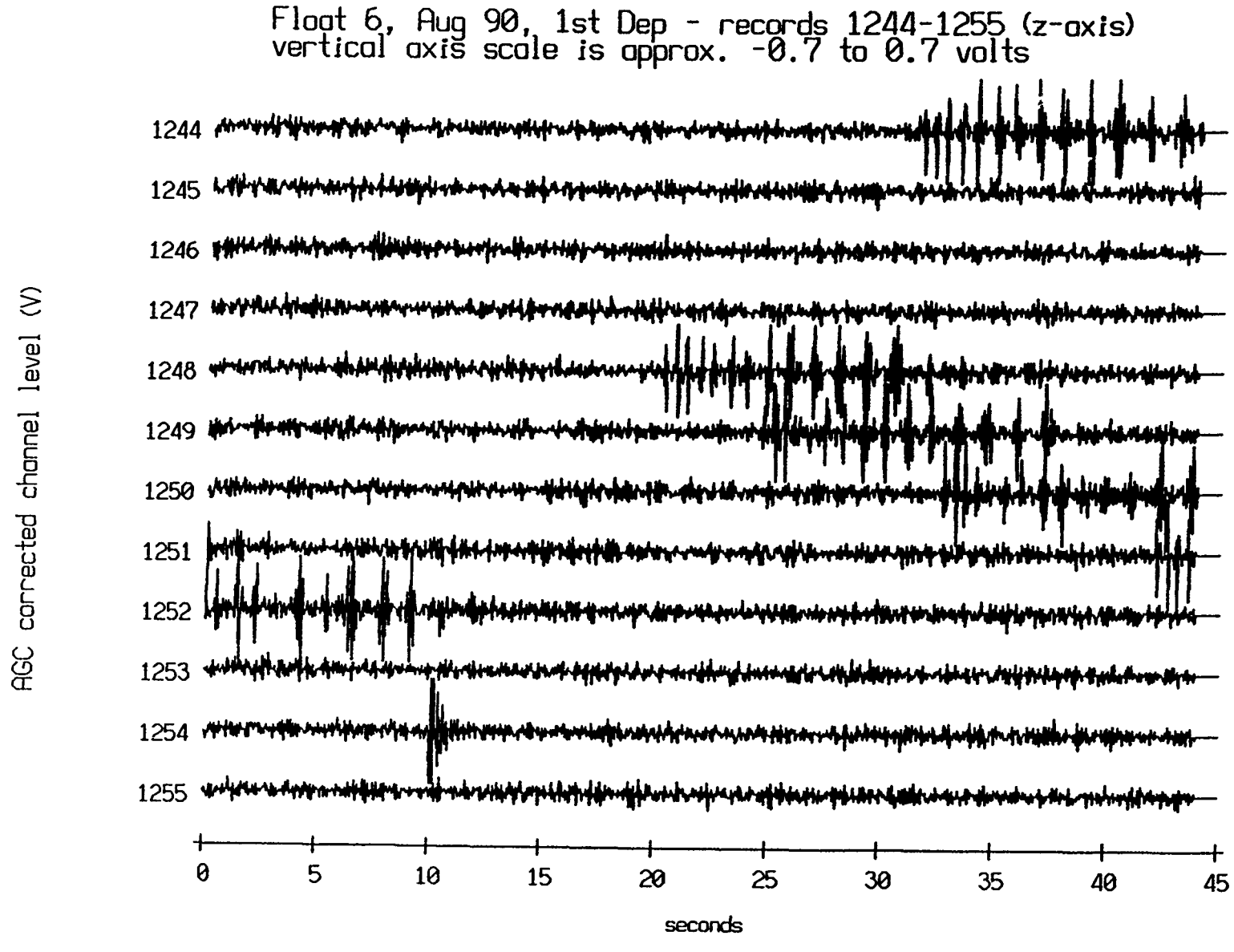
Float 6, Aug 90, 1st Dep - records 1244-1255 (z-axis)
vertical axis scale is approx. -0.7 to 0.7 volts
AGC corrected channel level (V)
1244
1245
1246
1247
1248
1249
1250
1251
1252
1253
1254
1255
0
5
10
15
20
25
30
35
40
45
seconds

Figure IX.3c

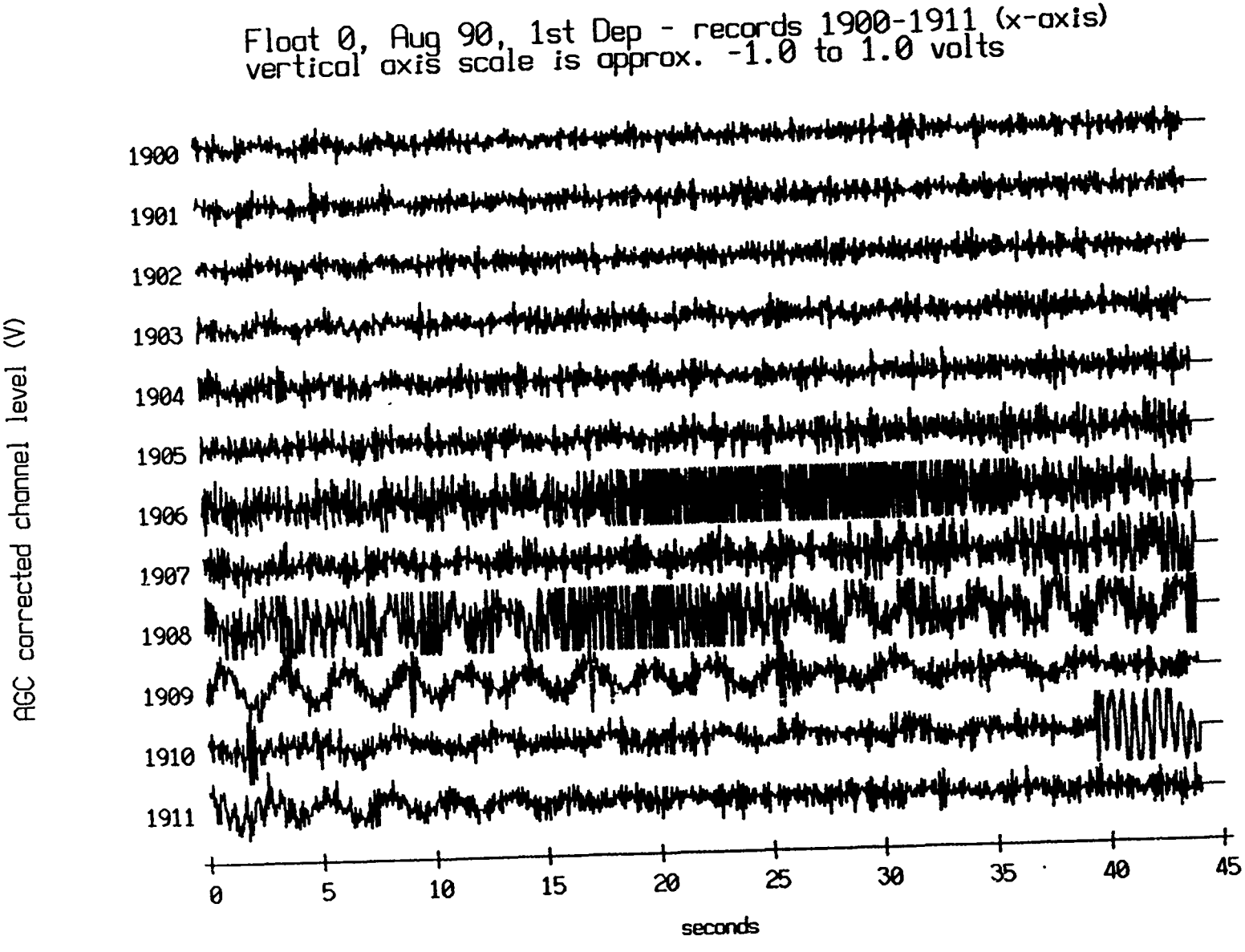
Float 0, Aug 90, 1st Dep - records 1900-1911 (x-axis)
vertical axis scale is approx. -1.0 to 1.0 volts
AGC corrected channel level (V)
1900
1901
1902
1903
1904
1905
1906
1907
1908
1909
1910
1911
0
5
10
15
20
25
30
35
40
45
seconds

Figure IX.4a

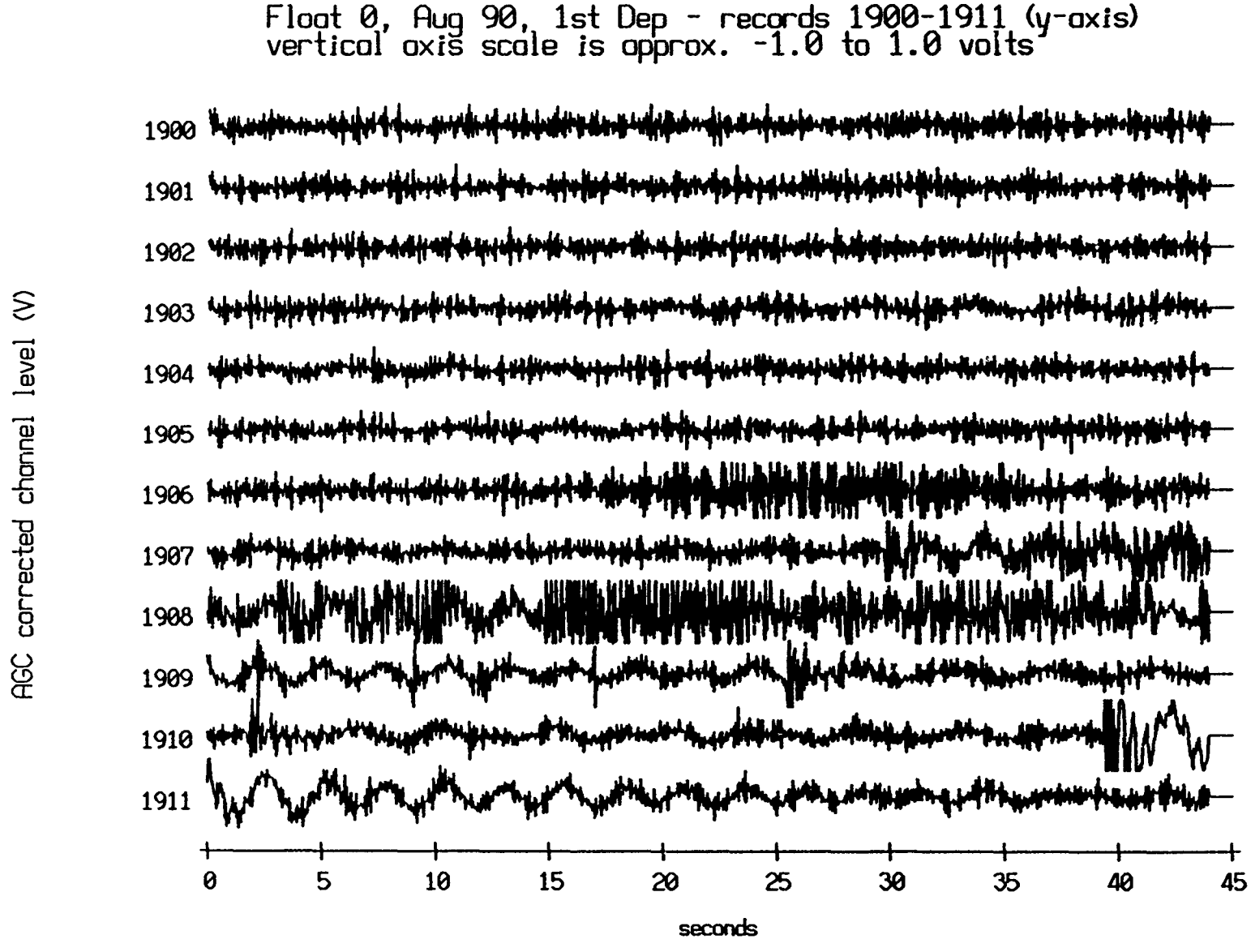
Float 0, Aug 90, 1st Dep - records 1900-1911 (y-axis)
vertical axis scale is approx. -1.0 to 1.0 volts
AGC corrected channel level (V)
1900
1901
1902
1903
1904
1905
1906
1907
1908
1909
1910
1911
0
5
10
15
20
25
30
35
40
45
seconds

Figure IX.4b

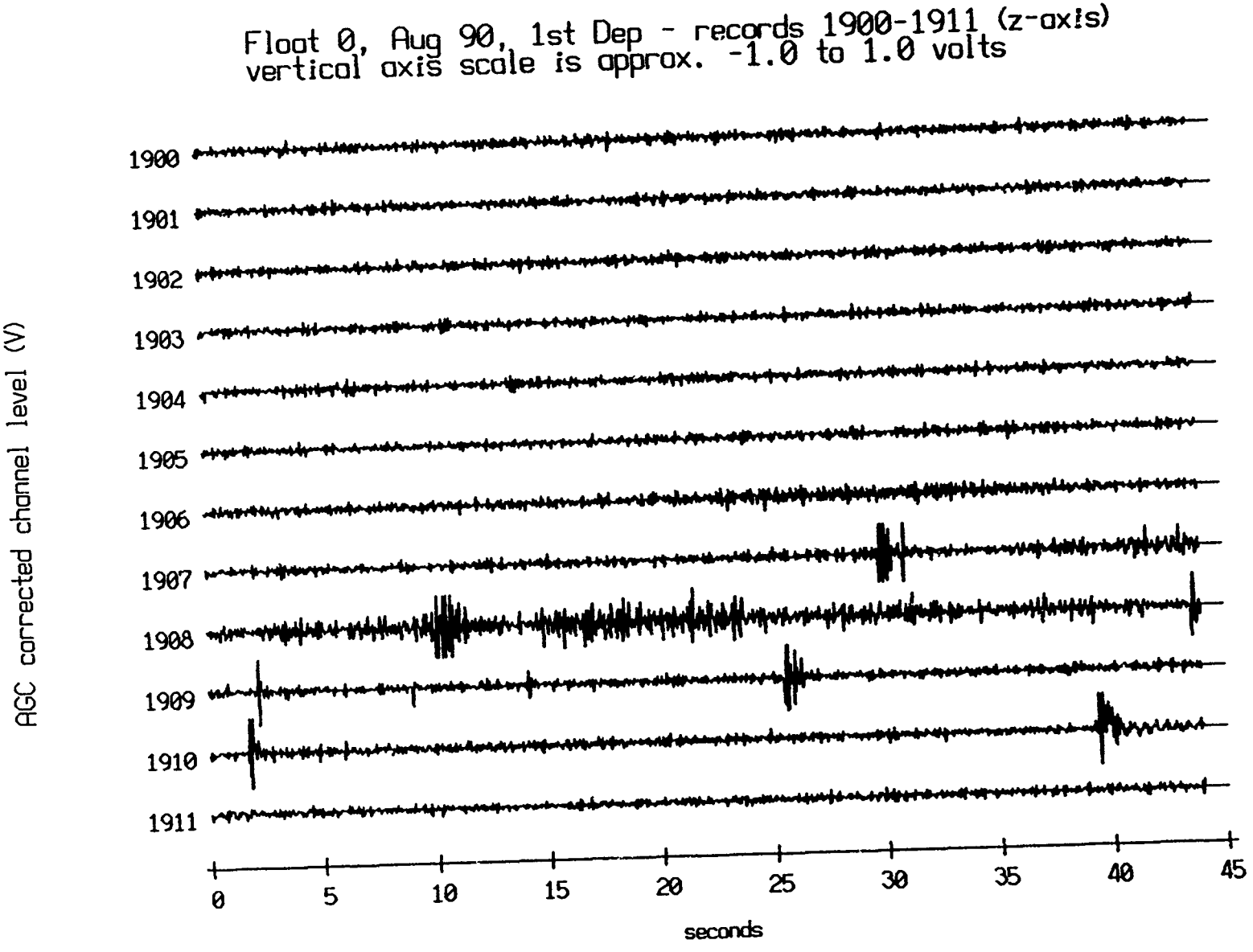
Float 0, Aug 90, 1st Dep - records 1900-1911 (z-axis)
vertical axis scale is approx. -1.0 to 1.0 volts
AGC corrected channel level (V)
1900
1901
1902
1903
1904
1905
1906
1907
1908
1909
1910
1911
0
5
10
15
20
25
30
35
40
45
seconds

Figure IX.4c

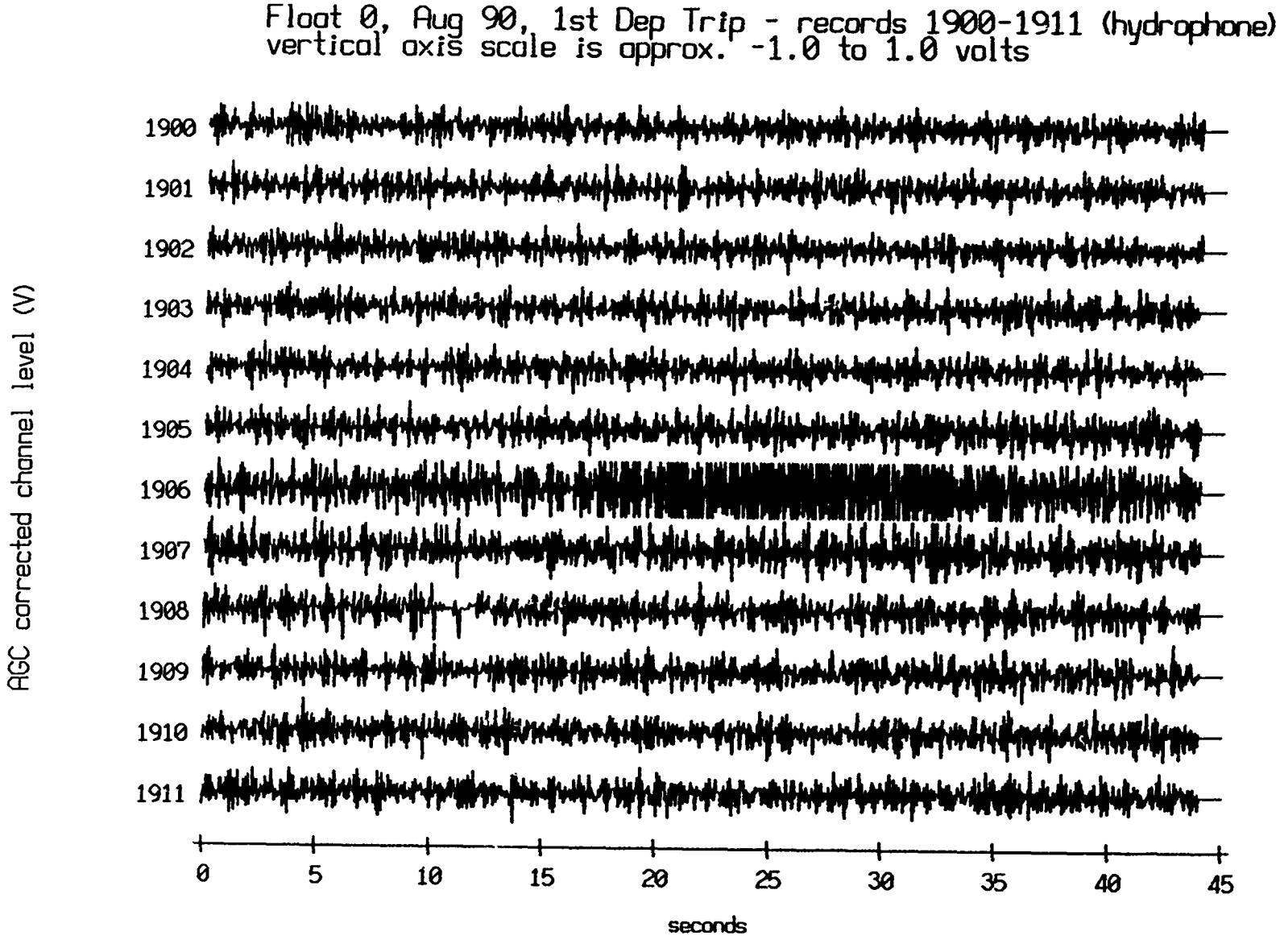
Float 0, Aug 90, 1st Dep Trip - records 1900-1911 (hydrophone)
vertical axis scale is approx. -1.0 to 1.0 volts
AGC corrected channel level (V)
1900
1901
1902
1903
1904
1905
1906
1907
1908
1909
1910
1911
0
5
10
15
20
25
30
35
40
45
seconds

Figure IX.4d

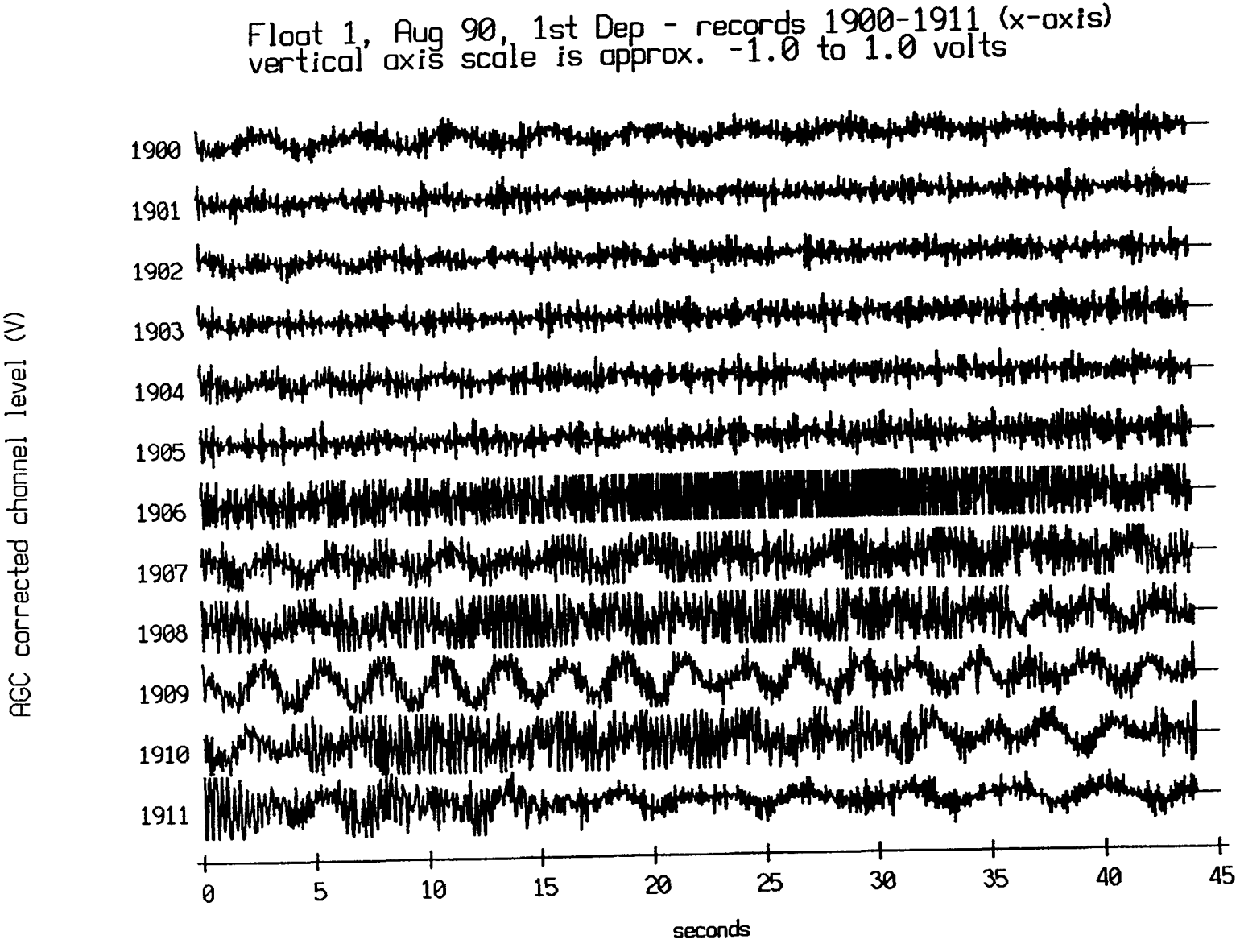
Float 1, Aug 90, 1st Dep - records 1900-1911 (x-axis)
vertical axis scale is approx. -1.0 to 1.0 volts
AGC corrected channel level (V)
1900
1901
1902
1903
1904
1905
1906
1907
1908
1909
1910
1911
0
5
10
15
20
25
30
35
40
45
seconds

Figure IX.5a

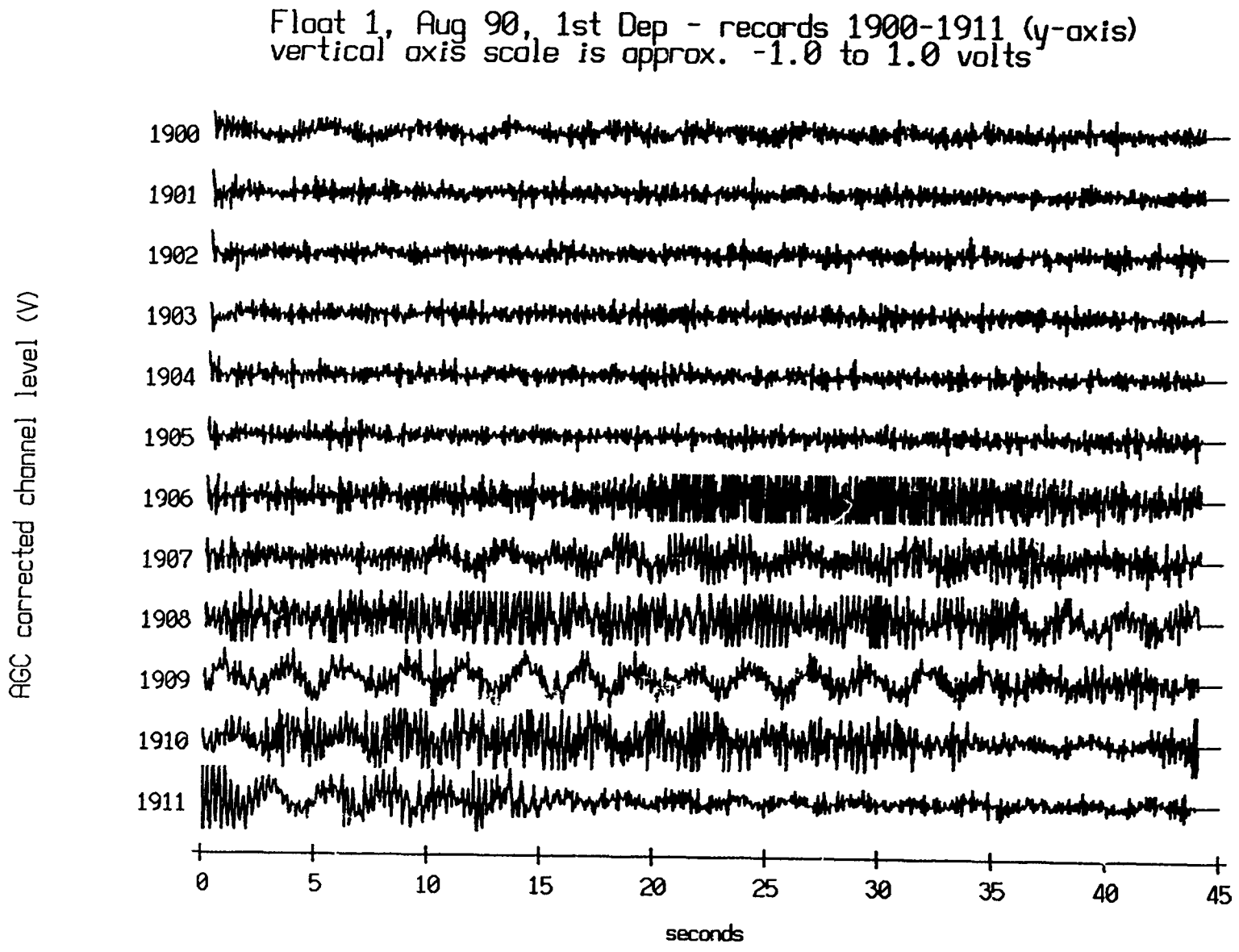
Float 1, Aug 90, 1st Dep - records 1900-1911 (y-axis)
vertical axis scale is approx. -1.0 to 1.0 volts
AGC corrected channel level (V)
1900
1901
1902
1903
1904
1905
1906
1907
1908
1909
1910
1911
0
5
10
15
20
25
30
35
40
45
seconds

Figure IX.5b

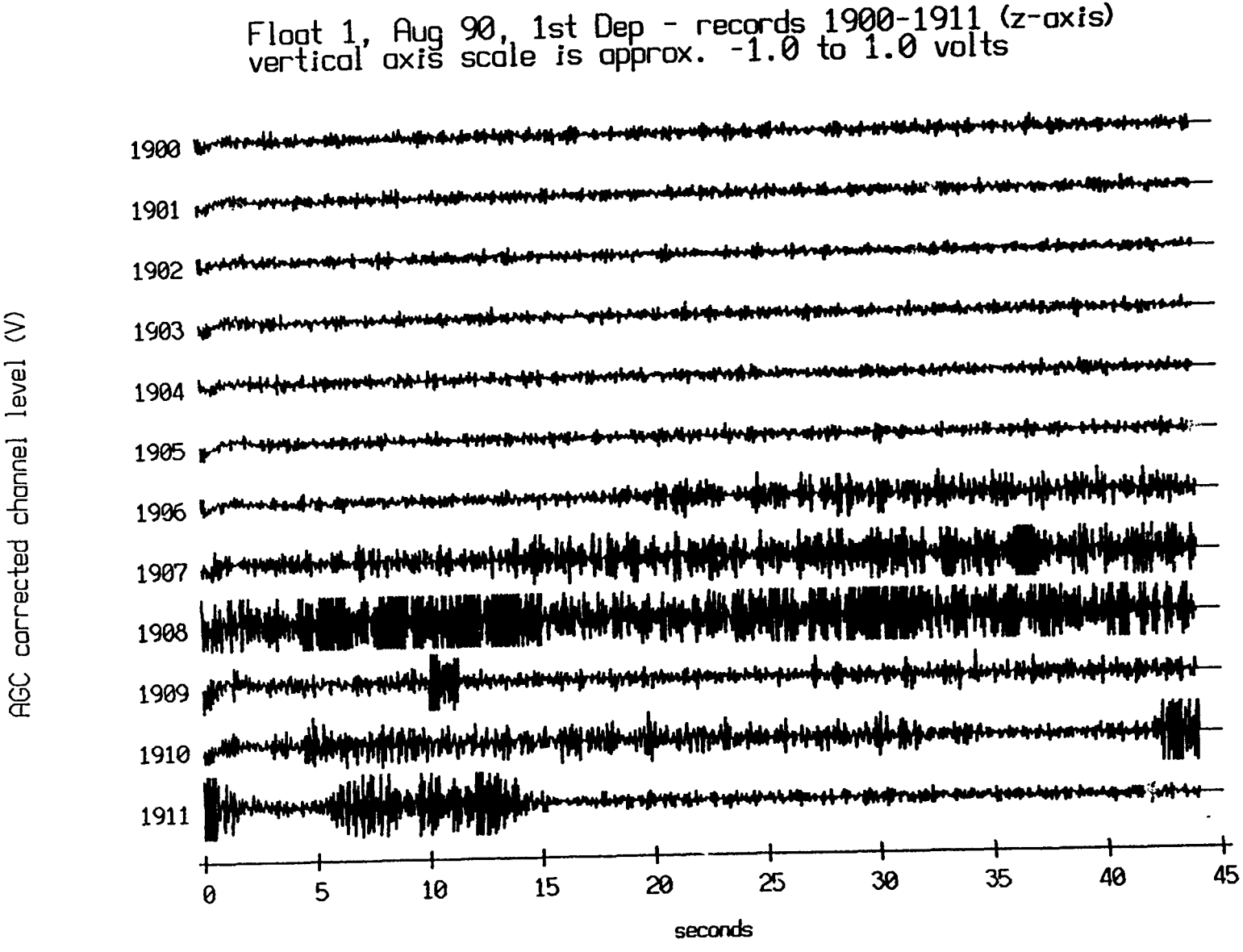
Float 1, Aug 90, 1st Dep - records 1900-1911 (z-axis)
vertical axis scale is approx. -1.0 to 1.0 volts
AGC corrected channel level (V)
1900
1901
1902
1903
1904
1905
1906
1907
1908
1909
1910
1911
0
5
10
15
20
25
30
35
40
45
seconds

Figure IX.5c

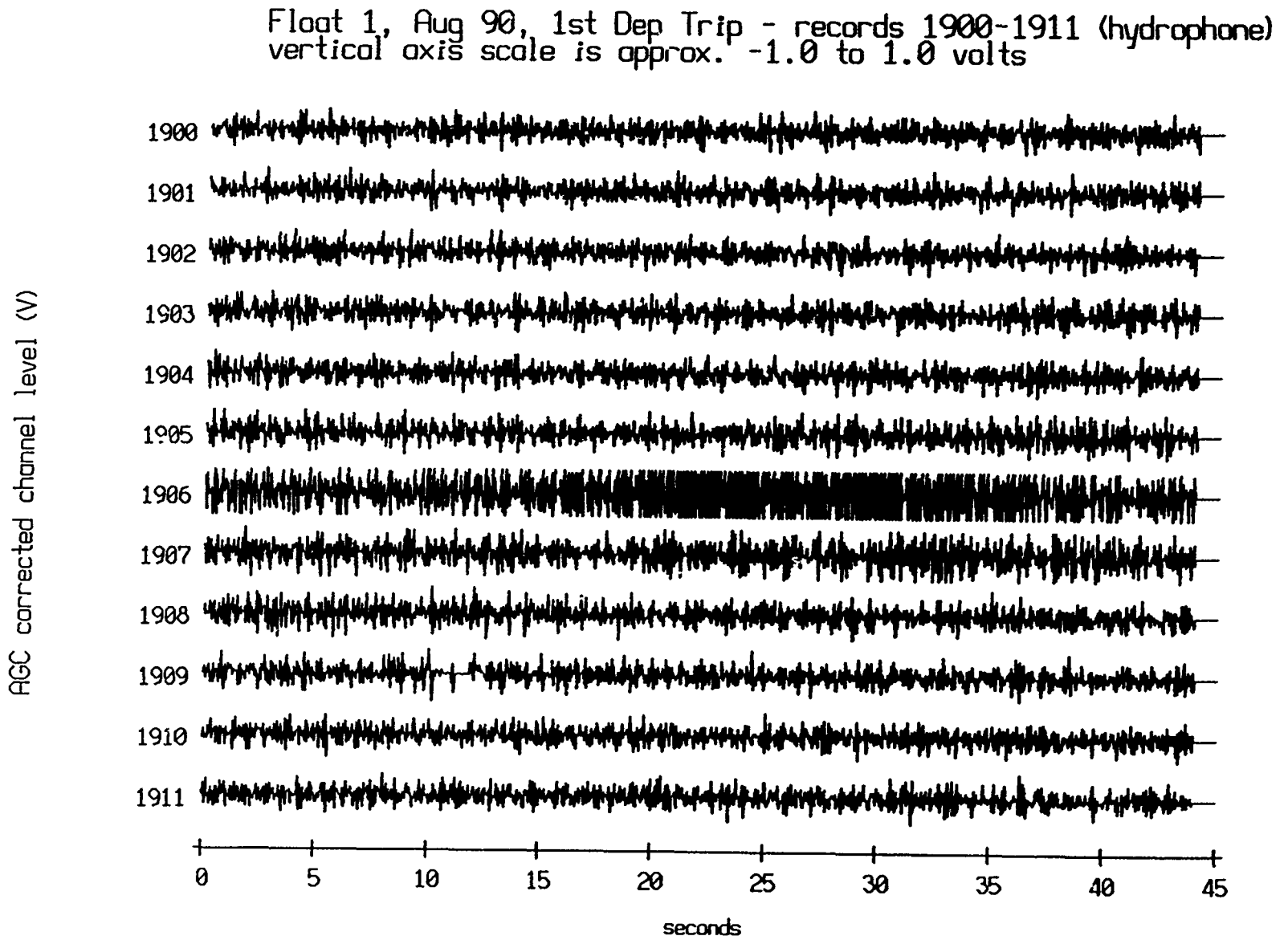
Float 1, Aug 90, 1st Dep Trip - records 1900-1911 (hydrophone)
vertical axis scale is approx. -1.0 to 1.0 volts
1900
1901
1902
1903
1904
1905
1906
1907
1908
1909
1910
1911
0
5
10
15
20
25
30
35
40
45
seconds
AGC corrected channel level (V)

Figure IX.5d

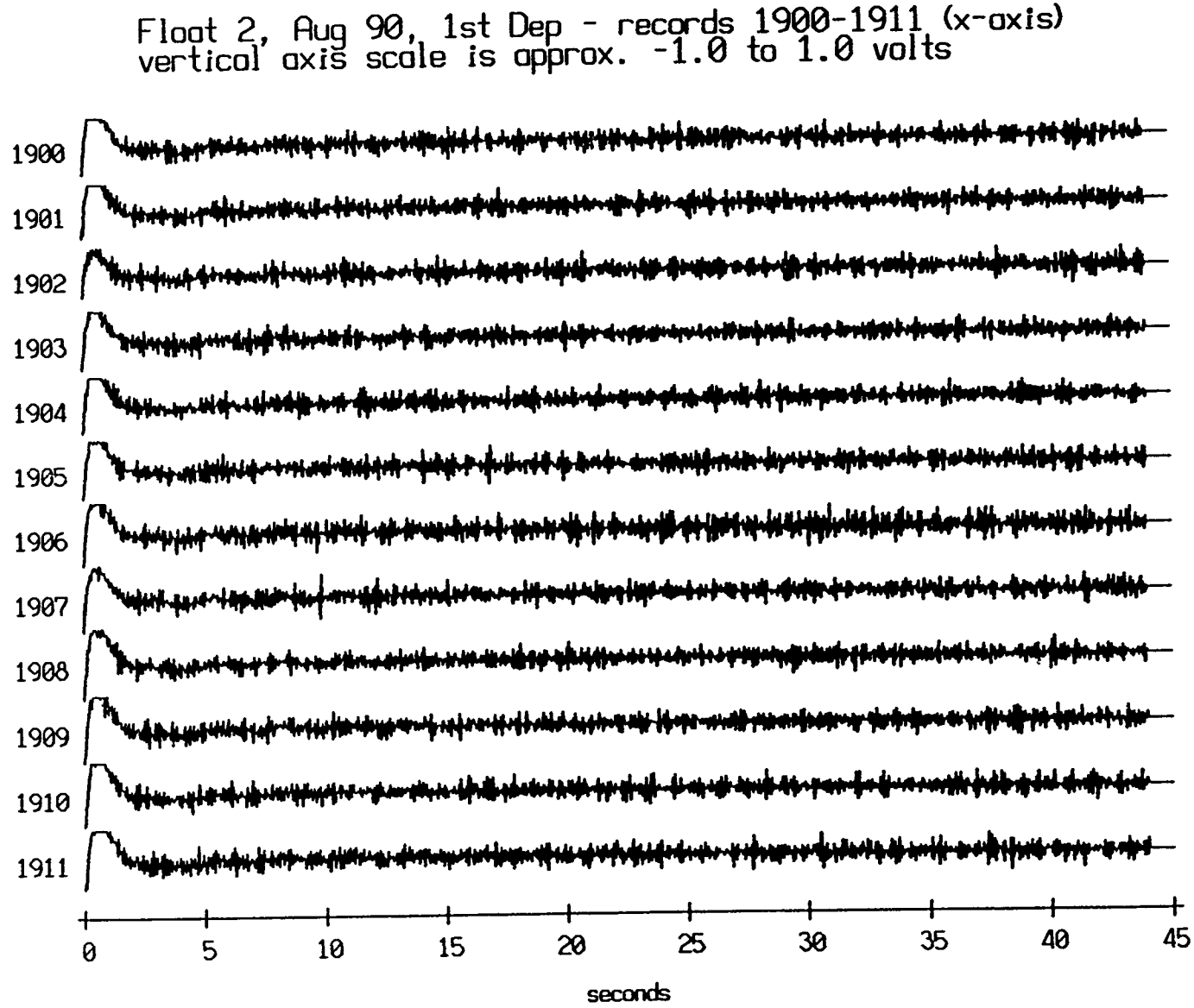
Float 2, Aug 90, 1st Dep - records 1900-1911 (x-axis)
vertical axis scale is approx. -1.0 to 1.0 volts
AGC corrected channel level (V)
1900
1901
1902
1903
1904
1905
1906
1907
1908
1909
1910
1911
0
5
10
15
20
25
30
35
40
45
seconds

Figure IX.6a

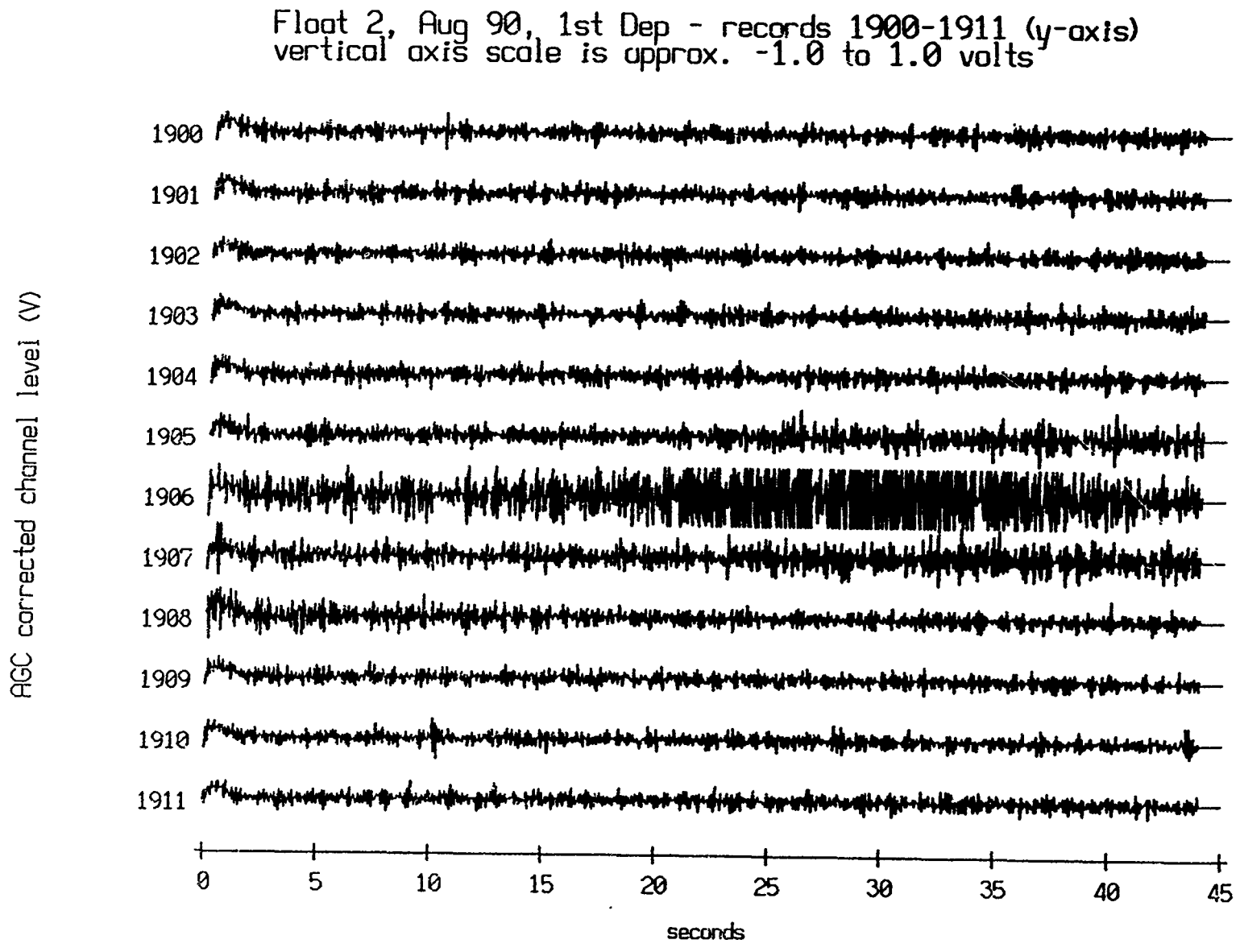
Float 2, Aug 90, 1st Dep - records 1900-1911 (y-axis)
vertical axis scale is approx. -1.0 to 1.0 volts
AGC corrected channel level (V)
1900
1901
1902
1903
1904
1905
1906
1907
1908
1909
1910
1911
0
5
10
15
20
25
30
35
40
45
seconds

Figure IX.6b

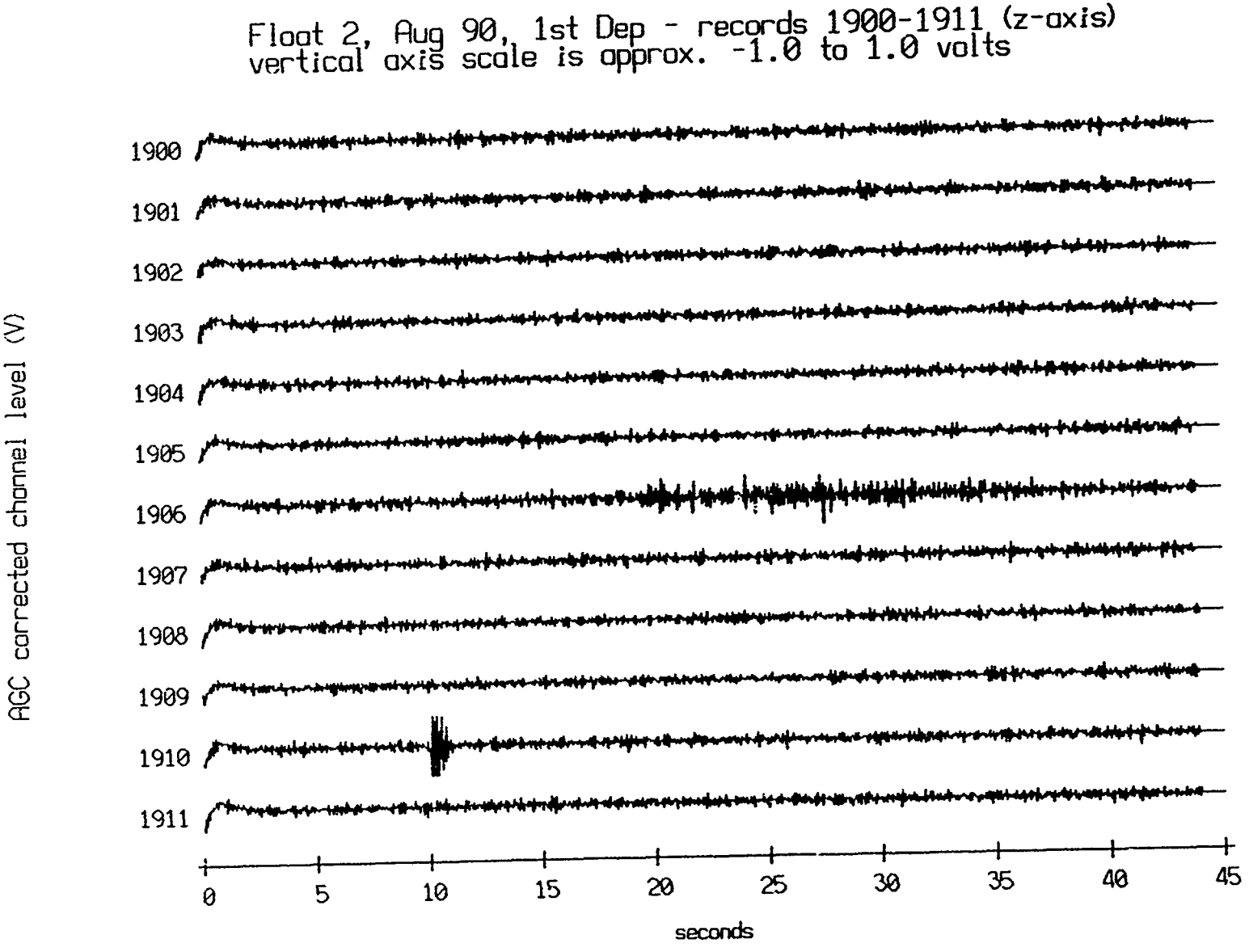
Float 2, Aug 90, 1st Dep - records 1900-1911 (z-axis)
vertical axis scale is approx. -1.0 to 1.0 volts
AGC corrected channel level (V)
1900
1901
1902
1903
1904
1905
1906
1907
1908
1909
1910
1911
0
5
10
15
20
25
30
35
40
45
seconds

Figure IX.6c

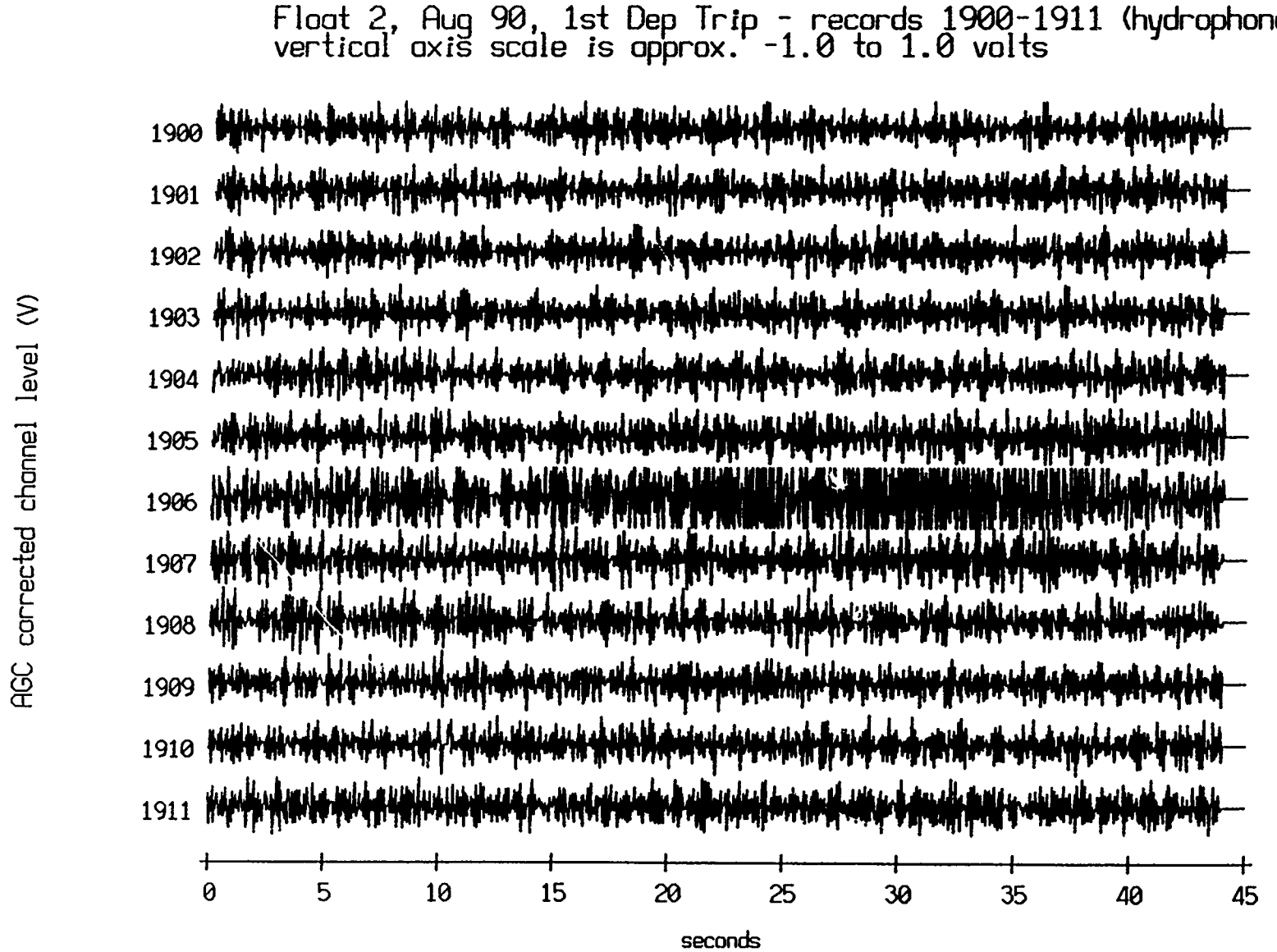
Float 2, Aug 90, 1st Dep Trip - records 1900-1911 (hydrophone)
vertical axis scale is approx. -1.0 to 1.0 volts
AGC corrected channel level (V)
1900
1901
1902
1903
1904
1905
1906
1907
1908
1909
1910
1911
0
5
10
15
20
25
30
35
40
45
seconds

Figure IX.6d

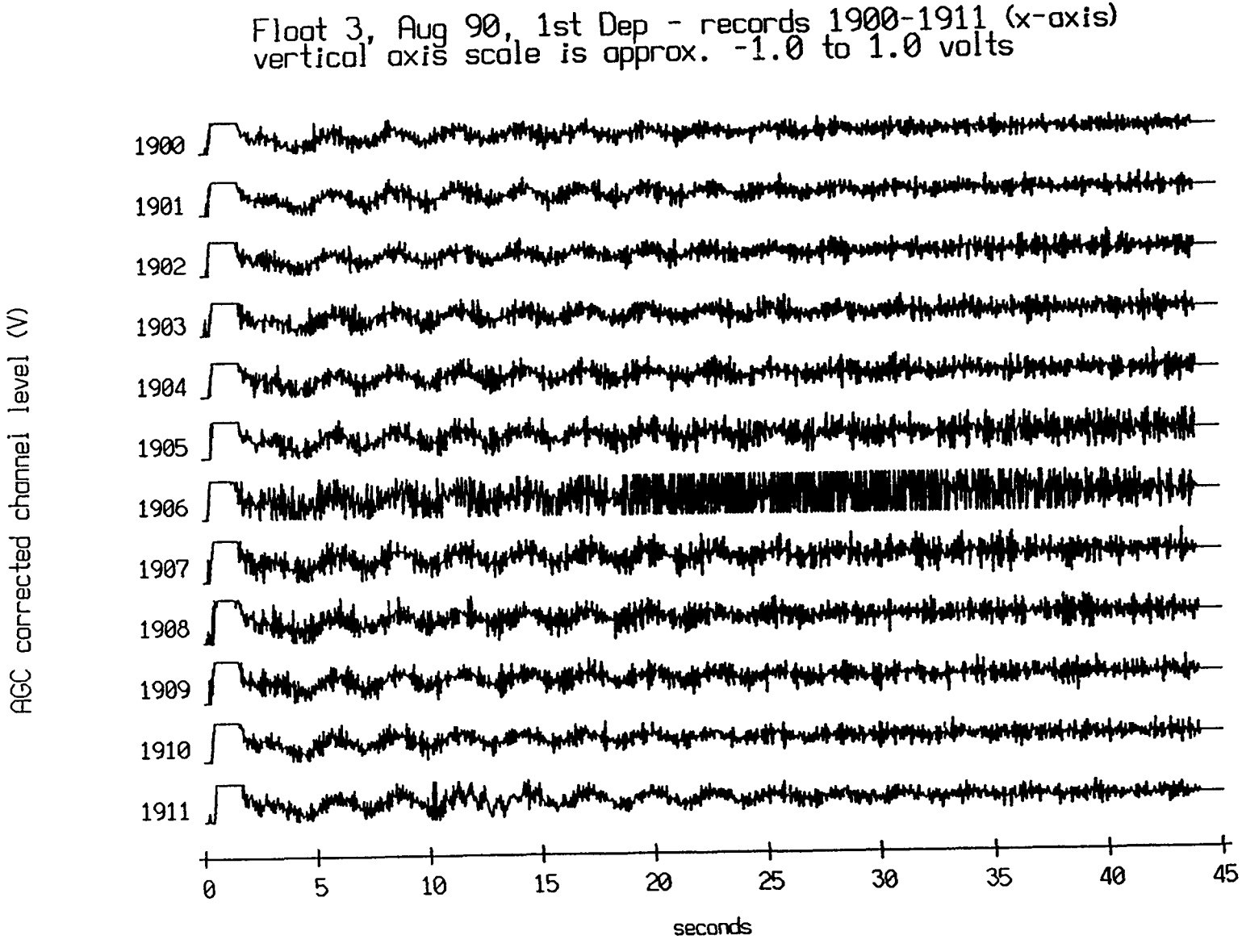
Float 3, Aug 90, 1st Dep - records 1900-1911 (x-axis)
vertical axis scale is approx. -1.0 to 1.0 volts
AGC corrected channel level (V)
1900
1901
1902
1903
1904
1905
1906
1907
1908
1909
1910
1911
0
5
10
15
20
25
30
35
40
45
seconds

Figure IX.7a

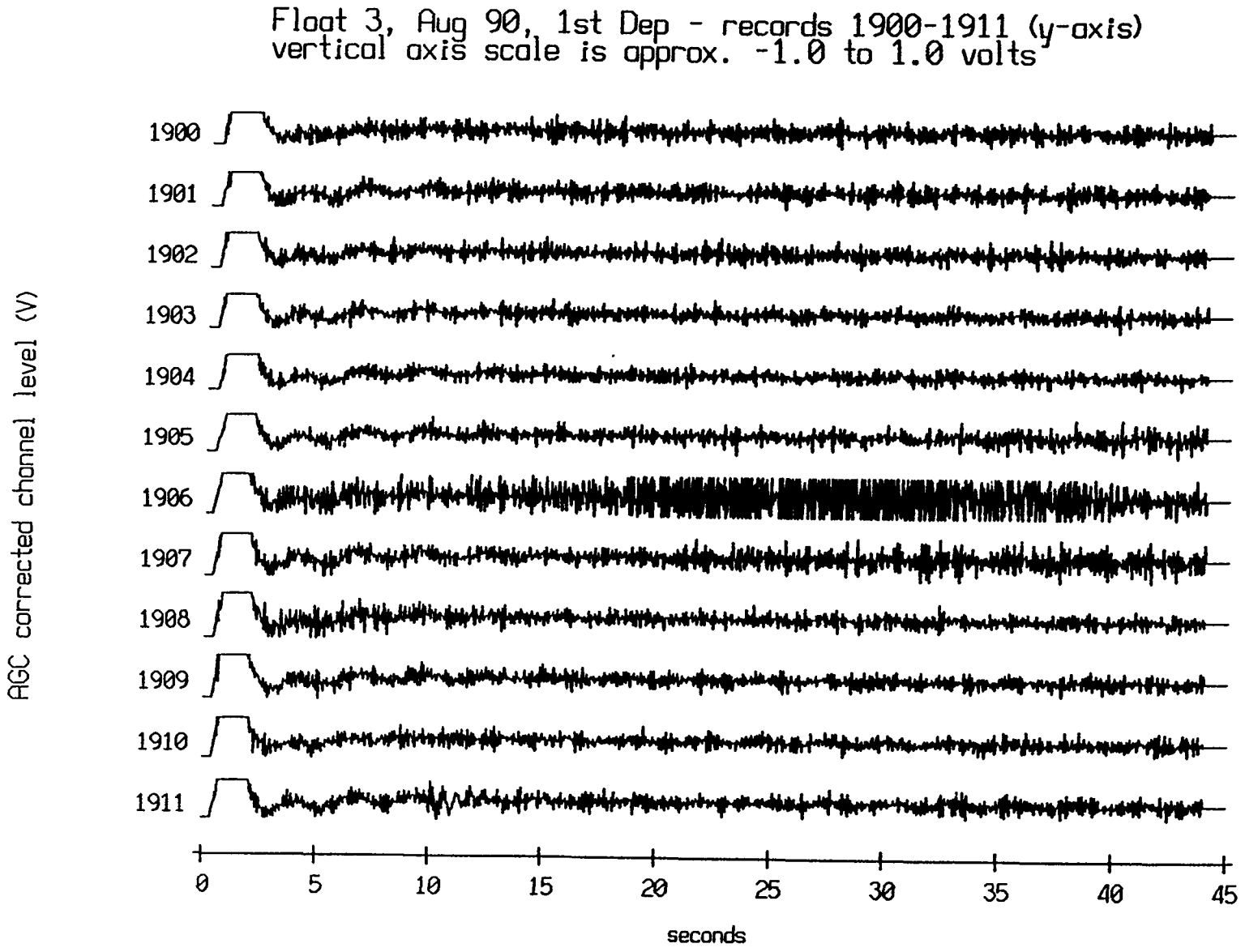
Float 3, Aug 90, 1st Dep - records 1900-1911 (y-axis)
vertical axis scale is approx. -1.0 to 1.0 volts
AGC corrected channel level (V)
1900
1901
1902
1903
1904
1905
1906
1907
1908
1909
1910
1911
0
5
10
15
20
25
30
35
40
45
seconds

Figure IX.7b

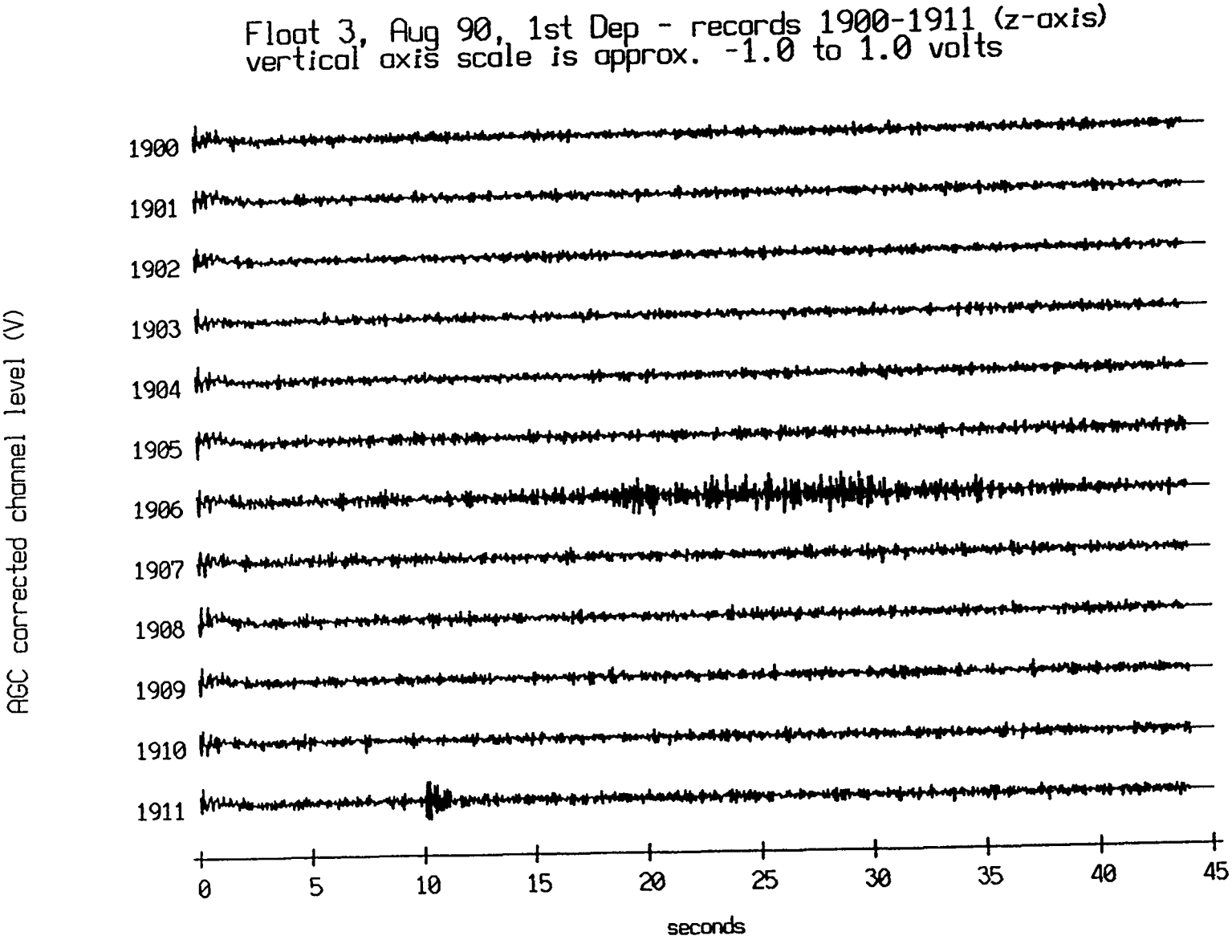
Float 3, Aug 90, 1st Dep - records 1900-1911 (z-axis)
vertical axis scale is approx. -1.0 to 1.0 volts
AGC corrected channel level (V)
1900
1901
1902
1903
1904
1905
1906
1907
1908
1909
1910
1911
0
5
10
15
20
25
30
35
40
45
seconds

Figure IX.7c

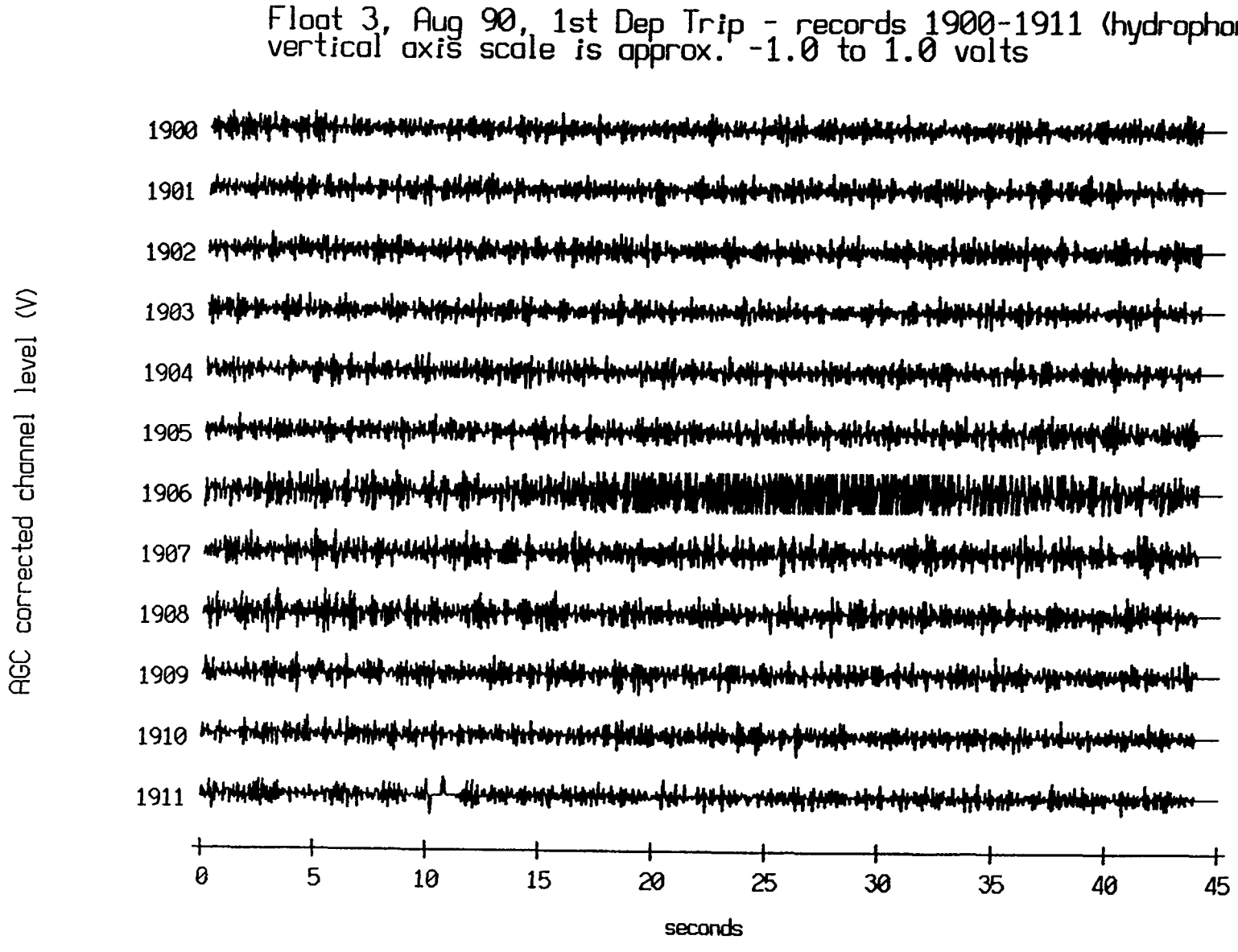
Float 3, Aug 90, 1st Dep Trip - records 1900-1911 (hydrophone)
vertical axis scale is approx. -1.0 to 1.0 volts
AGC corrected channel level (V)
1900
1901
1902
1903
1904
1905
1906
1907
1908
1909
1910
1911
0
5
10
15
20
25
30
35
40
45
seconds

Figure IX.7.d

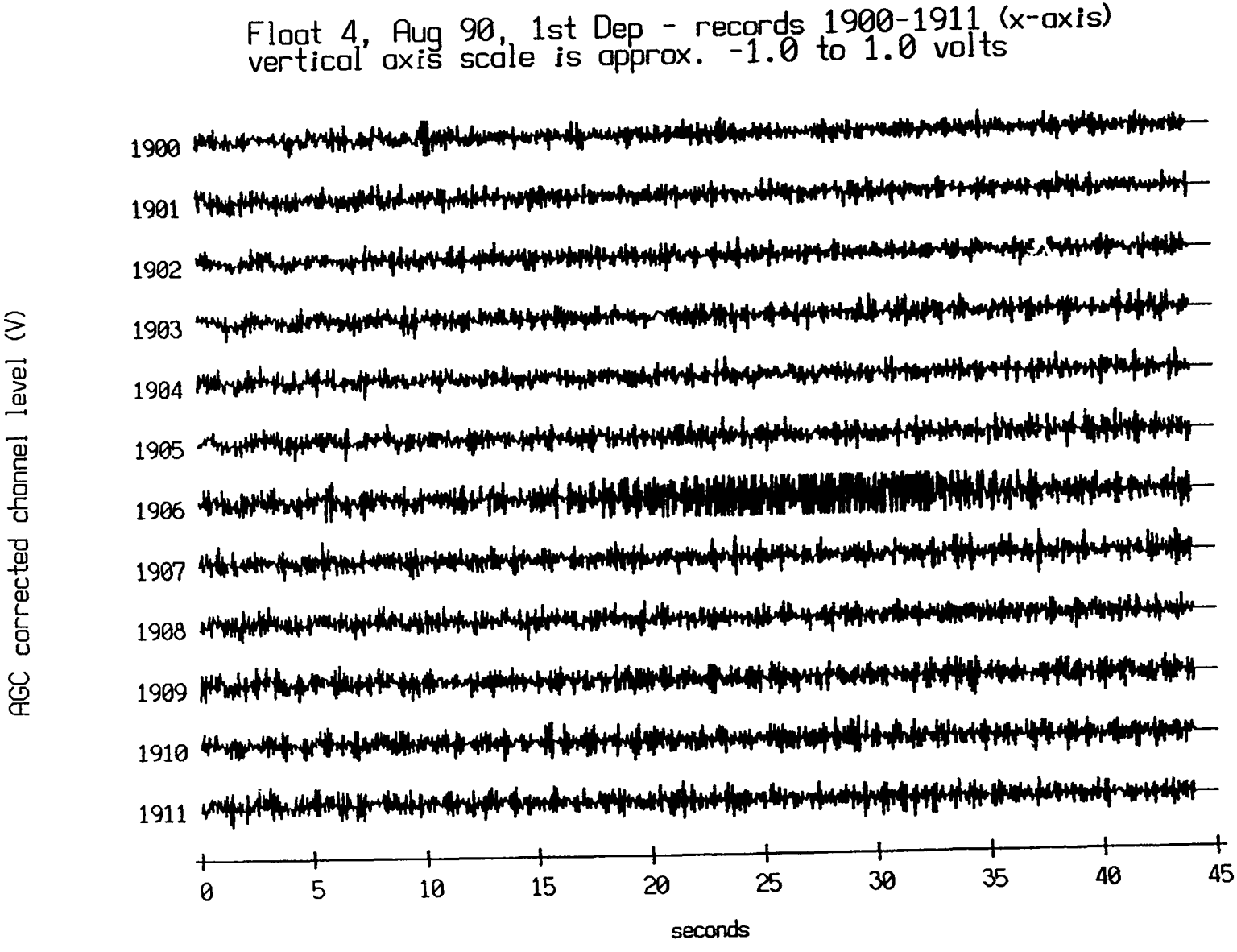
Float 4, Aug 90, 1st Dep - records 1900-1911 (x-axis)
vertical axis scale is approx. -1.0 to 1.0 volts
AGC corrected channel level (V)
1900
1901
1902
1903
1904
1905
1906
1907
1908
1909
1910
1911
0
5
10
15
20
25
30
35
40
45
seconds

Figure IX.8a

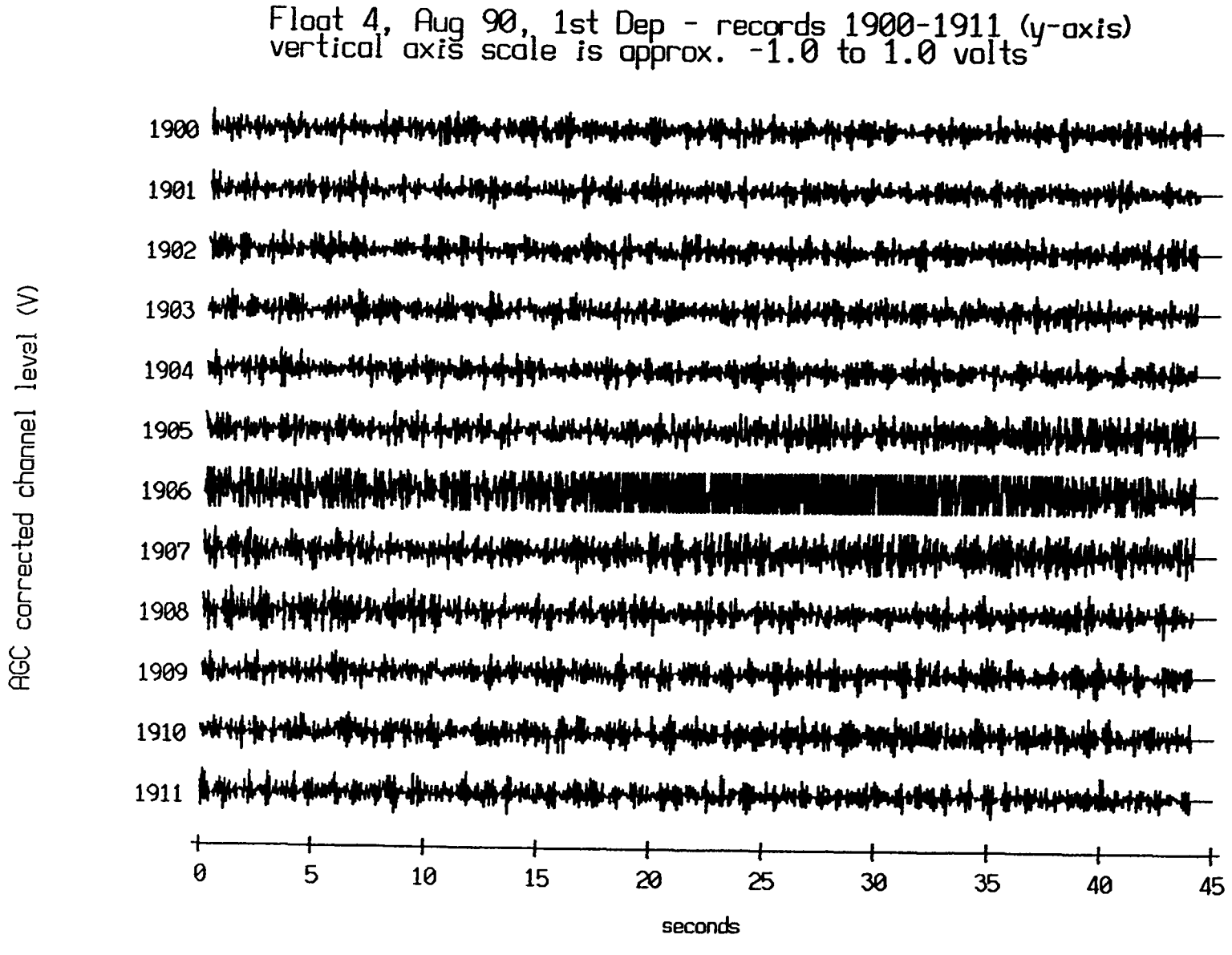
Float 4, Aug 90, 1st Dep - records 1900-1911 (y-axis)
vertical axis scale is approx. -1.0 to 1.0 volts
AGC corrected channel level (V)
1900
1901
1902
1903
1904
1905
1906
1907
1908
1909
1910
1911
0
5
10
15
20
25
30
35
40
45
seconds

Figure IX.8b

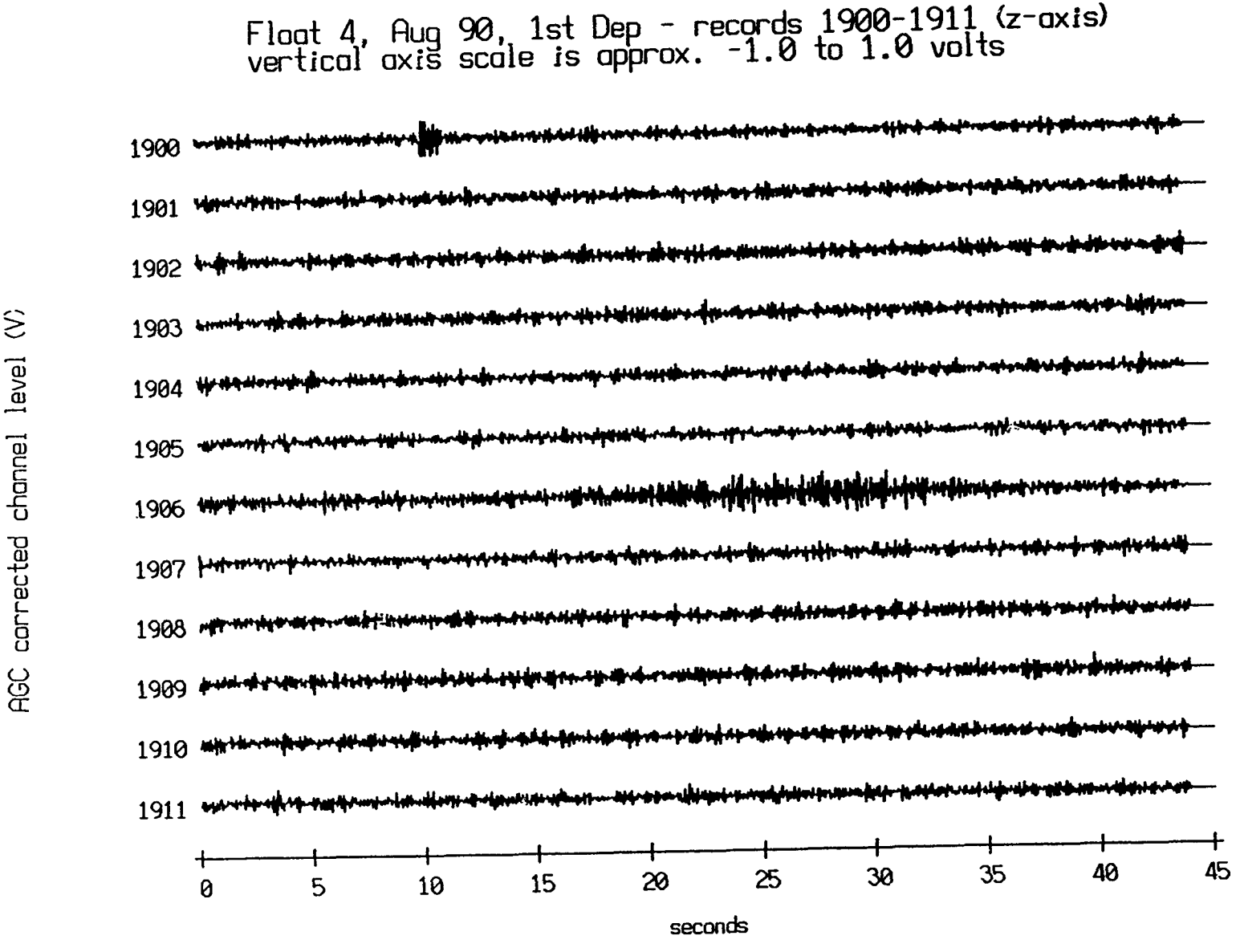
Float 4, Aug 90, 1st Dep - records 1900-1911 (z-axis)
vertical axis scale is approx. -1.0 to 1.0 volts
AGC corrected channel level (V)
1900
1901
1902
1903
1904
1905
1906
1907
1908
1909
1910
1911
0
5
10
15
20
25
30
35
40
45
seconds

Figure IX.8c

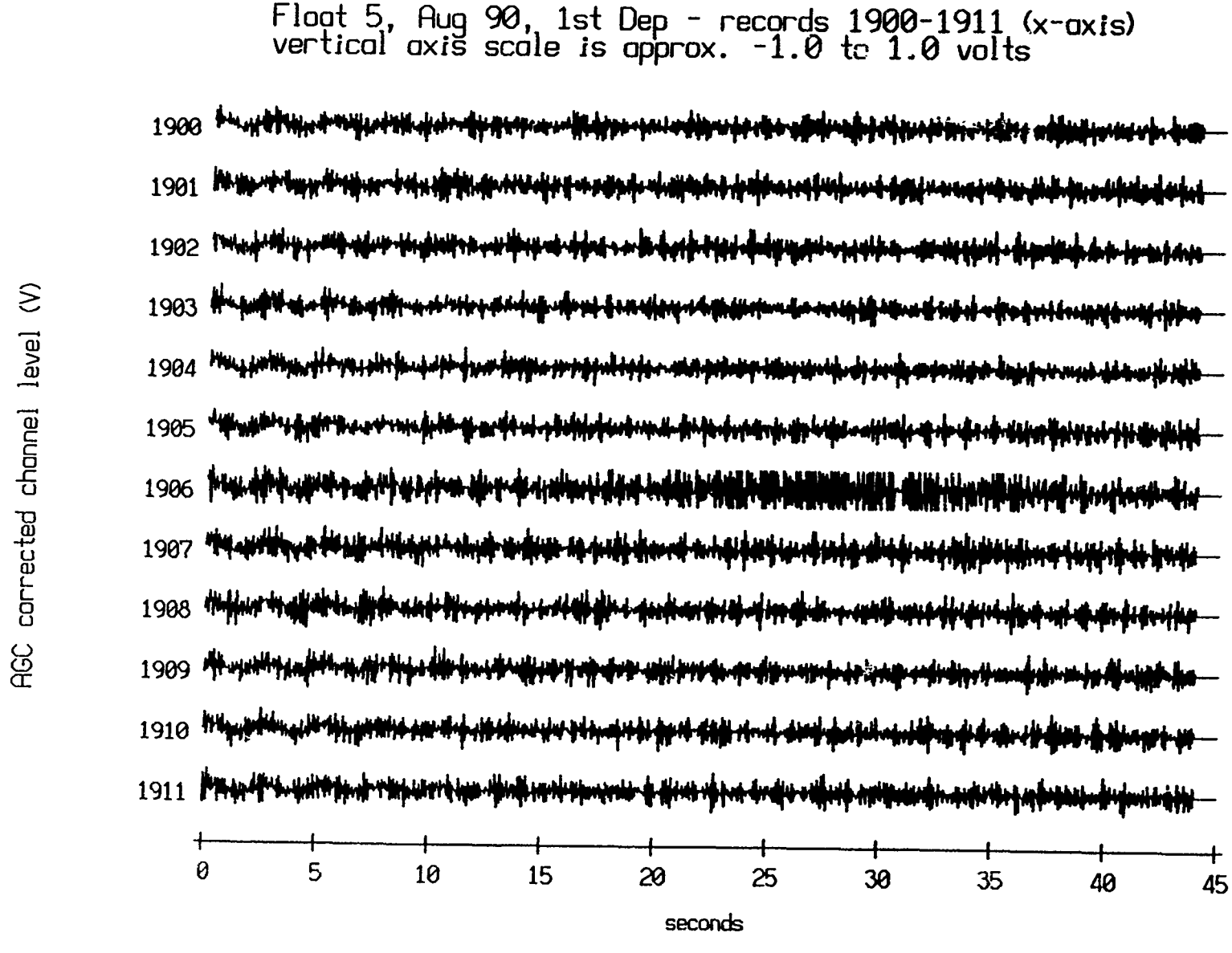
Float 5, Aug 90, 1st Dep - records 1900-1911 (x-axis)
vertical axis scale is approx. -1.0 to 1.0 volts
AGC corrected channel level (V)
1900
1901
1902
1903
1904
1905
1906
1907
1908
1909
1910
1911
0
5
10
15
20
25
30
35
40
45
seconds

Figure IX.9a

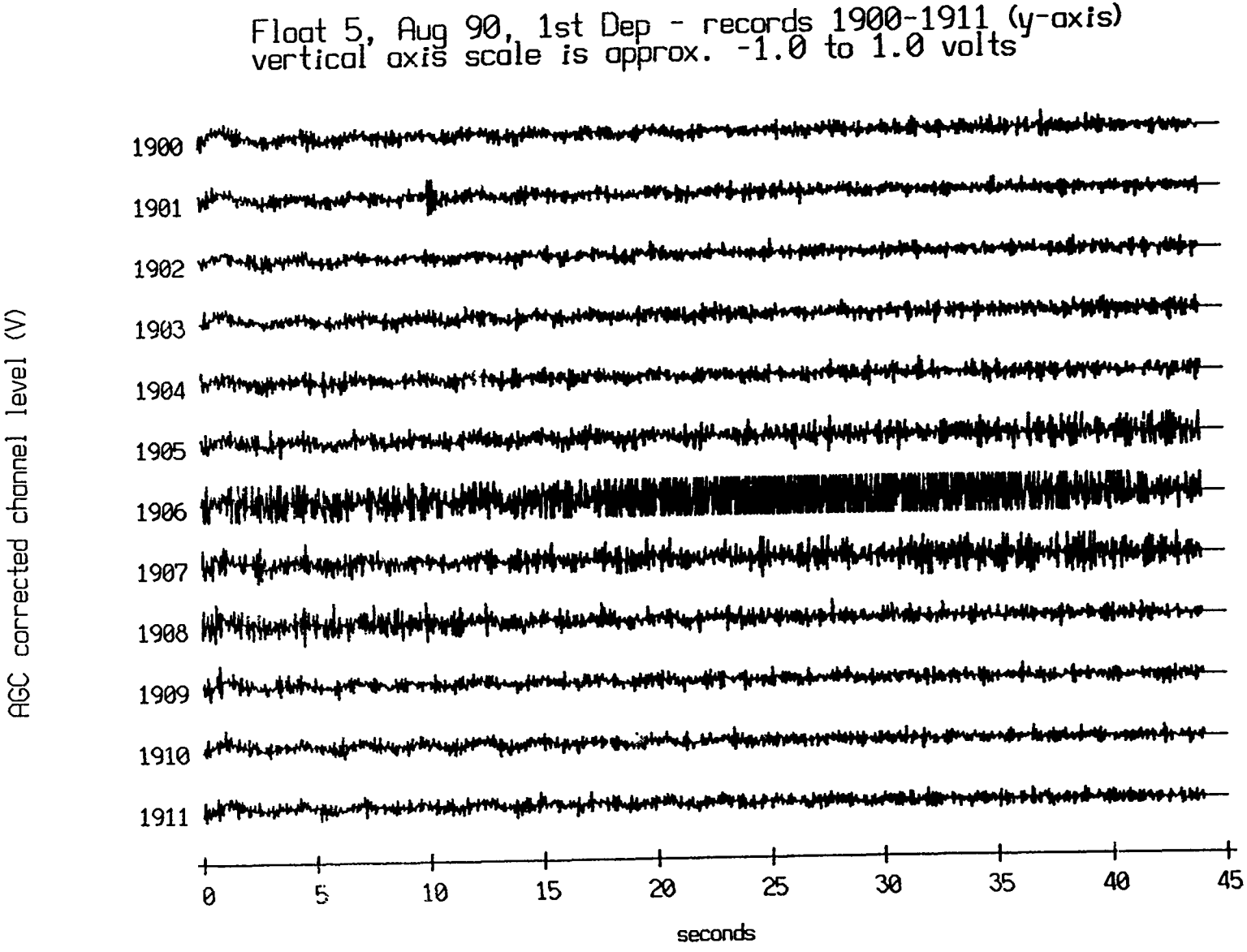
Float 5, Aug 90, 1st Dep - records 1900-1911 (y-axis)
vertical axis scale is approx. -1.0 to 1.0 volts
AGC corrected channel level (V)
1900
1901
1902
1903
1904
1905
1906
1907
1908
1909
1910
1911
0
5
10
15
20
25
30
35
40
45
seconds

Figure IX.9b

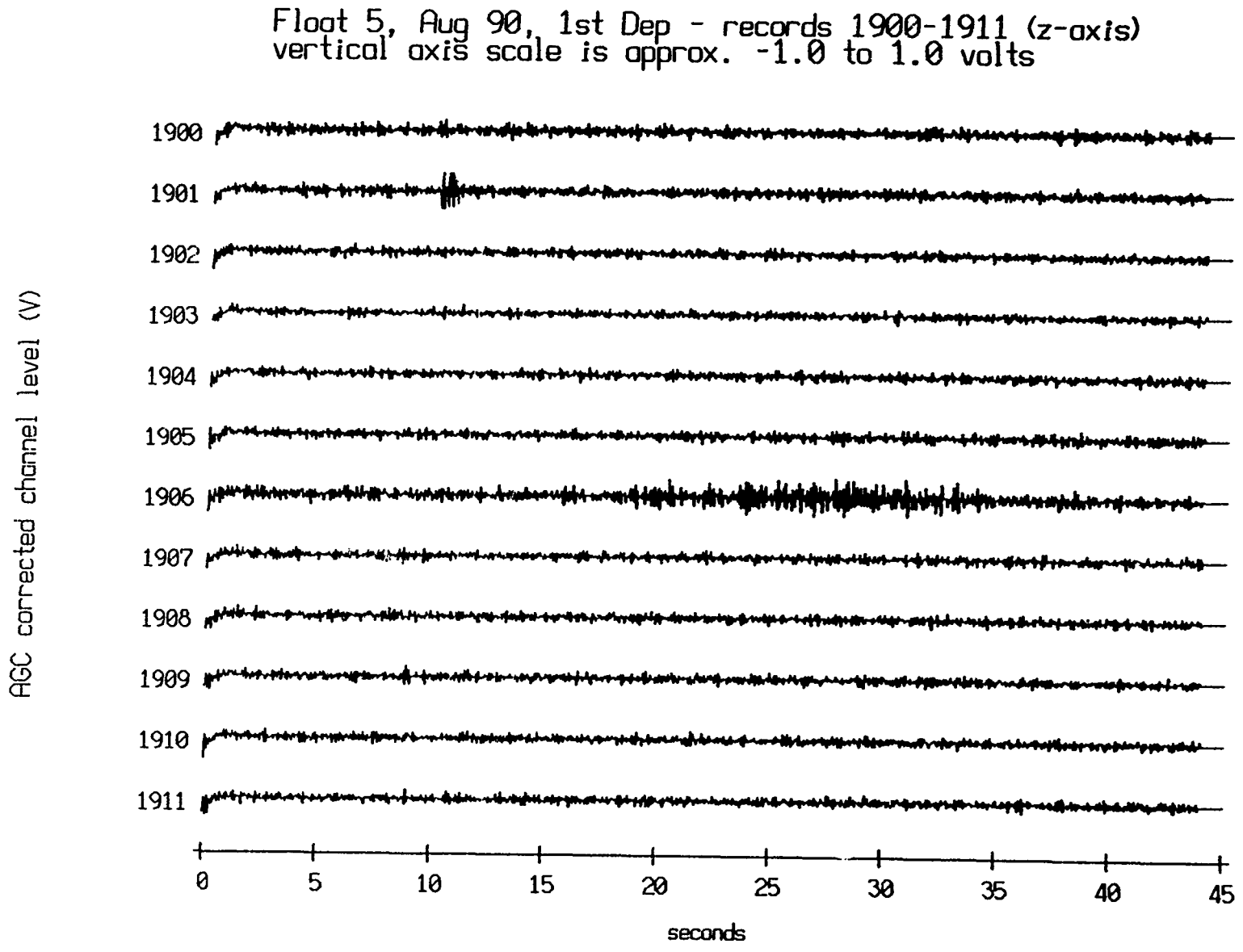
Float 5, Aug 90, 1st Dep - records 1900-1911 (z-axis)
vertical axis scale is approx. -1.0 to 1.0 volts
1900
1901
1902
1903
1904
1905
1906
1907
1908
1909
1910
1911
0
5
10
15
20
25
30
35
40
45
seconds
AGC corrected channel level (V)

Figure IX.9c

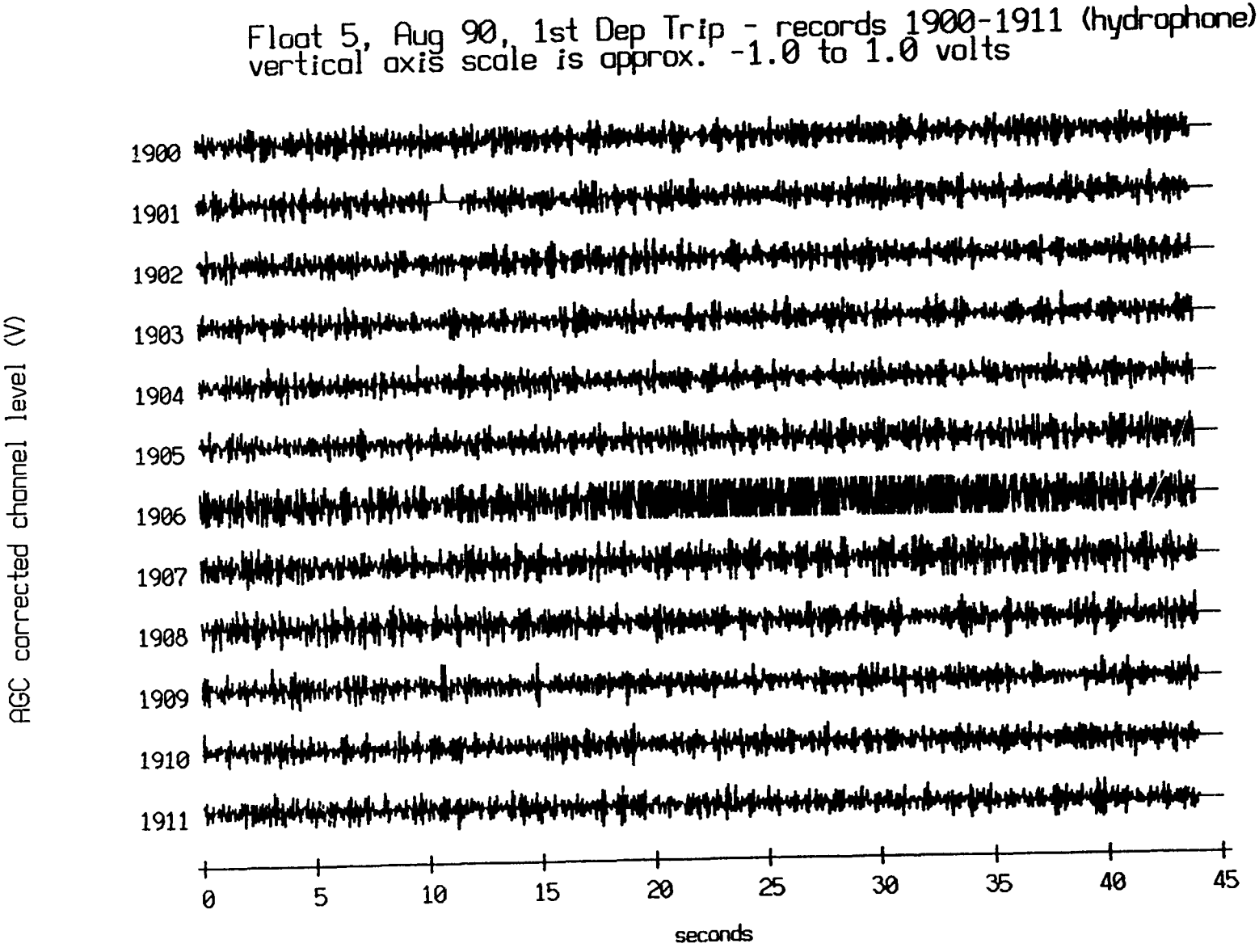
Float 5, Aug 90, 1st Dep Trip - records 1900-1911 (hydrophone)
vertical axis scale is approx. -1.0 to 1.0 volts
AGC corrected channel level (V)
1900
1901
1902
1903
1904
1905
1906
1907
1908
1909
1910
1911
0
5
10
15
20
25
30
35
40
45
seconds

Figure IX.9d

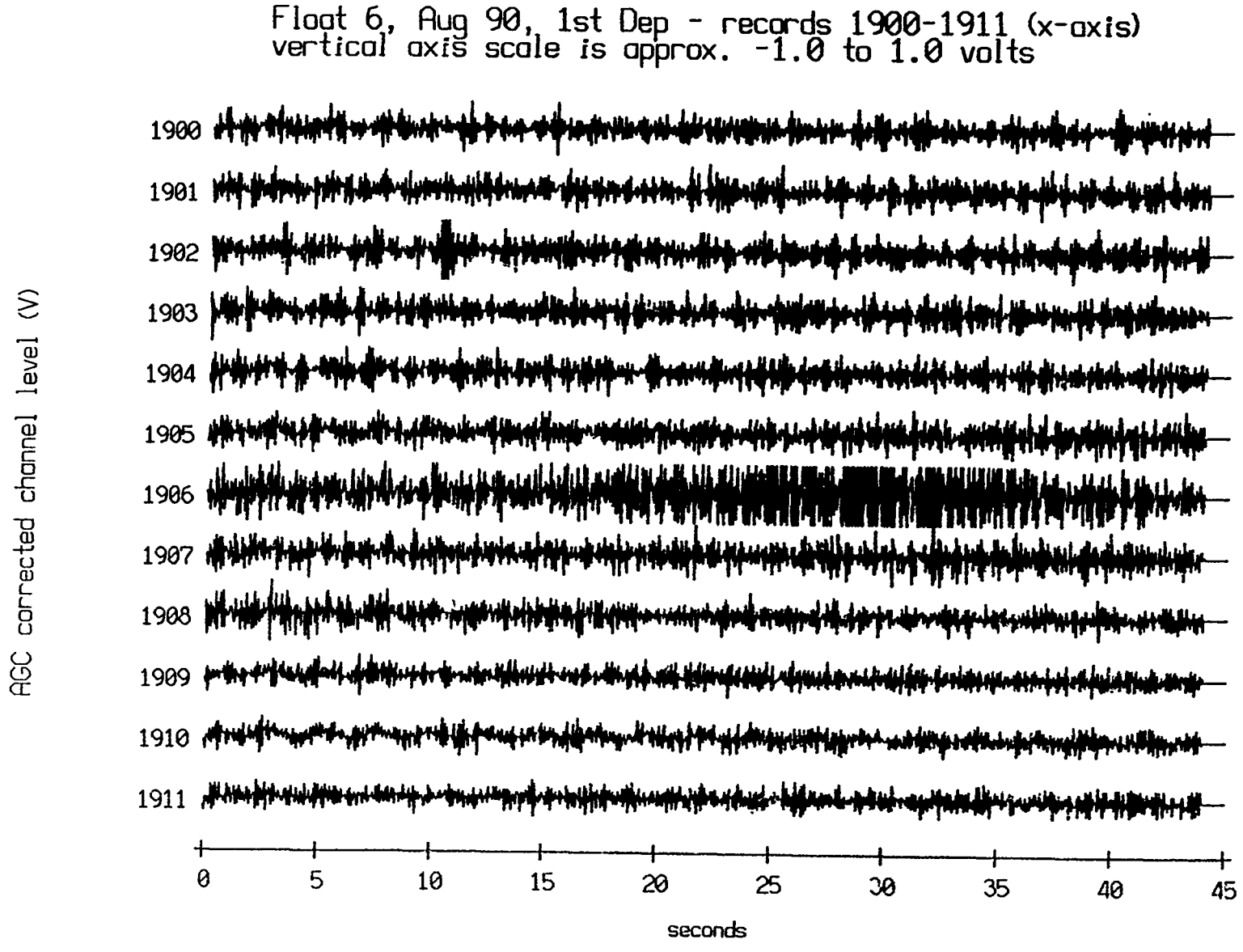

Figure IX.10a

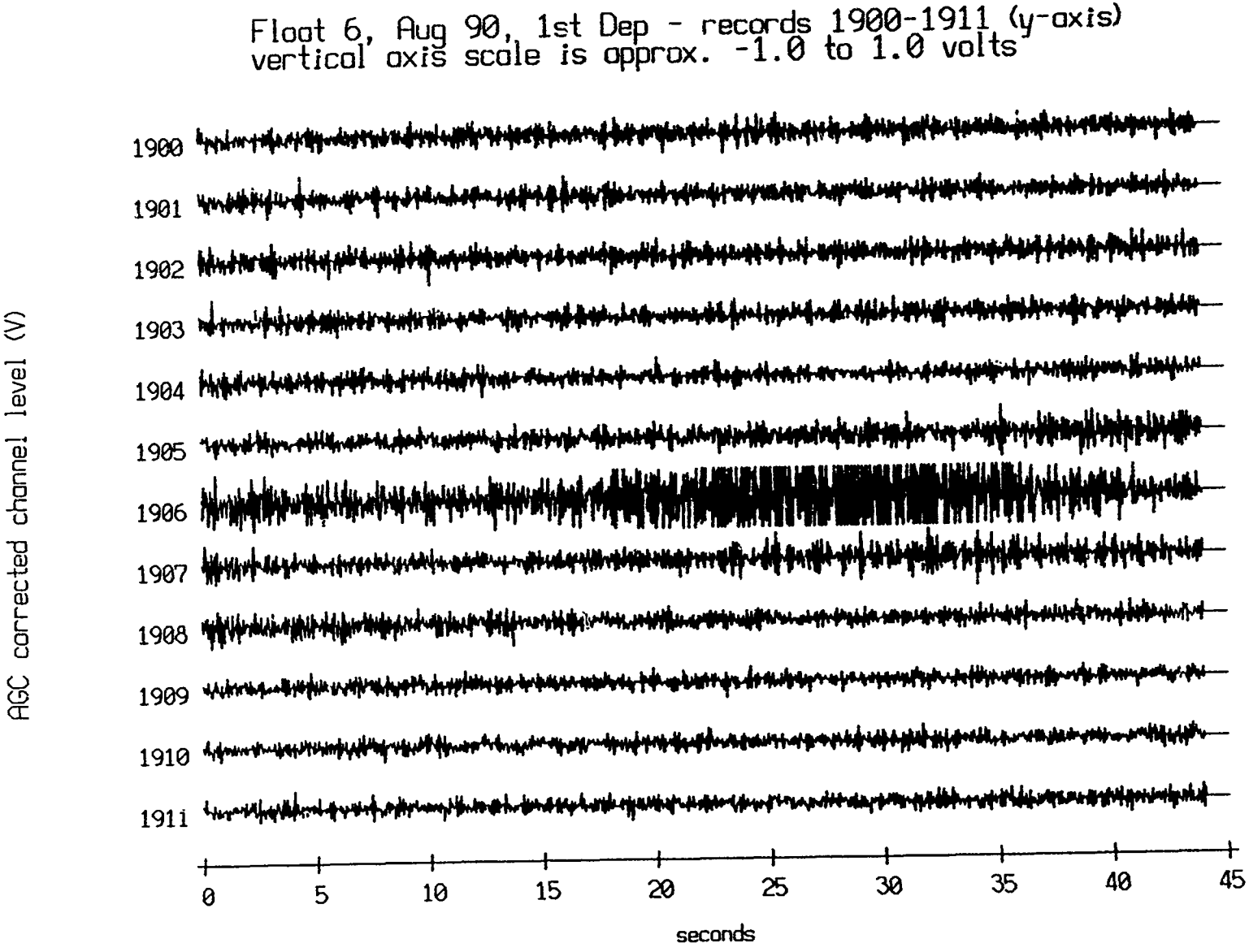

Figure IX.10b

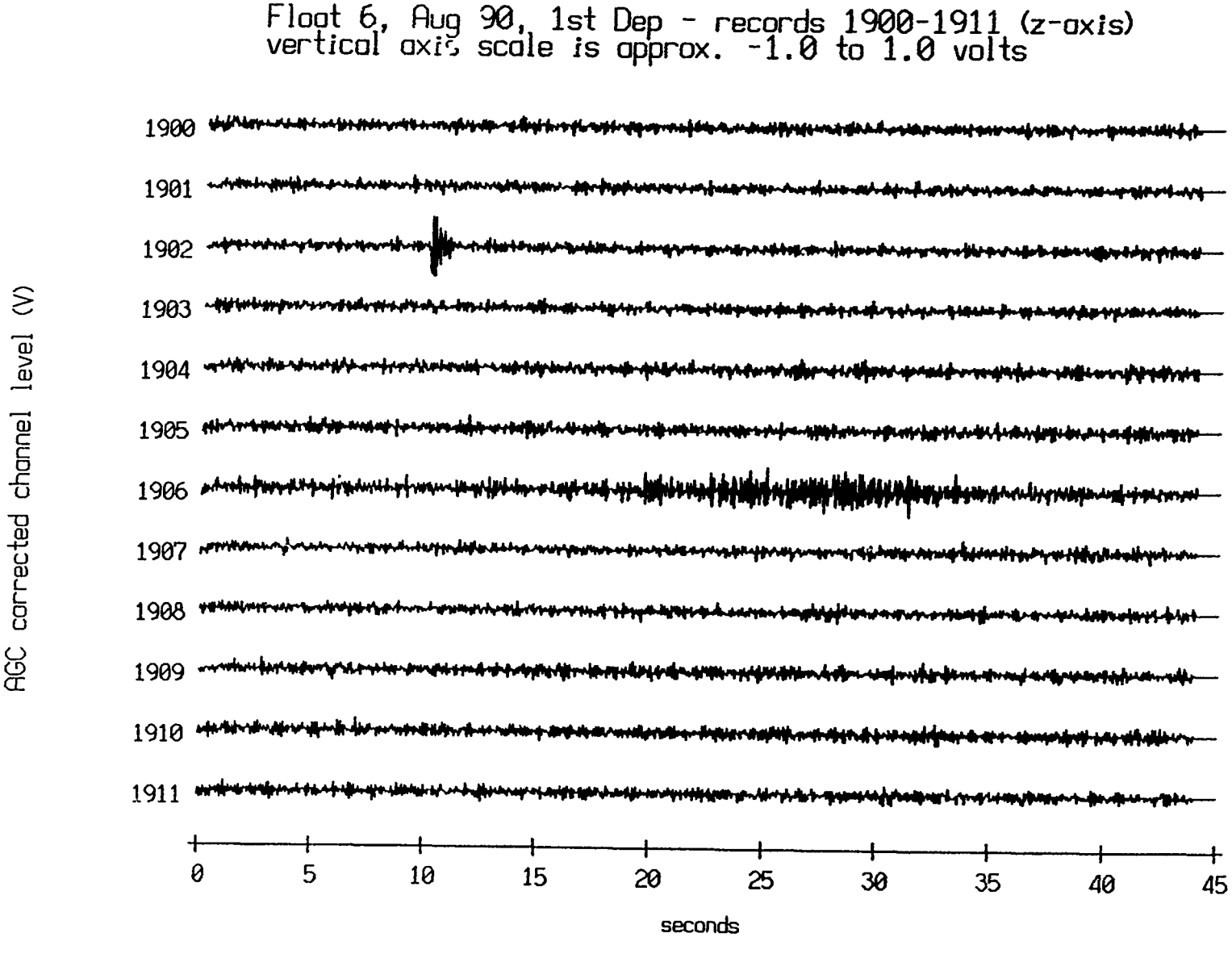

Figure IX.10c

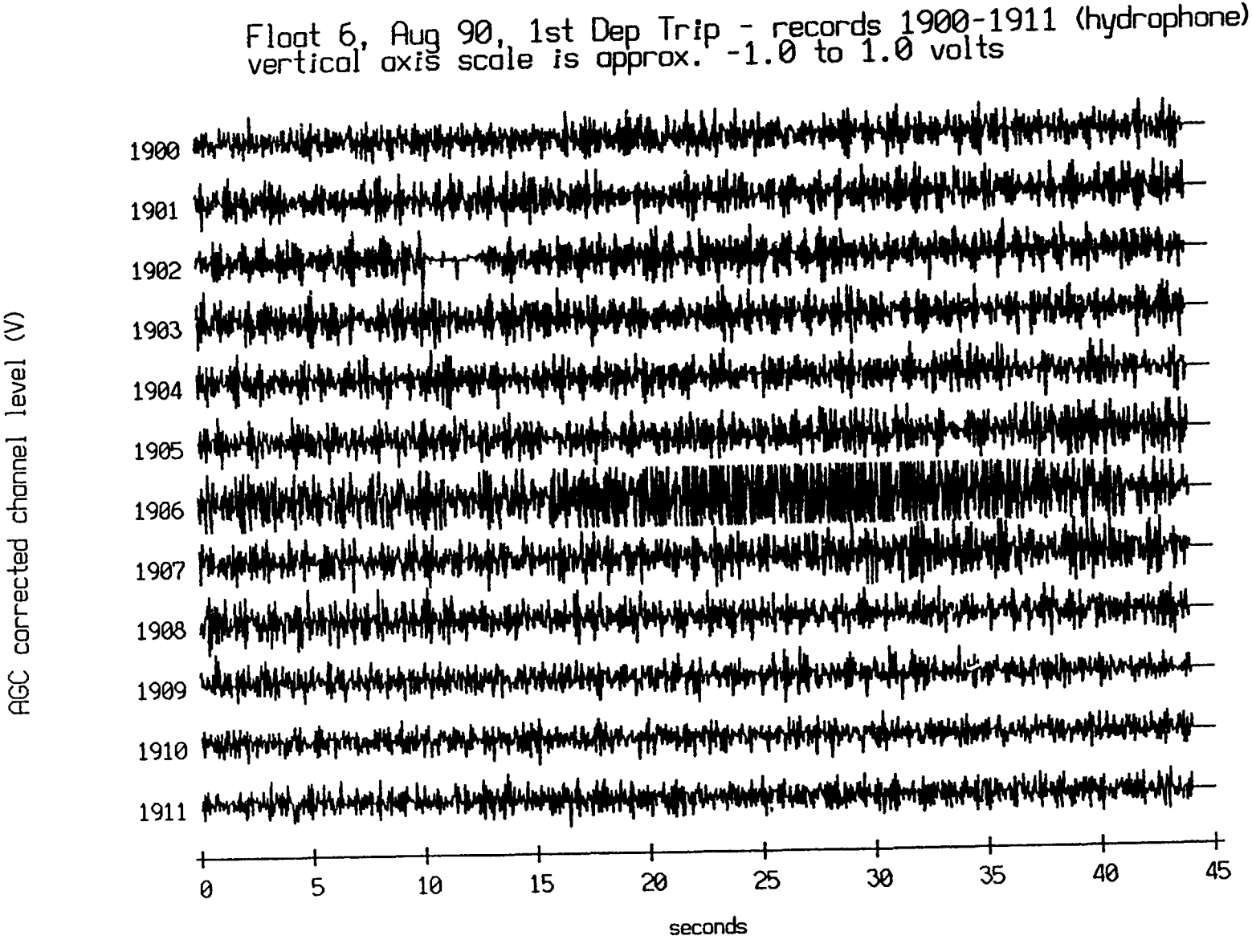

Figure IX.10d

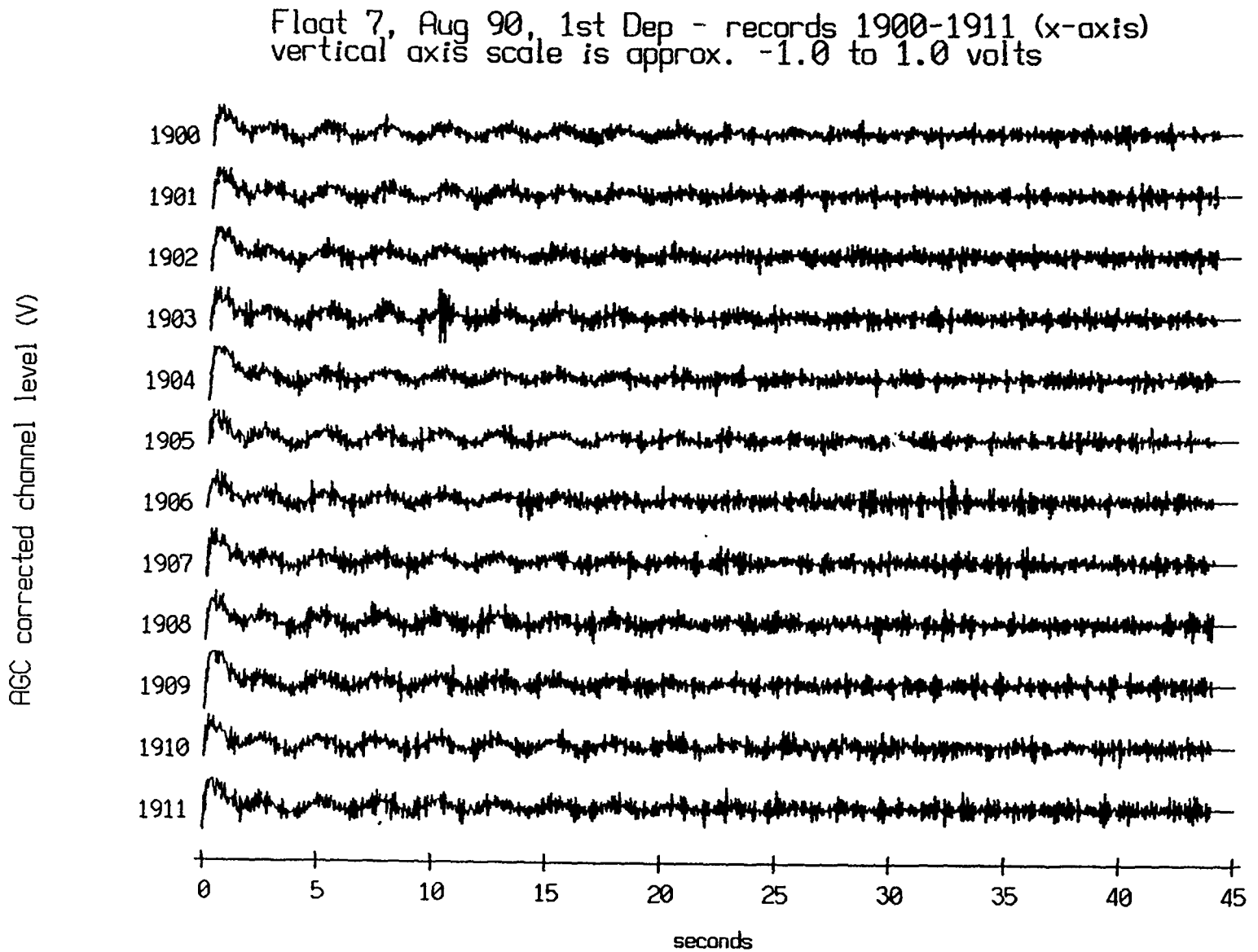

Figure IX.11a

Figure IX.11b

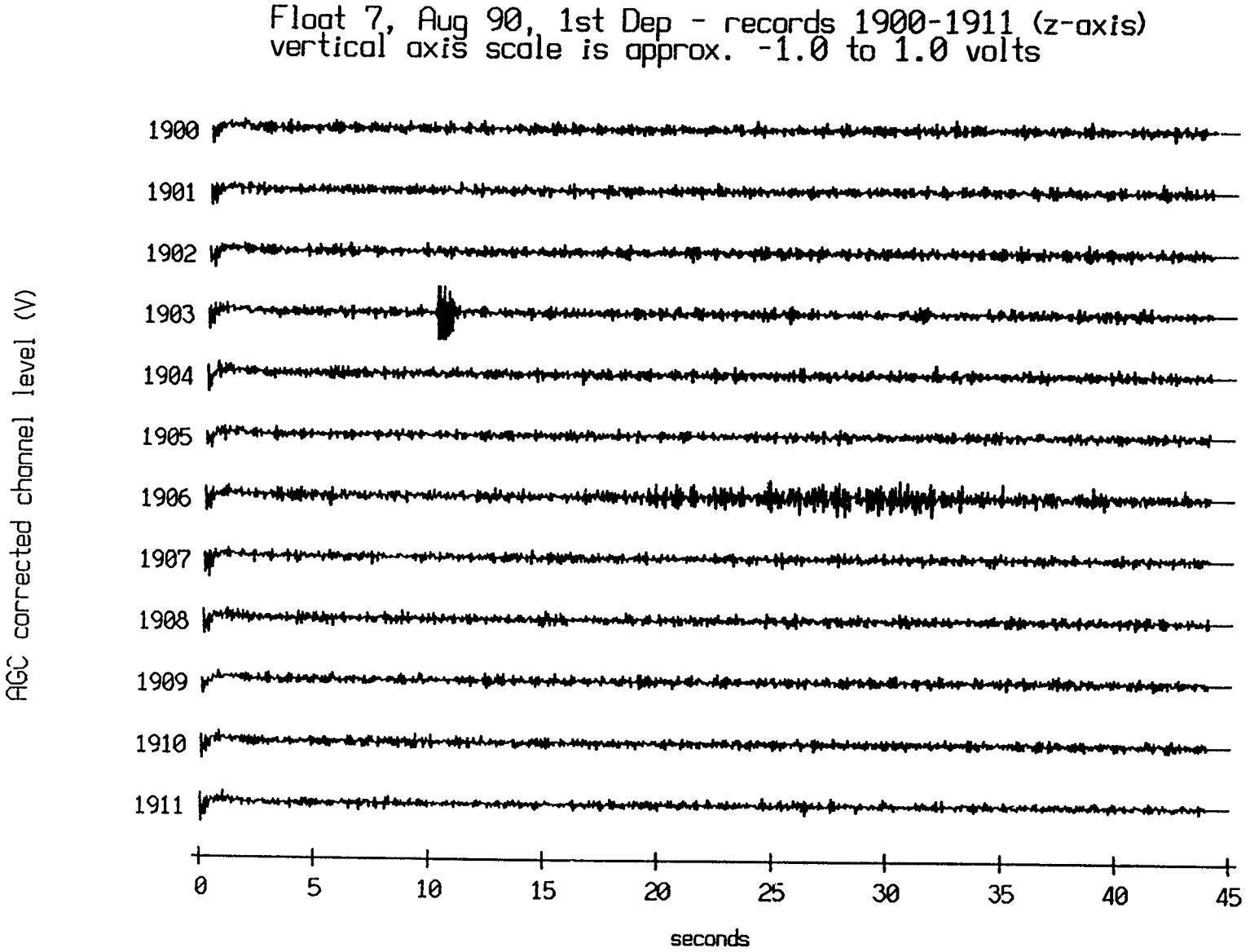

Figure IX.11c

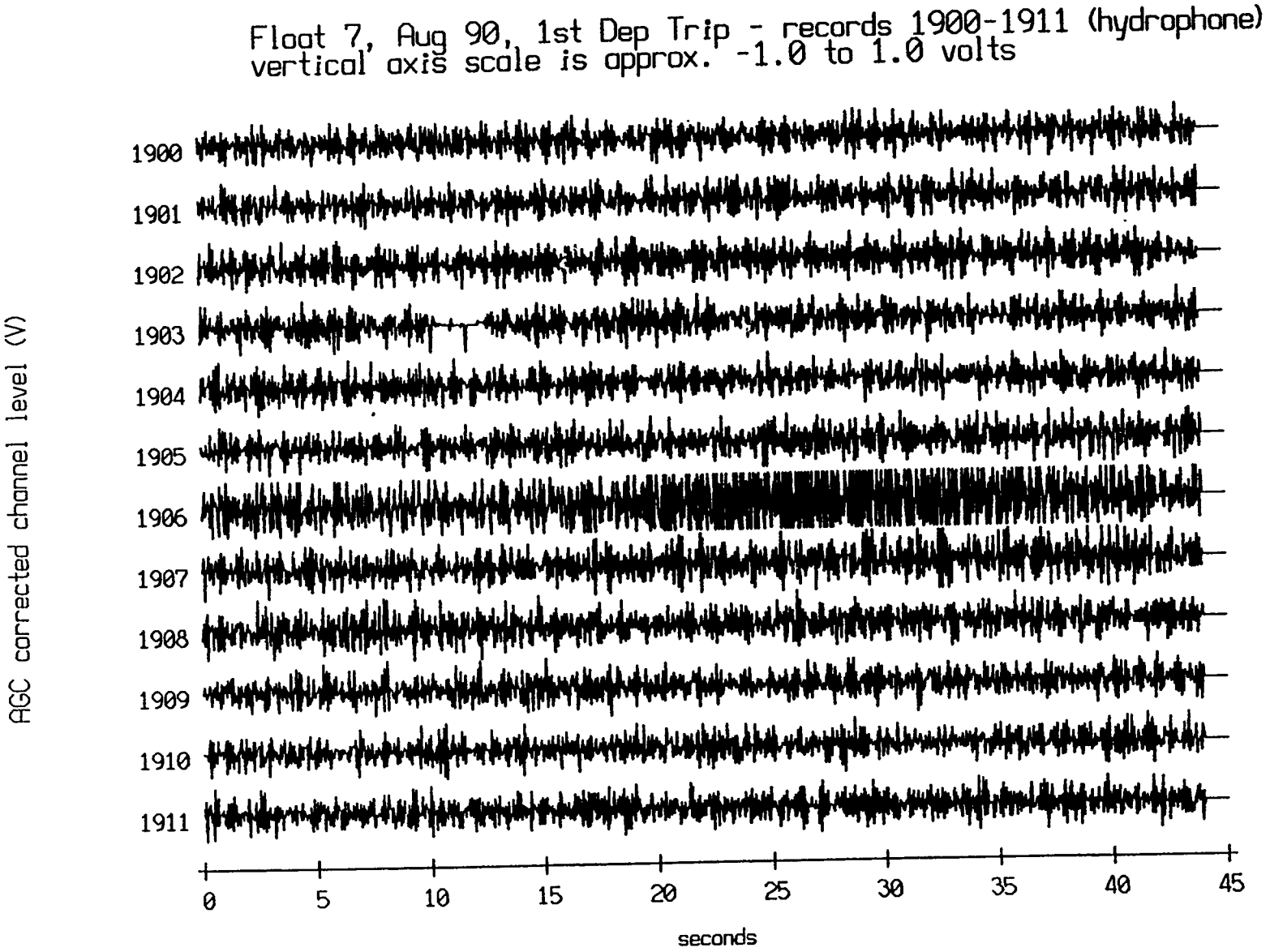

Figure IX.11d

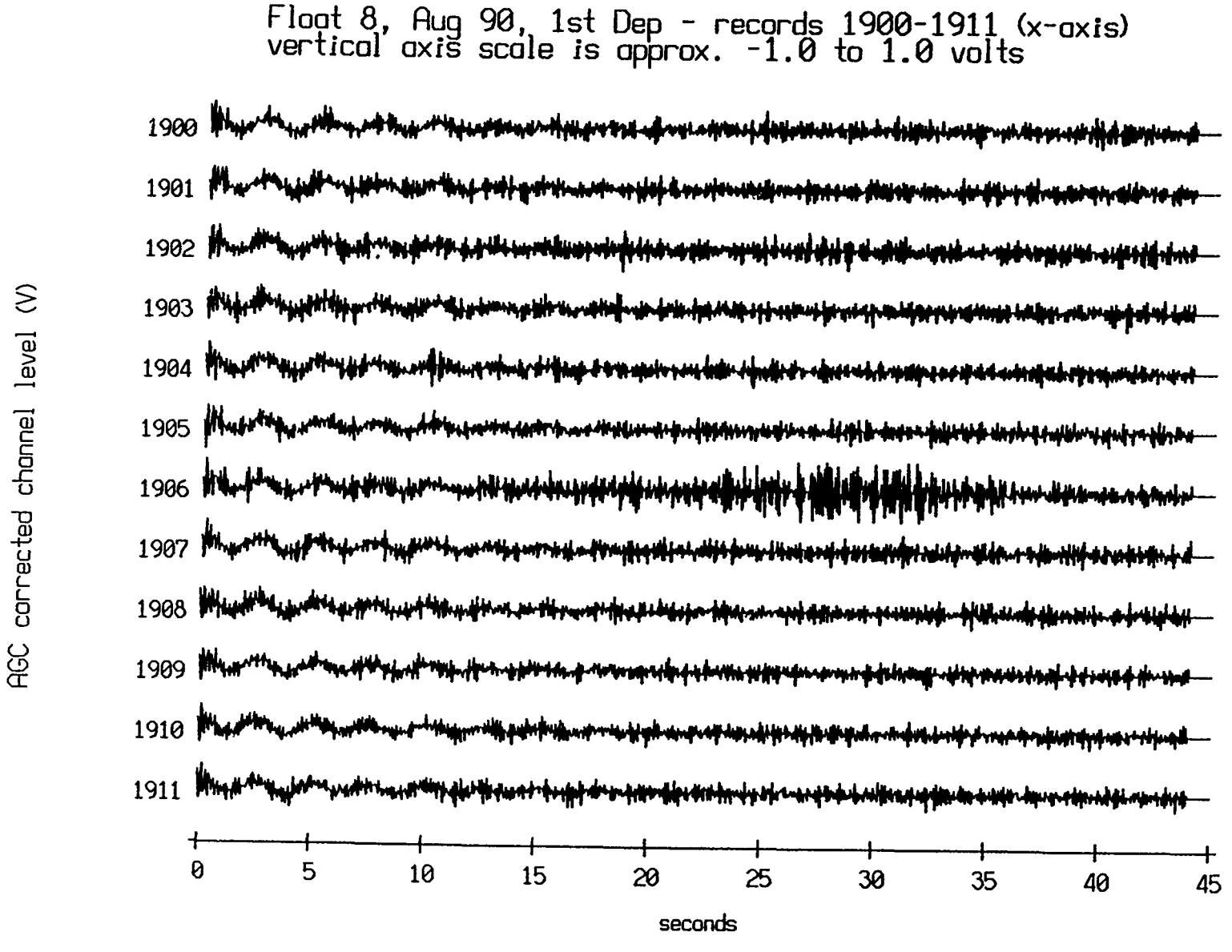

Figure IX.12a

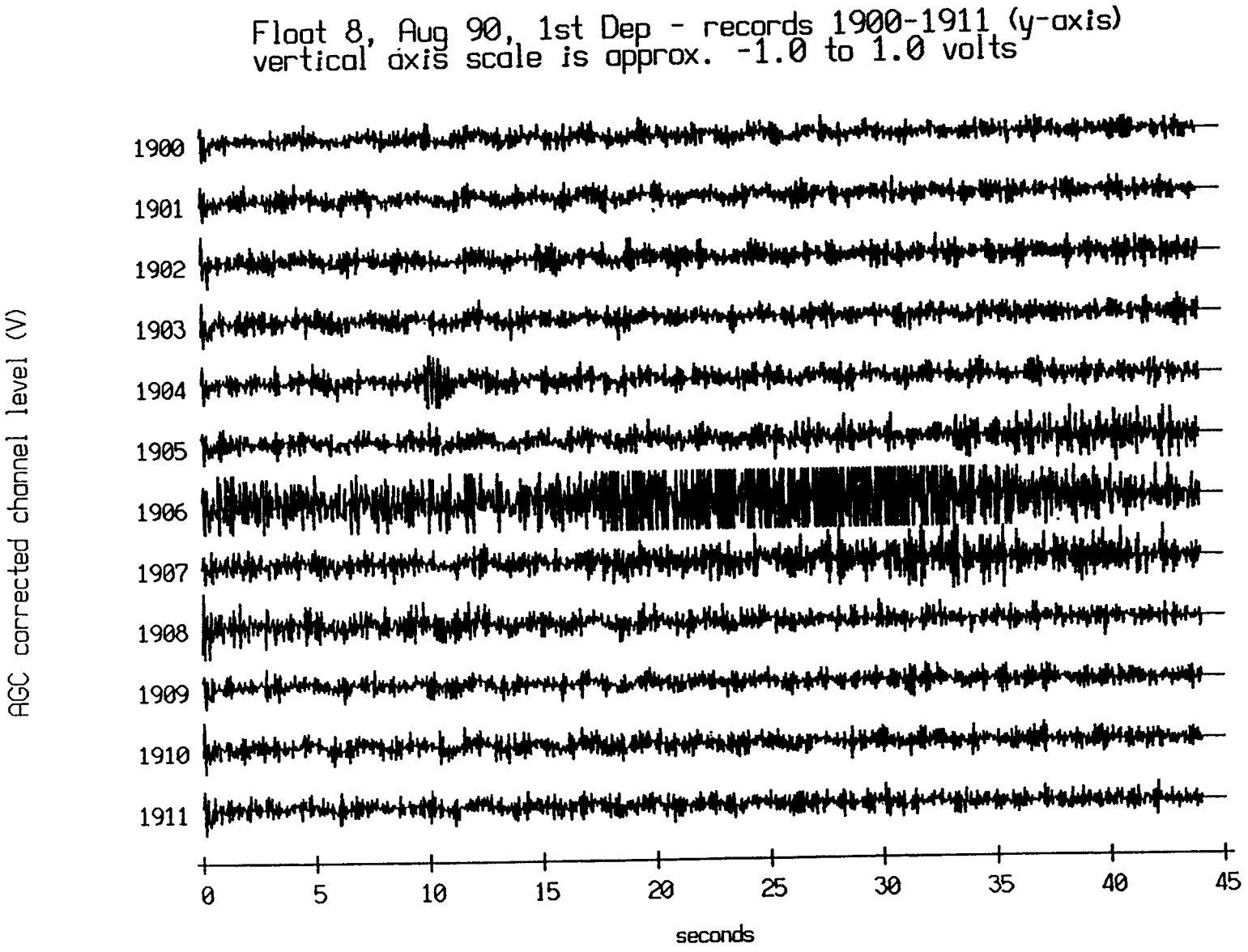

Figure IX.12b

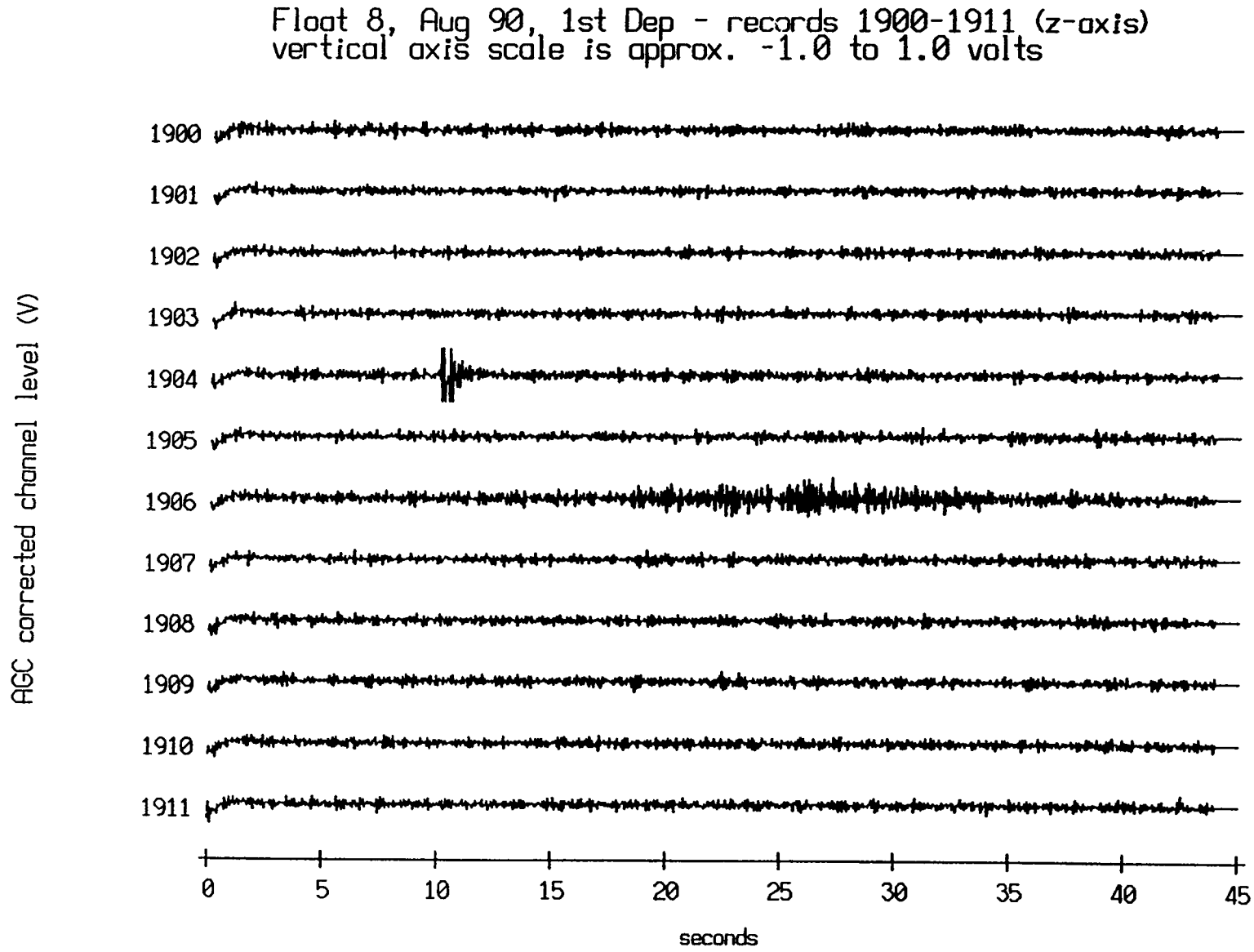

Figure IX.12c

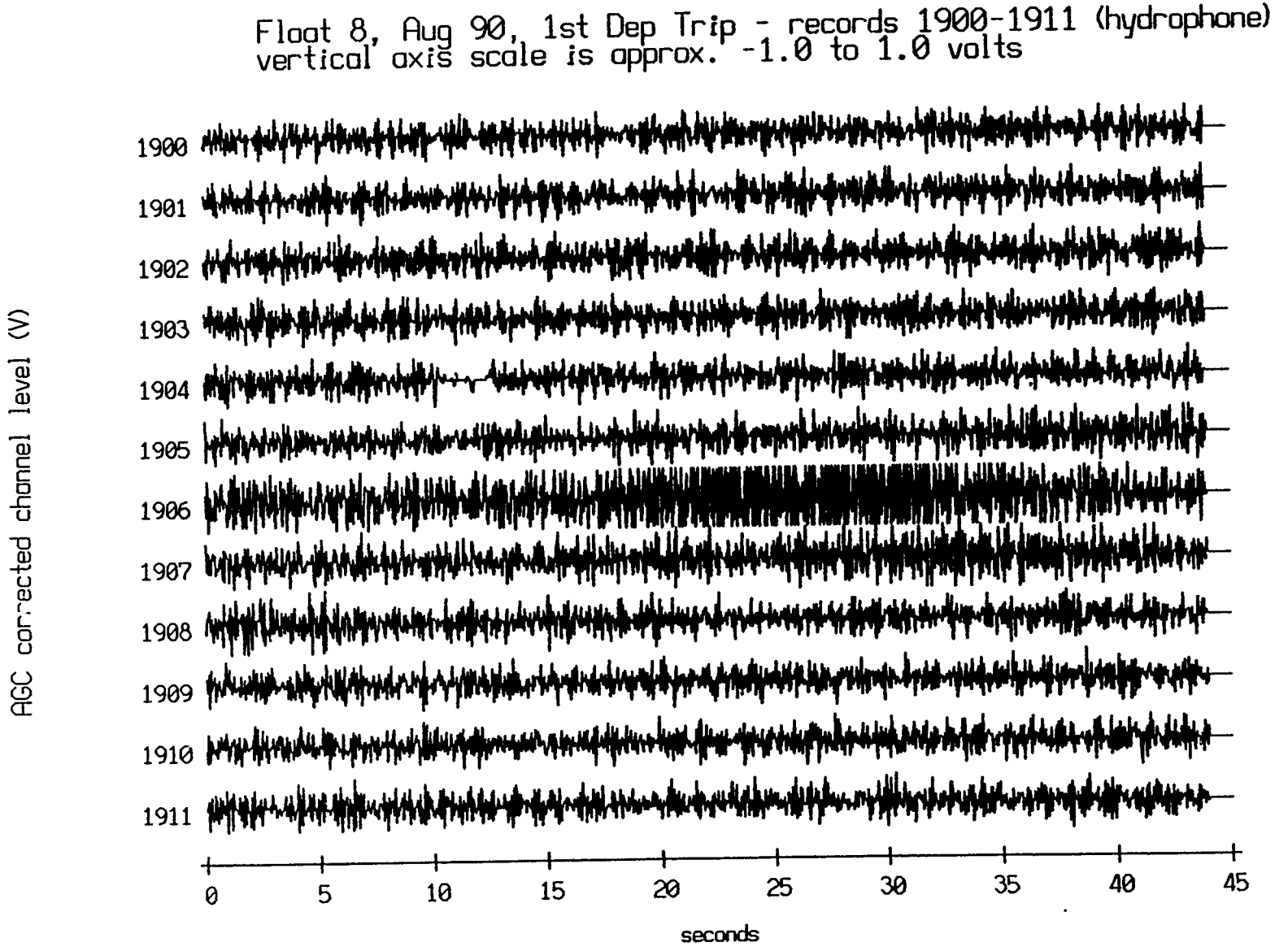

Figure IX.12d

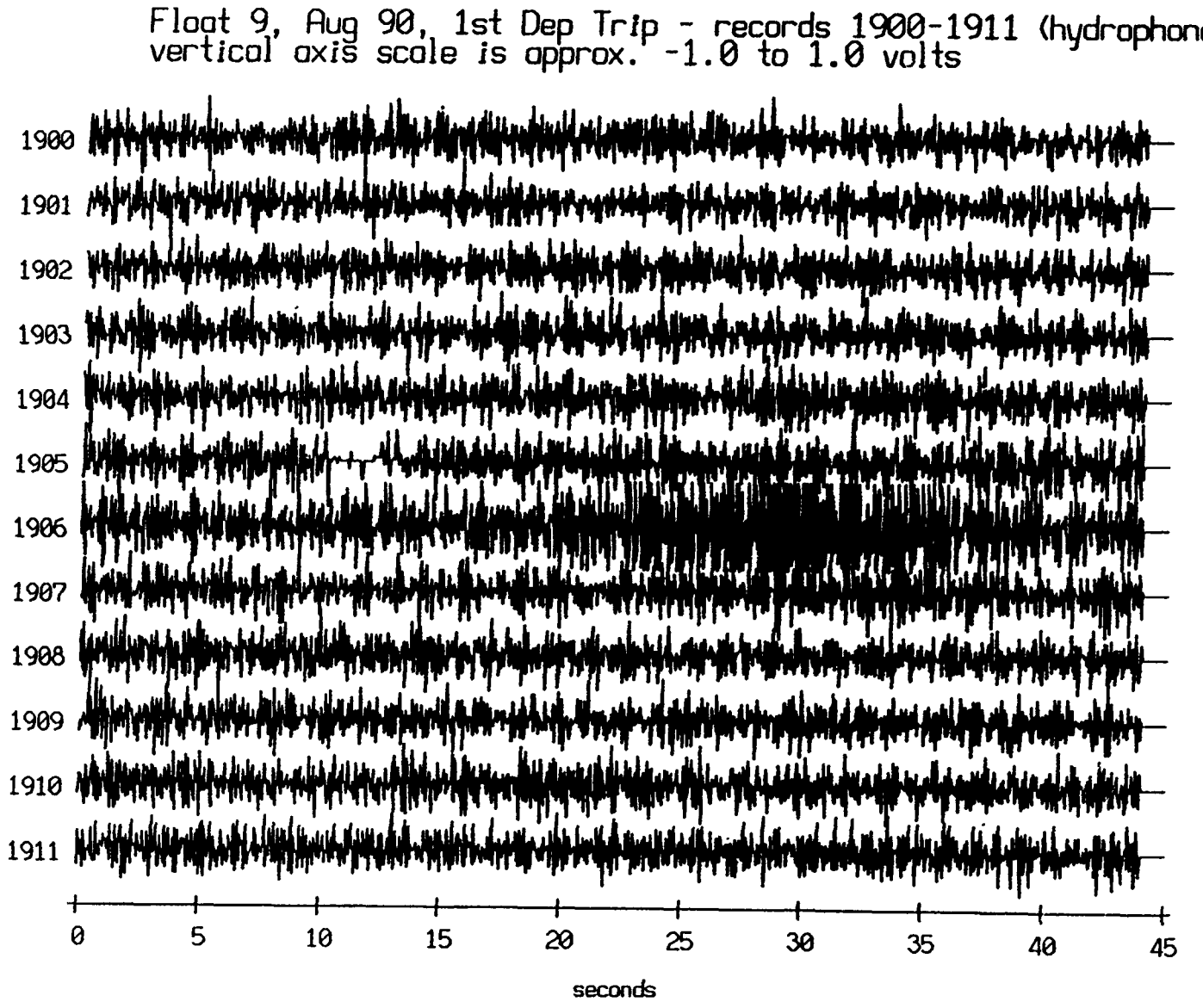
Float 9, Aug 90, 1st Dep Trip - records 1900-1911 (hydrophone)
vertical axis scale is approx. -1.0 to 1.0 volts
1900
1901
1902
1903
1904
1905
1906
1907
1908
1909
1910
1911
0
5
10
15
20
25
30
35
40
45
seconds
AGC corrected channel level (V)

Figure IX.13

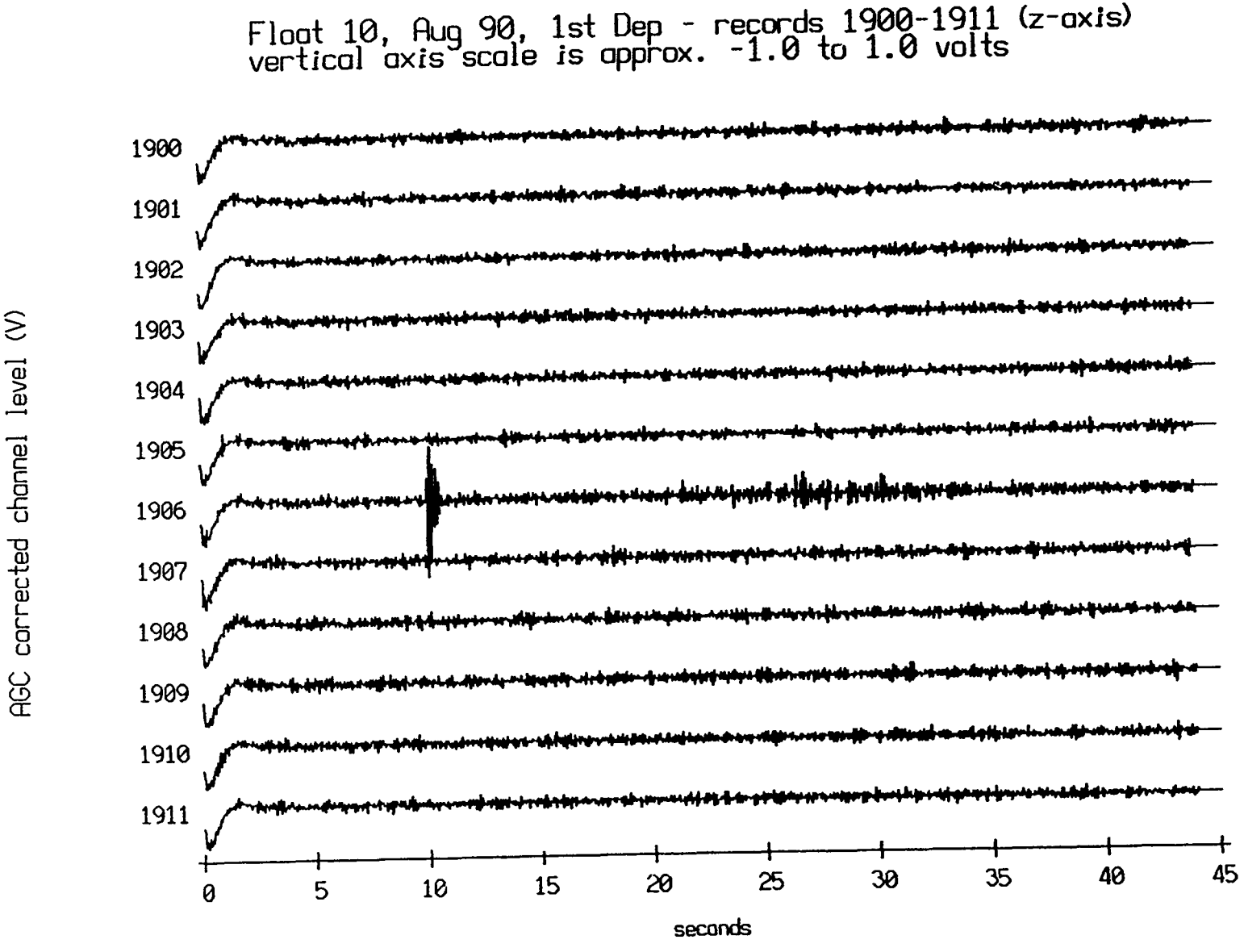

Figure IX.14a

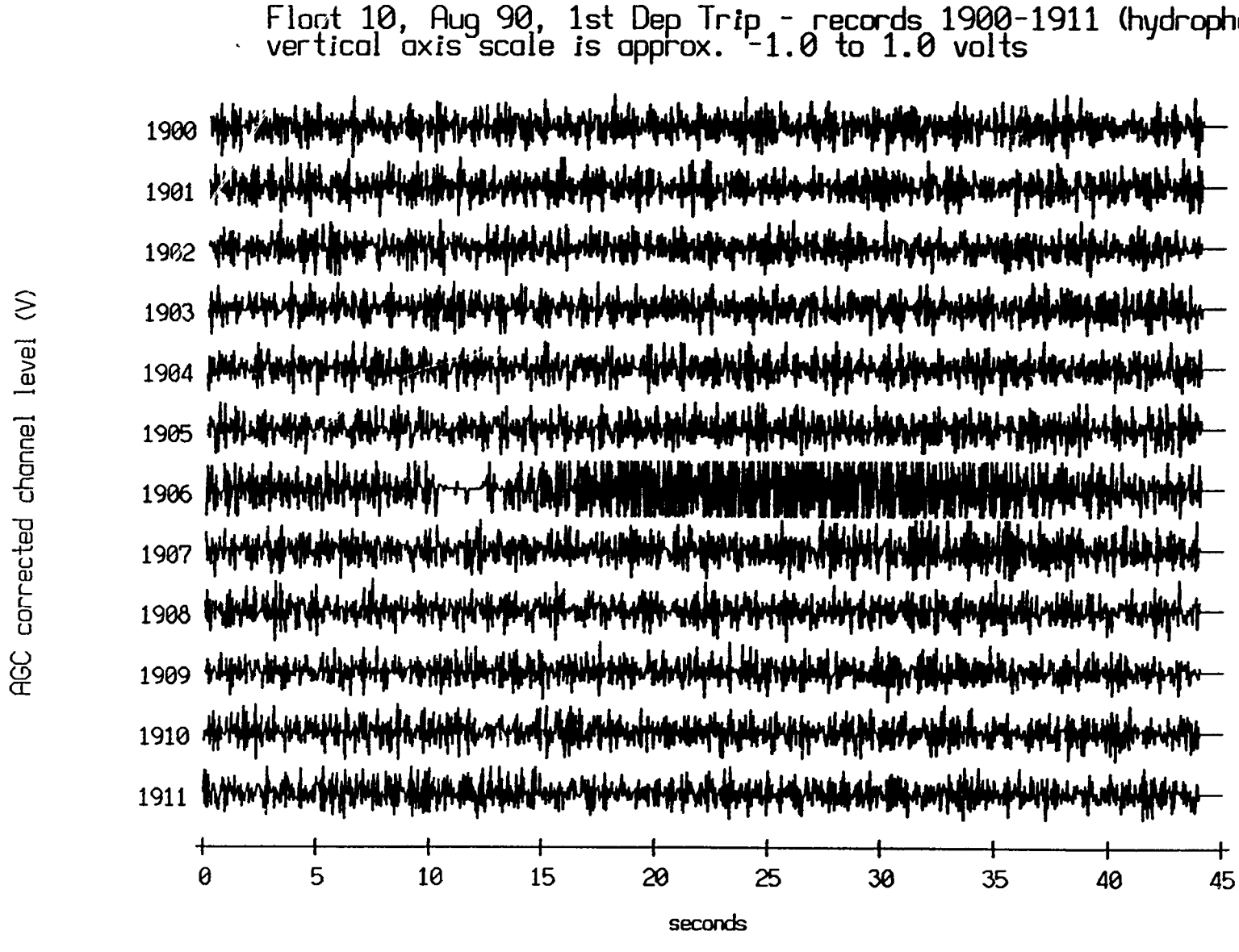

Figure IX.14b

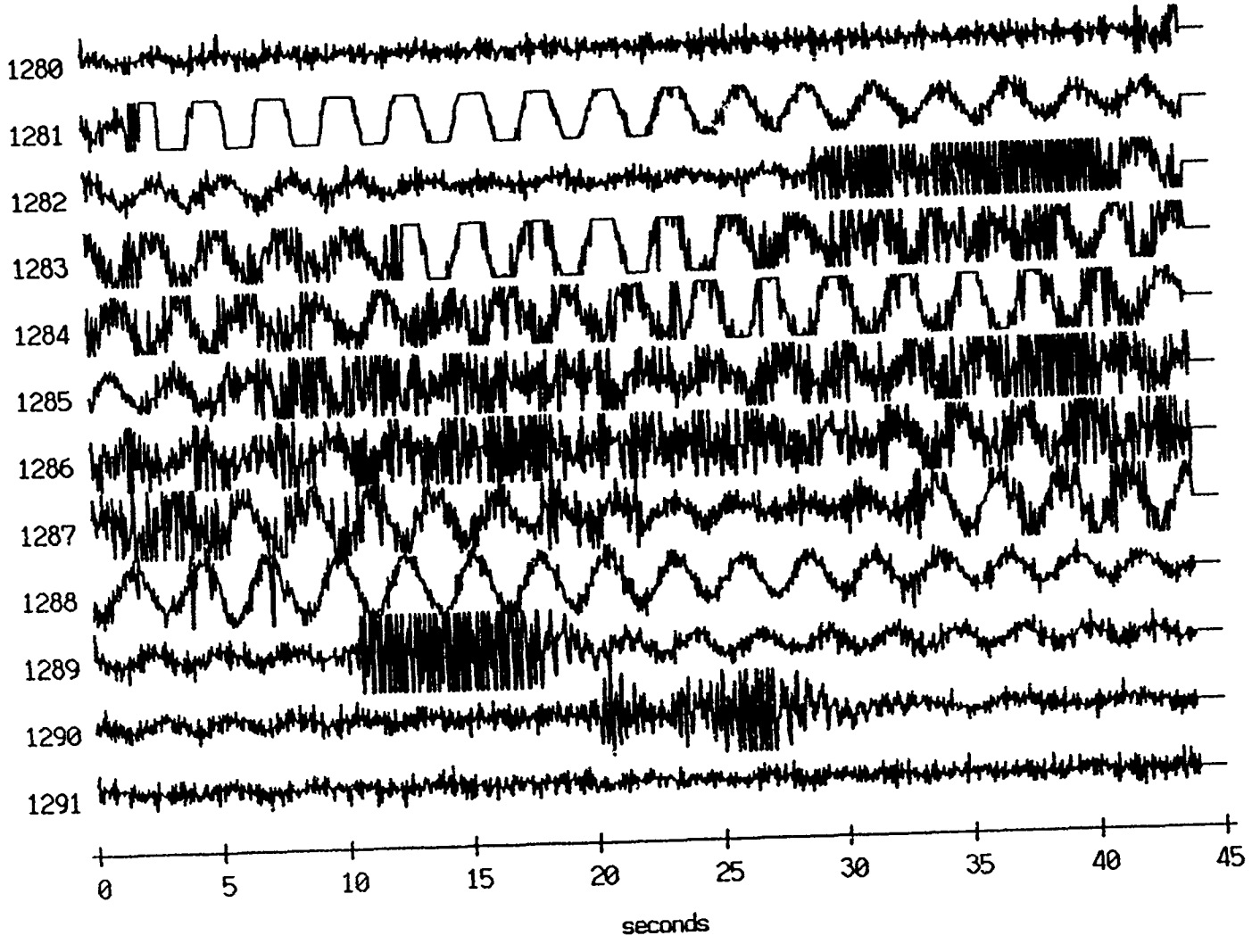

Figure IX.15a

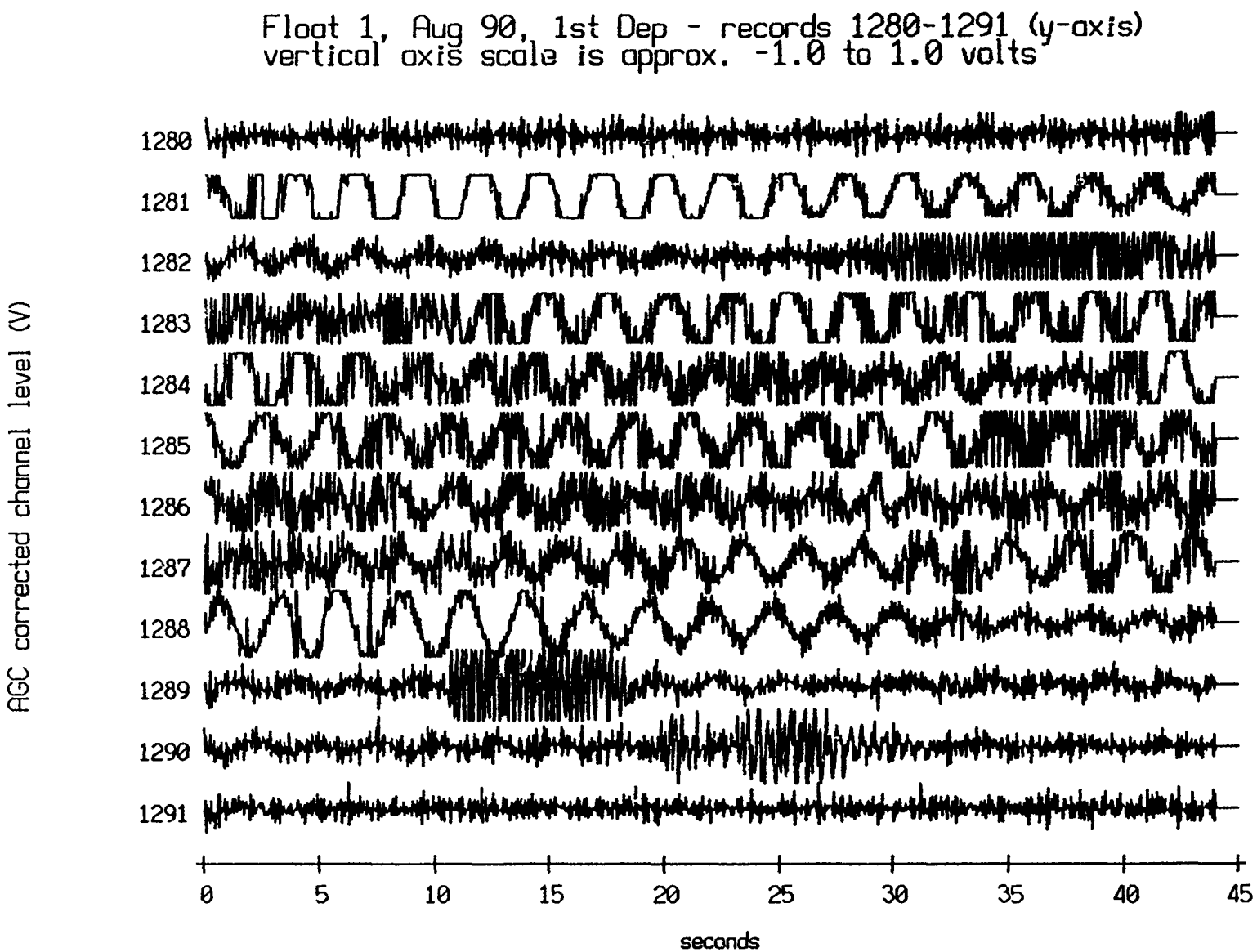

Figure IX.15b

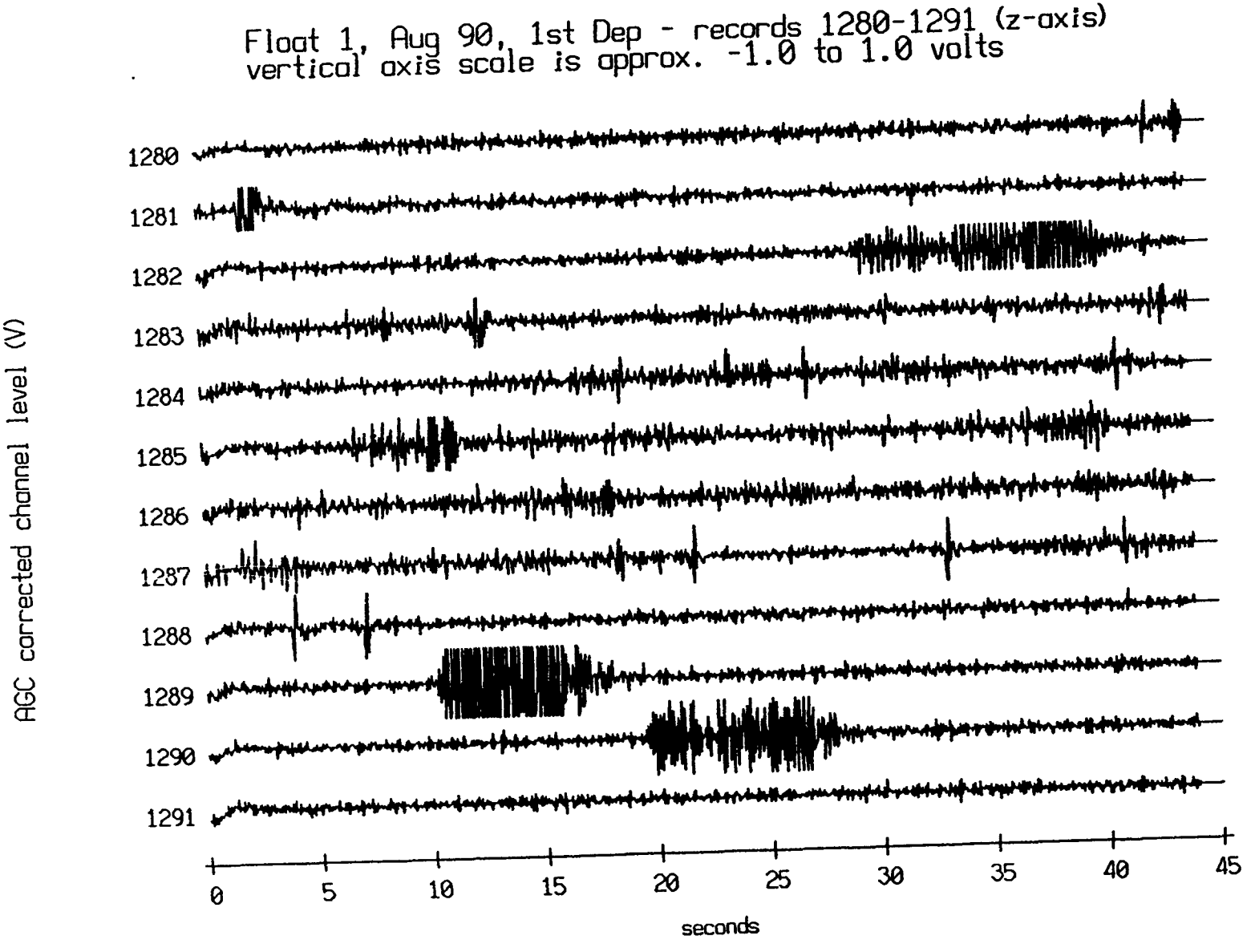

Figure IX.15c

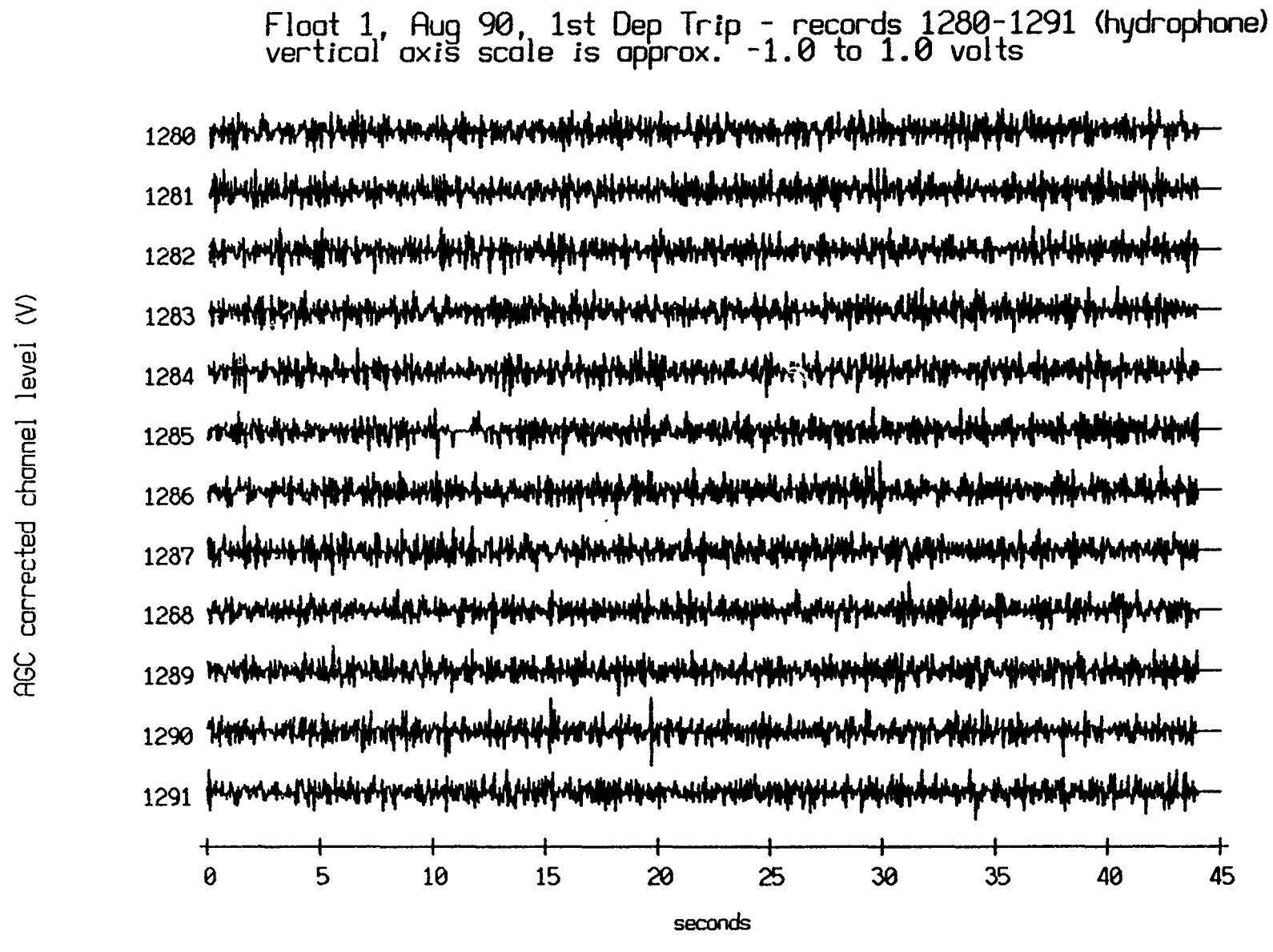

Figure IX.15d

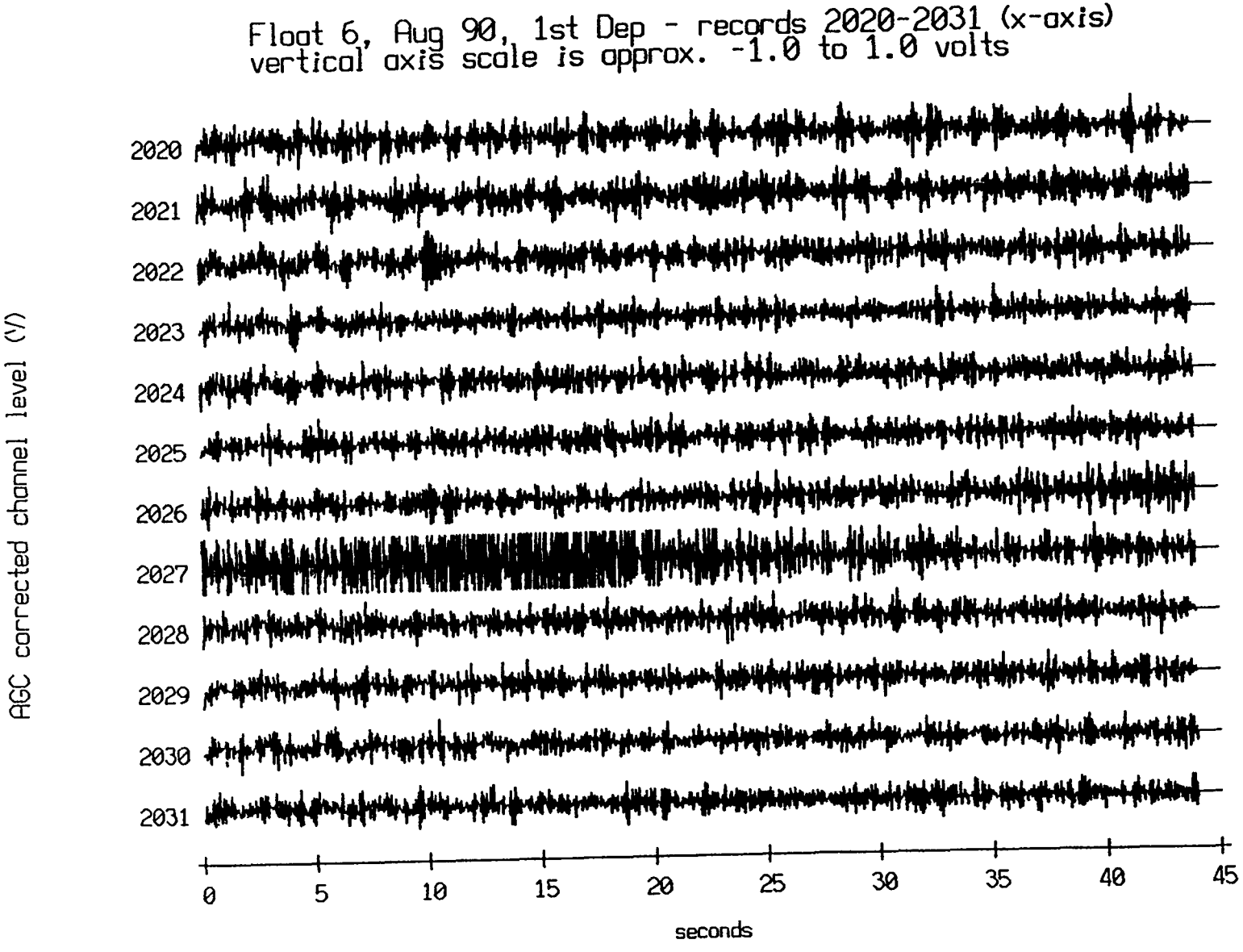

Figure IX.16a

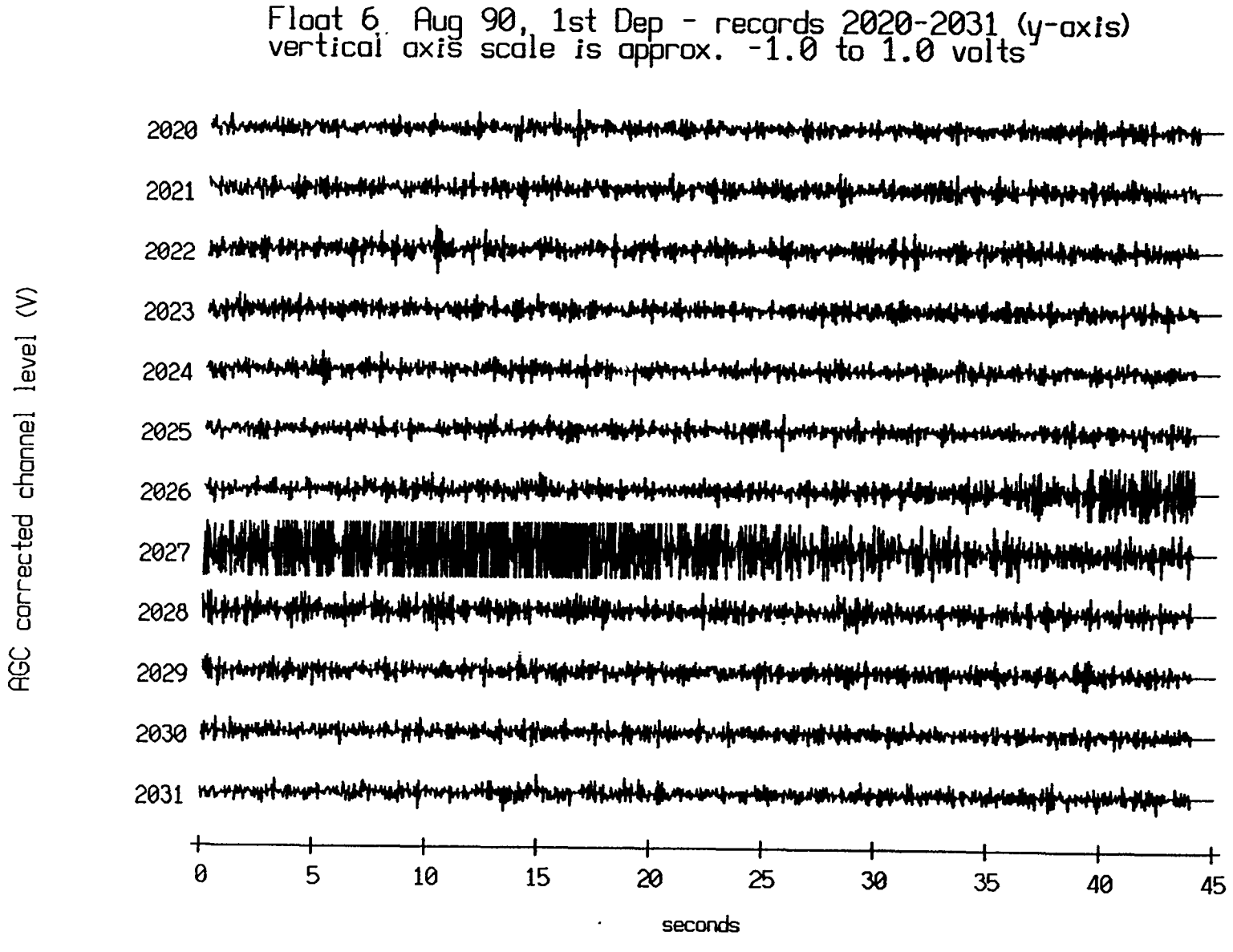

Figure IX.16b

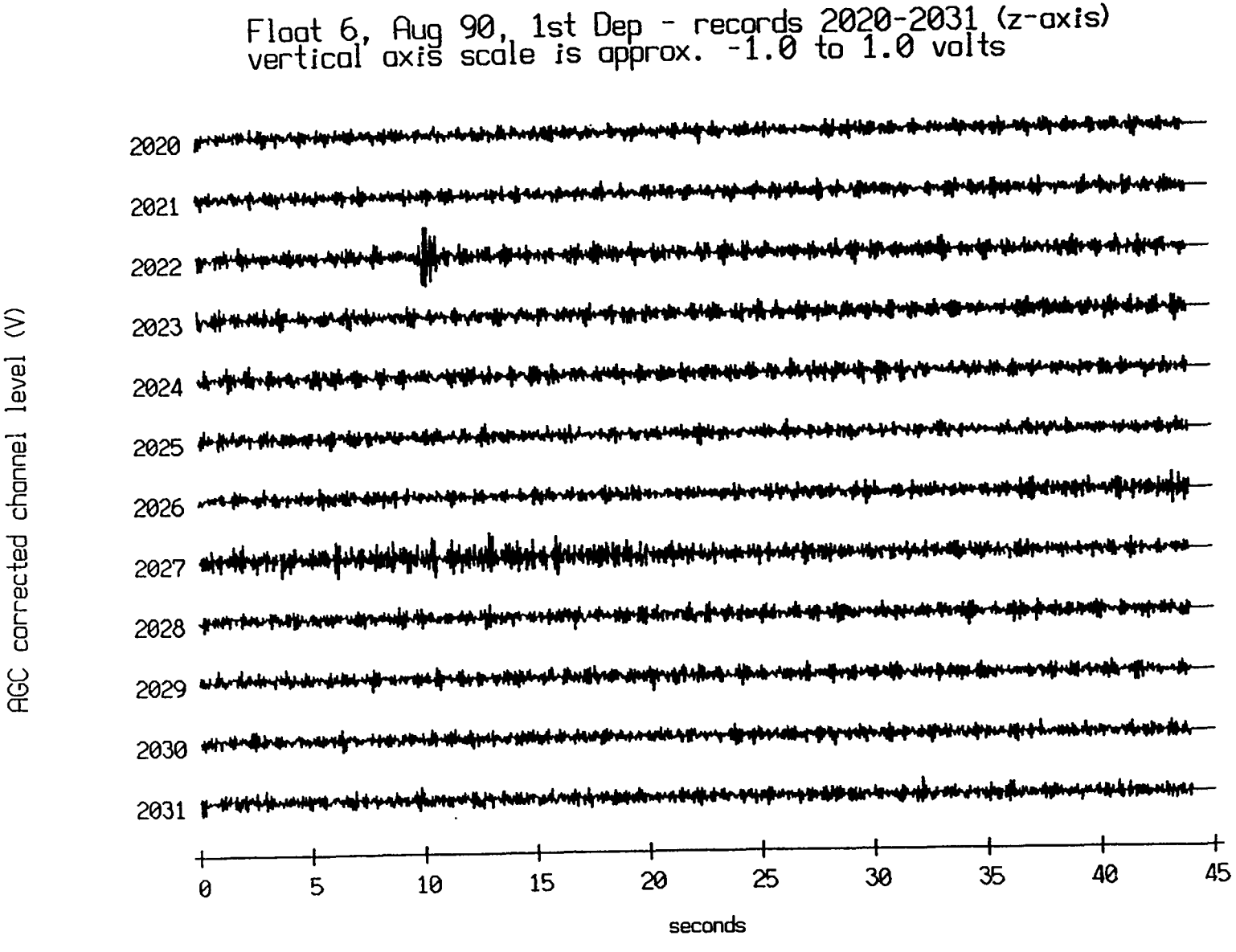

Figure IX.16c

Figure IX.16d

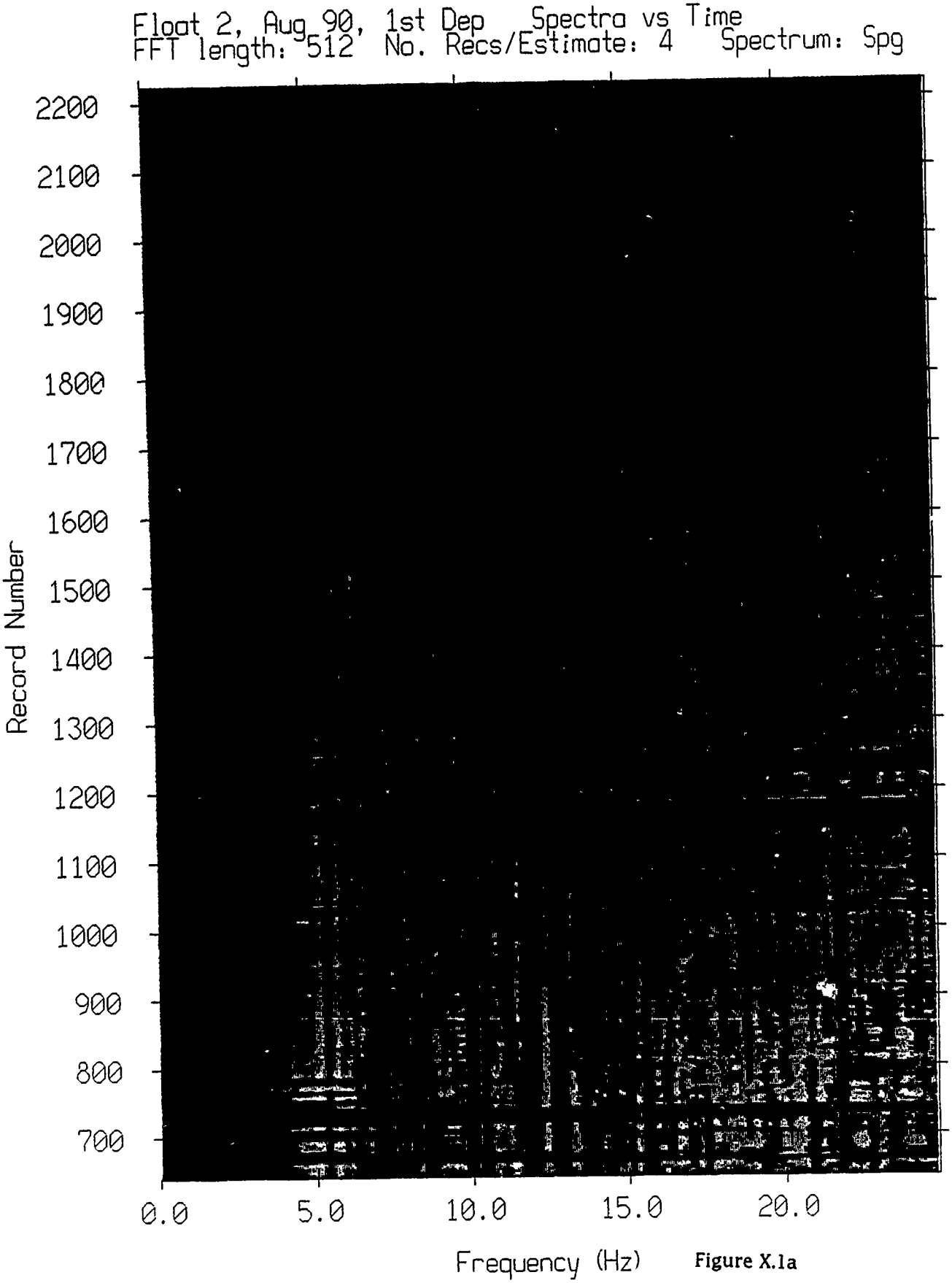
Float 2, Aug 90, 1st Dep Spectra vs Time
FFT length: 512 No. Recs/Estimate: 4 Spectrum: Spg
Record Number
2200
2100
2000
1900
1800
1700
1600
1500
1400
1300
1200
1100
1000
900
800
700
0.0
5.0
10.0
15.0
20.0
Frequency (Hz)

Figure X.1a

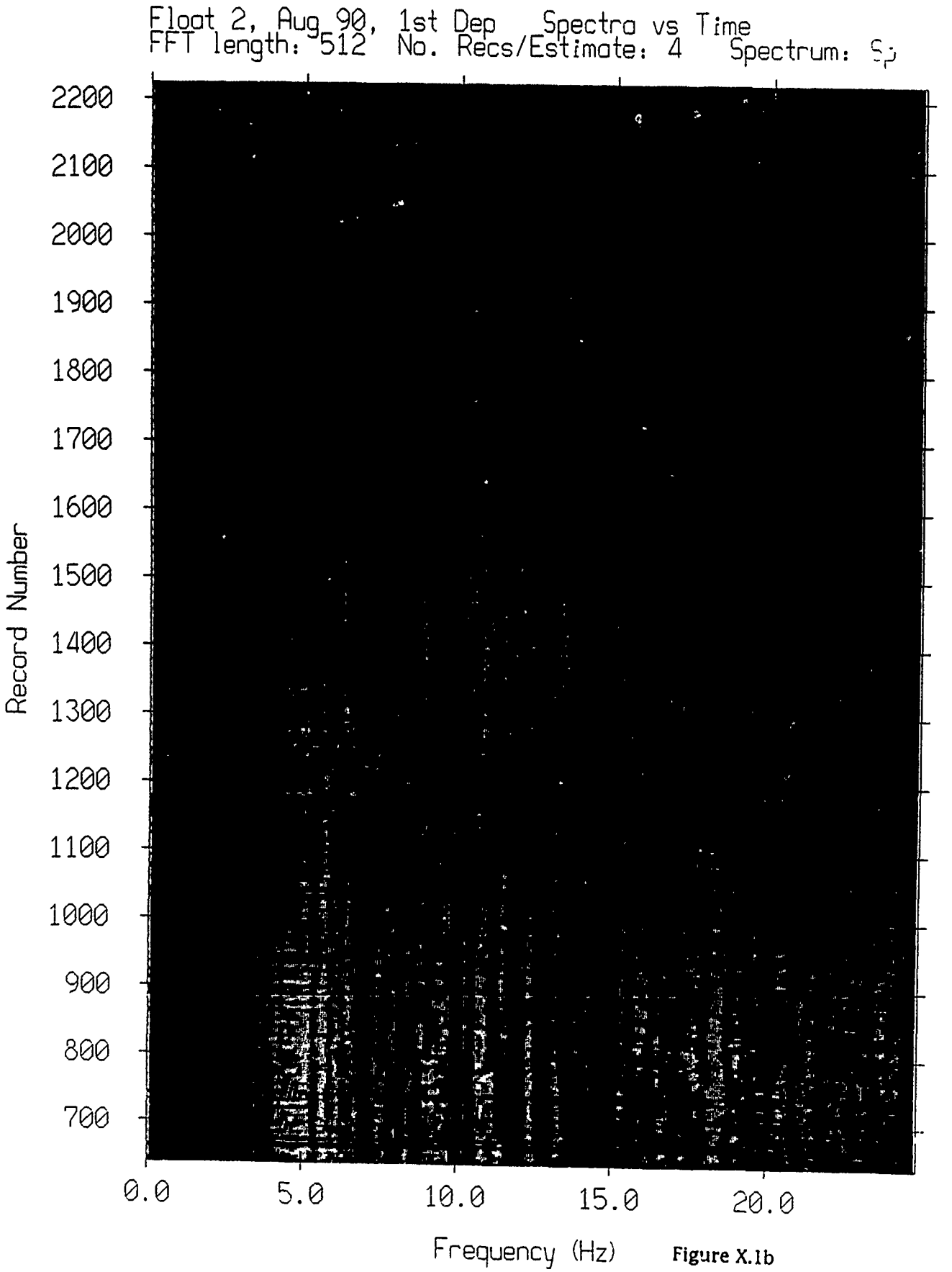
Float 2, Aug 90, 1st Dep Spectra vs Time
FFT length: 512 No. Recs/Estimate: 4 Spectrum: Sp
Record Number
2200
2100
2000
1900
1800
1700
1600
1500
1400
1300
1200
1100
1000
900
800
700
0.0
5.0
10.0
15.0
20.0
Frequency (Hz)

Figure X.1b

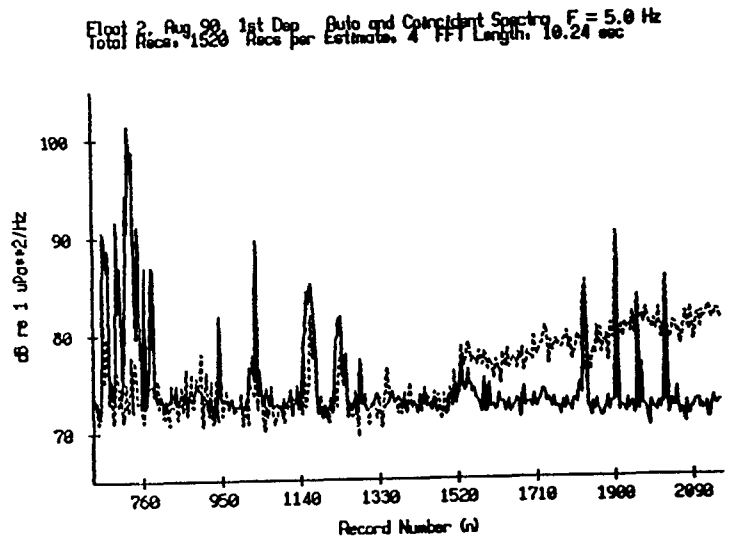
Float 2, Aug 90, 1st Dep Auto and Coincident Spectra, F = 5.0 Hz
Total Recs. 1520 Recs per Estimate. 4 FFT Length. 10.24 sec
dB re 1 uPa**2/Hz
100
90
80
70
760
950
1140
1330
1520
1710
1900
2090
Record Number (n)

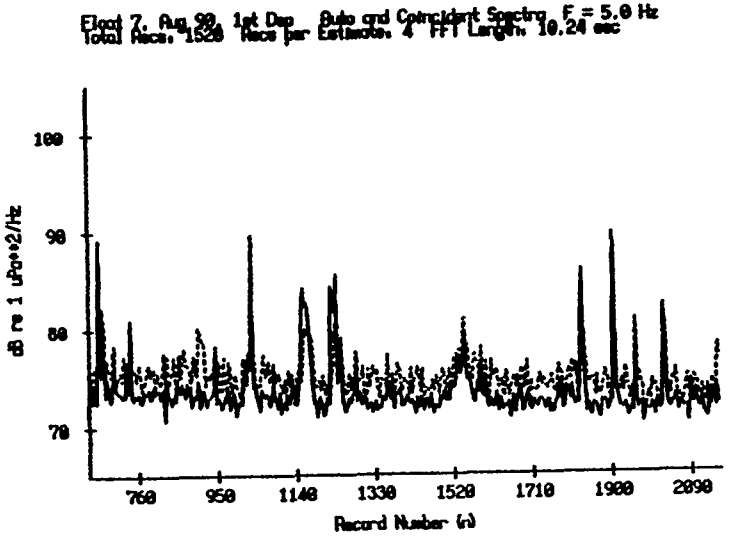
Float 7, Aug 90, 1st Dep Auto and Coincident Spectra, F = 5.0 Hz
Total Recs. 1520 Recs per Estimate. 4 FFT Length. 10.24 sec
dB re 1 uPa**2/Hz
100
90
80
70
760
950
1140
1330
1520
1710
1900
2090
Record Number (n)

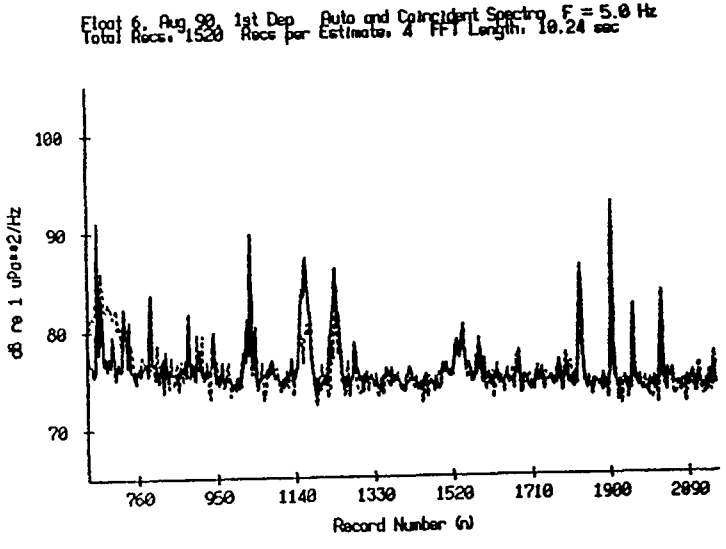
Float 6, Aug 90, 1st Dep Auto and Coincident Spectra, F = 5.0 Hz
Total Recs. 1520 Recs per Estimate. 4 FFT Length. 10.24 sec
dB re 1 uPa**2/Hz
100
90
80
70
760
950
1140
1330
1520
1710
1900
2090
Record Number (n)

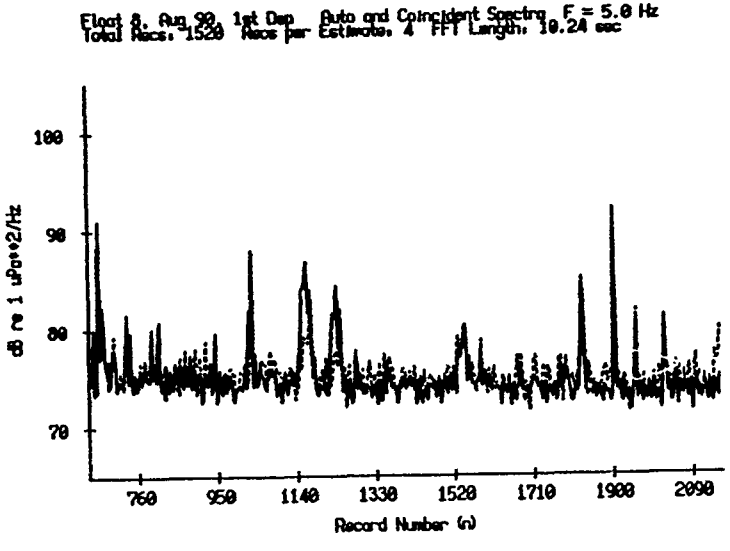
Float 8, Aug 90, 1st Dep Auto and Coincident Spectra, F = 5.0 Hz
Total Recs. 1520 Recs per Estimate. 4 FFT Length. 10.24 sec
dB re 1 uPa**2/Hz
100
90
80
70
760
950
1140
1330
1520
1710
1900
2090
Record Number (n)

Figure X.2

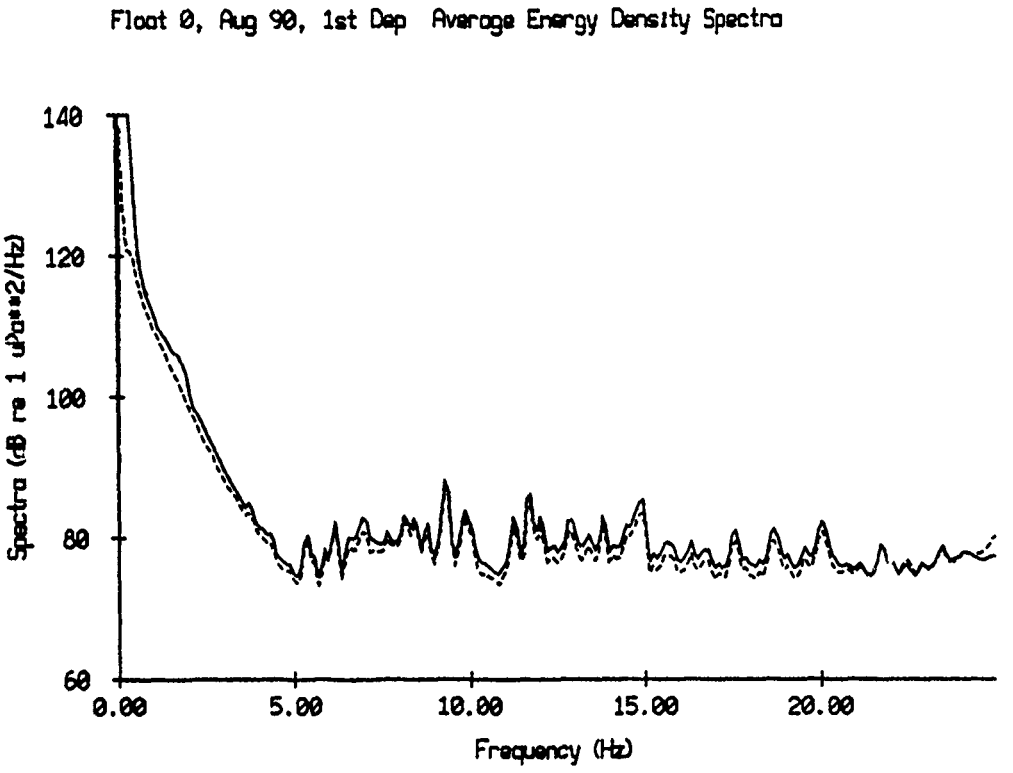
Float 0, Aug 90, 1st Dep Average Energy Density Spectra
Spectra (dB re 1 uPa**2/Hz)
140
120
100
80
60
0.00
5.00
10.00
15.00
20.00
Frequency (Hz)

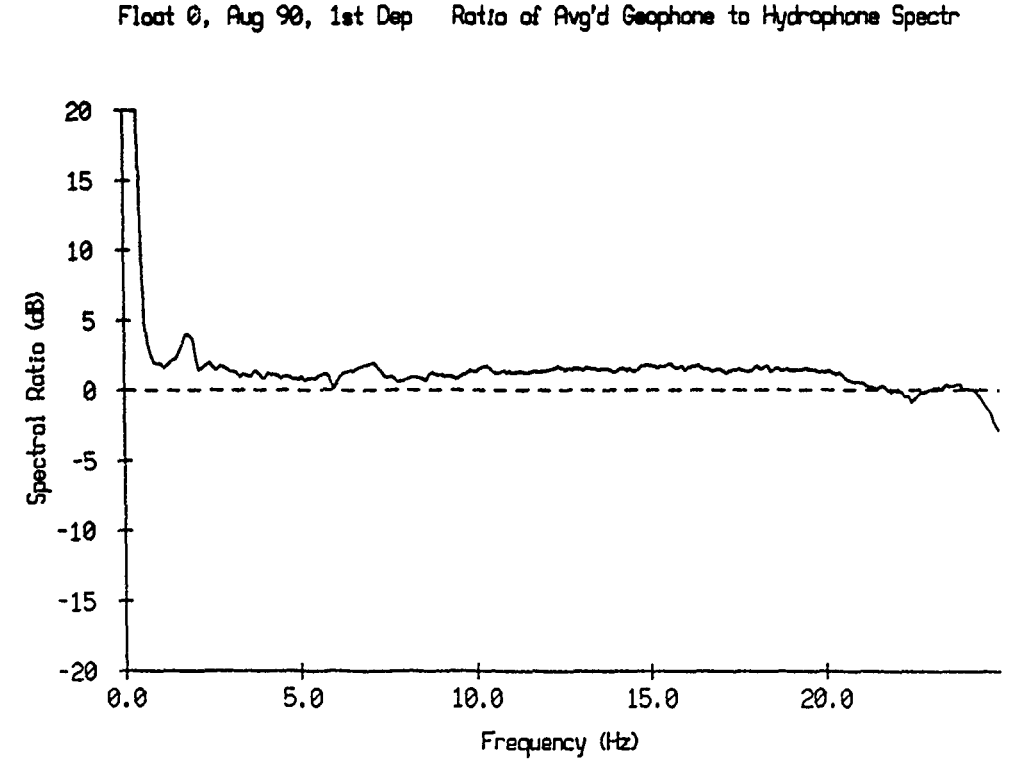
Float 0, Aug 90, 1st Dep Ratio of Avg'd Geophone to Hydrophone Spectr
Spectral Ratio (dB)
20
15
10
5
0
-5
-10
-15
-20
0.0
5.0
10.0
15.0
20.0
Frequency (Hz)

Figure X.3

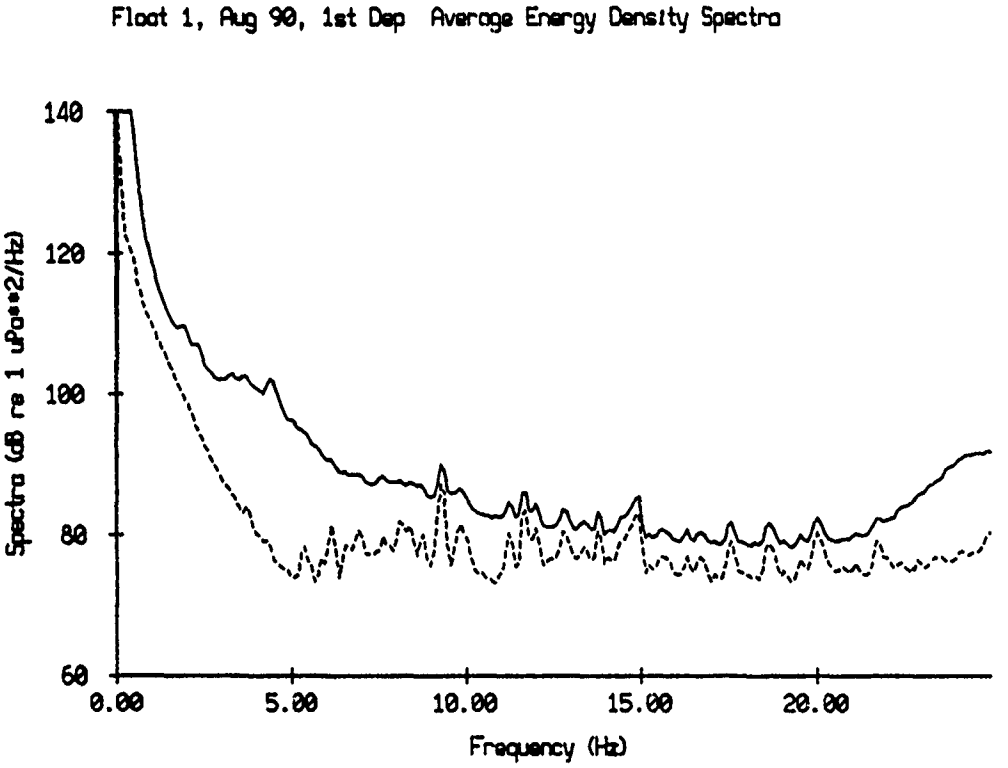
Float 1, Aug 90, 1st Dep Average Energy Density Spectra
Spectra (dB re 1 uPa**2/Hz)
140
120
100
80
60
0.00
5.00
10.00
15.00
20.00
Frequency (Hz)

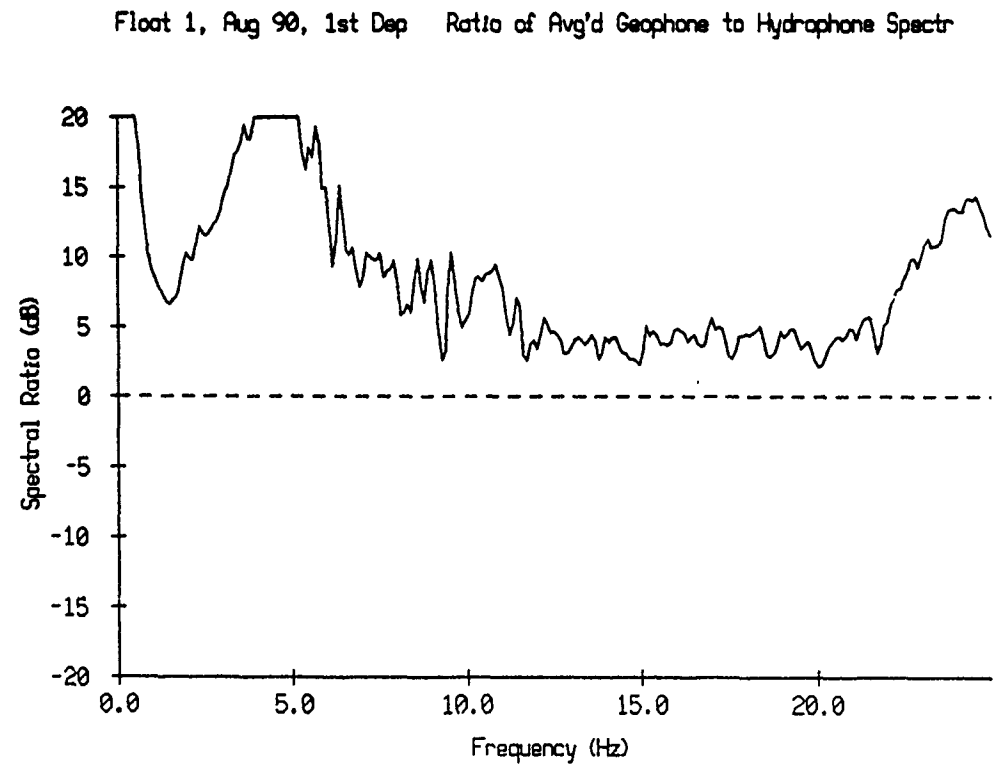
Float 1, Aug 90, 1st Dep Ratio of Avg'd Geophone to Hydrophone Spectr
Spectral Ratio (dB)
20
15
10
5
0
-5
-10
-15
-20
0.0
5.0
10.0
15.0
20.0
Frequency (Hz)

Figure X.4

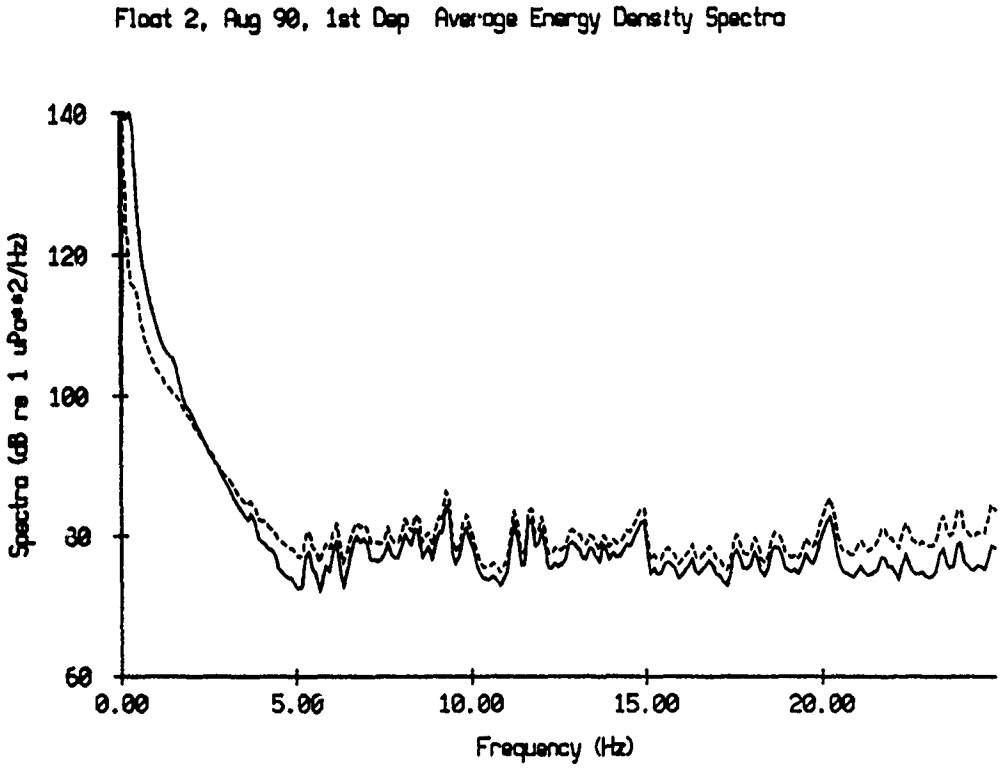
Float 2, Aug 90, 1st Dep Average Energy Density Spectra
140
120
100
80
60
Spectra (dB re 1 uPa**2/Hz)
0.00
5.00
10.00
15.00
20.00
Frequency (Hz)

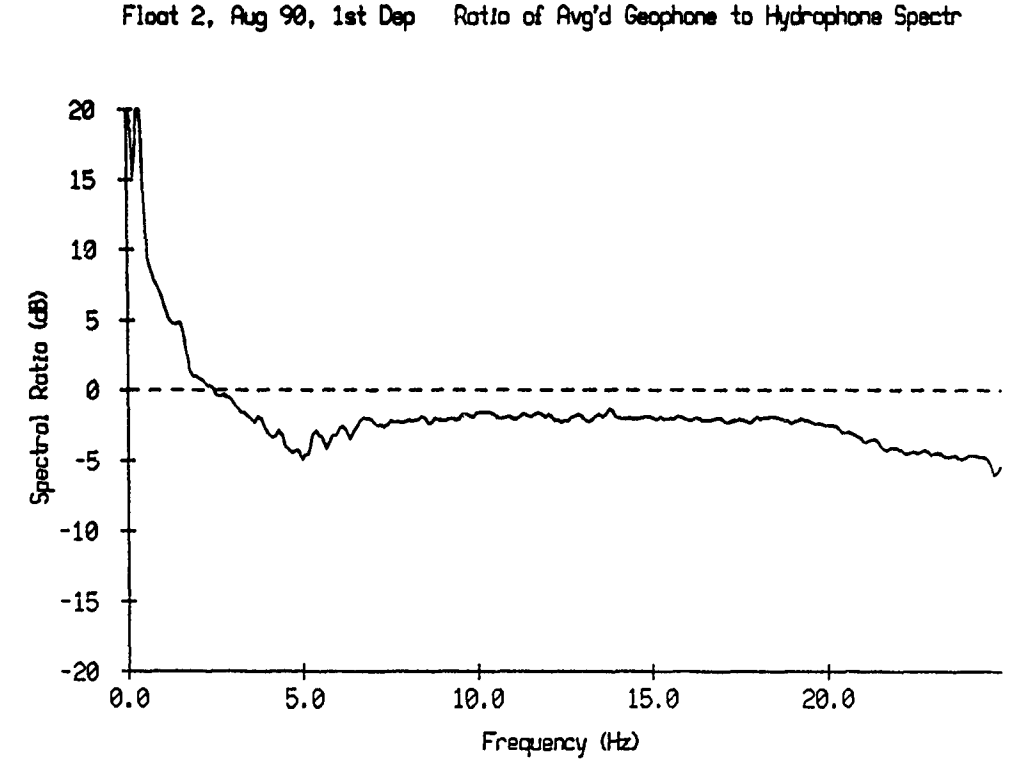
Float 2, Aug 90, 1st Dep Ratio of Avg'd Geophone to Hydrophone Spectr
20
15
10
5
0
-5
-10
-15
-20
Spectral Ratio (dB)
0.0
5.0
10.0
15.0
20.0
Frequency (Hz)

Figure X.5

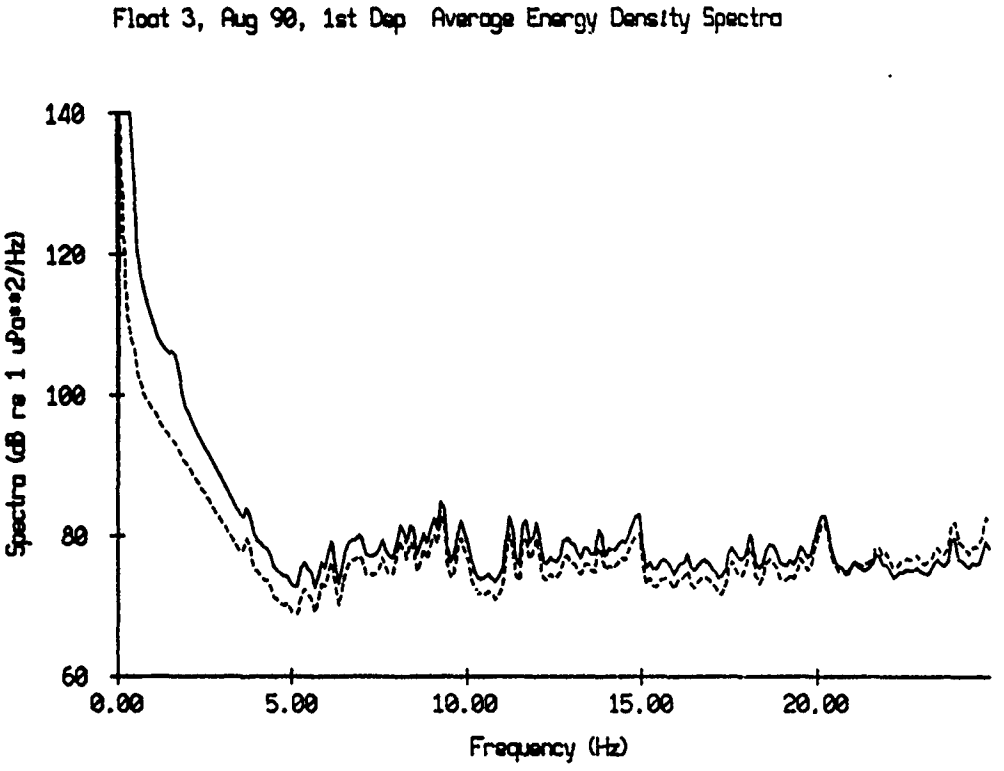
Float 3, Aug 90, 1st Dep Average Energy Density Spectra
Spectra (dB re 1 uPa**2/Hz)
140
120
100
80
60
0.00
5.00
10.00
15.00
20.00
Frequency (Hz)

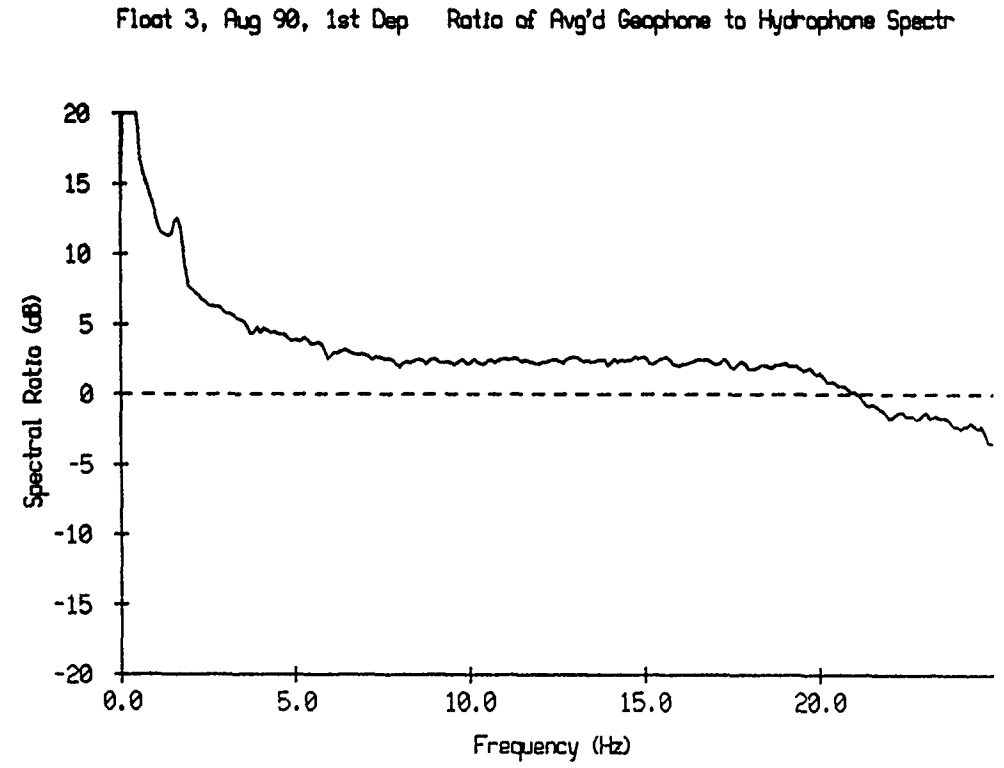
Float 3, Aug 90, 1st Dep Ratio of Avg'd Geophone to Hydrophone Spectr
Spectral Ratio (dB)
20
15
10
5
0
-5
-10
-15
-20
0.0
5.0
10.0
15.0
20.0
Frequency (Hz)

Figure X.6

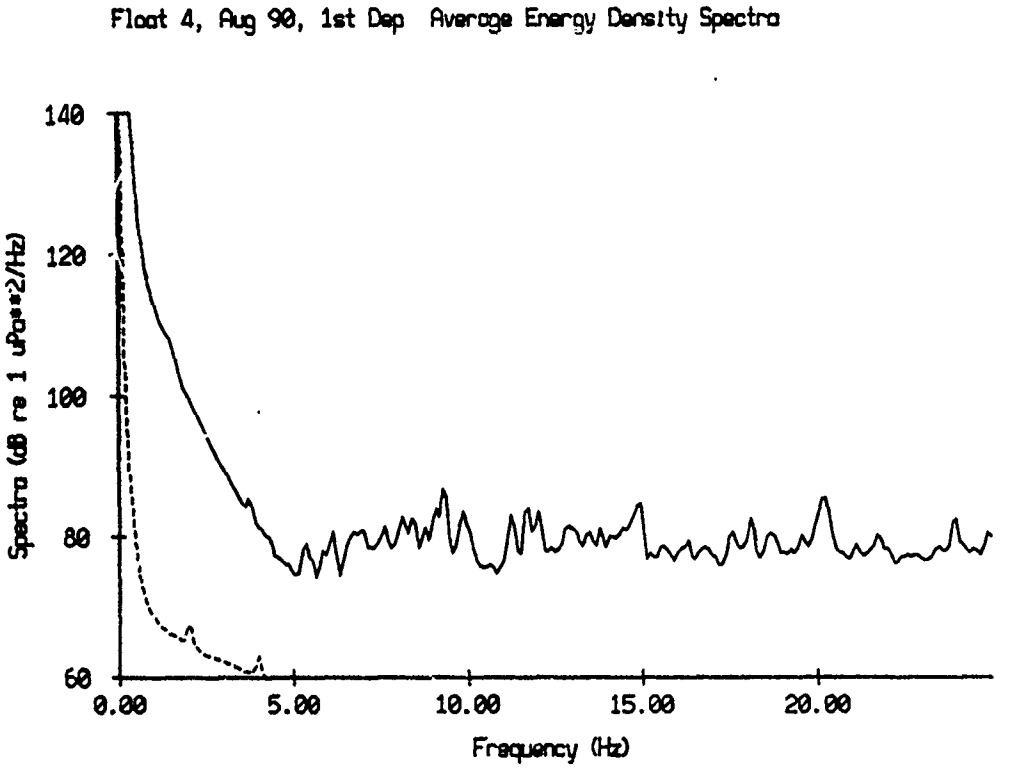
Float 4, Aug 90, 1st Dep Average Energy Density Spectra
140
120
100
80
60
Spectra (dB re 1 uPasa2/Hz)
0.00
5.00
10.00
15.00
20.00
Frequency (Hz)

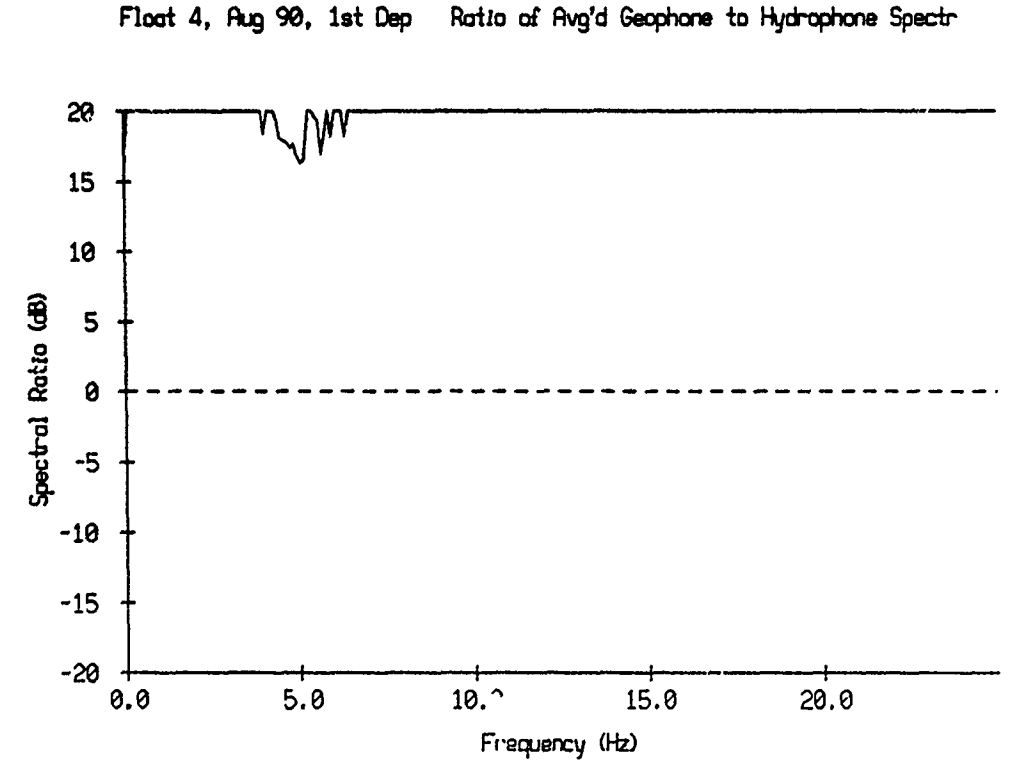
Float 4, Aug 90, 1st Dep Ratio of Avg'd Geophone to Hydrophone Spectr
20
15
10
5
0
-5
-10
-15
-20
Spectral Ratio (dB)
0.0
5.0
10.0
15.0
20.0
Frequency (Hz)

Figure X.7

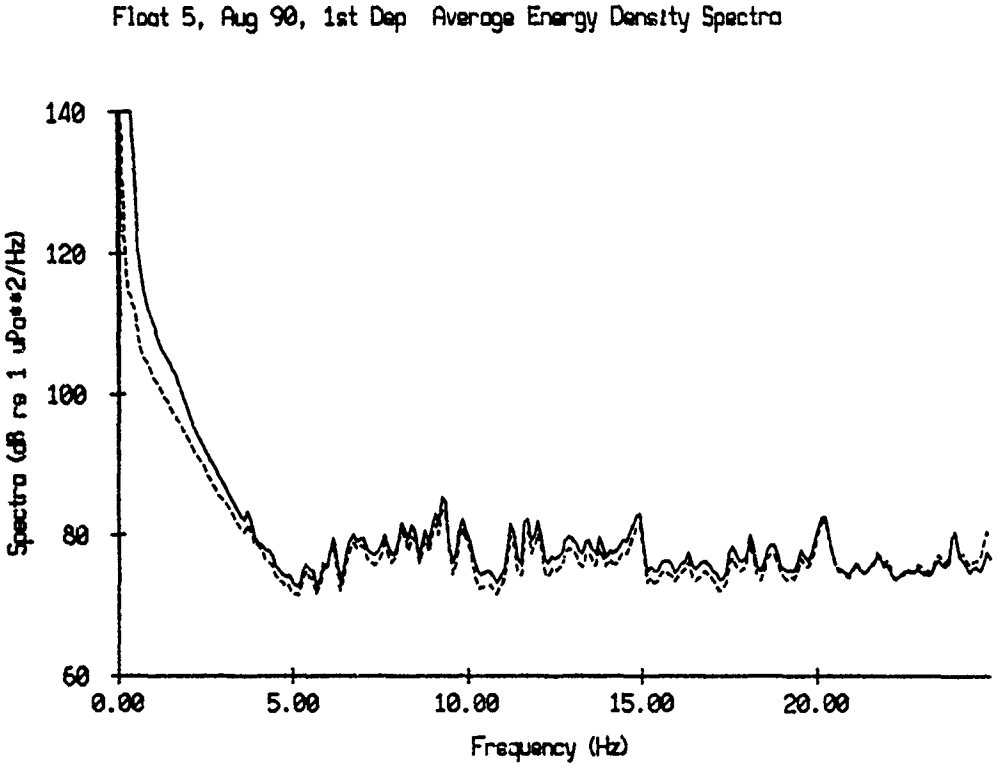
Float 5, Aug 90, 1st Dep Average Energy Density Spectra
Spectra (dB re 1 uPa**2/Hz)
140
120
100
80
60
0.00
5.00
10.00
15.00
20.00
Frequency (Hz)

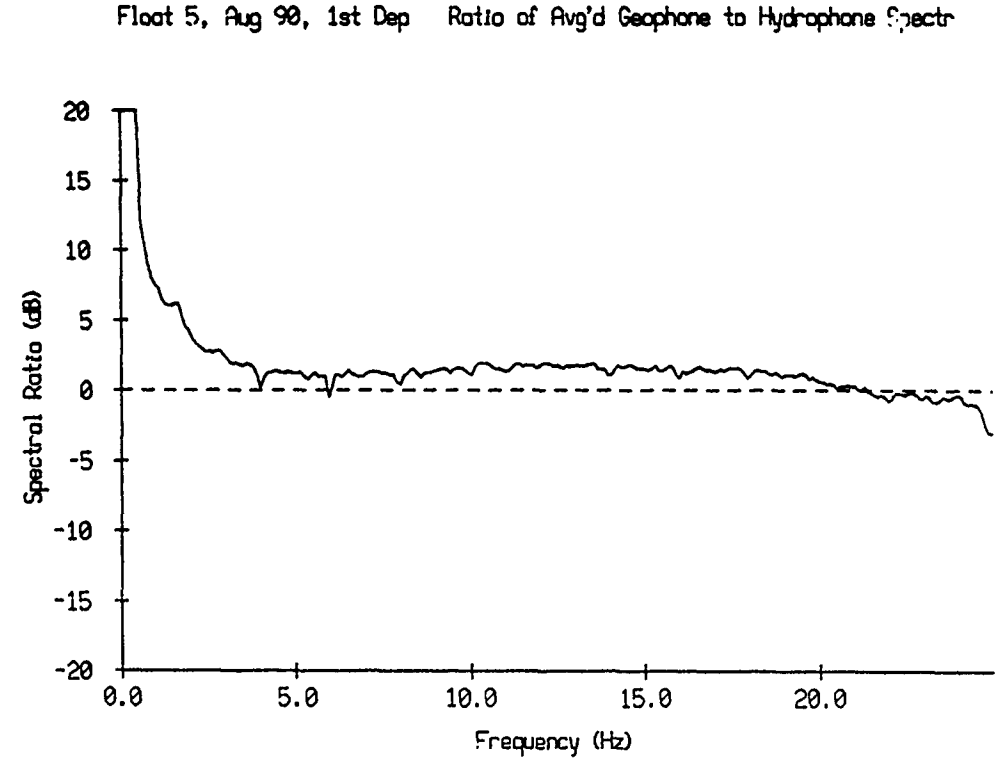
Float 5, Aug 90, 1st Dep Ratio of Avg'd Geophone to Hydrophone Spectr
Spectral Ratio (dB)
20
15
10
5
0
-5
-10
-15
-20
0.0
5.0
10.0
15.0
20.0
Frequency (Hz)

Figure X.8

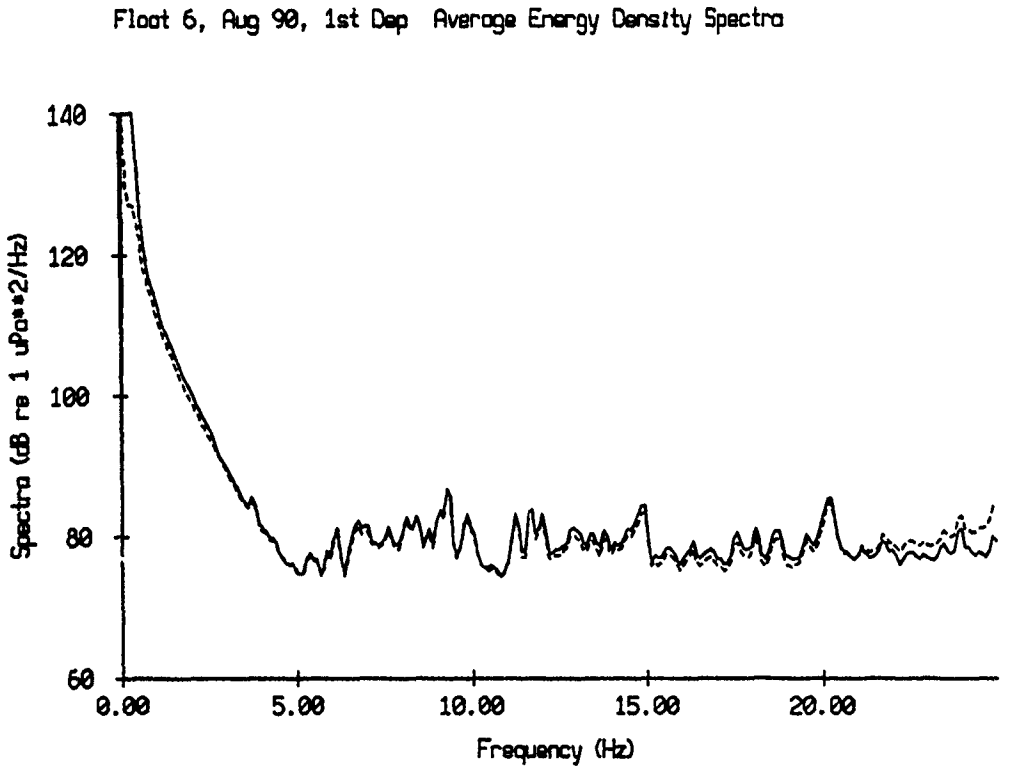
Float 6, Aug 90, 1st Dep Average Energy Density Spectra
140
120
100
80
60
Spectra (dB re 1 uPa**2/Hz)
0.00
5.00
10.00
15.00
20.00
Frequency (Hz)

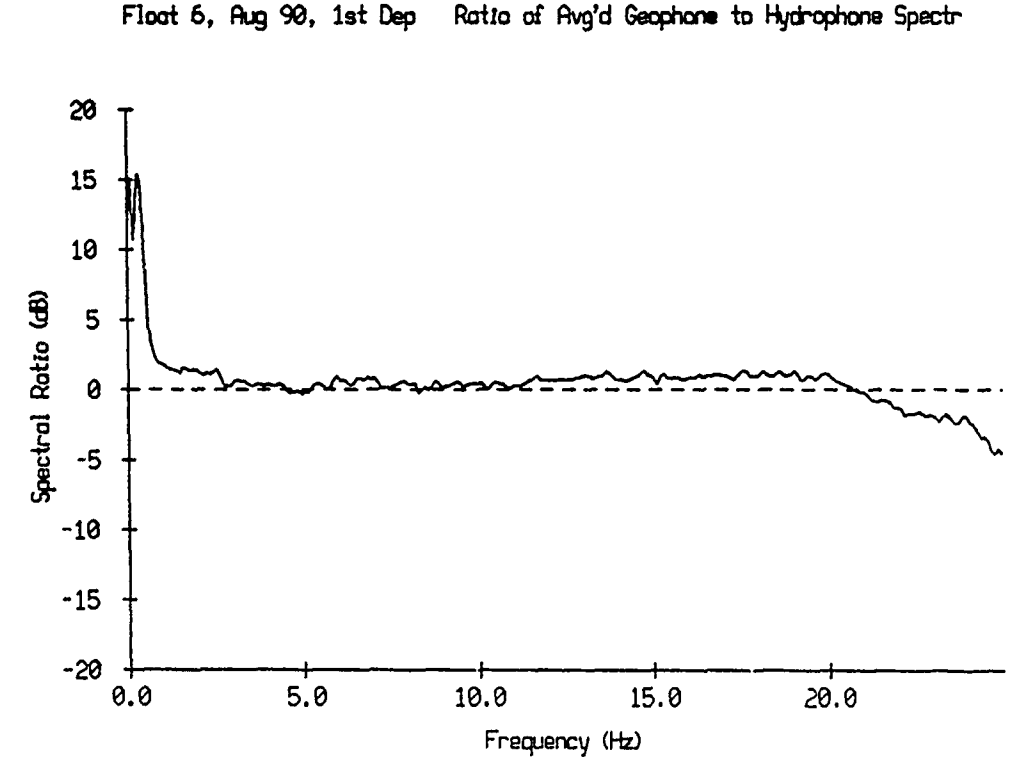
Float 6, Aug 90, 1st Dep Ratio of Avg'd Geophone to Hydrophone Spectr
20
15
10
5
0
-5
-10
-15
-20
Spectral Ratio (dB)
0.0
5.0
10.0
15.0
20.0
Frequency (Hz)

Figure X.9

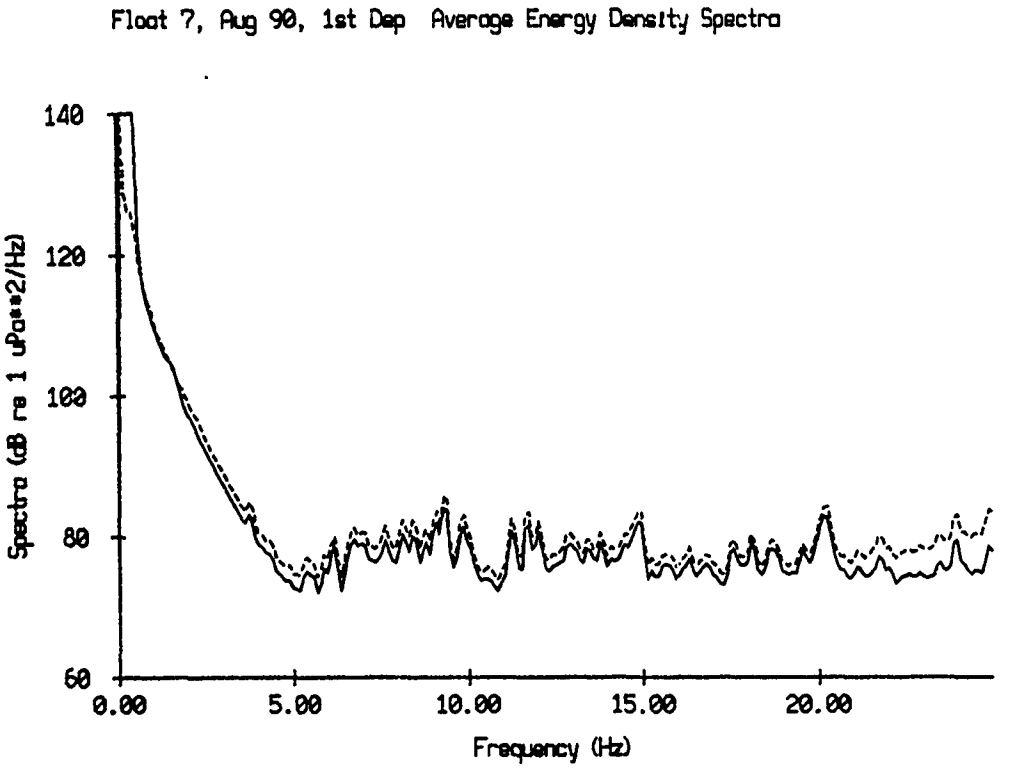
Float 7, Aug 90, 1st Dep Average Energy Density Spectra
Spectra (dB re 1 uPa**2/Hz)
140
120
100
80
60
0.00
5.00
10.00
15.00
20.00
Frequency (Hz)

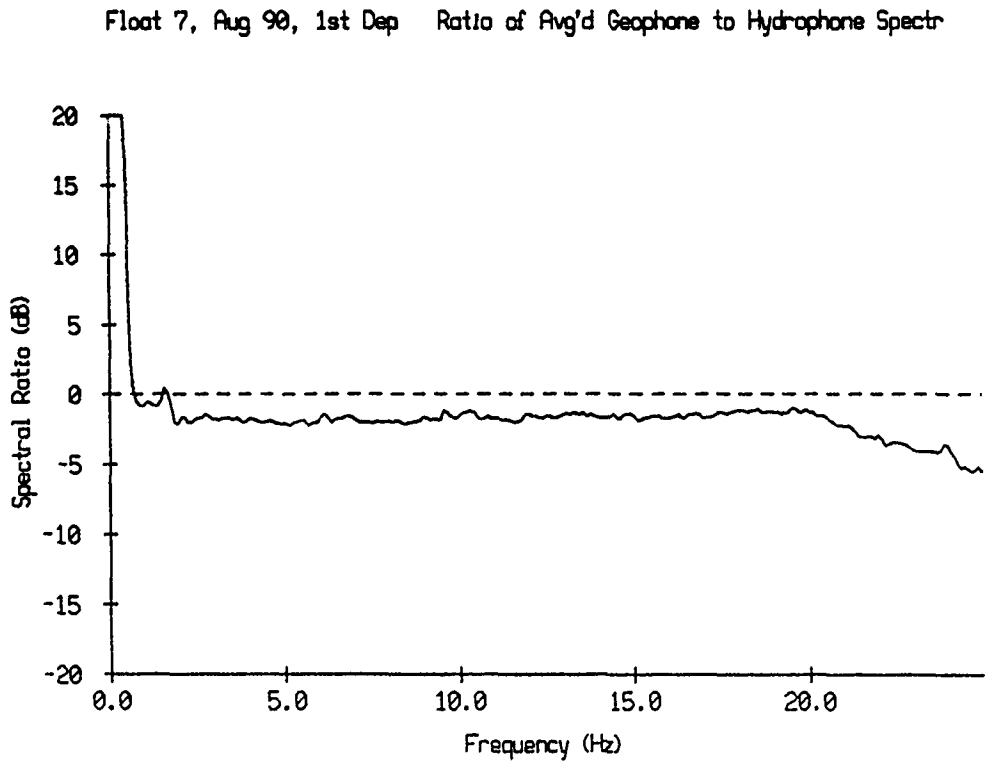
Float 7, Aug 90, 1st Dep Ratio of Avg'd Geophone to Hydrophone Spectr
Spectral Ratio (dB)
20
15
10
5
0
-5
-10
-15
-20
0.0
5.0
10.0
15.0
20.0
Frequency (Hz)

Figure X.10

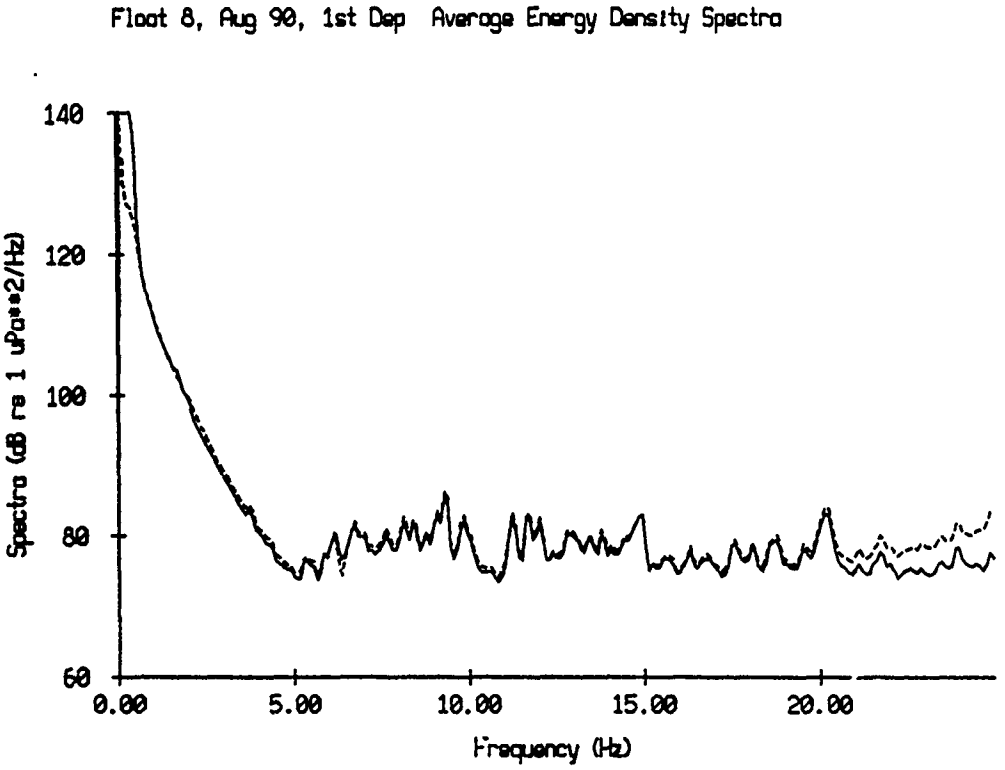
Float 8, Aug 90, 1st Dep Average Energy Density Spectra
Spectra (dB re 1 uPa**2/Hz)
140
120
100
80
60
0.00
5.00
10.00
15.00
20.00
Frequency (Hz)

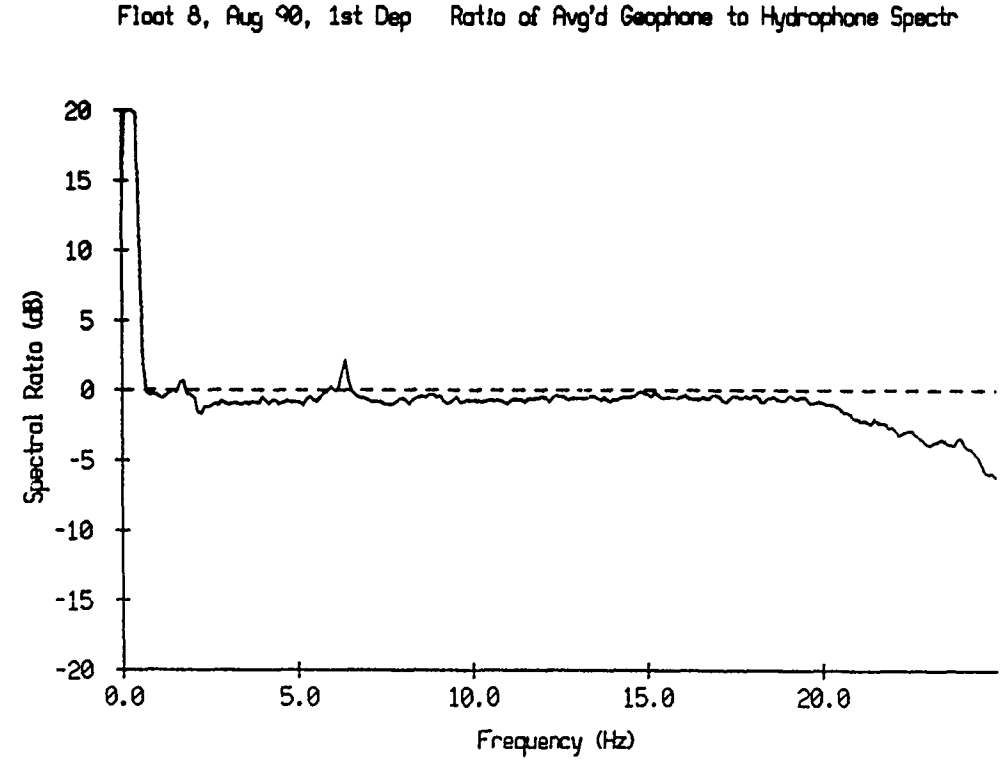
Float 8, Aug 90, 1st Dep Ratio of Avg'd Geophone to Hydrophone Spectr
Spectral Ratio (dB)
20
15
10
5
0
-5
-10
-15
-20
0.0
5.0
10.0
15.0
20.0
Frequency (Hz)

Figure X.11

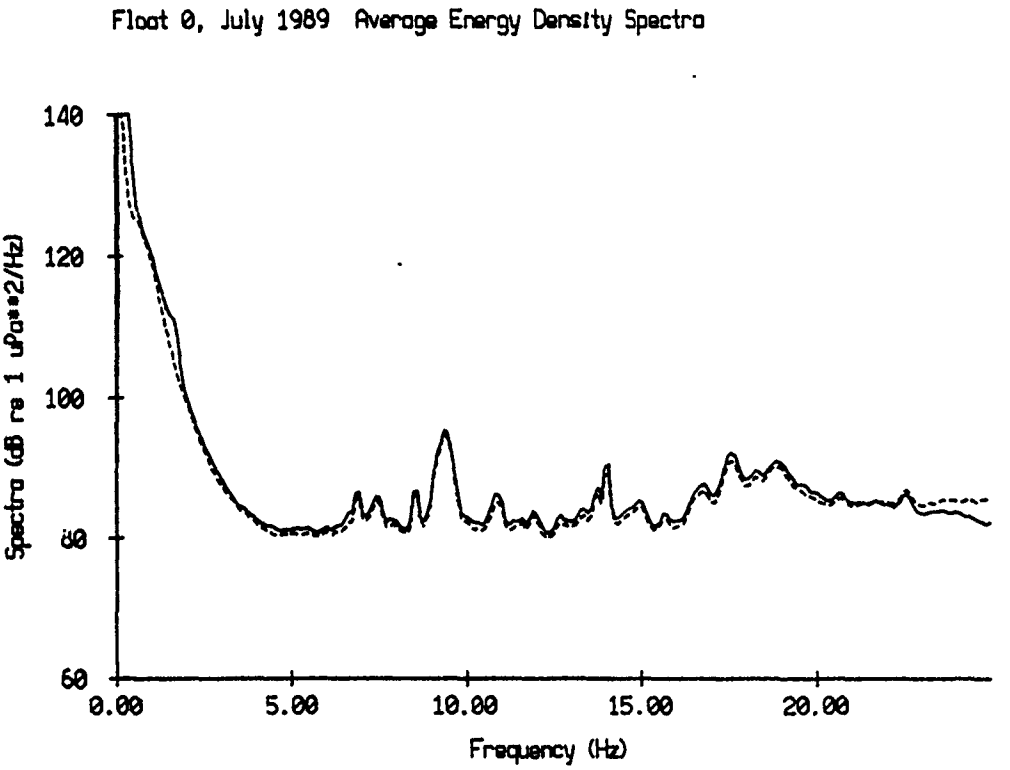
Float 0, July 1989 Average Energy Density Spectra
Spectra (dB re 1 uPa**2/Hz)
140
120
100
80
60
0.00
5.00
10.00
15.00
20.00
Frequency (Hz)

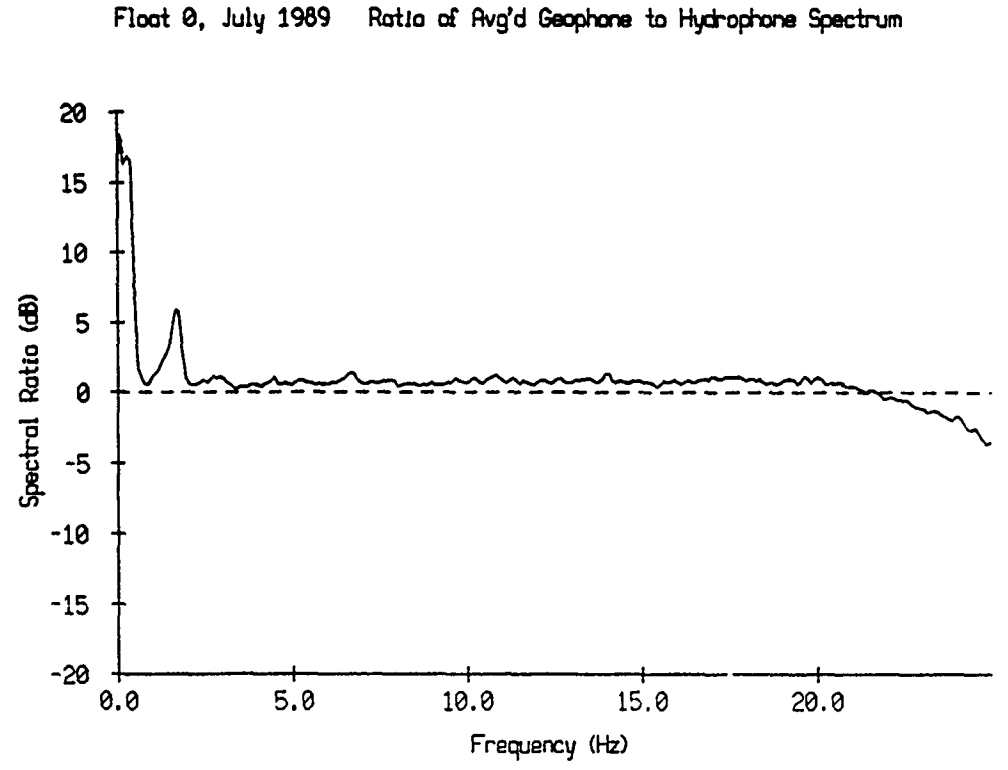
Float 0, July 1989 Ratio of Avg'd Geophone to Hydrophone Spectrum
Spectral Ratio (dB)
20
15
10
5
0
-5
-10
-15
-20
0.0
5.0
10.0
15.0
20.0
Frequency (Hz)

Figure X.12

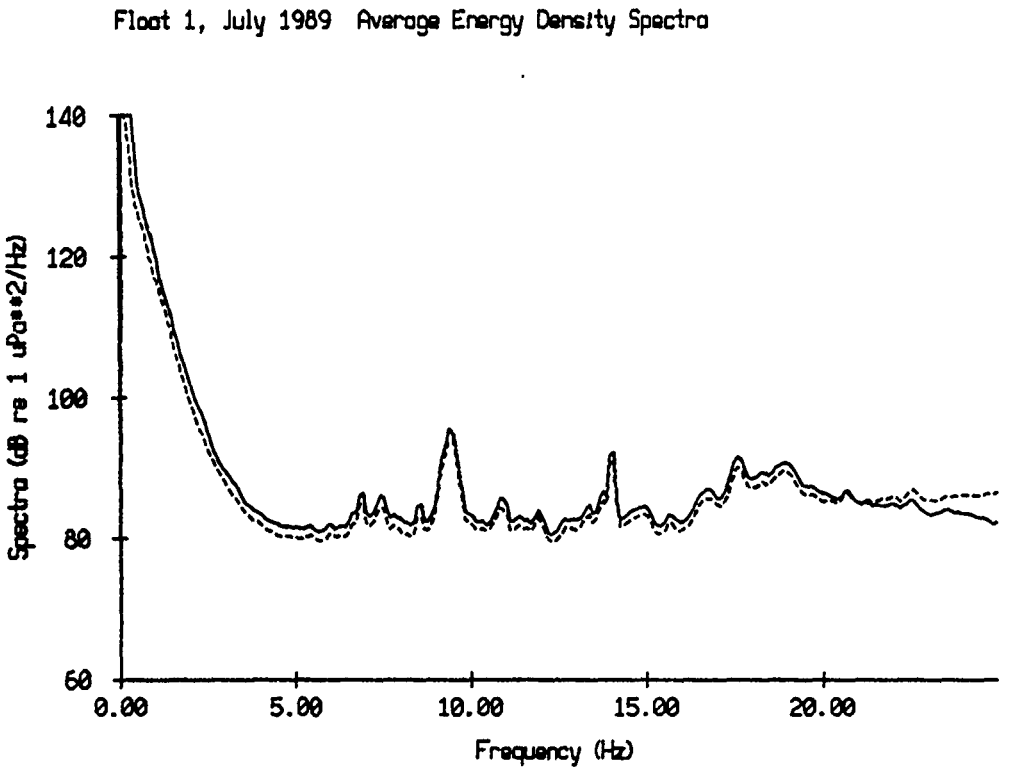
Float 1, July 1989 Average Energy Density Spectra
Spectra (dB re 1 uPa**2/Hz)
140
120
100
80
60
0.00
5.00
10.00
15.00
20.00
Frequency (Hz)

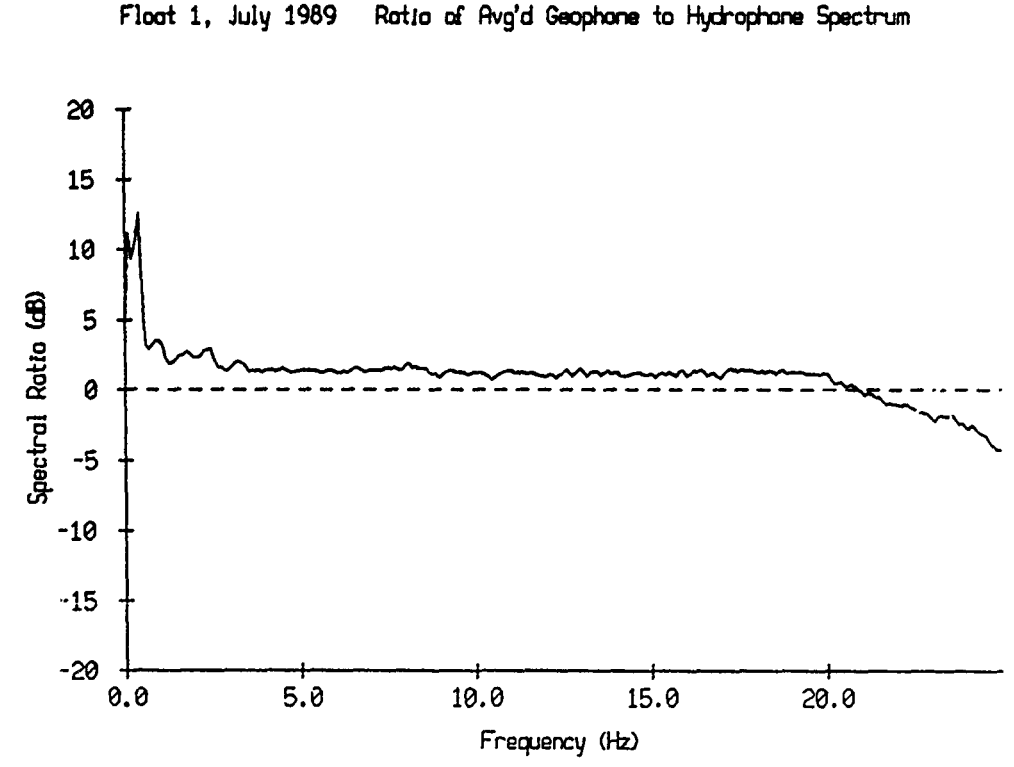
Float 1, July 1989 Ratio of Avg'd Geophone to Hydrophone Spectrum
Spectral Ratio (dB)
20
15
10
5
0
-5
-10
-15
-20
0.0
5.0
10.0
15.0
20.0
Frequency (Hz)

Figure X.13

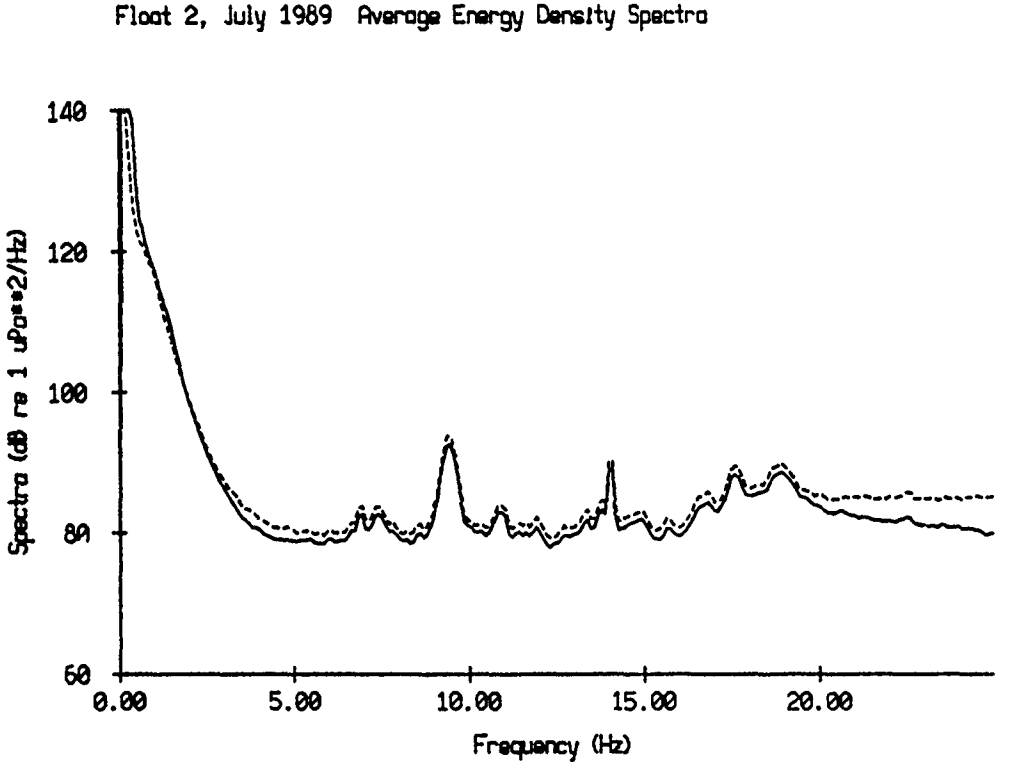
Float 2, July 1989 Average Energy Density Spectra
Spectra (dB re 1 uPa**2/Hz)
140
120
100
80
60
0.00
5.00
10.00
15.00
20.00
Frequency (Hz)

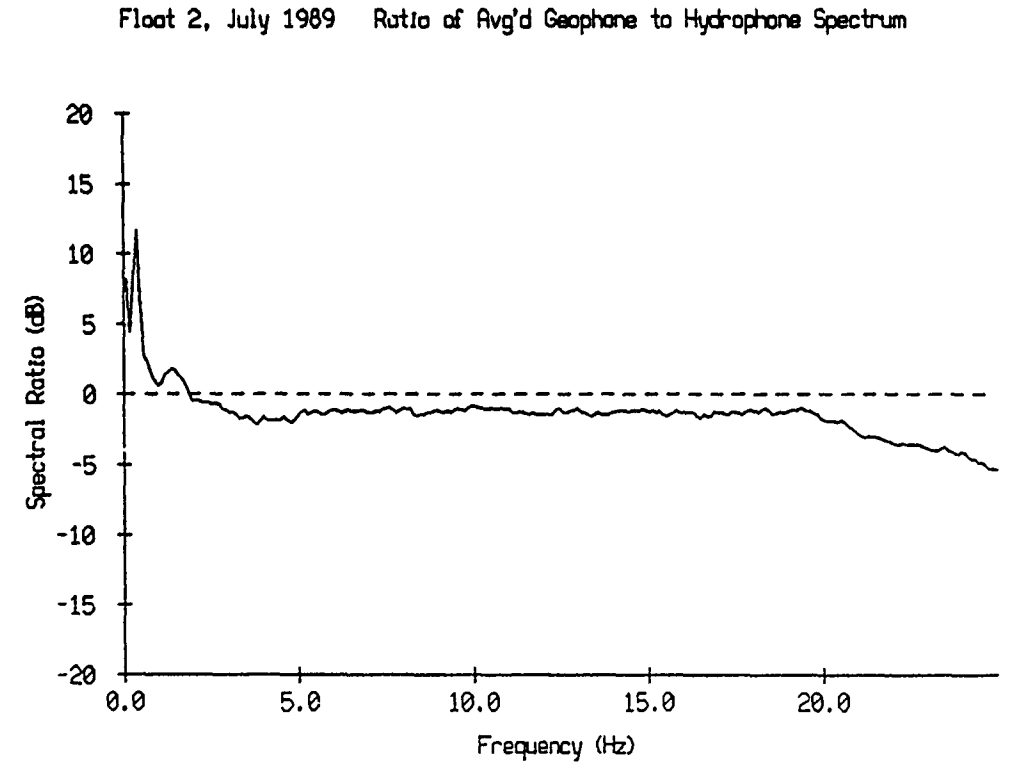
Float 2, July 1989 Ratio of Avg'd Geophone to Hydrophone Spectrum
Spectral Ratio (dB)
20
15
10
5
0
-5
-10
-15
-20
0.0
5.0
10.0
15.0
20.0
Frequency (Hz)

Figure X.14

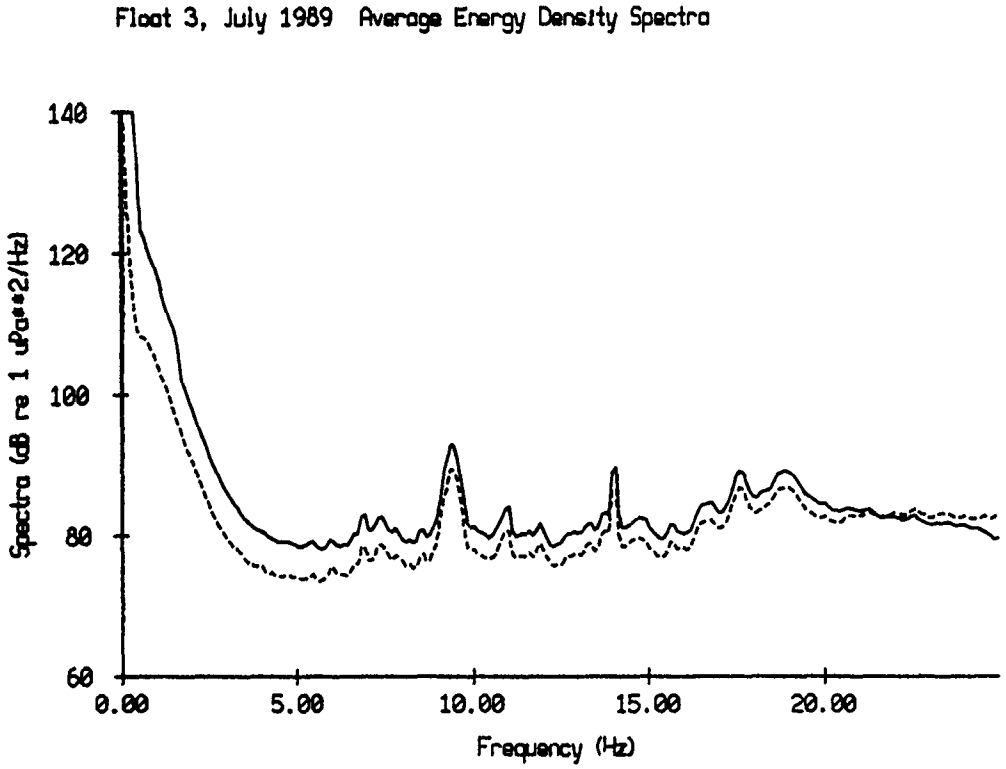
Float 3, July 1989 Average Energy Density Spectra
140
120
100
80
60
Spectra (dB re 1 uPa**2/Hz)
0.00
5.00
10.00
15.00
20.00
Frequency (Hz)

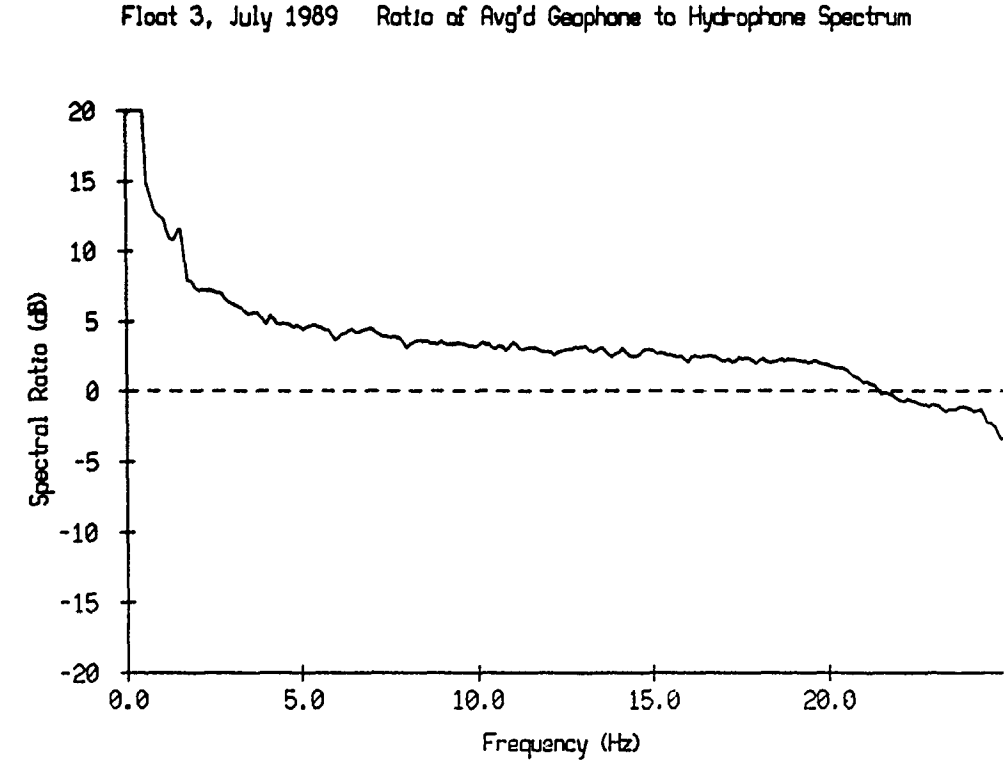
Float 3, July 1989 Ratio of Avg'd Geophone to Hydrophone Spectrum
20
15
10
5
0
-5
-10
-15
-20
Spectral Ratio (dB)
0.0
5.0
10.0
15.0
20.0
Frequency (Hz)

Figure X.15

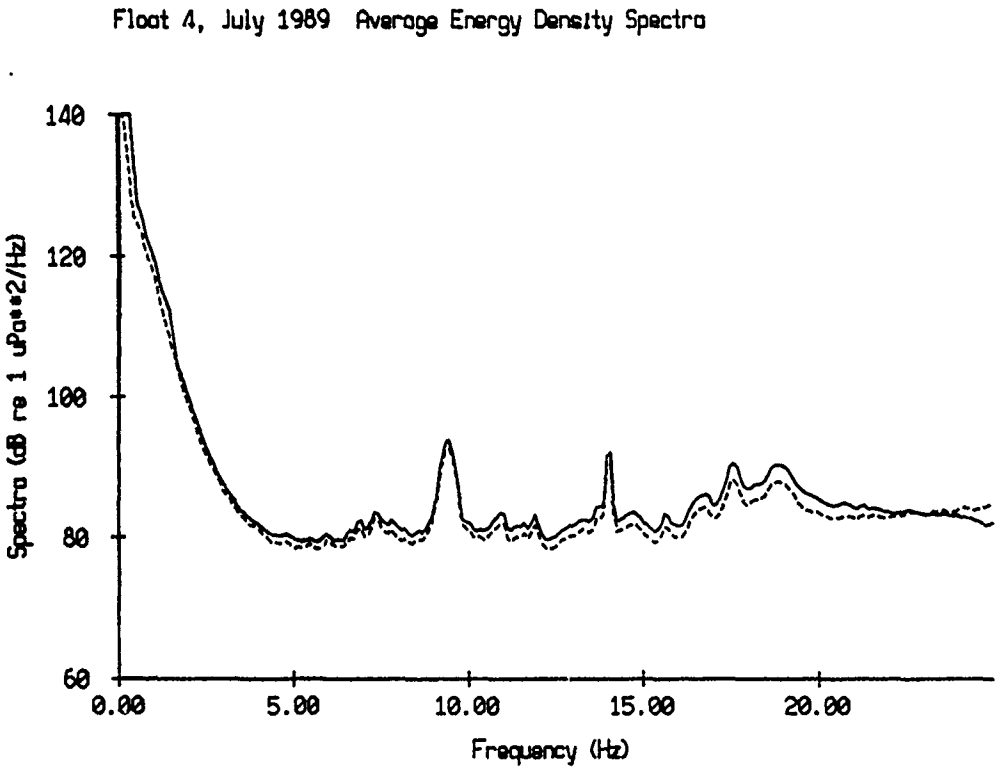
Float 4, July 1989 Average Energy Density Spectra
Spectra (dB re 1 uPa**2/Hz)
140
120
100
80
60
0.00
5.00
10.00
15.00
20.00
Frequency (Hz)

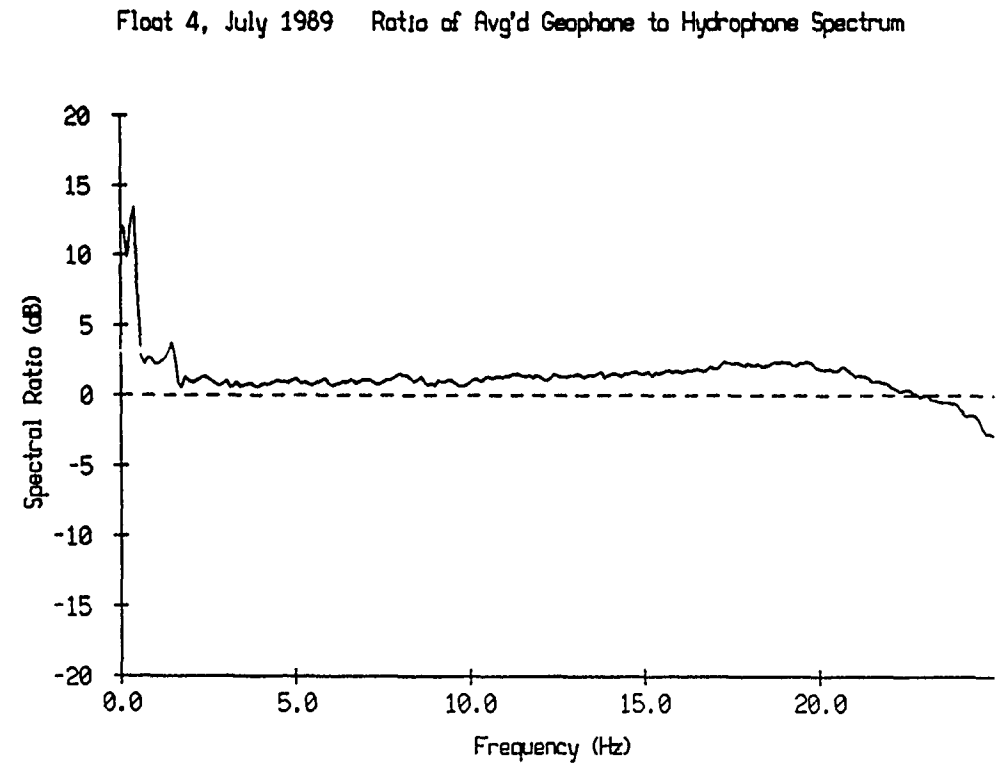
Float 4, July 1989 Ratio of Avg'd Geophone to Hydrophone Spectrum
Spectral Ratio (dB)
20
15
10
5
0
-5
-10
-15
-20
0.0
5.0
10.0
15.0
20.0
Frequency (Hz)

Figure X.16

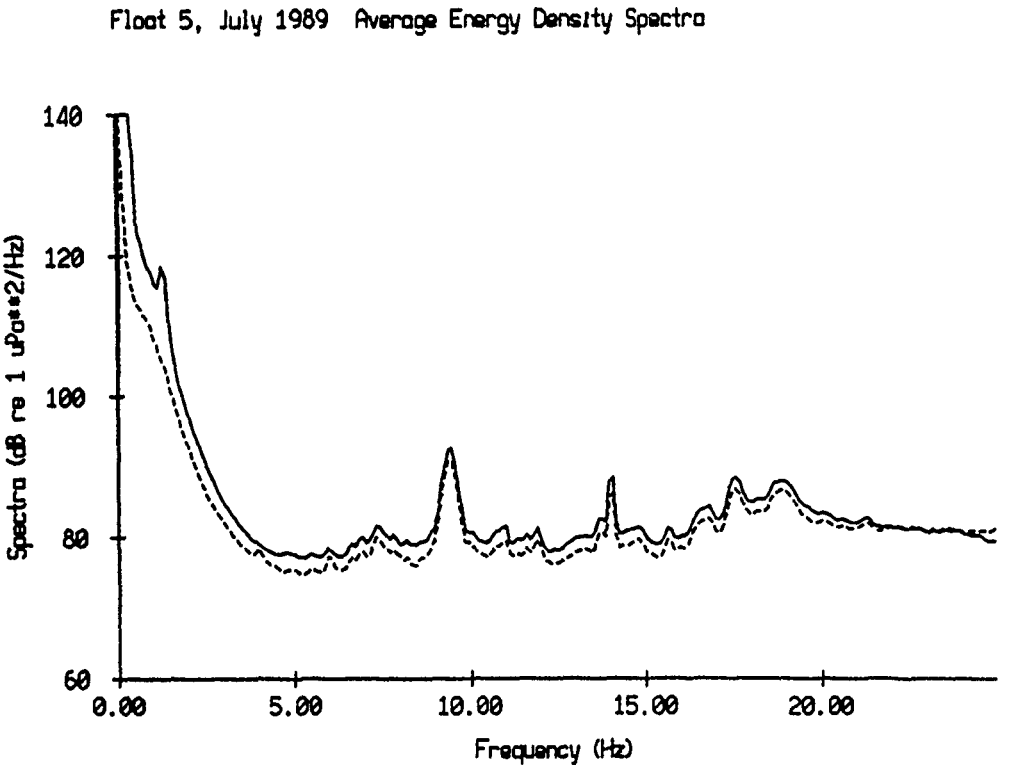
Float 5, July 1989 Average Energy Density Spectra
140
120
100
80
60
Spectra (dB re 1 uPa**2/Hz)
0.00
5.00
10.00
15.00
20.00
Frequency (Hz)

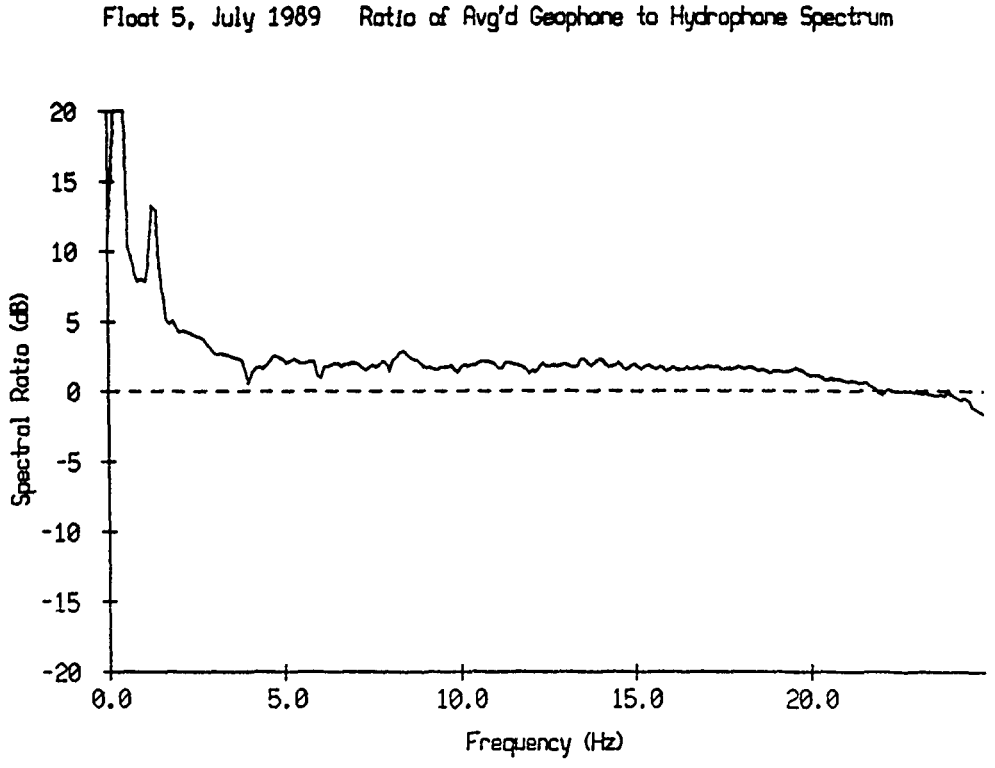
Float 5, July 1989 Ratio of Avg'd Geophone to Hydrophone Spectrum
20
15
10
5
0
-5
-10
-15
-20
Spectral Ratio (dB)
0.0
5.0
10.0
15.0
20.0
Frequency (Hz)

Figure X.17

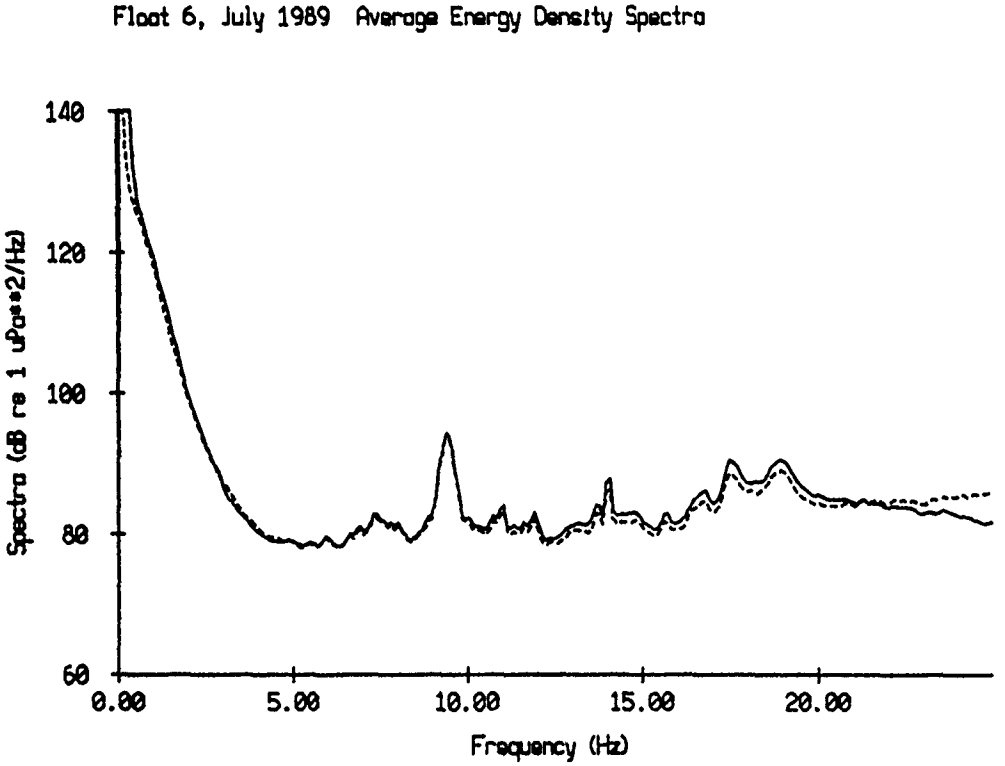
Float 6, July 1989 Average Energy Density Spectra
Spectra (dB re 1 uPa**2/Hz)
140
120
100
80
60
0.00
5.00
10.00
15.00
20.00
Frequency (Hz)

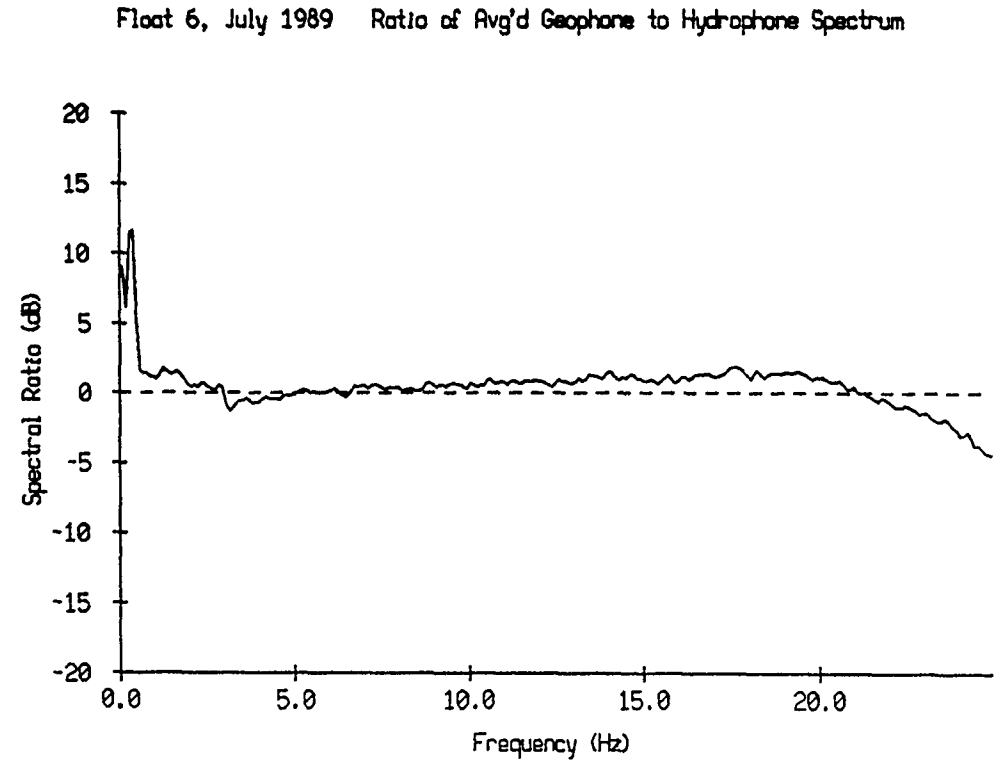
Float 6, July 1989 Ratio of Avg'd Geophone to Hydrophone Spectrum
Spectral Ratio (dB)
20
15
10
5
0
-5
-10
-15
-20
0.0
5.0
10.0
15.0
20.0
Frequency (Hz)

Figure X.18

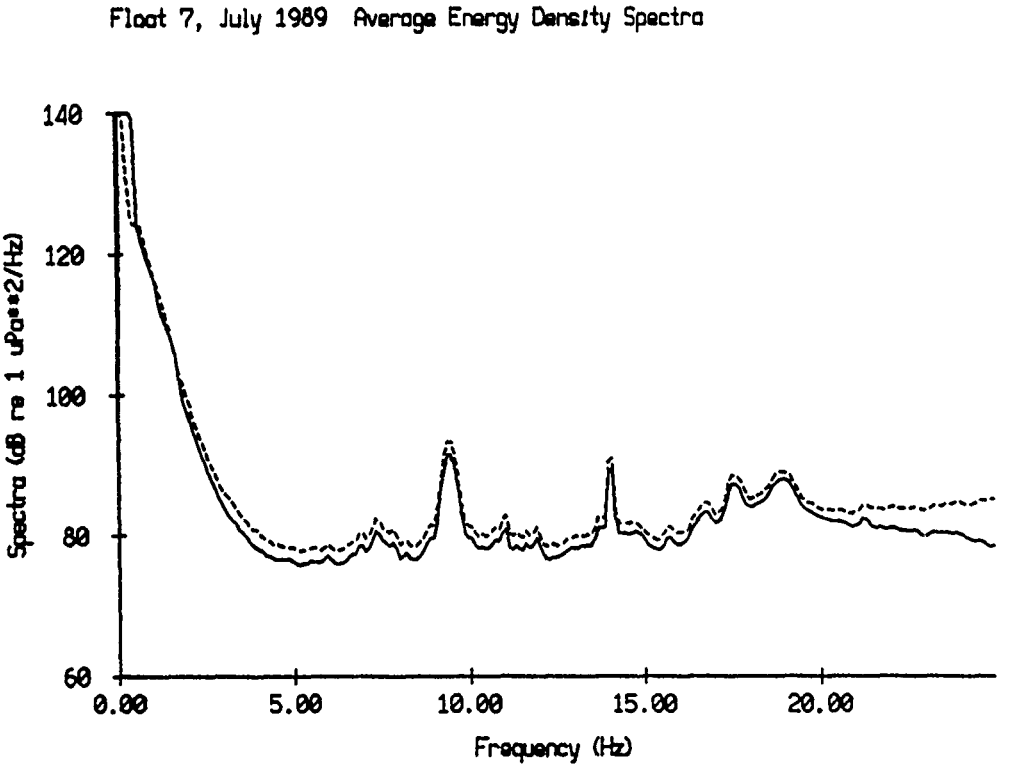
Float 7, July 1989 Average Energy Density Spectra
140
120
100
80
60
Spectra (dB re 1 uPa**2/Hz)
0.00
5.00
10.00
15.00
20.00
Frequency (Hz)

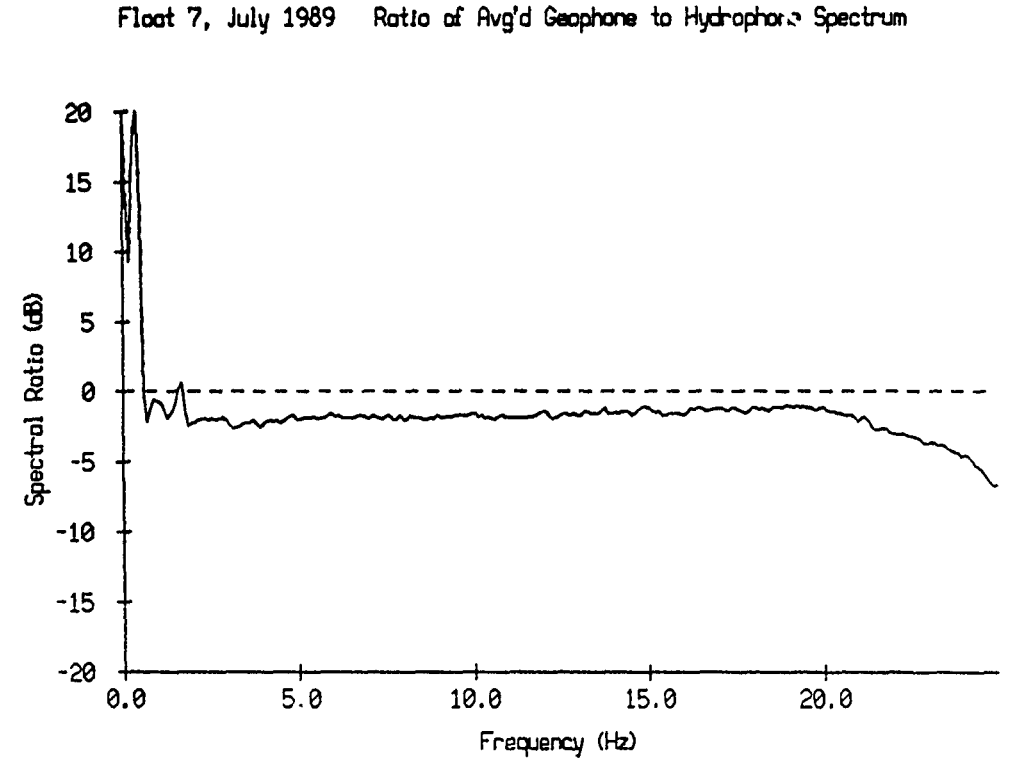
Float 7, July 1989 Ratio of Avg'd Geophone to Hydrophone Spectrum
20
15
10
5
0
-5
-10
-15
-20
Spectral Ratio (dB)
0.0
5.0
10.0
15.0
20.0
Frequency (Hz)

Figure X.19

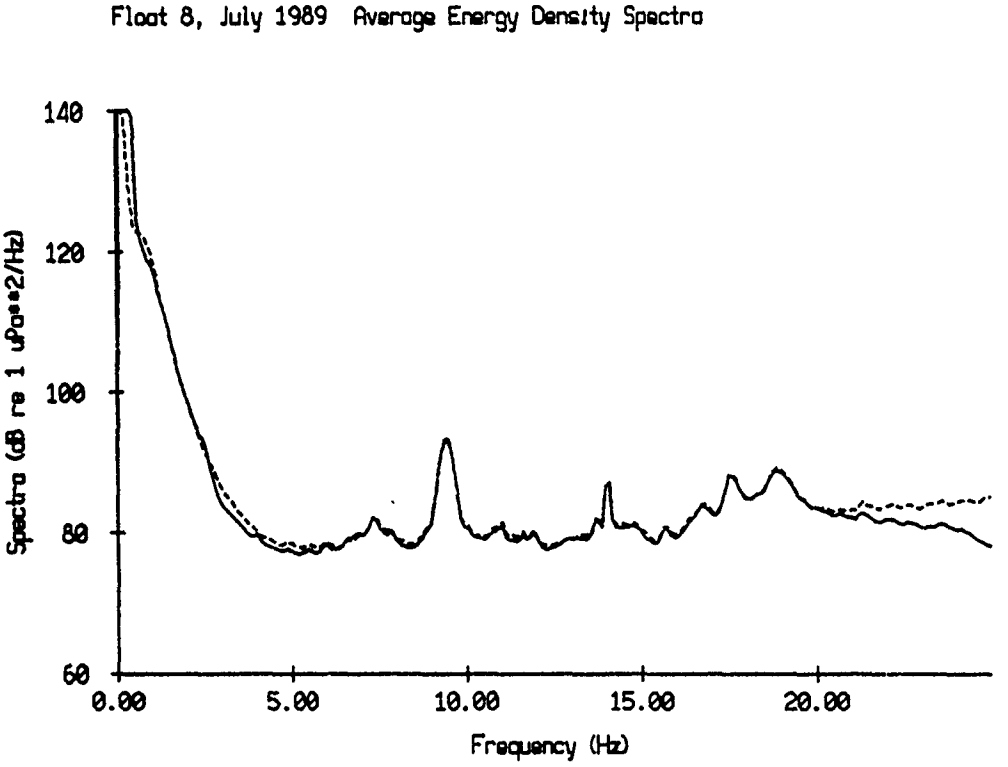
Float 8, July 1989 Average Energy Density Spectra
140
120
100
80
60
Spectra (dB re 1 uPa**2/Hz)
0.00
5.00
10.00
15.00
20.00
Frequency (Hz)

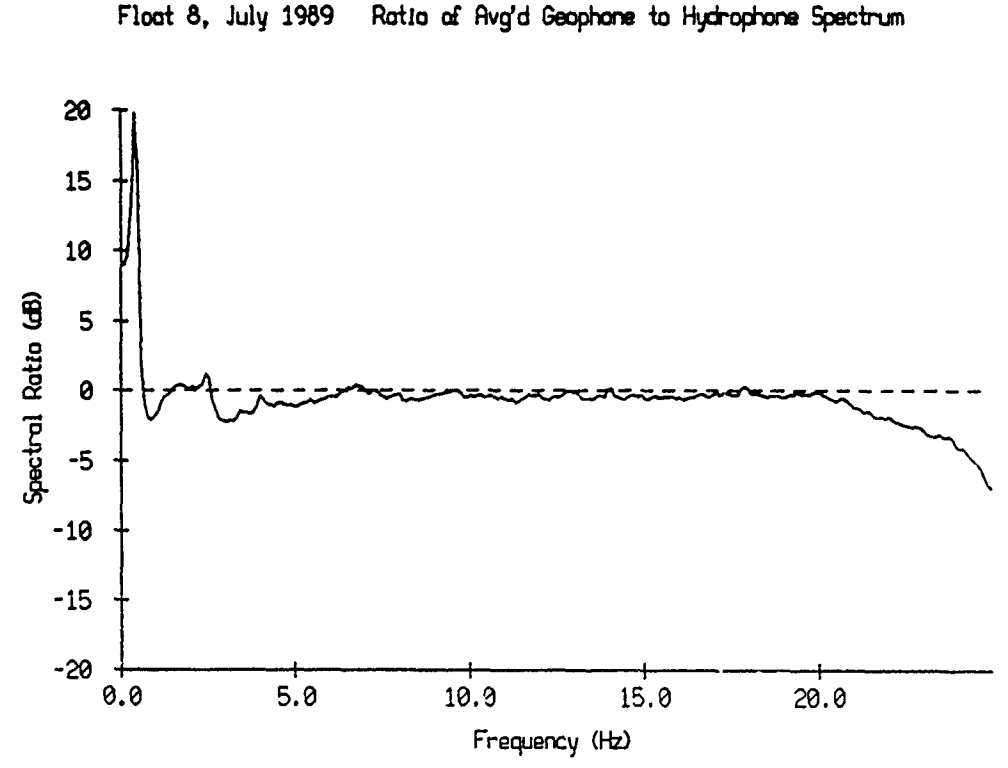
Float 8, July 1989 Ratio of Avg'd Geophone to Hydrophone Spectrum
20
15
10
5
0
-5
-10
-15
-20
Spectral Ratio (dB)
0.0
5.0
10.0
15.0
20.0
Frequency (Hz)

Figure X.20

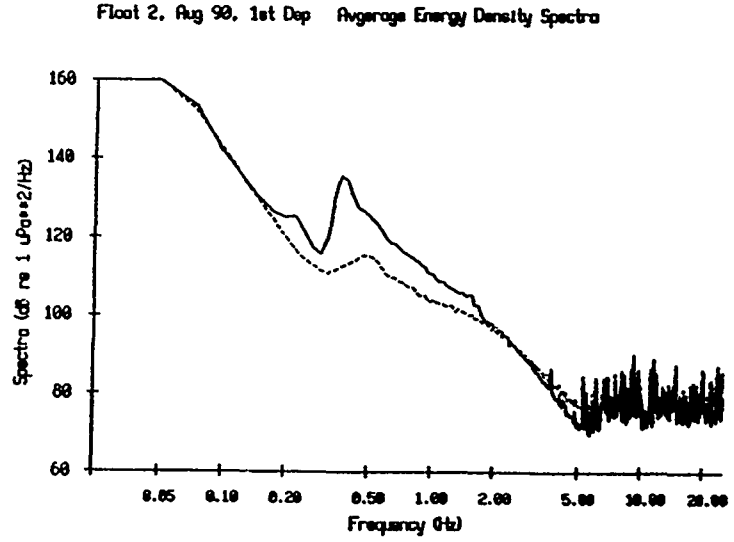
Float 2, Aug 90, 1st Dep Avgerage Energy Density Spectra
Spectra (dB re 1 uPa**2/Hz)
160
140
120
100
80
60
0.05
0.10
0.20
0.50
1.00
2.00
5.00
10.00
20.00
Frequency (Hz)

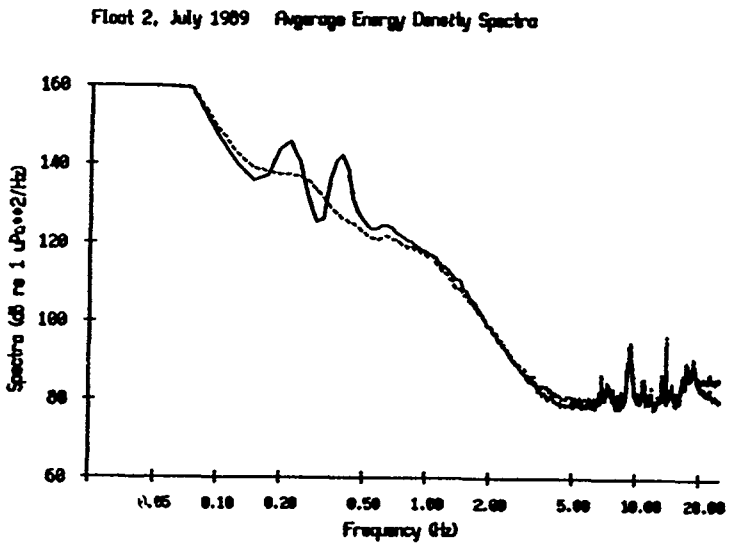
Float 2, July 1989 Avgerage Energy Density Spectra
Spectra (dB re 1 uPa**2/Hz)
160
140
120
100
80
60
0.05
0.10
0.20
0.50
1.00
2.00
5.00
10.00
20.00
Frequency (Hz)

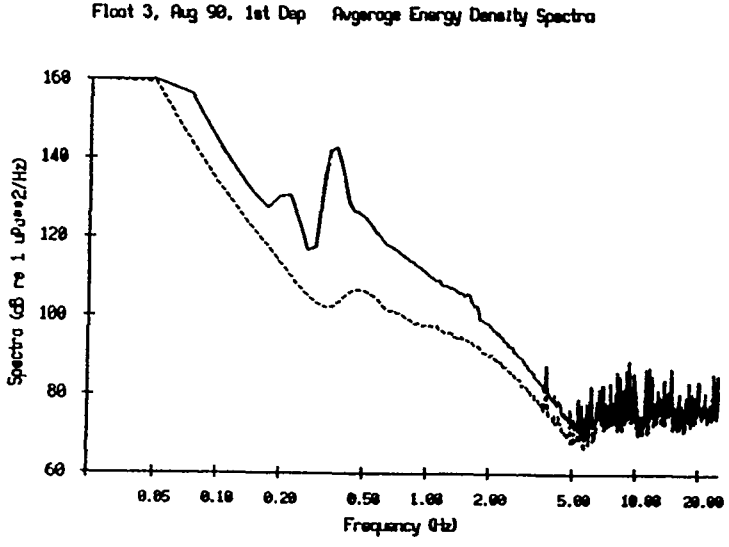
Float 3, Aug 90, 1st Dep Avgerage Energy Density Spectra
Spectra (dB re 1 uPa**2/Hz)
160
140
120
100
80
60
0.05
0.10
0.20
0.50
1.00
2.00
5.00
10.00
20.00
Frequency (Hz)

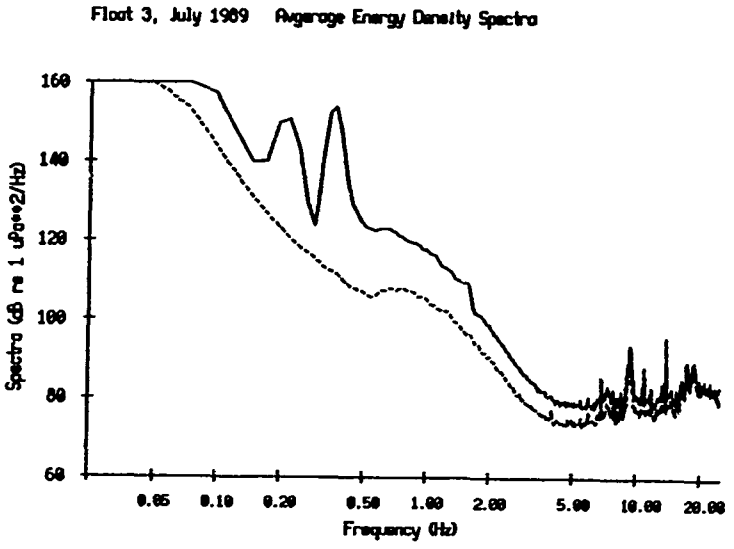
Float 3, July 1989 Avgerage Energy Density Spectra
Spectra (dB re 1 uPa**2/Hz)
160
140
120
100
80
60
0.05
0.10
0.20
0.50
1.00
2.00
5.00
10.00
20.00
Frequency (Hz)

Figure X.21

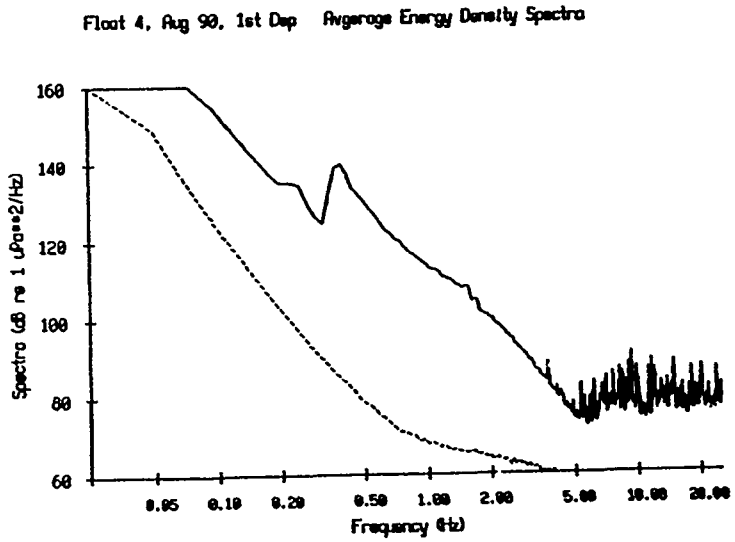
Float 4, Aug 90, 1st Dep Avgerage Energy Density Spectra
Spectra (dB re 1 uPa**2/Hz)
160
140
120
100
80
60
0.05
0.10
0.20
0.50
1.00
2.00
5.00
10.00
20.00
Frequency (Hz)

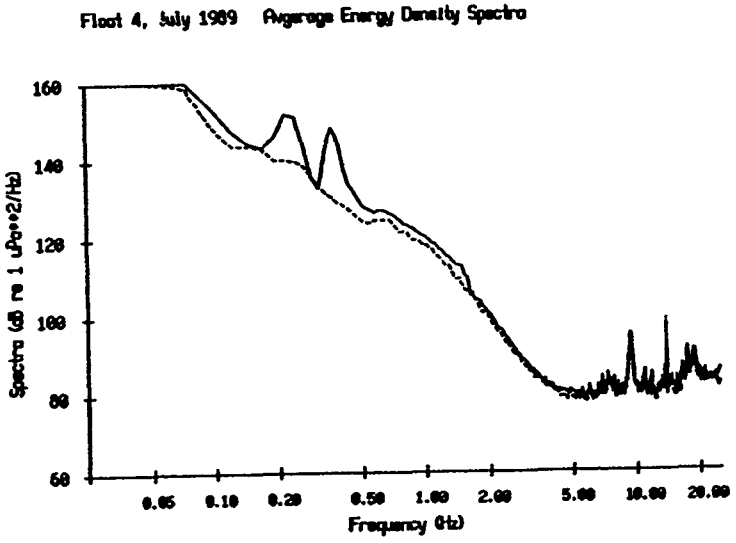
Float 4, July 1989 Avgerage Energy Density Spectra
Spectra (dB re 1 uPa**2/Hz)
160
140
120
100
80
60
0.05
0.10
0.20
0.50
1.00
2.00
5.00
10.00
20.00
Frequency (Hz)

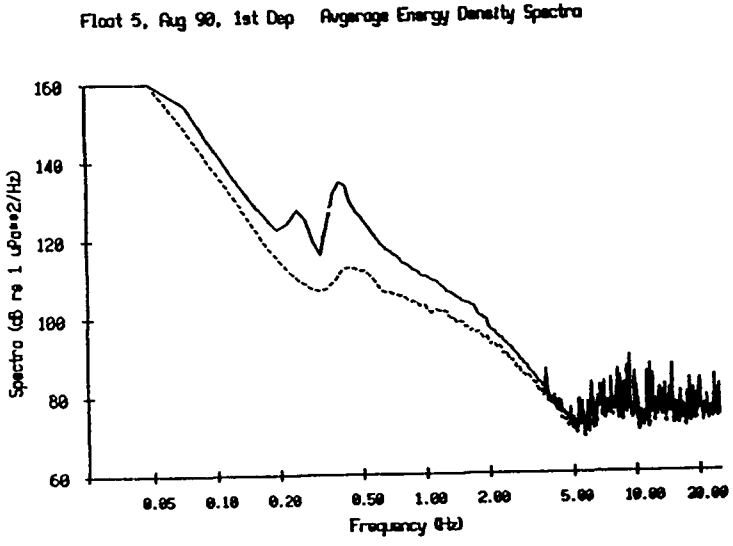
Float 5, Aug 90, 1st Dep Avgerage Energy Density Spectra
Spectra (dB re 1 uPa**2/Hz)
160
140
120
100
80
60
0.05
0.10
0.20
0.50
1.00
2.00
5.00
10.00
20.00
Frequency (Hz)

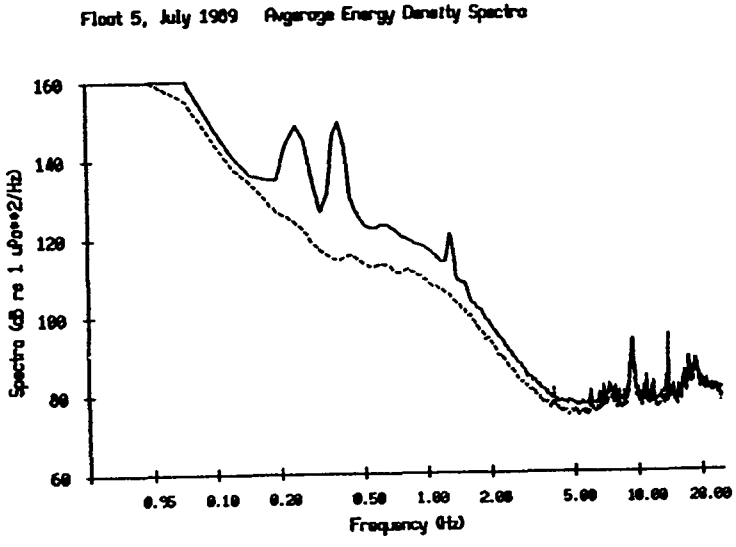
Float 5, July 1989 Avgerage Energy Density Spectra
Spectra (dB re 1 uPa**2/Hz)
160
140
120
100
80
60
0.05
0.10
0.20
0.50
1.00
2.00
5.00
10.00
20.00
Frequency (Hz)

Figure X.22

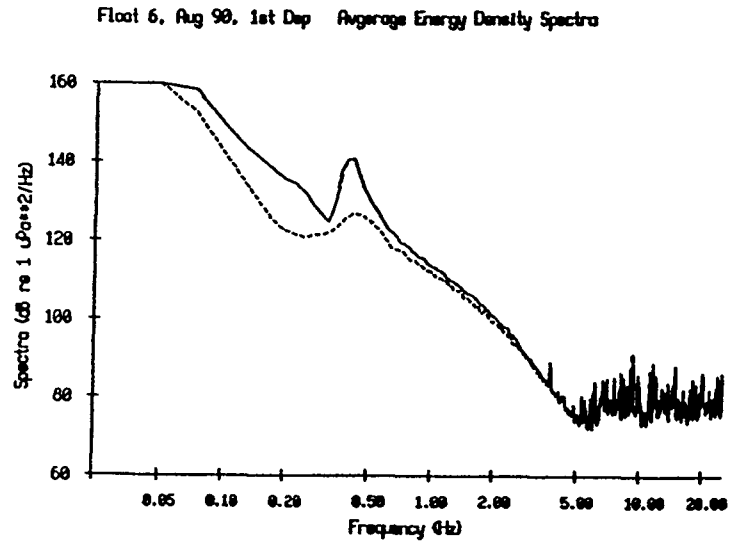
Float 6, Aug 90, 1st Dep Avgerage Energy Density Spectra
Spectra (dB re 1 uPasec2/Hz)
160
140
120
100
80
60
0.05
0.10
0.20
0.50
1.00
2.00
5.00
10.00
20.00
Frequency (Hz)

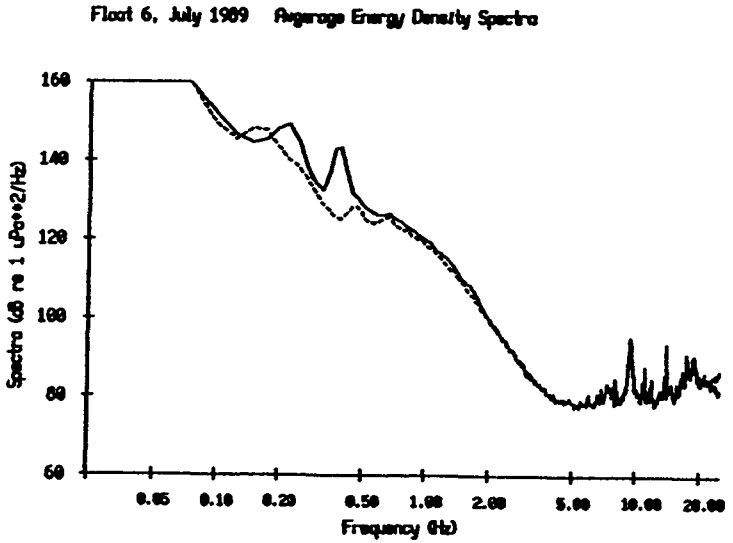
Float 6, July 1989 Avgerage Energy Density Spectra
Spectra (dB re 1 uPasec2/Hz)
160
140
120
100
80
60
0.05
0.10
0.20
0.50
1.00
2.00
5.00
10.00
20.00
Frequency (Hz)

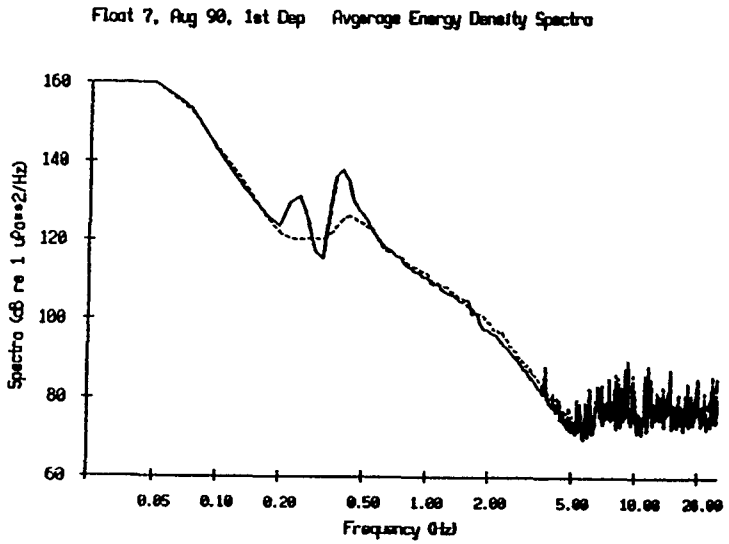
Float 7, Aug 90, 1st Dep Avgerage Energy Density Spectra
Spectra (dB re 1 uPasec2/Hz)
160
140
120
100
80
60
0.05
0.10
0.20
0.50
1.00
2.00
5.00
10.00
20.00
Frequency (Hz)

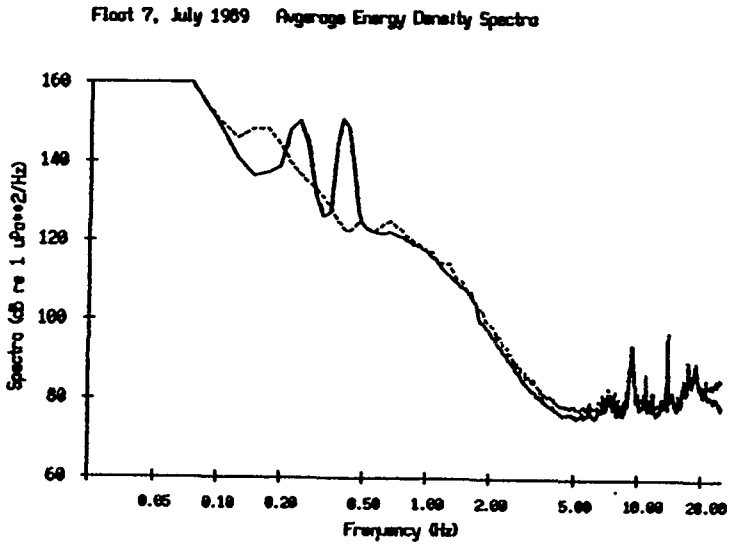
Float 7, July 1989 Avgerage Energy Density Spectra
Spectra (dB re 1 uPasec2/Hz)
160
140
120
100
80
60
0.05
0.10
0.20
0.50
1.00
2.00
5.00
10.00
20.00
Frequency (Hz)

Figure X.23

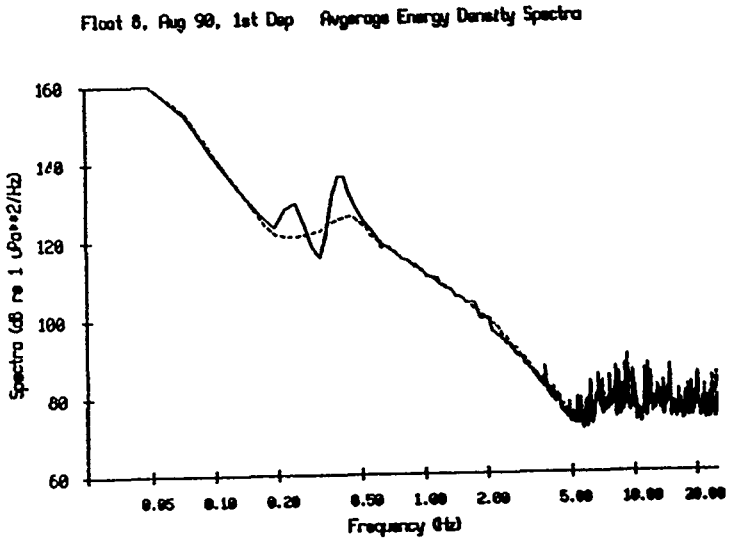
Float 8, Aug 90, 1st Dep Avgerage Energy Density Spectra
Spectra (dB re 1 uPa**2/Hz)
160
140
120
100
80
60
0.05
0.10
0.20
0.50
1.00
2.00
5.00
10.00
20.00
Frequency (Hz)

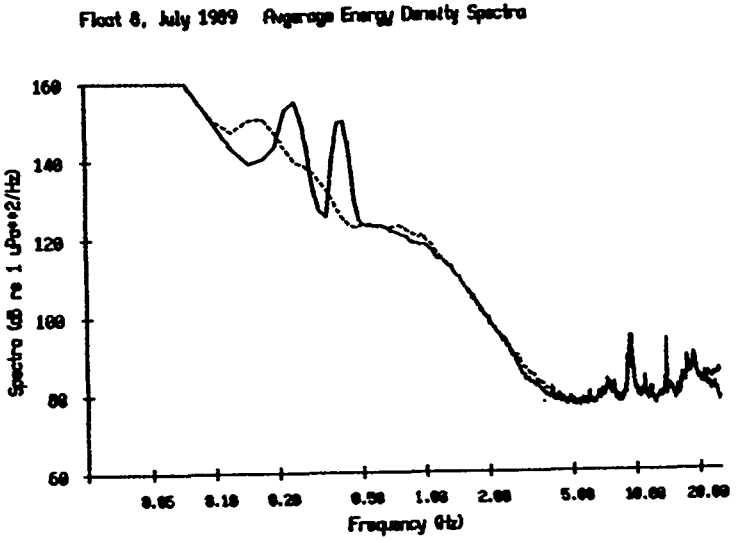
Float 8, July 1989 Avgerage Energy Density Spectra
Spectra (dB re 1 uPa**2/Hz)
160
140
120
100
80
60
0.05
0.10
0.20
0.50
1.00
2.00
5.00
10.00
20.00
Frequency (Hz)

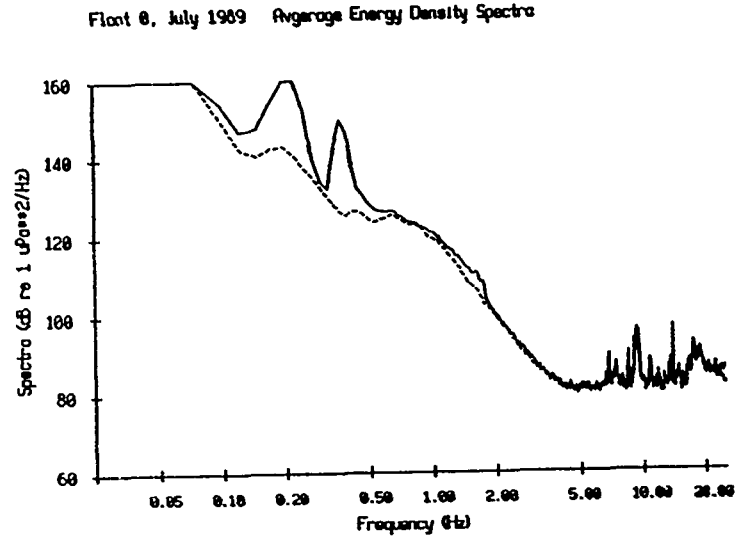
Float 8, July 1989 Avgerage Energy Density Spectra
Spectra (dB re 1 uPa**2/Hz)
160
140
120
100
80
60
0.05
0.10
0.20
0.50
1.00
2.00
5.00
10.00
20.00
Frequency (Hz)

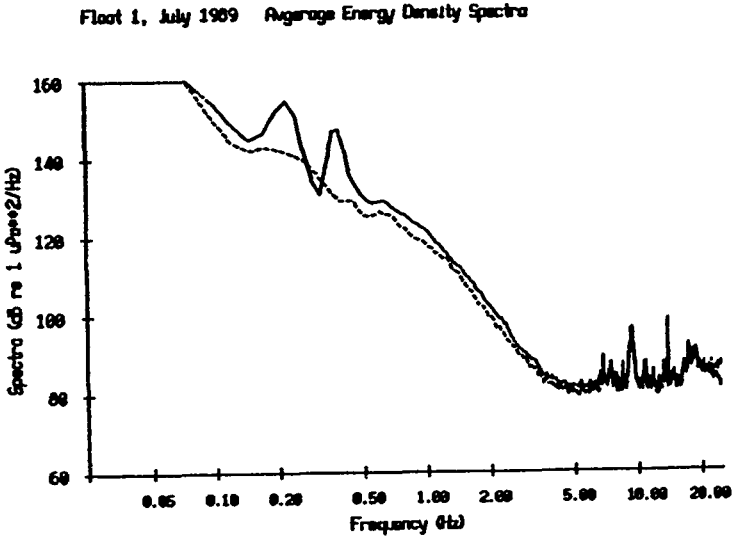
Float 1, July 1989 Avgerage Energy Density Spectra
Spectra (dB re 1 uPa**2/Hz)
160
140
120
100
80
60
0.05
0.10
0.20
0.50
1.00
2.00
5.00
10.00
20.00
Frequency (Hz)

Figure X.24

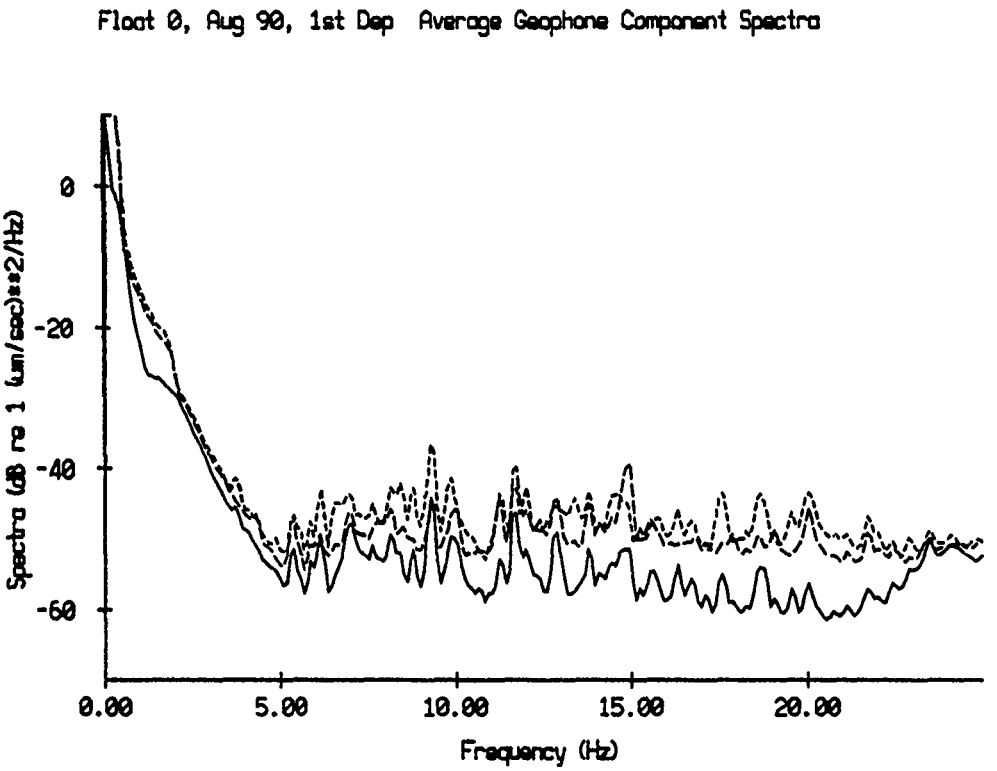
Float 0, Aug 90, 1st Dep Average Geophone Component Spectra
Spectra (dB re 1 (um/sec)**2/Hz)
0
-20
-40
-60
0.00
5.00
10.00
15.00
20.00
Frequency (Hz)

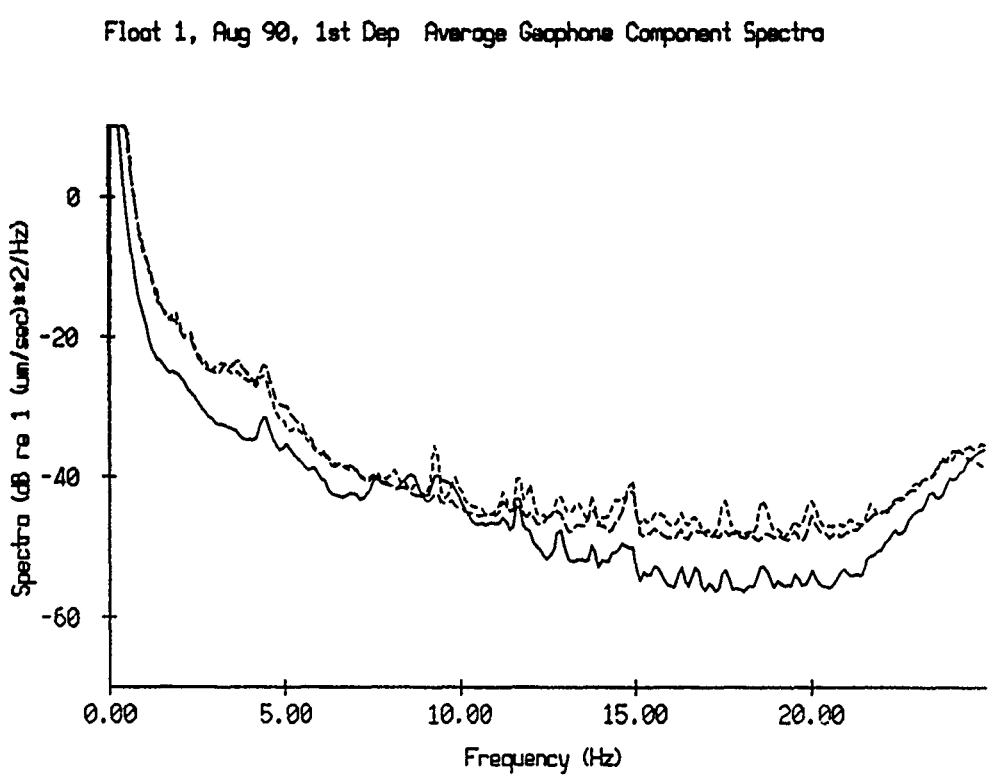
Float 1, Aug 90, 1st Dep Average Geophone Component Spectra
Spectra (dB re 1 (um/sec)**2/Hz)
0
-20
-40
-60
0.00
5.00
10.00
15.00
20.00
Frequency (Hz)

Figure X.25

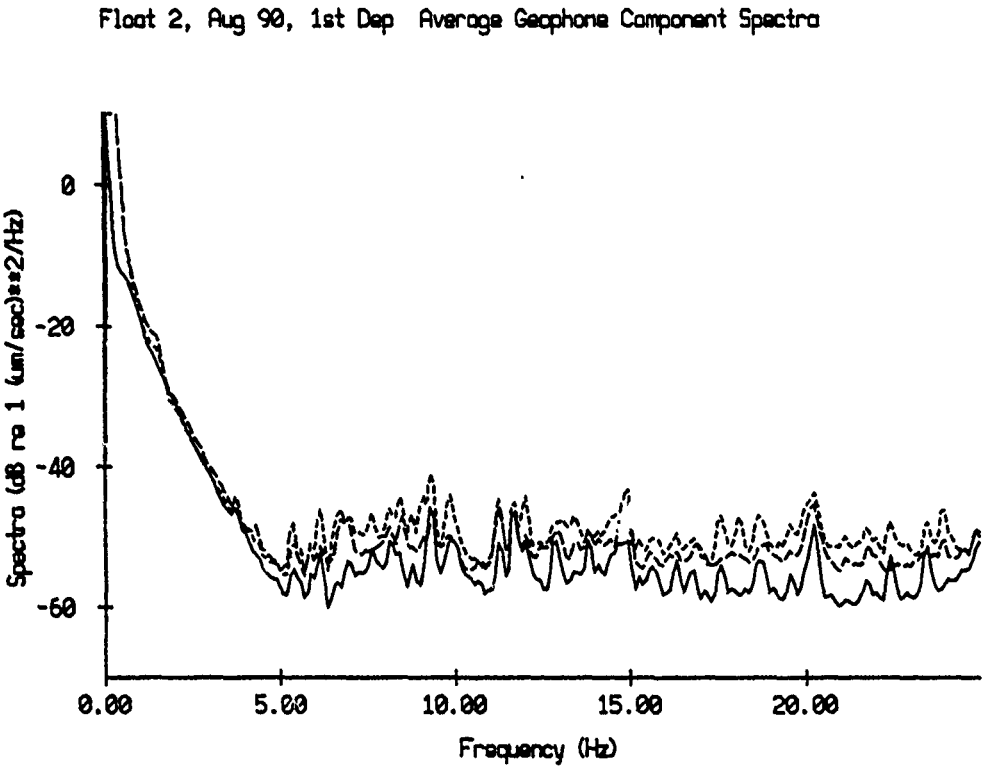
Float 2, Aug 90, 1st Dep Average Geophone Component Spectra
Spectra (dB re 1 (um/sec)**2/Hz)
0
-20
-40
-60
0.00
5.00
10.00
15.00
20.00
Frequency (Hz)

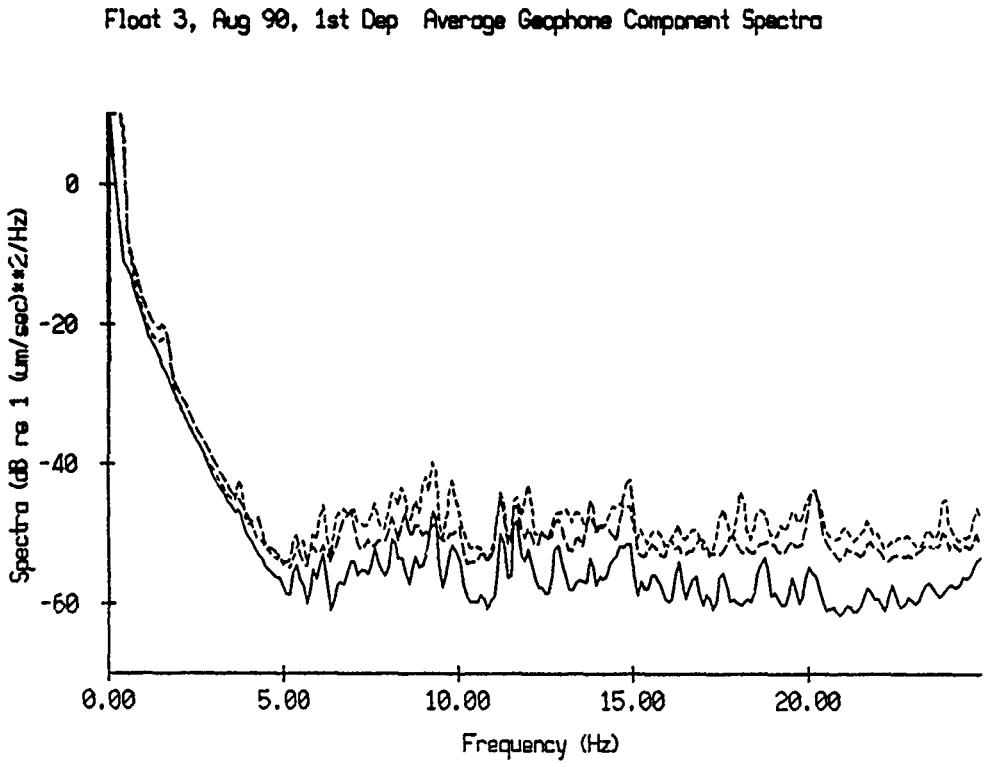
Float 3, Aug 90, 1st Dep Average Geophone Component Spectra
Spectra (dB re 1 (um/sec)**2/Hz)
0
-20
-40
-60
0.00
5.00
10.00
15.00
20.00
Frequency (Hz)

Figure X.26

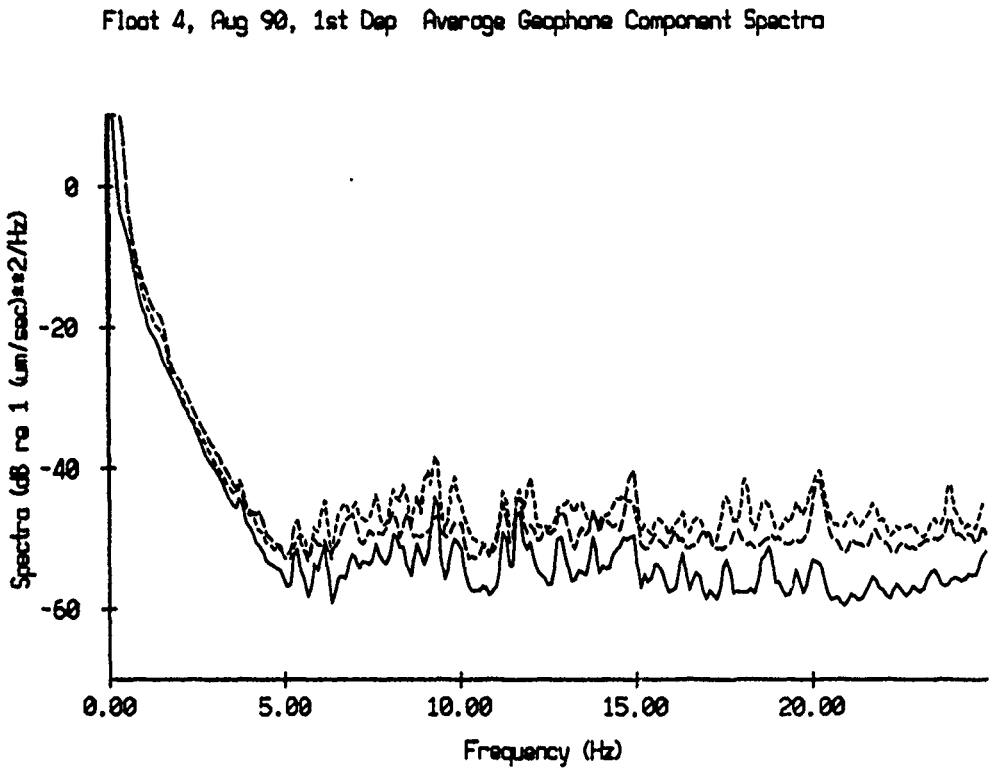
Float 4, Aug 90, 1st Dep Average Geophone Component Spectra
Spectra (dB re 1 (um/sec)**2/Hz)
0
-20
-40
-60
0.00
5.00
10.00
15.00
20.00
Frequency (Hz)

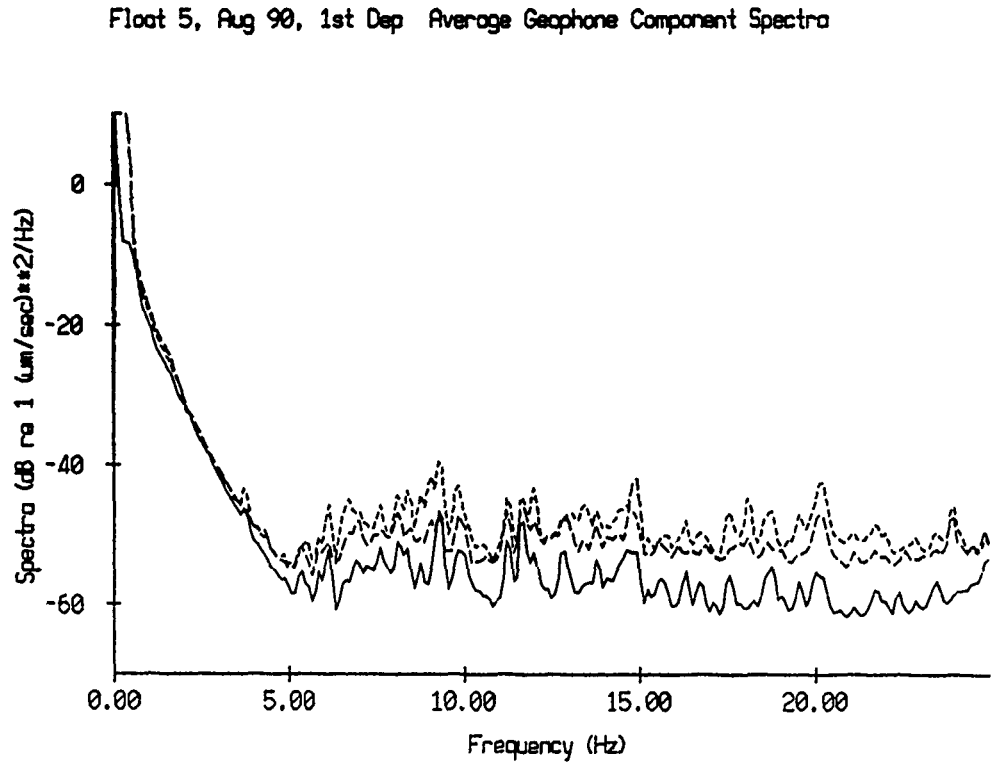
Float 5, Aug 90, 1st Dep Average Geophone Component Spectra
Spectra (dB re 1 (um/sec)**2/Hz)
0
-20
-40
-60
0.00
5.00
10.00
15.00
20.00
Frequency (Hz)

Figure X.27

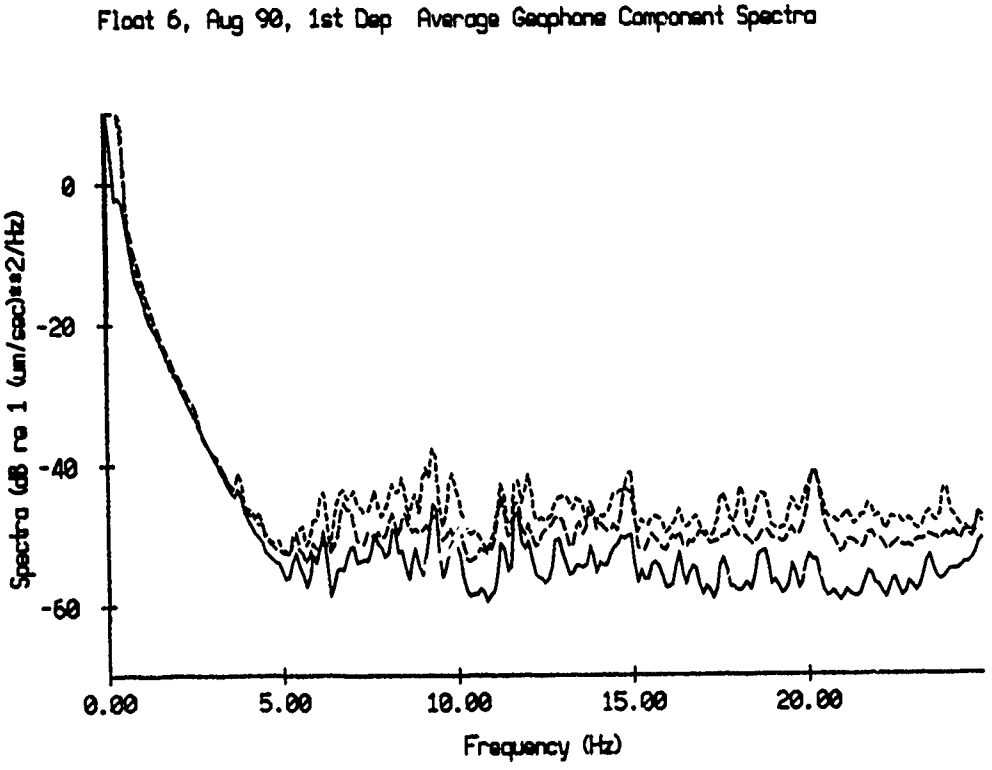
Float 6, Aug 90, 1st Dep Average Geophone Component Spectra
Spectra (dB re 1 (um/sec)**2/Hz)
0
-20
-40
-60
0.00
5.00
10.00
15.00
20.00
Frequency (Hz)

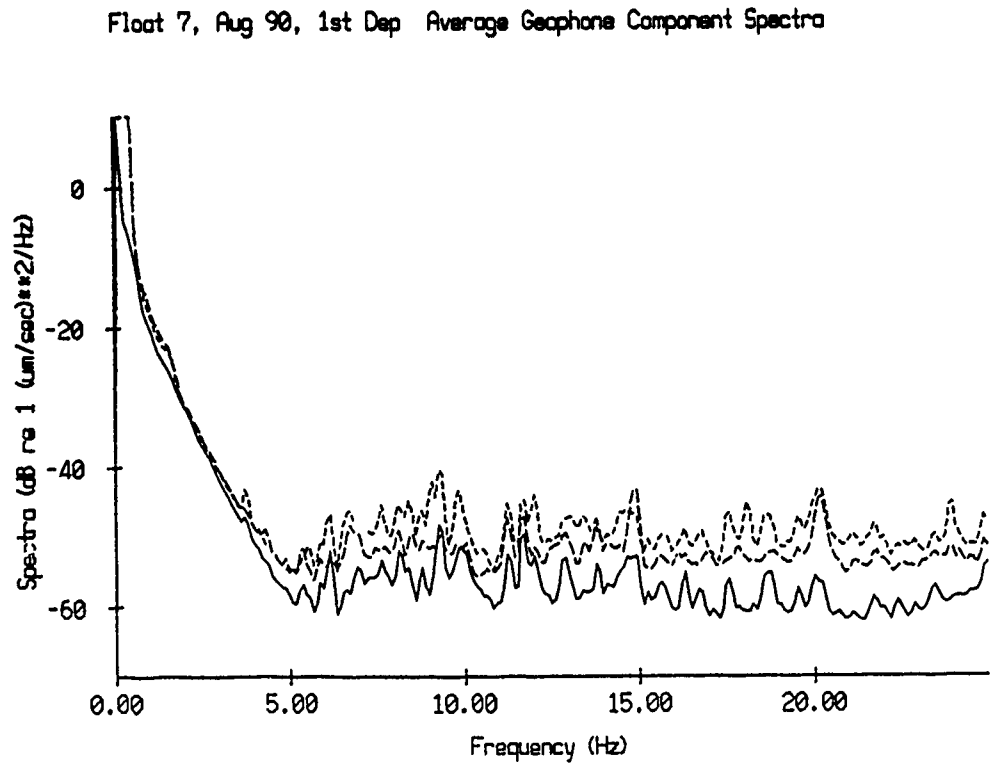
Float 7, Aug 90, 1st Dep Average Geophone Component Spectra
Spectra (dB re 1 (um/sec)**2/Hz)
0
-20
-40
-60
0.00
5.00
10.00
15.00
20.00
Frequency (Hz)

Figure X.28

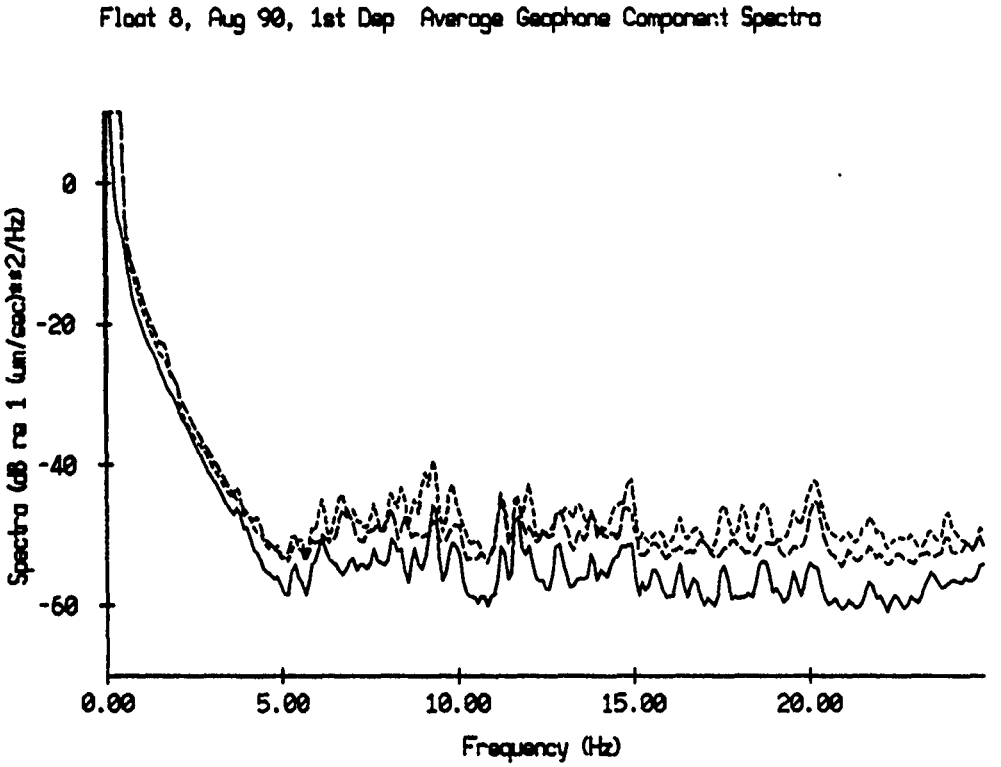
Float 8, Aug 90, 1st Dep Average Geophone Component Spectra
Spectra (dB re 1 (um/sec)s2/Hz)
0
-20
-40
-60
0.00
5.00
10.00
15.00
20.00
Frequency (Hz)

Figure X.29

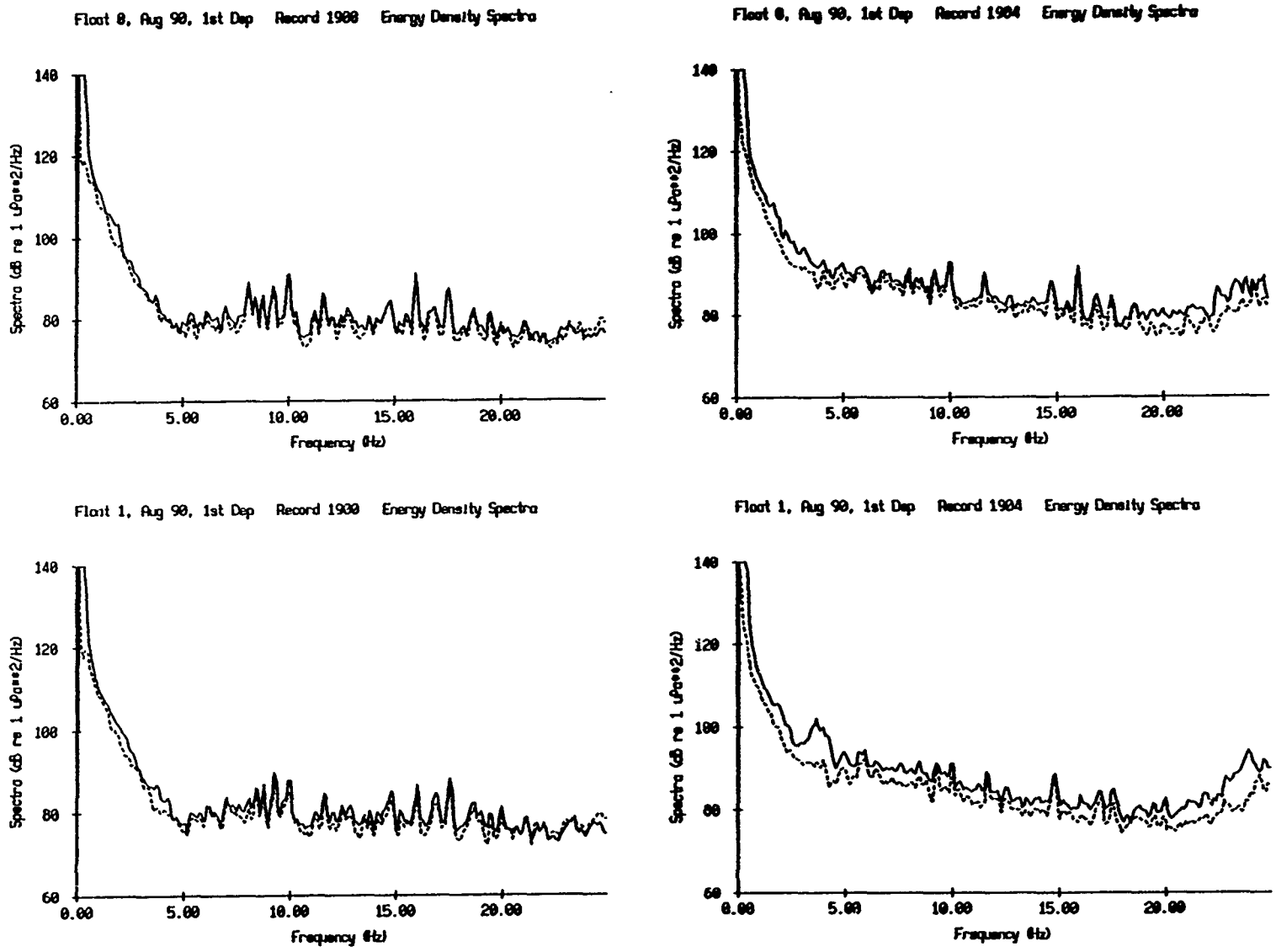
Float 0, Aug 90, 1st Dep Record 1900 Energy Density Spectra
Float 0, Aug 90, 1st Dep Record 1904 Energy Density Spectra
Float 1, Aug 90, 1st Dep Record 1900 Energy Density Spectra
Float 1, Aug 90, 1st Dep Record 1904 Energy Density Spectra
Spectra (dB re 1 uPa**2/Hz)
140
120
100
80
60
0.00
5.00
10.00
15.00
20.00
Frequency (Hz)

Figure X.30

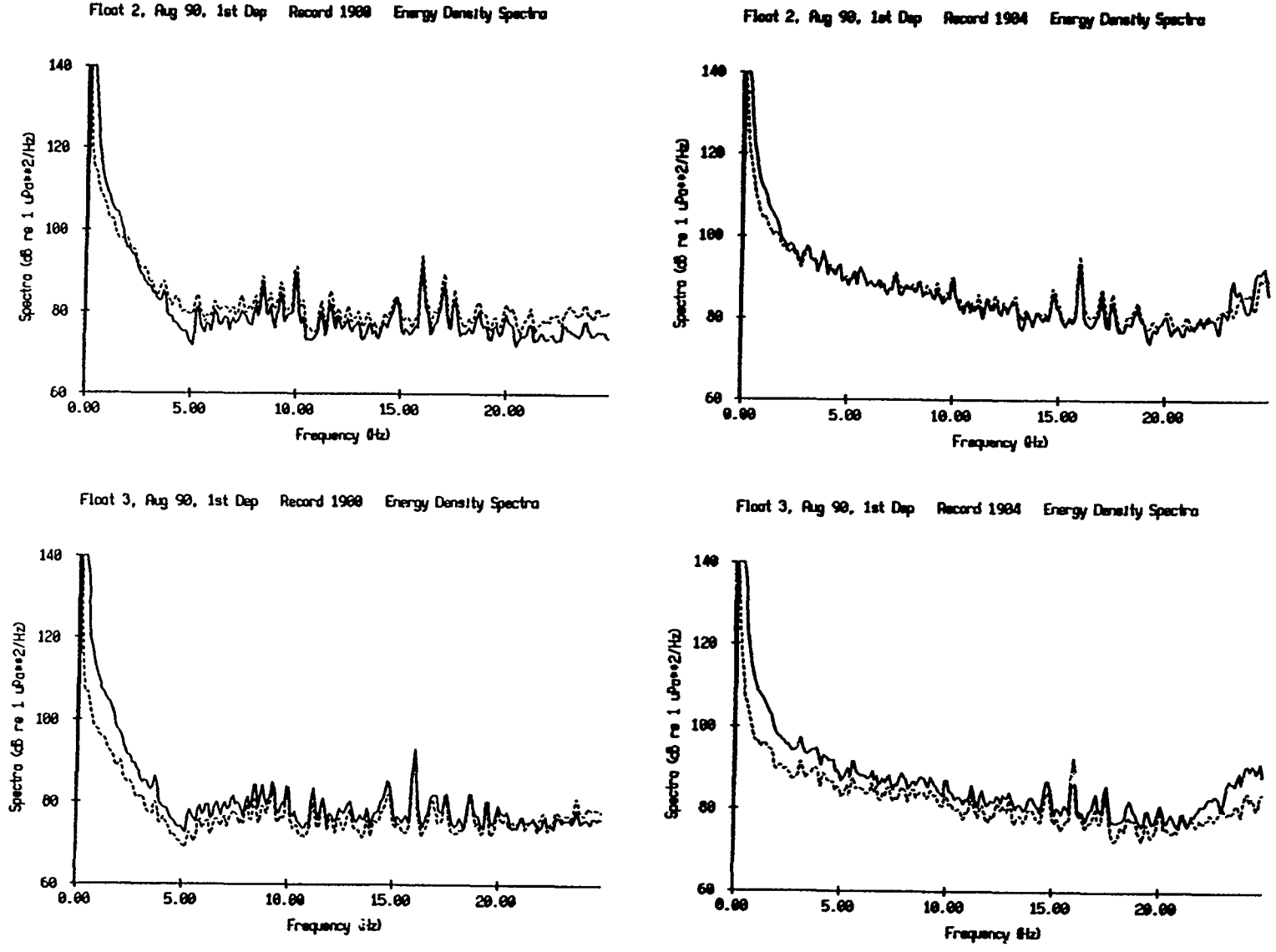
Float 2, Aug 90, 1st Dep Record 1900 Energy Density Spectra
Spectra (dB re 1 uPa**2/Hz)
140
120
100
80
60
0.00
5.00
10.00
15.00
20.00
Frequency (Hz)
Float 2, Aug 90, 1st Dep Record 1904 Energy Density Spectra
Spectra (dB re 1 uPa**2/Hz)
140
120
100
80
60
0.00
5.00
10.00
15.00
20.00
Frequency (Hz)
Float 3, Aug 90, 1st Dep Record 1900 Energy Density Spectra
Spectra (dB re 1 uPa**2/Hz)
140
120
100
80
60
0.00
5.00
10.00
15.00
20.00
Frequency (Hz)
Float 3, Aug 90, 1st Dep Record 1904 Energy Density Spectra
Spectra (dB re 1 uPa**2/Hz)
140
120
100
80
60
0.00
5.00
10.00
15.00
20.00
Frequency (Hz)

Figure X.31

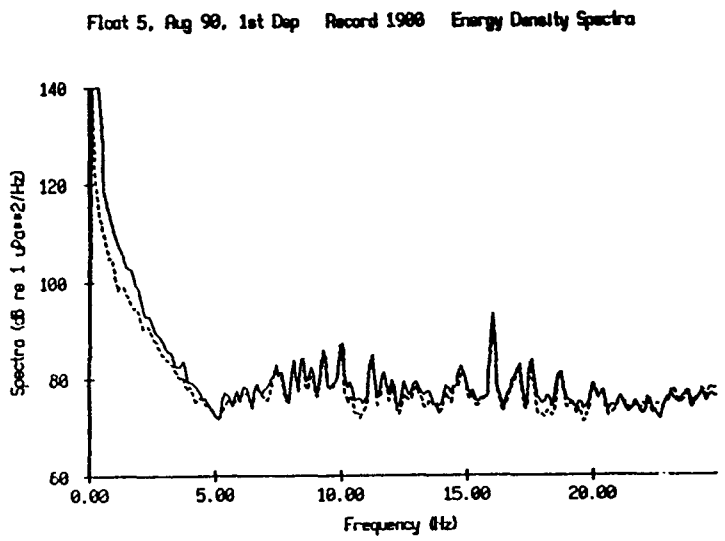
Float 5, Aug 90, 1st Dep Record 1900 Energy Density Spectra
Spectra (dB re 1 uPa**2/Hz)
140
120
100
80
60
0.00
5.00
10.00
15.00
20.00
Frequency (Hz)

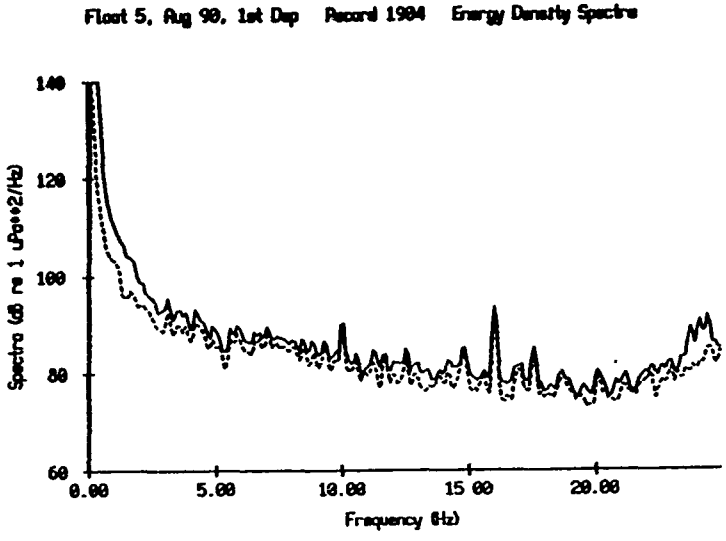
Float 5, Aug 90, 1st Dep Record 1904 Energy Density Spectra
Spectra (dB re 1 uPa**2/Hz)
140
120
100
80
60
0.00
5.00
10.00
15 00
20.00
Frequency (Hz)

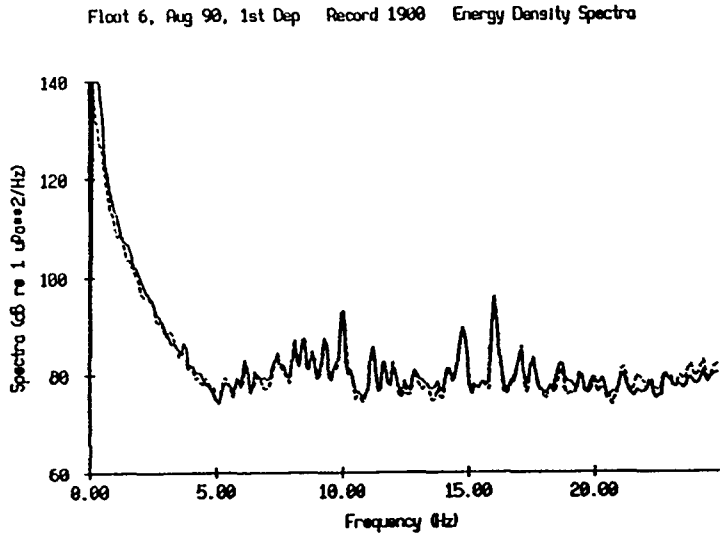
Float 6, Aug 90, 1st Dep Record 1900 Energy Density Spectra
Spectra (dB re 1 uPa**2/Hz)
140
120
100
80
60
0.00
5.00
10.00
15.00
20.00
Frequency (Hz)

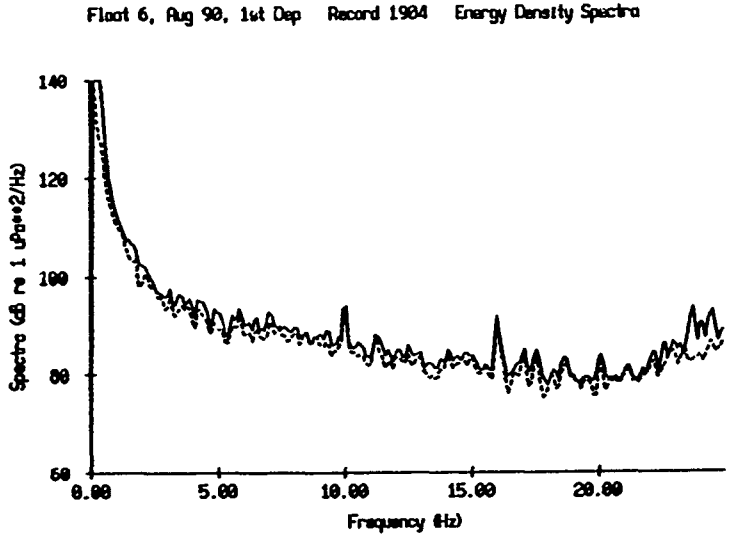
Float 6, Aug 90, 1st Dep Record 1904 Energy Density Spectra
Spectra (dB re 1 uPa**2/Hz)
140
120
100
80
60
0.00
5.00
10.00
15.00
20.00
Frequency (Hz)

Figure X.32

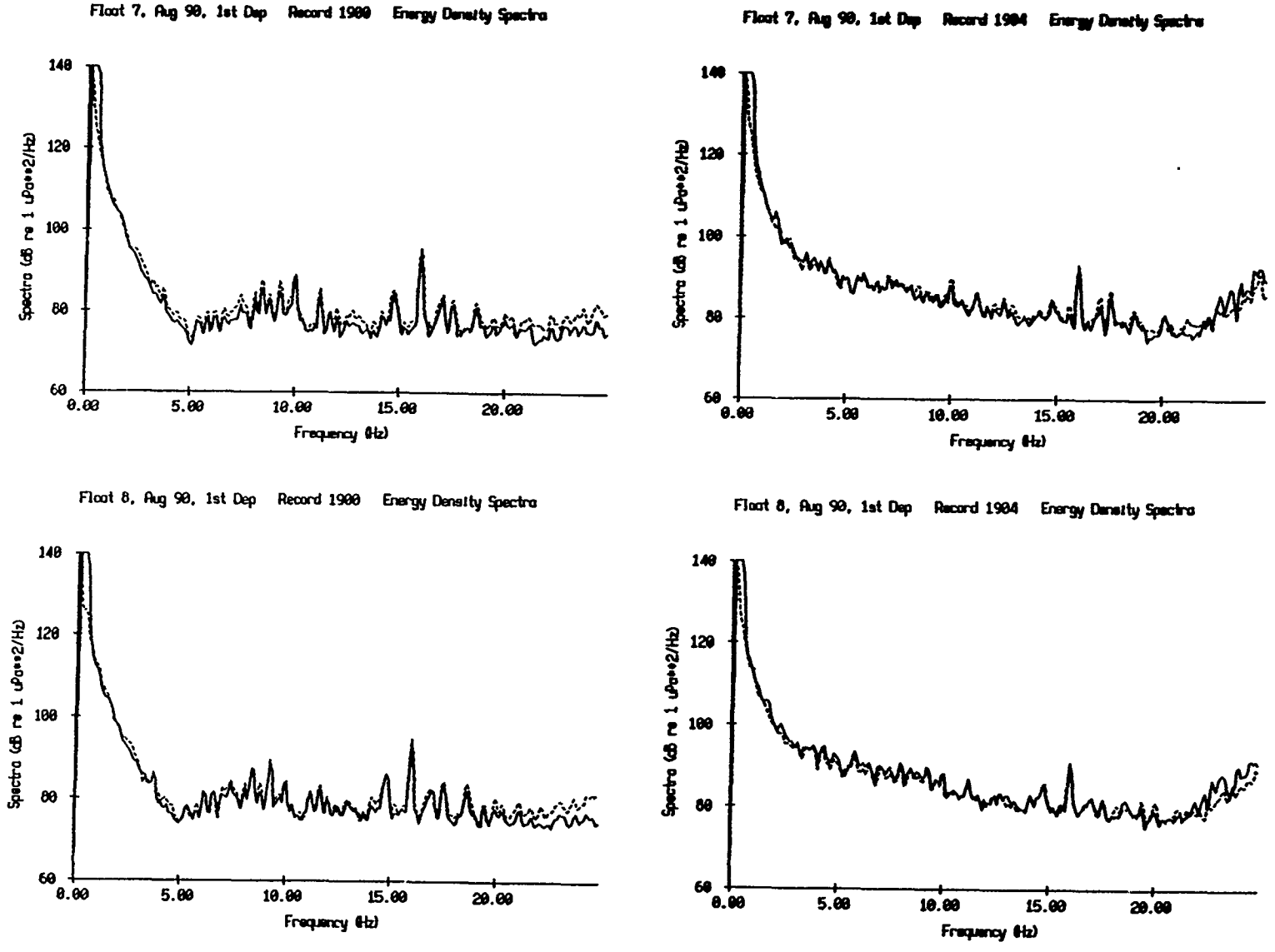
Float 7, Aug 90, 1st Dep Record 1900 Energy Density Spectra
Spectra (dB re 1 uPa**2/Hz)
140
120
100
80
60
0.00
5.00
10.00
15.00
20.00
Frequency (Hz)
Float 7, Aug 90, 1st Dep Record 1904 Energy Density Spectra
Spectra (dB re 1 uPa**2/Hz)
140
120
100
80
60
0.00
5.00
10.00
15.00
20.00
Frequency (Hz)
Float 8, Aug 90, 1st Dep Record 1900 Energy Density Spectra
Spectra (dB re 1 uPa**2/Hz)
140
120
100
80
60
0.00
5.00
10.00
15.00
20.00
Frequency (Hz)
Float 8, Aug 90, 1st Dep Record 1904 Energy Density Spectra
Spectra (dB re 1 uPa**2/Hz)
140
120
100
80
60
0.00
5.00
10.00
15.00
20.00
Frequency (Hz)

Figure X.33

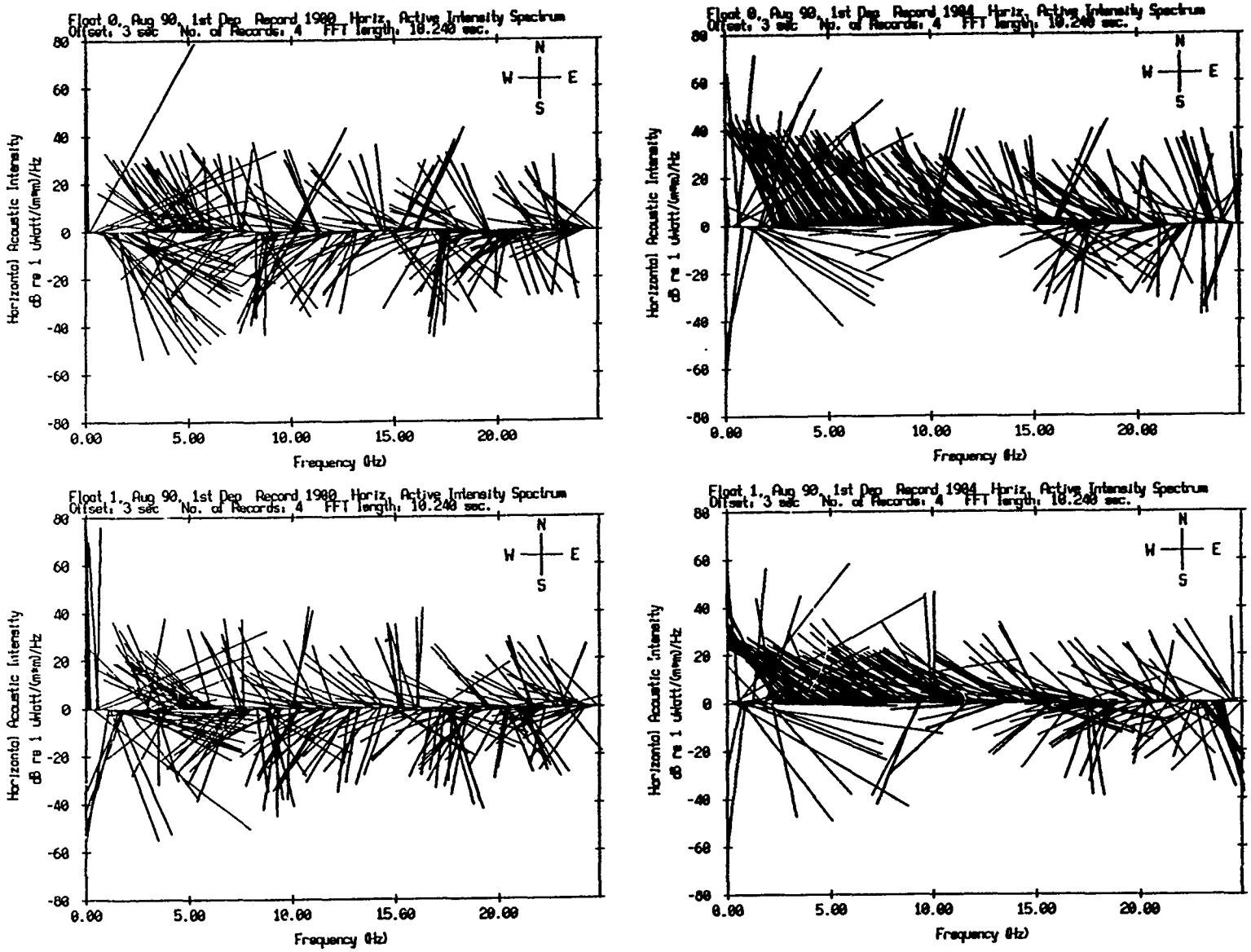
Float 0, Aug 90, 1st Dep Record 1980 Horiz. Active Intensity Spectrum
Offset: 3 sec No. of Records: 4 FFT length: 10.240 sec.
Horizontal Acoustic Intensity
dB re 1 uWatt/(m*m)/Hz
Frequency (Hz)
N
W
E
S
Float 0, Aug 90, 1st Dep Record 1984 Horiz. Active Intensity Spectrum
Offset: 3 sec No. of Records: 4 FFT length: 10.240 sec.
Horizontal Acoustic Intensity
dB re 1 uWatt/(m*m)/Hz
Frequency (Hz)
Float 1, Aug 90, 1st Dep Record 1980 Horiz. Active Intensity Spectrum
Offset: 3 sec No. of Records: 4 FFT length: 10.240 sec.
Horizontal Acoustic Intensity
dB re 1 uWatt/(m*m)/Hz
Frequency (Hz)
Float 1, Aug 90, 1st Dep Record 1984 Horiz. Active Intensity Spectrum
Offset: 3 sec No. of Records: 4 FFT length: 10.240 sec.
Horizontal Acoustic Intensity
dB re 1 uWatt/(m*m)/Hz
Frequency (Hz)

Figure X.34

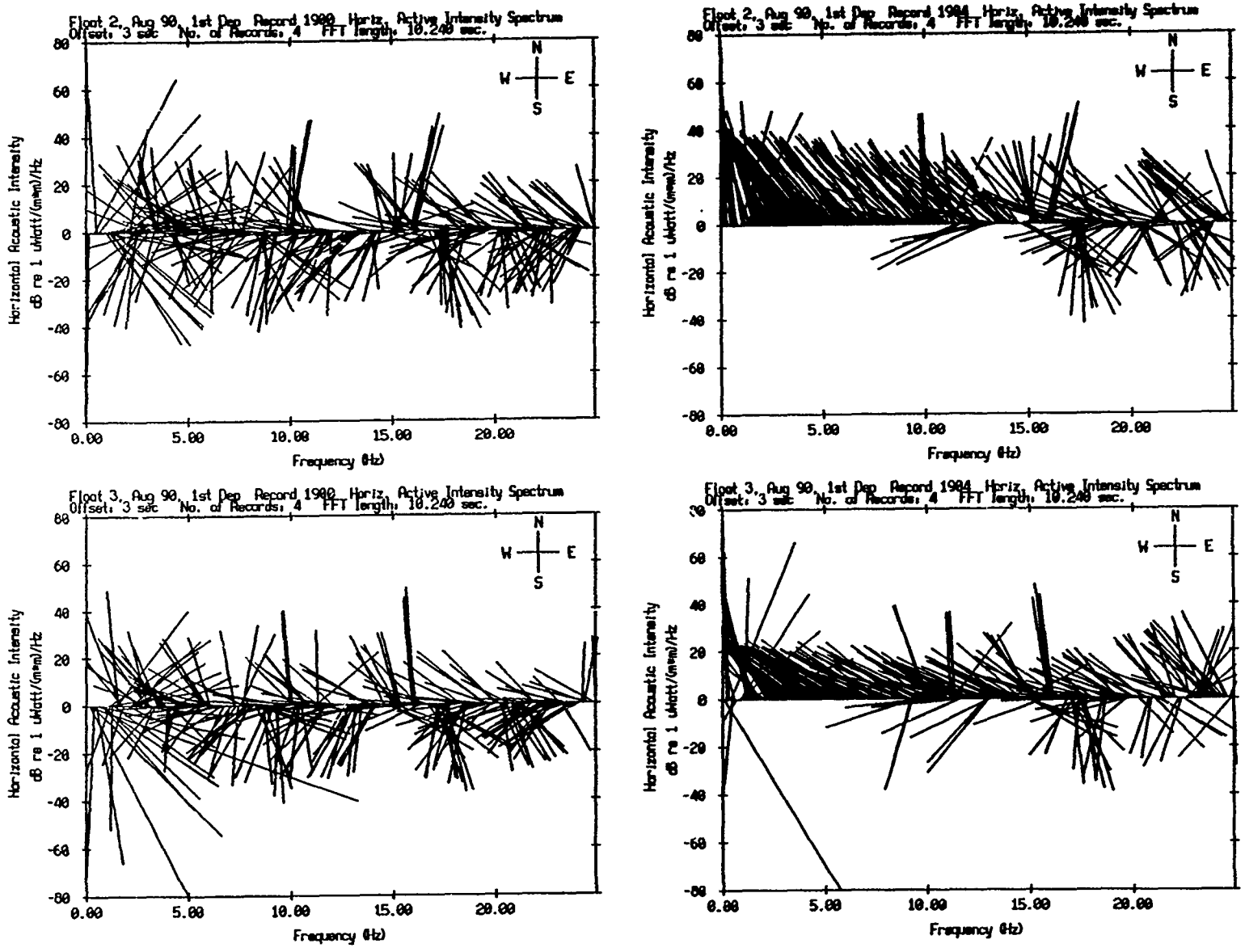
Float 2, Aug 90, 1st Dep Record 1980 Horiz. Active Intensity Spectrum
Offset: 3 sec No. of Records: 4 FFT length: 10.240 sec.
Horizontal Acoustic Intensity
dB re 1 uWatt/(m*m)/Hz
Frequency (Hz)
N
W
E
S
Float 2, Aug 90, 1st Dep Record 1984 Horiz. Active Intensity Spectrum
Offset: 3 sec No. of Records: 4 FFT length: 10.240 sec.
Horizontal Acoustic Intensity
dB re 1 uWatt/(m*m)/Hz
Frequency (Hz)
Float 3, Aug 90, 1st Dep Record 1980 Horiz. Active Intensity Spectrum
Offset: 3 sec No. of Records: 4 FFT length: 10.240 sec.
Horizontal Acoustic Intensity
dB re 1 uWatt/(m*m)/Hz
Frequency (Hz)
Float 3, Aug 90, 1st Dep Record 1984 Horiz. Active Intensity Spectrum
Offset: 3 sec No. of Records: 4 FFT length: 10.240 sec.
Horizontal Acoustic Intensity
dB re 1 uWatt/(m*m)/Hz
Frequency (Hz)

Figure X.35

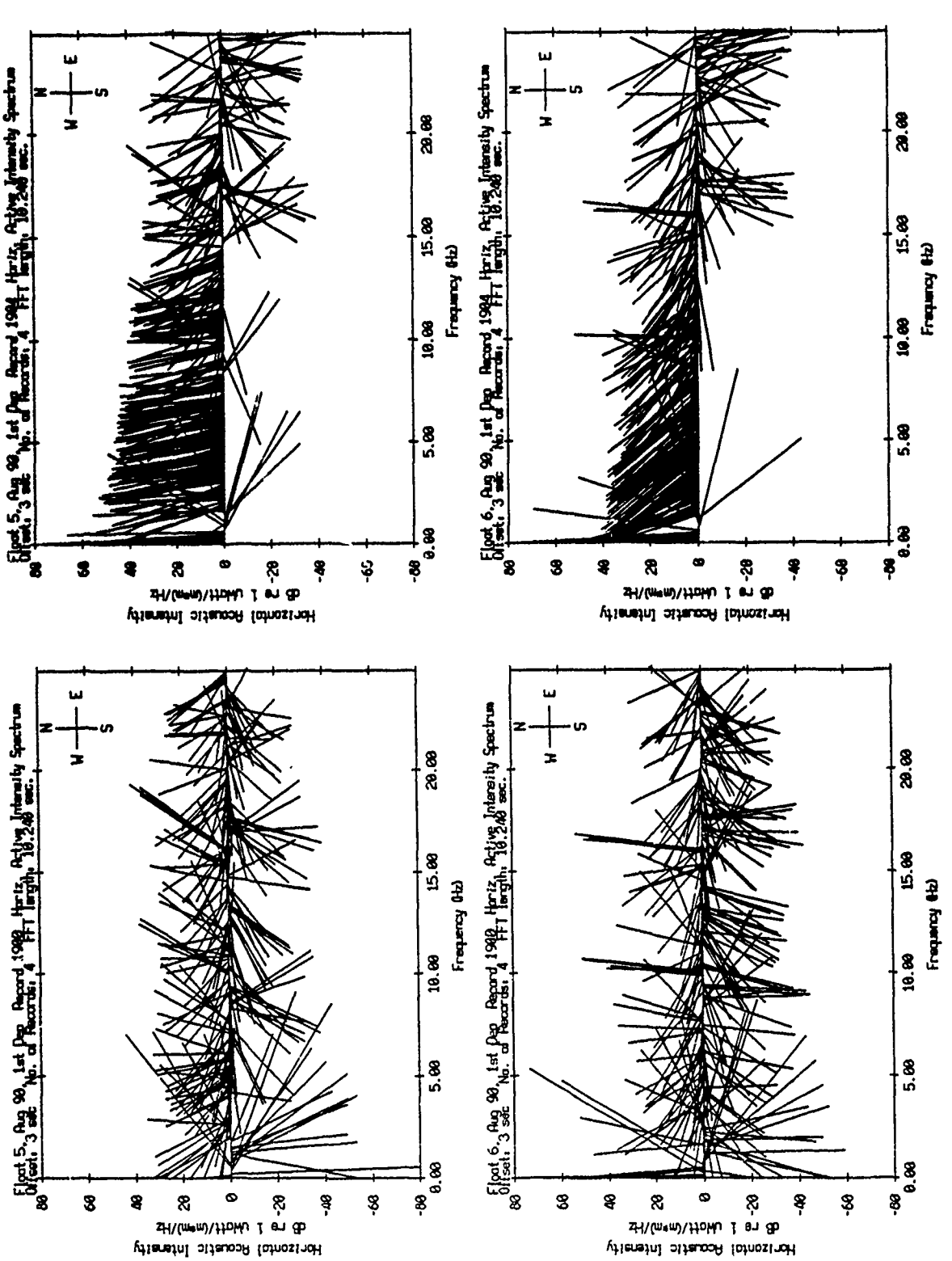
Float 5, Aug 90, 1st Dep. Record 1900, Horiz. Active Intensity Spectrum
Offset: 3 sec No. of Records: 4 FFT length: 10.240 sec.
Horizontal Acoustic Intensity
dB re 1 uWatt/(m*m)/Hz
Frequency (Hz)
Float 6, Aug 90, 1st Dep. Record 1904, Horiz. Active Intensity Spectrum
Offset: 3 sec No. of Records: 4 FFT length: 10.240 sec.
Horizontal Acoustic Intensity
dB re 1 uWatt/(m*m)/Hz
Frequency (Hz)
Float 5, Aug 90, 1st Dep. Record 1900, Horiz. Active Intensity Spectrum
Offset: 3 sec No. of Records: 4 FFT length: 10.240 sec.
Horizontal Acoustic Intensity
dB re 1 uWatt/(m*m)/Hz
Frequency (Hz)
Float 6, Aug 90, 1st Dep. Record 1904, Horiz. Active Intensity Spectrum
Offset: 3 sec No. of Records: 4 FFT length: 10.240 sec.
Horizontal Acoustic Intensity
dB re 1 uWatt/(m*m)/Hz
Frequency (Hz)

Figure X.36

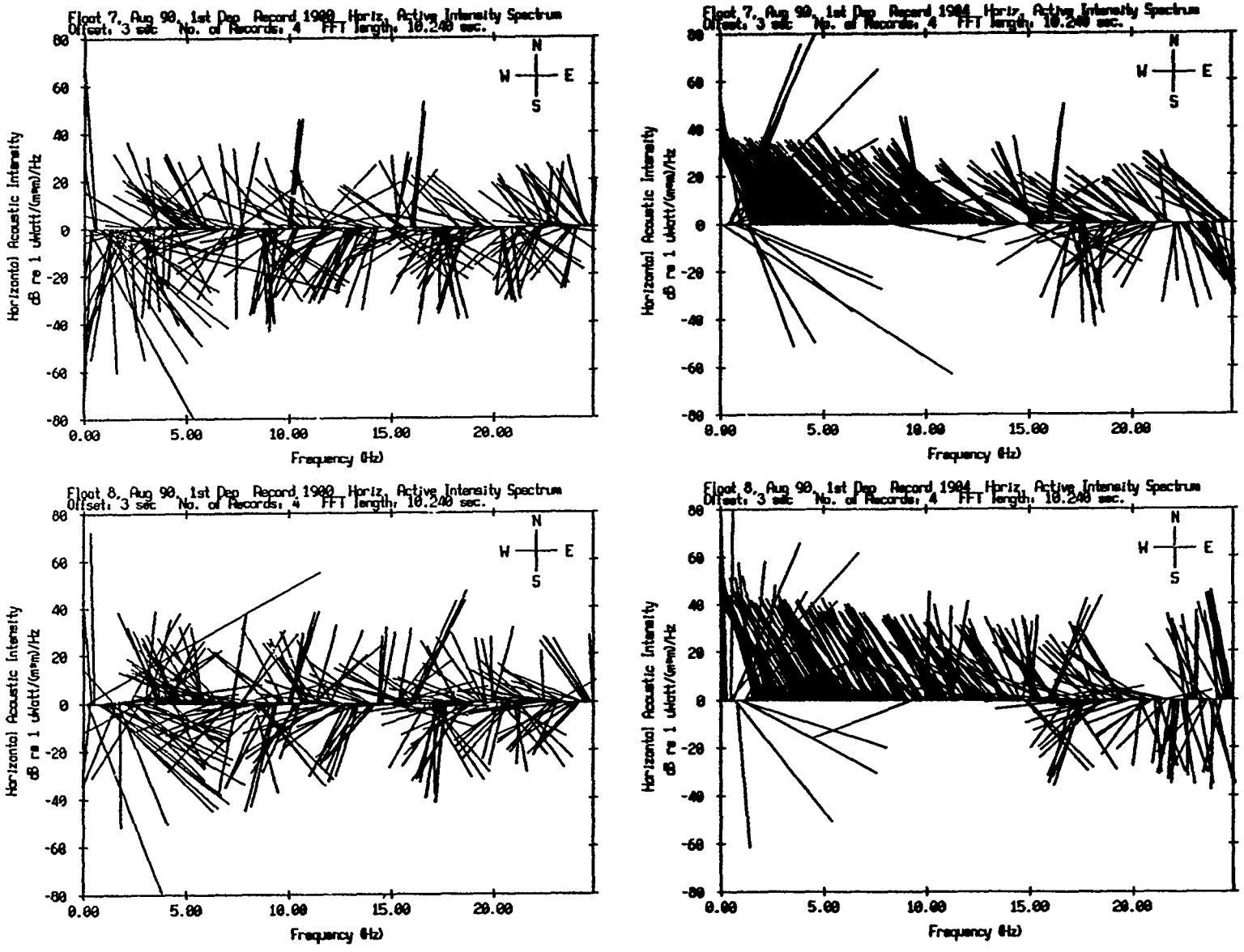
Float 7, Aug 90, 1st Dep Record 1900 Horiz. Active Intensity Spectrum
Offset: 3 sec No. of Records: 4 FFT length: 10.240 sec.
Horizontal Acoustic Intensity
dB re 1 uWatt/(m*m)/Hz
Frequency (Hz)
Float 7, Aug 90, 1st Dep Record 1904 Horiz. Active Intensity Spectrum
Offset: 3 sec No. of Records: 4 FFT length: 10.240 sec.
Horizontal Acoustic Intensity
dB re 1 uWatt/(m*m)/Hz
Frequency (Hz)
Float 8, Aug 90, 1st Dep Record 1900 Horiz. Active Intensity Spectrum
Offset: 3 sec No. of Records: 4 FFT length: 10.240 sec.
Horizontal Acoustic Intensity
dB re 1 uWatt/(m*m)/Hz
Frequency (Hz)
Float 8, Aug 90, 1st Dep Record 1904 Horiz. Active Intensity Spectrum
Offset: 3 sec No. of Records: 4 FFT length: 10.240 sec.
Horizontal Acoustic Intensity
dB re 1 uWatt/(m*m)/Hz
Frequency (Hz)

Figure X.37

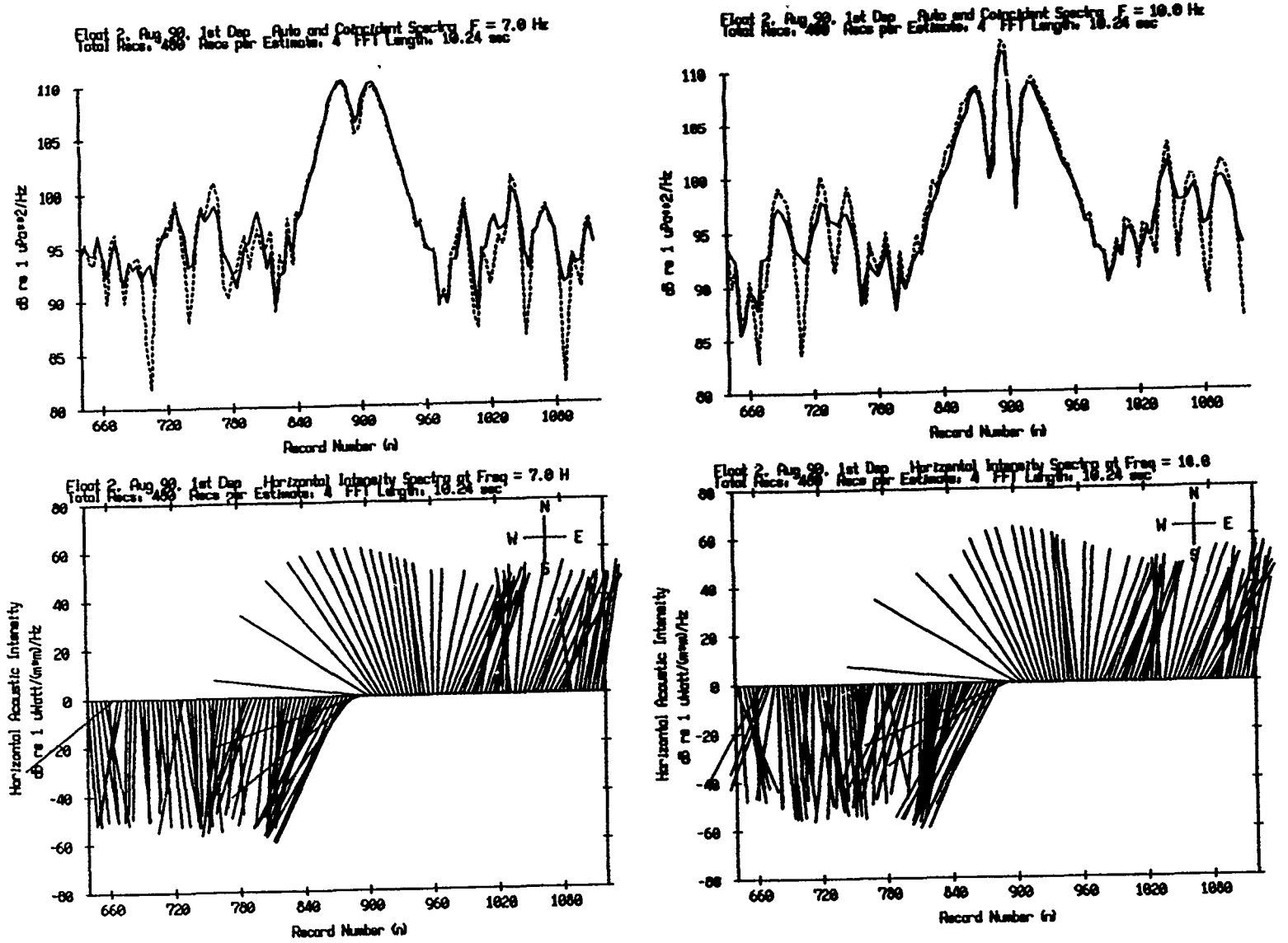
Float 2, Aug 90, 1st Dep Auto and Coincident Spectra, F = 7.0 Hz
Total Recs: 480 Recs per Estimate: 4 FFT Length: 10.24 sec
dB re 1 uPasc2/Hz
Record Number (n)
Float 2, Aug 90, 1st Dep Auto and Coincident Spectra, F = 10.0 Hz
Total Recs: 480 Recs per Estimate: 4 FFT Length: 10.24 sec
dB re 1 uPasc2/Hz
Record Number (n)
Float 2, Aug 90, 1st Dep Horizontal Intensity Spectra at Freq = 7.0 H
Total Recs: 480 Recs per Estimate: 4 FFT Length: 10.24 sec
N
W E
S
Horizontal Acoustic Intensity
dB re 1 uWatt/(um)2/Hz
Record Number (n)
Float 2, Aug 90, 1st Dep Horizontal Intensity Spectra at Freq = 10.0
Total Recs: 480 Recs per Estimate: 4 FFT Length: 10.24 sec
N
W E
S
Horizontal Acoustic Intensity
dB re 1 uWatt/(um)2/Hz
Record Number (n)

Figure X.38

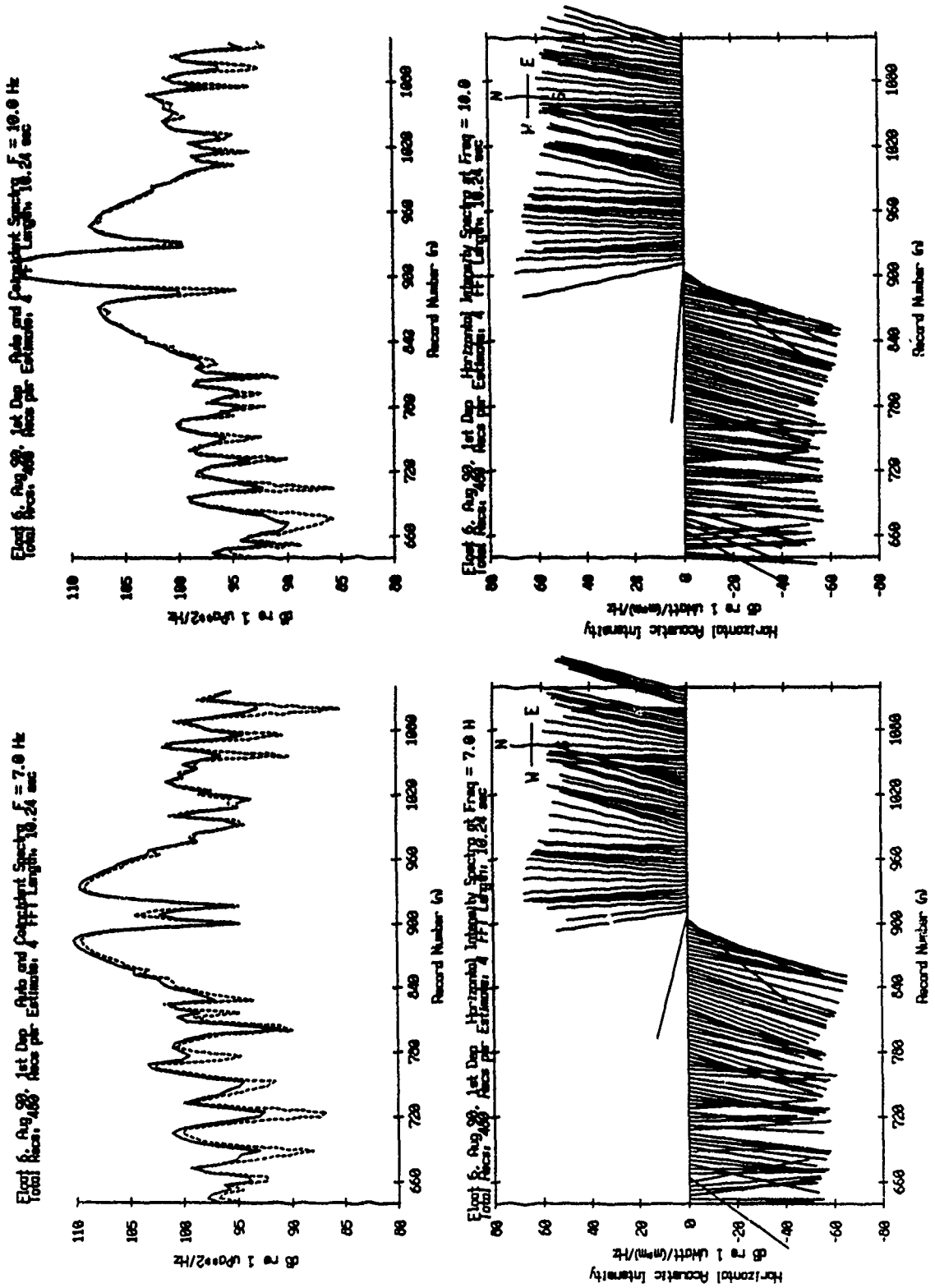
Record Number (n)
dB re 1 uPa**2/Hz
Horizontal Acoustic Intensity
dB re 1 uWatt/(m**m)/Hz
N
E
W

Figure X.39

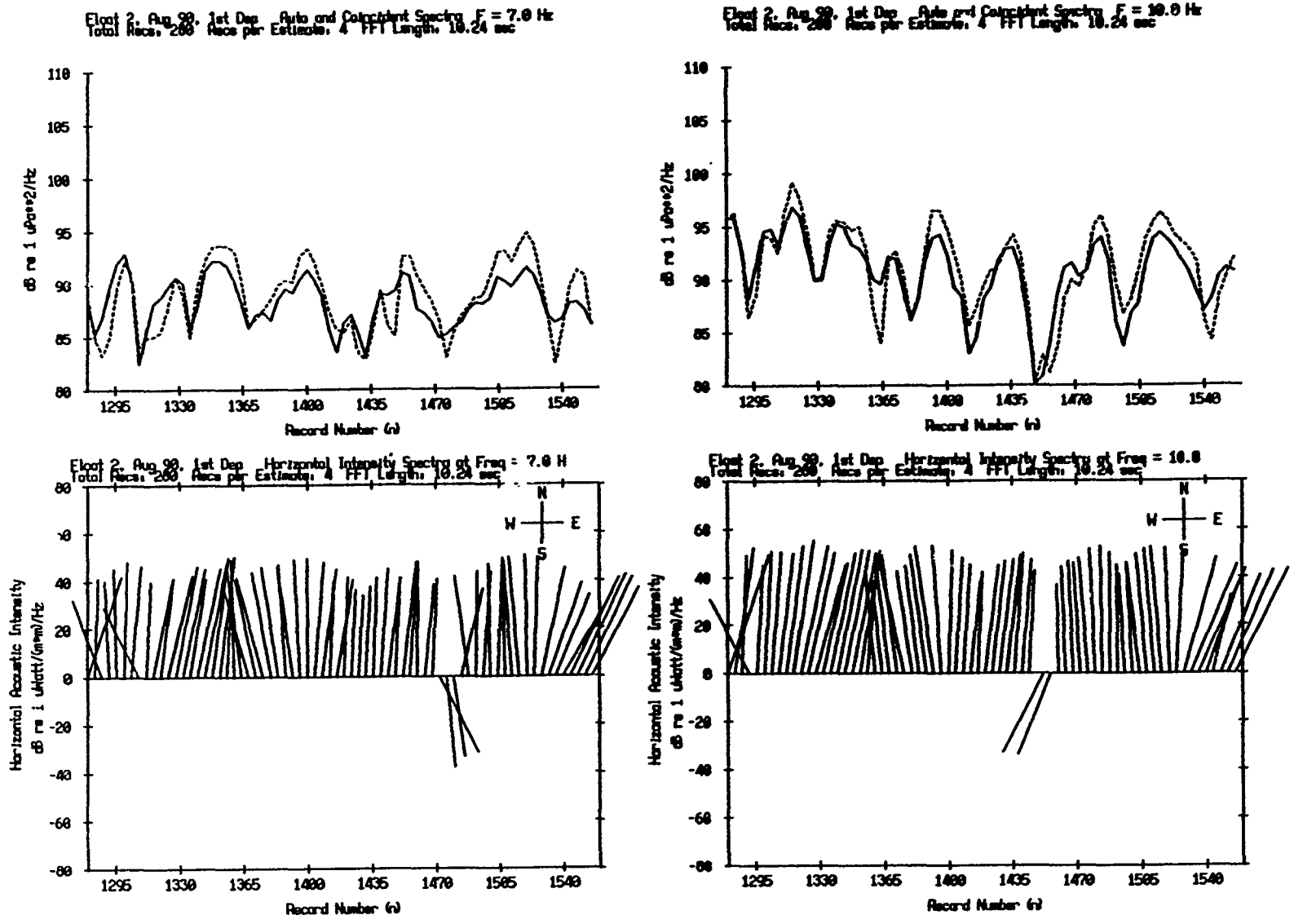
Float 2, Aug 90, 1st Dep Auto and Coincident Spectra, F = 7.0 Hz
Total Recs: 200 Recs per Estimate: 4 FFT Length: 10.24 sec
dB re 1 uPa**2/Hz
Record Number (n)
Float 2, Aug 90, 1st Dep Auto and Coincident Spectra, F = 10.0 Hz
Total Recs: 200 Recs per Estimate: 4 FFT Length: 10.24 sec
dB re 1 uPa**2/Hz
Record Number (n)
Float 2, Aug 90, 1st Dep Horizontal Intensity Spectra at Freq = 7.0 H
Total Recs: 200 Recs per Estimate: 4 FFT Length: 10.24 sec
Horizontal Acoustic Intensity
dB re 1 uWatt/(m**2)/Hz
N
W
E
S
Record Number (n)
Float 2, Aug 90, 1st Dep Horizontal Intensity Spectra at Freq = 10.0
Total Recs: 200 Recs per Estimate: 4 FFT Length: 10.24 sec
Horizontal Acoustic Intensity
dB re 1 uWatt/(m**2)/Hz
N
W
E
S
Record Number (n)

Figure X.40

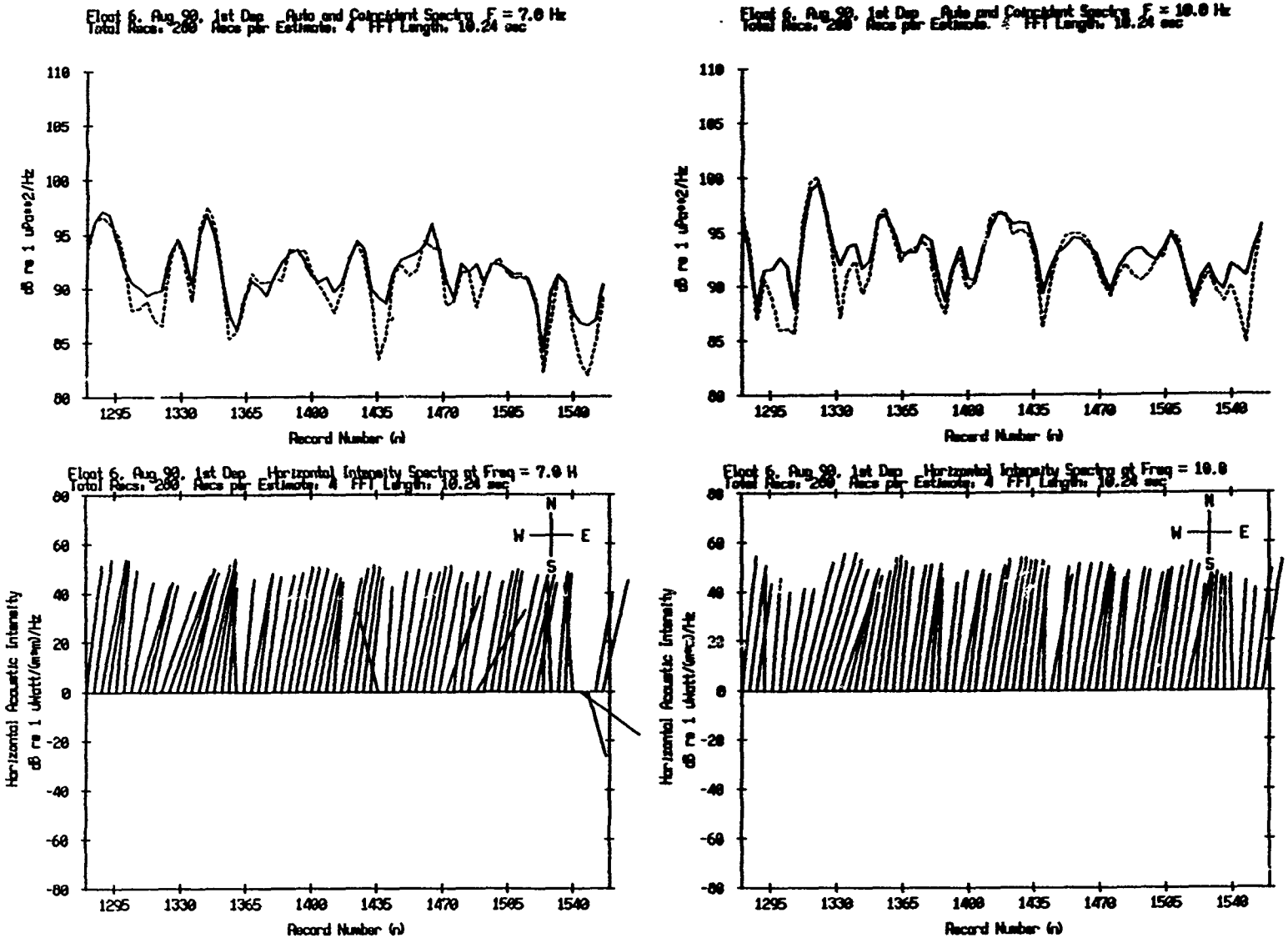
Float 6, Aug 99, 1st Dep Auto and Coincident Spectra @ F = 7.0 Hz
Total Recs: 280 Recs per Estimate: 4 FFT Length: 10.24 sec
dB re 1 uPa**2/Hz
Record Number (n)
Float 6, Aug 99, 1st Dep Auto and Coincident Spectra @ F = 10.0 Hz
Total Recs: 280 Recs per Estimate: 4 FFT Length: 10.24 sec
dB re 1 uPa**2/Hz
Record Number (n)
Float 6, Aug 99, 1st Dep Horizontal Intensity Spectra at Freq = 7.0 H
Total Recs: 280 Recs per Estimate: 4 FFT Length: 10.24 sec
Horizontal Acoustic Intensity
dB re 1 uWatt/(cm2)/Hz
N
W
E
S
Record Number (n)
Float 6, Aug 99, 1st Dep Horizontal Intensity Spectra at Freq = 10.0
Total Recs: 280 Recs per Estimate: 4 FFT Length: 10.24 sec
Horizontal Acoustic Intensity
dB re 1 uWatt/(cm2)/Hz
N
W
E
S
Record Number (n)

Figure X.41

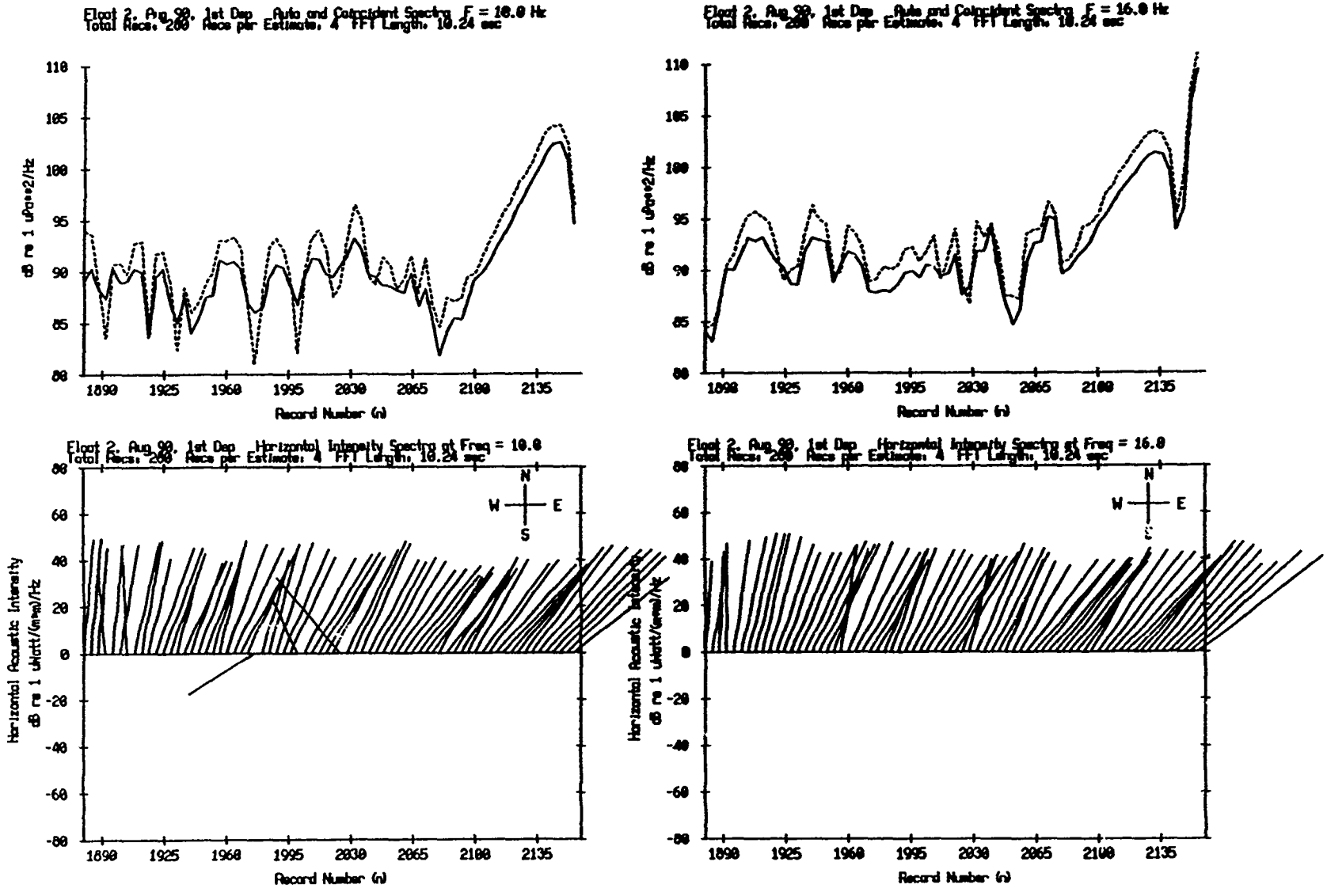
Float 2, Aug 90, 1st Dep Auto and Coincident Spectra F = 10.0 Hz
Total Recs: 200 Recs per Estimate: 4 FFT Length: 10.24 sec
dB re 1 uPa**2/Hz
Record Number (n)
Float 2, Aug 90, 1st Dep Auto and Coincident Spectra F = 16.0 Hz
Total Recs: 200 Recs per Estimate: 4 FFT Length: 10.24 sec
dB re 1 uPa**2/Hz
Record Number (n)
Float 2, Aug 90, 1st Dep Horizontal Intensity Spectra at Freq = 10.0
Total Recs: 200 Recs per Estimate: 4 FFT Length: 10.24 sec
Horizontal Acoustic Intensity
dB re 1 uWatt/(m**2)/Hz
N
W
E
S
Record Number (n)
Float 2, Aug 90, 1st Dep Horizontal Intensity Spectra at Freq = 16.0
Total Recs: 200 Recs per Estimate: 4 FFT Length: 10.24 sec
Horizontal Acoustic Intensity
dB re 1 uWatt/(m**2)/Hz
N
W
E
Record Number (n)

Figure X.42

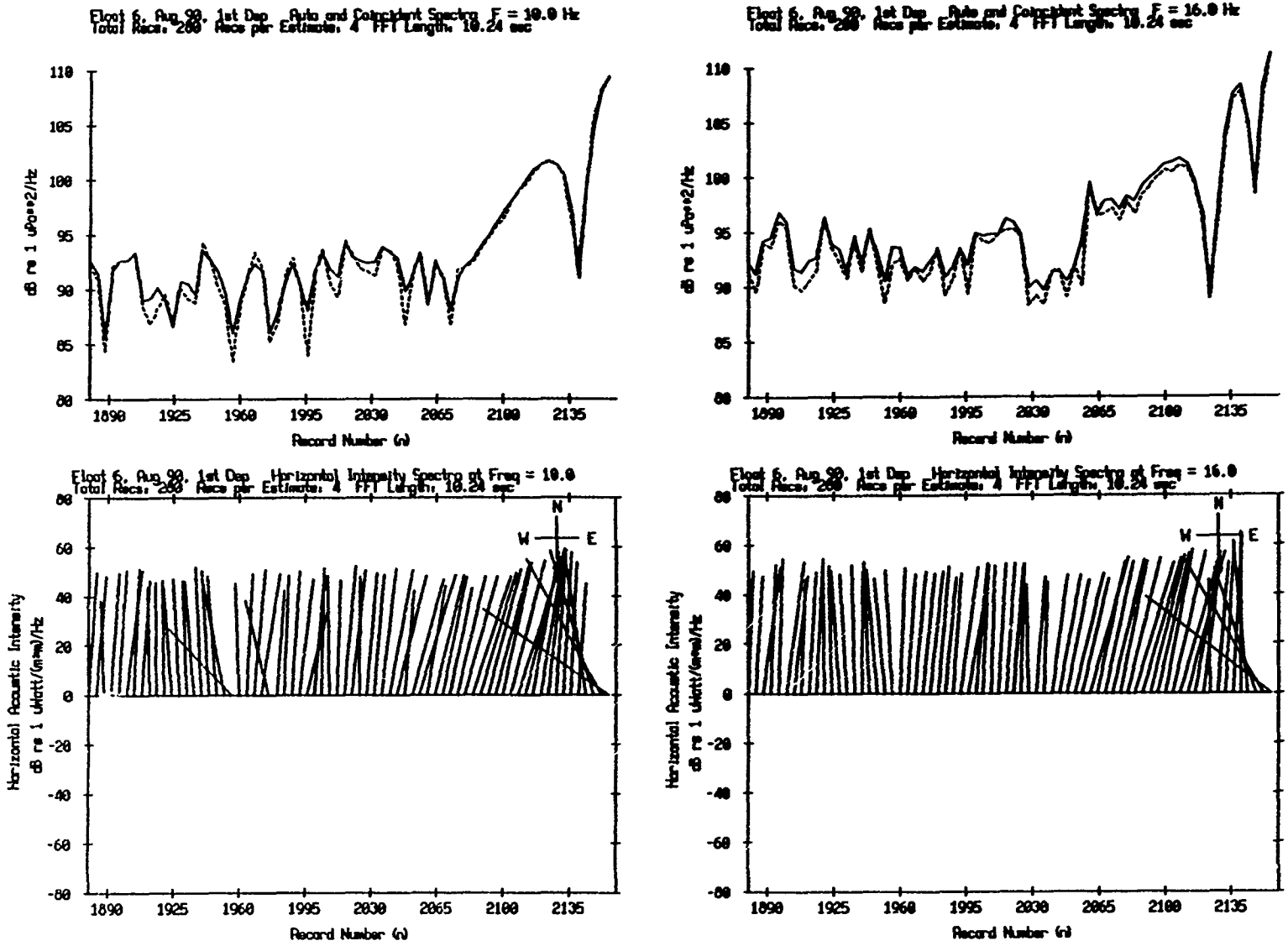
Float 6, Aug 99, 1st Dep Auto and Coincident Spectra, F = 10.0 Hz
Total Recs: 260 Recs per Estimate: 4 FFT Length: 10.24 sec
dB re 1 uPa**2/Hz
Record Number (n)
Float 6, Aug 99, 1st Dep Auto and Coincident Spectra, F = 16.0 Hz
Total Recs: 260 Recs per Estimate: 4 FFT Length: 10.24 sec
dB re 1 uPa**2/Hz
Record Number (n)
Float 6, Aug 99, 1st Dep Horizontal Intensity Spectra at Freq = 10.0
Total Recs: 260 Recs per Estimate: 4 FFT Length: 10.24 sec
N
W
E
Horizontal Acoustic Intensity
dB re 1 uWatt/(m**2)/Hz
Record Number (n)
Float 6, Aug 99, 1st Dep Horizontal Intensity Spectra at Freq = 16.0
Total Recs: 260 Recs per Estimate: 4 FFT Length: 10.24 sec
N
W
E
Horizontal Acoustic Intensity
dB re 1 uWatt/(m**2)/Hz
Record Number (n)

Figure X.43

BLOCK DIAGRAM OF THE SWALLOW FLOAT INFRASONIC DATA ACQUISITION SYSTEM

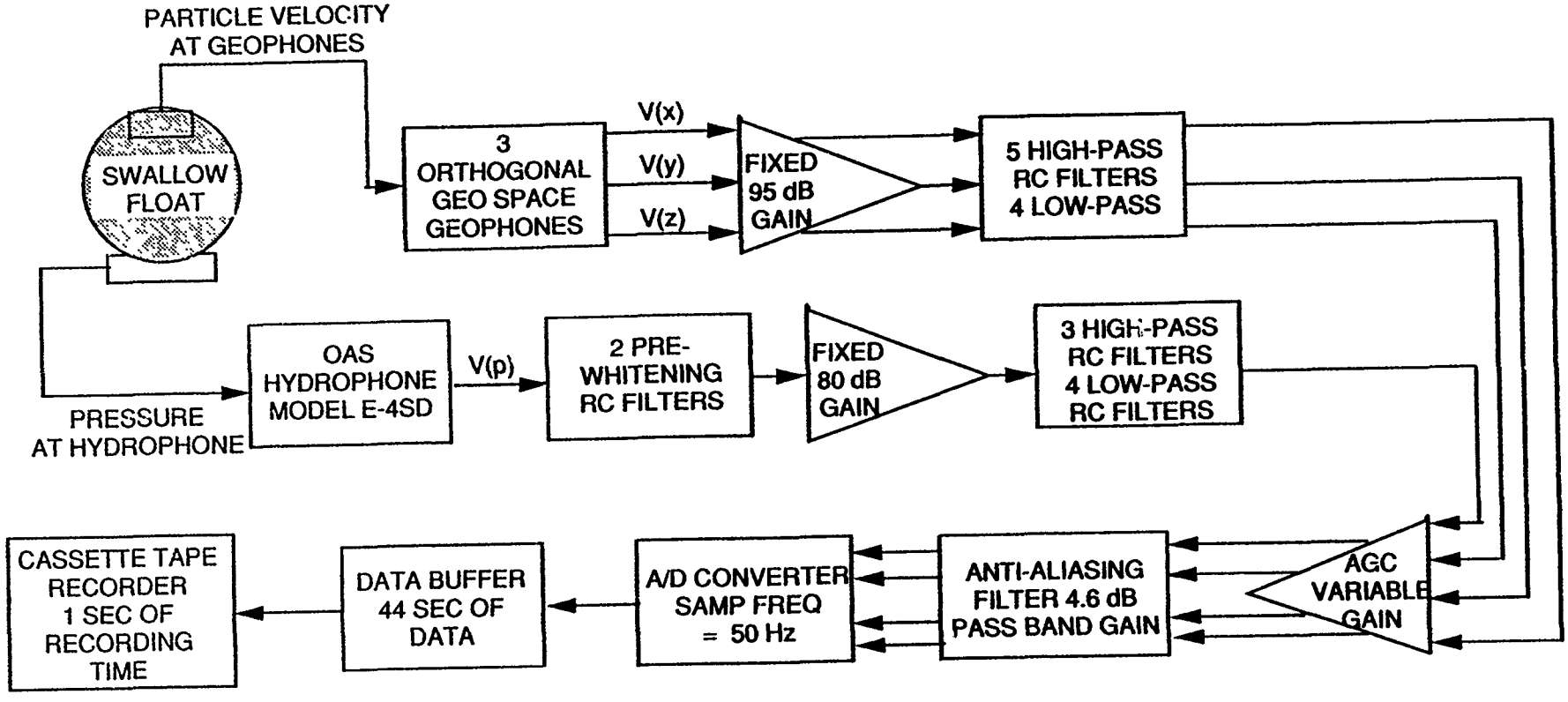

Figure A1.1

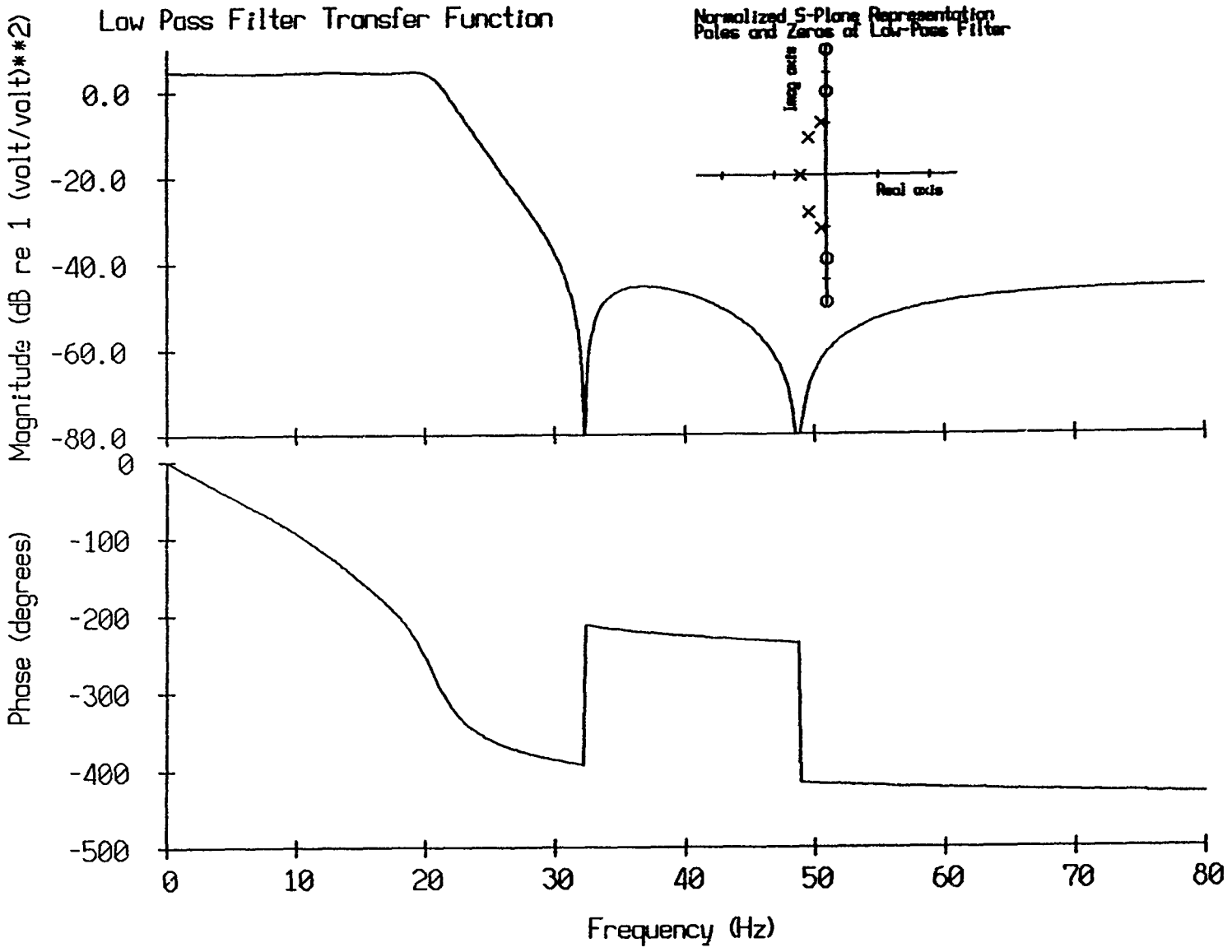
Low Pass Filter Transfer Function
Normalized S-Plane Representation
Poles and Zeros of Low-Pass Filter
Imag axis
Real axis
Magnitude (dB re 1 (volt/volt)**2)
0.0
-20.0
-40.0
-60.0
-80.0
Phase (degrees)
0
-100
-200
-300
-400
-500
0
10
20
30
40
50
60
70
80
Frequency (Hz)

Figure A1.2

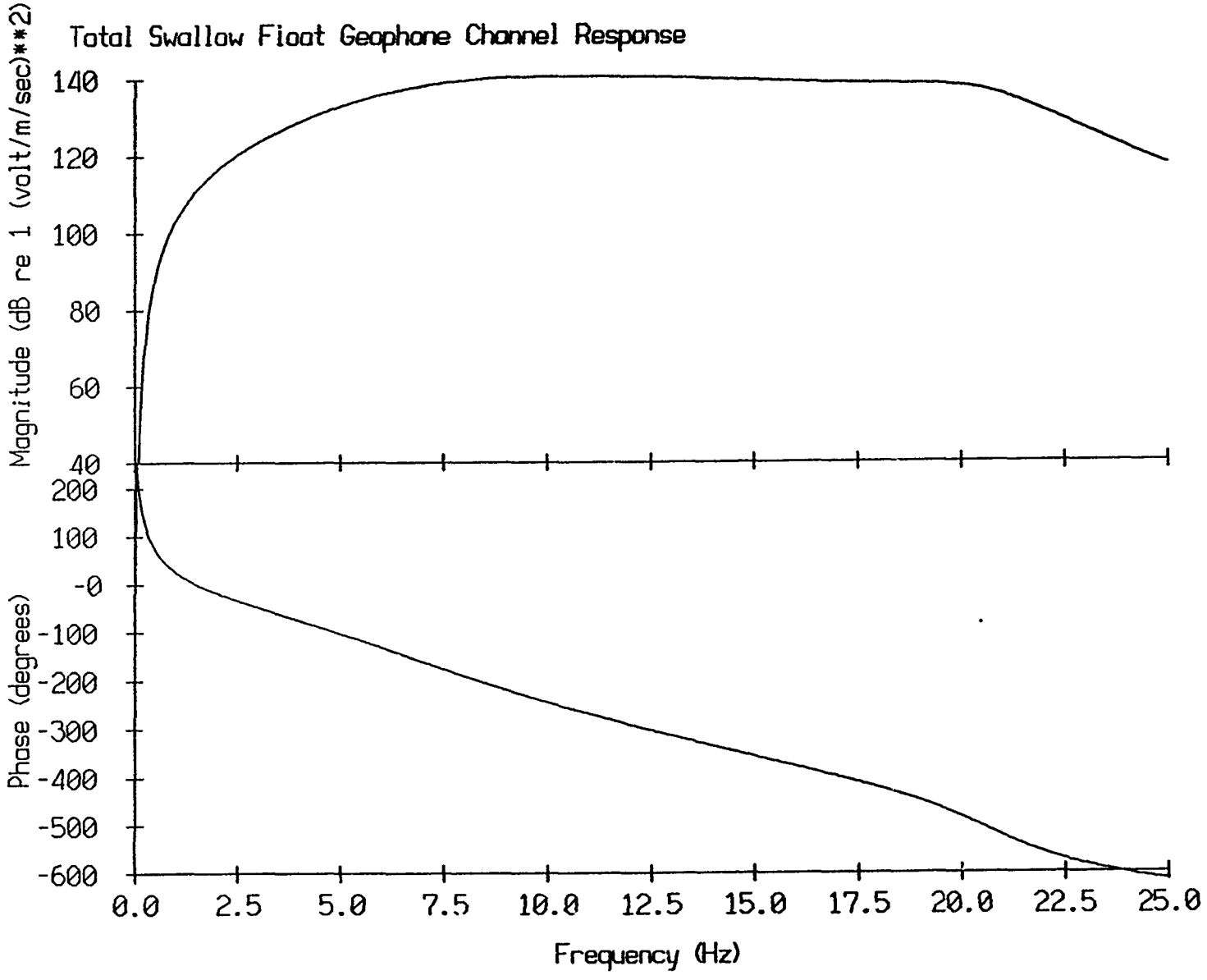
Total Swallow Float Geophone Channel Response
Magnitude (dB re 1 (volt/m/sec)**2)
140
120
100
80
60
40
Phase (degrees)
200
100
-0
-100
-200
-300
-400
-500
-600
0.0
2.5
5.0
7.5
10.0
12.5
15.0
17.5
20.0
22.5
25.0
Frequency (Hz)

Figure A1.3

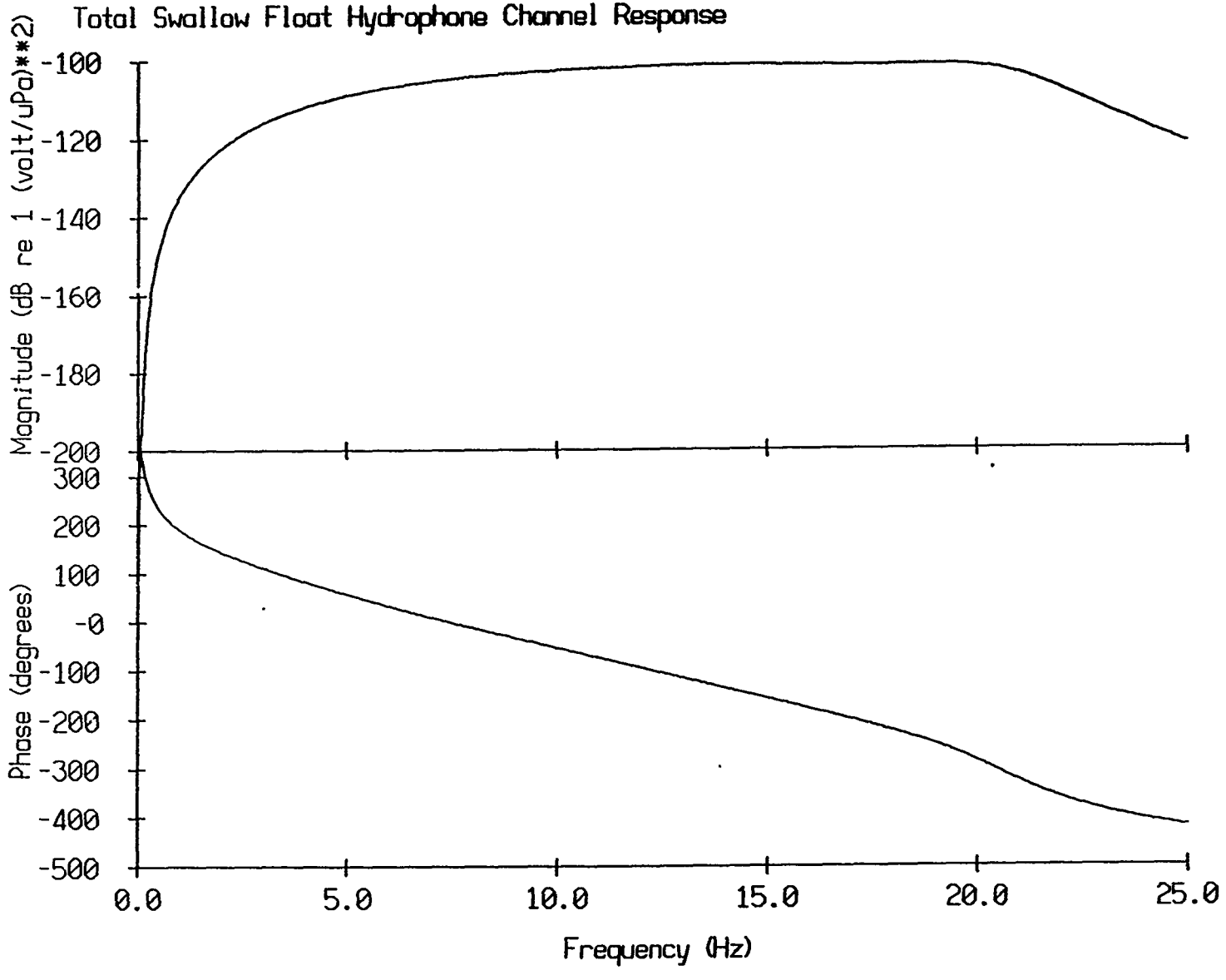
Total Swallow Float Hydrophone Channel Response
Magnitude (dB re 1 (volt/uPa)**2)
-100
-120
-140
-160
-180
-200
300
200
100
-0
-100
-200
-300
-400
-500
Phase (degrees)
0.0
5.0
10.0
15.0
20.0
25.0
Frequency (Hz)

Figure A1.4